EMERGING INFECTIOUS DISEASES®

U.S. CENTERS FOR DISEASE CONTROL AND PREVENTION

Fungal Infections

May 2025

CHAMPIGNONS. — *PLANCHE II.* (C. *Comestible*; I. *Indifférent*; S. *Suspect*; V. *Vénéneux*) : 1. *Lenzite* flasque, I. — 2. *Dédalée* du chêne, I. — *Polyporées* : 3. Luisant, I.; 4. Soufré, I.; 5. De couleurs variées, I.; 6. Du bouleau, I.; 7. Amadouvier, I. — *Bolets* : 8. Comestible (Cèpe de Bordeaux), C. — 9. Pomme de pin, C.; 10. Amer, V.; 11. Bronzé (Tête de nègre), C.; 12. Jaune, C.; 13. Raboteux, C.; 14. Raboteux (variété orangée), C.; 15. Satan, V.; 16. Blafard, S.; 17. Poivré, V.; 18. Bai brun, C.; 19. Des bœufs, C.; 20. Granulé, C. — 21. *Fistuline* foie (Foie ou Langue de bœuf), C. — *Hydnes* : 22. Imbriqué, C.; 23. Bosselé, C.; 24. Coralloïde, C.; 25. Hérisson, C. — 26. *Sparassis* crépu, C. — *Clavaires* : 27. Jaune, C.; 28. Dorée, S.; 29. Belle, C.; 30. Pilon, I. — 31. *Craterelle* corne d'abondance (Trompette des morts), C. — 32. *Stérée* pulvin, I. — 33. *Phallie* vulgaire, V. — 34. *Clathre* grillagé, I. — 35. *Cyathe* soyeux, I. — *Lycoperdons* : 36. A pierreries, I.; 37. En poire, I. — 38. *Scléroderme* vulgaire, I. — 39. *Géaster* hygrométrique, I. — 40. *Calocère* visqueux, I. — 41. *Tremelle* mésentérique, I. — 42. *Auriculaire* (oreille de Judas), I. — *Pezizes* : 43. Vésiculeuse, C.; 44. En coupe, C.; 45. Orangée, C.; 46. Cochenille, C.; 47. Oreille d'âne, C. — 48. *Bulgarie* salissante, I. — *Morilles* : 49. Comestible (blanche), C.; 50. Comestible (noire), C.; 51. A pied ridé, C.; 52. Conique, C. — *Helvelles* : 53. Crépue, C.; 54. Lacuneuse, C.; 55. Elastique, C. — 56. *Xylaire* du bois, I. — *Truffes* : 57. A spores noires, C.; 58. D'hiver, C.; 59. A veines plissées, C.; 60. D'été, C. — 61. *Ergotia* incarnat (très grossi). — 62. *Ergot* du seigle. — 63. *Ergot* du blé. — 64. *Charbon* du blé. — 65. *Torubia* militaire sur une guêpe. — 66. *Oïdium*. — 67. *Mildew*. — 68. *Black-rot*. — 69. *Anthracnose*. (*Les plantes — sauf 61 à 69 — sont toutes figurées au quart de gr. nat.*)

Adolphe Philippe Millot (1857–1921), *Champignons-couleurs 2 (Mushrooms colour plate 02)*. Public domain illustration from Larousse du XXe siècle, 1932 Éditions.

EMERGING INFECTIOUS DISEASES®

Emerging Infectious Diseases is published monthly by the Centers for Disease Control and Prevention, 1600 Clifton Rd NE, Mailstop H16-2, Atlanta, GA 30329-4018, USA. Telephone 404-639-1960; email eideditor@cdc.gov

EMERGING INFECTIOUS DISEASES®

Vol. 31, No. 5 May 2025

On the Cover

Adolphe Philippe Millot (1857–1921). *Champignons-couleurs 2 (Mushrooms color plate 02)*. Public domain illustration from Larousse du XXe siècle, 1932 Éditions.

About the Cover p. 1062

Synopses

Medscape EDUCATION ACTIVITY

Research

Medscape EDUCATION ACTIVITY

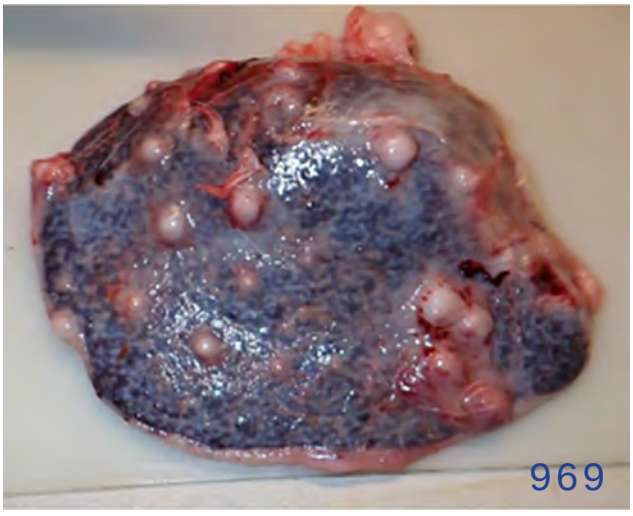

EMERGING INFECTIOUS DISEASES®
May 2025

Dispatches

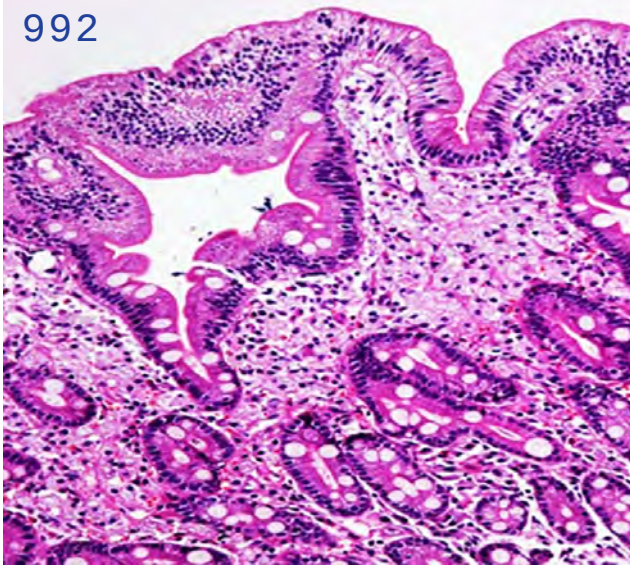

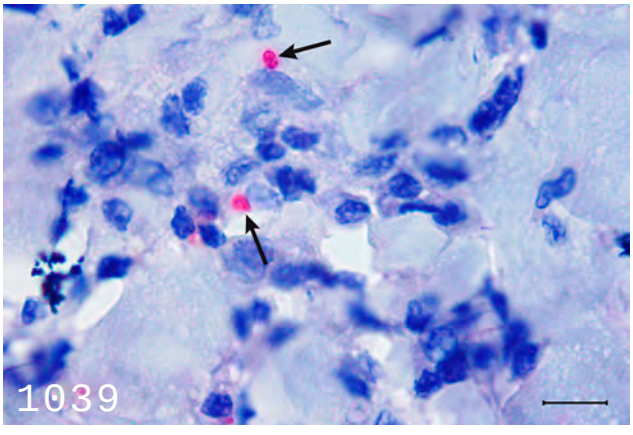

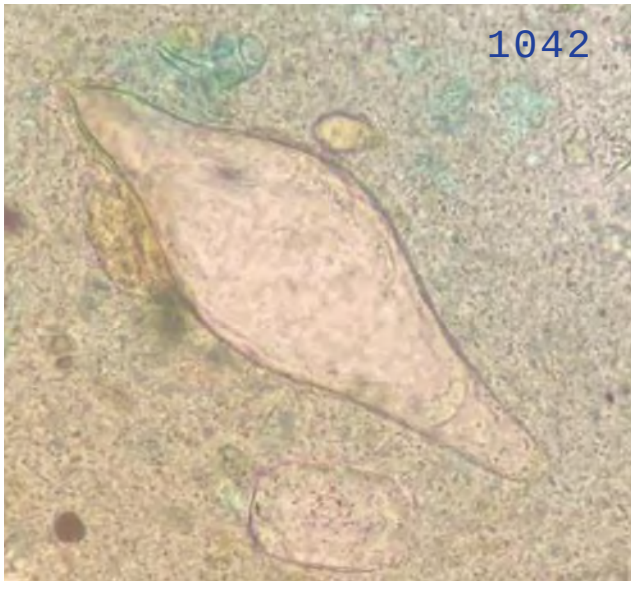

EMERGING INFECTIOUS DISEASES®
May 2025

Research Letters

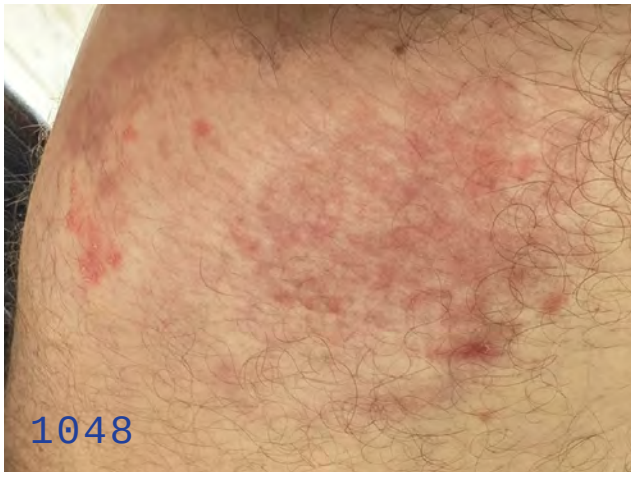

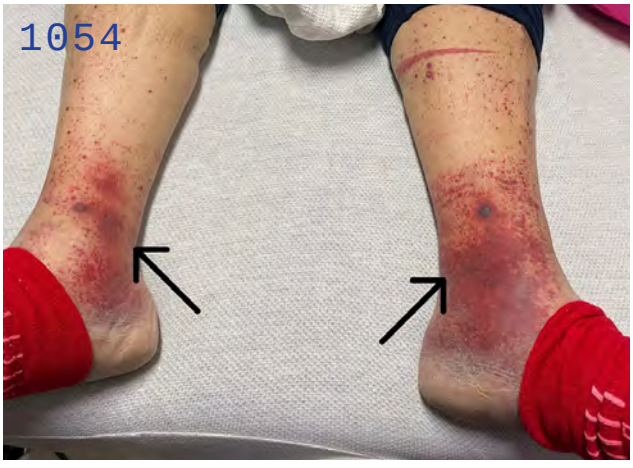

About the Cover

Etymologia

Corrections

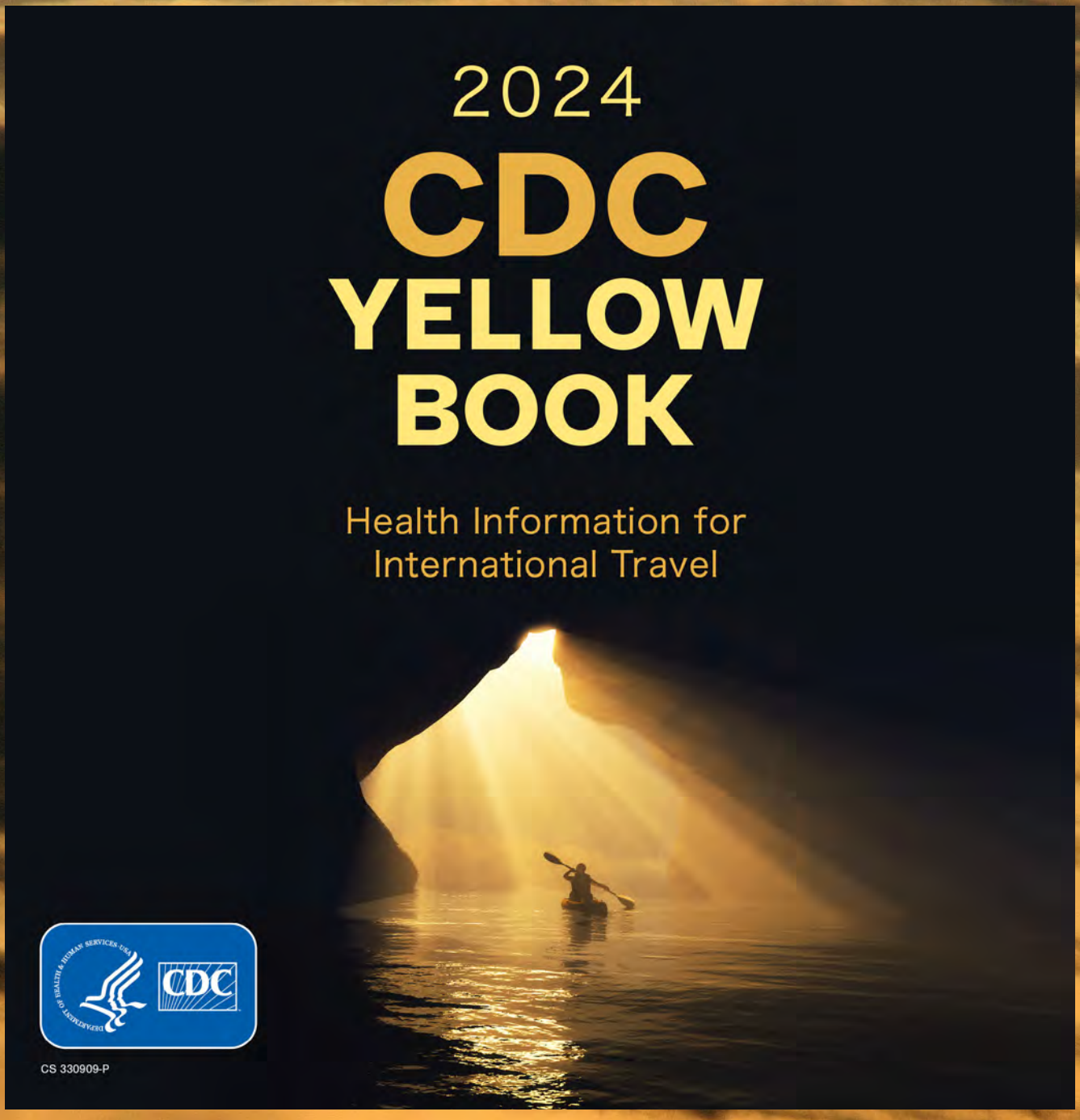

Launch of CDC Yellow Book 2024 – A Trusted Travel Medicine Resource

CDC is pleased to announce the launch of the CDC Yellow Book 2024. The CDC Yellow Book is a source of the U.S. Government's recommendations on travel medicine and has been a trusted resource among the travel medicine community for over 50 years. Healthcare professionals can use the print and digital versions to find the most up-to-date travel medicine information to better serve their patients' healthcare needs.

The CDC Yellow Book is available in print through Oxford University Press and online at www.cdc.gov/yellowbook.

Outbreak of Marburg Virus Disease, Equatorial Guinea, 2023

Stephanie Ngai, Egmond Samir Evers, Angela Katherine Lao Seoane, George Ameh, Julienne N. Anoko, Céline Barnadas, Mary J. Choi, Janet Diaz, Luca Fontana, Pierre Formenty, Ingrid Hammermeister Nezu, Frédérique Jacquerioz, John Klena, Henry Laurenson-Schafer, Olivier le Polain de Waroux, Anaïs Legand, Raquel Medialdea Carrera, Tatiana Metcalf, Joel Montgomery, Silvia Morreale, María E. Negrón, Justino Obama Nvé, Mitoha Ondo'o Ayekaba, Boris I. Pavlin, Trevor Shoemaker, Yaimara Torres Hernandez, Mabel Varona Venta, Emily Z. Gutierrez, Florentino Abaga Ondo Ndoho, on behalf of the Marburg Virus Disease Outbreak Response Working Group[1]

In February 2023, the government of Equatorial Guinea declared an outbreak of Marburg virus disease. We describe the response structure and epidemiologic characteristics, including case-patient demographics, clinical manifestations, risk factors, and the serial interval and timing of symptom onset, treatment seeking, and recovery or death. We identified 16 laboratory-confirmed and 23 probable cases of Marburg virus disease in 5 districts and noted several unlinked chains of transmission and a case-fatality ratio of 90% (35/39 cases). Transmission was concentrated in family clusters and healthcare settings. The median serial interval was 18.5 days; most transmission occurred during late-stage disease. Rapid isolation of symptomatic case-patients is critical in preventing transmission and improving patient outcomes; community engagement and surveillance strengthening should be prioritized in emerging outbreaks. Further analysis of this outbreak and a One Health surveillance approach can help prevent and prepare for future potential spillover events.

Marburg virus disease (MVD) is a severe infectious illness caused by 2 closely related viruses (Marburg virus [MARV] and Ravn virus, within the genus *Orthomarburgvirus*) of the family *Filoviridae* (*1*). Before 2023, at least 15 outbreaks of MVD had been identified; most involved sporadic or small numbers of cases (*2*). The 2 largest known outbreaks occurred during 1998–2000 in the Democratic Republic of the Congo (154 total cases) (*3*) and during 2004–2005 in northern Angola (252 confirmed and 374 total cases) (*4*,*5*).

MVD is characterized by the onset of nonspecific symptoms, typically including fever, headache, chills, fatigue, and myalgia, followed by a rapid progression to severe illness that may include nausea, vomiting, diarrhea, and hemorrhagic symptoms (*6*). Case-fatality rates (CFRs) range from 23% to 88%, and death often follows shock and multiorgan failure (*7*–*9*). Human-to-human transmission of MARV occurs through direct contact with blood or other bodily fluids of MVD patients, contaminated materials, and blood, fluids, or tissues from bodies of persons who have died from MVD (*9*).

Egyptian rousette fruit bats (*Rousettus aegyptiacus*) have been identified as a primary reservoir host for MARV (*10*–*12*). Outbreaks of MVD have been linked to exposure to mines or caves, where Egyptian rousettes typically roost (*13*), and have been found to be infected with MARV (*3*,*8*,*11*,*12*,*14*–*16*). Although models have identified that Equatorial Guinea falls within the zoonotic niche of MVD (*17*) and the virus has been identified in bat populations in neighboring Gabon (*18*), no previous outbreaks of filovirus disease (Marburg or Ebola disease) have been identified in

Author affiliations: World Health Organization, Geneva, Switzerland (S. Ngai, E.S. Evers, A.K. Lao Seoane, G. Ameh, J.N. Anoko, C. Barnadas, J. Diaz, L. Fontana, P. Formenty, I. Hammermeister Nezu, H. Laurenson-Schafer, O. le Polain de Waroux, A. Legand, R. Medialdea Carrera, T. Metcalf, S. Morreale, B.I. Pavlin, Y. Torres Hernandez); Centers for Disease Control and Prevention, Atlanta, Georgia, USA (M.J. Choi, J. Klena, J. Montgomery, M.E. Negrón, T. Shoemaker, E.Z. Gutierrez); Hôpitaux Universitaires de Genève, Geneva (F. Jacquerioz); Ministerio de Sanidad y Bienestar Social, Malabo, Equatorial Guinea (J.O. Nvé, M. Ondo'o Ayekaba, F. Abaga Ondo Ndoho); Brigada Médica Cubana, Malabo (M. Varona Venta).

DOI: https://doi.org/10.3201/eid3105.241749

[1]Members of this group are listed at the end of this article.

Equatorial Guinea, and MARV has not been identified in humans in neighboring countries (*19*).

On February 7, 2023, the Ministry of Health and Social Welfare of Equatorial Guinea (MINSABS) was notified about a cluster of deaths with suspected hemorrhagic fever in 2 villages in Nsok Nsomo District, Kié-Ntem Province, on the border with Cameroon and Gabon. MINSABS sent blood samples from 10 persons from the cluster and identified through active case finding to 2 World Health Organization (WHO) collaborating centers for viral hemorrhagic fevers, Centre Interdisciplinaire de Recherches Médicales de Franceville in Gabon (8 samples) and Institut Pasteur Dakar (IPD) in Senegal (5 repeat and 2 additional samples). One of the additional samples, from a hospitalized patient in Ebibeyín District who died on February 10 with an unclear epidemiologic link to the cluster of deaths, tested positive for MARV by real-time reverse transcription PCR at IPD on February 12. The government of Equatorial Guinea declared an outbreak of MVD the following day. We describe the epidemiologic characteristics of the 2023 MVD outbreak in Equatorial Guinea.

Methods

Geographic Area of the Outbreak

We identified all cases within the mainland continental region of Equatorial Guinea, which is dominated by lush rainforests within the Congo Basin rainforest. The population is concentrated in urban areas, although the small geographic area lends itself to movement between districts. Economic windfall from oil production has funded substantial investment in the country's infrastructure and road networks in recent years.

Response Structure

The response to the outbreak in Equatorial Guinea was led by MINSABS, with support from national and international partners. A response structure was organized around key pillars, including coordination, surveillance and epidemiology, case management, laboratory, infection prevention and control (IPC), risk communication and community engagement, operational support and logistics, and finance and administration. Strategic decisions were made by the Political Committee for Health Emergencies, chaired by the Vice President of Equatorial Guinea.

The response structure was activated immediately after the outbreak declaration. The initial response coordination was based in Ebibeyín and later relocated to Bata, Equatorial Guinea's largest city and economic hub, in mid-March, after the identification of a confirmed case in Bata with indication of earlier probable cases and secondary household transmission.

Case Investigation and Contact Tracing

We used the WHO-recommended case definition (*20*) and later adapted it (Appendix, https://wwwnc.cdc.gov/EID/article/31/5/24-1749-App1.pdf), once all identified ongoing transmission was located in Bata, to emphasize human-to-human transmission over exposure to mines, caves, and wild animals and to reflect symptoms observed among confirmed MVD case-patients managed in the Marburg treatment center (MTC), including rash and back pain. An alert cell coordinated the management of alerts about possible suspected cases received through an established national hotline. Investigators used a standardized case investigation form, based on the WHO template (*21*), to collect information on patient demographics, clinical history and symptoms, exposure history, and patient movements during the potential infectious period. We conducted investigations prospectively for cases identified after the declaration of the outbreak and retrospectively for initial cases; those included interviews with families and community contacts of patients and health facility records, where available. Contacts of confirmed and probable cases (Appendix) were quarantined at home, and we followed them in person daily for 21 days after their last exposure. We managed contacts who had onset of symptoms during the follow-up period as suspected cases.

Laboratory Testing

We collected whole blood for diagnostic testing from suspected case-patients and oral swab samples from deceased persons suspected of having MVD. After laboratory confirmation of the first confirmed case at IPD, we established a field laboratory in Ebibeyín within 1 week, with considerable support from partners, but were delayed in initiating laboratory testing until March 10. We consolidated the field laboratory with the Bome laboratory facility in Bata in mid-March, alongside the epicenter of the outbreak and the response coordination, to reduce laboratory testing turnaround time.

The laboratory in Ebibeyín used the BioFire FilmArray system (bioMérieux, https://www.biomerieux.com) using Warrior Panel test cartridges; the use of the cartridges is restricted to laboratories designated by the US Department of Defense. After the laboratory was relocated, the BioFire Global Fever Panel was used. All samples tested in Ebibeyín were

retested in Bata by using the RealStar Filovirus Screen 1.0 RT-PCR kit (altona Diagnostics, https://altona-diagnostics.com) for result confirmation, according to manufacturer instructions.

Patient Management

Suspected patients were hospitalized in designated temporary transit or treatment centers; confirmed patients were transferred and managed in a dedicated MTC, where they received supportive care (*22*,*23*). The initial isolation and treatment ward was established in Ebibeyín; after transmission was identified in Bata, an isolation and treatment ward was designated within Bata Regional Hospital. A dedicated MTC was opened in the Mondong INSESO Hospital in Bata on March 28 and had capacity to manage 16 patients. Subsequently, all confirmed MVD patients in the continental region and suspected MVD patients in Bata and those referred from other districts were managed at the Mondong MTC. Teams deployed from health facilities were trained to conduct safe and dignified burials for deceased patients.

Data Management and Statistical Analysis

We entered case investigation forms into a standardized Excel database (Microsoft, https://www.microsoft.com). We conducted analyses by using R version 4.2.2 (The R Project for Statistical Computing, https://www.r-project.org) and produced maps by using ArcGIS (Esri, https://www.esri.com). We excluded from analyses 1 confirmed sample (collected in Kié-Ntem Province) that could not be linked to any patient data; we included all other confirmed and probable cases in analyses. We excluded missing or unknown information from calculations of proportions. We calculated the serial interval (the time between symptom onset dates of an infector–infectee pair) and the time from illness onset to hospitalization and death for case-patients with reliable information on exposure, illness onset, or both. Cases were categorized by number of days spent being symptomatic in the community before isolation, and we calculated the proportion of cases with possible or probable onward transmission.

MINSABS authorized the analysis and publication of these data. Analyses in this report were a retrospective review of data that were collected for surveillance and operational response purposes during the outbreak, outside of a research context; as such, no further ethical approval was required.

Results

Epidemiologic Description of the Outbreak

We identified 16 laboratory-confirmed and 23 probable MVD cases during this outbreak. The onset date for symptoms of confirmed cases ranged from February 3 to April 19, 2023; the earliest identified probable case had an estimated onset of symptoms during

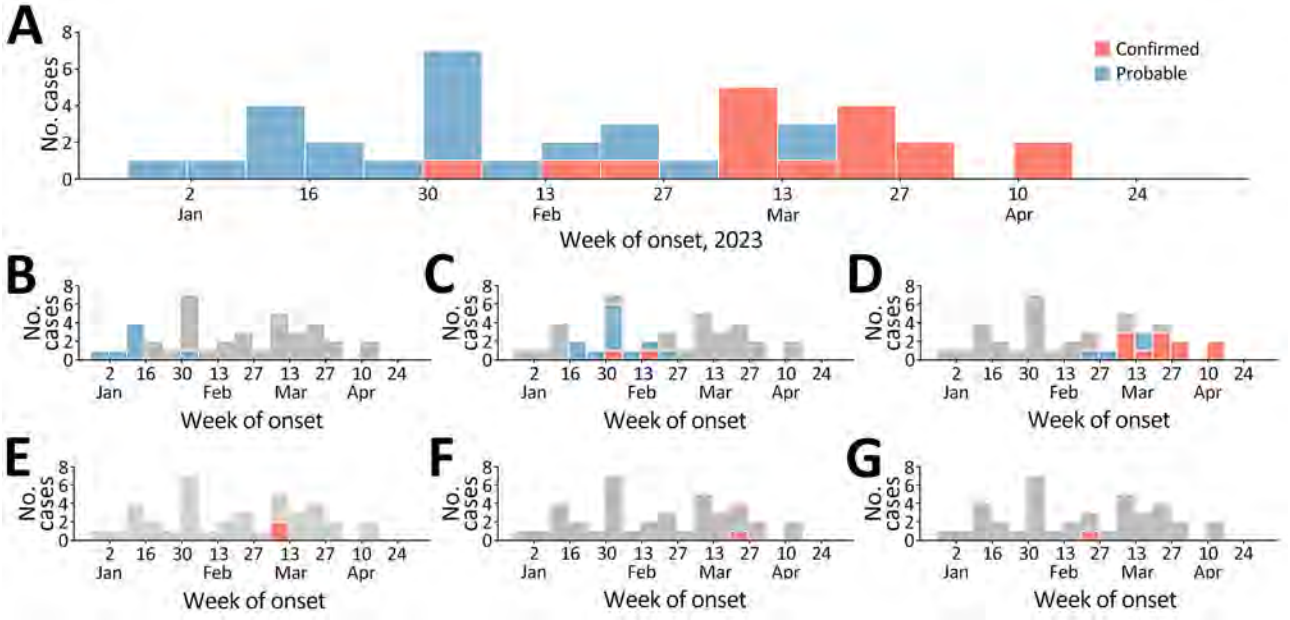

Figure 1. Confirmed and probable cases of Marburg virus disease, Equatorial Guinea, December 2022–April 2023. A) Confirmed and probable cases of Marburg virus disease, by week of illness onset and case classification. Where date of symptom onset was unavailable (1 case), estimated date of sample collection was used. B–G) Confirmed and probable cases of Marburg virus disease (as in shown in panel A), by district: B) Nsok Nsomo; C) Ebibeyín; D) Bata; E) Evinayong; F) Nsork; G) Unknown. Gray shading indicates total number of cases in the country.

the last week of December 2022 (Figure 1, panel A). We identified cases in 5 districts in 4 provinces: Bata (Litoral Province; 11 confirmed, 4 probable), Ebibeyín (Kié-Ntem Province; 2 confirmed, 11 probable), Nsok Nsomo (Kié-Ntem Province; 8 probable), Evinayong (Centro Sur Province; 2 confirmed), and Nsork (Wele-Nzas Province; 1 confirmed) (Figure 1, panel B–G; Figure 2). We recorded 166 alerts and listed 1,451 contacts.

We identified 5 chains of transmission that could not be epidemiologically linked. Two clusters accounted for 60% of cases: the initial cluster of 14 cases in Nsok Nsomo and Ebibeyín Districts (35% of cases), linked to several funerals, and a household cluster of 10 cases in Bata District (25% of cases) (Figure 3). We identified smaller chains of transmission in the districts of Ebibeyín, Bata, and Evinayong (including 1 confirmed case in Nsork District and contacts in Nsork and Mongomo Districts). Initial genomic sequencing results from IPD suggest that all confirmed cases were linked to a single introduction of MARV into the population. Of the 16 confirmed case-patients, 9 (56%) were known contacts at the time of detection and 8 (50%) were identified during daily contact follow-up.

The median serial interval was 18.5 days (range 12–19 days) among 4 pairs of case-patients with known contact history. Among case-patients with reliable symptom onset date, the median time from symptom onset to case-patient isolation or burial was 8 days (n = 17; range 1–13 days); this period was shorter (4 days) among the subset of cases from Bata (n = 9; range 1–10 days). We observed onward transmission more frequently from case-patients who spent more time while symptomatic in the community: 58% (7/12) of case-patients who spent ≥5 days while symptomatic in the community had documented secondary transmission, compared with 20% (1/5) of case-patients who spent <5 days.

Participation in a funeral was a commonly reported risk factor for infection (56% [13/23]), as was contact with another case-patient in the same household (31% [12/39]). We identified 8 (21%) healthcare workers (HCWs): 5 confirmed and 3 probable case-patients, 1 of whom was a traditional healer. Five of the 8 HCWs died.

At least 3 confirmed case-patients sought care at private clinics after the onset of MVD. One of those clinics had poor IPC practices, and record keeping was minimal in a sample of clinics, complicating tracing of potential contacts. Although several probable case-patients visited traditional healers during their illness and we identified 1 probable MVD death in a traditional healer, we could not identify definitive transmission in these settings, which also had limited record keeping and are not included in routine health facility surveillance systems.

We suspect that all but 1 (who had other epidemiologic links) of the HCWs were infected through occupational exposure, although we only identified definitive exposure for 3 HCWs: infection followed invasive procedures (endotracheal intubation, IV insertion, and urinary catherization), with minimal or no personal protective equipment, performed on patients who were within hours of death and later confirmed to have MVD. An additional 2 HCWs with confirmed infection worked in the same service of a hospital and had illness onset within 1 day of one another, suggesting a common occupational exposure.

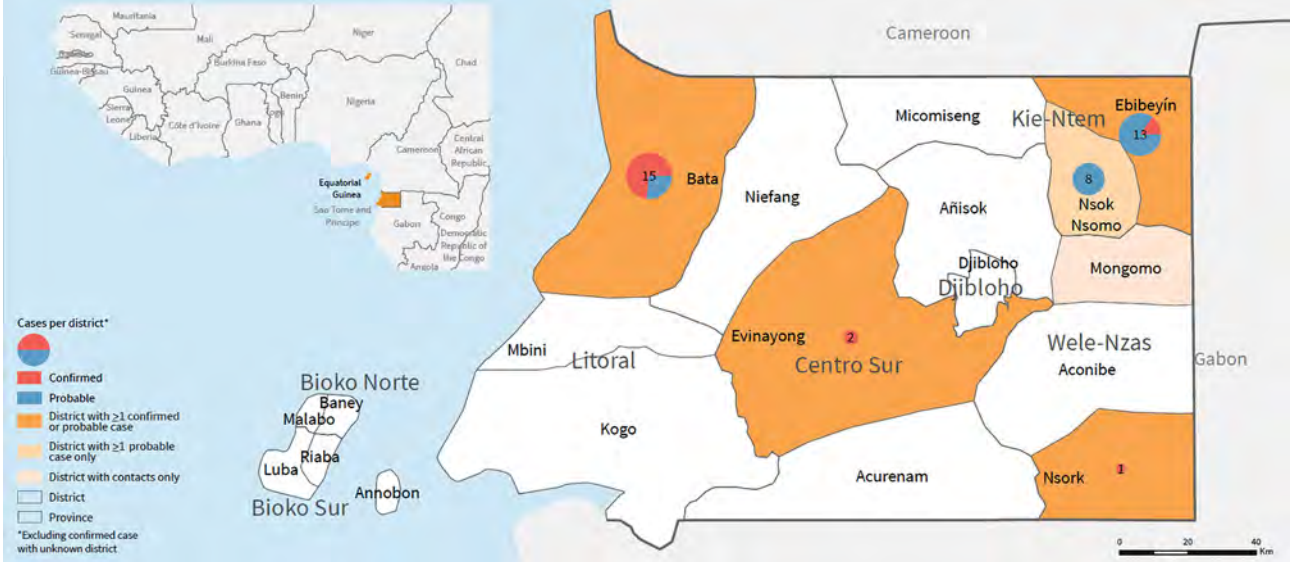

Figure 2. Confirmed and probable cases of Marburg virus disease, by district, Equatorial Guinea, January–April 2023.

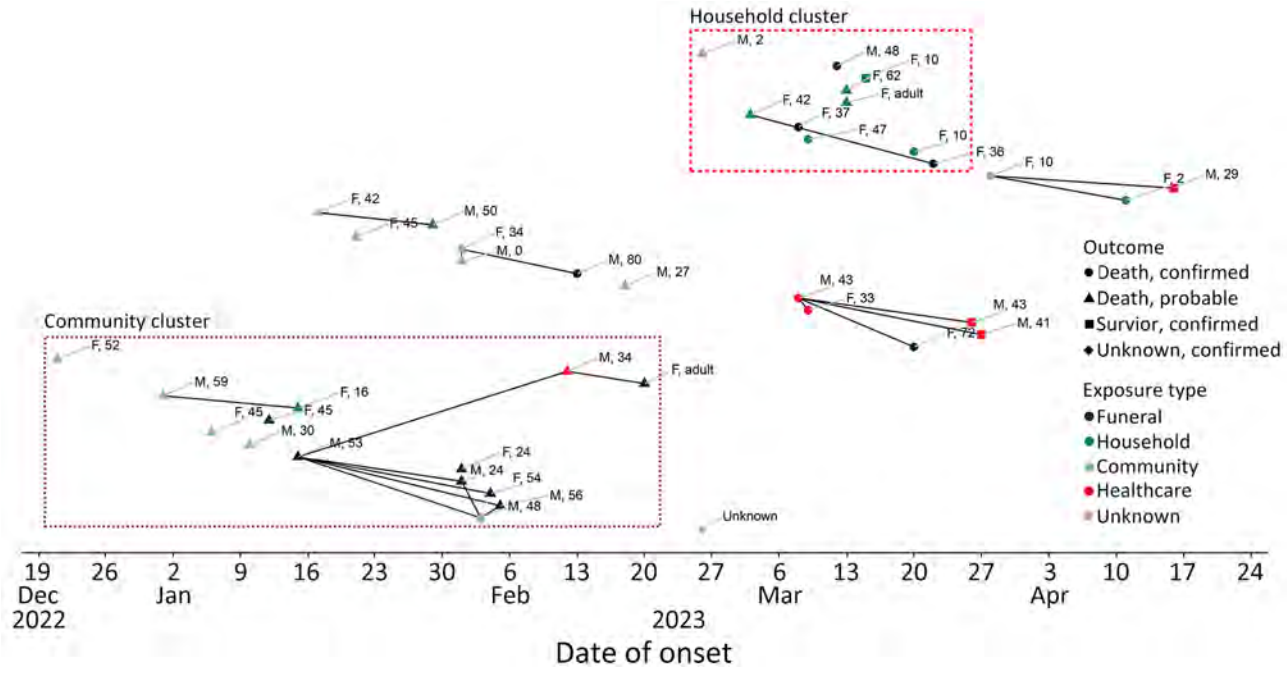

Figure 3. Chain of transmission of Marburg virus disease cases, by date of symptom onset and district, Equatorial Guinea, December 2022–April 2023. Where date of symptom onset was unavailable (1 case), estimated date of sample collection was used. Cases are labeled by sex and age in years. Solid black lines indicate known contact links suspected to be associated with transmission events. A degree of uncertainty is associated with some links shown. In the context of epidemiologically linked clusters with numerous contact links, infector–infectee pairs could not be determined in some cases. Boxes around cases indicate groups of cases with known epidemiologic links (i.e., clusters).

Case Management

Among case-patients with known outcomes, the CFR was 75% (12/16) among confirmed case-patients and 90% (35/39) among all case-patients. The median age of case-patients was 42 years (n = 37; range 7 months–80 years); 22 (56%) case-patients were female and 17 (44%) were male (Figure 4). We identified no pregnant women. The most frequently reported symptoms were fever (94% [32/34]), nausea or vomiting (79% [26/33]), and fatigue or general malaise (65% [22/34]). Diarrhea was reported in 13% (2/15) of confirmed and 83% (15/18) of probable case-patients, and hemorrhagic signs were reported in 57% (21/37) of all case-patients (Table).

Among cases never managed in a designated MTC (confirmed case-patients with MVD diagnosed postmortem and probable case-patients), 77% (20/26) sought healthcare in a hospital setting before death. The median time from illness onset to initial hospitalization among hospitalized case-patients with reliable information on date of illness onset was 4 days (n = 15; range 1–9 days).

No confirmed case-patients were managed in the Ebibeyín treatment ward; 5 confirmed case-patients were admitted to the isolation unit in Bata Regional Hospital, of whom 1 survived. The Mondong MTC managed 5 confirmed case-patients, of whom 3 survived. The 4 surviving case-patients were admitted soon after illness onset (median 1 day; range 1–2 days), and the median time from onset to recovery was 14 days (range 10–15 days). Among deceased confirmed case-patients, the median time from illness onset to hospitalization was 6 days (n = 9; range 4–9 days); those case-patients admitted to a treatment center died shortly after admission (n = 7; median 2 days; range 1–4 days).

Discussion

This outbreak of MVD in Equatorial Guinea had 39 identified confirmed and probable cases across 5 districts, plus 1 confirmed sample from a patient who was never identified. Transmission was concentrated in family clusters and often involved contact with deceased case-patients; more than half of all case-patients had a known household or funeral exposure. The mechanisms of community transmission events were not described for most cases, and the demographic distribution, with no clear overrepresentation of adult female case-patients, does not support caregiving as the principal risk factor (*4*,*5*). We never identified the initial case and exposure, but no case-patients reported exposures to bats or visits to mines (*3*).

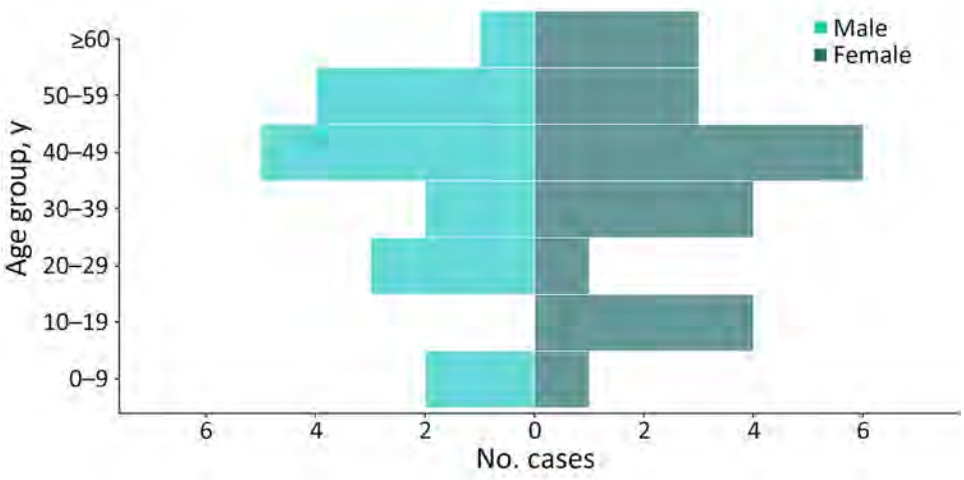

Figure 4. Age group and sex distribution of persons with confirmed or probable Marburg virus disease, Equatorial Guinea, January–April 2023.

Rapid isolation of symptomatic case-patients remains critical: those who survived sought care sooner at the MTC than did those who died. Three of the 4 survivors were HCWs and sought care immediately after symptom onset because of their familiarity with MVD. Case-patients who were isolated quickly after symptom onset also contributed less frequently to downstream transmission, and the relatively long serial interval among patients with reliable data suggests that most documented transmission occurred during late-stage disease. Those improved outcomes and decreased transmission risks underscore the importance of strong risk communication, community engagement, contact tracing programs, and early care in improving patient outcomes and preventing secondary transmission.

The number of unconnected chains of transmission raised concerns about undetected community circulation and highlighted the need for additional case-finding strategies. Many case-patients sought healthcare in hospital settings but did not have MVD diagnosed. Although most case-patients were managed in a hospital at some point during their illness, for most, no secondary nosocomial transmission was documented. However, limited IPC capacities combined with care-seeking behavior indicate a high potential risk for transmission. Although not observed during this outbreak, vertical transmission has been documented during other filovirus disease outbreaks (*24*), as has viral persistence in the placenta after recovery (*25*). Improved hospital record keeping would aid case finding and contact tracing, particularly for unconnected chains of transmission. The identified cases of nosocomial transmission occurred among HCWs who had inadequate protection and high-risk exposures to severely ill patients; better IPC standards, particularly in the midst of an outbreak, might have prevented these infections. Healthcare exposures were not limited to hospital settings; care seeking involved both traditional healers and small, low-cost private clinics. The role of small neighborhood clinics and traditional healers with inadequate IPC measures remains important in terms of limiting healthcare-related exposures and the potential as foci of infection for other patients in future outbreaks.

Fewer case-patients reported so-called wet symptoms than is typically expected during an outbreak of filovirus disease: only 13% of confirmed case-patients reported diarrhea, in contrast to 46% of a subset of confirmed case-patients from the 2004–2005 outbreak in Angola (*4*,*5*). Although information on nausea and vomiting was collected jointly, many confirmed case-patients reported nausea without vomiting. Wet symptoms were more frequently reported among probable cases, with 83% reporting diarrhea, although probable cases are representative of late-stage disease and this elevated prevalence might be partially attributable to recall bias during retrospective investigations. Among confirmed case-patients, convulsions and hemorrhagic signs were observed only in the hours preceding death. A case series further describes the clinical and laboratory progression of the 5 confirmed case-patients managed at the Mondong MTC (*23*). Case-patients often were positive for malaria at the time of MVD diagnosis; the high malaria prevalence and diversity of malaria species in Equatorial Guinea underscores the need to enhance malaria treatment during MVD outbreaks to avoid unnecessary confusion with MVD.

Although the origin of the outbreak was not identified, zoonotic spillover is the most likely route of infection, considering close proximity of the initially affected communities to wild bats and widespread consumption of wild animals, including bats (*26*). Genomic sequencing of the virus isolated from the first confirmed case-patient in this outbreak found

that the isolate was most closely related to MARVs isolated from Egyptian rousettes in Sierra Leone (*27*), which in turn were similar to isolates collected from humans during the 2004–2005 outbreak in Angola (*28*). Detailed genomic sequencing results on samples from the Equatorial Guinea outbreak are not available; integration of additional sequencing results with epidemiologic data could further elucidate details on and connect chains of transmission.

We encountered several challenges during the response. Because there had not been a previous response to a filovirus disease outbreak in the country, the government of Equatorial Guinea requested support from some international partners, but simultaneous spread to multiple districts stretched resources thin from both the government and partners with presence in the country. After a delay between identifying and reporting initial cases, processes were established for regular information sharing. Because of limited existing field epidemiology and outbreak investigation capacity, along with community resistance, few alerts were triggered, documentation of alerts was incomplete, and identification of contacts was limited, particularly early in the response. Mortality surveillance, including systematic sampling of deaths, was not implemented. Weak existing disease surveillance and data management systems precluded further epidemiologic analyses to inform response activities. Inadequate risk perception was partly addressed through countrywide risk communication and community engagement efforts, although the lack of familiarity with filovirus diseases, severity of the cases, and tendency of the virus to infect entire families contributed to ongoing concerns among the population that MVD was related to witchcraft. We encountered challenges in implementing standardized contact definitions; during initial investigations, entire villages in which case-patients resided were listed as contacts. Poor communication and widespread enforcement of quarantine probably caused reluctance to engage with contact tracing and educational messaging. Standard IPC measures were limited; a national IPC program was established, although implementation was delayed at several facilities. Remdesivir was provided to 4 patients at the MTC on a compassionate use basis (*23*), but other potential treatments and candidate vaccines for MVD were not approved for use at the time of the outbreak.

Some data in this report, in particular those from initial investigations, are incomplete; we discarded values that were missing, unknown, or thought to be unreliable, resulting in small sample sizes. Information on clinical manifestations, particularly for probable case-patients, might not be reliable, because medical records were infrequently available and symptom information was ascertained during retrospective investigations. Information on risk factors was not complete for all case-patients. Retrospective identification of probable case-patients was biased toward identification of deaths; that bias might have inflated the CFR because nonfatal cases, particularly early in the outbreak, might have been missed. Individual-level contact tracing data were not entered into centralized databases and were not available for decision-making or analysis. We identified several unlinked chains of transmission, spanning multiple generations of transmission; we could not further analyze transmission dynamics. Laboratory data were not systematically linked to case investigation data and were not available for analysis.

The government declared the end of the MVD outbreak in Equatorial Guinea on June 8, 2023, nearly 4 months after its initial detection. The epidemiology

Table. Reported symptoms among case-patients with Marburg virus disease, Equatorial Guinea, January–April 2023*

Symptom	Death, confirmed	Survivor, confirmed	Total, confirmed	Total, probable	Total, confirmed and probable
Fever	12/12 (100.0)	4/4 (100.0)	16/16 (100.0)	16/18 (88.9)	32/34 (94.1)
Abdominal pain	3/4 (75.0)	3/3 (100.0)	6/7 (85.7)	ND	6/7 (85.7)
Fatigue	8/12 (66.7)	4/4 (100.0)	12/16 (75.0)	10/18 (55.6)	22/34 (64.7)
Nausea/vomiting	8/11 (72.7)	2/4 (50.0)	10/15 (66.7)	16/18 (88.9)	26/33 (78.8)
Anorexia/loss of appetite	5/10 (50.0)	4/4 (100.0)	9/14 (64.3)	2/4 (50.0)	11/18 (61.1)
Convulsions	5/5 (100.0)	0/3 (0.0)	5/8 (62.5)	ND	5/8 (62.5)
Rash	0/2 (0.0)	3/3 (100.0)	3/5 (60.0)	ND	3/5 (60.0)
Any hemorrhagic sign	8/12 (66.7)	0/4 (0.0)	8/16 (50.0)	13/21 (61.9)	21/37 (56.8)
Joint or muscle pain	3/10 (30.0)	3/4 (75.0)	6/14 (42.9)	7/18 (38.9)	13/32 (40.6)
Headache	4/9 (44.4)	1/4 (25.0)	5/13 (38.5)	2/5 (40.0)	7/18 (38.9)
Conjunctivitis	2/3 (66.7)	0/3 (0.0)	2/6 (33.3)	ND	2/6 (33.3)
Hematemesis	4/11 (36.4)	0/4 (0.0)	4/15 (26.7)	13/18 (72.2)	17/33 (51.5)
Difficulty breathing	3/11 (27.3)	0/4 (0.0)	3/15 (20.0)	2/18 (11.1)	5/33 (15.2)
Difficulty swallowing	0/9 (0.0)	2/4 (50.0)	2/13 (15.4)	0/4 (0.0)	2/17 (11.8)
Bloody diarrhea	2/9 (22.2)	0/4 (0.0)	2/13 (15.4)	12/18 (66.7)	14/31 (45.2)
Diarrhea	2/11 (18.2)	0/4 (0.0)	2/15 (13.3)	15/18 (83.3)	17/33 (51.5)

*Values are no./no. (%). Denominators exclude case-patients where information on the symptom was unknown or not collected. ND, no data were available.

of this outbreak adds to the limited knowledge about MVD, most of which is based on data from 2 large outbreaks with distinct epidemiologic characteristics (*3*–*5*), and reinforces the importance of early detection of cases to prevent transmission and improve outcomes for patients. The identification of this outbreak follows an increasing trend in the number of detected filovirus outbreaks (*29*–*31*). The unknown origin of the outbreak underscores the importance of incorporating a One Health approach to strengthening surveillance systems to understand the history of this outbreak and to prevent and prepare for future spillover events. Further investigation and seroprevalence studies should be considered to determine the number of unidentified cases and geographic areas to target for enhanced surveillance for MVD and other filovirus diseases. Overall limited International Health Regulations core capacities before the outbreak, which were assessed during the most recent WHO Joint External Evaluation and became apparent during the course of the outbreak, underscore the need for a WHO National Action Plan for Health Security for the country to develop its capacity to prevent, detect, and adequately respond to future health threats.

Members of the Marburg Virus Disease Outbreak Response Working Group: Marie-Roseline Belizaire, Ishata Conteh, Aura Rocio Escobar Corado Waeber, Abdou Salam Gueye, Robert Holden, Zyleen Kassamali, Abdi Rahman Mahamud, Charles Okot, Patrick Otim (World Health Organization, Geneva, Switzerland); Crisanta Pilar Mikue Ndong Bile, Ladislao E. Ngomo Mikue, Cándido O. Ondo Avomo (Ministerio de Sanidad y Bienestar Social, Malabo, Equatorial Guinea); Brian Baker, Ana Cecilia Bardossy, Christopher Brown, Loren Cadena, Kristie Clarke, Fatima Coronado, Miguel Cruz, Elizabeth Garza, Brandon Hugueley, Cecilia Kato, Susan Kaydos-Daniels, William Lonergan, Jason Malenfant, Oren Mayer, Nancy Ortiz, Leah Pao, Vanessa Sandoval, Florine Scholte, Elizabeth Soda, Diana Valencia, Stephen Welch (CDC, Atlanta, Georgia, USA).

Acknowledgments

The authors acknowledge the HCWs in Equatorial Guinea, particularly those who provided care to patients with MVD, and to the patients, their families, and community members who were directly affected by this outbreak.

All data included in this report belong to the Ministry of Health and Social Welfare of Equatorial Guinea. Any requests to access or analyze these data should be presented to the Ministry of Health for approval.

Relevant work on the outbreak response was funded by WHO and the US Centers for Disease Control and Prevention. Many persons across these and other organizations were involved in all aspects of the outbreak response. The findings and conclusions in this report are those of the authors and do not necessarily represent the official position of the National Institute for Occupational Safety and Health, CDC.

The designations employed and the presentation of the material in this publication do not imply the expression of any opinion whatsoever on the part of WHO concerning the legal status of any country, territory, city, or area of its authorities, or concerning the delimitation of its frontiers or boundaries.

Author contributions: S.N. and E.E. contributed to the conception and design of this work. S.N., A.K.L.S., J.N.A., C.B., M.J.C., J.D., L.F., P.F., F.J., J.K., O.L.P.W., R.M.C., T.M., S.M., M.E.N., B.I.P., Y.T.H., M.V.V., and E.Z.G. were involved in investigations and data collection during the outbreak. H.L.S., S.N., and I.H.M. verified and analyzed the data. S.N. and E.E. drafted the manuscript with the support of M.J.C., O.L.P.W., A.L., M.E.N., and E.Z.G. E.E., A.K.L.S., G.A., J.O.N., M.O.A., E.Z.G., F.A.O.N., J.M., and T.S. coordinated the outbreak response. All authors had substantial contributions to management of the outbreak and acquisition and interpretation of the data. All authors have approved the final manuscript and are accountable for the results therein.

About the Author

Ms. Ngai is an epidemiologist working in global health. She worked with the WHO Health Emergencies Program at the time of this research. Her interests include infectious disease surveillance and outbreak response in low-resource and conflict-affected settings.

References

1. Biedenkopf N, Bukreyev A, Chandran K, Di Paola N, Formenty PBH, Griffiths A, et al. ICTV virus taxonomy profile: *Filoviridae* 2024. J Gen Virol. 2024;105:001955. https://doi.org/10.1099/jgv.0.001955
2. Centers for Disease Control and Prevention. History of Marburg outbreaks. 2024 [cited 2024 Nov 9]. https://www.cdc.gov/marburg/outbreaks/index.html
3. Bausch DG, Nichol ST, Muyembe-Tamfum JJ, Borchert M, Rollin PE, Sleurs H, et al.; International Scientific and Technical Committee for Marburg Hemorrhagic Fever Control in the Democratic Republic of the Congo. Marburg hemorrhagic fever associated with multiple genetic lineages of virus. N Engl J Med. 2006;355:909–19. https://doi.org/10.1056/NEJMoa051465
4. Towner JS, Khristova ML, Sealy TK, Vincent MJ, Erickson BR, Bawiec DA, et al. Marburgvirus genomics and association with a large hemorrhagic fever outbreak in

Angola. J Virol. 2006;80:6497–516. https://doi.org/10.1128/JVI.00069-06
5. Roddy P, Thomas SL, Jeffs B, Nascimento Folo P, Pablo Palma P, Moco Henrique B, et al. Factors associated with Marburg hemorrhagic fever: analysis of patient data from Uige, Angola. J Infect Dis. 2010;201:1909–18. https://doi.org/10.1086/652748
6. Ristanović ES, Kokoškov NS, Crozier I, Kuhn JH, Gligić AS. A forgotten episode of Marburg virus disease: Belgrade, Yugoslavia, 1967. Microbiol Mol Biol Rev. 2020;84:e00095–19. https://doi.org/10.1128/MMBR.00095-19
7. Brauburger K, Hume AJ, Mühlberger E, Olejnik J. Forty-five years of Marburg virus research. Viruses. 2012;4:1878–927. https://doi.org/10.3390/v4101878
8. Abir MH, Rahman T, Das A, Etu SN, Nafiz IH, Rakib A, et al. Pathogenicity and virulence of Marburg virus. Virulence. 2022;13:609–33. https://doi.org/10.1080/21505594.2022.2054760
9. World Health Organization. Marburg virus disease fact sheet. 2021 Aug 7 [cited 2023 Jun 3]. https://www.who.int/news-room/fact-sheets/detail/marburg-virus-disease
10. Swanepoel R, Smit SB, Rollin PE, Formenty P, Leman PA, Kemp A, et al.; International Scientific and Technical Committee for Marburg Hemorrhagic Fever Control in the Democratic Republic of Congo. Studies of reservoir hosts for Marburg virus. Emerg Infect Dis. 2007;13:1847–51. https://doi.org/10.3201/eid1312.071115
11. Amman BR, Carroll SA, Reed ZD, Sealy TK, Balinandi S, Swanepoel R, et al. Seasonal pulses of Marburg virus circulation in juvenile *Rousettus aegyptiacus* bats coincide with periods of increased risk of human infection. PLoS Pathog. 2012;8:e1002877. https://doi.org/10.1371/journal.ppat.1002877
12. Towner JS, Amman BR, Sealy TK, Carroll SA, Comer JA, Kemp A, et al. Isolation of genetically diverse Marburg viruses from Egyptian fruit bats. PLoS Pathog. 2009;5:e1000536. https://doi.org/10.1371/journal.ppat.1000536
13. Kingdon J. *Rousettus aegyptiacus*. In: Happold M, Happold D, editors. Mammals of Africa. Volume IV. Hedgehogs, shrews and bats. London: Bloomsbury Publishing; 2013. p. 289–91.
14. Nyakarahuka L, Shoemaker TR, Balinandi S, Chemos G, Kwesiga B, Mulei S, et al. Marburg virus disease outbreak in Kween District Uganda, 2017: epidemiological and laboratory findings. PLoS Negl Trop Dis. 2019;13:e0007257. https://doi.org/10.1371/journal.pntd.0007257
15. Asaah Denkyira S, Olamilekan Adesola R, Idris I, et al. Marburg virus in Ghana: a public health threat to Ghanaians and to Africans. Public Health Chall. 2022;1:e32. https://doi.org/10.1002/puh2.32
16. Adjemian J, Farnon EC, Tschioko F, Wamala JF, Byaruhanga E, Bwire GS, et al. Outbreak of Marburg hemorrhagic fever among miners in Kamwenge and Ibanda Districts, Uganda, 2007. J Infect Dis. 2011;204(Suppl 3):S796–9. https://doi.org/10.1093/infdis/jir312
17. Pigott DM, Deshpande A, Letourneau I, Morozoff C, Reiner RC Jr, Kraemer MUG, et al. Local, national, and regional viral haemorrhagic fever pandemic potential in Africa: a multistage analysis. Lancet. 2017;390:2662–72. https://doi.org/10.1016/S0140-6736(17)32092-5
18. Towner JS, Pourrut X, Albariño CG, Nkogue CN, Bird BH, Grard G, et al. Marburg virus infection detected in a common African bat. PLoS One. 2007;2:e764. https://doi.org/10.1371/journal.pone.0000764
19. World Health Organization. Geographic distribution of Marburg virus disease outbreaks on bats of Pteropodidae family. 2023 [cited 2025 Feb 3]. https://cdn.who.int/media/docs/default-source/documents/emergencies/geographic-distribution-of-marburg-virus-disease-outbreaks-on-bats-of-pteropodidae-family-2023.pdf
20. World Health Organization. Case definition recommendations for Ebola or Marburg virus diseases: interim guideline. 2014 Aug 9 [cited 2023 Jun 3]. https://www.who.int/publications/i/item/WHO-EVD-CaseDef-14-1
21. World Health Organization. Ebola and Marburg virus disease epidemics: preparedness, alert, control, and evaluation. 2014 [cited 2025 Feb 3]. https://www.who.int/publications/i/item/ebola-and-marburg-virus-disease-epidemics-preparedness-alert-control-and-evaluation
22. World Health Organization. Optimized supportive care for Ebola virus disease: clinical management standard operating procedures. 2019 [cited 2025 Feb 3]. https://www.who.int/publications/i/item/optimized-supportive-care-for-ebola-virus-disease
23. Fontana L, Ondo Avomo CO, Ngomo Mikue LE, Fuga Eyemam DÑ, Nguere MA, Mometolo IE, et al. Case series of patients with Marburg virus disease, Equatorial Guinea, 2023. N Engl J Med. 2024;391:283–5. https://doi.org/10.1056/NEJMc2313181
24. Kayem ND, Benson C, Aye CYL, Barker S, Tome M, Kennedy S, et al. Ebola virus disease in pregnancy: a systematic review and meta-analysis. Trans R Soc Trop Med Hyg. 2022;116:509–22. https://doi.org/10.1093/trstmh/trab180
25. Caluwaerts S, Fautsch T, Lagrou D, Moreau M, Modet Camara A, Günther S, et al. Dilemmas in managing pregnant women with Ebola: 2 case reports. Clin Infect Dis. 2016;62:903–5. https://doi.org/10.1093/cid/civ1024
26. Jagadesh S, Zhao C, Mulchandani R, Van Boeckel TP. Mapping global bushmeat activities to improve zoonotic spillover surveillance by using geospatial modeling. Emerg Infect Dis. 2023;29:742–50. https://doi.org/10.3201/eid2904.221022
27. Sall AA, Ondo'o Ayekaba M, Faye O, et al. First emergence of Marburg virus in Equatorial Guinea, 2023. 2023 Mar 1 [cited 2023 May 25]. https://virological.org/t/first-emergence-of-marburg-virus-in-equatorial-guinea-2023/924
28. Amman BR, Bird BH, Bakarr IA, Bangura J, Schuh AJ, Johnny J, et al. Isolation of Angola-like Marburg virus from Egyptian rousette bats from West Africa. Nat Commun. 2020;11:510. https://doi.org/10.1038/s41467-020-14327-8
29. World Health Organization. Marburg virus disease—Ghana. 2022 Sep 26 [cited 2023 May 24]. https://www.who.int/emergencies/disease-outbreak-news/item/2022-DON409
30. Makenov MT, Boumbaly S, Tolno FR, Sacko N, N'Fatoma LT, Mansare O, et al. Marburg virus in Egyptian rousettus bats in Guinea: investigation of Marburg virus outbreak origin in 2021. PLoS Negl Trop Dis. 2023;17:e0011279. https://doi.org/10.1371/journal.pntd.0011279
31. World Health Organization. Marburg virus disease—the United Republic of Tanzania. 2023 Jun 2 [cited 2023 Jun 13]. https://www.who.int/emergencies/disease-outbreak-news/item/2023-DON471

Address for correspondence: Stephanie Ngai, World Health Organization, c/o WHE, Avenue Appia 20, 1211 Geneva, Switzerland; email: ngai.stephanie.m@gmail.com

Features of Invasive Aspergillosis Caused by *Aspergillus flavus*, France, 2012–2018

Lise Bertin-Biasutto, Olivier Paccoud, Dea Garcia-Hermoso, Blandine Denis, Karine Boukris-Sitbon, Olivier Lortholary, Stéphane Bretagne, Maud Gits-Muselli, Raoul Herbrecht, Valérie Letscher-Bru, François Danion, Sophie Cassaing, Florent Morio, Céline Nourrisson, Marc Pihet, Milène Sasso, Guillaume Desoubeaux, Marie-Fleur Durieux, Julie Bonhomme, Elisabeth Chachaty, Taieb Chouaki, Nicole Desbois-Nogard, Alexandre Alanio,[1] Jean-Pierre Gangneux,[1] Fanny Lanternier

Medscape CME Activity

In support of improving patient care, this activity has been planned and implemented by Medscape, LLC and Emerging Infectious Diseases. Medscape, LLC is jointly accredited with commendation by the Accreditation Council for Continuing Medical Education (ACCME), the Accreditation Council for Pharmacy Education (ACPE), and the American Nurses Credentialing Center (ANCC), to provide continuing education for the healthcare team.

Medscape, LLC designates this Journal-based CME activity for a maximum of 1.00 ***AMA PRA Category 1 Credit(s)™***. Physicians should claim only the credit commensurate with the extent of their participation in the activity.

Successful completion of this CME activity, which includes participation in the evaluation component, enables the participant to earn up to 1.0 MOC points in the American Board of Internal Medicine's (ABIM) Maintenance of Certification (MOC) program. Participants will earn MOC points equivalent to the amount of CME credits claimed for the activity. It is the CME activity provider's responsibility to submit participant completion information to ACCME for the purpose of granting ABIM MOC credit.

All other clinicians completing this activity will be issued a certificate of participation. To participate in this journal CME activity: (1) review the learning objectives and author disclosures; (2) study the education content; (3) take the post-test with a 75% minimum passing score and complete the evaluation at https://www.medscape.org/qna/processor/74135?showStandAlone=true&src=prt_jcme_eid_mscpedu; and (4) view/print certificate. For CME questions, see page 1067.

NOTE: It is Medscape's policy to avoid the use of Brand names in accredited activities. However, in an effort to be as clear as possible, trade names are used in this activity to distinguish between the mixtures and different tests. It is not meant to promote any particular product.

Release date: April 29, 2025; Expiration date: April 29, 2026

Learning Objectives

Upon completion of this activity, participants will be able to:

- Analyze common risk factors for immune aspergillosis (IA)
- Assess the clinical presentation and course of IA based on baseline risk factors
- Compare clinical data based on the anatomic location of IA
- Evaluate the treatment and outcomes of IA

CME Editor

Amy J. Guinn, BA, MA, Technical Writer/Editor, Emerging Infectious Diseases. *Disclosure: Amy J. Guinn, BA, MA, has no relevant financial relationships.*

CME Author

Charles P. Vega, MD, Health Sciences Clinical Professor of Family Medicine, University of California, Irvine School of Medicine, Irvine, California. *Disclosure: Charles P. Vega, MD, has the following relevant financial relationships: served as a consultant or advisor for: Boehringer Ingelheim; Exact Sciences.*

Authors

Lise Bertin-Biasutto, MD; Olivier Paccoud, MD; Dea Garcia-Hermoso, PhD; Blandine Denis, MD, PhD; Karine Boukris-Sitbon, MD; Olivier Lortholary, MD, PhD; Stéphane Bretagne, MD, PhD; Maud Gits-Muselli, MD, PhD; Raoul Herbrecht, MD, PhD; Valérie Letscher-Bru, PharmD, PhD; François Danion, MD, PhD; Sophie Cassaing, MD, PhD; Florent Morio, PharmD, PhD; Céline Nourrisson, MD; Marc Pihet, MD; Milène Sasso, MD; Guillaume Desoubeaux, MD, PhD; Marie-Fleur Durieux, MD; Julie Bonhomme, MD; Elisabeth Chachaty, PharmD, PhD; Taieb Chouaki, PharmD; Nicole Desbois-Nogard, MD, PhD; Alexandre Alanio, MD, PhD; Jean-Pierre Gangneux, MD, PhD; Fanny Lanternier, MD, PhD.

Invasive aspergillosis (IA) caused by *Aspergillus flavus* remains poorly described. We retrospectively analyzed 54 cases of IA caused by *A. flavus* reported in France during 2012–2018. Among cases, underlying IA risk factors were malignancy, solid organ transplantation, and diabetes. Most (87%, 47/54) infections were localized, of which 33 were pleuropulmonary and 13 were ear-nose-throat (ENT) infection sites. Malignancy (70% [23/33]) and solid organ transplantation (21% [7/33]) were the main risk factors in localized pulmonary infections, and diabetes mellitus was associated with localized ENT involvement (61.5%, [8/13]). Fungal co-infections were frequent in pulmonary (36%, 12/33) but not ENT IA (0 cases). Antifungal monotherapy was prescribed in 45/50 (90%) cases, mainly voriconazole (67%, 30/45). All-cause 30-day case-fatality rates were 39.2% and 90-day rates were 47.1%, and rates varied according to risk factor, IA site, and fungal co-infections. Clinicians should remain vigilant for *A. flavus* and consider it in the differential diagnosis for IA.

After invasive candidiasis and pneumocystosis, invasive aspergillosis (IA) is the third most frequent invasive fungal infection in Europe. IA occurs primarily in immunocompromised patients, including those with a hematologic malignancy (HM) and those who receive solid organ transplants or immunosuppressive treatments (*1*). After *A. fumigatus*, *A. flavus* is the second most frequently reported *Aspergillus* species isolated from clinical specimens in invasive and noninvasive aspergillosis, but *A. flavus* IA has marked differences in infection sites and geographic locations. Indeed, *A. flavus* is reported as the main etiologic agent of sinusitis, keratitis, and invasive aspergillosis in the Middle East, northern Africa, and South Asia (*2*–*4*). In stark contrast, *A. flavus* accounts for <10% of IA cases reported in Europe and North America (*5*,*6*). For instance, according to data from the Fungal Infection Surveillance Network (RESSIF; RESeau de Surveillance des Infections Fongiques) in France, *A. flavus* represented 8.7% (74/845) of all IA during 2012–2018, second only to the 86% of IA caused by *A. fumigatus*.

Data regarding the epidemiology, risk factors, clinical manifestations, and management of IA caused by *A. flavus* remain scarce, particularly in Europe. We sought to describe patient characteristics, underlying conditions, clinical presentations, and outcomes of IA cases caused by *A. flavus* reported in France.

Material and Methods

Database Management and Case Definition

The RESSIF (*1*,*7*), based at the French National Reference Center for Invasive Mycoses and Antifungals (NRCMA), Institut Pasteur, Paris, is a nationwide surveillance network for cases of invasive mycoses in France. RESSIF relies on the active participation of 21 collaborative centers in 15 of the 18 regions of France, including overseas territories. Case details are sent to the NRCMA by referent medical mycologists in collaboration with clinicians.

We included all patients registered in RESSIF during 2012–2018 with proven or probable IA caused by *A. flavus*, according to the 2020 European Organization for Research and Treatment of Cancer/Mycoses Study Group Education and Research Consortium criteria (*8*), which include diabetes mellitus and severe burns as additional risk factors for probable IA. We excluded cases for which data were unavailable and cases of noninvasive aspergillosis (e.g., aspergilloma). We considered the date of IA diagnosis to be the date of the first microbiological criteria leading to diagnosis.

Data Collection and Classification

Data were collected by using a standardized case report form that included patient demographic characteristics, clinical and radiologic manifestations, time

Author affiliations: Hopital Necker-Enfants Malades, Paris, France (L. Bertin-Biasutto, O. Paccoud, O. Lortholary, F. Lanternier); Université de Paris, Paris (L. Bertin-Biasutto, O. Lortholary, F. Lanternier); Institut Pasteur, Paris (D. Garcia-Hermoso, K. Boukris-Sitbon, O. Lortholary, S. Bretagne, A. Alanio, F. Lanternier); Hôpital Saint Louis, Paris (B. Denis, S. Bretagne, M. Gits-Muselli, A. Aliano); Institut de Cancérologie de Strasbourg, Strasbourg, France (R. Herbrecht); Hôpitaux Universitaires de Strasbourg, Strasbourg (V. Letscher-Bru, F. Danion); Toulouse University Hospital, Toulouse, France (S. Cassaing); Nantes University Hospital, Nantes, France (F. Morio); CHU Clermont-Ferrand, Clermont-Ferrand, France (C. Nourrisson); CHU d'Angers, Angers, France (M. Pihet); CHU Nîmes and Université de Montpellier, Nîmes, France (M. Sasso); Hôpital Bretonneau, Tours, France (G. Desoubeaux); Limoges University, Limoges, France (M.-F. Durieux); Unicaen Université Normandie, Caen, France (J. Bonhomme); Gustave Roussy, Villejuif, France (E. Chachaty); CHU Amiens-Picardie, Amiens, France (T. Chouaki); Inserm U1285, University of Lille, Lille, France (T. Chouaki); Centre Hospitalier Universitaire de Martinique, Fort-de-France, France (N. Desbois-Nogard); Université de Rennes, CHU Rennes, Rennes, France (J.-P. Gangneux); Rennes Teaching Hospital, Rennes (J.-P. Gangneux)

DOI: https://doi.org/10.3201/eid3105.241392

[1]These authors contributed equally contributed to this article.

from symptom onset to diagnosis, diagnostic methods, treatment regimen, and 30- and 90-day case-fatality rates (CFRs). We assigned each patient to 1 of 6 main underlying condition categories: HM, including acute leukemia (myeloid or lymphoid) and other lymphoid malignancies; solid organ tumors; solid organ transplant; diabetes mellitus; severe burns; other risk factors, such as HIV and iatrogenic agranulocytosis; or no risk factors, in the absence of all other conditions. For patients with multiple potential risk factors, we prioritized HM and solid organ transplantation. We considered patients with HM, solid organ tumors under chemotherapy treatment, solid organ transplants, and other risk factors to be severely immunocompromised and grouped them for statistical comparisons; we did not include patients with severe burns in that group because, although immunocompromised, those case-patients have specific features. We considered patients with diabetes moderately immunocompromised and considered patients without risk factors to be immunocompetent.

We defined dissemination as infection in ≥2 noncontiguous sites. We separated localized IA into pleuropulmonary, ear-nose-throat (ENT), central nervous system (CNS), and skin disease. We considered cases with ENT and skull base infection sites as localized ENT infections with contiguous skull base extension. We considered cases with pleuropulmonary and ENT sites of infection as localized pulmonary infections with a contiguous sinus localization. We defined neutropenia as a neutrophil polymorphonuclear cell count of $<0.5 \times 10^6$ cells/mL. We considered positive galactomannan (GM) antigen in blood samples only, with a positivity threshold of ≥0.5 optical density. We defined bacterial, viral, or fungal co-infections as microbial pathogens found in the same microbiological samples as *A. flavus* at time of diagnosis and compatible with the patient's clinical manifestations.

Because *A. flavus* has higher prevalence in dry and warm regions (*2*–*4*), we evaluated seasonality of infections in France. We chose April 1–October 31 as the warmest months of the year in France, with average temperatures of ≥14°C, compared with November 1–March 31, during which average temperatures were <10°C, according to the 2018 report from the national meteorological organization in France (*9*).

Species Identification and Antifungal Susceptibility Testing

NRCMA centralized all isolates for identification confirmation. NMRCA identified *A. flavus* by morphology and partial DNA sequence analysis of the calmodulin gene. We only retained *A. flavus* var. *flavus*. We performed in vitro susceptibility testing according to the European Committee on Antimicrobial Susceptibility Testing (EUCAST) broth microdilution method (https://www.eucast.org/fileadmin/src/media/PDFs/EUCAST_files/AFST/Files/EUCAST_EDef_9.4_method_for_susceptibility_testing_of_moulds.pdf) with some modifications. NRCMA determined MICs for 7 antifungal agents, including liposomal amphotericin B (L-AmB), isavuconazole, voriconazole, posaconazole, itraconazole, caspofungin, and micafungin.

Statistical Analyses

We calculated continuous variables by using Mann-Whitney nonparametric test and expressed results as medians and interquartile range (IQRs). We used Fisher exact test for categorical variables and expressed results as frequencies and percentages. We performed all analyses in Stata 17 (StataCorp LLC, https://www.stata.com) and considered $p<0.05$ to be statistically significant.

Ethics

This research was performed in compliance with French law and the Declaration of Helsinki as adopted in 2000. NRCMA monitoring was approved by the Institute Pasteur institutional review board 1 (approval no. 2009–34 IRB) and the Commission Nationale de l'Informatique et des Libertés (National Commission for Information Technology and Civil Liberties) according to regulations in France.

Results

Patient Characteristics and Underlying Conditions

During January 2012–December 2018, a total of 54 patients with proven (44.4%) or probable (55.6%) IA caused by *A. flavus* were reported to RESSIF. Median patient age was 58 (IQR 48–70) years; 48.1% were male and 51.8% were female (Table 1). The main underlying condition was HM (53.7%, 29/54), most frequently acute leukemia (20/54, including 10 with acute myeloid leukemia and 10 with acute lymphoid leukemia) (Table 1). Almost all (90%, 26/29) HM patients had neutropenia at diagnosis. The second most frequent underlying condition was solid organ transplant (16.7%, 9/54), including kidney (n = 3), heart (n = 3), lung (n = 2), and liver (n = 1) transplantation. Median time between transplantation and IA was 5 months, with differences according to the type of organ transplant, from 1 month for heart transplant recipients to 36 months for kidney transplant recipients. Eight (14.8%) patients had diabetes mellitus as

Table 1. Characteristics of 54 patients with probable or proven invasive aspergillosis caused by *Aspergillus flavus*, France, 2012–2018*

Characteristics	Value
Median age, y (IQR)	58 (48–70)
Originating from Africa, n = 50	14 (28)
Diagnosis during April 1–Oct 31	32 (59.2)
Sex	
M	26 (48.1)
F	28 (51.8)
Primary underlying risk factor	
Malignancy	31 (57.4)
Solid organ cancer	2 (3.7)
Hematologic malignancy, n = 29	29 (54)
Acute myeloid leukemia	10 (34.5)
Acute lymphoid leukemia	10 (34.5)
Lymphoma	2 (6.9)
Chronic lymphoid leukemia	2 (6.9)
Other hematologic malignancy	5 (17.2)
Solid organ transplant, n = 9	9 (16.7)
Kidney	3 (33.3)
Heart	3 (33.3)
Lung	2 (22.2)
Liver	1 (11.1)
Diabetes mellitus	8 (14.8)
Severe burns	2 (3.7)
Other immunodeficiency, n = 2	2 (3.7)
HIV	1 (50)
Iatrogenic agranulocytosis	1 (50)
No risk factor	2 (3.7)
Median time between onset of symptoms and diagnosis, d (IQR)	20 (10–50)
Site of infection	
Localized infections, n = 47	47 (87)
Pulmonary†	33 (70.2)
Ear-nose-throat†	13 (27.7)
Cerebral contiguous extension‡	10 (21.3)
Skin and soft tissue	1 (2.1)
Disseminated infections, n = 7	7 (13)
Pulmonary	6 (85.7)
Ear-nose-throat	2 (28.8)
Cerebral	2 (28.8)
Skin and soft tissue	5 (71.4)
Fungemia	2 (28.6)
Positive serum galactomannan antigen, n = 38	23 (60.5)
Proven infection	24 (44.4)
Fungal coinfection at same site as *A. flavus*, n = 16§	16 (29.7)
A. fumigatus	6 (37.5)
A. niger	3 (18.8)
Mucorales	5 (31.2)
Pneumocystis jirovecii	3 (18.8)
Candidemia	1 (6.2)
Influenza coinfection	2 (3.7)
First-line antifungal therapy, including combinations, n = 50	
Voriconazole	32 (64)
Posaconazole	3 (6)
Itraconazole	2 (4)
Isavuconazole	2 (4)
Liposomal amphotericin B	9 (18)
Echinocandin	7 (14)
Antifungal combination	5 (10)
Death, n = 51 patients with outcome data	
30-day case-fatality, all causes	20 (39.2)
90-day case-fatality, all causes	24 (47.1)

*Values are no. (%) patients except as indicated.
†Four patients had lung and ear-nose-throat infections.
‡All were sinus infections with contiguous cerebral lesions.
§Including 1 case with 3 fungal co-infections.

Table 2. Main underlying risk factors for 54 patients with probable or proven invasive aspergillosis caused by *Aspergillus flavus*, France, 2012–2018*

Characteristics	HM, n = 29	SOC, n = 2	SOT, n = 9	DM, n = 8	Other, n = 2	Severe burns, n = 2	No risk factors, n = 2	p value†
Median age, y (IQR)	53 (28–66)	73 (66–80)	60 (57–70)	72.5 (70–74)	49 (48–50)	60 (50–69)	21 (16–25)	**<0.001**
Originating from Africa, n = 26	5/26 (19.2)	0	2/8 (25)	5 (62.5)	0	0	2 (100)	**0.02**
Sex								
M	12 (41.4)	1 (50)	5 (55.6)	5 (62.5)	1 (50)	0	1 (50)	0.46
F	17 (58.6)	1 (50)	4 (44.4)	3 (37.5)	1 (50)	2 (100)	1 (50)	0.46
Median delay to diagnosis, d (IQR)	17 (5–30)	5 (2–7)	20 (13.5–54)	105 (68–163)	32 (20–43)	7 (5–9)	NA	**<0.001**
Neutropenia‡§	26 (89.6)	0	1/8 (12)	0	1 (50)	0	0	**<0.001**
Positive serum galactomannan antigen§	15/22 (68.1)	1/1 (100)	3/7 (43)	2/4 (50)	1 (50)	1 (50)	0	0.63
Infection site								
Disseminated infection	4 (13.7)	1 (50)	1 (11.1)	0	0	1 (50)	0	0.57
Localized infection	25 (86.2)	1 (50)	8 (88.9)	8 (100)	2 (100)	1 (50)	2 (100)	0.57
Pleuropulmonary	23/25 (92)	0	7/8 (87.5)	0	2 (100)	0	1 (50)	**<0.001**
ENT	2/25 (8)	1/1 (100)	1/8 (12.5)	8/8 (100)	0	0	1 (50)	**<0.001**
CNS	0	1/1 (100)	1/8 (12.5)	7/8 (87.5)	0	0	1 (50)	**<0.001**
Skin and soft tissue	0	0	0	0	0	1 (100)	0	>0.999
First-line antifungal therapy¶	n = 27		n = 7					
Voriconazole	18 (66.7)	2 (100)	3 (4.8)	6/8 (75)	1 (50)	1 (50)	1 (50)	0.69
L-AmB	5 (18.5)	0	2 (28.6)	0/8 (0)	1 (50)	1 (50)	0	0.32
Other agent	6 (22.2)	0	2 (28.6)	3/8 (37.5)	1 (50)	0	1 (50)	0.41
Death	n = 28	n = 1	n = 8					
30-d CFR	13 (46.4)	0	4 (44.4)	0	1 (50)	2 (100)	0	**0.017**
90-d CFR	15 (53.6)	0	5 (55.6)	1 (12.5)	1 (50)	2 (100)	0	0.052

*Values are no. (%) except as indicated. Bold font indicates statistical significance. CFR, case-fatality rate; CNS, central nervous system; DM, diabetes mellitis; ENT, ear-nose-throat; HM, hemolytic malignancy; IQR, interquartile range; L-AmB, liposomal amphotericin B; NA, not applicable; SOC, solid organ cancer; SOT, solid organ transplant.
†For solid organ transplant, solid organ cancer, hemolytic malignancy, and other versus diabetes mellitis.
‡<0.5 × 10^3 cells/mL.
§No. positive/no. tested (%).
¶Including combination therapy. Other first-line agents included posaconazole, itraconazole, isavuconazole, and echinocandin.

the sole risk factor. The other patients had solid organ tumors under chemotherapy (n = 2), severe burns (n = 2), HIV infection (n = 1), or carbimazole-induced agranulocytosis (n = 1); 2 patients had no identified risk factors.

Patients with diabetes were significantly older (median age 72.5 [IQR 70–74] years) than patients with malignancy, either HM or solid organ cancer (median age 54 [IQR 32–66] years), or solid organ transplantation (median age 60 [IQR 53.5–70.5] years) (p<0.001) (Table 2). Patients with diabetes also had longer time between symptom onset and diagnosis (median 105 [IQR 68–163] days) than HM patients (median 16 [IQR 5–30] days) or patients with solid organ transplant (median 20 [IQR 13.5–54] days). Pleuropulmonary involvement was more frequent in patients with HM, solid organ tumors, or solid organ transplant (88%, 30/34) than those with diabetes (0/8) (p<0.001). In contrast, all 8 patients with diabetes mellitus had ENT infections, and most (88%, 7/8) had extension to the skull bases, but ENT infections were much less frequent (12%, 4/34) among HM, solid organ tumor, and solid organ transplant patients (p<0.001). We noted no cases of disseminated IA in patients with diabetes, compared with 5 cases (16%, 5/31) in HM patients and 1 (11%, 1/16) case in a solid organ transplant patient (p = 0.57).

Infection Sites and Clinical Manifestations

Of the 54 cases, 47 (87%) were localized (Table 3) and 7 (12.3%) disseminated (Table 4). Among the 47 localized infections, 33 were (70.2%) pleuropulmonary infections and 13 (27.6%) were ENT infections; 10 (77%) of the ENT infections had extension to the skull bases. No isolated CNS infections and only 1 case of localized skin and soft tissue infection were reported.

Compared with patients with pleuropulmonary IA, those with ENT infections were significantly older (median age 72 [IQR 61–74] years vs. 57 [IQR 48–67] years; p = 0.03) and had a longer duration of symptoms before diagnosis (median 90 [IQR 42–163] days vs. 19 [IQR 12–30] days; p = 0.0005). Patients with pleuropulmonary IA had higher rates of HM and solid organ transplantation than patients with

Table 3. Characteristics of localized invasive aspergillosis cases caused by *Aspergillus flavus*, France, 2012–2018*

Characteristics	Localized pleuropulmonary infection, n = 33	Localized ENT infection, n = 13	p value
Median age, y (IQR)	57 (48–67)	72 (61–74)	**0.03**
Originating from Africa	6/29 (21)	7/13 (54)	0.068
Sex			
M	16 (48.5)	7 (53.8)	>0.999
F	17 (51.5)	6 (46.2)	>0.999
Primary risk factors			**<0.001**
Hemolytic malignancy	23 (69.7)	2 (15.4)	**0.001**
Solid organ cancer	0	1 (7.7)	0.28
Solid organ transplant	7 (21.2)	1 (7.7)	0.41
Diabetes mellitus	0	8 (61.5)	**<0.001**
Other	2 (6.1)	0	>0.999
No risk factors	1 (3)	1 (7.7)	0.49
Clinical signs and symptoms			
Fever	22 (66.7)	5 (38.5)	0.1
Dyspnea	18 (54.5)	0	**<0.001**
Cough	11 (33.3)	0	**0.02**
Hemoptysis	4 (12.1)	0	0.09
Otalgia, otorrhea	0	8 (61.5)	**<0.001**
Chemosis, exophthalmia	2 (6.1)	2 (15.4)	0.56
Facial nerve palsy, headache	2 (6.1)	3 (23.1)	0.13
No symptoms	1 (3)	0	>0.999
Imaging features			
Nodules, mass lesion	17 (51.5)	0	0.11
Alveolar consolidation, ground-glass opacities	32 (96.9)	0	**<0.001**
Pleural effusion	18 (54.5)	0	0.11
Sinus opacification	4 (12.1)	12 (92.3)	**<0.001**
Sinus or mastoids lytic lesions	2 (6.1)	9 (69.2)	**<0.001**
Median time to diagnosis, d (IQR)	19 (12–30)	90 (42–163)	**<0.001**
Positive serum galactomannan antigen†	14/26 (53.8)	4/7 (57.1)	1
Diagnostic method‡			>0.999
Smear sputum	9/10 (90)	0	**<0.001**
BAL direct examination	15/25 (60)	NA	NA
BAL culture	24/25 (96)	NA	NA
Biopsy direct examination	5/7 (71)	10 (76.9)	>0.999
Biopsy culture	6/7 (86)	13 (100)	0.35
Proven cases	6 (18)	13 (100)	**<0.001**
Associated localizations			
Pulmonary	NA	0	NA
Ear, nose, throat	4 (12.1)	NA	NA
Central nervous system	0	10 (76.9)	**<0.001**
Mediastinal	1 (3)	0	**<0.001**
Fungal coinfection at same site§	12 (36.3)	0	**0.01**
Aspergillus fumigatus	5(15.1)	0	0.31
A. niger	3 (9.1)	0	0.55
Mucorales	4 (12.1)	0	0.31
Pneumocystis jirovecii	2 (6.1)	0	>0.999
Influenza co-infection	2 (6.1)	0	>0.999
First-line antifungal monotherapy¶	26/30 (86.7)	11/12 (91.7)	>0.999
Voriconazole	16/26 (61.5)	8/11 (72.7)	0.71
Other triazole	4/26 (15.3)	3/11 (27.3)	0.40
Echinocandin	2/26 (7.7)	0/11	>0.999
Liposomal amphotericin B	4/26 (15.4)	0/11	0.30
Antifungal combination therapy¶	4/30 (13.3)	1/12 (8.3)	>0.999
Curative surgery	3 (9.1)	6 (46.1)	**0.01**
Death	N = 31	N = 12	
30-day case-fatality	14 (45.2)	1 (8.3)	**0.03**
3-month case-fatality	17 (54.8)	2 (16.7)	**0.04**

*Values are no. (%) except as indicated. BAL, bronchoalveolar lavage; IQR, interquartile range.
†Positive galactomannan antigen in blood with an optical density index cutoff value of ≥0.5.
‡Values are no. positive/no. tested (%).
§13 cases with pulmonary fungal coinfections, including one with more than 1 coinfection.
¶Values are no. positive/no. treated (%).

Table 4. Main characteristics of patients with disseminated infections in a study of features of invasive aspergillosis caused by *Aspergillus flavus*, France, 2012–2018*

Characteristics	Value
Median age, y (IQR)	36 (14.5–58)
Sex	
M	3 (42.8)
F	4 (57.1)
Main risk factor	
Hematologic malignancy	4 (57.1)
Solid organ cancer	1 (14.3)
Solid organ transplant	1 (14.3)
Others, severe burns	1 (14.3)
Fever as primary clinical sign	5 (71.4)
Site of infection	
Pulmonary	6 (85.7)
Ear, nose, throat	2 (28.6)
Central nervous system	2 (28.6)
Skin and soft tissues	3 (42.8)
Fungemia	2 (28.6)
Median time to diagnosis, d (IQR)	5 (4.5–28)
Positive serum galactomannan antigen, n = 5	5 (100)
Proven cases	5 (71.4)
Fungal co-infection	3 (42.8)
Voriconazole first-line antifungal therapy	6 (85.7)
3-month case-fatality	4 (57.1)

*IQR, interquartile range.

ENT IA (69.7% [23/33]) vs. 15.4% [2/13] for HM, and 21.2% [7/33] vs. 15.4% [1/13] for solid organ transplantation; p<0.001). In contrast, diabetes mellitis was the most common underlying condition in patients with ENT IA (61.5% [8/13]), compared with no diabetes mellitis in patients with pleuropulmonary IA (p<0.001).

We also assessed available imaging results for the 54 included IA cases. All 33 patients with pleuropulmonary IA had chest computed tomography scans, 17 (51.5%) of whom had nodules, 32 (96.6%) had alveolar consolidations or ground-glass opacities, and 18 (54.5%) had pleural effusion. All 13 ENT IA patients had computed tomography scans of the sinuses, ear, or brain, showing sinus opacification in 12 (92.3%) and lytic lesions of sinus, mastoid, or skull base walls in 9 (69.2%) cases. When performed, serum GM testing was positive in 53.8% (14/26) of cases of pleuropulmonary IA and in 57.1% (4/7) of ENT IA cases.

Among pulmonary IA cases, 36.4% (12/33) of patients had ≥1 fungal co-infection at the same site; 11 had 1 co-infection and 1 had 3 fungal co-infections. Co-infections included 5 *A. fumigatus*, 3 *A. niger*, 4 Mucorales, and 2 *Pneumocystis jirovecii*. Patients with ENT IA did not exhibit relevant fungal co-infections. Of note, influenza co-infection was reported in 6.1% (2/33) of pulmonary IA. In those cases, influenza was diagnosed before IA, and the diagnosis was considered influenza-associated pulmonary aspergillosis.

Among the 7 disseminated IA cases, the most frequent underlying condition was HM in 4 (57%) cases, followed by 1 (14.3%) case each of solid-organ tumor under chemotherapy, solid organ transplant, and severe burns. Patients with disseminated IA infections were younger (median age 36 [IQR 14–66] years) than patients with localized IA (median age 60 [IQR 50–70] years; p = 0.04). The most frequent sites involved in disseminated IA were pulmonary (85.7%), skin and soft tissues (42.8%), ENT (28.6%), and CNS (28.6%). Serum galactomannan was positive in all disseminated cases. Two patients had *A. flavus* fungemia (1 patient had metastatic cholangiocarcinoma and 1 had severe burns). Fungal co-infections were found in 43% (3/7) of cases, including various pathogens identified in different sites: 1 *P. jirovecii* in a bronchoalveolar lavage sample associated with *A. flavus* cutaneous infection, and 1 candidemia and 1 sinusal mucormycosis associated with *A. flavus* found in a puncture of a frontonasal subcutaneaous collection. Finally, disseminated IA with pulmonary involvement (6/7) accounted for 15.4% (6/39) of all cases of pulmonary IA, and disseminated IA with ENT involvement (2/7) accounted for 13.3% (2/15) of all ENT IA.

Treatment and Outcomes

Before invasive *A. flavus* infection, only 3 patients, all of whom had HM, had been receiving antifungal prophylaxis (1 fluconazole and 2 L-AmB). An antifungal treatment was recorded in 50 (92.6%) of 54 cases. The other 4 (7.4%) patients did not receive antifungal therapy: 3 patients had localized pleuropulmonary IA cases diagnosed postmortem, and the fourth patient had a complete curative surgical treatment for ENT IA. Antifungal monotherapy was prescribed as the first-line treatment for 45 (90%) of the 50 patients who received antifungal treatment, most (66.7%, 30) of whom received voriconazole, but other azoles (posaconazole in 7%, itraconazole in 4%, and isavuconazole in 4%) were also administered, as were L-AmB in 13% (n = 6) and an echinocandin in 4% (n = 2). Five (10%) patients received combined antifungal therapy, including L-AmB and an echinocandin in 3 cases and voriconazole and an echinocandin in 2 cases. Of the 54 ctotal cases, curative surgery was performed in 9 (16.6%), more frequently in ENT IA (46.1%, 6/13) cases than in pleuropulmonary IA (3%, 1/33) cases (p = 0.01).

We determined EUCAST MICs for itraconazole, posaconazole, voriconazole, isavuconazole, L-AmB, caspofungin, and micafungin on 46 isolates (Table 5). The MICs for amphotericin B ranged from 0.5 to >4 mg/L, and the MICs for voriconazole ranged from 0.125 to 1 mg/L. *A. flavus* showed lower susceptibility to amphotericin B (MIC_{50} of 2 mg/L and MIC_{90} of

4 mg/L) than to voriconazole (MIC_{50} of 0.5 mg/L and MIC_{90} of 1 mg/L).

Among 51 patients with available outcome data, 20 patients died, yielding a 30-day CFR of 39.2% (95% CI 25.8%–53.9%) (Table 1). The CFR was higher (46%) for patients with malignancy or solid organ transplant than for patients with diabetes mellitus (n = 0) (p = 0.013) (Table 2). Although not statistically significant, CFR was higher for disseminated (57%) than localized (36%) infections (p = 0.4). Among the different localized IA, pleuropulmonary IA had a higher CFR than did ENT IA (45% vs. 8%; p = 0.03) (Table 3). IA associated with fungal co-infections tended to have a higher 30-day CFR than those without fungal coinfections (44% [7/16] vs. 37% [13/35]; p = 0.8).

Discussion

Herein, we describe 54 cases of invasive aspergillosis caused by *A. flavus* reported in France during 2012–2018. Few data on *A. flavus* IA in the Northern Hemisphere are available, probably because *A. flavus* is scarce in high-income countries, cases are underdiagnosed because of nonspecific clinical manifestations and absence of diagnostic confirmation in mildly immunocompromised patients, and most countries do not have specific fungal surveillance programs. Thus, we sought to identify risk factors specific to *A. flavus* and the association of risk factors with clinical manifestations and outcomes.

Although some characteristics of our patients, such as median age (58 years) and CFR (42%), were similar to cases of IA (all species combined) reported in France during 2005–2007 (*7*) and 2012−2018 (*1*), we found a relatively lower percentage (55%) of patients with HM and a higher percentage (14.8%) with diabetes among the underlying factors, compared with 71% for patients with HM and <10% for those with diabetes mellitus from in an earlier study (*1*). Because *A. flavus* has a higher prevalence in dry and warm regions (*2*–*4*), we also investigated the possibility of *A. flavus* acquisition in tropical or subtropical countries such as northern or southern Africa and East Asia, where patients might have lived. Of note, although recent travel history was not recorded for all patients in our study, 28% of patients originated from Africa, suggesting acquisition of *A. flavus* in the Southern Hemisphere.

We also assessed seasonality of infections in France. We found a higher rate (59.2%) of diagnoses of IA caused by *A. flavus* in the hottest months (Table 1), highlighting the probable influence of hot temperatures on *A. flavus* development, as previously reported (*10*).

We identified 2 distinct patterns of disease: pulmonary IA in highly immunocompromised patients, and ENT IA primarily occurring in patients with diabetes mellitus. Most (87%) cases of IA in our study were localized pleuropulmonary infections. Characteristics of infection were similar in terms of underlying condition, clinical manifestations, and prognosis to previously reported IA cases caused by *A. fumigatus* (*11*). HM and solid organ transplantation accounted for 91% of underlying risk factors in IA cases, consistent with the >85% reported on pulmonary IA from all species combined in a previous study (*11*). Clinical manifestations of *A. flavus* pulmonary IA among our patient cohort were similar to those for pulmonary IA caused by *A. fumigatus*, including acute symptom onset and a short diagnostic delay. ENT IA was the second main site of infection in our study, which is consistent with prior data reporting *A. flavus* as the main causative species in ENT IA in tropical and subtropical countries (*2*–*4*). ENT infection might be related to the larger size of *A. flavus* conidia compared with that of *A. fumigatus* (*12*,*13*), making progression through the lower airways difficult.

The main underlying condition among our cohort was uncontrolled diabetes mellitus, which we noted in 61.5% of cases. The association between diabetes mellitus and IA was previously observed in aspergillosis otitis in a study where all 12 patients had diabetes mellitis (*14*) and another in which where 46.2% of patients were diabetic (*15*). The association between diabetes mellitus and IA has been assumed to be the result of susceptibility to functional impairment of innate immunity because of alteration of phagocytosis and efficiency of neutrophil polymorphonuclear cells that are known to play a pivotal role in antifungal immunity (*16*). We noted a higher (54%) percentage of patients originating from North Africa, where environmental prevalence of *A. flavus* is high, among cases of ENT IA compared with 21% among patients with pulmonary

Table 5. MICs of first-line antifungal drugs used for 46 cases of invasive aspergillosis caused by *Aspergillus flavus*, France, 2012–2018*

Antifungal drug	Range, mg/L	MIC_{50}	MIC_{90}
Voriconazole	0.125–1	0.5	1
Isavuconazole	0.25–2	0.5	1
Itraconazole	0.06–0.5	0.125	0.25
Posaconazole	<0.015–0.25	0.125	0.25
Liposomal amphotericin B	0.5 to >4	1	4
Caspofungin	0.125–0.5	0.25	0.5
Micafungin	0.007–0.03	0.007	0.015

*Values according to European Committee on Antimicrobial Susceptibility Testing broth microdilution method (https://www.eucast.org/fileadmin/src/media/PDFs/EUCAST_files/AFST/Files/EUCAST_EDef_9.4_method_for_susceptibility_testing_of_moulds.pdf). MIC_{50}, MIC that inhibited 50% of tested microorganisms; MIC_{90}, that inhibited 90% of tested microorganisms.

IA (p = 0.068). Despite less acute progression of infection in those forms, ENT IA cannot be considered benign, considering the frequent (77%) extension to the skull base reported in our study. That finding is similar to 2 meta-analyses of osteoarticular aspergillosis reported during 1936–2013 (*17*,*18*), wherein skull base osteomyelitis accounted for 18% of cases, 68% of which were related to a contiguous ENT injury.

Concerning antifungal drug therapy, voriconazole, the first-line recommended treatment in current guidelines (*19*), was only used in 64% of cases in this study, similar to data reported in previous epidemiologic studies (*7*). The use of other first-line antifungal drugs, mainly in L-AmB (23%) and echinocandins (20%) in pulmonary IA, could be explained by initial disease severity and diagnostic uncertainty in severely immunocompromised patients with frequent fungal co-infections. Consistent with prior studies (*20*), we found that MICs for L-AmB were high. However, because of the retrospective design of the study, we could not evaluate whether the use of L-AmB as initial therapy was associated with increased mortality rates. Curative surgical management was also prevalent (46%) for ENT IA in our study, consistent with a previous case series of ENT aspergillosis (*15*). Research on surgical therapy, which has been shown to influence illness and death, deserves to be better codified (*21*). Despite rapid initiation of treatment, overall mortality rates remained high (47% at 3 months), with notable variability according to underlying risk factors and IA localizations (17% in ENT vs. 55% in pulmonary infections).

One of the main limitations of our study remains the low number of cases reported, which limits the statistical power of comparisons between groups, needing further collaborative studies among countries in Europe or more broadly to increase the number of cases assessed. Another limitation is a lack of comparison between groups. We compared general characteristics of *A. flavus* IA patients, including sex ratio, age, underlying conditions at diagnosis, and mortality rates, to all cases of IA reported from RESSIF for all *Aspergillus* species, >86% of which were *A. fumigatus*, for the same period (2012–2018) (*1*). However, we could not compare specific subgroups, such as those with localized infections, because of the absence of individual patient data. International studies would also increase the number of cases studied and enable comparisons with infections caused by other non–*A. fumigatus* species.

A. flavus IA could represent an increasing issue in the Northern Hemisphere, and further studies are needed to clarify its prevalence and risk factors. Indeed, during 2005–2007 in France, 3% of reported IA cases were caused by *A. flavus* (*7*), which increased to 8.7% during 2012–2018 (*1*). That increase is probably to the result of multiple reasons, including climate, migration, and rates of immunodeficiency. First, global warming could create a more favorable ecosystem for *A. flavus*, as observed in the seasonal pattern in North America, which has seen increased cases in summer months (*10*). Second, migrating populations could be at risk for IA after long-term carriage of *A. flavus* previously acquired in more southern countries, as noted by the high percentage of patients originating from North Africa among our *A. flavus* IA cohort. Finally, increases in the population of patients with acquired immunodeficiency, such as organ recipients (*22*), could mean that more patients are susceptible to present *A. flavus* infection and have more severe outcomes.

In conclusion, we found that IA caused by *A. flavus* shared many similarities with IA caused by *A. fumigatus*. Clinical manifestations mainly showed 2 distinct patterns: aggressive pleuropulmonary or disseminated infection in highly immunocompromised patients, with a high rate of co-infection and a high mortality rate despite antifungal treatment; and ENT infections, usually occurring in patients with uncontrolled diabetes mellitus, frequently among persons originating from countries in North Africa, and showing low mortality rates after curative surgery and antifungal treatment. Surveillance studies such as ours can raise awareness of non–*A. fumigatus* IA, including in Western countries, where their incidence may increase in the future because of climate change. Clinicians should remain vigilant for *A. flavus* and consider it during differential diagnosis for IA.

Acknowledgments

We thank Françoise Dromer for her tremendous input in the conceptualization of this study, particularly for the expansion of the RESSIF surveillance network and her continuous investment in its management.

This work was supported by recurrent financial support from Santé Publique France and Institut Pasteur.

Author contributions: L.B. and F.L. conceptualized the study; L.B., O.P., and F.L. developed study methodology; J.P.G, K.B.S., D.G.H, O.L., S.B., A.A., R.H., F.D., G.D., S.C., F.M., S.D., C.N., J.B., M.P., E.C, T.C., M.S., N.D.B., and F.L. curated study data; L.B. and O.P. wrote the original draft; J.P.G, K.B.S., D.G.H, O.L., S.B., A.A., R.H., F.D., G.D., S.C., F.M., S.D., C.N., J.B., M.P., E.C, T.C., M.S., N.D.B., and F.L. reviewed and edited the draft article. Methods and results were reported according to STROBE guidelines.

About the Author

Dr. Bertin is an internal medicine physician currently pursuing a PhD at the University of Paris-Cité, France. Her primary research interests include infectious diseases and immunology, notably mucosal-associated invariant T cells.

References

1. Bretagne S, Sitbon K, Desnos-Ollivier M, Garcia-Hermoso D, Letscher-Bru V, Cassaing S, et al.; French Mycoses Study Group. Active surveillance program to increase awareness on invasive fungal diseases: the French RESSIF Network (2012 to 2018). MBio. 2022;13:e0092022. https://doi.org/10.1128/mbio.00920-22
2. Chakrabarti A, Kaur H, Savio J, Rudramurthy SM, Patel A, Shastri P, et al. Epidemiology and clinical outcomes of invasive mould infections in Indian intensive care units (FISF study). J Crit Care. 2019;51:64–70. https://doi.org/10.1016/j.jcrc.2019.02.005
3. Chakrabarti A, Chatterjee SS, Das A, Shivaprakash MR. Invasive aspergillosis in developing countries. Med Mycol. 2011;49:S35–47. https://doi.org/10.3109/13693786.2010.505206
4. Zanganeh E, Zarrinfar H, Rezaeetalab F, Fata A, Tohidi M, Najafzadeh MJ, et al. Predominance of non-*fumigatus* *Aspergillus* species among patients suspected to pulmonary aspergillosis in a tropical and subtropical region of the Middle East. Microb Pathog. 2018;116:296–300. https://doi.org/10.1016/j.micpath.2018.01.047
5. Ragozzino S, Goldenberger D, Wright PR, Zimmerli S, Mühlethaler K, Neofytos D, et al. Distribution of *Aspergillus* species and prevalence of azole resistance in respiratory samples from Swiss tertiary care hospitals. Open Forum Infect Dis. 2021;9:ofab638. https://doi.org/10.1093/ofid/ofab638
6. Steinbach WJ, Marr KA, Anaissie EJ, Azie N, Quan SP, Meier-Kriesche HU, et al. Clinical epidemiology of 960 patients with invasive aspergillosis from the PATH Alliance registry. J Infect. 2012;65:453–64. https://doi.org/10.1016/j.jinf.2012.08.003
7. Lortholary O, Gangneux JP, Sitbon K, Lebeau B, de Monbrison F, Le Strat Y, et al.; French Mycosis Study Group. Epidemiological trends in invasive aspergillosis in France: the SAIF network (2005–2007). Clin Microbiol Infect. 2011;17:1882–9. https://doi.org/10.1111/j.1469-0691.2011.03548.x
8. Donnelly JP, Chen SC, Kauffman CA, Steinbach WJ, Baddley JW, Verweij PE, et al. Revision and update of the consensus definitions of invasive fungal disease from the European Organization for Research and Treatment of Cancer and the Mycoses Study Group Education and Research Consortium. Clin Infect Dis. 2020;71:1367–76. https://doi.org/10.1093/cid/ciz1008
9. Meteo France. Climate report for the year 2018 [in French] [cited 2019 Jan 8]. https://meteofrance.fr/sites/meteofrance.fr/files/files/editorial/Bilan-climatique-annee2018.pdf
10. Panackal AA, Li H, Kontoyiannis DP, Mori M, Perego CA, Boeckh M, et al. Geoclimatic influences on invasive aspergillosis after hematopoietic stem cell transplantation. Clin Infect Dis. 2010;50:1588–97. https://doi.org/10.1086/652761
11. Ledoux MP, Herbrecht R. Invasive pulmonary aspergillosis. J Fungi (Basel). 2023;9:131. https://doi.org/10.3390/jof9020131
12. Pasqualotto AC. Differences in pathogenicity and clinical syndromes due to *Aspergillus fumigatus* and *Aspergillus flavus*. Med Mycol. 2009;47:S261–70. https://doi.org/10.1080/13693780802247702
13. Wong SSW, Venugopalan LP, Beaussart A, Karnam A, Mohammed MRS, Jayapal JM, et al. Species-specific immunological reactivities depend on the cell-wall organization of the two *Aspergillus*, *Aspergillus fumigatus* and *A. flavus*. Front Cell Infect Microbiol. 2021;11:643312. https://doi.org/10.3389/fcimb.2021.643312
14. Marchionni E, Parize P, Lefevre A, Vironneau P, Bougnoux ME, Poiree S, et al. *Aspergillus* spp. invasive external otitis: favourable outcome with a medical approach. Clin Microbiol Infect. 2016;22:434–7. https://doi.org/10.1016/j.cmi.2015.12.027
15. Pichon M, Joly V, Argy N, Houze S, Bretagne S, Alanio A, et al. *Aspergillus flavus* malignant external otitis in a diabetic patient: case report and literature review. Infection. 2020;48:193–203. https://doi.org/10.1007/s15010-020-01394-8
16. Daryabor G, Atashzar MR, Kabelitz D, Meri S, Kalantar K. The effects of type 2 diabetes mellitus on organ metabolism and the immune system. Front Immunol. 2020;11:1582. https://doi.org/10.3389/fimmu.2020.01582
17. Gabrielli E, Fothergill AW, Brescini L, Sutton DA, Marchionni E, Orsetti E, et al. Osteomyelitis caused by *Aspergillus* species: a review of 310 reported cases. Clin Microbiol Infect. 2014;20:559–65. https://doi.org/10.1111/1469-0691.12389
18. Gamaletsou MN, Rammaert B, Bueno MA, Moriyama B, Sipsas NV, Kontoyiannis DP, et al. *Aspergillus* osteomyelitis: epidemiology, clinical manifestations, management, and outcome. J Infect. 2014;68:478–93. https://doi.org/10.1016/j.jinf.2013.12.008
19. Ullmann AJ, Aguado JM, Arikan-Akdagli S, Denning DW, Groll AH, Lagrou K, et al. Diagnosis and management of *Aspergillus* diseases: executive summary of the 2017 ESCMID-ECMM-ERS guideline. Clin Microbiol Infect. 2018;24(Suppl 1):e1–38. https://doi.org/10.1016/j.cmi.2018.01.002
20. Rudramurthy SM, Paul RA, Chakrabarti A, Mouton JW, Meis JF. Invasive aspergillosis by *Aspergillus flavus*: epidemiology, diagnosis, antifungal resistance, and management. J Fungi (Basel). 2019;5:55. https://doi.org/10.3390/jof5030055
21. Serris A, Benzakoun J, Danion F, Porcher R, Sonneville R, Wolff M, et al.; CEREAL study group. Cerebral aspergillosis in the era of new antifungals: the CEREALS national cohort study Nationwide CEREbral Aspergillosis Lesional Study (CEREALS). J Infect. 2022;84:227–36. https://doi.org/10.1016/j.jinf.2021.11.014
22. Agence de la biomédecine. 2024 organ retrieval and transplantation activity in 2023 and 2024 opinion barometer [in French] [cited 2025 Jan 11]. https://presse.agence-biomedecine.fr/?p=3744

Address for correspondence: Fanny Lanternier, Department of Infectious Diseases and Tropical Medicine, Necker–Enfants Malades University Hospital, Assistance Publique–Hôpitaux de Paris (AP-HP), IHU Imagine, Paris 75014, France; email: fanny.lanternier@aphp.fr

Comprehensive Survival Analysis of Alveolar Echinococcosis Patients, University Hospital Zurich, Zurich, Switzerland, 1973–2022

Ansgar Deibel,[1] Yanick Kindler,[1] Rubens Mita, Soleen Ghafoor, Cordula Meyer zu Schwabedissen, Barbara Brunner-Geissmann, Alexander Schweiger, Felix Grimm, Michael Reinehr, Achim Weber, Cäcilia S. Reiner, Andreas E. Kremer, Henrik Petrowsky, Pierre-Alain Clavien, Peter Deplazes, Stefanie von Felten, Beat Müllhaupt

Alveolar echinococcosis (AE) is a zoonotic disease of increasing concern worldwide. Before benzimidazole drug therapy, 10-year death rates were 90% without surgical resection. In unresectable patients, long-term benzimidazole therapy is highly effective in stabilizing the disease course. We performed a retrospective study of 334 AE patients treated at the University Hospital Zurich, Zurich, Switzerland, during 1973–2022. Annual diagnoses increased over time, and more cases were detected by chance at earlier stages. Ninety patients died, mostly from causes unrelated to AE. Relative survival of AE patients compared with the population of Switzerland demonstrated a steady decrease 5 years after diagnosis. Patient age at diagnosis was the primary variable associated with overall survival. In a propensity-score matched survival analysis, early curative surgery was associated with overall improvement but not AE-specific survival. We conclude that survival of patients with AE is limited by non-AE causes and that early curative surgery does not improve AE-specific survival.

Alveolar echinococcosis (AE) is an orphan zoonosis caused by the metacestode stage of the fox tapeworm, *Echinococcus multilocularis*. This parasite is endemic across large parts of the Northern Hemisphere, including Switzerland, Germany, and France (*1*). Although rare, AE is of increasing concern because of rising incidences (*2*–*6*). Previously nonendemic regions such as North America and eastern central Europe are reporting an increasing number of AE patients (*7*–*10*). Proposed explanations for this phenomenon include the habitat expansion of a growing fox population, an increased use of imaging in healthcare, and a more susceptible population (*4*,*5*,*11*).

AE is a silently progressing and infiltrative disease that primarily affects the liver and can become symptomatic through mass effect and occlusion of bile ducts or blood vessels (*12*). Various complications can occur, such as obstructive jaundice, cholangitis, portal vein occlusion or thrombosis, or secondary Budd Chiari syndrome with or without portal hypertension (*13*). On occasion, distant metastasis is observed (*12*). For staging of the disease the PNM classification (parasite location in the liver, neighboring organ involvement, metastasis) was proposed (*14*).

Without adequate treatment, 90% of AE patients died within 10 years of disease onset (*15*). Cure can only be achieved through complete resection and adjuvant benzimidazole drug recurrence prophylaxis (*16*). Curative resection is often not possible because of advanced disease (*16*). The use of palliative surgery was abandoned in the early 2000s because of a lack of survival benefit over benzimidazole drug therapy alone (*17*). Liver transplantation is associated with frequent disease recurrence and remains a rescue measure in select cases (*18*). In inoperable AE cases, long-term benzimidazole drug therapy is highly effective at stopping disease progression (*19*). Treating icteric patients because of biliary obstruction with benzimidazole drugs alone, rather than performing biliary tract intervention, might be as effective and safer (*20*). Today,

Author affiliations: University Hospital Zurich, Zurich, Switzerland (A. Deibel, Y. Kindler, S. Ghafoor, C. Meyer zu Schwabedissen, B. Brunner-Geissmann, M. Reinehr, A. Weber, C.S. Reiner, A.E. Kremer, H. Petrowsky, P.-A. Clavien, B. Müllhaupt); University of Zurich, Zurich (R. Mita, F. Grimm, P. Deplazes, S. von Felten); Cantonal Hospital Zug, Zug, Switzerland (A. Schweiger)

DOI: https://doi.org/10.3201/eid3105.241608

[1]These first authors contributed equally to this article.

selected inoperable patients can be considered for treatment discontinuation (*21*,*22*).

The life expectancy of AE patients has increased since benzimidazole drug therapy was introduced (*19*,*23*). Excess deaths caused by AE were reported to be highest in the first 2 years after diagnosis (*23*). The main death risk was attributed to hilar involvement of the AE and the age of patients when AE was diagnosed (*19*,*23*). Radical surgery and benzimidazole drug therapy have improved overall survival of AE patients (*19*,*23*).

The aim of this study was to assess changes in the clinical manifestation, treatment, and survival of AE patients treated at the University Hospital Zurich, Zurich, Switzerland, over a 50-year period. This study followed the Strengthening the Reporting of Observational Studies in Epidemiology statement checklist.

Patients and Methods

Patients

The Zurich Echinococcosis Cohort Study was launched in November 2020 after receiving ethical approval (Business Administration System for Ethics Committees approval no. 2020-00495). The study included all patients who underwent consultations for AE at Zurich University Hospital from 1973–2022, identified by the hospital's electronic system and an AE cohort registry (*2*,*19*,*24*). We obtained informed consent during outpatient visits or by letter; for deceased patients, consent was waived by the ethics committee. We sourced clinical data from the old cohort registry and reviewed from both archived and electronic patient records.

AE Diagnosis, Staging, Symptoms, and Complications

We classified AE diagnoses according to World Health Organization criteria as possible (imaging finding or positive serologic test), probable (imaging finding confirmed by 2 serologic tests), and definitive (confirmation through histopathologic test or PCR) (*14*). For staging AE, we applied the PNM classification through review of available imaging data at diagnosis (*14*). When no computed tomography or magnetic resonance imaging images were available for review, we cross-verified staging data entries from the cohort registry database with available imaging reports, which a radiologist with experience in AE imaging corrected in case of conflicting results (n = 10). We recorded the presence of any AE-associated symptoms, such as right upper quadrant pain, and the presence of any biliary, vascular, or infectious (nonbiliary) complications at the time of diagnosis. Biliary complications comprised biliary tract occlusion with jaundice or cholangitis. Vascular complications included portal vein, liver vein, or inferior vena cava occlusion or thrombosis with signs of portal-hypertension or inferior vena cava obstruction, which included the presence of ascites, esophageal varices, or lower leg edema. We defined infectious complications as AE-associated infections other than cholangitis, mainly cyst infections, empyema, or peritonitis.

AE Treatment

We classified initial surgical resection of AE lesions by intent (curative or palliative) and by involvement of the liver (hepatic or nonhepatic). In case of curatively intended liver resection, we defined the resection margin as R0 or R1, depending on whether the AE lesion extended into the resection margin on histopathologic examination. We classified liver resection as mentioned in the case surgical report into segmentectomy, hemihepatectomy (segments I–IV or V–VIII), extended hemihepatectomy (segments I–VI or IV–VIII), or liver transplantation. We assessed the time from diagnosis to surgical intervention and classified into early (≤12 months) and late (>12 months) resection. After curatively intended liver resection, we defined the detection of any new AE-typical lesions on repeat cross-sectional imaging as recurrence.

We recorded the initial benzimidazole drug therapy, the type (albendazole or mebendazole) of drug, and time from diagnosis to start of treatment. Curatively resected patients receive a postoperative recurrence prophylaxis with benzimidazole drugs for ≥2 years (*16*). In case of R1, palliative resection, or inoperable disease, benzimidazole drug therapy is continued indefinitely (*16*). In addition, if benzimidazole drug treatment was prematurely discontinued, we recorded the reason. We considered a structured treatment discontinuation in patients meeting the criteria of inactive disease, negative results on Em18/EmII (*3*–*10*) serologic testing, and no metabolic activity of AE lesions on positron emission tomography–computed tomography (*22*). We considered any physician-initiated treatment discontinuation outside those criteria nonstructured.

Follow-Up and Survival Data

We recorded the date of last follow-up, follow-up duration, and clinical course of AE. Complete follow-up included patient history, imaging report (computed tomography or magnetic resonance imaging), serologic testing, and blood analysis until last contact or study closure date (by September 30, 2023). We recorded the occurrence of symptomatic

events, including biliary complications (cholestasis or cholangitis) or vascular obstruction (ascites or variceal bleeding), cyst rupture, infection, or fistula formation. We considered patients cured if parasitic tissue was completely surgically removed and the disease did not reoccur during follow-up. In addition, we recorded date of death, obtained through patient charts or from the hospital administration that obtained the information through the national civil register, and cause of death. If the cause of death was not noted in the patient charts, we contacted the last treating physician or local hospital to provide that information. We grouped causes of death other than AE into 6 groups: malignant, cardiovascular, neurologic, hepatic (non-AE), infectious, and other diseases.

Statistical Analysis

We conducted all analysis by using R (The R Project for Statistical Computing Team, https://www.r-project.org). We compared the survival of AE patients with the population of Switzerland by estimating relative survival curves and by using additive relative survival models as implemented in the R functions rs.surv and rsadd (with the method of expectation-maximization) from the relsurv package (*25*). We retrieved the life tables of the population of Switzerland from the Human Mortality Database (https://www.mortality.org).

Table 1. Baseline characteristics of alveolar echinococcosis patients, University Hospital Zurich, Zurich, Switzerland, 1973–2022*

Baseline characteristics	Value
No. patients	334
Age at diagnosis, y, median (IQR)	57.5 (44.0–65.8)
Sex	
M	142 (42.5)
F	192 (57.5)
World Health Organization diagnosis criteria	
Possible	4 (1.2)
Probable	144 (43.1)
Definitive	186 (55.7)
Alveolar echinococcosis stage	
I	93 (27.8)
II	42 (12.6)
IIIa	50 (15.0)
IIIb	74 (22.2)
IV	68 (20.4)
Unclassified	7 (2.1)
Symptoms at diagnosis	
Yes	201 (60.2)
No	127 (38.0)
Missing	6 (1.8)
Complication at diagnosis	
Biliary	46 (13.8)
Vascular	8 (2.4)
Infectious	6 (1.8)
Missing	1 (0.3)

*Values are no. (%) except as indicated.

To evaluate whether early curative surgery (within a year of diagnosis) improved overall and disease-specific survival compared with no, delayed, or palliative surgery, we used propensity score matching to balance baseline characteristics and applied Cox proportional hazards models on the matched set. We estimated the propensity score, the probability of receiving curative surgery within 1 year, by using logistic regression with patient age at AE diagnosis, year of diagnosis, PNM classification (MX was considered M0), incidental finding of AE, benzimidazole drug therapy within 1 year, and presence of AE complications at diagnosis as explanatory variables. We performed matching once by using 1:1 nearest neighbor matching on the propensity score without replacement and once by using 1:1 genetic matching, both targeting the average treatment effect on the treated, as implemented in the R package MatchIt (*26*).

Results

Patient Cohort

In total, we included 334 (93.8%) of 356 identified AE patients in the study (Table 1; Appendix Figure 1, https://wwwnc.cdc.gov/EID/article/31/5/24-1608-App1.pdf). Diagnosis was probable in 144 (43.1%) cases and definitive in 186 (55.7%) cases, according to World Health Organization criteria (*14*). Only in 4 patients (1.2%) was the diagnosis solely on the basis of typical imaging findings. The median patient age at diagnosis was 57.5 years of age, and there was a slight female predominance (57.5% female vs. 42.5% male). The liver was affected in most patients (97%, n = 331), whereas 96 (28.7%) patients demonstrated involvement of a neighboring organ, and 41 patients (12.3%) demonstrated distant metastasis (Appendix Table 1). AE manifested in a limited stage (I–II) in 135 (40.4%) patients and in an advanced stage (IIIa–IV) in 192 (57.6%) patients; in 7 patients (2.1%) AE could not be staged because of missing data. Most (60.2%, n = 201) patients had symptoms attributable to AE, whereas 127 (38.0%) patients had AE diagnosed incidentally. If complications were observed at diagnosis, biliary complications were reported most frequently (13.8%, n = 46), whereas vascular complications and nonbiliary infections occurred only in rare cases.

Pursued Treatment and Observed Clinical Course

We observed different treatment strategies and clinical courses in our study (Table 2; Appendix Table 2). Surgical resection was performed in 151 (45.2%)

patients after a median of 1 month. Only 10 patients had surgery >12 months after diagnosis. Twenty-five (16.6%) patients underwent an a priori palliative debulking resection. In 126 (83.4%) patients, a curative resection was intended, which was confirmed by histologic testing in 105 (83.3%) patients (R0 resection), whereas in 21 (16.7%) patients the resection margin was positive (R1 resection). Of the 126 patients who underwent curatively intended surgery, 13 suffered disease recurrence, most in cases of R1 resection (n = 8). All recurrences were in the liver, in 10 patients at the resection margin, whereas 3 patients showed new liver lesions. R1 resection resulted in a prolongation of benzimidazole drug therapy to a median of 79 months (median 26 months in R0 resected patients), and 10 patients were on drug therapy at last follow-up. Four patients with R0 resection received no recurrence prophylaxis because of suspected inactive disease. In all 4 patients, surgery was performed under the assumption of cancer metastasis to the liver, and AE infection was an incidental diagnosis. Serologic testing performed shortly after surgery was completely negative.

Most commonly, patients underwent segmentectomy (n = 51) or hemihepatectomy (n = 53). Only 17 had an extended hemihepatectomy, and 3 patients underwent liver transplantation. Only 1 transplant was performed because of AE, whereas the other 2 had independent indications (hepatocellular and perihilar cholangiocellular carcinoma). Two patients underwent nonhepatic resection, 1 of an isolated cerebral lesion and 1 of an isolated lesion in the thoracic spine.

Benzimidazole drug therapy, mainly albendazole, was initiated in most patients (94.3%, n = 315) after a median of 1 month. In 212 (63.5%) patients who underwent palliative or no resection, albendazole was the mainstay of treatment. Only 15 nonresected patients did not receive benzimidazole drug therapy because of suspected inactive disease. Twenty (6.0%) patients who underwent palliative or no resection had a symptomatic progression event during follow-up. Twelve of those events were recurrent or new onset of cholestasis with or without cholangitis; 4 had portal-hypertensive complications including ascites or variceal bleeding, whereas another 5 had cyst rupture, infection, or fistula formation.

In 33 (9.9%) resected and nonresected patients, benzimidazole drug therapy was discontinued prematurely at various time points during follow-up, most commonly because of treatment-related adverse events (n = 10), followed by nonstructured discontinuations in R1 and palliative resected patients (n = 8), terminal illness other than AE (n = 7), patient choice (n = 4), intended pregnancy (n = 2), and other or unknown 2 (n = 2) (Appendix Table 2). Of all inoperable patients that discontinued benzimidazole drug therapy because of intolerance, only 1 patient died of AE, 95 months after treatment discontinuation (Table 3). Another 28 (8.5%) patients on long-term benzimidazole therapy underwent a structured treatment discontinuation after a median of 58.5 months.

Table 2. Treatments used for alveolar echinococcosis patients, University Hospital Zurich, Zurich, Switzerland, 1973–2022*

Treatment	Value
No. patients	334
Surgical therapy	151 (45.2)
Time to surgery, mo, median (IQR)	1 (0–4)
Surgery aim	
Palliative	25 (7.5)
After >12 mo	5 (1.5)
Curative	126 (37.7)
After >12 mo	5 (1.5)
Resection margins	
R0	105 (31.4)
R1	21 (6.3)
Surgery type	
Segmentectomy	51 (15.3)
Hemihepatectomy	53 (15.9)
Extended hemihepatectomy	17 (5.1)
Liver transplantation	3 (0.9)
Nonhepatic surgery	2 (0.6)
Benzimidazole drug therapy	315 (94.3)
Time to benzimidazole start, mo, median (IQR)	1 (0–2)
>12 mo	17 (5.1)
Benzimidazole drug type	
Albendazole	241 (72.2)
Mebendazole	74 (22.2)
Clinical setting	
After curatively intended surgery	122 (36.5)
R0 margin	97 (29.0)
Duration, mo, median (IQR)	26 (23–31.5)
R1 margin	21 (6.3)
Duration, mo, median (IQR)	79 (44–152)
Palliative surgery and nonresected	212 (63.5)

*Values are no. (%) except as indicated.

Changes in Clinical Manifestation and Treatment over Time

Over the decades of the study period, patient demographics remained similar (Appendix Table 4). Since 2000, a steady increase in new AE diagnosis per year was noted, with an increasing proportion attributable to incidental diagnosis (Figure 1). In fact, during the last 3 years of the study period, most of the patients with newly diagnosed AE had incidental diagnoses. Concordantly, a shift toward earlier AE stages was observed (Figure 2, panel A). With time, fewer patients underwent palliative resection; the last was performed in 2007 (Figure 2, panel B). Although the proportion of patients undergoing curatively intended resections rose at first, it decreased sharply in the

last decade of the study period (Figure 2, panel B). Of interest, patients were also followed without treatment (Figure 2, panel B).

Symptomatic versus Incidental Diagnosis

As expected, patients with incidental diagnoses showed more frequently a limited stage of the disease (Appendix Table 3). In contrast, those patients were slightly older at diagnosis than were patients with symptomatic disease (Appendix Table 3). Furthermore, patients with incidental diagnoses less often underwent surgery. The reported reason to forgo surgery was either disease inactivity, personal choice or presence of comorbidity, and, less frequently, disease extent. Benzimidazole drug treatment was also slightly less frequently initiated. Of interest, no AE related death was observed in the incidental group.

Causes of Death

In total, 90 (26.9%) patients died after a median of 176 months, but causes of death were predominantly non-AE related (Figures 3, 4). AE-related death occurred more frequently in symptomatic patients whose AE was diagnosed in earlier decades (Figures 3, 4; Appendix Table 3). Most of those patients had biliary or vascular complications when AE was diagnosed (Table 3). Only 1 patient had undergone curatively intended resection, and 5 had palliative resections. The median time to AE-related death was 159 months.

The cause of death could not be determined in 13 patients. Their AE was diagnosed in an advanced stage but without any biliary, vascular, or infectious complication at diagnosis. The median age at death in this group was 89 years, and at last clinical visit, AE was considered as cured or stable, making AE unlikely as the cause of death (Appendix Table 5).

Table 3. Characteristics of patients who died because of AE, University Hospital Zurich, Zurich, Switzerland, 1973–2022*

ID	Year diag	Age, y/sex	Stage	Symp	Comp	Surgery	Time to surgery, mo†	Aim	BMZ	Time to BMZ†	Survival time, mo†	Direct cause of death
1	1973	26/M	IV	Yes	None	Yes	37	Palliative, with biliodigestive anastomosis	Yes‡	94	384	Biliocutaneous fistula, recurrent biliary infections, secondary biliary cirrhosis
2	1975	57/M	IV	Yes	Vascular	Yes	0	Curative	Yes	80	238	Retroperitoneal recurrence, total IVC occlusion, GI hemorrhage
3	1975	54/F	IV	Yes	None	NA	NA	NA	Yes	77	104	Cerebral AE manifestation
4	1978	68/F	II	Yes	Biliary	Yes	0	Palliative, with biliodigestive anastomosis	Yes	0	35	Recurrent biliary infections, secondary biliary cirrhosis
5	1979	44/F	IIIa	Yes	Vascular	NA	NA	NA	Yes	0	281	ERCP for pancreatitis, decompensation, peritonitis
6	1980	61/F	IV	Yes	Biliary	NA	NA	NA	Yes	0	133	Secondary biliary cirrhosis
7	1982	67/M	IV	Yes	Vascular	NA	NA	NA	Yes	0	159	Variceal bleeding
8	1983	64/F	IIIb	Yes	Biliary	NA	NA	NA	Yes	0	53	Cholangitis with liver abscess
9	1983	47/F	II	Yes	None	Yes	0	Palliative	Yes	0	233	Progressive disease, secondary surgery, postoperative multiorgan failure
10	1988	67/M	IIIa	Yes	Biliary	Yes	0	Palliative	Yes	1	149	PTCD for cholangitis
11	2001	48/M	IV	Yes	None	Yes	0	Palliative, nonhepatic	Yes	0	193	Cerebral AE manifestation
12	2001	56/F	IIIb	Yes	Vascular	NA	NA	NA	Yes	0	187	Liver failure because of portal and liver vein thrombosis
13	2017	60/F	IV	Yes	Biliary	NA	NA	NA	Yes	0	70	PTCD for cyst infection with rupture and peritoneal dissemination

*AE, alveolar echinococcosis; BMZ, benzimidazole drug therapy; comp, complications at diagnosis; diag, diagnosed; ERCP, endoscopic retrograde cholangiopancreaticography; ID, identification number; IVC, inferior vena cava; PTCD, percutaneous transhepatic cholangiography and drainage; symp, symptoms at diagnosis; surg, surgery.
†Time after diagnosis.
‡Discontinued after 195 months because of intolerance (95 months before death).

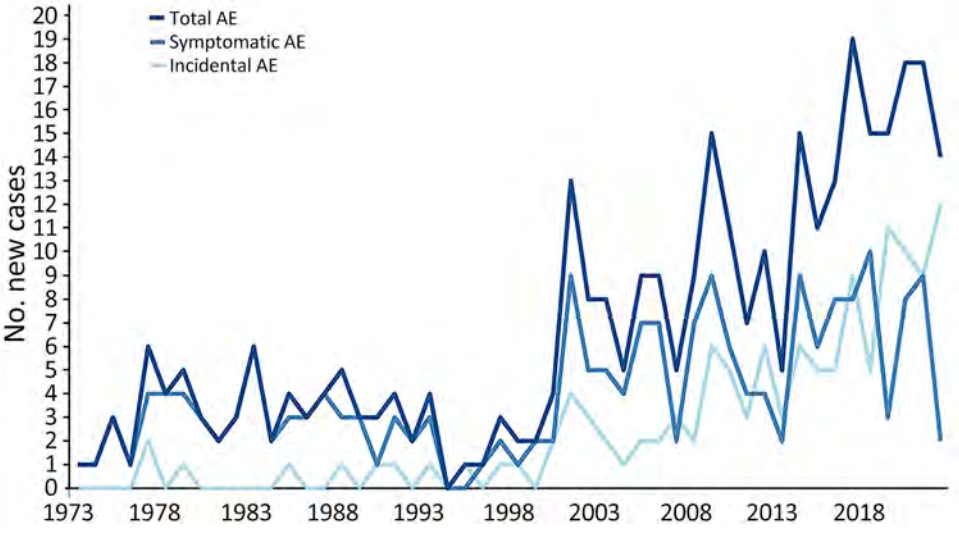

Figure 1. Total number of new, symptomatic, and incidental AE diagnosis by calendar year, University Hospital Zurich, Zurich, Switzerland, 1973–2022. AE, alveolar echinococcosis.

Survival Analysis

Relative survival of our cohort of AE patients compared with the population of Switzerland started with a survival ratio around 1.0 but decreased over time (Figure 5). The survival ratio was higher in younger compared with the elderly AE patients; in particular, patients <40 years of age demonstrated a survival ratio of 1.0 over 20 years after diagnosis (Figure 5). Of note, those figures leave out 1 patient who had AE diagnosed in 2008 at 86 years of age (above the average life expectancy for men in Switzerland) and died at 99 years of age, resulting in a bump in the relative survival curves after 13 years (Appendix Figure 2). In the additive relative survival model, only age at diagnosis was significantly associated with overall survival (Table 4). AE-specific variables, in particular stage of the disease but also treatment initiation (surgery or benzimidazole drug treatment) within 1 year, did not show significantly associated coefficient estimates (Table 4).

Before propensity score matching, baseline characteristics of patients undergoing curatively intended surgery within 1 year were considerably different from the remaining patients (curatively intended surgery after 1 year, palliative surgery, or medical treatment only) (Appendix Table 6). Both 1:1 nearest neighbor and 1:1 genetic matching resulted in 112 matched pairs of patients, including all patients with curative surgery within 1 year (all treated patients), with much better balance of baseline characteristics (Appendix Tables 7, 8). The absolute standardized mean difference was considerably reduced for all characteristics and was <0.2 after matching, except for age at AE diagnosis and overall distance (Appendix Figure 3). In both matched analyses, patients with curative surgery within 1 year showed a better overall survival, with a hazard ratio (HR) of 0.48 (95% CI 0.30–0.77) for 1:1 nearest neighbor matching and 0.49 (95% CI 0.29–0.84) for 1:1 genetic matching (Figure 6, panels A, B). Regarding the occurrence of AE death, matching resulted in an even lower number of events (n = 7 with 1:1 nearest neighbor matching, n = 6 with genetic matching) than observed in the whole cohort

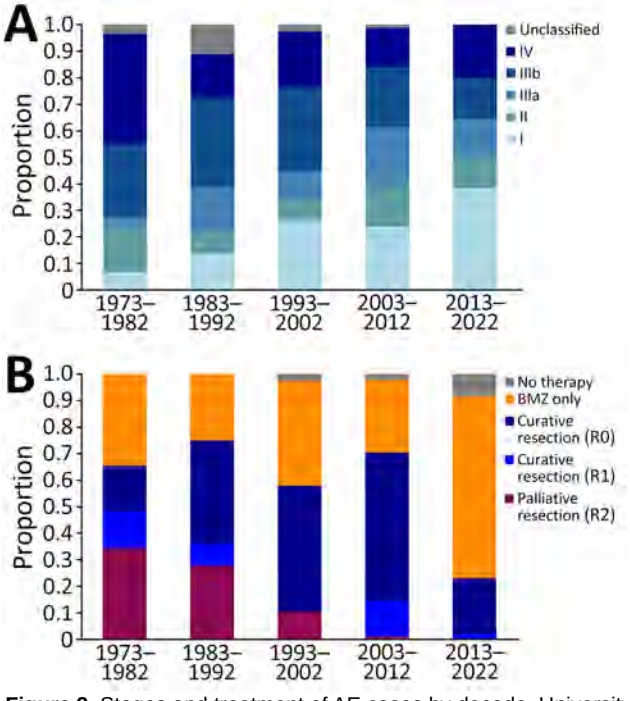

Figure 2. Stages and treatment of AE cases by decade, University Hospital Zurich, Zurich, Switzerland, 1973–2022. A) AE stages; B) treatment strategies. Although palliative surgery was discontinued in the early 2000s, curative surgery was less frequently pursued in the last decade of the study period. AE, alveolar echinococcosis; BMZ, benzimidazole drug therapy.

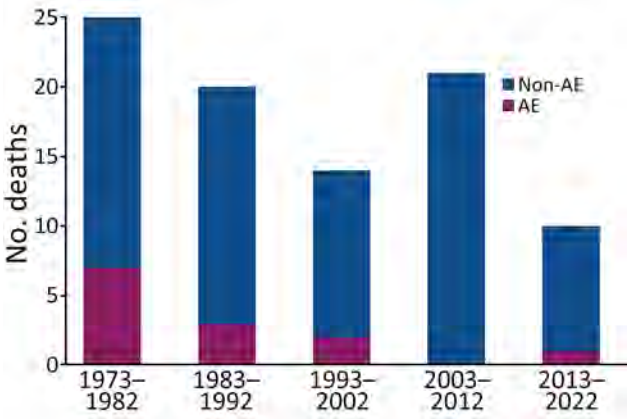

Figure 3. AE and non-AE associated causes of death for AE patients, by decade of AE diagnosis, University Hospital Zurich, Zurich, Switzerland, 1973–2022. AE associated death was observed more frequently in earlier decades of the study period. AE, alveolar echinococcosis.

(n = 13). Curative surgery within 1 year was not associated with a significant disease-specific survival benefit (HR 0.15 [95% CI 0.02–1.27] after nearest neighbor matching; HR 0.18 [95% CI 0.02–1.56] after genetic matching) (Figure 6, panels A, B).

Discussion

Our study demonstrates major changes in the clinical manifestations and treatment of AE patients over a 50-year period in Zurich, Switzerland. In addition, survival was mainly limited by non-AE causes, and early curative surgery did not provide a survival benefit in our cohort.

Historically, AE prognosis depended on complete surgical removal of all parasitic tissue. The 2010 World Health Organization guidelines recommend radical resections for all suitable patients (*16*). Despite a shift toward earlier AE stages, our cohort did not show an expected rise in curative surgeries, especially in the last decade of the study period, which might be explained by 2 factors. First, incidentally diagnosed AE cases were more frequently considered inactive, and patients were more likely to refuse surgery. Second, whereas many patients were considered inoperable because of disease extent, the perception of operability or willingness to perform more extensive operations and risk incomplete (R1) resection could have changed over the decades because of the increasingly positive experience with benzimidazole therapy in inoperable patients.

We made several observations about patients who died from AE. Most of those cases were diagnosed before 2000 and in an advanced stage with biliary or vascular complications. For patients who had palliative surgery, it is unclear whether complications leading to death were because of the disease or the surgery itself; only 1 patient in the entire cohort met the criteria for surgical death, defined as

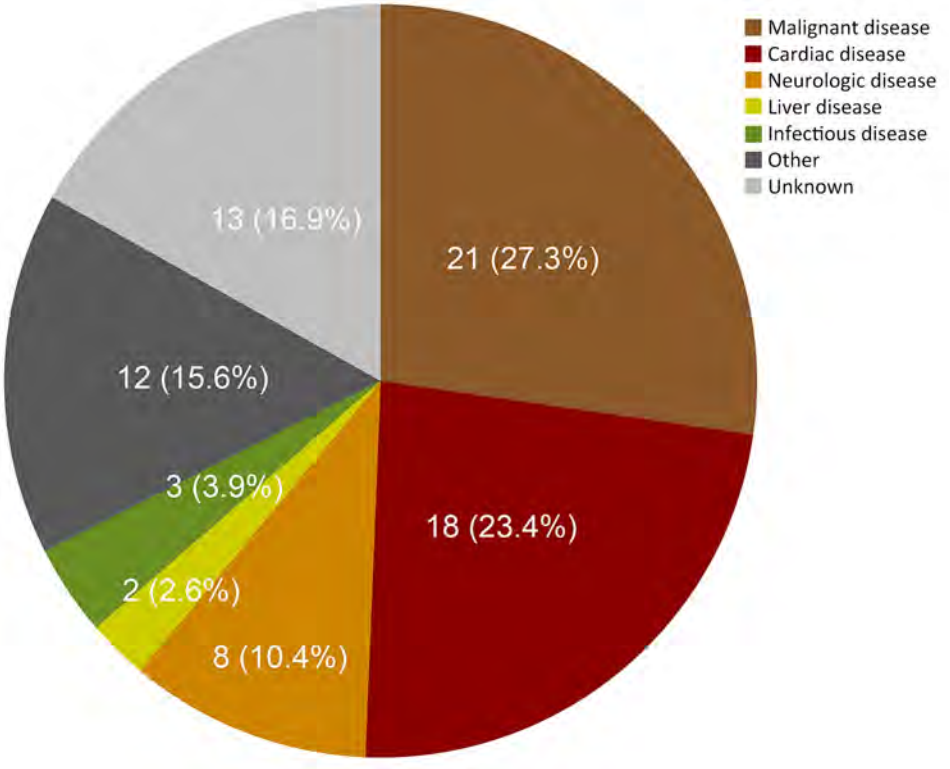

Figure 4. Causes of death other than alveolar echinococcosis in alveolar echinococcosis cases, University Hospital Zurich, Zurich, Switzerland, 1973–2022.

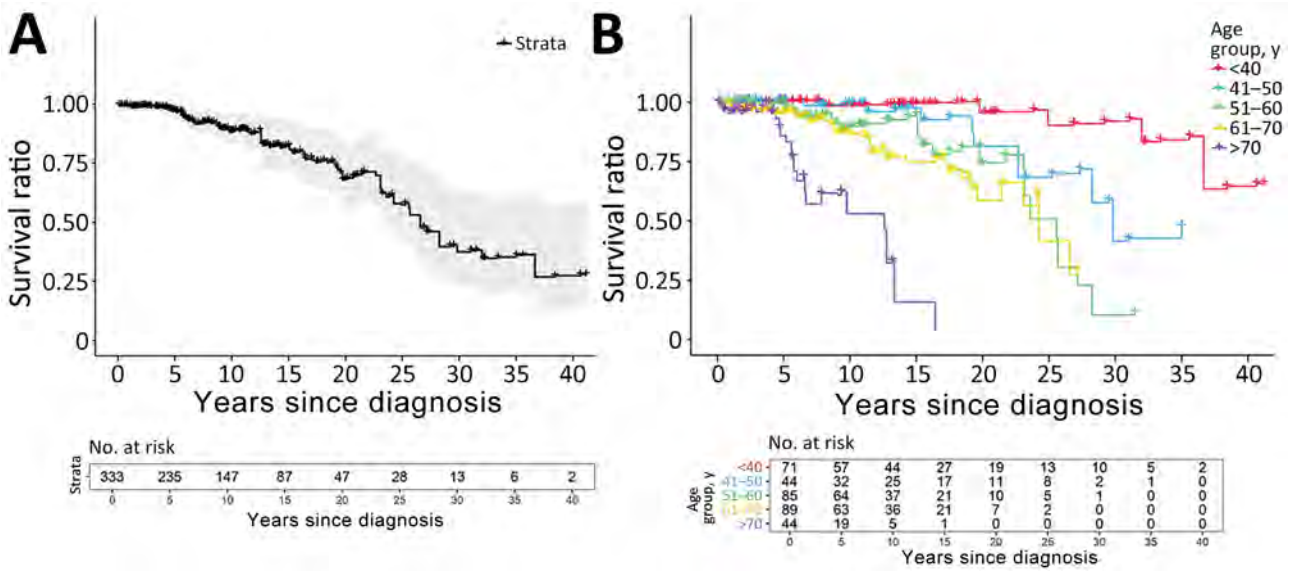

Figure 5. Relative survival analysis of alveolar echinococcosis cases, University Hospital Zurich, Zurich, Switzerland, 1973–2022. A) Relative survival of alveolar echinococcosis patients compared with the population of Switzerland. B) Relative survival grouped by age at alveolar echinococcosis diagnosis. One patient with an alveolar echinococcosis diagnosis at 86 years of age and died at age 99 was excluded for better visualization (Appendix Figure 2, https://wwwnc.cdc.gov/EID/article/31/5/24-1608-App1.pdf).

any death within 30 days or during the same hospitalization (*27*). After an in-house study, University Hospital Zurich stopped performing palliative resections, and now its care providers would not consider surgery for most patients (*17*). University Hospital Zurich has also become more restrictive concerning biliary tract interventions because of the risk for infectious complication (*20*). Despite receiving mainly palliative or no surgery, the median survival of patients who died of AE was 159 months, highlighting the effectiveness of benzimidazole drugs in slowing disease progression.

Relative survival analysis of AE patients compared with the population of Switzerland revealed several key findings. Unlike a cohort in France that reported excess death in the first 2 years after diagnosis (*23*), our analysis showed a steady decline in relative survival starting 5 years after diagnosis. The decline was age dependent and observed particularly in younger patients (<40 years of age at AE diagnosis), who showed similar survival to the general population over a very long time. Disease-specific factors, such as stage and year of diagnosis or treatment within 1 year, were not linked to survival, contrasting with the France study (*23*). That finding might be because most of the patients in this study received timely benzimidazole drug treatment. However, direct comparison is limited because of the absence of baseline treatment data in the France study (*23*). Our findings suggest AE is not the main determinant of life expectancy in infected patients, and the gradual decline of relative survival 5 years after diagnosis could reflect a generally sicker population.

To analyze the effect of early curative surgery on the outcome of our patients, we used propensity-score matching, focusing on AE-specific variables related to treatment and outcomes to avoid overfitting the model. Because perception of operability varies among surgeons, we used the PNM classification as a proxy for operability (*14*,*28*). Palliative surgery patients remained in the control group because of their benefit from benzimidazole drug therapy, despite surgery potentially contributing to death in some cases. Whereas our approach may overestimate

Table 4. Parameters of the relative survival analysis by using an additive model for cases of alveolar echinococcosis, University Hospital Zurich, Zurich, Switzerland, 1973–2022*

Characteristic	Estimate	95% CI	p value
Age at diagnosis	0.078	0.05–0.11	<0.0001
Year of diagnosis	−0.018	−0.04 to 0.00	0.11
Sex, male vs. female	0.033	−0.47 to 0.53	0.90
Stage	−0.036	−0.29 to 0.22	0.78
Surgery within 1 year	−0.411	−0.93 to 0.10	0.12
Benzimidazole within 1 year	−0.514	−1.13 to 0.10	0.10

*The additive survival model provides covariate estimates that reflect the direct effect of each covariate on the excess risk. Compared with a Cox proportional hazard, this effect is absolute and not exponential.

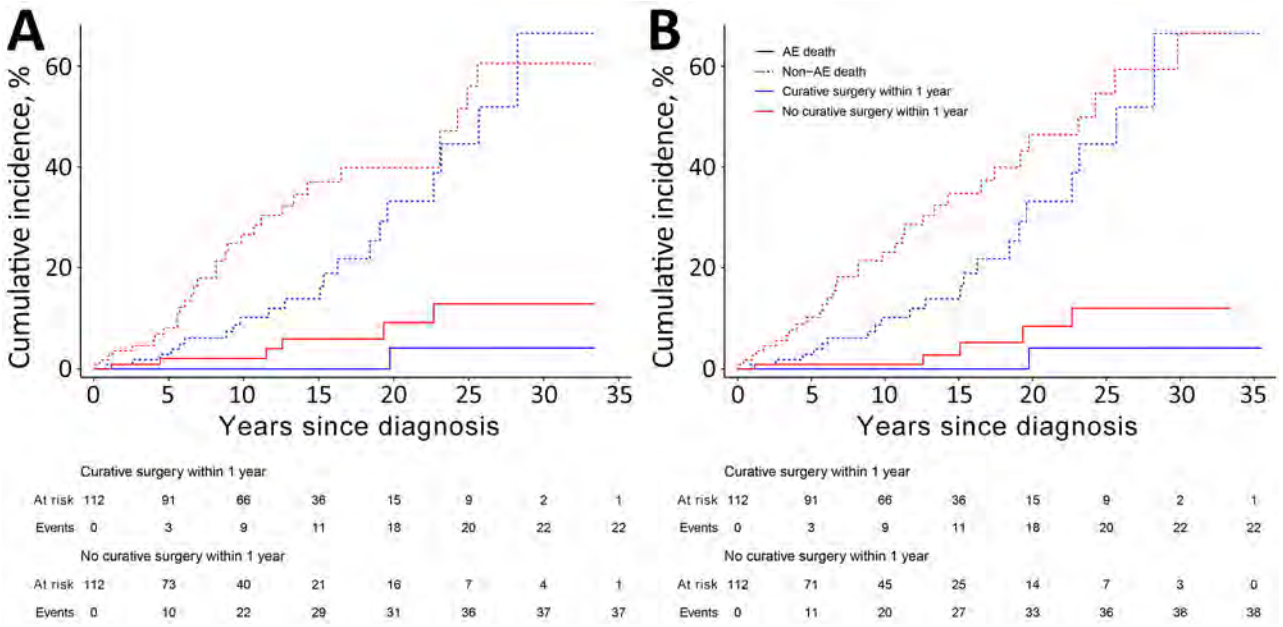

Figure 6. Matched survival analysis of AE cases, University Hospital Zurich, Zurich, Switzerland, 1973–2022. A) Results of nearest neighbor matching. Non-AE death hazard ratio (HR) = 0.48 (95% CI 0.30–0.77), p = 0.002; AE death HR = 0.15 (95% CI 0.02–1.27), p = 0.082. B) Results after genetic matching. Non-AE death HR = 0.49 (95% CI 0.29–0.84), p = 0.009; AE death HR = 0.18 (95% CI 0.02–1.56), p = 0.12. Patients undergoing curatively intended surgery within 1 year of diagnosis showed better overall survival. AE-related death did not differ after matching. AE, alveolar echinococcosis.

operability in the control group, the analysis showed no disease-specific survival benefit for early curative surgery performed within 1 year of diagnosis. The analysis is, however, limited by the small number of AE-related deaths in our cohort and the long survival times of patients who died from AE. The difference in overall survival between groups likely reflects residual confounding, no differences were observed for non-AE causes of death.

Finally, we confirm previous observations of rising AE cases since 2000 and great improvement of patient survival in patients with inoperable disease (*3*,*4*,*19*). In our cohort, the rise of annual AE cases was accompanied by a substantial increase in incidental findings and a shift toward earlier stages, although symptomatic patients with an advanced disease stage remained the majority. This difference might be because of advances in classification of lesions on imaging and histopathology (*29*–*31*). Contrary to expectation, patients with incidental findings were on average not younger but older at diagnosis. This finding has 2 implications. First it eliminates the possibility of a lead-time bias in our survival analysis. Second, the speculation arises if some of those patients would ever have become symptomatic or suffered complications or death because of AE.

In conclusion, our study shows that because of the excellent disease control with benzimidazole drug therapy, curatively intended surgery is only associated with a marginal disease-specific survival benefit. Those findings give reason to change our perception of optimal medical care in AE patients. Today, treatment decisions should be made on the basis of the patient's expected remaining years with the disease and the potential complications and cost-effectiveness of either a surgical or conservative approach. Although younger patients will most likely benefit from radical resection, older patients may not.

Acknowledgments

We thank all patients participating in our cohort study for providing their health-related personal data for research. We also thank the Fontana Foundation for supporting our research in the field of alveolar echinococcosis.

This study was supported by the Fontana Foundation, a nonprofit organization that supports echinococcosis research in Switzerland. The funders had no role in study design, data collection and analysis, decision to publish, or preparation of the manuscript.

Authors contributions: A.D. and B.M. conceived the study. A.D. obtained ethical approval and designed and supervised the study. Y.K. and A.D. retrieved retrospective data, performed descriptive data analysis, and wrote the manuscript. R.M. performed relative-survival analysis, supervised by S.V.F. S.V.F. performed

propensity score matched analysis. C.M.Z.S. recruited and consulted alveolar echinococcosis patients for the study. B.B.G. is the involved study nurse. F.G. supervised and interpreted alveolar echinococcosis serology. S.G. and C.S.R. supervised and interpreted cross-sectional imaging. H.P. and P.A.C. supervised and performed surgical resections. M.R. and A.W. supervised and interpreted histopathological analysis. A.S. provided registry data from before 2005. R.M., S.G., C.M.Z.S., A.S., F.G., M.R., A.W., C.S.R., A.E.K., H.P., P.A.C., P.D., S.V.F., and B.M. critically revised the manuscript for important intellectual content. All authors approved the final version of the manuscript.

About the Author

Dr. Deibel is an attending physician in the Department of Gastroenterology and Hepatology of the University Hospital Zurich. He oversees outpatient echinococcosis consultations, and his research focuses on the field of alveolar echinococcosis.

References

1. Deplazes P, Rinaldi L, Alvarez Rojas CA, Torgerson PR, Harandi MF, Romig T, et al. Global distribution of alveolar and cystic echinococcosis. Adv Parasitol. 2017;95:315–493. https://doi.org/10.1016/bs.apar.2016.11.001
2. Schweiger A, Ammann RW, Candinas D, Clavien PA, Eckert J, Gottstein B, et al. Human alveolar echinococcosis after fox population increase, Switzerland. Emerg Infect Dis. 2007;13:878–82. https://doi.org/10.3201/eid1306.061074
3. Grüner B, Kern P, Mayer B, Gräter T, Hillenbrand A, Barth TEF, et al. Comprehensive diagnosis and treatment of alveolar echinococcosis: a single-center, long-term observational study of 312 patients in Germany. GMS Infect Dis. 2017;5:Doc01.
4. Chauchet A, Grenouillet F, Knapp J, Richou C, Delabrousse E, Dentan C, et al.; FrancEchino Network. Increased incidence and characteristics of alveolar echinococcosis in patients with immunosuppression-associated conditions. Clin Infect Dis. 2014;59:1095–104. https://doi.org/10.1093/cid/ciu520
5. Deibel A, Meyer Zu Schwabedissen C, Husmann L, Grimm F, Deplazes P, Reiner CS, et al. Characteristics and clinical course of alveolar echinococcosis in patients with immunosuppression-associated conditions: a retrospective cohort study. Pathogens. 2022;11:441. https://doi.org/10.3390/pathogens11040441
6. Paternoster G, Boo G, Wang C, Minbaeva G, Usubalieva J, Raimkulov KM, et al. Epidemic cystic and alveolar echinococcosis in Kyrgyzstan: an analysis of national surveillance data. Lancet Glob Health. 2020;8:e603–11. https://doi.org/10.1016/S2214-109X(20)30038-3
7. Massolo A, Klein C, Kowalewska-Grochowska K, Belga S, MacDonald C, Vaughan S, et al. European *Echinococcus multilocularis* identified in patients in Canada. N Engl J Med. 2019;381:384–5. https://doi.org/10.1056/NEJMc1814975
8. Houston S, Belga S, Buttenschoen K, Cooper R, Girgis S, Gottstein B, et al. Epidemiological and clinical characteristics of alveolar echinococcosis: an emerging infectious disease in Alberta, Canada. Am J Trop Med Hyg. 2021;104:1863–9. https://doi.org/10.4269/ajtmh.20-1577
9. Nahorski WL, Knap JP, Pawłowski ZS, Krawczyk M, Polański J, Stefaniak J, et al. Human alveolar echinococcosis in Poland: 1990–2011. PLoS Negl Trop Dis. 2013;7:e1986. https://doi.org/10.1371/journal.pntd.0001986
10. Bruzinskaite R, Marcinkute A, Strupas K, Sokolovas V, Deplazes P, Mathis A, et al. Alveolar echinococcosis, Lithuania. Emerg Infect Dis. 2007;13:1618–9. https://doi.org/10.3201/eid1310.061161
11. Deplazes P, Hegglin D, Gloor S, Romig T. Wilderness in the city: the urbanization of *Echinococcus multilocularis*. Trends Parasitol. 2004;20:77–84. https://doi.org/10.1016/j.pt.2003.11.011
12. Eckert J, Deplazes P. Biological, epidemiological, and clinical aspects of echinococcosis, a zoonosis of increasing concern. Clin Microbiol Rev. 2004;17:107–35. https://doi.org/10.1128/CMR.17.1.107-135.2004
13. Kern P, Menezes da Silva A, Akhan O, Müllhaupt B, Vizcaychipi KA, Budke C, et al. The echinococcoses: diagnosis, clinical management and burden of disease. Adv Parasitol. 2017;96:259–369. https://doi.org/10.1016/bs.apar.2016.09.006
14. Kern P, Wen H, Sato N, Vuitton DA, Gruener B, Shao Y, et al. WHO classification of alveolar echinococcosis: principles and application. Parasitol Int. 2006;55 (Suppl):S283–7. https://doi.org/10.1016/j.parint.2005.11.041
15. Ammann RW, Hoffmann AF, Eckert J. Swiss study of chemotherapy of alveolar echinococcosis—review of a 20-year clinical research project. Schweiz Med Wochenschr. 1999;129:323–32.
16. Brunetti E, Kern P, Vuitton DA; Writing Panel for the WHO-IWGE. Expert consensus for the diagnosis and treatment of cystic and alveolar echinococcosis in humans. Acta Trop. 2010;114:1–16. https://doi.org/10.1016/j.actatropica.2009.11.001
17. Kadry Z, Renner EC, Bachmann LM, Attigah N, Renner EL, Ammann RW, et al. Evaluation of treatment and long-term follow-up in patients with hepatic alveolar echinococcosis. Br J Surg. 2005;92:1110–6. https://doi.org/10.1002/bjs.4998
18. Bresson-Hadni S, Koch S, Beurton I, Vuitton DA, Bartholomot B, Hrusovsky S, et al. Primary disease recurrence after liver transplantation for alveolar echinococcosis: long-term evaluation in 15 patients. Hepatology. 1999;30:857–64. https://doi.org/10.1002/hep.510300426
19. Torgerson PR, Schweiger A, Deplazes P, Pohar M, Reichen J, Ammann RW, et al. Alveolar echinococcosis: from a deadly disease to a well-controlled infection. Relative survival and economic analysis in Switzerland over the last 35 years. J Hepatol. 2008;49:72–7. https://doi.org/10.1016/j.jhep.2008.03.023
20. Müller S, Ghafoor S, Meyer Zu Schwabedissen C, Grimm F, Murray FR, Husmann L, et al. Management of biliary obstruction in patients with newly diagnosed alveolar echinococcosis: a Swiss retrospective cohort study. Swiss Med Wkly. 2023;153:40116. https://doi.org/10.57187/smw.2023.40116
21. Caoduro C, Porot C, Vuitton DA, Bresson-Hadni S, Grenouillet F, Richou C, et al. The role of delayed 18F-FDG PET imaging in the follow-up of patients with alveolar echinococcosis. J Nucl Med. 2013;54:358–63. https://doi.org/10.2967/jnumed.112.109942
22. Ammann RW, Stumpe KD, Grimm F, Deplazes P, Huber S, Bertogg K, et al. Outcome after discontinuing

long-term benzimidazole treatment in 11 patients with non-resectable alveolar echinococcosis with negative FDG-PET/CT and anti-EmII/3-10 serology. PLoS Negl Trop Dis. 2015;9:e0003964. https://doi.org/10.1371/journal.pntd.0003964
23. Piarroux M, Piarroux R, Giorgi R, Knapp J, Bardonnet K, Sudre B, et al. Clinical features and evolution of alveolar echinococcosis in France from 1982 to 2007: results of a survey in 387 patients. J Hepatol. 2011;55:1025–33. https://doi.org/10.1016/j.jhep.2011.02.018
24. Kern P, Bardonnet K, Renner E, Auer H, Pawlowski Z, Ammann RW, et al.; European Echinococcosis Registry. European echinococcosis registry: human alveolar echinococcosis, Europe, 1982–2000. Emerg Infect Dis. 2003;9:343–9. https://doi.org/10.3201/eid0903.020341
25. Perme MP, Pavlic K. Nonparametric relative survival analysis with the R package relsurv. J Stat Softw. 2018;87:1–27. https://doi.org/10.18637/jss.v087.i08
26. Ho D, Imai K, King G, Stuart EA. MatchIt: nonparametric preprocessing for parametric causal inference. J Stat Softw. 2011;42:1–28. https://doi.org/10.18637/jss.v042.i08
27. Jacobs JP, Mavroudis C, Jacobs ML, Maruszewski B, Tchervenkov CI, Lacour-Gayet FG, et al.; STS Congenital Database Taskforce; Joint EACTS-STS Congenital Database Committee. What is operative mortality? Defining death in a surgical registry database: a report of the STS congenital database taskforce and the joint EACTS-STS congenital database committee. Ann Thorac Surg. 2006;81:1937–41. https://doi.org/10.1016/j.athoracsur.2005.11.063
28. Ignatavicius P, Oberkofler CE, Chapman WC, DeMatteo RP, Clary BM, D'Angelica MI, et al. Choices of therapeutic strategies for colorectal liver metastases among expert liver surgeons: a throw of the dice? Ann Surg. 2020;272:715–22. https://doi.org/10.1097/SLA.0000000000004331
29. Graeter T, Kratzer W, Oeztuerk S, Haenle MM, Mason RA, Hillenbrand A, et al. Proposal of a computed tomography classification for hepatic alveolar echinococcosis. World J Gastroenterol. 2016;22:3621–31. https://doi.org/10.3748/wjg.v22.i13.3621
30. Kodama Y, Fujita N, Shimizu T, Endo H, Nambu T, Sato N, et al. Alveolar echinococcosis: MR findings in the liver. Radiology. 2003;228:172–7. https://doi.org/10.1148/radiol.2281020323
31. Reinehr M, Micheloud C, Grimm F, Kronenberg PA, Grimm J, Beck A, et al. Pathology of echinococcosis: a morphologic and immunohistochemical study on 138 specimens with focus on the differential diagnosis between cystic and alveolar echinococcosis. Am J Surg Pathol. 2020;44:43–54. https://doi.org/10.1097/PAS.0000000000001374

Address for correspondence: Ansgar Deibel, University Hospital Zurich, Raemistrasse 100, 8091 Zurich, Switzerland; email: rudolfansgar.deibel@usz.ch

etymologia revisited

Salmonella

[sal''mo-nel'ə]

Named in honor of Daniel Elmer Salmon, an American veterinary pathologist, *Salmonella* is a genus of motile, gram-negative bacillus, nonspore-forming, aerobic to facultatively anaerobic bacteria of the family Enterobacteriaceae. In 1880, Karl Joseph Eberth was the first to observe *Salmonella* from specimens of patients with typhoid fever (from the Greek *typhōdes* [like smoke; delirious]), which was formerly called *Eberthella typhosa* in his tribute. In 1884, Georg Gaffky successfully isolated this bacillus (later described as *Salmonella* Typhi) from patients with typhoid fever, confirming Eberth's findings. Shortly afterward, Salmon and his assistant Theobald Smith, an American bacteriologist, isolated *Salmonella* Choleraesuis from swine, incorrectly assuming that this germ was the causative agent of hog cholera. Later, Joseph Lignières, a French bacteriologist, proposed the genus name *Salmonella* in recognition of Salmon's efforts.

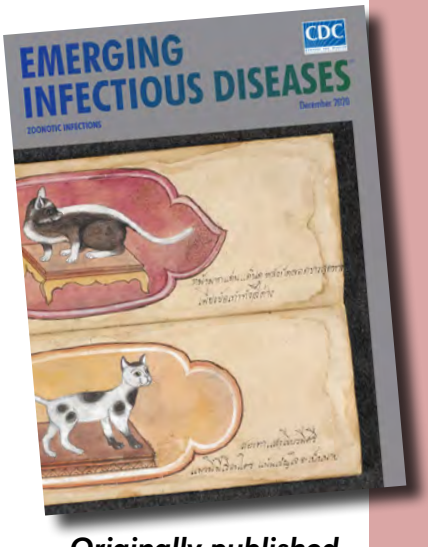

Originally published in December 2020

References:

1. Dorland's Illustrated Medical Dictionary. 32nd ed. Philadelphia: Elsevier Saunders; 2012.
2. Gossner CM, Le Hello S, de Jong B, Rolfhamre P, Faensen D, Weill FX, et al. Around the world in 1,475 Salmonella geo-serotypes [Another Dimension]. Emerg Infect Dis. 2016;22:1298–302.
3. Issenhuth-Jeanjean S, Roggentin P, Mikoleit M, Guibourdenche M, de Pinna E, Nair S, et al. Supplement 2008-2010 (no. 48) to the White-Kauffmann-Le Minor scheme. Res Microbiol. 2014;165:526–30.
4. Salmon DE. The discovery of the germ of swine-plague. Science. 1884;3:155–8.
5. Su LH, Chiu CH. Salmonella: clinical importance and evolution of nomenclature. Chang Gung Med J. 2007;30:210–9.

https://wwwnc.cdc.gov/eid/article/26/12/et-2612_article

Nationwide Observational Case–Control Study of Risk Factors for *Aerococcus* Bloodstream Infections, Sweden

John Walles, Malin Inghammar, Magnus Rasmussen, Torgny Sunnerhagen

Medscape CME Activity

In support of improving patient care, this activity has been planned and implemented by Medscape, LLC and Emerging Infectious Diseases. Medscape, LLC is jointly accredited with commendation by the Accreditation Council for Continuing Medical Education (ACCME), the Accreditation Council for Pharmacy Education (ACPE), and the American Nurses Credentialing Center (ANCC), to provide continuing education for the healthcare team.

Medscape, LLC designates this Journal-based CME activity for a maximum of 1.00 ***AMA PRA Category 1 Credit(s)™***. Physicians should claim only the credit commensurate with the extent of their participation in the activity.

Successful completion of this CME activity, which includes participation in the evaluation component, enables the participant to earn up to 1.0 MOC points in the American Board of Internal Medicine's (ABIM) Maintenance of Certification (MOC) program. Participants will earn MOC points equivalent to the amount of CME credits claimed for the activity. It is the CME activity provider's responsibility to submit participant completion information to ACCME for the purpose of granting ABIM MOC credit.

All other clinicians completing this activity will be issued a certificate of participation. To participate in this journal CME activity: (1) review the learning objectives and author disclosures; (2) study the education content; (3) take the post-test with a 75% minimum passing score and complete the evaluation at https://www.medscape.org/qna/processor/74096?showStandAlone=true&src=prt_jcme_eid_mscpedueid; and (4) view/print certificate. For CME questions, see page 1068.

NOTE: It is Medscape's policy to avoid the use of Brand names in accredited activities. However, in an effort to be as clear as possible, trade names are used in this activity to distinguish between the mixtures and different tests. It is not meant to promote any particular product.

Release date: April 22, 2025; Expiration date: April 22, 2026

Learning Objectives

Upon completion of this activity, participants will be able to:

- Distinguish the most common anatomic site of infection with aerococci
- Assess the epidemiology of aerococcal bloodstream infections (BSIs)
- Analyze chronic disease risk factors for aerococcal BSIs
- Identify antibiotics associated with a higher risk for aerococcal BSIs

CME Editor

Susan Zunino, PhD, Technical Writer/Editor, Emerging Infectious Diseases. *Disclosure: Susan Zunino, PhD, has no relevant financial relationships.*

CME Author

Charles P. Vega, MD, Health Sciences Clinical Professor of Family Medicine, University of California, Irvine School of Medicine, Irvine, California. *Disclosure: Charles P. Vega, MD, has the following relevant financial relationships: served as consultant or advisor for Boehringer Ingelheim; Exact Sciences.*

Authors

John Walles, MD, PhD; Malin Inghammar, MD, PhD; Magnus Rasmussen, MD, PhD; Torgny Sunnerhagen, MD, PhD.

Risk factors for developing bloodstream infections (BSIs) caused by *Aerococcus* bacteria remain insufficiently examined. In this nationwide case–control study in Sweden, 19 of 23 clinical microbiological laboratories identified patients who had aerococcal BSIs during 2012–2016. We compared each of those index patients with 4 controls matched for age, sex, and county of residence. Overall, 588 episodes of aerococcal BSI occurred over 39.6 million person-years, corresponding to an average incidence of 1.48/100,000 person-years (95% CI 1.37–1.60/100,000 person-years). Most infections developed in men >65 years of age. Aerococcal BSI was associated with neurologic (adjusted odds ratio 2.89 [95% CI 2.26–3.70]) and urologic (adjusted odds ratio 2.15 [95% CI 1.72—2.68]) conditions and previous hospitalization or infection treatment. Our findings support the previously observed predilection for aerococcal BSIs developing in elderly men with urinary tract disorders. Awareness of *Aerococcus* spp. in patients, especially elderly men, will be needed to manage invasive infections.

Invasive infections caused by bacteria of the genus *Aerococcus* have been increasingly recognized; however, because of difficulties in identification during routine care, patients at risk for those infections have been insufficiently examined. *Aerococcus* bacteria were first described in 1953 (*1*), identified as relatives of bacteria belonging to *Streptococcus* and *Enterococcus* genera. Since then, specific species have been discovered, of which *A. urinae* and *A. sanguinicola* are most commonly observed in human infections (*2*–*4*).

Before matrix-assisted laser desorption/ionization time-of-flight (MALDI-TOF) mass spectrometry was introduced, accurate identification of *Aerococcus* at the species level was difficult. Consequently, the characteristics of aerococcal infections and infected patients were not described extensively until about 2016, primarily through case series reports (*5*–*8*).

Aerococcus spp. are a fundamental cause of urinary tract infections (*9*–*11*). However, the rates of severe infections, such as aerococcal bloodstream infections (BSIs), most notably found in elderly men and persons with urinary tract disorders (*6*,*12*–*17*), and aerococcal infective endocarditis have also increased in recent years (*5*,*14*,*17*–*20*). Despite previous studies indicating that most patients with aerococcal infective endocarditis tend to be elderly and have underlying illnesses, the prognosis appears to be favorable (*18*). The increased number of reported cases is likely attributed to MALDI-TOF mass spectrometry, a reliable tool for correctly identifying aerococci and the preferred method for determining *Aerococcus* species in most clinical microbiology laboratories (*7*,*21*). Aerococci have been suggested to adhere to urinary catheters and urothelium and, thus, form biofilms, but the precise mechanisms by which they do so remain unknown (*22*–*24*). Epidemiologic studies have been limited primarily to case series. In this national study, we examined the incidence of and risk factors for aerococcal BSI in Sweden during 2012–2016. This study was approved by the regional ethics review board of Lund University, Sweden (approval no. 2016/938). The retrospective nature of the study obviated the need to obtain informed consent.

Author affiliations: Central Hospital Kristianstad, Kristianstad, Sweden (J. Walles); Lund University, Malmö, Sweden (J. Walles); Lund University, Lund, Sweden (J. Walles, M. Inghammar, M. Rasmussen, T. Sunnerhagen); Skåne University Hospital, Lund (J. Walles, M. Inghammar, M. Rasmussen, T. Sunnerhagen)

DOI: https://doi.org/10.3201/eid3105.240424

Materials and Methods

Study Design and Setting

In a retrospective, matched case–control study, we compared a population of persons who had culture-proven aerococcal BSI with a matched control population by using a set of potential predisposing conditions that existed for >1 month before the detection of the BSI. Predisposing conditions were predefined by registered care and drug prescriptions data in national healthcare registers of Sweden. Healthcare in Sweden is publicly financed and provided regardless of a person's financial or health insurance status. Permanent residents of Sweden are assigned a unique and lifelong 10-digit personal identification number, enabling cross-referencing of health data sources (*25*).

Retrieval of Cases and Controls

Clinical microbiology laboratories (19 of 23) in Sweden identified patients with ≥1 episode of aerococcal BSI (defined as the detection of *Aerococcus* bacteria in blood culture, regardless of the species or the presence of other bacteria) during 2012–2016; the remaining 4 laboratories declined participation (Figure 1). For each case, Statistics Sweden (https://www.scb.se) selected 4 controls matched for sex, age (±2 years difference), and county of residence by using the Population Register of Sweden (*26*). We required that each person designated as a control had been alive on the date the aerococcal BSI was detected in the corresponding study patient. We intended the controls to reflect a similar distribution of age, sex, and county of residence as the case-patients, irrespective of any interaction with the healthcare system. Sweden's

National Board of Health and Welfare linked study participants to registered diagnosis codes (classified according to the International Classification of Diseases, 10th revision [ICD-10]) from hospital admissions data (National Inpatient Register) and specialized ambulatory care data (National Outpatient Register) (*25*,*27*); diagnoses registered in primary care were not included. The National Board of Health and Welfare also linked study participants to drugs prescribed during specialized and primary healthcare (classified by the Anatomic Therapeutic Chemical classification system) from the National Prescribed Drug Register (*25*). We defined repeat aerococcal BSI episodes as relapses if they occurred within 90 days; we excluded relapse episodes from all analyses. We defined reinfection as an aerococcal BSI occurring >90 days after the index episode; we retained those cases for incidence calculations but excluded them from other analyses.

Rationale and Definitions of Predisposing Conditions

We defined a set of mechanisms that we considered plausible contributors to the risk for aerococcal BSI: ecologic dysregulation, compromise of local dermal and mucosal barriers, compromise of systemic immune competence, displacement of urogenital or fecal microbiota, healthcare exposure, and frailty (Table 1). Subsequently, we selected a set of specific, defined predisposing conditions to capture ≥1 of those mechanisms (Table 1). For example, we considered the treatment for infection variable to be relevant for capturing aspects of ecologic dysregulation, healthcare exposure, and compromise of local barriers, whereas we considered diabetes mellitus to capture ecologic dysregulation, immune competence, healthcare exposure, and frailty.

We included the following variables in multivariable analyses: number of hospital admissions (categorized as 0, 1–2, 3–5, 6–10, or >10), total number of prescribed drugs, pulmonary disease, gastrointestinal disease, malignant disease, structural urologic condition, corticosteroid treatment, rheumatologic disease, chronic kidney disease, neurologic condition, diabetes mellitus, cardiovascular disease, and previous treatment for infection (categorized as a filled prescription for any antimicrobial drug or registered treatment for infectious disease before the index date: 1–3 months, 4–9 months, 10–24 months, >24 months, or never). To capture conditions that were preexisting and relevant at the time of the aerococcal BSI but avoid conditions that were caused or aggravated by the infection, we only considered diagnoses and prescribed drugs registered from 2 years to 30 days

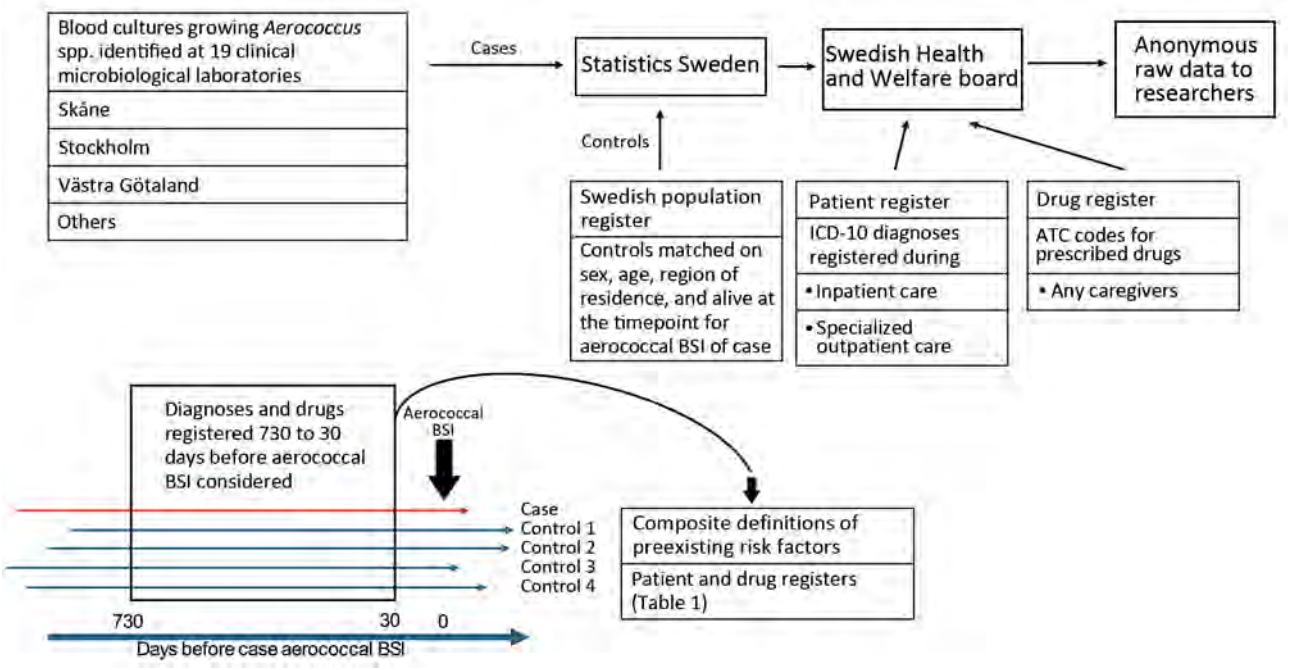

Figure 1. Overview of data collection and curation in nationwide observational case–control study of risk factors for *Aerococcus* BSIs, Sweden. Cases of aerococcal BSI were identified at 19 clinical microbiological laboratories across Sweden during 2012–2016. Matched control data were obtained from the Swedish Population Register. Registered diagnoses were collected from the National Patient Register, and prescribed drug data were collected from the National Drug Register. Registrations performed 30–730 days before aerococcal BSI detection were used to define medical conditions and characteristics hypothesized to contribute to aerococcal BSI. ATC, Anatomic Therapeutic Chemical; BSI, bloodstream infection; ICD-10, International Classification of Diseases, 10th Revision.

Table 1. Hypothesized mechanisms for and operational definitions of participants' medical conditions in nationwide observational case–control study of risk factors for *Aerococcus* BSIs, Sweden, 2012–2016*

	Hypothesized mechanisms linking conditions to aerococcal BSI					Operational definitions	
Conditions	Ecologic dysregulation/ displacement	Compromised local barriers	Lowered immune competence	Healthcare exposure	Frailty	Patient register, ICD-10 codes	Drug register, ATC codes
Hospital admissions	No	No	No	**Yes**	**Yes**	Registered admissions	NA
Prescribed drugs	No	No	No	**Yes**	**Yes**	NA	Registered prescriptions
Treatment for infection	**Yes**	**Yes**	No	**Yes**	No	A, B, M00–03, G00–08, I33, I38–40, J0–2, N10	J01
Pulmonary disease	No	**Yes**	No	**Yes**	**Yes**	J3–9	R03
Gastrointestinal disease	**Yes**	**Yes**	No	**Yes**	No	K2–9	NA
Malignant disease, nonurologic	No	**Yes**	Yes	**Yes**	**Yes**	C0–4, C50, C54–58, C69, C7–9, Z923, Z926	NA
Urologic conditions, including malignancy	No	**Yes**	No	No	No	C51–53, C60–68, R3, N2–5, N7–9, Q5, Q60–64, Z935–36	G04c, G04bd, G04bx
Neurologic conditions	**Yes**	No	No	**Yes**	**Yes**	G0–3, G6–8, F0, F7, F8, I6	N06d, N04
Corticosteroid treatment	No	No	Yes	No	No	NA	H02ab, H02aa02, A07ea
Diabetes mellitus	**Yes**	No	**Yes**	**Yes**	**Yes**	E10–14	A10a, A10b
Heart disease	No	No	No	**Yes**	**Yes**	I0, I2–5, I7, Z45, Q2	C03c
Rheumatic disease	No	No	**Yes**	**Yes**	**Yes**	M	NA
Kidney disease	No	No	**Yes**	**Yes**	**Yes**	N0, N11–19	NA

*Condition or characteristic considered to capture aspects of ≥1 prehoc hypothesized mechanisms for aerococcal BSI. Bold font indicates positive association. Conditions were defined operationally by the presence of any criteria listed in the final 2 columns (registered diagnosis or drug prescription); absence of a condition was defined as lack of all listed criteria for that condition. Conditions were considered for registrations made 1–24 months (excluding the most recent month) preceding the aerococcal BSI detection or control date. ATC, Anatomic Therapeutic Chemical; BSI, bloodstream infection; ICD-10, International Classification of Diseases, 10th Revision; NA, not applicable.

before aerococcal BSI detection; the same dates were applied for the matched controls. When no component of the definition for a particular condition was registered, we considered those patients did not have that condition.

Statistical Analysis

We extracted publicly available data from Statistics Sweden and stratified by age and sex for the total population that inhabited the uptake areas of the participating laboratories during the study period (*28*). We calculated crude, age-stratified, and sex-stratified incidence as the number of cases that occurred within the strata divided by the number of persons within the respective strata of the source population and the study period in years. We included repeat episodes of aerococcal BSI for this analysis if they were separated by >90 days.

We applied conditional logistic regression models to analyze multivariable associations between underlying conditions and aerococcal BSIs, accounting for matching. We selected the variables for the final model by structured backward selection according to likelihood-ratio tests and a p value of <0.10 as the threshold that defined a loss of model fitness after elimination of a variable. For each model, we assessed multicollinearity and used a variance inflation factor threshold of 2.4 to discard variables affected by multicollinearity, even if it led to loss of model fitness.

We performed secondary analyses by using models stratified by sex and age (in tertiles) and presented those data as forest plots. We conducted statistical analyses and generated graphs by using R version 4.3.1 (The R Project for Statistical Computing, https://www.r-project.org). We used the clogit function of the survival package for conditional logistic regression, the lmtest function to perform likelihood-ratio tests, the car function to assess variance inflation, and the forestplot function to construct forest plots.

Results

Of all 23 clinical microbiology laboratories in Sweden, 19 provided data for this study; those laboratories collectively serve 8.78 million persons and correspond to ≈90% of the country's population. The laboratories contributed data on cases within a 2- to 5-year period

(depending on the time of introduction of MALDI-TOF mass spectrometry for *Aerococcus* spp. identification), yielding a total observation of 39.6 million person-years.

We identified a total of 591 episodes of aerococcal BSI in 581 persons. Among those episodes, 3 were considered relapses (<90-day interval) and excluded from our incidence calculations. The average incidence of aerococcal BSI was 1.48/100,000 person-years (95% CI 1.37–1.60/100,000 person-years). Most aerococcal BSIs occurred in older persons; the median age was 82 (interquartile range 74–87) years, and 78.6% (452 cases) of infected patients were men (Figure 2, panels A, B). Other than 2 cases that occurred in children ≤1 year of age, the age-stratified incidence was ≈0 in persons <60 years of age for both sexes, after which a substantial increase in the number of cases occurred, especially in men (maximum incidence 62.8/100,000 person-years [95% CI 46.9–78.6/100,000 person-years] in men 90–94 years of age) (Figure 2, panel C).

Most (n = 422 [71.7%]) aerococcal BSI episodes were caused by *A. urinae*, whereas 61 (10.4%) episodes were attributed to *A. sanguinicola* and 91 (15.5%) episodes were caused by other or unspecified aerococci; 14 (2.4%) patients had 2 concomitant species of aerococci in their blood cultures. Additional species of bacteria were identified in blood cultures from 201 (34.2%) cases, including 62 (10.5%) cultures containing coagulase-negative staphylococci, 35 (6.0%) with *Escherichia coli*, 26 (4.4%) with *Actinotignum schaali*, 17 (2.9%) with *Enterococcus faecalis*, and 15 (2.6%) with *Staphylococcus aureus*.

Comparison with Matched Controls

We identified 4 matched controls for each of 577 (99.3%) of 581 patients with aerococcal BSIs; the resulting 2,885 persons constituted the study population. Crude analyses revealed significantly higher proportions of most medical conditions in participants with aerococcal BSIs than in controls, including structural urologic (331/577 [57.4%] vs. 753/2308 [31.8%]; p<0.001) and neurologic (227/577 [39.3%] vs. 318/2308 [13.8%]; p<0.001) conditions (Table 2).

Structured progressive modeling yielded a final conditional logistic regression model in which aerococcal BSI was associated with structural urologic conditions (adjusted odds ratio [aOR] 2.15 [95% CI 1.72–2.68]; p<0.001), neurologic conditions (aOR 2.89 [95% CI 2.26–3.70]; p<0.001), number of hospital admissions (aOR 6.81 [95% CI 2.51–8.5]; p<0.001 for >10 vs. 0 hospitalizations), and previous treatment for infection (for treatment 1–3 months before infection compared with >2 years or never, aOR 1.88 [95% CI 1.38–2.56]; p<0.001) (Table 3). A borderline significant negative association with rheumatologic diseases was also observed (aOR 0.77 [95% CI 0.59–1.00]; p = 0.05).

In age-stratified models, the associations between aerococcal BSI and hospital admission, previous treatment for infection, malignancy, and neurologic or structural urologic conditions were slightly more pronounced in the lower age tertiles (Figure 3). The sex-stratified models revealed male or female sex did not strongly affect other risk factors for aerococcal BSI (Figure 4).

Post Hoc Analyses

We performed univariable post hoc analyses according to the primary multivariable modeling. Prescriptions of oral antimicrobial drugs commonly used during 30 days–2 years before aerococcal BSI diagnosis for lower urinary tract infections, such as pivmecillinam, nitrofurantoin, and trimethoprim (odds ratio [OR] 3.02 [95% CI 2.36–3.85]; p<0.001), and upper urinary tract infections, such as ciprofloxacin (OR 3.23

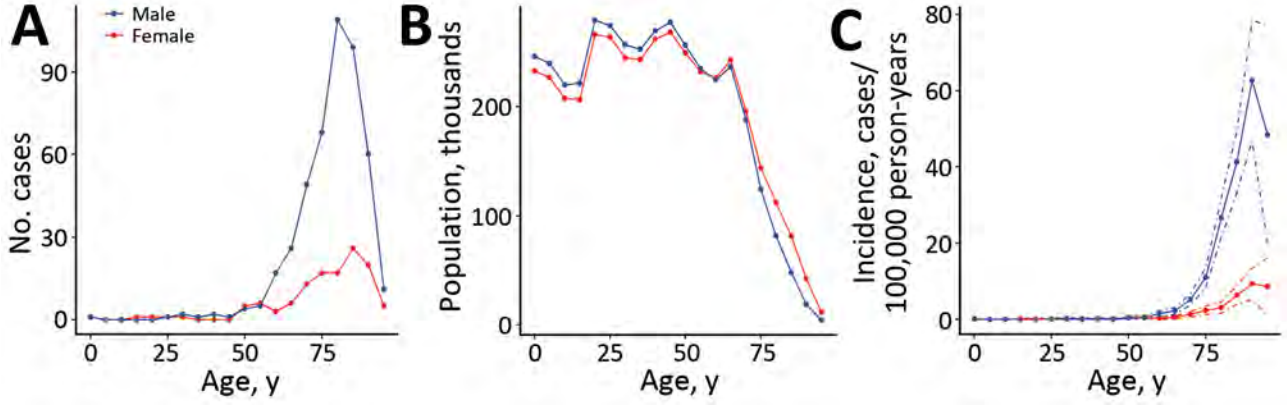

Figure 2. Age and sex distribution of patients in nationwide observational case–control study of risk factors for *Aerococcus* bloodstream infections (BSIs), stratified by age in 5-year intervals and sex, Sweden, 2012–2016. A) Number of patients with aerococcal BSI. B) Populations within the uptake area at risk for aerococcal BSI. C) Incidence of aerococcal BSI.

Table 2. Characteristics of participants in nationwide observational case–control study of risk factors for *Aerococcus* BSIs, Sweden, 2012–2016*

Characteristics	Controls, n = 2,308	Aerococcal BSI, n = 577	p value
Age, y			
Median (IQR)	82 (74–87)	82 (74–87)	1.0
0–5	8 (0.3)	2 (0.3)	
6–18	0	0	
19–76	796 (34.5)	199 (34.5)	
77–85	740 (32.1)	185 (32.1)	
>85	764 (33.1)	191 (33.1)	
Sex			1.0
M	1,816 (78.7)	454 (78.7)	
F	492 (21.3)	123 (21.3)	
Residence, regional council			1.0
Skåne	584 (25.3)	146 (25.3)	
Stockholm	396 (17.2)	99 (17.2)	
Västra Götaland	376 (16.3)	94 (16.3)	
Kalmar	124 (5.4)	31 (5.4)	
Uppsala	100 (4.3)	25 (4.3)	
Other†	728 (31.5)	182 (31.5)	
Previous treatment for another infection,‡ mo			<0.001
1–3	231 (10.0)	129 (22.4)	
>3–9	281 (12.2)	100 (17.3)	
>9–24	416 (18.0)	122 (21.1)	
>24 or never	1,380 (59.8)	226 (39.2)	
Malignant disease, nonurologic	182 (7.9)	75 (13.0)	<0.001
Urologic conditions§	753 (31.8)	331 (57.4)	<0.001
Neurologic conditions	318 (13.8)	227 (39.3)	<0.001
Hospital admissions, median (IQR)	0 (0–1)	1 (0–3)	<0.001
Kidney disease	93 (4.0)	52 (9.0)	<0.001
Pulmonary disease	346 (15.0)	122 (21.1)	0.001
Gastrointestinal disease	255 (11.0)	105 (18.2)	<0.001
Diabetes mellitus	324 (14.0)	113 (19.6)	<0.001
Cardiovascular disease	814 (35.3)	292 (50.6)	<0.001
Number of prescribed drugs, median (IQR)	7 (4–12)	11 (7–16)	<0.001
Rheumatological disease	390 (16.9)	130 (22.5)	0.002
Corticosteroid therapy	309 (13.4)	96 (16.6)	0.05

*Values are no. (%) except as indicated. The matching variables age, sex, and geographic region were distributed equally, but patients with aerococcal BSI were disproportionately affected by all investigated conditions. p values were calculated by χ^2 or Mann-Whitney U tests as appropriate. BSI, bloodstream infection; IQR, interquartile range.
†Other regions were Östergötland, Jönköping, Kronoberg, Blekinge, Halland, Värmland, Örebro, Västmanland, Dalarna, and Norrbotten.
‡Time in months indicates when treatment for another infection occurred before the aerococcal BSI was detected.
§Including urologic malignancies.

[95% CI 2.55–4.10]; p<0.001) and trimethoprim/sulfamethoxazole (OR 2.76 [95% CI 1.71–4.40]; p<0.001), were associated with aerococcal BSI (Table 4). Penicillins other than pivmecillinam had only a modest association (OR 1.37 [95% CI 1.11–1.68]; p = 0.003). Clindamycin, macrolides, and tetracyclins were not associated with aerococcal BSI (Table 4).

Among urologic conditions, benign prostatic hyperplasia was a common condition, having a modest association with aerococcal BSI (OR 1.54 [95% CI 1.23–1.92]; p<0.001). Prostate cancer (which constituted most urologic malignancies in this group) also correlated with aerococcal BSI (OR 2.02 [95% CI 1.45–2.79]; p<0.001). Diagnoses related to urinary tract stones, especially hydronephrosis (OR 10.8 [95% CI 5.36–23.7]; p<0.001), were rare but strongly associated with aerococcal BSI. Conditions involving kidneys and ureters generally had more robust associations with aerococcal BSI than those involving the bladder and urethra. In women, gynecologic cancers were rare and were not significantly associated with aerococcal BSI (OR 3.27 [95% CI 0.80–12.6]; p = 0.081).

Malignant tumors of the colon and skin did not correlate with aerococcal BSI, whereas lung cancer (OR 14.2 [95% CI 3.41–95.2]; p<0.001) and hematologic malignancies (OR 2.47 [95% CI 1.23–4.78]; p = 0.008) were rare risk factors for this infection. Among neurologic conditions, dementia (OR 3.99 [95% CI 3.01–5.27]; p<0.001), cerebrovascular insult (OR 3.17 [95% CI 2.37–4.23]; p<0.001), Parkinson's disease (OR 3.12 [95% CI 2.07–4.67]; p<0.001), paraparesis or tetraparesis (OR 4.50 [95% CI 2.53–8.03]; p<0.001), and multiple sclerosis (OR 11.2 [95% CI 3.81–40.5]; p<0.001) were strongly associated with aerococcal BSI.

Discussion

In this nationwide population-based study in Sweden, we identified associations between aerococcal

Table 3. Multivariable models used in nationwide observational case–control study of risk factors for *Aerococcus* BSIs, Sweden, 2012–2016*

Characteristics	First model		Final model	
	Adjusted odds ratio (95% CI)	p value	Adjusted odds ratio (95% CI)	p value
Previous treatment for infection,† mo				
Never	Referent	NA	Referent	NA
1–3	1.77 (1.28–2.45)	<0.001	1.88 (1.38–2.56)	<0.001
>3–9	1.15 (0.83–1.58)	0.40	1.21 (0.89–1.65)	0.23
>9–24	1.19 (0.90–1.59)	0.22	1.22 (0.92–1.61)	0.16
Malignant disease, nonurologic	1.40 (1.01–1.95)	0.046	1.39 (1.00–1.93)	0.052
Structural urologic conditions‡	2.05 (1.63–2.57)	<0.001	2.15 (1.72–2.68)	<0.001
Neurologic conditions	2.74 (2.13–3.52)	<0.001	2.89 (2.26–3.70)	<0.001
Hospital admissions				
None	Referent	NA	Referent	NA
1–2	1.80 (1.37–2.37)	<0.001	1.74 (1.34–2.25)	<0.001
3–5	3.56 (2.46–5.14)	<0.001	3.50 (2.50–4.88)	<0.001
6–10	4.30 (2.39–7.75)	<0.001	4.34 (2.57–7.66)	<0.001
>10	5.99 (2.08–17.2)	<0.001	6.81 (2.51–18.5)	<0.001
Rheumatologic disease	0.77 (0.57–0.01)	0.061	0.77 (0.59–1.00)	0.050
Kidney disease	1.15 (0.80–1.66)	0.4	NA	NA
Pulmonary conditions	1.00 (0.75–1.34)	0.98	NA	NA
Gastrointestinal conditions	0.86 (0.63–1.16)	0.33	NA	NA
Diabetes mellitus	0.97 (0.72–1.29)	0.81	NA	NA
Cardiovascular disease	0.84 (0.65–1.08)	0.18	NA	NA
No. prescribed drugs	1.03 (1.00–1.05)	0.019	NA	NA
Corticosteroid therapy	0.72 (0.52–0.99)	0.040	NA	NA

*First model included variables that had univariable associations with aerococcal BSI. Age, sex, and county were included in the models but were hidden because matching on those variables prevented appropriate interpretation of their respective estimates. Likelihood-ratio tests and variance inflation analyses were used to guide progressive refinement of the model. BSI, bloodstream infection; NA, not applicable.
†Time in months indicates when treatment for another infection occurred before the aerococcal BSI was detected.
‡Included urological malignancies.

BSI and urogenital diagnoses in general and urologic malignancy in particular, consistent with previous observations. We also identified associations with neurologic conditions, such as dementia, which has been infrequently reported. Our findings support a considerable predilection for elderly men to acquire aerococcal BSIs and also support the hypothesis that aerococci enter the bloodstream through the urogenital tract and renal mucosa (*24*). That hypothesis is strengthened by the observation that previous prescriptions of antimicrobial drug classes commonly administered for urinary

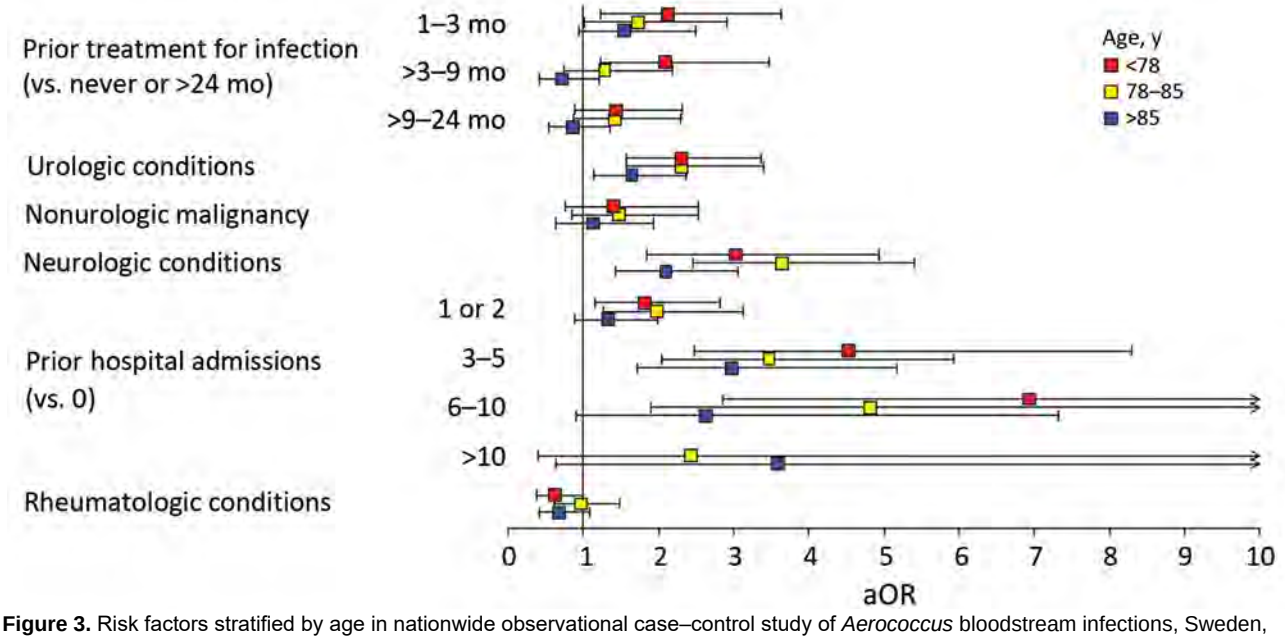

Figure 3. Risk factors stratified by age in nationwide observational case–control study of *Aerococcus* bloodstream infections, Sweden, 2012–2016. Forest plots depicting 3 conditional multivariable logistic regression analyses, 1 analysis each/age tertile. Squares indicate the aOR; error bars indicate 95% CIs. aOR, adjusted odds ratio.

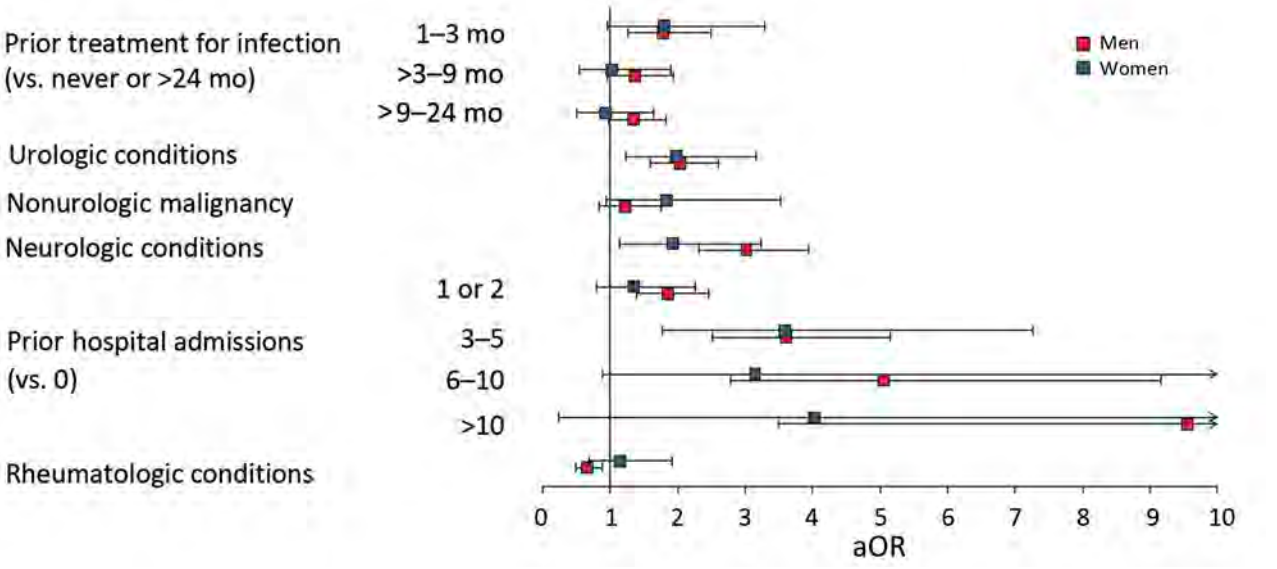

Figure 4. Risk factors stratified by sex in nationwide observational case–control study of *Aerococcus* bloodstream infections, Sweden, 2012–2016. Forest plots depicting 2 conditional multivariable logistic regression analyses, 1 each for male and female patients. Squares indicate the aOR; error bars indicate 95% CIs. aOR, adjusted odds ratio.

tract infections were positively associated with aerococcal BSI.

We noted a higher incidence of aerococcal BSI in this study than in previous reports on *A. urinae* and *A. sanguinicola*, although the number of studies estimating rates has been low (*5*,*6*,*12*,*13*,*29*). As in previous studies, we observed sex differences in the tendency toward developing aerococcal BSIs; men had a greater incidence (*5*–*7*,*12*–*14*,*18*,*29*), but the mechanisms of this differential pattern of infection remain unknown. We found male urogenital tract disorders were more common in patients with aerococcal BSI than in controls. We speculate that the disproportionate male prevalence of aerococcal BSI can be explained in part by the preponderance of prostate disorders in elderly men.

The mechanisms of susceptibility to aerococcal BSI in male and female patients warrant further study. Because aerococcal BSIs are more frequent in elderly men, *Aerococcus* spp. have been proposed to enter the bloodstream through the prostate (*3*,*5*–*7*,*12*–*14*,*18*,*29*,*30*). Our findings indicate prostate cancer increases the risk for aerococcal BSI, whereas the association between infection and benign prostate hyperplasia was modest compared with conditions in other structures of the urogenital system. Our results indicate that clinical conditions in the kidneys and ureters were also associated with a higher risk for aerococcal BSI than those in the bladder, prostate, or urethra. A link between neurologic conditions in general, particularly dementia and paresis, and aerococcal BSI has been suggested in a small case series from Denmark, although only for *A. sanguinicola* (*31*). It is possible that a connection between neurologic diseases and aerococcal BSI is mediated by immobility issues in some patients (e.g., cerebrovascular insults leading to immobility) and, in the case of paresis, through catheterization of the urinary tract. Rheumatologic disease and aerococcal BSI had a negative association in multivariable analysis but had a positive crude association; however, the association was relatively modest and borderline significant and might have been a spurious effect of multiple comparisons.

In women, the levels of *A. urinae* and *A. sanguinicola* in vaginal microbiota increase during hormone replacement therapy (*32*). We did not, however, observe an increased risk for aerococcal BSI in women who had been prescribed estrogen medication, although the validity of that finding is limited by the low number of female study participants. One possible explanation is that urogenital carriage of aerococci is less likely to lead to bacteremia in women. That interpretation is consistent with smaller studies in Scotland and southern Sweden in which a larger proportion of men compared with women had *Aerococcus* spp. in blood but not urinary cultures (*11*,*12*,*33*,*34*).

The main strengths of this study are that it is population-based, examined the incidence of and risk factors for aerococcal BSI, and had a follow-up of ≈40 million person-years and a matched control group from the source population, enabling

high-precision estimates and robust control for confounding. Access to healthcare in Sweden is not restricted by having private insurance, which might have otherwise introduced bias and possibly caused underestimation of aerococcal BSI incidence and limited the generalizability of our results to persons in lower socioeconomic strata or vulnerable subgroups (*25*). Second, in contrast to previous studies in which species were identified by using varied methods (often involving hospital-based or local inclusion of patients), the participating laboratories used MALDI-TOF mass spectrometry throughout the study period, and we included persons from multiple regions in a population-based manner (*12*–*14*). MALDI-TOF mass spectrometry has been shown to reliably identify *Aerococcus* spp. and has rectified the misclassification of *A. sanguinicola* as *A. viridans* and of aerococci in general as streptococci (*35*). Third, using population-based selection of matched controls enabled relevant comparisons with aerococcal BSIs among persons of the same age, sex distribution, and county of residence. That setup promoted a more efficient analysis of risk factors other than age and sex and

Table 4. Post hoc analyses of risk factors for *Aerococcus* BSIs in nationwide observational case–control study, Sweden, 2012–2016*

Risk factor	Controls, no. (%)	Aerococcal BSI, no. (%)	Odds ratio (95% CI)	p value	Codes†
Prescribed antimicrobial drugs					
Phenoxymethylpenicillin, amoxicillin, or flucloxacillin	512 (22.2)	162 (28.1)	1.37 (1.11–1.68)	0.003	ATC: J01CE02, J01CF05, J01CA04
Macrolides or clindamycin	90 (3.9)	24 (4.2)	1.07 (0.66–1.67)	0.8	ATC: J01F
Tetracyclins	171 (7.4)	49 (8.5)	1.16 (0.82–1.60)	0.4	ATC: J01A
Pivmecillinam, nitrofurantoin, or trimethoprim	201 (8.7)	129 (22.4)	3.02 (2.36–3.85)	<0.001	ATC: J01XE01, J01CA08, J01EA01
Ciprofloxacin	208 (9.0)	140 (24.3)	3.23 (2.55–4.10)	<0.001	ATC: J01MA02
Trimethoprim or sulfamethoxazole	45 (1.9)	30 (5.2)	2.76 (1.71–4.40)	<0.001	ATC: J01EE01
Urologic conditions, including malignancy	753 (31.8)	331 (57.4)	2.88 (2.39–3.47)	<0.001	See Table 1
Renal or ureteral conditions	31 (1.3)	43 (7.5)	5.91 (3.71–9.55)	<0.001	C64–66, D300–302, D410–412, N13, N20, Q60–63, S370–371
Vesical or urethral conditions	40 (1.7)	25 (4.3)	2.57 (1.53–4.24)	<0.001	C67–68, D303–304, D090, D413–414, N21, Q64, S372–373
Prostate and other male reproductive organs	241 (10.4)	123 (27.2)	2.43 (1.89–3.11)	<0.001	C60–63, D074–76, D29, D40, N40–42
Urologic malignancy	152 (6.6)	70 (12.2)	1.96 (1.45–2.63)	<0.001	C51–53, C60–68
Urologic malignancy except prostate	36 (1.6)	15 (2.6)	1.68 (0.89–3.04)	0.094	C51–53, C60, C62–68
Prostate cancer, men	121 (5.2)	58 (10.1)	2.02 (1.45–2.79)	<0.001	C61
Gynecologic cancer, women	5 (1.0)	4 (3.3)	3.27 (0.80–12.6)	0.081	C51–59
Prescription of drugs for prostatic hyperplasia, men	367 (20.2)	130 (28.6)	1.54 (1.23–1.92)	<0.001	ATC: G04C
Urinary tract stones	25 (1.1)	25 (4.5)	4.31 (2.46–7.55)	<0.001	N20–21
Hydronephrosis	10 (0.4)	26 (4.5)	10.8 (5.36–23.7)	<0.001	N13
Malignant disease, nonurologic	182 (7.9)	75 (13.0)	1.75 (1.30–2.31)	<0.001	See Table 1
Lung cancer	2 (0.1)	7 (1.2)	14.2 (3.41–95.2)	<0.001	C34
Skin cancer	112 (4.9)	29 (5.0)	1.04 (0.67–1.56)	0.9	C43–44
Colon cancer	11 (0.5)	5 (0.9)	1.83 (0.57–5.04)	0.3	C18–20
Hematologic malignancy	23 (1.0)	14 (2.4)	2.47 (1.23–4.78)	0.008	C8–9
Neurologic conditions					
Cerebrovascular insult	124 (5.4)	88 (15.3)	3.17 (2.37–4.23)	<0.001	I61–63, I69
Paraparesis or tetraparesis	23 (1.0)	25 (4.3)	4.50 (2.53–8.03)	<0.001	G8
Dementia	122 (5.3)	105 (18.2)	3.99 (3.01–5.27)	<0.001	G30–31, F00–03, F051; ATC: N06D
Parkinson's disease	58 (2.5)	43 (7.5)	3.12 (2.07–4.67)	<0.001	G20–22; ATC: N04
Multiple sclerosis	4 (0.2)	11 (1.9)	11.2 (3.81–40.5)	<0.001	G35
Estrogen prescription, women	111 (22.5)	23 (18.7)	0.80 (0.48–1.30)	0.4	G03C

*Descriptive analysis of subdivisions of risk factor categories identified in multivariable analyses. ATC, Anatomic Therapeutic Chemical; BSI, bloodstream infection.
†Diagnostic codes were derived from the International Classification of Diseases, 10th Revision; drug prescription codes were derived from the ATC classification system (as indicated).

reduced potential biases from variabilities in the structure or care registration between counties in Sweden. Moreover, considering the low incidence of aerococcal BSI, we consider it highly unlikely that a substantial proportion of the control population would have had an aerococcal BSI outside of the study uptake area or before the study period. Finally, the use of structured backward selection, according to variance likelihood ratio and variance inflation, enabled additional control for confounding and multicollinearity.

The first limitation of our study is that, despite our approach to control for confounding, residual confounding from factors that were not included in the registers cannot be ruled out. Despite efforts to limit potential sources of bias, claims on causality cannot be made by using a register-based study design. We also acknowledge that our findings might not be generalizable to children and young adults because of the limited number of those participants in this study. Second, information on over-the-counter drugs and drugs given during inpatient care was unavailable; however, except for topical estrogen, no drug reported in this study was available over the counter. Third, iatrogenic immune suppression caused by drugs (other than corticosteroids), especially chemotherapeutics, was not possible to define operationally by using the available registers because those drugs are often administered directly at the clinic and not filled by prescription in a pharmacy outside of the hospital. Thus, the relative effects of treatments for malignancy versus treatments for aerococcal BSI were not possible to evaluate in this study. Fourth, information on intermittent catheterization and the use of medical devices, including permanent urinary catheters, was lacking. Therefore, it was not possible to study the extent to which urinary catheterization might explain the link between neurologic conditions and aerococcal BSI. Finally, *A. urinae* has recently been proposed to comprise a cluster of related species (*36*). Because our study data were collected before that publication appeared, potential clustering was not possible to include in our analyses.

Previous validation studies of inpatient registry data in Sweden have shown that 85%–95% of diagnoses are correct, inasmuch as the ICD-10 code corresponds to the diagnosis entered into the medical records (*27*). However, diagnoses made during primary healthcare are unavailable in the patient register. That lack of accessibility could lead to selection bias, wherein each predisposing condition would only be represented by the stratum of disease severity that justified specialized care, potentially causing low power and inflated OR estimates because milder disease would be undetected. To minimize that risk, we combined registered ICD-10 codes with drug prescription data to capture the conditions of interest more robustly, which is especially critical for conditions such as diabetes mellitus, benign prostatic hyperplasia, and less severe infectious diseases that are generally managed during primary care in Sweden.

We defined aerococcal BSI according to the detection of aerococci in a blood culture. In ≈33% of cases, >1 bacteria species grew in the blood culture. We do not believe that polymicrobial growth reflects contamination of blood cultures by aerococci to any appreciable extent, because they are not known to routinely colonize the skin. It was not possible to determine the relative significance of aerococci when identified with other bacteria; however, we consider the presence of *Aerococcus* spp. in a patient's blood to represent true bacteremia. A high degree of co-isolation with other established uropathogens, including *E. coli*, *E. faecalis*, and *A. schaali*, also suggests bacteremia originated from a urinary tract infection. Furthermore, prescriptions of antimicrobial drugs commonly taken for urinary tract infections were strongly associated with the development of aerococcal BSI. Whereas that association might reflect a chronic predilection for urinary tract infections, it is also possible that antimicrobial drug treatment promotes ecologic dysregulation, causing aerococcal overgrowth and invasive disease.

In conclusion, our findings substantially strengthen the proposed link between urologic conditions and aerococcal BSI. Neurologic conditions were also strongly associated with aerococcal BSI, although this association might be mediated by bacterial entry through the urothelium. Further study of the mechanisms that underly the associations between urologic and neurologic conditions and aerococcal bacteremia might be especially valuable in light of our findings. Awareness of *Aerococcus* spp. in patients, especially elderly men, will be needed to manage invasive infections.

Acknowledgments

We thank the clinical microbiology laboratories of Sweden for contributing data on episodes of aerococcal BSI and the Department for Registries and Statistics at the National Board of Health and Welfare Sweden and the Department for Microdata at Statistics Sweden for registry data.

The study was supported by grants from Sweden's governmental ALF funds (to J.W. and M.R.) and by grants

from the Swedish Society for Medical Research, Swedish Medical Association, and Royal Physiographic Society of Lund (to T.S.). M.I. is supported by grants from the Swedish Society for Medical Research and ALF.

Study data will be shared by authors upon reasonable request.

About the Author

Dr. Walles is a clinical microbiology resident at Lund University Hospital in Lund, Sweden. His main research is on tuberculosis and other mycobacterial infections.

References

1. Williams RE, Hirch A, Cowan ST. *Aerococcus*, a new bacterial genus. J Gen Microbiol. 1953;8:475–80. https://doi.org/10.1099/00221287-8-3-475
2. Christensen JJ, Korner B, Kjaergaard H. *Aerococcus*-like organism—an unnoticed urinary tract pathogen. APMIS. 1989;97:539–46. https://doi.org/10.1111/j.1699-0463.1989.tb00828.x
3. Rasmussen M. *Aerococcus*: an increasingly acknowledged human pathogen. Clin Microbiol Infect. 2016;22:22–7. https://doi.org/10.1016/j.cmi.2015.09.026
4. Aguirre M, Collins MD. Phylogenetic analysis of some *Aerococcus*-like organisms from urinary tract infections: description of *Aerococcus urinae* sp. nov. J Gen Microbiol. 1992;138:401–5. https://doi.org/10.1099/00221287-138-2-401
5. de Jong MFC, Soetekouw R, ten Kate RW, Veenendaal D. *Aerococcus urinae*: severe and fatal bloodstream infections and endocarditis. J Clin Microbiol. 2010;48:3445–7. https://doi.org/10.1128/JCM.00835-10
6. Senneby E, Petersson AC, Rasmussen M. Clinical and microbiological features of bacteraemia with *Aerococcus urinae*. Clin Microbiol Infect. 2012;18:546–50. https://doi.org/10.1111/j.1469-0691.2011.03609.x
7. Senneby E, Göransson L, Weiber S, Rasmussen M. A population-based study of aerococcal bacteraemia in the MALDI-TOF MS–era. Eur J Clin Microbiol Infect Dis. 2016;35:755–62. https://doi.org/10.1007/s10096-016-2594-z
8. Cattoir V, Kobal A, Legrand P. *Aerococcus urinae* and *Aerococcus sanguinicola*, two frequently misidentified uropathogens. Scand J Infect Dis. 2010;42:775–80. https://doi.org/10.3109/00365548.2010.485576
9. Melnyk AI, Toal C, Glass Clark S, Bradley M. Home urinary tract infection testing: patient experience and satisfaction with polymerase chain reaction kit. Int Urogynecol J. 2023;34:1055–60. PubMed https://doi.org/10.1007/s00192-022-05309-z
10. Forsvall A, Wagenius M, Rasmussen M. Perigenital necrotizing soft tissue infection caused by *Aerococcus urinae*. IDCases. 2019;18:e00590. https://doi.org/10.1016/j.idcr.2019.e00590
11. Oskooi M, Sunnerhagen T, Senneby E, Rasmussen M. A prospective observational treatment study of aerococcal urinary tract infection. J Infect. 2018;76:354–60. https://doi.org/10.1016/j.jinf.2017.12.009
12. Senneby E, Eriksson B, Fagerholm E, Rasmussen M. Bacteremia with *Aerococcus sanguinicola*: case series with characterization of virulence properties. Open Forum Infect Dis. 2014;1:ofu025. https://doi.org/10.1093/ofid/ofu025
13. Sihvonen R, Turunen M, Lehtola L, Pakarinen L, Grönroos JO, Rantakokko-Jalava K, et al. Clinical and microbiological characterization of *Aerococcus urinae* bacteraemias at Helsinki metropolitan area, Finland. Eur J Clin Microbiol Infect Dis. 2022;41:751–60. https://doi.org/10.1007/s10096-022-04415-6
14. Tai DBG, Go JR, Fida M, Saleh OA. Management and treatment of *Aerococcus* bacteremia and endocarditis. Int J Infect Dis. 2021;102:584–9. https://doi.org/10.1016/j.ijid.2020.10.096
15. Narayanasamy S, King K, Dennison A, Spelman DW, Aung AK. Clinical characteristics and laboratory identification of *Aerococcus* infections: an Australian tertiary centre perspective. Int J Microbiol. 2017;2017:5684614. https://doi.org/10.1155/2017/5684614
16. Yaban B, Kikhney J, Musci M, Petrich A, Schmidt J, Hajduczenia M, et al. *Aerococcus urinae*—a potent biofilm builder in endocarditis. PLoS One. 2020;15:e0231827. https://doi.org/10.1371/journal.pone.0231827
17. Yonetani S, Hirao C, Ohnishi H. Background of patients with *Aerococcus* spp. detected in blood cultures, and drug sensitivity of *Aerococcus* spp. Diagn Microbiol Infect Dis. 2021;101:115506. https://doi.org/10.1016/j.diagmicrobio.2021.115506
18. Sunnerhagen T, Nilson B, Olaison L, Rasmussen M. Clinical and microbiological features of infective endocarditis caused by aerococci. Infection. 2016;44:167–73. https://doi.org/10.1007/s15010-015-0812-8
19. Berge A, Kronberg K, Sunnerhagen T, Nilson BHK, Giske CG, Rasmussen M. Risk for endocarditis in bacteremia with *Streptococcus*-like bacteria: a retrospective population-based cohort study. Open Forum Infect Dis. 2019;6:ofz437. https://doi.org/10.1093/ofid/ofz437
20. Stelling J, Read JS, Fritch W, O'Brien TF, Peters R, Clark A, et al. Surveillance of antimicrobial resistance and evolving microbial populations in Vermont: 2011–2018. Expert Rev Anti Infect Ther. 2020;18:1055–62. https://doi.org/10.1080/14787210.2020.1776114
21. Rodríguez-Sánchez B, Cercenado E, Coste AT, Greub G. Review of the impact of MALDI-TOF MS in public health and hospital hygiene, 2018. Euro Surveill. 2019;24:1800193. https://doi.org/10.2807/1560-7917.ES.2019.24.4.1800193
22. Senneby E, Sunnerhagen T, Hallström B, Lood R, Malmström J, Karlsson C, et al. Identification of two abundant *Aerococcus urinae* cell wall–anchored proteins. Int J Med Microbiol. 2019;309:151325. https://doi.org/10.1016/j.ijmm.2019.06.005
23. Yu Y, Tsitrin T, Bekele S, Thovarai V, Torralba MG, Singh H, et al. *Aerococcus urinae* and *Globicatella sanguinis* persist in polymicrobial urethral catheter biofilms examined in longitudinal profiles at the proteomic level. Biochem Insights. 2019;12:1178626419875089. https://doi.org/10.1177/1178626419875089
24. Gilbert NM, Choi B, Du J, Collins C, Lewis AL, Putonti C, et al. A mouse model displays host and bacterial strain differences in *Aerococcus urinae* urinary tract infection. Biol Open. 2021;10:bio058931. https://doi.org/10.1242/bio.058931
25. Laugesen K, Ludvigsson JF, Schmidt M, Gissler M, Valdimarsdottir UA, Lunde A, et al. Nordic health registry-based research: a review of health care systems and key registries. Clin Epidemiol. 2021;13:533–54. https://doi.org/10.2147/CLEP.S314959
26. Ludvigsson JF, Almqvist C, Bonamy AK, Ljung R, Michaëlsson K, Neovius M, et al. Registers of the Swedish total population and their use in medical research. Eur J

Epidemiol. 2016;31:125–36. https://doi.org/10.1007/s10654-016-0117-y
27. Ludvigsson JF, Andersson E, Ekbom A, Feychting M, Kim JL, Reuterwall C, et al. External review and validation of the Swedish national inpatient register. BMC Public Health. 2011;11:450. https://doi.org/10.1186/1471-2458-11-450
28. SCB Statistics Sweden. Population statistics [cited 2023 Sep 1]. https://www.scb.se/en/finding-statistics
29. Christensen JJ, Jensen IP, Faerk J, Kristensen B, Skov R, Korner B; Danish ALO Study Group. Bacteremia/septicemia due to *Aerococcus*-like organisms: report of seventeen cases. Clin Infect Dis. 1995;21:943–7. https://doi.org/10.1093/clinids/21.4.943
30. Rasmussen M. Aerococci and aerococcal infections. J Infect. 2013;66:467–74. https://doi.org/10.1016/j.jinf.2012.12.006
31. Ibler K, Truberg Jensen K, Ostergaard C, Sönksen UW, Bruun B, Schønheyder HC, et al. Six cases of *Aerococcus sanguinicola* infection: clinical relevance and bacterial identification. Scand J Infect Dis. 2008;40:761–5. https://doi.org/10.1080/00365540802078059
32. Geng L, Huang W, Jiang S, Zheng Y, Zhou Y, Zhou Y, et al. Effect of menopausal hormone therapy on the vaginal microbiota and genitourinary syndrome of menopause in Chinese menopausal women. Front Microbiol. 2020;11:590877. https://doi.org/10.3389/fmicb.2020.590877
33. Htwe SS, Inkster T. Epidemiology and urological pathogenic potential of *Aerococcus* species in greater Glasgow and Clyde (descriptive study of *Aerococcus urinae* in blood culture and urinary samples: clinical importance and potential marker of urinary tract pathology). J Med Microbiol. 2023;72. https://doi.org/10.1099/jmm.0.001690
34. Senneby E, Petersson AC, Rasmussen M. Epidemiology and antibiotic susceptibility of aerococci in urinary cultures. Diagn Microbiol Infect Dis. 2015;81:149–51. https://doi.org/10.1016/j.diagmicrobio.2014.11.009
35. Senneby E, Nilson B, Petersson AC, Rasmussen M. Matrix-assisted laser desorption ionization time-of-flight mass spectrometry is a sensitive and specific method for identification of aerococci. J Clin Microbiol. 2013;51:1303–4. https://doi.org/10.1128/JCM.02637-12
36. Choi BI, Ene A, Du J, Johnson G, Putonti C, Schouw CH, et al. Taxonomic considerations on *Aerococcus urinae* with proposal of subdivision into *Aerococcus urinae*, *Aerococcus tenax* sp. nov., *Aerococcus mictus* sp. nov., and *Aerococcus loyolae* sp. nov. Int J Syst Evol Microbiol. 2023;73. https://doi.org/10.1099/ijsem.0.006066

Address for correspondence: John Walles, Clinical Infection Medicine, Lund University, Ruth Lundskogs gata 3, 214 28, Malmö, Sweden; email: john.walles@med.lu.se

etymologia revisited

Mycobacterium chimaera

[mi'ko-bak-tēr'e-əm ki-mēr'ə]

Formerly an unnamed *Mycobacterium* sequevar within the *M. avium–M. intracellulare–M. scrofulaceum* group (MAIS), *M. chimaera* is an emerging opportunistic pathogen that can cause infections of heart valve prostheses, vascular grafts, and disseminated infections after open-heart surgery. Heater–cooler units used to regulate blood temperature during cardiopulmonary bypass have been implicated, although most isolates are respiratory. In 2004, Tortoli et al. proposed the name *M. chimaera* for strains that a reverse hybridization–based line probe assay suggested belonged to MAIS but were different from *M. avium, M. intracellulare*, or *M. scrofulaceum*. The new species name comes from the chimera, a mythological being made up of parts of 3 different animals.

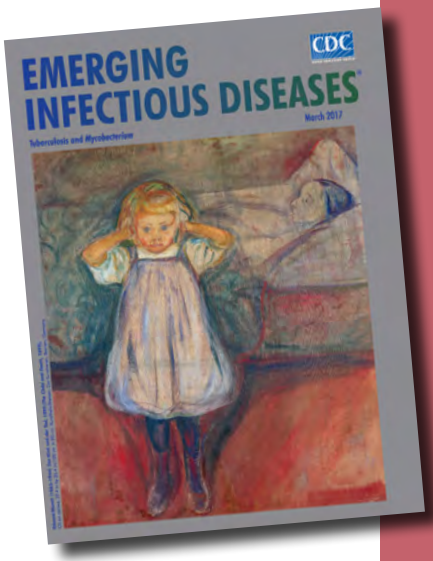

Originally published in March 2017

References

1. Schreiber PW, Kuster SP, Hasse B, Bayard C, Rüegg C, Kohler P, et al. Reemergence of *Mycobacterium chimaera* in heater–cooler units despite intensified cleaning and disinfection protocol. Emerg Infect Dis. 2016;22:1830–3.
2. Struelens MJ, Plachouras D. *Mycobacterium chimaer*a infections associated with heater-cooler units (HCU): closing another loophole in patient safety. Euro Surveill. 2016;21:1–3.
3. Tortoli E, Rindi L, Garcia MJ, Chiaradonna P, Dei R, Garzelli C, et al. Proposal to elevate the genetic variant MAC-A, included in the *Mycobacterium avium* complex, to species rank as *Mycobacterium chimaera* sp. nov. Int J Syst Evol Microbiol. 2004;54:1277–85.

https://wwwnc.cdc.gov/eid/article/23/3/et-2303_article

Powassan and Eastern Equine Encephalitis Virus Seroprevalence in Endemic Areas, United States, 2019–2020

Hannah Padda, Claire Y.-H. Huang, Kacie Grimm, Brad J. Biggerstaff, Jeremy P. Ledermann, Janae Raetz, Karen Boroughs, Eric C. Mossel, Stacey W. Martin, Jennifer A. Lehman, Rebecca L. Townsend, David Krysztof, Paula Saá, Emily T.N. Dinh, Mary Grace Stobierski, Brenda Esponda-Morrison, Karen Ann A. Wolujewicz, Matthew Osborne, Catherine M. Brown, Brandi Hopkins, Elizabeth K. Schiffman, Alex Garvin, Xia Lee, Rebecca A. Osborn, Ryan J. Wozniak, Aaron C. Brault, Sridhar V. Basavaraju, Susan L. Stramer, J. Erin Staples, Carolyn V. Gould

Powassan virus (POWV) and Eastern equine encephalitis virus (EEEV) are regionally endemic arboviruses in the United States that can cause neuroinvasive disease and death. Recent identification of EEEV transmission through organ transplantation and POWV transmission through blood transfusion have increased concerns about infection risk. After historically high numbers of cases of both viruses were reported in 2019, we conducted a seroprevalence survey using blood donation samples from selected endemic counties. Specimens were screened for virus-specific neutralizing antibodies, and population seroprevalence was estimated using weights calibrated to county population census data. For POWV, median county seroprevalence in 4 states was 0.84%, ranging from 0% (95% CI 0%–2.28%) to 11.5% (95% CI 0.82%–40.9%). EEEV infection was identified in a single county (estimated seroprevalence 1.62% [95% CI 0.04%–8.75%]). Although seroprevalence estimates in sampled areas were generally low, additional investigation of higher-prevalence areas could inform risk for transmission from asymptomatic blood and organ donors.

Powassan virus (POWV) and Eastern equine encephalitis virus (EEEV) are geographically focal arthropodborne viruses (arboviruses) in the United States (*1*–*3*). Most human infections are asymptomatic, but both viruses can cause disease ranging from acute febrile illness to severe encephalitis that can cause long-term disability or death. Recent increases in disease cases, outbreaks with high rates of illness and deaths, and identification of blood and organ donor–transmitted infections have led to greater concerns about human risk.

POWV, a flavivirus in the tickborne encephalitis serogroup, is spread to humans primarily by *Ixodes* spp. ticks in eastern Canada and the upper Midwest and Northeast United States (*2*). The number of POWV disease cases reported to the Centers for Disease Control and Prevention (CDC) has been rising; an average of 10 cases were reported annually before 2016, compared with 30 cases reported annually during 2016–2022 (*4*). In 2018, a probable case of blood transfusion transmission of POWV from a Wisconsin donor was identified in a kidney transplant recipient with neuroinvasive disease (*5*).

EEEV is an alphavirus spread to humans by several species of mosquitoes, most often near freshwater hardwood swamps in US states of the Atlantic, Gulf

Author affiliations: Centers for Disease Control and Prevention, Fort Collins, Colorado, USA (H. Padda, C.Y.-H. Huang, B.J. Biggerstaff, J.P. Ledermann, J. Raetz, K. Boroughs, E.C. Mossel, S.W. Martin, J.A. Lehman, A.C. Brault, J.E. Staples, C.V. Gould); American Red Cross, Rockville, Maryland, USA (K. Grimm, R.L. Townsend, D. Krysztof, P. Saá); Michigan Department of Health and Human Services, Lansing, Michigan, USA (E.T.N. Dinh, M.G. Stobierski); Connecticut Department of Public Health, Hartford, Connecticut, USA (B. Esponda-Morrison, K.A.A. Wolujewicz); Massachusetts Department of Public Health, Boston, Massachusetts, USA (M. Osborne, C.M. Brown, B. Hopkins); Minnesota Department of Health, Saint Paul, Minnesota, USA (E.K. Schiffman, A. Garvin); Wisconsin Department of Health Services, Madison, Wisconsin, USA (X. Lee, R.A. Osborn, R.J. Wozniak); Centers for Disease Control and Prevention, Atlanta, Georgia, USA (S.V. Basavaraju); Infectious Disease Consultant, North Potomac, Maryland, USA (S.L. Stramer)

DOI: https://doi.org/10.3201/eid3105.240893

Coast, and Great Lakes regions (*6*). EEEV disease has the highest reported case-fatality rate among arboviral diseases endemic to the United States; 78 (41%) deaths were reported among 189 neurologic cases of EEEV disease during 2003–2022 (*7*). In 2017, EEEV disease developed in 3 organ transplant recipients who received an organ from an infected donor, and 2 died (*8*). In 2019, a record number of EEEV disease cases was reported during a multistate outbreak of 34 cases in 7 states with 12 (35%) fatalities (*9*,*10*).

Few POWV and EEEV seroprevalence studies have been performed to assess the burden of infection. We conducted a seroprevalence study using residual blood donation samples collected from persons residing in selected POWV- and EEEV-endemic areas during 2019–2020 to determine infection risk among county residents and to assess potential risk to the blood supply for these pathogens.

Methods

Ethics Considerations

Routine informed consent obtained at the time of blood donation includes potential use of samples and demographic information for research purposes. The protocol for this study was approved by the American Red Cross Institutional Review Board (protocol no. 2021-038).

Study Population

We obtained residual serum and plasma samples from blood donations collected by the American Red Cross during December 2019–July 2020 from a selected number of states and counties. We restricted the study population to unique blood donors (all ≥16 years of age) who resided in a county endemic for either POWV or EEEV, which we defined as having either ≥2 human disease cases in 2019 or 1 case in 2019 and ≥1 case during 2010–2018 reported to CDC's ArboNET, the national arboviral disease surveillance system. We designed the criteria to capture counties with suitable habitats for the sustained circulation of the viruses resulting in human disease cases; however, we limited counties assessed to those with available blood donor samples.

Sampling Strategy

We selected samples using proportional-to-size stratified sampling by county. We specified the expected seroprevalences and acceptable margins of error (ME) on the basis of the only known previously published seroprevalence estimates, both from focal areas of New Jersey that experienced outbreaks of human POWV disease in 2019 (*11*) and EEEV disease in 1959 (*12*). For POWV, the expected seroprevalence was 0.5% and the ME 0.4%. Given the low expected seroprevalence, we used the available blood donor population, rather than the county population, to calculate sample sizes. For EEEV, the expected seroprevalence was 3% and the ME 2%. We used the 2020 United States Census Bureau County population of adults to determine the sample size needed to calculate EEEV population seroprevalence (*13*). We randomly chose samples from the available pool of donor samples in each county.

Laboratory Testing

We first screened samples for the presence of neutralizing antibodies against POWV, EEEV, or both, depending on the endemic county (Table 1). For initial POWV screening, we used a reporter virus–based microfocus neutralization reduction test (R-mFRNT) to identify positive samples as those with a 90% R-mFRNT (R-mFRNT$_{90}$) titer ≥10. For EEEV, we used plaque reduction neutralization test (PRNT) to identify positive samples as those with a 90% PRNT (PRNT$_{90}$) titer ≥10 (*14*). The high-throughput R-mFRNT method is based on the same principle as PRNT in measuring virus infection foci (plaques) reduction by neutralizing antibodies (*15*). The method uses live reporter–POWV and reporter–West Nile virus (WNV) that were engineered using the chimeric platform previously described (*16*). We validated the R-mFRNT$_{90}$ using reporter viruses against PRNT$_{90}$ using wild-type viruses with panels of positive POWV or WNV samples before use in this study and found strong correlation of the 90% effective concentrations between the R-mFRNT$_{90}$ and PRNT$_{90}$ assays.

We also endpoint titrated samples that screened positive for POWV neutralizing antibodies for both POWV and WNV by R-mFRNT$_{90}$ to assess potential cross-reactivity between the 2 flaviviruses. We conducted the endpoints of R-mFRNT$_{90}$ in 2-fold serial dilutions of samples in triplicate to determine the effective concentration for 90% neutralization (EC$_{90}$; concentration is the $\log_{10}$ reciprocal of dilutions) by the 4-parameter logistic curve analysis using GraphPad Prism version 10.1.2 (GraphPad Software Inc., https://www.graphpad.com). We used a ≥4-fold difference in the R-mFRNT$_{90}$ to confirm exposure to POWV or WNV. We considered similar titers (<4-fold difference) to both viruses as undifferentiated flavivirus exposures and did not include them in POWV seroprevalence estimates. We then tested samples positive for POWV- and EEEV-neutralizing antibodies for presence of IgM using IgM capture ELISA

Table 1. Demographics of blood donors tested for POWV and EEEV and disease cases and population census of selected counties of residence in study of seroprevalence in endemic areas, United States, 2019–2020*

Demographics	No. disease cases reported, 2010–2019		2020 US Census population, age ≥15 y	No. (%) specimens tested	
	POWV	EEEV		POWV	EEEV
Sex					
F				835 (47.2)	276 (48.7)
M				935 (52.8)	291 (51.3)
Age group, y					
16–29				225 (12.7)	65 (11.5)
30–49				436 (24.6)	147 (25.9)
50–64				751 (42.4)	243 (42.9)
≥65				358 (20.2)	112 (19.8)
State/county of residence					
Connecticut					
Fairfield	3		771,950	420	
Litchfield	2		155,110	164	
New London		3	224,538		17
Massachusetts					
Barnstable	5		187,694	21	
Bristol		4	467,915		36
Essex	9	3	650,007	184	49
Middlesex	10	3	1,343,808	337	100
Norfolk	2		583,823	206	
Plymouth		4	428,646		32
Worcester	2	4	684,405	160	52
Michigan					
Berrien		2	126,184		81
Cass		2	42,929		24
Kalamazoo		5	216,792		137
Van Buren		2	60,928		39
Minnesota					
Anoka	5		284,136	141	
Cass	2		24,286	3	
Itasca	7		37,544	8	
Morrison	3		26,551	8	
Wisconsin					
Jackson	2		16,881	16	
Shawano	2		33,692	3	
Trempealeau	2		23,357	19	
Wood	2		59,811	80	
Total				1,770	567

*Blank cells indicate not applicable. EEEV, Eastern equine encephalitis virus; POWV, Powassan virus.

(MAC-ELISA) for POWV and a microsphere immunoassay for EEEV to assess for evidence of recent infection, as previously described (*17*,*18*).

Statistical Analysis

We calculated seroprevalence estimates and 95% CIs at the county population level by calibrating the sample design weights to population age group distributions obtained from the 2020 US Census Bureau data (*13*). We calibrated sample weights using poststratification to the census data on the basis of the age group of the blood donors and county population. For the weighting calibration, we grouped age into 4 categories (Table 1) according to previously described methods (*19*). We computed estimates both for presence of neutralizing antibodies (any previous infection) and for presence of both neutralizing antibodies and IgM (recent infection) (*20*). We excluded counties with ≤5 blood donor samples because of instability in the estimates. For the county in which the source of infection was most likely outside the county of residence according to previous case investigations by the state health department, we restricted seroprevalence estimates to the county blood donor population, rather than to the general population.

To estimate the percentage of EEEV infections that resulted in neuroinvasive disease, we multiplied estimated county IgM seroprevalence (with 95% CI) by the county population (≥15 years of age, the closest available census data age category to the blood donor population) for the expected number of recent infections. We then divided the reported number of EEEV disease cases during June 2019–July 2020 by the expected number of recent infections (95% CI). We assumed IgM against EEEV persisted for up to 6 months for this calculation (*21*,*22*). We analyzed data using R version 4.3.1 using the survey package version 4.2 (*23*).

Results

POWV Seroprevalence

We tested a total of 1,770 samples from 15 counties in 4 states (Connecticut, Massachusetts, Minnesota, and Wisconsin) for evidence of POWV infection (Table 1; Figure 1). We found 50 (2.8%) samples had neutralizing antibodies for either POWV or WNV; 3 of those samples had WNV-specific neutralizing antibodies and 31 had indistinguishable results. Sixteen samples had POWV-specific neutralizing antibodies: 4 from Connecticut, 5 from Massachusetts, 3 from Minnesota, and 4 from Wisconsin (Table 2). County estimates by state among counties with locally acquired POWV infections ranged from 0% (95% CI 0%–2.28%) to 11.5% (95% CI 0.82%–40.9%). The highest and almost equivalent estimates were in 2 neighboring counties in Wisconsin: 11.5% (95% CI 0.82%–40.9%) and 11.5% (95% CI 0.87%–40.3%). Of the 16 samples with POWV-specific neutralizing antibodies, 6 (38%) were IgM positive. Recent seroprevalence estimates by county ranged from 0% (95% CI 0%–2.28%) to 1.68% (95% CI 0.14%–6.70%) (Table 2). In Anoka County, Minnesota, where cases were considered likely to be travel-associated, estimated county blood donor seroprevalence was 1.42% (95% CI 0.39%–5.02%) for any infection and 0.71% (95% CI 0.04%–3.91%) for recent infection (Table 2).

EEEV Seroprevalence

We tested a total of 567 samples from 10 counties in 3 states (Connecticut, Massachusetts, and Michigan) for evidence of EEEV infection (Table 1; Figure 2). Only 1 sample in Worcester County, Massachusetts, was positive for both neutralizing antibodies and IgM against EEEV, for an estimated recent infection seroprevalence of 1.62% (95% CI 0.04%–8.75%) (Table 3). The demographics of this blood donor did not match any of the EEEV disease case-patients reported to ArboNET; therefore, the donor most likely had an asymptomatic infection or nonneuroinvasive disease that was not diagnosed. The estimated total number of recent infections in Worcester was 11,086 (95% CI 272–59,912), and 3 human EEEV neuroinvasive disease cases were reported in the county in 2019, for a neuroinvasive disease–to-infection percentage of 0.027% (95% CI 0.005%–1.10%).

Discussion

On the basis of this blood donor serosurvey, we estimated that population seroprevalence for POWV and EEEV in the counties sampled is generally low. The finding of a low number of infections suggests the risk to the blood supply is minimal in most areas surveyed. However, 2 adjacent counties in Wisconsin had higher POWV seroprevalence than the others, suggesting a potential risk for blood donor infection, although the estimates were imprecise because of small numbers of blood donor samples available from those locations.

Limited data are published on human seroprevalence for POWV and EEEV. For POWV, in a household survey conducted after a 2019 cluster of POWV disease cases in a focal area of New Jersey, estimated neutralizing antibody seroprevalence was 1.1% (95% CI 0%–2.3%) and IgM seroprevalence was 0.31% (95%

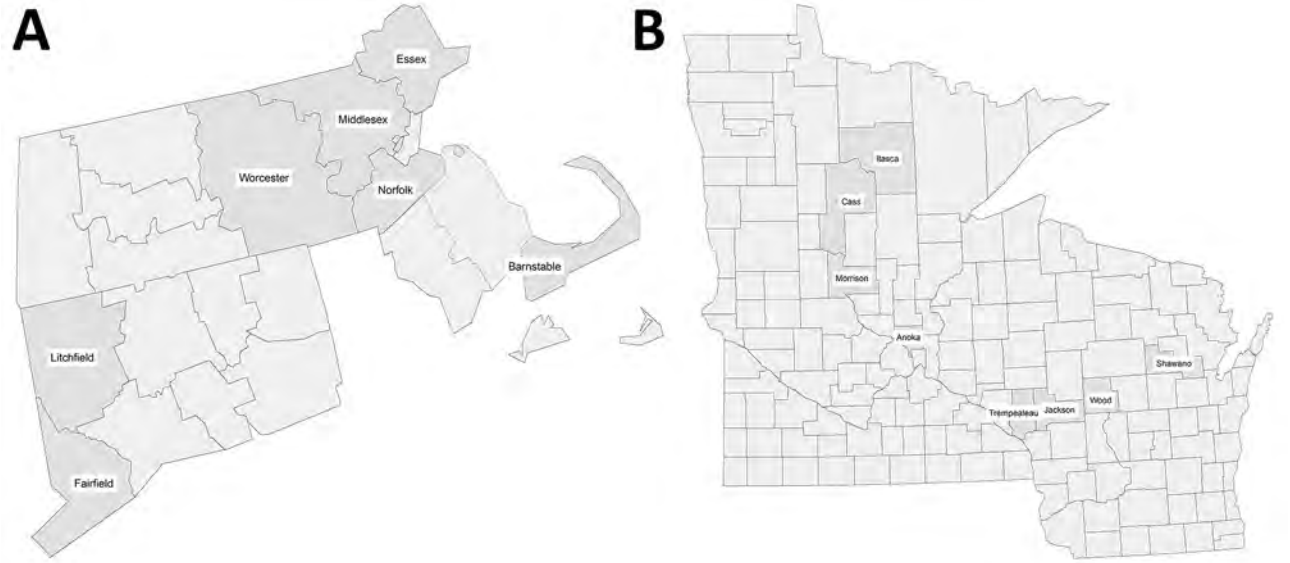

Figure 1. Selected counties for Powassan virus sampling in in study of Powassan virus and Eastern equine encephalitis virus seroprevalence in endemic areas, United States, 2019–2020. A) Connecticut and Massachusetts; B) Minnesota and Wisconsin.

Table 2. Blood donor and estimated population seroprevalence for Powassan virus in selected endemic counties in study of Powassan virus and Eastern equine encephalitis virus seroprevalence in endemic areas, United States, 2019–2020

			No. (%) donors			
	Calculated sample size	No. samples tested	Neutralizing antibody positive	Neutralizing antibody and IgM positive	% Seroprevalence (95% CI) Estimated*	Estimated recent†
Connecticut						
Fairfield	422	420	2 (0.48)	1 (0.24)	0.29 (0.04–1.04)	0.15 (0.00–0.81)
Litchfield	164	164	2 (1.2)	2 (1.2)	1.68 (0.14–6.70)	1.68 (0.14–6.63)
Massachusetts						
Barnstable	21	21	0	0	0 (0–16.1)	0 (0–16.1)
Essex	184	184	3 (1.6)	2 (1.1)	1.12 (0.22–3.32)	0.81 (0.09–2.96)
Middlesex	339	337	2 (0.59)	0	0.98 (0.10–3.67)	0 (0–1.09)
Norfolk	206	206	1 (0.49)	0	0.70 (0.02–3.81)	0 (0–1.77)
Worcester	160	160	0	0	0 (0–2.28)	0 (0–2.28)
Minnesota						
Anoka‡	141	141	2 (1.4)	1 (0.71)	1.42 (0.39–5.02)	0.71 (0.04–3.91)
Cass§	3	3	0	0	–	–
Itasca	8	8	0	0	0 (0–36.9)	0 (0–36.9)
Morrison	8	8	0	0	0 (0–36.9)	0 (0–36.9)
Wisconsin						
Jackson	16	16	1 (6.3)	0	11.48 (0.82–40.92)	0 (0–20.59)
Shawano§	3	3	0	0	–	–
Trempealeau	19	19	1 (5.3)	0	11.47 (0.87–40.3)	0 (0–17.65)
Wood	78	80	2 (2.5)	0	2.12 (0.27–7.37)	0 (0–4.51)

*Neutralizing antibodies present.
†Neutralizing antibodies and IgM present.
‡County where cases were suspected to be travel-associated rather than locally acquired.
§Counties with ≤5 samples were excluded from seroprevalence calculations.

CI 0.04%–1.0%) (*11*). Those estimates fell within the range of our county estimates for the 2 East Coast states in this study, Connecticut and Massachusetts, despite differences in methodologies and locations sampled. However, we did find higher POWV seroprevalence estimates in some Wisconsin counties. Geographic variation in occurrence and seroprevalence has been well documented for vectorborne diseases and is likely dependent on several factors, such as vector density, infection prevalence in vectors and animal reservoirs, climate effects on ecology, and human behavior affecting a person's risk for infection (*24*). Further study is warranted to obtain a more precise estimate of POWV seroprevalence in these counties in Wisconsin, the state of residence for the blood donor implicated in the only reported transfusion-transmitted POWV infection (*5*), to determine whether risk for infection might be heightened in that region.

The imprecision in the POWV estimates, particularly in the Midwestern states, precluded us from calculating the proportion of infections that resulted in neuroinvasive disease. Vahey et al. (*11*) reported that 23% (95% CI 7%–100%) of POWV infections result in neuroinvasive disease. That estimate is higher than those for WNV, in which neuroinvasive disease develops in <1% of infected persons (*25*–*27*).

Although we sampled from EEEV-endemic areas affected by the 2019 multistate EEEV disease outbreak (*10*), we found only 1 positive blood donor, for a county seroprevalence estimate of 1.6%. This finding was slightly lower but within the range of the only known published estimate of 2.3% (range by township 0.9%–6.2%) from a 1959 EEEV outbreak in New Jersey, despite differences in serologic methods used (*12*). The finding of just 1 blood donor with antibodies to EEEV after the large outbreak in the season before the samples were collected suggests that human infections are uncommon and the risk to the blood supply is limited.

Our estimate of the percentage of EEEV-infected persons who develop neuroinvasive disease was lower than that of the 1959 New Jersey study, which estimated 4.4% and ranged from 2% in younger adults to 13% in young children (*12*,*28*). Differences in the setting and methodologies of the studies make comparisons of estimates challenging; however, the upper limit of our 95% CI (1.1%) supports the approximation that <5% of EEEV infections result in neuroinvasive disease, although the risk varies by age group (*12*,*28*–*30*). Additional seroprevalence studies conducted after an outbreak could be done to calculate more precise estimates.

The first limitation of our study is that use of a convenience sample of blood donations collected by a single collection agency resulted in small sample sizes in some areas, limiting the precision of the estimates and our ability to assess all areas endemic for these viruses. The lack of blood donor samples from endemic areas such as New Jersey or New York precluded estimates and comparisons in those areas.

Figure 2. Selected counties for Eastern equine encephalitis virus sampling in study of Powassan virus and Eastern equine encephalitis virus seroprevalence in endemic areas, United States, 2019–2020. A) Connecticut and Massachusetts; B) Michigan.

Also, sample size calculations were based on the only known seroprevalence estimates from focal New Jersey outbreaks (11,12), which might have led to undersampling in some areas.

The blood donor population is not likely to be representative of the general population in all respects. In addition, the blood donor samples used for this study were collected during the early part of the COVID pandemic, which might have affected the characteristics of the donor population; donors in March 2020–February 2022 were more likely to be repeat donors who were older, white, and women than were donors in the previous 2 years (*31*). However, those demographic factors are not known to be associated with risk for arboviral disease. To address that limitation, we used similar weighting methods to other published studies to generate population estimates from blood donor seroprevalence (*19*,*25*,*32*). Our estimates are similar to those of previous household seroprevalence surveys for the target viruses (*11*,*12*), suggesting our results are plausible.

By testing for antibodies, we cannot directly determine the chance of viremia being present in a blood donor for these pathogens. However, the overall low occurrence of antibodies, including IgM, suggests that having a viremic blood donor would be even less common; for other arboviruses, IgM can persist for months

Table 3. Blood donor and estimated population seroprevalence for Eastern equine encephalitis virus in selected counties in study of Powassan virus and Eastern equine encephalitis virus seroprevalence in endemic areas, United States, 2019–2020

State/county	Calculated sample size	No. samples tested	No. (%) donors: Neutralizing antibody positive	No. (%) donors: Neutralizing antibody and IgM positive	% Seroprevalence (95% CI): Estimated*	% Seroprevalence (95% CI): Estimated recent†
Connecticut						
New London	17	17	0	0	0 (0–19.5)	0 (0–19.5)
Massachusetts						
Bristol	36	36	0	0	0 (0–9.74)	0 (0–9.74)
Essex	49	49	0	0	0 (0–7.25)	0 (0–7.25)
Middlesex	100	100	0	0	0 (0–3.62)	0 (0–3.62)
Plymouth	32	32	0	0	0 (0–10.9)	0 (0–10.9)
Worcester	52	52	1 (1.9)	1 (1.9)	1.62 (0.04–8.75)	1.62 (0.04–8.75)
Michigan						
Berrien	81	81	0	0	0 (0–4.45)	0 (0–4.45)
Cass	27	24	0	0	0 (0–14.3)	0 (0–14.3)
Kalamazoo	137	137	0	0	0 (0–2.66)	0 (0–2.66)
Van Buren	39	39	0	0	0 (0–9.03)	0 (0–9.03)

*Neutralizing antibodies present.
†Neutralizing antibodies and IgM present.

to years after infection, and viremia is present for up to 2 weeks (*21*,*33*,*34*). In addition, studies of WNV-infected blood donors suggest that viremic donors with IgM are less likely to be infectious than those without IgM (*21*,*35*). Consistent with that hypothesis, in the only report of POWV transmission through blood transfusion, the implicated donation was RNA positive and IgM negative (*5*). The duration of IgM persistence in POWV and EEEV is unknown. Although nucleic acid testing could have identified potentially infectious donors, given the low seroprevalence of infection, the likelihood of detecting RNA in an asymptomatic person would have been so low as to require a much larger sample size. Finally, we could have underestimated the seroprevalence of POWV, given that >50% of the flavivirus-positive specimens could not be differentiated between POWV and WNV.

In conclusion, in POWV- and EEEV-endemic areas of the United States sampled during 2019–2020, seroprevalence estimates for POWV and EEEV infection were generally low, suggesting a low risk for transmission by blood transfusion or organ transplantation. Further studies in the Wisconsin counties with higher seroprevalence estimates using high-throughput molecular assays and larger sample sizes could lead to improved understanding of risk. Potential blood donors could lower their risk for tick and mosquito bites by taking such steps as wearing long sleeves and pants, using Environmental Protection Agency–registered insect repellent, and treating clothing and gear with permethrin. Of note, POWV can be transmitted within 15 minutes of tick attachment, so preventing ticks from attaching and removing them before attachment is key (*36*). CDC will continue to work with partners to monitor infectious threats to blood transfusions and organ transplantation and identify prevention and control interventions to reduce the risk among transfusion and transplant recipients.

About the Author

Dr. Padda is an Epidemic Intelligence Service Officer in the Arboviral Diseases Branch, the Division of Vector-Borne Diseases, National Center for Emerging and Zoonotic Infectious Diseases, Centers for Disease Control and Prevention, Fort Collins, CO. Her research interests include infectious disease epidemiology and One Health.

References

1. Calisher CH. Medically important arboviruses of the United States and Canada. Clin Microbiol Rev. 1994;7:89–116. https://doi.org/10.1128/CMR.7.1.89
2. Krow-Lucal ER, Lindsey NP, Fischer M, Hills SL. Powassan virus disease in the United States, 2006–2016. Vector Borne Zoonotic Dis. 2018;18:286–90. https://doi.org/10.1089/vbz.2017.2239
3. Lindsey NP, Staples JE, Fischer M. Eastern equine encephalitis virus in the United States, 2003–2016. Am J Trop Med Hyg. 2018;98:1472–7. https://doi.org/10.4269/ajtmh.17-0927
4. Centers for Disease Control and Prevention. Powassan virus: historic data (2004–2023) [cited 2024 Oct 1]. https://www.cdc.gov/powassan/data-maps/historic-data.html
5. Taylor L, Stevens T, Destrampe EM, Brown JA, McGavic J, Gould CV, et al. Powassan virus infection likely acquired through blood transfusion presenting as encephalitis in a kidney transplant recipient. Clin Infect Dis. 2020.
6. Ciota AT. Eastern equine encephalitis virus taxonomy, genomics, and evolution. J Med Entomol. 2022;59:14–9. https://doi.org/10.1093/jme/tjab079
7. Centers for Disease Control and Prevention. Eastern equine encephalitis virus: historic data (2003–2023) [cited 2024 Oct 1]. https://www.cdc.gov/eastern-equine-encephalitis/data-maps/historic-data.html
8. Pouch SM, Katugaha SB, Shieh WJ, Annambhotla P, Walker WL, Basavaraju SV, et al. Transmission of eastern equine encephalitis virus from an organ donor to three transplant recipients. Clin Infect Dis. 2018.
9. Hill V, Koch RT, Bialosuknia SM, Ngo K, Zink SD, Koetzner CA, et al. Dynamics of eastern equine encephalitis virus during the 2019 outbreak in the Northeast United States. Curr Biol. 2023;33:2515–2527.e6. https://doi.org/10.1016/j.cub.2023.05.047
10. Lindsey NP, Martin SW, Staples JE, Fischer M. Notes from the field: multistate outbreak of eastern equine encephalitis virus—United States, 2019. MMWR Morb Mortal Wkly Rep. 2020;69:50–1. https://doi.org/10.15585/mmwr.mm6902a4
11. Vahey GM, Wilson N, McDonald E, Fitzpatrick K, Lehman J, Clark S, et al. Seroprevalence of Powassan virus infection in an area experiencing a cluster of disease cases: Sussex County, New Jersey, 2019. Open Forum Infect Dis. 2022;9:ofac023. https://doi.org/10.1093/ofid/ofac023
12. Goldfield M, Sussman O. The 1959 outbreak of Eastern encephalitis in New Jersey. I. Introduction and description of outbreak. Am J Epidemiol. 1968;87:1–10. https://doi.org/10.1093/oxfordjournals.aje.a120789
13. United States Census Bureau. American community survey [cited 2023 Oct 1]. https://www.census.gov/programs-surveys/acs/data.html
14. Beaty BJ, Calisher CH, Shope RE. Arboviruses. In: Lennette EH, Lennette DA, Lennette ET, editors. Diagnostic procedures for viral, rickettsial and chlamydial infections. 7th edition. Washington: American Public Health Association; 1995. p. 189–212.
15. Calvert AE, Horiuchi K, Boroughs KL, Ong YT, Anderson KM, Biggerstaff BJ, et al. The specificity of the persistent IgM neutralizing antibody response in Zika virus infections among individuals with prior dengue virus exposure. J Clin Microbiol. 2021;59:e0040021. https://doi.org/10.1128/JCM.00400-21
16. Baldwin WR, Livengood JA, Giebler HA, Stovall JL, Boroughs KL, Sonnberg S, et al. Purified inactivated Zika vaccine candidates afford protection against lethal challenge in mice. Sci Rep. 2018;8:16509. https://doi.org/10.1038/s41598-018-34735-7

17. Basile AJ, Horiuchi K, Panella AJ, Laven J, Kosoy O, Lanciotti RS, et al. Multiplex microsphere immunoassays for the detection of IgM and IgG to arboviral diseases. PLoS One. 2013;8:e75670. https://doi.org/10.1371/journal.pone.0075670
18. Martin DA, Biggerstaff BJ, Allen B, Johnson AJ, Lanciotti RS, Roehrig JT. Use of immunoglobulin M cross-reactions in differential diagnosis of human flaviviral encephalitis infections in the United States. Clin Diagn Lab Immunol. 2002;9:544–9.
19. Jones JM, Stone M, Sulaeman H, Fink RV, Dave H, Levy ME, et al. Estimated US infection- and vaccine-induced SARS-CoV-2 seroprevalence based on blood donations, July 2020–May 2021. JAMA. 2021;326:1400–9. https://doi.org/10.1001/jama.2021.15161
20. Korn EL, Graubard BI. Confidence intervals for proportions with small expected number of positive counts estimated from survey data. Surv Methodol. 1998;24:193–201.
21. Busch MP, Kleinman SH, Tobler LH, Kamel HT, Norris PJ, Walsh I, et al. Virus and antibody dynamics in acute West Nile virus infection. J Infect Dis. 2008;198:984–93. https://doi.org/10.1086/591467
22. Prince HE, Tobler LH, Yeh C, Gefter N, Custer B, Busch MP. Persistence of West Nile virus–specific antibodies in viremic blood donors. Clin Vaccine Immunol. 2007;14:1228–30. https://doi.org/10.1128/CVI.00233-07
23. Lumley T. Survey: analysis of complex survey samples. J Stat Software. 2004;9:1–19. https://doi.org/10.18637/jss.v009.i08
24. de Souza WM, Weaver SC. Effects of climate change and human activities on vector-borne diseases. Nat Rev Microbiol. 2024;22:476–91. https://doi.org/10.1038/s41579-024-01026-0
25. Busch MP, Wright DJ, Custer B, Tobler LH, Stramer SL, Kleinman SH, et al. West Nile virus infections projected from blood donor screening data, United States, 2003. Emerg Infect Dis. 2006;12:395–402. https://doi.org/10.3201/eid1205.051287
26. Mostashari F, Bunning ML, Kitsutani PT, Singer DA, Nash D, Cooper MJ, et al. Epidemic West Nile encephalitis, New York, 1999: results of a household-based seroepidemiological survey. Lancet. 2001;358:261–4. https://doi.org/10.1016/S0140-6736(01)05480-0
27. Williamson PC, Custer B, Biggerstaff BJ, Lanciotti RS, Sayers MH, Eason SJ, et al. Incidence of West Nile virus infection in the Dallas-Fort Worth metropolitan area during the 2012 epidemic. Epidemiol Infect. 2017;145:2536–44. https://doi.org/10.1017/S0950268816000042
28. Goldfield M, Welsh JN, Taylor BF. The 1959 outbreak of Eastern encephalitis in New Jersey. 5. The inapparent infection:disease ratio. Am J Epidemiol. 1968;87:32–3. https://doi.org/10.1093/oxfordjournals.aje.a120807
29. Deresiewicz RL, Thaler SJ, Hsu L, Zamani AA. Clinical and neuroradiographic manifestations of eastern equine encephalitis. N Engl J Med. 1997;336:1867–74. https://doi.org/10.1056/NEJM199706263362604
30. Luethy D. Eastern, western, and Venezuelan equine encephalitis and West Nile viruses: clinical and public health considerations. Vet Clin North Am Equine Pract. 2023;39:99–113. https://doi.org/10.1016/j.cveq.2022.11.007
31. Conti G, Notari EP IV, Dodd RY, Kessler D, Custer B, Bruhn R, et al.; U.S. Transfusion-Transmissible Infections Monitoring System (TTIMS). Changes in transfusion-transmissible infection prevalence and demographics among US blood donors during the COVID-19 pandemic. Transfusion. 2024;64:1040–9. https://doi.org/10.1111/trf.17851
32. Lindsey NP, Menitove JE, Biggerstaff BJ, Turabelidze G, Parton P, Peck K, et al. Seroprevalence of Heartland virus antibodies in blood donors, northwestern Missouri, USA. Emerg Infect Dis. 2019;25:358–60. https://doi.org/10.3201/eid2502.181288
33. Griffin I, Martin SW, Fischer M, Chambers TV, Kosoy O, Falise A, et al. Zika virus IgM detection and neutralizing antibody profiles 12–19 months after illness onset. Emerg Infect Dis. 2019;25:299–303. https://doi.org/10.3201/eid2502.181286
34. Staples JE, Gibney KB, Panella AJ, Prince HE, Basile AJ, Laven J, et al. Duration of West Nile virus immunoglobulin M antibodies up to 81 months following West Nile virus disease onset. Am J Trop Med Hyg. 2022;106:1721–4. https://doi.org/10.4269/ajtmh.21-1234
35. Pealer LN, Marfin AA, Petersen LR, Lanciotti RS, Page PL, Stramer SL, et al.; West Nile Virus Transmission Investigation Team. Transmission of West Nile virus through blood transfusion in the United States in 2002. N Engl J Med. 2003;349:1236–45. https://doi.org/10.1056/NEJMoa030969
36. Ebel GD, Kramer LD. Short report: duration of tick attachment required for transmission of powassan virus by deer ticks. Am J Trop Med Hyg. 2004;71:268–71. https://doi.org/10.4269/ajtmh.2004.71.3.0700268

Address for correspondence: Carolyn Gould, Centers for Disease Control and Prevention, 3156 Rampart Rd, Mailstop P-02, Fort Collins, CO 80521, USA; email: cgould@cdc.gov

Highly Pathogenic Avian Influenza A(H5N1) Outbreak in Endangered Cranes, Izumi Plain, Japan, 2022–23

Mana Esaki,[1] Kosuke Okuya,[1] Kaori Tokorozaki, Yuko Haraguchi, Taichi Hasegawa, Makoto Ozawa

During the 2022–23 winter season, >1,500 endangered cranes, including hooded cranes (*Grus monacha*) and white-naped cranes (*Grus vipio*), were found debilitated or dead in the Izumi Plain, Japan. Most of the cranes, particularly those collected in November, were infected with highly pathogenic avian influenza (HPAI) H5N1 viruses; virus shedding was higher from the trachea than from the cloaca. The isolation rate from the cranes' roost water was not markedly higher than that of previous seasons, suggesting that the viruses might be more effectively transmitted among cranes via the respiratory route than through feces. Most wild bird–derived H5N1 isolates were phylogenetically distinct from viruses isolated on nearby chicken farms, indicating limited relationship between the wild bird and chicken isolates. Serologic analyses suggested that herd immunity had little effect on outbreak subsidence. This study deepens our understanding of the circumstances surrounding the unexpected HPAI outbreaks among these endangered cranes.

The Izumi Plain in Kagoshima Prefecture, Japan, is an internationally important wetland registered under the Ramsar Convention. It serves as a crucial wintering site for ≈70% of the global population of hooded cranes (*Grus monacha*) (*1*–*3*) and 20% of white-naped cranes (*Grus vipio*) (*1*,*2*,*4*). To support the conservation of those endangered species, artificial wet paddies are systematically established to provide roosting areas every winter. The roosting sites are also frequented by wild ducks, such as mallards (*Anas platyrhynchos*) and Eurasian wigeons (*Mareca penelope*). Of note, wild waterfowl belonging to the orders Anseriformes and Charadriiformes are known natural reservoirs of avian influenza viruses (AIVs) (*5*,*6*), which raises concerns about possible transmission of AIVs to cranes through shared roost water. We established efficient methods to isolate AIVs from the roost water of cranes and have been monitoring AIVs every winter season since 2012 (*7*–*15*).

We previously isolated highly pathogenic avian influenza (HPAI) subtype H5 viruses from the roost water of cranes and dead or debilitated cranes in the Izumi Plain during the 2014–15, 2016–17, 2020–21, and 2021–22 winter seasons (*12*–*15*). Despite the frequent isolation of HPAI viruses (HPAIVs) from the roost water of cranes, only a few cranes were confirmed to be infected with HPAI H5 virus. For example, during the 2020–21 winter season, we isolated 29 HPAI H5N8 viruses from the roost water of cranes and confirmed 6 cases of HPAI H5N8 infection in dead cranes (*13*). Overall, our previous reports suggested that endangered cranes have low susceptibility to HPAI infection and that the viruses have been circulating primarily among wild ducks in the Izumi Plain.

During the 2022–23 winter season, we encountered a large HPAI outbreak among the endangered cranes in the Izumi Plain. More than 1,500 cranes, most of which were hooded and white-naped cranes, died likely because of HPAI H5N1 infection (*16*). Of note, 11 HPAI outbreaks on chicken farms were reported from the Izumi Plain during the same winter season (*17*), leading us to speculate that the HPAIVs circulating among the endangered cranes may have accidentally and repeatedly invaded the nearby chicken farms. Here, we aimed to describe the details of the unexpected HPAI outbreak among the wild birds in the Izumi Plain, including the results of genetic and serologic analyses of the isolated viruses.

Materials and Methods

Ethics Statement

We conducted this study in compliance with the International Guiding Principles for Biomedical Research

Author affiliations: Kagoshima University, Kagoshima, Japan (M. Esaki, K. Okuya, M. Ozawa); Crane Park Izumi, Kagoshima, Japan (K. Tokorozaki, Y. Haraguchi); Matsuoka Research Institute for Science, Tokyo, Japan (T. Hasegawa)

DOI: https://doi.org/10.3201/eid3105.241410

[1]These authors contributed equally to this article.

Involving Animals, Japan's Act on Conservation of Endangered Species of Wild Fauna and Flora, and the regulations of the Kagoshima University Research Ethics Committee. No animal experiments were conducted as part of this study. Veterinary staff at the crane observatory center collected swab samples for analysis from wild cranes during the wintering period. We carried out all handling procedures to minimize stress and ensure the welfare of the animals.

Sample Collection

We collected tracheal and cloacal swab samples from 317 debilitated or dead wild birds (295 cranes and 22 other bird species) that were found in the Izumi Plain during November 2022–April 2023. We suspended the collected swab samples in BD Universal Viral Transport Medium (BD, https://www.bd.com) and stored at ≤4°C until further use.

We collected environmental water samples weekly (50 mL/sample) from 2 crane roost sites, a total of 14 spots/week, at the Izumi Plain, following the same protocol as in the 2020–21 (*13*) and 2021–22 (*18*) winter seasons. We collected a total of 196 samples during November 7, 2022–February 20, 2023 and stored them at ≤4°C until further use (Appendix Figure 1, https://wwwnc.cdc.gov/EID/article/31/5/24-1410-App1.pdf).

AIV Isolation

For AIV isolation, we filtered the collected swab samples through a 0.22-μm pore membrane (Sartorius, https://www.sartorius.com) and inoculated into the allantoic cavity of 10-day-old embryonated chicken eggs (2 eggs/sample), as described previously (*8*). We isolated AIVs from the collected water samples as described previously (*14*). In brief, we added chicken red blood cells to roost water samples of cranes that potentially contained AIVs and subsequently inoculated those cells into the allantoic cavity of 10-day-old embryonated chicken eggs (4 eggs/sample). We incubated the inoculated eggs at 37°C for 2 days. We used hemagglutination assay (*8*) to confirm AIV isolation.

AIV Gene Detection from Swab Samples and Allantoic Fluids

We extracted RNA from swab samples and allantoic fluids using the innuPREP Virus DNA/RNA Kit (Analytik Jena AG, https://www.analytik-jena.com) and used for influenza A viral gene detection via 1-step real-time reverse transcription PCR RT-PCR with the iTaq Universal SYBR Green One-Step Kit (Bio-Rad Laboratories, https://www.bio-rad.com) and primer sets specific for the H5 hemagglutinin (HA), H7 HA, and matrix (M) genes (*10*). To calculate gene copy number from swab samples, we used plasmids (pCR-Blunt II-TOPO; Thermo Fisher Scientific, https://www.thermofisher.com) inserted with the M gene of A/California/04/2009 (H1N1) for constructing standard curves.

Targeted Sequencing of H5 HA Cleavage Site

We subjected the sample-derived RNAs in which the H5 HA gene was detected to sequence the H5 HA cleavage site to genetically evaluate viral pathogenicity. Using H5 HA gene–positive samples as a template, we amplified the H5 HA cleavage site through PCR with the PrimeScript One-Step RT-PCR Kit Version Two (TaKaRa Bio Inc., https://www.takara-bio.com) and a primary primer set specific for the full-length H5 HA gene; 5′-CAGGGGTTCAMTCTGTCAAAATGGA-3′ (H5-uni-f_mod) and 5′-ACAAGGGTGTTTTTAACTACAATCTGA-3′ (H5-uni-r_mod), followed by nested PCR with the Tks Gflex DNA Polymerase (TaKaRa Bio Inc.) and a secondary primer set; 5′-AACGTGGAAGAATGGAYTTC-3′ (H5_713F) and 5′-TGTCTGCAGCGTACCCACT-3′ (H5_cle-1149R). We determined nucleotide sequences of the cleavage sites in the H5 HA gene through Sanger sequencing (Azenta Inc., https://www.azenta.com).

HA and NA Subtyping

To identify potential singular isolates from the allantoic fluids inoculated with the roost water samples of cranes, we subjected the M gene–positive RNA samples to additional scrutiny through real-time RT-PCR with primer sets specific to the H1, H3, H4, H6, and H10 HA genes; those genes have been frequently detected in the Izumi Plain since 2012 (*13*). RNA samples that responded exclusively to a single HA subtype–specific primer set were subjected to reverse transcription using SuperScript IV reverse transcription (Thermo Fisher Scientific) for complementary DNA (cDNA) synthesis. cDNA served as the template for conventional PCR-based HA and NA subtyping using Tks Gflex DNA Polymerase (TaKaRa Bio Inc.), along with a set of subtype-specific primer sets (*19*).

Comprehensive Sequencing of AIV Genes

Using AIV cDNA as the template, we amplified each gene segment using Tks Gflex DNA Polymerase and KOD One PCR Master Mix-Blue (TOYOBO Co., Ltd., https://www.toyobo-global.com), in conjunction with gene segment-specific primer sets (*20*), through conventional PCR. Subsequently, we determined the nucleotide sequences of the open reading frames for all viral gene segments through nanopore sequencing

using the MinION Mk1b system (Oxford Nanopore Technologies, https://nanoporetech.com), as described previously (*21*). In brief, we purified PCR amplicons and performed adaptor ligation using a direct cDNA sequencing kit (Oxford Nanopore Technologies), along with a native barcoding expansion kit (Oxford Nanopore Technologies). We conducted sequencing using the Flongle flow cells (Oxford Nanopore Technologies).

We generated consensus sequences for each gene segment using Geneious Prime version 2021.1.1 (Biomatters Ltd, https://www.geneious.com). The nucleotide sequences have been deposited in the GISAID database (http://www.gisaid.org) (Table 1; Appendix Tables 2, 3).

Phylogenetic Analyses

We conducted phylogenetic analysis on the nucleotide sequences of viral gene segments obtained from the isolates, along with their representative counterparts retrieved from the GISAID database; the analysis captured the temporal and spatial distribution of AIVs. We aligned the sequences using the MUSCLE program (*22*) and constructed phylogenetic trees for each viral gene using the maximum-likelihood method in MEGA 7 software (*23*) with a bootstrapping set of 1,000 replicates.

Hemagglutination Inhibition Assay

We evaluated neutralizing antibody titers against HPAI H5 viruses using hemagglutination inhibition (HI) assays as described in the World Health Organization standards (*24*). We treated 30 crane serum samples with receptor destroying enzyme (Denka-Seiken, https://www.denka.co.jp), according to the manufacturer's instructions. Those samples were collected from the debilitated or dead wild cranes found in the Izumi Plain during November 2021–March 2023 (Appendix Table 4). For the viral antigens, we selected 5 genetically diverse HPAI H5 viruses isolated from the Izumi Plain: A/hooded crane/Kagoshima/KU-106/2021 (H5N8) (G1 group), A/hooded crane/Kagoshima/

Table. HI titers for HA antigen in serum samples of cranes tested for influenza A, Izumi Plain, Japan*

Crane sample	Genetic testing for HPAI H5N1	HA antigen titer				
		A/hooded crane/Kagoshima/KU-106/2021 (H5N8) G1 group	A/hooded crane/Kagoshima/KU-5T/2021 (H5N8) G2a subgroup	A/crane/Kagoshima/KU-93/2021 (H5N8) G2a subgroup	A/Environment/Kagoshima/KU-B20/2021 (H5N1) G2b subgroup	A/hooded crane/Kagoshima/KU-105/2022 (H5N1) G2c subgroup
2021–22						
21–8	Neg	ND	ND	ND	4	ND
21–11	Neg	ND	ND	ND	ND	ND
21–14	Neg	8	ND	ND	4	4
21–15	Neg	ND	ND	ND	ND	ND
21–21	Neg	ND	ND	ND	ND	ND
21–19	Neg	ND	ND	ND	ND	ND
21–20	Neg	ND	ND	ND	ND	ND
21–10	Neg	ND	ND	ND	ND	4
21–36	Neg	ND	ND	ND	ND	ND
21–38	Neg	ND	ND	ND	ND	ND
21–51	Neg	ND	ND	ND	ND	ND
21–52	Neg	ND	ND	ND	ND	ND
21–53	Neg	ND	ND	ND	ND	ND
2022–23						
22–105	Pos	4	ND	ND	8	8
22–151	Pos	8	4	4	8	16
22–152	Pos	ND	ND	ND	8	8
22–265	Neg	ND	ND	ND	ND	ND
22–272	Pos	4	ND	ND	4	4
22–278	Neg	ND	ND	ND	ND	ND
22–280	Neg	ND	ND	ND	ND	ND
22–281	Neg	ND	ND	ND	ND	ND
22–282	Neg	ND	ND	ND	ND	ND
22–283	Neg	ND	ND	ND	ND	ND
22–285	Neg	ND	ND	ND	ND	ND
22–286	Neg	ND	ND	ND	ND	ND
22–287	Neg	8	8	4	16	16
22–288	Neg	8	4	ND	16	16
22–289	Neg	ND	ND	ND	ND	4
22–313	Neg	ND	ND	ND	ND	ND
22–318	Neg	ND	ND	ND	ND	ND

*HI, hemagglutination inhibition; HPAI, highly pathogenic avian influenza; ND, specific antibody was not detected (detection limit: 4 HI titer); Neg, negative; Pos, positive.

KU-5T/2021 (H5N8) (G2a subgroup), A/crane/Kagoshima/KU-93/2021 (H5N8) (G2a subgroup), A/environment/Kagoshima/KU-B20/2021 (H5N1) (G2b subgroup), and A/hooded crane/Kagoshima/KU-105/2022 (H5N1) (G2c subgroup) (*7*,*13*,*14*).

Results

Large-Scale Mortality of Endangered Cranes in the Izumi Plain

During the 2022–23 winter season, 1,425 hooded and 79 white-naped cranes were found debilitated or dead in the Izumi Plain (Appendix Table 1). The peak daily collection number reached 92 cranes on November 18, 2022 (Figure 1, panel A). The number of collected cranes gradually decreased; daily collections averaged ≤10 cranes from mid-December onward. We collected swab samples from 295/1,504 cranes and subjected them to genetic testing for influenza A viral M and H5 HA genes. We further analyzed the H5 HA-positive samples by sequencing the H5 HA cleavage site, revealing that 170 (57.6%) cranes tested positive for HPAI H5N1 viruses (Figure 1, panel B). Although most (132/138 [95.7%]) of the samples collected in November were positive for HPAI H5N1 viruses, the positivity ratio began to decrease in samples collected in December (Figure 2). Of note, a swab sample collected on March 20, 2023, tested positive, indicating the circulation of HPAIVs by the end of the winter season in the Izumi Plain.

To isolate HPAI viruses from the samples that tested positive for HPAI H5N1, we inoculated all swab samples from the 170 cranes into embryonated chicken eggs. We isolated 136 HPAI H5N1 viruses from the swab samples (Appendix Table 1).

HPAI H5N1 Virus Shedding of in Endangered Cranes

To compare oral and cloacal virus shedding from the HPAI H5N1–infected cranes, we measured numbers of copies of influenza A viral M gene in their tracheal and cloacal swab specimens individually. However, we combined the tracheal and cloacal swab specimens collected from the same cranes before analysis beginning November 22, 2022, because of the drastic increase in the number of cases and shortage of equipment. In total, we tested tracheal and cloacal swab samples from 86 cranes collected during November 1–21, 2022, in this study (Figure 3; Appendix Table 2, Figure 2). In addition, we included RNA extracted from the swab samples of 7 HPAI-infected cranes from previous seasons as comparison controls (*13*,*14*). We found that the gene copy numbers in tracheal swab samples were significantly higher than those in cloacal swab samples during the 2022–23 season, as confirmed by a paired *t*-test ($p<0.05$); however, we observed no significant difference during the 2020–21 and 2021–22 seasons (Figure 3). Our results suggest that virus shedding in the cranes was more pronounced in the trachea than in the cloaca.

Limited Number of HPAI Virus Isolates from Roost Water

A total of 53 of 196 allantoic fluid samples acquired from the eggs inoculated with roost water samples of

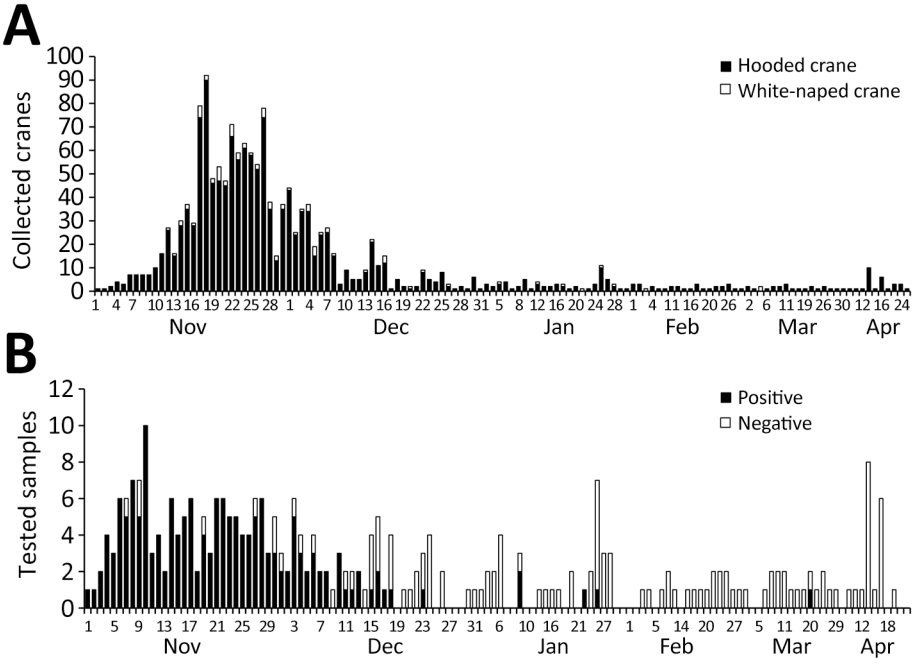

Figure 1. Numbers of collected cranes in the Izumi Plain, Japan, and the samples subjected to genetic testing for influenza A viral matrix (M) and H5 hemagglutinin (HA) genes during the 2022–23 winter season. A) Number of debilitated and dead cranes collected in the Izumi Plain per day. B) Number of cranes subjected to genetic testing for influenza A viral M and H5 HA genes per day.

cranes tested positive for influenza A viral M gene. We identified HA genes of multiple subtypes, including the H5 genes, in 15/53 samples; we excluded those 15 samples from further genetic analyses. Genetic analyses of the HA and NA genes revealed that the remaining 38 AIVs were singular isolates; we classified 24 as subtype H5N1, 8 as H3N8, and 6 as H10N6 (Appendix Table 3). Despite the large HPAI H5N1 outbreak among the endangered cranes, the number of HPAIV isolates from the roost water of cranes during the 2022–23 season was not markedly higher than that in previous seasons; we identified 107 (42.46%) HPAIV-containing isolates out of 252 samples during the 2020–21 season (*13*) and 29 (14.80%) HPAIV-containing isolates out of 196 samples during the 2021–22 winter season (*18*) (Figure 4). The ratio of HPAIV-containing isolates during the 2022–23 season (37/196 [18.88%] samples) was significantly lower than that in the 2020–21 season ($p<0.05$ by χ^2 test); no significant difference was observed between the 2022–23 and 2021–22 seasons. Those results suggest that virus shedding from the HPAIV-infected cranes into environmental water was minimal. Furthermore, considering that virus shedding in the cranes was more evident in the tracheal swab than in the cloacal swab samples, HPAI H5N1 viruses might be effectively transmitted via the respiratory route among the cranes, rather than through waterborne transmission.

AIV Isolation from Other Bird Species

We isolated 2 HPAI H5N1 virus strains, A/northern pintail/Kagoshima/KU-64/2022 (H5N1) and A/black kite/Kagoshima/KU-140/2022 (H5N1), and 1 low pathogenicity avian influenza (LPAI) H11N9 virus, A/mallard/Kagoshima/KU-131/2022 (H11N9), from 22 wild birds other than cranes collected in the Izumi Plain (Appendix Table 2). The results indicated that HPAI H5N1 viruses were spread not only among cranes but also among other species of wild birds in the Izumi Plain during the 2022–23 season.

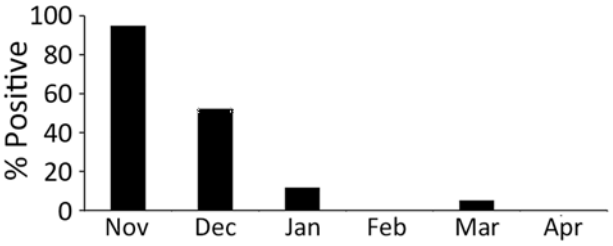

Figure 2. Monthly rate of highly pathogenic avian influenza A(H5N1) infection among tested cranes in the Izumi Plain, Japan, 2022–23 winter season.

Detection of Multiple Genotypes of HPAI H5N1 Viruses

We phylogenetically genotyped the HPAI H5N1 isolates for genetic characterization of each gene segment (Appendix Table 5); we constructed phylogenetic trees for representative H5N1 isolates from each genotype (Figure 5; Appendix Figure 3). We categorized the HA genes of the H5N1 isolates, except those of A/hooded crane/Kagoshima/KU-40/2022 (H5N1), into the G2c subgroup (Figure 5, panel A). The HA gene of A/hooded crane/Kagoshima/KU-40/2022 (H5N1) formed a cluster with HPAI H5 viruses

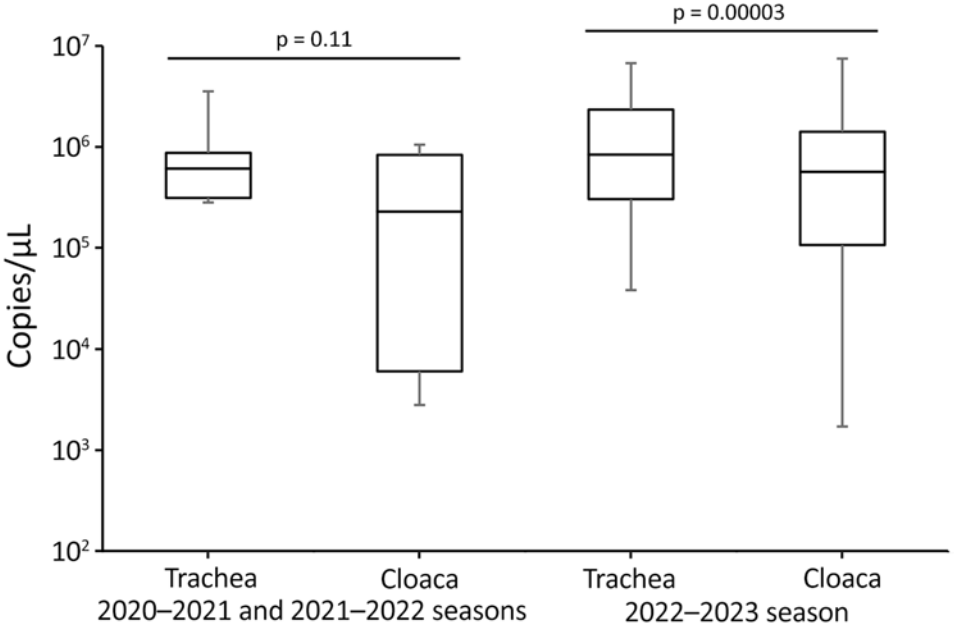

Figure 3. Box-and-whisker plot showing the distribution of copy numbers of the avian influenza virus (AIV) matrix (M) gene in swabs from AIV gene–positive cranes from the 2022–23 winter season compared with the combined 2020–21 and 2021–22 seasons in the Izumi Plain, Japan. We used RNA extracted from each AIV gene–positive swab sample for quantifying the copy number of the AIV M gene using real-time reverse transcription PCR. Boxes represent interquartile ranges; horizontal lines inside boxes indicates median; whiskers indicate maximum and minimum values. We evaluated significant differences between groups by paired *t*-test; $p<0.05$ was considered statistically significant.

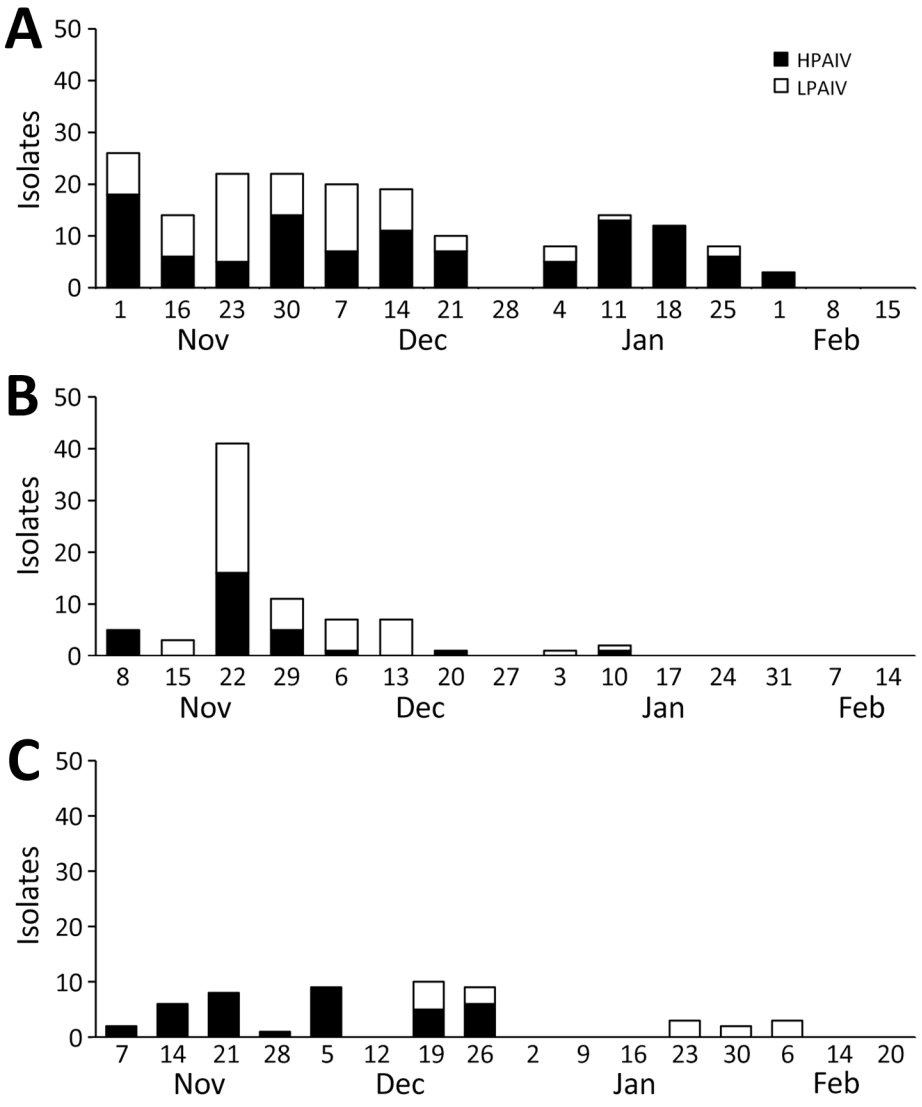

Figure 4. Avian influenza virus (AIV) isolation from roost water of cranes in the Izumi Plain, Japan. Weekly representation illustrates the numbers of AIV-positive allantoic fluid samples during the 2020–21 (A) (*13*), 2021–22 (B) (*18*), and 2022–23 (C) winter seasons. Bars show AIV isolates containing HPAIV H5 and those containing LPAIV. The weekly chart displays the number of AIV-positive allantoic fluid samples. HPAIV, highly pathogenic avian influenza virus; LPAIV, low pathogenicity avian influenza virus.

mainly isolated from chicken farms in Japan, including 9 farms in the Izumi Plain (https://www.maff.go.jp/j/syouan/douei/tori/220929.html#2) (*25*), during the 2022–23 winter season and was categorized into the G2b subgroup (Figure 5, panel A). Those results indicate that HPAI H5N1 virus strains circulating among the crane population were genetically distinct from those isolated from chicken farms, suggesting that the invasion of HPAIV in the farms was not attributable to the crane species.

Genetic analyses revealed that the N1 NA genes could be classified into 2 genetic clusters, N1-I and N1-II (Figure 5, panel B). Similarly, we classified the PB2, NP, and NS genes into 6 genetic clusters, the PB1 and PA genes into 7 genetic clusters, and the M gene into 5 genetic clusters (Appendix Table 5, Figure 3). According to the genetic clusters of the remaining 6 gene segments, we classified HPAI H5N1 virus strains isolated in this study into 13 genotypes (H5N1-I to -XIII) (Appendix Table 5). Furthermore, genetic analyses of LPAI viruses revealed that 4 genotypes of H3N8 (H3N8-I to -IV) and 2 genotypes of H10N6 (H10N6-I and -II) were introduced into the Izumi Plain during the 2022–23 winter season (Appendix Table 5, Figure 4). We found that multiple genotypes of H5N1 HPAIVs were introduced into the Izumi Plain in the early winter season. Of note, the PA gene of A/hooded crane/Kagoshima/KU-38/2022 (H5N1), whose HA gene was categorized to the G2c subgroup, was almost identical to that of A/hooded crane/Kagoshima/KU-40/2022 (H5N1), whose HA gene was categorized into the G2b subgroup (Appendix Figure 3, panel C). Those results suggest that a genetic reassortment event occurred among the H5N1 HPAIVs circulating in the Izumi Plain.

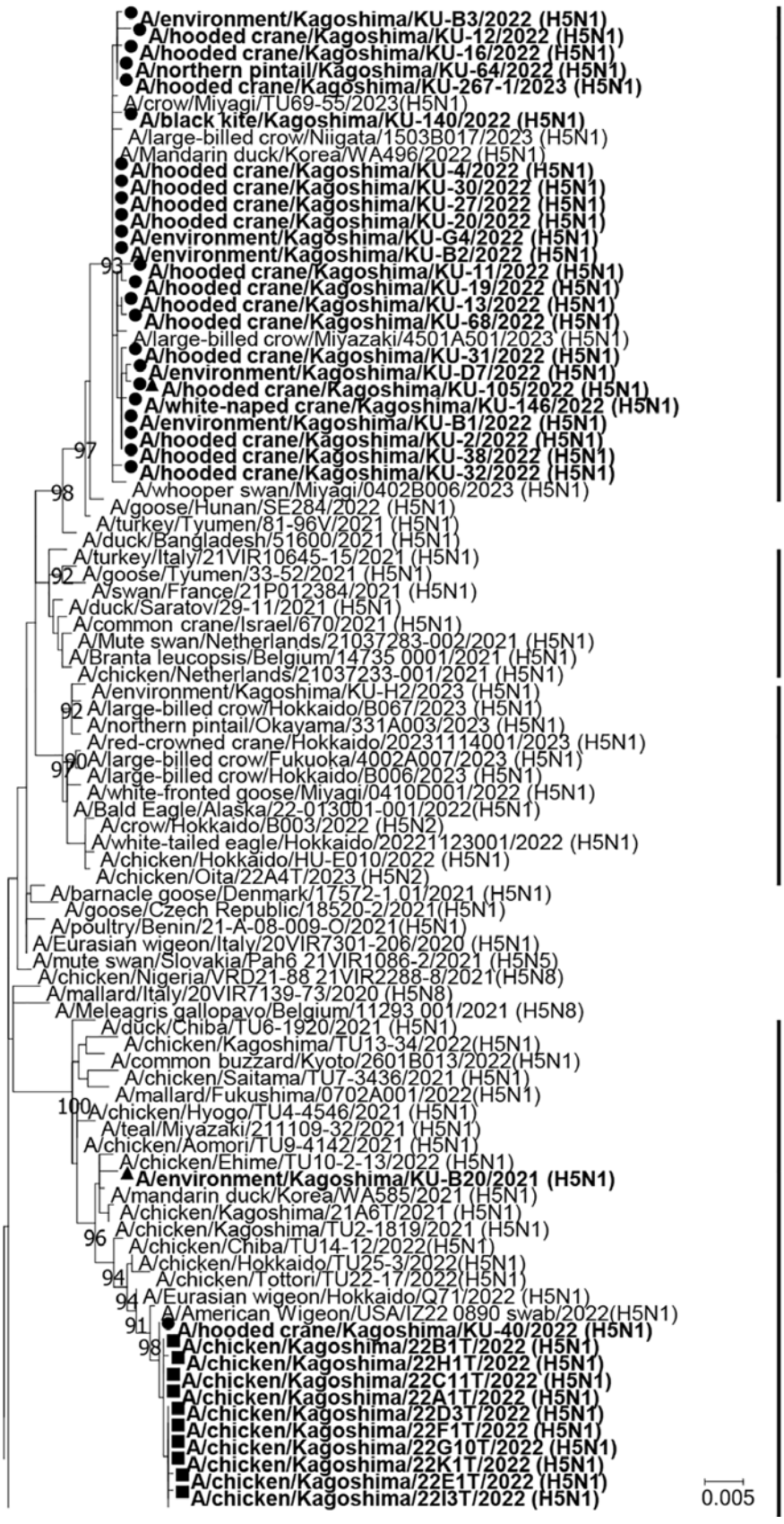

Figure 5. A portion of the phylogenetic tree of H5 hemagglutinin (HA) genes from avian influenza virus gene–positive cranes from the 2022–23 winter season in the Izumi Plain, Japan, compared with reference sequences. Tree was constructed using the maximum-likelihood method with a bootstrapping set of 1,000 replicates. Circles indicate isolates from wild birds and cranes' roost water during the 2022–23 winter season. Squares indicate isolates from chickens during the same season. Triangles indicate H5 HA genes of highly pathogenic avian influenza viruses used for the hemagglutination inhibition assay. Scale bar indicates nucleotide substitutions per site. An expanded figure showing the full tree is available online (https://wwwnc.cdc.gov/EID/article/31/5/24-1410-F5.htm).

Figure 6. A portion of the phylogenetic tree of N1 neuraminidase (NA) genes from avian influenza virus gene–positive cranes from the 2022–23 winter season in the Izumi Plain, Japan, compared with reference sequences. Tree was constructed using the maximum-likelihood method with a bootstrapping set of 1,000 replicates. Nodes with bootstrap values >90% are shown. Circles indicate isolates from the 2022–23 winter season. Triangles indicate H5 NA genes of highly pathogenic avian influenza viruses used for the hemagglutination inhibition assay. Scale bar indicates of nucleotide substitutions per site. An expanded figure showing the full tree is available online (https://wwwnc.cdc.gov/EID/article/31/5/24-1410-F6.htm).

HI Titer against H5 HPAIVs in Crane Serum

To assess herd immunity against HPAIV infection among endangered cranes, we measured antibody titers using HI assay in 30 crane serum samples: 13 serum samples collected during the 2021–22 winter season and 17 serum samples collected during the 2022–23 winter season (Appendix Table 4). Of note, 14/17 serum samples were collected during January–February 2023, after the large outbreak of HPAI H5N1 infection in the Izumi Plain. Among 17 cranes from which serum samples collected during the 2022–23 winter season, 4 cranes (i.e., cranes 22-105, 22-151, 22-152, and 22-272) had been confirmed to be infected with H5N1 HPAIV. We selected 5 phylogenetically distant HPAI H5 viruses as viral antigens: A/hooded crane/Kagoshima/KU-106/2021 (H5N8) from G1 group, A/hooded crane/Kagoshima/KU-5T/2021 (H5N8) from G2a subgroup, A/crane/Kagoshima/KU-93/2021 (H5N8) from G2a subgroup, A/environment/Kagoshima/KU-B20/2021 (H5N1) from G2b subgroup, and A/hooded crane/Kagoshima/KU-105/2022 (H5N1) from G2c subgroup (Figure 5).

We detected specific antibodies against ≥1 HPAI H5 viruses in 3 (23.1%) of 13 serum samples collected during the 2021–22 winter season and in 7 (41.2%) of 17 samples from the 2022–23 winter season (Table 1). Although the antibody-positive rate in crane serum samples collected during the 2022–23 winter season was higher than that for samples collected during the 2021–22 winter season, it was unexpectedly lower even after the large HPAI outbreak (*26*–*28*). Those results suggest the limited contribution of herd immunity to the subsidence of the outbreak among endangered cranes.

Discussion

We report a large HPAI outbreak among endangered cranes. In total, 1,504 debilitated or dead endangered cranes were collected during the 2022–23 winter season in the Izumi Plain, Japan (Figure 1, panel A). We confirmed that most of the debilitated or dead cranes, particularly those collected in November (95.7%), were infected with H5N1 viruses (Figure 1, panel B).

In wild ducks, LPAI viruses mainly replicate in the intestine and are thus shed in the feces (*5*,*6*). Environmental water contaminated with the feces of wild ducks has been effectively used for AIV surveillance in the Izumi Plain since 2012 (*10*,*11*,*13*,*14*,*18*,*29*). During the 2022–23 winter season, we isolated 24 HPAI H5N1 virus strains from the roost water of cranes (Appendix Table 3). Despite the large outbreak of HPAI H5N1 among endangered cranes, the number of water HPAI isolates during the 2022–23 winter season was not markedly higher than that in previous seasons (Figure 4). In addition, the gene copy numbers of HPAIVs in tracheal swabs from the infected cranes were higher than those in cloacal swabs (Figure 3), indicating high virus shedding in the respiratory tracts. Overall, these findings suggest that HPAI H5N1 circulating among the endangered cranes during the 2022–23 season might have been transmitted more efficiently via the respiratory route rather than through environmental water.

We isolated 162 HPAI H5N1 viruses of the G2c subgroup from wild birds and roost water of cranes during the 2022–23 winter season; we categorized 1 isolate, A/hooded crane/Kagoshima/KU-40/2022 (H5N1), in the G2b subgroup. Of note, all HPAIVs isolated from 9 chicken farms in the Izumi Plain during the 2022–23 winter season belonged to the G2b subgroup (Figure 5, panel A) (*22*). Those results suggest that the HPAI outbreaks in the chicken farms in the Izumi Plain are not closely associated with the HPAIVs circulating among nearby wild birds. Although our findings do not diminish the importance of wild birds as a major source of HPAIVs causing outbreaks on chicken farms (*29*), further studies are urgently needed to identify other factors contributing to HPAIV invasion in chicken farms.

Phylogenetic analyses revealed that the H5 HA gene of the G2c subgroup was located on a lower branch of the G2e subgroup (Figure 5, panel A), indicating that the H5 HPAIVs of G2c subgroup are progeny viruses of the G2e subgroup, which had caused large-scale mortality of common cranes (*Grus grus*) in Israel in 2021 (https://www.woah.org/app/uploads/2022/01/hpai-situation-report-20220117.pdf). Although specific factors affecting the pathogenicity and transmissibility of HPAI H5 in crane species remain unclear, the H5 subtype of G2e and G2c subgroups may share genetic background related to high mortality rates in crane species.

Serologic analyses revealed that only 41.2% of crane serum samples collected during the 2022–23 winter season were seropositive for HPAI H5 circulating in the same crane populations after the large HPAI outbreak in that season (Table 1). A limitation of our study is that the sample size was insufficient and the samples might contain potential biases. Nevertheless, the results suggest that the HPAI H5 outbreak among cranes has not subsided because of herd immunity resulting from widespread infection in the Izumi Plain. One possible factor contributing to the low seropositive rate is the dispersal of dense crane gatherings at their roosts around mid-November, which likely reduced opportunities for

uninfected birtds to contract the infection. Therefore, the potential for another HPAI H5 outbreak among endangered cranes remains. Preventive measures, including intentional dispersal of crane wintering sites to avoid excessive concentration of birds in a single location (*30*–*33*), are urgently needed to protect the endangered cranes in the Izumi Plain.

In conclusion, HPAI H5N1 viruses caused large-scale mortality of endangered cranes, including hooded cranes and white-naped cranes, in the Izumi Plain of Japan during the 2022–23 winter season. Our findings suggest that H5N1 circulated mainly via the respiratory route, but not the environmental waterborne route, among the endangered cranes. Most of the HPAIVs circulating in wild birds were genetically distant from those isolated from chicken farms. In addition, the endangered crane populations have not developed herd immunity against H5N1. Our study provides new insights into understanding the circumstances surrounding HPAI H5N1 outbreaks among endangered cranes and could help in their conservation.

Acknowledgments

We thank the Ministry of Agriculture, Forestry and Fisheries, the Ministry of the Environment, the Prefecture of Kagoshima, and the City of Izumi for their kind cooperation.

About the Author

Ms. Esaki is a PhD candidate at Joint Graduate School of Veterinary Medicine, Kagoshima University, Kagoshima, Japan. Her primary research focuses on the molecular diagnosis and epidemiology of avian influenza viruses.

References

1. United Nations Environment Program. CITES appendices I, II, and III. Updated February 14, 2021 [cited 2024 Dec 16]. https://cites.org/sites/default/files/eng/app/2021/E-Appendices-2021-02-14.pdf
2. The IUCN Red List of Threatened Species. *Grus monacha*. [cited 2024 Dec 16]. https://www.iucnredlist.org/species/22692151/93337861
3. Ministry of the Environment. Red list and red data book. 2020 [cited 2024 Dec 16]. https://www.env.go.jp/nature/kisho/hozen/redlist/index.html
4. The IUCN Red List of Threatened Species. *Antigone vipio*. [cited 2024 Dec 16]. https://www.iucnredlist.org/species/22692073/131927305
5. Olsen B, Munster VJ, Wallensten A, Waldenström J, Osterhaus AD, Fouchier RA. Global patterns of influenza A virus in wild birds. Science. 2006;312:384–8. https://doi.org/10.1126/science.1122438
6. Webster RG, Bean WJ, Gorman OT, Chambers TM, Kawaoka Y. Evolution and ecology of influenza A viruses. Microbiol Rev. 1992;56:152–79. https://doi.org/10.1128/mr.56.1.152-179.1992
7. Khalil AM, Fujimoto Y, Kojima I, Esaki M, Ri K, Masatani T, et al. Genetic characterization of H5N8 highly pathogenic avian influenza viruses isolated from falcated ducks and environmental water in Japan in November 2020. Pathogens. 2021;10:171. https://doi.org/10.3390/pathogens10020171
8. Nakagawa H, Okuya K, Kawabata T, Matsuu A, Takase K, Kuwahara M, et al. Genetic characterization of low-pathogenic avian influenza viruses isolated on the Izumi Plain in Japan: possible association of dynamic movements of wild birds with AIV evolution. Arch Virol. 2018;163:911–23. https://doi.org/10.1007/s00705-017-3698-1
9. Okamatsu M, Ozawa M, Soda K, Takakuwa H, Haga A, Hiono T, et al. Characterization of highly pathogenic avian influenza virus A(H5N6), Japan, November 2016. Emerg Infect Dis. 2017;23:691–5. https://doi.org/10.3201/eid2304.161957
10. Okuya K, Kawabata T, Nagano K, Tsukiyama-Kohara K, Kusumoto I, Takase K, et al. Isolation and characterization of influenza A viruses from environmental water at an overwintering site of migratory birds in Japan. Arch Virol. 2015;160:3037–52. https://doi.org/10.1007/s00705-015-2610-0
11. Okuya K, Khalil AM, Esaki M, Kojima I, Nishi N, Koyamada D, et al. Genetic characterization of avian influenza viruses isolated from the Izumi Plain, Japan in 2019–20 winter season. Pathogens. 2022;11:1013. https://doi.org/10.3390/pathogens11091013
12. Ozawa M, Matsuu A, Tokorozaki K, Horie M, Masatani T, Nakagawa H, et al. Genetic diversity of highly pathogenic H5N8 avian influenza viruses at a single overwintering site of migratory birds in Japan, 2014/15. Euro Surveill. 2015;20:21132. https://doi.org/10.2807/1560-7917.ES2015.20.20.21132
13. Okuya K, Khalil AM, Esaki M, Nishi N, Koyamada D, Saito R, et al. Newly emerged genotypes of highly pathogenic H5N8 avian influenza viruses in Kagoshima prefecture, Japan during winter 2020/21. J Gen Virol. 2023; https://doi.org/10.1099/jgv.0.001870
14. Okuya K, Mine J, Tokorozaki K, Kojima I, Esaki M, Miyazawa K, et al. Genetically diverse highly pathogenic avian influenza A(H5N1/H5N8) viruses among wild waterfowl and domestic poultry, Japan, 2021. Emerg Infect Dis. 2022;28:1451–5. https://doi.org/10.3201/eid2807.212586
15. Ozawa M, Matsuu A, Khalil AM, Nishi N, Tokorozaki K, Masatani T, et al. Phylogenetic variations of highly pathogenic H5N6 avian influenza viruses isolated from wild birds in the Izumi Plain, Japan, during the 2016–17 winter season. Transbound Emerg Dis. 2019;66:797–806. https://doi.org/10.1111/tbed.13087
16. Ministry of Environment, Government of Japan. Surveillance results and incidence during the 2022–2023 season. 2023 [cited 2024 Aug 30]. https://www.env.go.jp/content/000235617.pdf
17. Ministry of Agriculture. Forestry and Fisheries. Information on high pathogenicity avian influenza outbreaks in the winter of 2022–2023. 2023 [cited 2024 Aug 30]. https://www.maff.go.jp/j/syouan/douei/tori/220929.html#2
18. Okuya K, Esaki M, Tokorozaki K, Hasegawa T, Ozawa M. Isolation and genetic characterization of multiple genotypes of both H5 and H7 avian influenza viruses from environmental water in the Izumi Plain, Kagoshima prefecture, Japan during the 2021–22 winter season. Comp Immunol Microbiol Infect Dis. 2024;109:102182. https://doi.org/10.1016/j.cimid.2024.102182
19. Tsukamoto K, Ashizawa H, Nakanishi K, Kaji N, Suzuki K, Okamatsu M, et al. Subtyping of avian influenza viruses H1 to H15 on the basis of hemagglutinin

genes by PCR assay and molecular determination of pathogenic potential. J Clin Microbiol. 2008;46:3048–55. https://doi.org/10.1128/JCM.02386-07
20. Hoffmann E, Stech J, Guan Y, Webster RG, Perez DR. Universal primer set for the full-length amplification of all influenza A viruses. Arch Virol. 2001;146:2275–89. https://doi.org/10.1007/s007050170002
21. Khalil AM, Hatai H, Fujimoto Y, Kojima I, Okajima M, Esaki M, et al. A lethal case of natural infection with the H5N8 highly pathogenic avian influenza virus of clade 2.3.4.4 in a Mandarin duck. Zoonotic Dis. 2022;2:32–6. https://doi.org/10.3390/zoonoticdis2010004
22. Edgar RC. MUSCLE: multiple sequence alignment with high accuracy and high throughput. Nucleic Acids Res. 2004;32:1792–7. https://doi.org/10.1093/nar/gkh340
23. Tamura K, Peterson D, Peterson N, Stecher G, Nei M, Kumar S. MEGA5: molecular evolutionary genetics analysis using maximum likelihood, evolutionary distance, and maximum parsimony methods. Mol Biol Evol. 2011;28:2731–9. https://doi.org/10.1093/molbev/msr121
24. World Health Organization. WHO global influenza surveillance network: manual for the laboratory diagnosis and virological surveillance of influenza. Geneva: World Health Organization; 2011 [cited 2024 Aug 30]. https://apps.who.int/iris/bitstream/handle/10665/44518/9789241548090_eng.pdf
25. Takadate Y, Mine J, Tsunekuni R, Sakuma S, Kumagai A, Nishiura H, et al. Genetic diversity of H5N1 and H5N2 high pathogenicity avian influenza viruses isolated from poultry in Japan during the winter of 2022–2023. Virus Res. 2024;347:199425. https://doi.org/10.1016/j.virusres.2024.199425
26. Verhagen JH, Munster VJ, Majoor F, Lexmond P, Vuong O, Stumpel JB, et al. Avian influenza a virus in wild birds in highly urbanized areas. PLoS One. 2012;7:e38256. https://doi.org/10.1371/journal.pone.0038256
27. Wilson HM, Hall JS, Flint PL, Franson JC, Ely CR, Schmutz JA, et al. High seroprevalence of antibodies to avian influenza viruses among wild waterfowl in Alaska: implications for surveillance. PLoS One. 2013;8:e58308. https://doi.org/10.1371/journal.pone.0058308
28. Michalska-Smith M, Clements E, Rasmussen E, Culhane MR, Craft ME. Location, age, and antibodies predict avian influenza virus shedding in ring-billed and Franklin's gulls in Minnesota. Animals (Basel). 2024;14:1–18. https://doi.org/10.3390/ani14192781
29. Khalil AM, Kojima I, Fukunaga W, Okajima M, Mitarai S, Fujimoto Y, et al. Improved method for avian influenza virus isolation from environmental water samples. Transbound Emerg Dis. 2022;69:e2889–97. https://doi.org/10.1111/tbed.14639
30. Cai T, Huettmann F, Lee K, Guo Y. Analyzing stopover and wintering habitats of hooded cranes (*Grus monacha*): implications for conservation and species dispersion in the East Asia. Pak J Zool. 2019;51:1323–33. https://doi.org/10.17582/journal.pjz/2019.51.4.1323.1333
31. Convention on Migratory Species. Report of the meeting on suggestion of dispersal of wintering cranes at Izumi, Japan. 2001 [cited 2024 Dec 16]. https://www.cms.int/siberian-crane/sites/default/files/uploads/SiberianCrane/Report-of-the-Meeting-on-Suggestion-of-Dispersal-of-Wintering-Cranes-at-Izumi_2001.pdf
32. Farrington JD. Northeast Asia crane wintering sites: field observations and background on important crane wintering grounds in China, South Korea, and Japan. 2022 [cited 2024 Dec 16]. https://archive.org/details/farrington-2022-northeast-asia-crane-wintering-sites-v-1.0/page/46/mode/2up
33. Chan S. Atlas of key sites for cranes in the North East Asian flyway. 1999 [cited 2024 Dec 16]. https://www.wetlands.org/wp-content/uploads/2015/11/Atlas-of-Key-Sites-for-Cranes-in-the-North-East-Asian-Flyway.pdf

Address for correspondence: Makoto Ozawa, Department of Pathogenetic and Preventive Veterinary Science, Joint Faculty of Veterinary Medicine, Kagoshima University, 1-21-24 Korimoto, Kagoshima 890-0065, Japan; email: mozawa@vet.kagoshima-u.ac.jp

Metagenomic Identification of *Fusarium solani* Strain as Cause of US Fungal Meningitis Outbreak Associated with Surgical Procedures in Mexico, 2023

Charles Y. Chiu, Venice Servellita, Mikael de Lorenzi-Tognon, Patrick Benoit, Nanami Sumimoto, Abiodun Foresythe, Filipe M. Cerqueira, Natalie Williams-Bouyer, Ping Ren, Lauren Nicholas S. Herrera, David C. Gaston, Leanna Sayyad, Shannon L. Whitmer, John Klena, Holenarasipur R. Vikram, Jeremy A.W. Gold, Lalitha Gade, Lindsay Parnell, Elizabeth Misas, Tom M. Chiller, Isabel S. Griffin, Sridhar V. Basavaraju, Dallas J. Smith, Anastasia P. Litvintseva, Nancy A. Chow

We used metagenomic next-generation sequencing (mNGS) to investigate an outbreak of *Fusarium solani* meningitis in US patients who had surgical procedures under spinal anesthesia in Matamoros, Mexico, during 2023. Using a novel method called metaMELT (metagenomic multiple extended locus typing), we performed phylogenetic analysis of concatenated mNGS reads from 4 patients (P1–P4) in parallel with reads from 28 fungal reference genomes. Fungal strains from the 4 patients were most closely related to each other and to 2 cultured isolates from P1 and an additional case (P5), suggesting that all cases arose from a point source exposure. Our findings support epidemiologic data implicating a contaminated drug or device used for epidural anesthesia as the likely cause of the outbreak. In addition, our findings show that the benefits of mNGS extend beyond diagnosis of infections to public health outbreak investigation.

Whole-genome sequencing (WGS) of pathogens, including viruses, bacteria, and fungi, is a vital tool for detecting and investigating outbreaks (*1*–*3*). In addition to providing definitive identification of the causative organism, WGS can be used to construct phylogenetic trees, which in turn can be used to detect more cases, resolve disease transmission patterns, and identify potential outbreak sources. However, conventional WGS depends on the ability to grow the pathogen in culture. For fastidious organisms such as mycobacteria, fungi, and some viruses, successful culturing is often difficult and slow; growth of the organism requires weeks to months and sometimes is not possible at all. To bypass the requirement for culture, techniques such as multilocus sequence typing/multilocus sequence analysis (MLST/MLSA) have been developed, whereby specific regions of the microbial genome (loci) are targeted for PCR amplification directly from primary clinical material (*4*,*5*). A key limitation of MLST/MLSA, however, is the need to have the target organism identified, loci defined, and primers at hand a priori. Thus, MLST/MLSA is typically not useful for immediate outbreak situations caused by rare or unexpected pathogens.

Metagenomic next-generation sequencing (mNGS) is an agnostic diagnostic method with the potential to

Author affiliations: Chan-Zuckerberg Biohub, San Francisco (C.Y. Chiu); University of California San Francisco, San Francisco, (C.Y. Chiu, V. Servellita, M. de Lorenzi-Tognon, P. Benoit, N. Sumimoto, A. Foresythe); Abbott Pandemic Defense Coalition, Abbott Park, Illinois, USA (C.Y. Chiu, V. Servellita, M. de Lorenzi-Tognon, P. Benoit, N. Sumimoto, A. Foresythe); The University of Texas Medical Branch at Galveston, Galveston, Texas, USA (F.M. Cerqueira, N. Williams-Bouyer, P. Ren); Vanderbilt University Medical Center, Nashville, Tennessee, USA (L.N.S. Herrera, D.C. Gaston); Centers for Disease Control and Prevention, Atlanta, Georgia, USA (L. Sayyad, S.L. Whitmer, J. Klena, J.A.W. Gold, L. Gade, L. Parnell, E. Misas, T.M. Chiller, I.S. Griffin, S.V. Basavaraju, D.J. Smith, A.P. Litvintseva, N.A. Chow); Mayo Clinic, Phoenix, Arizona, USA (H.R. Vikram)

DOI: https://doi.org/10.3201/eid3105.241657

identify any pathogen, whether bacterial, viral, parasitic, or fungal, on the basis of shotgun sequencing of DNA or RNA (*6*). The use of mNGS testing from clinical samples has been shown to increase diagnostic yield and provide actionable results in multiple prospective studies (*7*–*11*). In addition, mNGS has proven to be an invaluable tool for identifying and initially characterizing emerging pathogens, such as SARS-CoV-2 (*12*). However, the use of mNGS to date has been mainly focused on pathogen detection for clinical diagnostic purposes, rather than outbreak investigation, because coverage of the pathogen genome recovered by mNGS is generally sparse and uneven.

On May 8, 2023, the Centers for Disease Control and Prevention (CDC) Emerging Infections Network reported cases of suspected fungal meningitis in US patients who had undergone surgical procedures performed under epidural anesthesia in the city of Matamoros in Durango state, Mexico (*13*). Using clinical mNGS testing, the University of California, San Francisco (UCSF), clinical microbiology laboratory reported identification of *Fusarium solani* species complex in cerebrospinal fluid from an affected patient (P1) with probable fungal meningitis in the United States on May 28, 2023 (*14*). That initial case and additional cases were subsequently confirmed independently by panfungal PCR followed by sequencing of the amplicon to confirm detection of *F. solani* (*13*). During the outbreak, a total of 184 patients in 22 US states were identified as persons potentially exposed, among whom 24 were identified with fungal meningitis and 12 died, mainly from severe vascular complications (*13*,*15*). Here, we describe a novel analytic technique called metaMELT, or metagenomic multiple extended locus typing, as a tool for simultaneously diagnosing infections and characterizing the interrelatedness of *F. solani* strains in patients from the Matamoros outbreak.

Methods

Human Sample Collection and Processing

Cerebrospinal fluid (CSF) samples from 5 patients (P1–P5) in the Matamoros outbreak were available for analysis. A CSF sample from patient P1 was sent to the UCSF Clinical Microbiology Laboratory for CSF mNGS testing and was processed and sequenced as previously described (*16*). Residual CSF, plasma, and brain tissue biopsy samples from patients P1–P4 were also processed and sequenced using mNGS. Cultures of *F. solani* were also obtained from P1 and P5 CSF samples.

For P1–P4 samples, we extracted DNA by using the MagMAX Viral/Pathogen II (MVP II) Nucleic Acid Isolation Kit (Thermo Fisher Scientific, https://www.thermofisher.com) and the KingFisher Flex Purification System with a 96 deep-well head (Thermo Fisher Scientific). We loaded the extracted DNA on the MagicPrep NGS instrument (Tecan Genomics, Inc., https://www.tecan.com) to undergo end repair, adaptor ligation and barcoding, amplification (25 cycles), and purification. We enriched some of the libraries for microbial DNA by using DepleteX (Jumpcode Genomics, https://www.jumpcodegenomics.com), an early release of a CRISPR-based human DNA depletion kit, according to the manufacturer's specifications. That kit leverages Cas9 depletion and exonuclease activity to efficiently remove human DNA from samples with high human content.

CRISPR-based host depletion increased the number of *Fusarium*-specific reads in the P1 CSF DNA library from 13 to 223 (16.4-fold enrichment increase), corresponding to an increase of 1.5 to 2.4 reads per million (RPM), a 1.6-fold enrichment increase. In the P3 plasma DNA library, the number of reads decreased from 60 to 36 after enrichment, but that decrease corresponded to an RPM increase from 0.12 to 0.16 (1.3-fold enrichment increase). We quantified and normalized the libraries by using the Qubit dsDNA HS Assay on the Qubit Flex (Thermo Fisher Scientific). We sequenced final pooled libraries as single-end reads on the NextSeq 550 (Illumina, https://www.illumina.com) by using the High-Output Kit or the NovaSeq Kit (Illumina) at 150 cycles.

F. solani WGS

We performed WGS of 18 *F. solani* isolates, including isolates cultured from 2 patients (P1 and P5) in the Matamoros outbreak as follows. We extracted DNA by using the DNeasy Blood and Tissue kit (QIAGEN, https://www.qiagen.com), and then used the NEBNext Ultra DNA Library Prep kit (New England Biolabs, https://www.neb.com) to construct DNA fungal genomic libraries for Illumina sequencing. We sequenced the isolate from patient P1 (genome B27264) on the Illumina MiSeq (250-bp paired-end sequencing, or 500 cycles). We sequenced the isolate from patient P5 (genome B27166) and 16 additional *F. solani* genomes unrelated to the Matamoros outbreak by using the NovaSeq 6000SP Reagent Kit (Illumina) at 500 cycles.

Bioinformatic Methods

We used the SURPI+ computational pipeline version 1.0.0 (https://github.com/chiulab/SURPI-plus-dist),

run as a container on either a secure server or cloud infrastructure, to identify pathogens from mNGS data (*16*,*17*). We preprocessed reads by trimming adapters and removing low-complexity and low-quality sequences and then performed computational subtraction of human reads by using SNAP version 1.0 (*16*) and Bowtie2 version 2.3.2 GTCh38/hg38 build (https://sourceforge.net/projects/bowtie-bio) to align and exclude reads mapping to the human genome. We aligned the remaining nonhuman reads to microbial reference sequences in the National Center for Biotechnology Information (NCBI) nucleotide database (https://www.ncbi.nlm.nih.gov/nucleotide; March 2019 build) using the SNAP nucleotide aligner (*18*). We performed filtering and taxonomic classification algorithms to remove spurious hits and classify each read at the species, genus, or family level, as previously described (*16*).

We further analyzed CSF mNGS reads from P1 by nucleotide BLASTn (https://blast.ncbi.nlm.nih.gov) alignment to the genome of an *F. solani* reference strain (ATCC strain no. MYA-4622) with an E-value of 1×10^{-8} and the remaining parameters set to corresponding default values (*19*). We visualized mapped reads by using Ensembl Fungi (*20*). Among the 28 *F. solani* cultured isolates included in the analysis, 10 were from genomes downloaded from GenBank. For the other 18 newly sequenced isolates, we obtained draft genomes by de novo assembly of raw reads using the SPADES genome assembler version 3.15.4 at default parameters (*21*).

We wrote Linux scripts and code to perform the metaMELT method for each patient as follows. For reads from patients P1–P4 identified as *F. solani* in SURPI+, we trimmed to the desired length and successively aligned reads by using BLASTn at a 1×10^{-8} E-value cutoff for each of the 28 *F. solani* reference genomes, including the assembled genomes from P1 and P5. If an alignment was successful, we extracted the mapped region corresponding to the read from the reference genome; otherwise, the system generated a synthetic dummy read consisting of a stretch of Ns (ambiguous nucleotides). We then concatenated reads from all 4 patients and the corresponding mapped regions in each reference genome by using a 50-bp spacer of Ns to separate each read or region. We performed multiple sequence alignment of the concatenated sequences by using MAFFT version 7.388 (*22*) and the following parameters: FFT-NS-2 algorithm, 200 PAM/k = 2 scoring matrix, gap open penalty = 3, and offset value = 0.123. We then constructed phylogenetic trees by using PhyML 3.0 (*23*) and substitution model TN93 with SH-like branch supports, in Geneious version 11.1.5 (*24*).

Inclusion and Ethics

Sequencing data from clinical CSF mNGS testing and deidentified residual samples from hospitalized patients who were part of the *F. solani* outbreak were analyzed under protocols approved by the UCSF institutional review board (protocol no. 11-05519). Clinical and demographic patient-level data were not collected because that information was not considered relevant to this study. All patients with sufficient remaining volume of residual samples were included in the study.

Results

We used clinical CSF mNGS testing and SURPI+ analysis to diagnose *F. solani* infection in case P1. Among the 8.7 million reads that we recovered from CSF, 13 (0.00015%) aligned most closely to the genome of

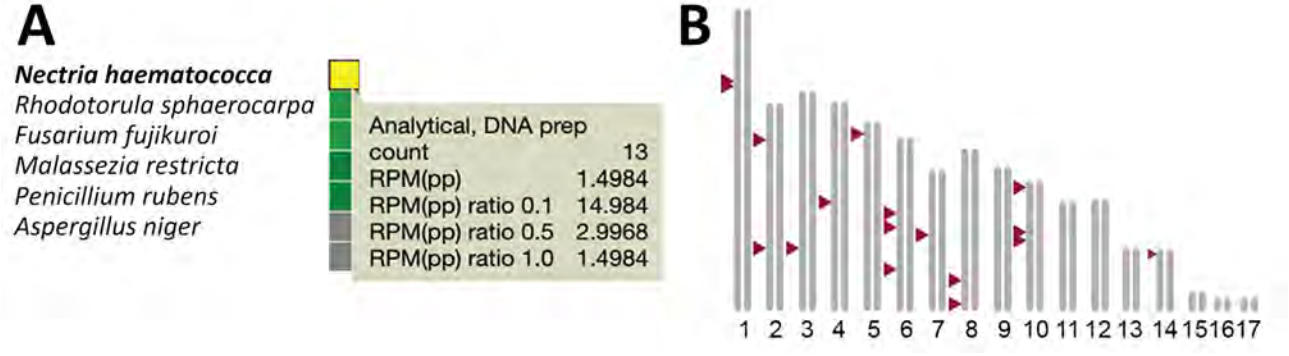

Figure 1. Identification of *Fusarium solani* in CSF from a patient with fungal meningitis associated with surgical procedures in Matamoros, Mexico, 2023. A) Heat map of 13 mNGS CSF reads from patient P1 showing reads aligning to *Nectria hematococca*, the anamorph of *F. solani.* That initial detection triggered a Centers for Disease Control and Prevention notification recommending testing for all patients in the outbreak who might have been exposed (*14*). B) Mapping of the 18 total *Fusarium* spp. mNGS reads recovered from patient P1 to the *F. solani* reference genome (ATCC MYA-4622). Arrows indicate the mapped positions of the 18 reads. CSF, cerebrospinal fluid; mNGS, metagenomic next-generation sequencing; RPM(pp), reads per million (preprocessed).

Nectria hematococca, the anamorph of *F. solani* (Figure 1, panel A). We did not observe any co-infections from viruses, bacteria, or parasites. The default SURPI+ pipeline uses the GenBank nucleotide database for its microbial reference database (*16*,*17*), which does not contain any fungal whole-genome sequences. Because fungal whole-genome sequences are found in the GenBank whole-genome shotgun database (*25*), we used that database to align the mNGS reads directly to an *F. solani* reference genome (ATCC strain no. MYA-4622) and identified an additional 5 fungal reads. We found that the 18 total mapped *F. solani* reads were distributed randomly across the ≈53 Mb genome (Figure 1, panel B).

We subsequently obtained more *F. solani* reads from the P1 CSF sample by additional sequencing and we also sequenced CSF, plasma, or brain tissue from 3 more patients (P2, P3, and P4) in the Matamoros outbreak who had PCR-confirmed *F. solani* meningitis. To maximize recovery of *F. solani* reads, we sequenced mNGS libraries both without and with enrichment for microbial DNA using DepleteX, although the level of enrichment was only 1.3–1.6 RPM using that kit. The total number of *F. solani* reads recovered from each patient ranged from 263 to 187,773.

The number of fungal mNGS reads was not sufficient to assemble the *F. solani* genome from any single patient. To achieve 30× coverage, we estimated that ≈10.6 million 150-bp *F. solani*–specific reads would need to be sequenced. The actual read numbers and percent coverage achieved from CSF mNGS from infected patients was extremely low; the number of reads ranged from 263 to 187,773 and the coverage ranged from 0.0005% to 0.35% of the fungal genome (Table 1). Thus, we developed metaMELT as a tool to enable comparison of fungal strains from individual patients using sparse mNGS data. The metaMELT method involves first extracting the regions defined by randomly selected mNGS reads from each patient sample from their corresponding locations (loci) in all available *F. solani* reference genomes (n = 28) (Figure 2). The total number of extracted reads or loci is equal to the product of the number of samples and the number of mNGS reads that are randomly selected from each sample. After concatenating the extracted reads, we performed phylogenetic analysis of the concatenated sequences, with each sequence derived from a single patient or a reference genome (Figure 3).

Table 1. Number of reads recovered from CSF, plasma, or brain tissue from 4 patients used for identification of *Fusarium solani* strain as cause of fungal meningitis US outbreak associated with surgical procedures in Mexico, 2023*

Patient ID	Location, USA	Sample type (no. reads)
P1†‡	State 1	CSF (263)
P2‡	State 2	CSF (187,773)
P3‡	State 2	CSF (2,669), plasma (96)
P4	State 2	CSF (4), brain tissue (608)

*Reads were recovered by using mNGS. CSF, cerebrospinal fluid; ID, identification; mNGS, metagenomic next-generation sequencing.
†Newly diagnosed case by mNGS testing of CSF.
‡Fatal case.

By early 2024, only 10 complete *F. solani* reference genomes were available for download in the GenBank whole-genome shotgun database (Figure 4, panel A). We performed de novo assembly on additional draft genomes from 18 cultured *F. solani* isolates in the CDC fungal biorepository from raw next-generation sequence data and included those in the phylogenetic analysis (Figure 4, panel B). Each draft genome consisted of a series of contigs (*26*), ranging from 1,057 to 7,216 contigs (Table 2). Of note, 2 draft genomes, B27264 from P1 and B27166 from P5, had been newly assembled from cultured outbreak isolates; patient P5 was part of the Matamoros outbreak for whom residual CSF was not available for mNGS. The accuracy of phylogenetic analysis relied on polymorphisms between an outbreak strain or cultured isolate and each

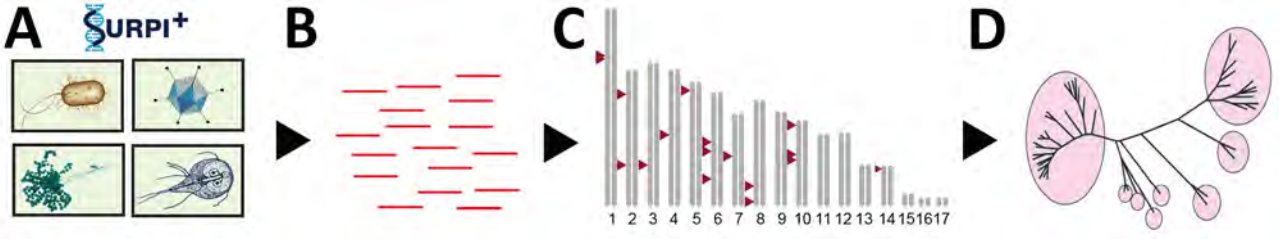

Figure 2. Flowchart showing the metaMELT analysis workflow used for identification of *Fusarium solani* strain as cause of fungal meningitis US outbreak associated with surgical procedures in Mexico, 2023. metaMELT (metagenomic multiple extended locus typing), is a novel analytic technique for simultaneously diagnosing the infection and characterizing the interrelatedness of *F. solani* strains. metaMELT uses the following steps: A) perform mNGS analysis of patient samples (i.e., cerebrospinal fluid, plasma, or brain tissue), using the SURPI+ computational pipeline (https://github.com/chiulab/SURPI-plus-dist) to identify pathogens; B) identify *F. solani* reads; C) map reads to the *F. solani* reference genome and then extract and concatenate; D) perform phylogenetic analysis on concatenated sequences. SURPI, sequence-based ultra-rapid pathogen identification.

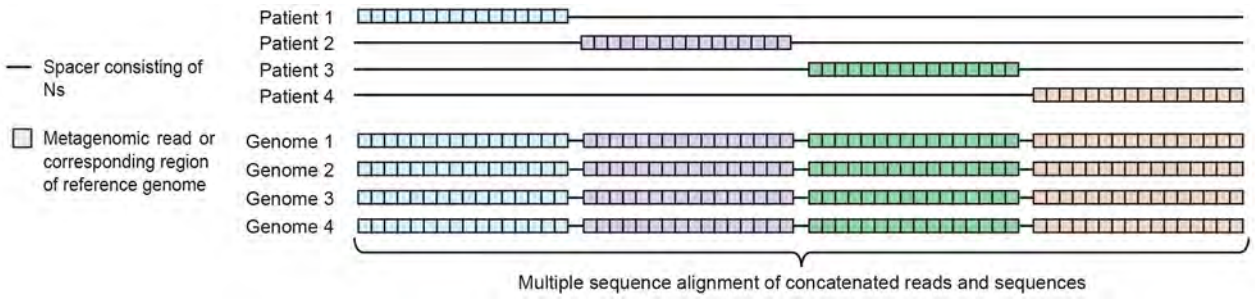

Figure 3. Diagram of concatenation and alignment step of the metaMELT procedure (metagenomic multiple extended locus typing, a novel analytic technique for simultaneously diagnosing the infection and characterizing the interrelatedness of *Fusarium solani* strains) used for identification of *F. solani* strain as cause of fungal meningitis US outbreak associated with surgical procedures in Mexico, 2023. The diagram shows concatenated metagenomic next-generation sequencing reads from 4 patients and the corresponding regions extracted from reference genomes, which are aligned to by using MAFFT version 7.388 (*22*). This diagram demonstrates the steps shown in Figure 2, panels C–D..

reference genome in the database and not on polymorphisms between individual strains or isolates, because the sparse mNGS reads recovered from the ≈53 Mb genome were unlikely to overlap.

We performed phylogenetic analysis of the concatenated sequences from P1−P4 and the 28 reference genomes. To evaluate the flexibility of metaMELT for different sample types, P1 and P2 included CSF reads, P3 included only plasma reads (n = 96), and P4 included mostly brain biopsy tissue reads (608 of 612 reads). Each concatenated sequence consisted of 90 randomly selected mNGS reads of 150-bp length because only 96 total plasma mNGS reads were available for patient P3. The topology of the resulting tree revealed that the *F. solani* strains from all 5 patients in the Matamoros outbreak were positioned together in a single cluster (Figure 4, panel A). To account for potential bias in the phylogenetic estimates because of the high proportion of ambiguous nucleotides in each of the concatenated sequences from patients P1–P4 (*27*), we reran the phylogenetic analysis including only 1 patient at a time, and all trees positioned the individual patient in the same cluster (Figure 4, panels B–E).

Next, we assessed whether clustering of mNGS reads from patients P1–P4 could still be visualized if only 1 outbreak-related reference genome from P5 was available for comparison or if no outbreak-related reference genome was available. We observed clustering of patients P1–P4 for both analyses (Figure 5, panels A, B), albeit with 11 unrelated genomes assigned to the cluster if no outbreak-related genome was included (Figure 5, panel B). Because only a few reference genomes might be in the existing reference databases for a given target pathogen, we then determined how the total number of available reference genomes affected patient clustering by metaMELT. Despite inclusion of only 10 or 5 total reference genomes, we still observed clustering of patients P1–P5 by phylogenetic analysis (Figure 5, panels C, D).

Based on MLST/MLSA analysis of the concatenated *ITS*, *rpb2*, and *tef1* genes (*28*), the predicted nucleotide pairwise identity between the 2 draft genomes from the Matamoros outbreak, B27264 (P1) and B27166 (P5), was 96% (Appendix Figure 1, panel A), and overall pairwise identities for the 28 reference genomes ranged from 89% to 96%. The high pairwise identity between the P1 and P5 isolates and positioning in the same subcluster by phylogenetic analysis (Appendix Figure 1, panel B) supported the notion of a single *F. solani* strain as the cause of the outbreak. Of note, the larger cluster consisting of an additional 11 genomes unrelated to the outbreak (Appendix Figure 1) was the same cluster that included the concatenated mNGS sequences from cases P1–P4 in all previous metaMELT phylogenetic analyses (Figures 4, 5).

We sought to ascertain the effect of read lengths and numbers on the clustering of the *F. solani* strains from patients P1−P5 by metaMELT. All 4 sequenced strains were correctly clustered at read lengths of ≥100 bp and ≥40 mNGS reads (Appendix Figure 2, panel A). To establish a quality control criterion for metaMELT at the empirically determined 40-read cutoff (Appendix Figure 2, panel A), we performed 20 bootstrap replicates in which we randomly sampled and analyzed 40 100-bp reads from patients P1–P4 by metaMELT. Phylogenetic trees from all 20 replicates correctly positioned patients P1–P4 in the same cluster (Appendix Figure 2, panel B).

Discussion

In this study, we used clinical mNGS testing to identify *F. solani* in a patient from a fungal meningitis outbreak associated with surgical procedures in Matamoros, Mexico. We used a novel analytic

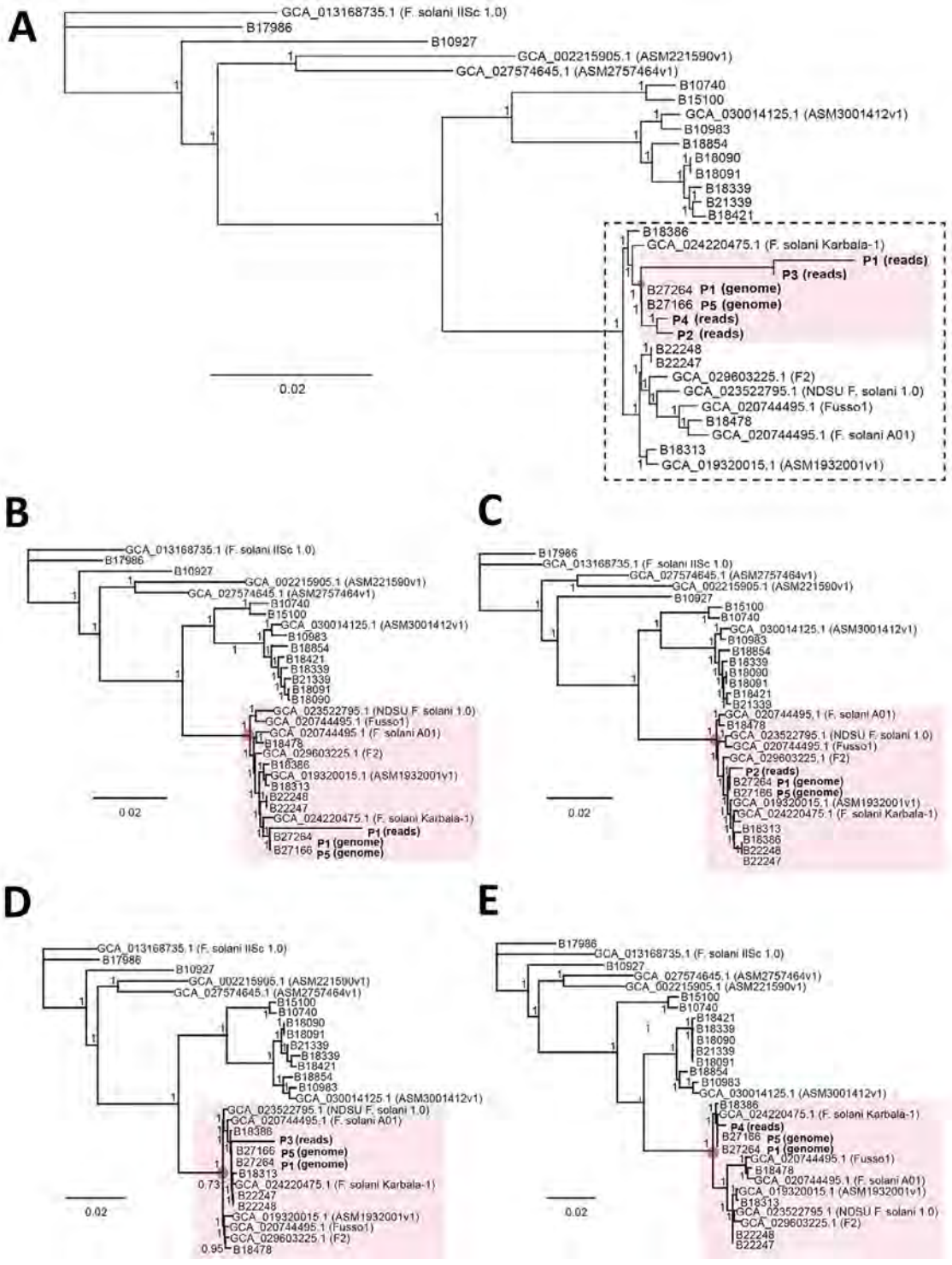

Figure 4. Phylogenetic analysis of concatenated metagenomic next-generation sequencing reads from US patients from a fungal meningitis outbreak associated with surgical procedures in Mexico, 2023. A) Phylogenetic trees showing clustering of strains from patients P1–P5 (pink shaded region) within a subclade that also includes fungal genomes unrelated to the outbreak (dotted rectangle). B–E) Phylogenetic trees of individual patients exhibiting similar topologies: B) P1; C) P2; D) P3; E) P4. Each patient is positioned in a cluster containing the same reference genomes, including the 2 outbreak genomes recovered from patients P1 and P5. Outbreak reads were mapped to corresponding regions from *Fusarium solani* reference genomes by using metaMELT (metagenomic multiple extended locus typing, a novel analytic technique for simultaneously diagnosing the infection and characterizing the interrelatedness of *F. solani* strains). Scale bars indicate nucleotide substitutions per site. P1–P5, patients 1–5.

Table 2. Data from de novo assembly of 18 draft genomes used for identification of *Fusarium solani* strain as cause of fungal meningitis US outbreak associated with surgical procedures in Mexico, 2023*

Genome assembly	No. contigs	Total contig length, bp	N50, bp
B10740	2,589	50,517,664	489,689
B10927	3,421	49,206,550	371,903
B10983	3,198	57,260,205	506,490
B15100	2,250	49,683,915	842,580
B17986	3,037	47,958,675	381,199
B18090	5,155	60,209,829	470,869
B18091	6,769	59,741,266	458,563
B18313	1,448	51,560,784	467,209
B18339	2,419	55,485,754	565,856
B18386	1,781	52,521,438	575,687
B18421	7,187	59,392,883	357,605
B18478	7,244	56,253,777	441,893
B18854	2,695	54,697,765	562,797
B21339	2,532	55,305,429	898,025
B22247	2,284	56,659,172	747,616
B22248	1,071	51,606,190	538,696
B27166	2,186	53,744,553	512,232
B27264	2,262	54,164,081	802,132

*bp, base pairs; N50, shortest contig length that needs to be included to cover 50% of the genome.

method, metaMELT, to leverage the mNGS data to aid the public health investigation. The metaMELT method is a powerful tool for species identification and evaluation of the interrelatedness of outbreak strains for pathogens that are difficult to culture. Clinical samples from 4 infected patients (P1–P4) and cultured isolates from P1 and another patient from the outbreak (P5) clustered together by phylogenetic analysis, showing that the strains from all 5 patients are the same or closely related. Those results indicate a high likelihood that all 5 infections, and, by extension, the US outbreak, originated from a single point source. The results of the CDC epidemiologic investigation, taken together with our findings, suggest a single point source and implicate a contaminated drug or device used for epidural anesthesia, either at the site of manufacturing or from breakdown of infection control practices at the clinics, as the likely cause of the outbreak.

The minimum number of reads necessary for accurate metaMELT analyses is dependent on multiple factors, including the sequence diversity of the species' genome, availability of closely related reference genomes, and the quality and length of reads. Given the high levels of sequence diversity and large number of potential outbreak pathogens, we propose an empirically derived quality control criterion for investigation of interrelatedness of outbreak samples that uses bootstrap sampling of randomly selected mNGS reads and a ≥95% accuracy cutoff (i.e., at least 19 of 20 trees with the correct topology) (Appendix Figure 2, panel B).

The usefulness of metaMELT for analysis of the Matamoros outbreak described is likely due in part to the high sequence diversity of circulating *Fusarium* species isolates. In a previously published international outbreak of *F. keratitis* associated with contact lens wear, 19 of 39 isolates tested had a unique multilocus genotype (*29*). For other pathogens with lower genetic diversity, the usefulness of metaMELT may be limited because determining the relatedness of outbreak strains can be challenging. Another potential limitation of metaMELT is the need for enough complete reference genomes in publicly available databases for comparison, which might not be the case for rare or unusual pathogens.

Our study also extends the utility of mNGS and subsequent metaMELT analyses to not only agnostic diagnosis of infections in clinical settings but also the monitoring and tracking of communicable diseases, which are relevant to infection control, public health surveillance, and outbreak investigation. To date, those activities have largely relied on microbial WGS and phylogenetic analysis of the assembled sequences. However, WGS can be problematic because many atypical bacteria, fungi, and viruses grow slowly in culture or do not grow at all. The requirement for culture also inevitably delays the generation of actionable results in time-critical scenarios, such as outbreak investigation. Targeted methods, such as tiled multiplex amplicon sequencing for viruses (*30*) and MLST/MLSA for bacteria, parasites, and fungi (*4*,*5*,*31*,*32*), including *F. solani* (*28*,*33*), can be applied in lieu of WGS-based phylogenetic analysis. However, those approaches require that the pathogen be identified a priori and depend on the assays being immediately available at the time of identification, which is usually not the case with rare or unexpected pathogens such as *F. solani*. Clustering and phylogeny inferred from MLST/MLSA are also known to be inferior for some organisms compared to more detailed WGS analyses (*34*,*35*). Unlike WGS, metaMELT can be useful with mNGS reads that can vary by several orders of magnitude in number from sample to sample but typically produce very sparse coverage of the genome. In addition, metaMELT analysis enables the leveraging of mNGS data generated at the time of diagnosis and thus has the potential of providing immediate and actionable information to guide infection control and public health efforts.

In summary, our mNGS findings support epidemiologic data implicating a contaminated drug or device used for epidural anesthesia as a common point

source and the likely cause of a *F. solani* meningitis outbreak in US patients associated with surgical procedures in Matamoros, Mexico. In addition, our findings show that mNGS could have benefits that extend beyond diagnosis of infections to more broadly assist in outbreak investigations.

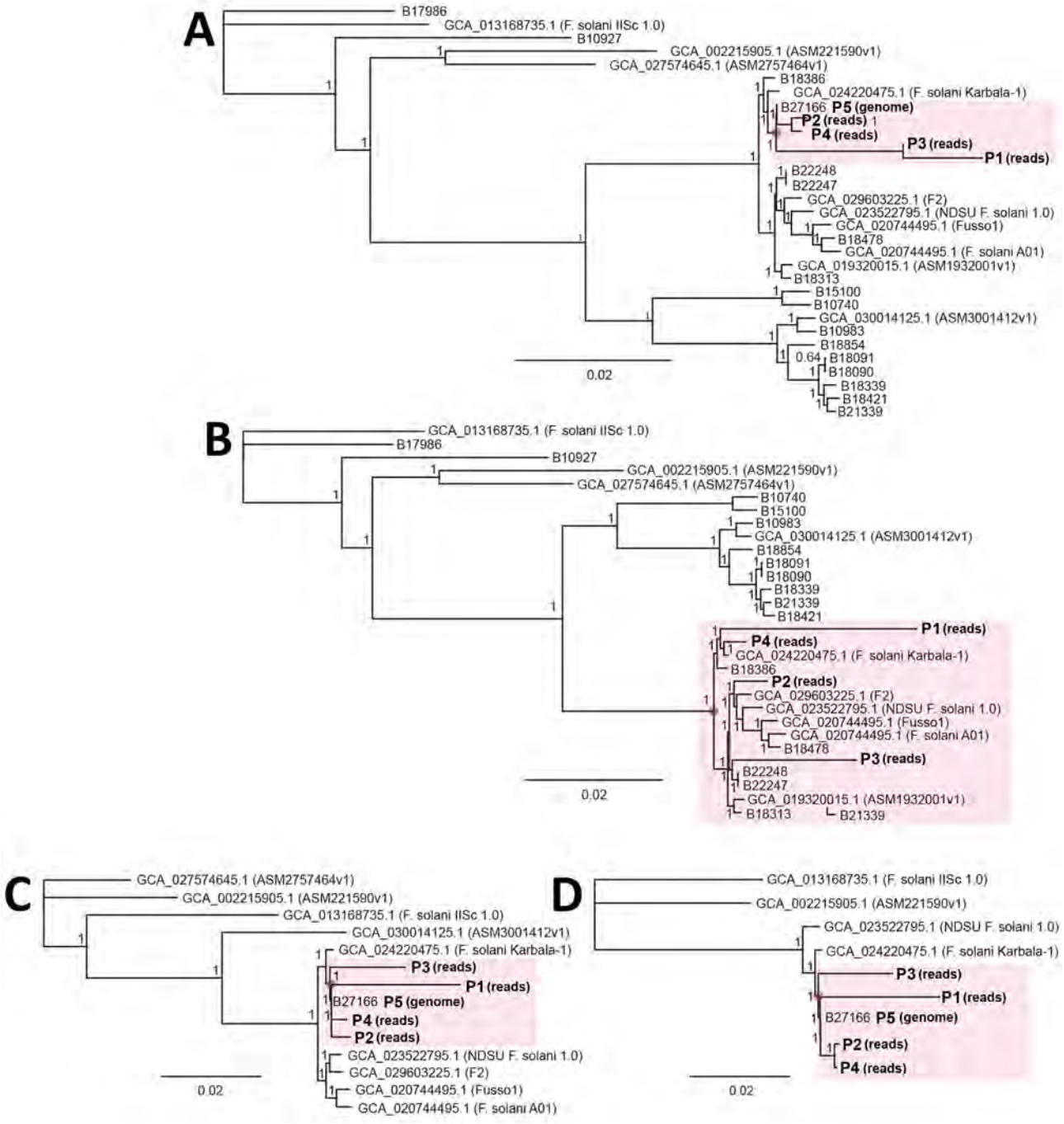

Figure 5. Effect of number of reference genomes on performance of metaMELT (metagenomic multiple extended locus typing, a novel analytic technique for simultaneously diagnosing the infection and characterizing the interrelatedness of *Fusarium solani* strains) for identification of *F. solani* strain as cause of fungal meningitis US outbreak associated with surgical procedures in Mexico, 2023. A, B) metaMELT phylogenetic trees that include mNGS reads from patients P1–P4 are shown with and without outbreak-related genomes: A) only 1 outbreak-related reference genome from P5; B) tree without any outbreak-related reference genomes. Note the clustering of patients P1–P4 (pink shaded regions) even in the absence of an outbreak-related reference genome. C, D) metaMELT phylogenetic trees that include mNGS reads from patients P1–P4 are shown with only 10 reference genomes, including patient P5 (C); and only 5 reference genomes, including patient P5 (D). Scale bars indicate nucleotide substitutions per site. P1–P5, patients 1–5.

Acknowledgments

We thank the staff at the UCSF Clinical Microbiology Laboratory for help in processing patient CSF samples for clinical mNGS testing.

Raw FASTQ sequence metadata, including deidentified mNGS data from patients with *Fusarium solani* infection depleted of human genomic sequences, were submitted a Zenodo data repository (https://doi.org/10.5281/zenodo.12572958) and the Sequence Read Archive database (BioProject accession no. PRJNA1130911 and umbrella BioProject accession no. PRJNA171119). Custom scripts and code for running metaMELT and draft genome assemblies from 18 cultured isolates of *F. solani* have also been deposited into the Zenodo data repository. Further information and requests for resources and reagents should be directed to and will be fulfilled by Charles Y. Chiu (charles.chiu@ucsf.edu).

This work was financially supported in part by funding from the following to C.Y.C.: BARDA EZ-BAA award no. 75A50122C00022, US Centers for Disease Control and Prevention grant nos. 75D30122C15360 and 75D30121C12641, Abbott Laboratories, and the Chan-Zuckerberg Biohub. The funders had no role in the design and conduct of the study; collection, management, analysis, and interpretation of the data; preparation, review, or approval of the manuscript; or decision to submit the manuscript for publication.

C.Y.C. is a founder of Delve Bio and on the scientific advisory board for Delve Bio, Flightpath Biosciences, Biomeme, Mammoth Biosciences, BiomeSense, and Poppy Health. He is also an inventor on US patent no. 11380421, Pathogen detection using next generation sequencing, under which algorithms for taxonomic classification, filtering, and pathogen detection are used by SURPI+ software. C.Y.C. receives research support from Delve Bio and Abbott Laboratories, Inc. The other authors declare no competing interests.

Author contributions: C.Y.C conceived and designed the study. V.S., N.S., A.F, L.G., L.P., and E.M. processed samples. C.Y.C., F.M.C., N.W.-B., P.R., L.N.S.H., D.C.G., L.S., S.W., J.K., J.A.W.G., L.G., L.P., I.G., and I.S.G. collected samples and clinical metadata. C.Y.C., V.S., M.D.L., P.B., E.M., D.J.S., and A.P.L. analyzed data. C.Y.C., P.R., J.K., T.M.C., S.V.B., D.J.S., A.P.L, and N.A.C. provided study oversight. C.Y.C. prepared the figures and wrote the manuscript. C.Y.C., M.D.L., P.B., P.R., H.R.V., E.M., D.J.S., A.P.L., and N.A.C. edited the manuscript. All authors read the manuscript and agree to its contents.

About the Author

Dr. Chiu is a professor in Laboratory Medicine and Infectious Diseases at University of California, San Francisco (UCSF), director of the UCSF Clinical Microbiology Laboratory, and a Chan-Zuckerberg Biohub Investigator. His research interests focus on clinical metagenomic assay development for infectious diseases and characterization of emerging outbreak viruses.

References

1. Popovich KJ, Snitkin ES. Whole genome sequencing—implications for infection prevention and outbreak investigations. Curr Infect Dis Rep. 2017;19:15.
2. Gilchrist CA, Turner SD, Riley MF, Petri WA Jr, Hewlett EL. Whole-genome sequencing in outbreak analysis. Clin Microbiol Rev. 2015;28:541–63. https://doi.org/10.1128/CMR.00075-13
3. Cuomo CA. Harnessing whole genome sequencing in medical mycology. Curr Fungal Infect Rep. 2017;11:52–9.
4. Maiden MC, Jansen van Rensburg MJ, Bray JE, Earle SG, Ford SA, Jolley KA, et al. MLST revisited: the gene-by-gene approach to bacterial genomics. Nat Rev Microbiol. 2013;11:728–36. https://doi.org/10.1038/nrmicro3093
5. Urwin R, Maiden MC. Multi-locus sequence typing: a tool for global epidemiology. Trends Microbiol. 2003;11:479–87.
6. Chiu CY, Miller SA. Clinical metagenomics. Nat Rev Genet. 2019;20:341–55.
7. Benoit P, Brazer N, de Lorenzi-Tognon M, Kelly E, Servellita V, Oseguera M, et al. Seven-year performance of a clinical metagenomic next-generation sequencing test for diagnosis of central nervous system infections. Nat Med. 2024;30:3522–33.
8. Bergin SP, Chemaly RF, Dadwal SS, Hill JA, Lee YJ, Haidar G, et al. Plasma microbial cell-free DNA sequencing in immunocompromised patients with pneumonia: a prospective observational study. Clin Infect Dis. 2024;78:775–84.
9. Blauwkamp TA, Thair S, Rosen MJ, Blair L, Lindner MS, Vilfan ID, et al. Analytical and clinical validation of a microbial cell-free DNA sequencing test for infectious disease. Nat Microbiol. 2019;4:663–74.
10. Fourgeaud J, Regnault B, Ok V, Da Rocha N, Sitterlé É, Mekouar M, et al. Performance of clinical metagenomics in France: a prospective observational study. Lancet Microbe. 2024;5:e52–61.
11. Wilson MR, Sample HA, Zorn KC, Arevalo S, Yu G, Neuhaus J, et al. Clinical metagenomic sequencing for diagnosis of meningitis and encephalitis. N Engl J Med. 2019;380:2327–40.
12. Zhu N, Zhang D, Wang W, Li X, Yang B, Song J, et al.; China Novel Coronavirus Investigating and Research Team. A novel coronavirus from patients with pneumonia in China, 2019. N Engl J Med. 2020;382:727–33. https://doi.org/10.1056/NEJMoa2001017
13. Smith DJ, Gold JAW, Chiller T, Bustamante ND, Marinissen MJ, Rodriquez GG, et al.; Fungal Meningitis Response Team. Update on outbreak of fungal meningitis among U.S. residents who received epidural anesthesia at two clinics in Matamoros, Mexico. Clin Infect Dis. 2024;78:1554–8.
14. US Centers for Disease Control and Prevention (CDC). Fungal meningitis outbreak associated with procedures performed under epidural anesthesia in Matamoros, Mexico [cited 2024 May 12]. https://www.cdc.gov/hai/outbreaks/meningitis-epidural-anesthesia.html

15. Strong N, Meeks G, Sheth SA, McCullough L, Villalba JA, Tan C, et al. Neurovascular complications of iatrogenic *Fusarium solani* meningitis. N Engl J Med. 2024;390:522–9.
16. Miller S, Naccache SN, Samayoa E, Messacar K, Arevalo S, Federman S, et al. Laboratory validation of a clinical metagenomic sequencing assay for pathogen detection in cerebrospinal fluid. Genome Res. 2019;29:831–42.
17. Naccache SN, Federman S, Veeraraghavan N, Zaharia M, Lee D, Samayoa E, et al. A cloud-compatible bioinformatics pipeline for ultrarapid pathogen identification from next-generation sequencing of clinical samples. Genome Res. 2014;24:1180–92. https://doi.org/10.1101/gr.171934.113
18. Zaharia M, Bolosky B, Curtis K, Patterson D, Fox A, Patterson D, et al. Alignment in a SNAP: cancer diagnosis in the genomic age. Abstract 1912: United States and Canadian Academy of Pathology Annual Meeting; March 17–23, 2012; Vancouver, British Columbia, Canada. Lab Invest. 2012; 92:458A.
19. Mount DW. Using the Basic Local Alignment Search Tool (BLAST). CSH Protoc. 2007;2007:pdb.top17.
20. Harrison PW, Amode MR, Austine-Orimoloye O, Azov AG, Barba M, Barnes I, et al. Ensembl 2024. Nucleic Acids Res. 2024;52(D1):D891–9.
21. Bankevich A, Nurk S, Antipov D, Gurevich AA, Dvorkin M, Kulikov AS, et al. SPAdes: a new genome assembly algorithm and its applications to single-cell sequencing. J Comput Biol. 2012;19:455–77.
22. Katoh K, Standley DM. MAFFT multiple sequence alignment software version 7: improvements in performance and usability. Mol Biol Evol. 2013;30:772–80.
23. Guindon S, Dufayard JF, Lefort V, Anisimova M, Hordijk W, Gascuel O. New algorithms and methods to estimate maximum-likelihood phylogenies: assessing the performance of PhyML 3.0. Syst Biol. 2010;59:307–21.
24. Kearse M, Moir R, Wilson A, Stones-Havas S, Cheung M, Sturrock S, et al. Geneious Basic: an integrated and extendable desktop software platform for the organization and analysis of sequence data. Bioinformatics. 2012;28:1647–9.
25. Sayers EW, Cavanaugh M, Clark K, Pruitt KD, Sherry ST, Yankie L, et al. GenBank 2024 Update. Nucleic Acids Res. 2024;52(D1):D134–7.
26. Galardini M, Mengoni A, Bazzicalupo M. Mapping contigs using CONTIGuator. Methods Mol Biol. 2015;1231:163–76.
27. Lemmon AR, Brown JM, Stanger-Hall K, Lemmon EM. The effect of ambiguous data on phylogenetic estimates obtained by maximum likelihood and Bayesian inference. Syst Biol. 2009;58:130–45.
28. Debourgogne A, Gueidan C, Hennequin C, Contet-Audonneau N, de Hoog S, Machouart M. Development of a new MLST scheme for differentiation of *Fusarium solani* Species Complex (FSSC) isolates. J Microbiol Methods. 2010;82:319–23.
29. Chang DC, Grant GB, O'Donnell K, Wannemuehler KA, Noble-Wang J, Rao CY, et al.; Fusarium Keratitis Investigation Team. Multistate outbreak of *Fusarium keratitis* associated with use of a contact lens solution. JAMA. 2006;296:953–63. https://doi.org/10.1001/jama.296.8.953
30. Quick J, Grubaugh ND, Pullan ST, Claro IM, Smith AD, Gangavarapu K, et al. Multiplex PCR method for MinION and Illumina sequencing of Zika and other virus genomes directly from clinical samples. Nat Protoc. 2017;12:1261–76. https://doi.org/10.1038/nprot.2017.066
31. Kilian M, Scholz CF, Lomholt HB. Multilocus sequence typing and phylogenetic analysis of *Propionibacterium acnes.* J Clin Microbiol. 2012;50:1158–65. https://doi.org/10.1128/JCM.r06129-11
32. Yeo M, Mauricio IL, Messenger LA, Lewis MD, Llewellyn MS, Acosta N, et al. Multilocus sequence typing (MLST) for lineage assignment and high resolution diversity studies in *Trypanosoma cruzi.* PLoS Negl Trop Dis. 2011;5:e1049. https://doi.org/10.1371/journal.pntd.0001049
33. O'Donnell K, Sutton DA, Fothergill A, McCarthy D, Rinaldi MG, Brandt ME, et al. Molecular phylogenetic diversity, multilocus haplotype nomenclature, and in vitro antifungal resistance within the *Fusarium solani* species complex. |J Clin Microbiol. 2008;46:2477–90. https://doi.org/10.1128/JCM.02371-07
34. Tsang AKL, Lee HH, Yiu SM, Lau SKP, Woo PCY. Failure of phylogeny inferred from multilocus sequence typing to represent bacterial phylogeny. Sci Rep. 2017;7:4536. https://doi.org/10.1038/s41598-017-04707-4
35. Bleidorn C, Gerth M. A critical re-evaluation of multilocus sequence typing (MLST) efforts in Wolbachia. FEMS Microbiol Ecol. 2018;94:1. https://doi.org/10.1093/femsec/fix163

Address for correspondence: Charles Y. Chiu, UCSF China Basin Campus, 185 Berry St, Box 0134, San Francisco, CA 94143, USA; email: charles.chiu@ucsf.edu

Detection of SARS-CoV-2 Reinfections Using Nucleocapsid Antibody Boosting

Eduard Grebe, Daniel Chacreton, Mars Stone, Bryan R. Spencer, James Haynes, Akintunde Akinseye, Marion C. Lanteri, Valerie Green, Hasan Sulaeman, Roberta Bruhn, Vivian I. Avelino-Silva, Paul Contestable, Brad J. Biggerstaff, Melissa M. Coughlin, Brian Custer, Jefferson M. Jones, David Wright,[1] Michael P. Busch[1]

More than 85% of US adults had been infected with SARS-CoV-2 by the end of 2023. Continued serosurveillance of transmission and assessments of correlates of protection require robust detection of reinfections. We developed a serologic method for identifying reinfections in longitudinal blood donor data by assessing nucleocapsid (N) antibody boosting using a total immunoglobulin assay. Receiver operating characteristic curve analysis yielded an optimal ratio of ≥1.43 (sensitivity 87.1%, specificity 96.0%). When prioritizing specificity, a ratio of ≥2.33 was optimal (sensitivity 75.3%, specificity 99.3%). In donors with higher anti-N reactivity levels before reinfection, sensitivity was reduced. Sensitivity could be improved by expanding the dynamic range of the assay through dilutional testing, from 38.8% to 66.7% in the highest reactivity group (signal-to-cutoff ratio before reinfection >150). This study demonstrated that longitudinal testing for N antibodies can be used to identify reinfections and estimate total infection incidence in a blood donor cohort.

In earlier phases of the COVID-19 pandemic, cross-sectional serosurveillance was informative for establishing cumulative incidence rates and the prevalence of previous infection in a population (*1*). In countries with spike (S)-based vaccines, previous SARS-CoV-2 infection could be detected using anti-nucleocapsid (N) serologic assays, which in combination with anti-S assays could discriminate vaccine-induced antibody reactivity from infection-induced antibody reactivity (*2*). However, because the epidemic evolved with increasing seroprevalence and most of the global population have experienced ≥1 SARS-CoV-2 infections, using serologic methods to estimate infection incidence now requires robust detection of reinfections. Furthermore, after the public health emergency declaration expired, case reporting and collection for public health surveillance decreased, limiting the ability to monitor transmission and disease burden, particularly rates of asymptomatic infection and subclinical reinfection.

The National Blood Donor Cohort (NBDC) is a longitudinal study of blood donors sponsored by the US Centers for Disease Control and Prevention and conducted in partnership with the 2 largest US blood collectors, Vitalant and the American Red Cross; their central testing laboratory, Creative Testing Solutions; and Westat (*3*). An earlier iteration of this program, the National Blood Donor Serosurvey, executed serial monthly cross-sectional serosurveys during July 2020–December 2021 (*1*,*4*–*7*) to provide population-weighted seroprevalence estimates. By the end of 2021, the proportion of donation specimens with vaccine-induced or infection-induced anti-S seroprevalence approached 95%, and infection-induced anti-N seroprevalence approached 30% (*6*). Because

Author affiliations: Vitalant Research Institute, San Francisco, California, USA (E. Grebe, M. Stone, H. Sulaeman, R. Bruhn, V.I. Avelino-Silva, B. Custer, M.P. Busch); Westat, Rockville, Maryland, USA (D. Chacreton, A. Akinseye, D. Wright); University of California San Francisco, San Francisco (M. Stone, R. Bruhn, B. Custer, M.P. Busch); American Red Cross, Dedham, Massachusetts, USA (B.R. Spencer); American Red Cross, Rockville (J.M. Haynes); Creative Testing Solutions, Tempe, Arizona, USA (M.C. Lanteri, V. Green); San Francisco State University, San Francisco (H. Sulaeman); QuidelOrtho, Rochester, New York, USA (P. Contestable); Centers for Disease Control and Prevention, Fort Collins, Colorado, USA (B.J. Biggerstaff); Centers for Disease Control and Prevention, Atlanta, Georgia, USA (M.M. Coughlin, J.M. Jones)

DOI: https://doi.org/10.3201/eid3105.250021

[1]These senior authors contributed equally to this article.

reinfections were known to become more common beginning in 2022 (*8*–*10*), we modified the blood donor study to a longitudinal design to enable detection of reinfections. Longitudinal testing is required to identify reinfections through boosting of infection-induced antibodies. Here, we describe the methods developed to detect reinfections in blood donors by detecting boosting of N antibodies, and measure the performance of those methods.

Materials and Methods

Study Population

Blood donors with a history of regular blood donation and with known prior SARS-CoV-2 infection and COVID-19 vaccination status (determined during the June 2020–June 2021 screening period) were selected for continued monitoring in the NBDC. Eligible donors were those who sought to donate blood at least twice during the screening period and met all blood donor eligibility criteria. The NBDC included 142,599 donors who were categorized into 4 groups by previous SARS-CoV-2 infection and vaccination status as of mid-2021. We established groups by testing donation specimens with the VITROS Anti-SARS-CoV-2 S total immunoglobulin (Ig) assay (QuidelOrtho, https://www.quidelortho.com) and Elecsys Anti-SARS-CoV-2 N total Ig assay (Roche, https://www.roche.com), as well as self-reported COVID-19 vaccination status (*1*,*3*,*6*,*11*). During follow-up, July 2021–December 2022, we identified donation specimens from donors in the cohort in real time and stored those specimens frozen. In 2022, we typically tested 1 donation specimen per donor per quarter (if the donor presented in that quarter), using VITROS Anti-SARS-CoV-2 IgG Quantitative test (Ortho anti-S IgG; QuidelOrtho) and VITROS Anti-SARS-CoV-2 Total N Antibody assay (Ortho anti-N total Ig; QuidelOrtho) at Creative Testing Solutions and Vitalant Research Institute. For certain substudies, more frequent longitudinal samples were tested.

Self-reported vaccination status was captured at each donation as part of routine donation procedures (M. Stone, unpub. data). We invited all cohort donors to respond to quarterly electronic surveys to report vaccination and infection history, including date and manufacturer of vaccine doses, which were not collected routinely at donation. Survey data enabled identification of swab-confirmed or physician-diagnosed first infections and reinfections, and associated symptoms and clinical outcomes. The overall survey response rate was 46.5%. We restricted this study to survey respondents with informative survey responses, i.e., responses that followed tested donation specimens.

Definition of Cases and Controls for Identifying Anti-N Boosting Criteria

We defined confirmed reinfections (cases) as survey-reported swab-confirmed reinfections. Methods for confirmation were a viral test, such as a rapid antigen test or laboratory-based PCR test, or a physician diagnosis (presumed to be on the basis of diagnostic testing). The first infections before the confirmed reinfections could be serologically identified by anti-N seroconversion or be reported as swab-confirmed infections. To classify a swab-confirmed infection as a reinfection, the reinfection had to occur ≥90 days after either seroconversion or a previous swab-confirmed infection. We identified a total of 2,681 cases of swab-confirmed reinfection.

We identified donors from early in the pandemic (the second half of 2020), when reinfections were rare (*12*). We selected donors for whom we had ≥2 longitudinal anti-N results, the first of which had been ≥56 days after seroconversion. Among those donors, we defined controls as donors who responded to the electronic survey and did not report any swab-confirmed or suspected infections during relevant interdonation intervals (IDIs). We identified a total of 5,150 controls.

Laboratory Testing and Anti-N Reactivity Trajectories

We tested donation specimens from cases and controls with the Ortho anti-N total Ig assay in accordance with the manufacturer's instructions. That semiquantitative assay reports signal-to-cutoff (S/CO) ratios, which we used to calculate changes in anti-N reactivity. The assay has high sensitivity to detect first infections in vaccinated (98.2% sensitivity) and unvaccinated (95.6% sensitivity) persons (*13*).

After initial results indicated insufficient dynamic range to detect boosting in persons who had high anti-N reactivity (S/CO >100), we developed a dilutional testing algorithm to extend the dynamic range of the assay. The algorithm implemented a 2-step dilution procedure: if the undiluted specimen (neat testing) yielded an S/CO ≥100, we retested the specimen in a 1:20 dilution. If the S/CO yielded by the 1:20 dilution (before multiplication) was still ≥100, we further tested the sample in a 1:400 dilution. We programmed and performed those dilutions on the VITROS instrument as reflex testing. The final estimated S/CO (reactivity) of the sample was then the S/CO obtained from the final dilution

(neat, 1:20, or 1:400) multiplied by the dilution factor (1, 20, or 400).

We plotted individual donors' anti-N trajectories, and derived average trajectories across all donors included in the analysis after first infection, before reinfection, and after reinfection. We stratified average trajectories by vaccination status.

Identifying Anti-N Boosting Criteria

We evaluated 2 methods to detect anti-N boosting for sensitivity and specificity. First, we estimated the slope in reactivity between 2 donation specimens (difference in log S/CO obtained on subsequent samples divided by time elapsed between samples). If the slope was positive (indicating an increase in reactivity) and exceeded a set threshold, we classified the IDI as a reinfection. We used the identified cases and controls for identifying optimal slope and ratio thresholds and to assess the performance of thresholds. We included only first reinfection (i.e., second infection) cases in the analysis.

Second, we derived a ratio of anti-N reactivity at the end of the IDI to reactivity at the start of the IDI, and if the ratio exceeded a threshold, we classified it as a reinfection. The first approach has the theoretical advantage over the second of accounting for lengths of IDIs, which are highly variable, but has the disadvantage of being more complicated to calculate.

Time to peak anti-N reactivity after first infections is variable. Misclassification can result from computing a ratio using sequential values observed during the initial ramp-up phase of anti-N reactivity after a first infection. That misclassification could result in an apparent reinfection-associated boost when in fact it represents continuing antibody reactivity increase (maturation) associated with 1 infection. For those reasons, we refined the method to only consider IDIs eligible for reinfection detection when the first specimen was collected ≥56 days after initial seroconversion (i.e., after first observed anti-N reactive donation). We chose the cutoff of 56 days on the basis of reported peak anti-N at 30–90 days after symptom onset, although that peak can be influenced by disease severity (*14*). Our reason was that a 56-day minimum was likely to reduce misclassification because of maturing antibody responses after first infection, while retaining most whole-blood donors for whom a minimum interdonation interval of 56 days applied. Furthermore, because very low S/COs can be unstable, and because very small absolute increases might exceed identified ratio thresholds, we set S/COs <1 to 1 for the purpose of calculating the ratio (Appendix, https://wwwnc.cdc.gov/EID/article/31/5/25-0021-App1.pdf). We imposed no maximum IDI length.

Statistical Analysis

Identification of Optimal Boosting Thresholds

We used ROC curve analysis to identify optimal anti-N boosting thresholds for detection of first reinfections, using the 2 approaches to quantify boosting we described. We defined optimality in 2 ways: first, on the basis of an equal weighting of sensitivity and specificity, as the threshold that maximized Youden's J statistic. Second, given that poor specificity would severely affect population-level estimates in a context in which reinfections are relatively rare, we defined optimality based on a weighted Youden's J, which prioritized specificity (Appendix). We chose the weight on the basis of the conservative assumption that 1 in 40 infections are reinfections. We therefore identified 2 sets of optimal thresholds, based on Youden's J and weighted Youden's J, for both the slope and ratio methods of classification. The weight could be adjusted or abandoned for later studies conducted when reinfections represented a larger proportion of all infections. Beyond sensitivity and specificity, we further evaluated only the ratio method in this analysis, given similar performance and reduced complexity. To further assess performance of anti-N boosting thresholds, we computed positive and negative predictive values (PPVs and NPVs) under different scenarios defined by hypothetical rates of reinfection.

Effect of Prereinfection Anti-N Reactivity Level on Sensitivity and Specificity

To assess the effect of assay saturation (limited dynamic range suppressing higher S/COs, which potentially limited the ability to observe reinfection-associated boosting), we stratified cases and controls by the anti-N S/CO at the start of the IDI and computed sensitivity and specificity using the thresholds derived from Youden's J and weighted Youden's J in each stratum. The strata were S/CO ≤50, >50 to ≤100, >100 to ≤150, and >150. We further computed the median ratio observed in cases and controls in each stratum.

Sensitivity of Dilutional Anti-N Testing for Detection of First Reinfections

Because we performed dilutional testing only on a subset of cases, and not controls, we could assess performance only in terms of sensitivity, which was the parameter affected by the reactivity level at the start

of the interval used to compute ratios. We computed the sensitivity (using both thresholds) in each stratum for the neat (undiluted) testing–only algorithm and the dilutional-testing algorithm. We further report the median observed ratios in cases for each testing algorithm. We conducted all analyses using SAS version 9.4 (SAS Institute Inc., https://www.sas.com) and Python version 3.10.11 (Python Software Foundation, https://www.python.org).

Results

Anti-N Boosting Associated with Reinfection

In donors reporting swab-confirmed reinfections, individual neat anti-N reactivity trajectories tended to wane slowly or remain stable after first infections with clear boosting of antibody reactivity after reinfection (Figure 1). As previously reported (*15*), vaccination history affected the level of reactivity observed;

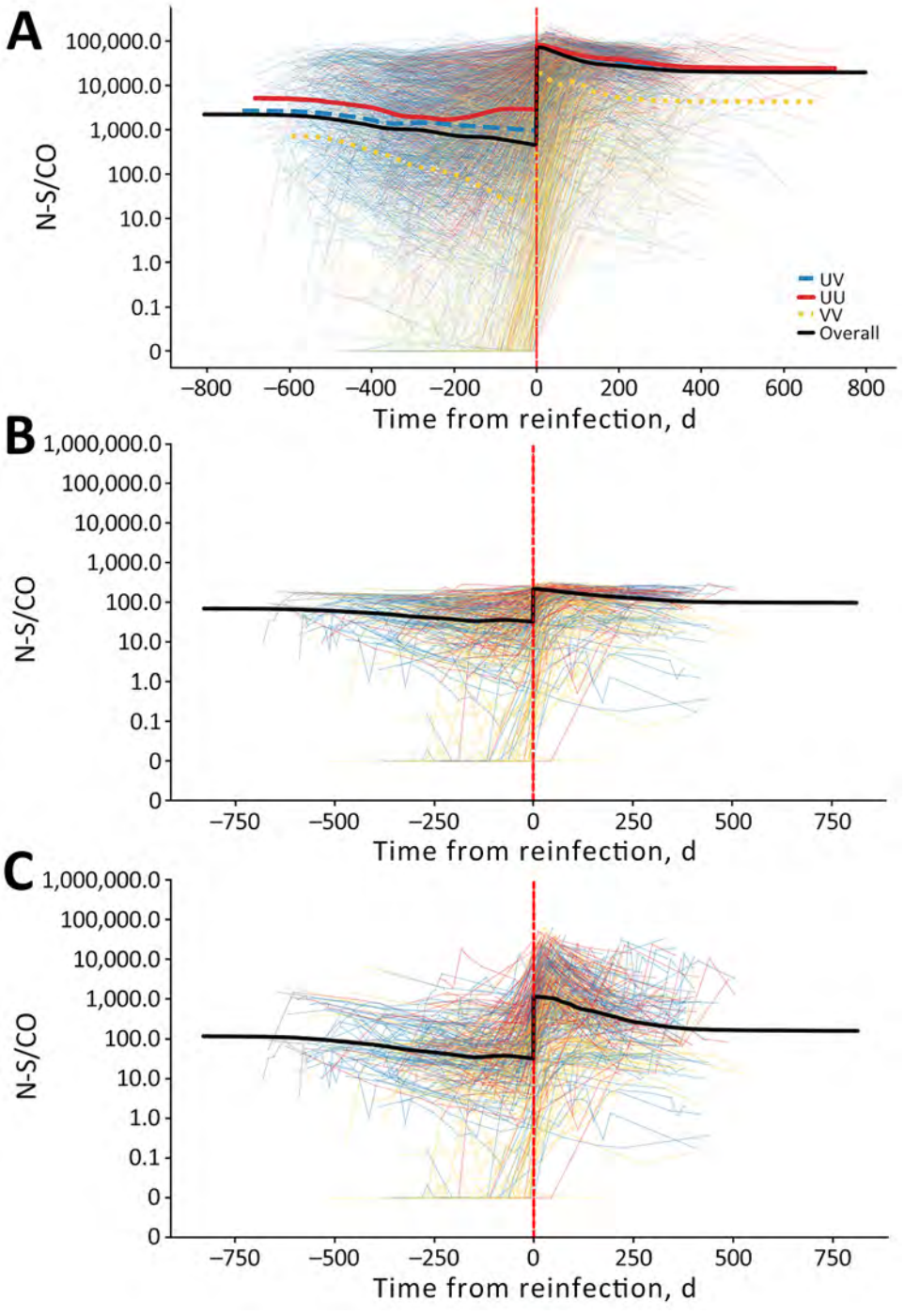

Figure 1. Individual anti-N S/CO trajectories before and after swab-confirmed reinfection in vaccinated and unvaccinated participants in study of detection of SARS-CoV-2 reinfections using nucleocapsid antibody boosting. A) S/CO trajectories with neat-only anti-N testing of all donors with reinfections in the study. B) Trajectories of test results from 434 donors with reinfections subjected to expanded dynamic range dilutional anti-N testing; neat results only. C) Trajectories of test results from the same 434 donors with reinfections subjected to dilutional anti-N testing; dilutional (expanded dynamic range) testing results only. Images show average anti-N trajectories of donors who experienced reinfections, with and without expanded dynamic range testing, stratified by vaccination status. Time represents days before or after swab-confirmed reinfection (vertical red dashed line). N, nucleocapsid; S/CO, signal-to-cutoff ratio; UU, unvaccinated at the time of first infection and reinfection; UV, unvaccinated at first infection and vaccinated at reinfection; VV, vaccinated at first infection and reinfection.

Table 1. Reinfection classification data determined from receiver operating characteristic curve analysis in study of SARS-CoV-2 reinfections detected by nucleocapsid antibody boosting*

Classification method	Statistic†	Optimal threshold (95% CI)	Sensitivity, % (95% CI),‡ n = 2,681	Specificity, % (95% CI),‡ n = 5,150
Pre–/post–anti-N slope	Unweighted Youden's J	0.003 (0.003–0.004)	87.24 (86.09–87.84)	96.97 (96.04–97.61)
Pre–/post–anti-N slope	Weighted Youden's J	0.006 (0.006–0.007)	78.78 (76.73–80.16)	99.38 (99.18–99.38)
Post–/pre–anti-N ratio	Unweighted Youden's J	1.43 (1.27–1.61)	87.09 (84.48–88.77)	95.96 (93.24–97.51)
Post–/pre–anti-N ratio	Weighted Youden's J	2.33 (2.12–2.56)	75.31 (72.7–77.88)	99.34 (99.13–99.38)

*N, nucleocapsid.
†Weighted method prioritized specificity by applying a weight to specificity (see Methods).
‡Sensitivity and specificity associated with lower and upper CI limits on optimal threshold.

unvaccinated donors exhibited higher postinfection anti-N reactivity than vaccinated donors. Donors who were vaccinated before their first infection showed overall lower reactivity levels than unvaccinated donors, and donors who were vaccinated between the 2 infection events showed reactivity that fell between donors who were vaccinated before the first infection and those who were not vaccinated (Figure 1, panel A). However, the relative magnitude of the anamnestic boost induced by reinfection was similar across vaccination groups.

Identification of Optimal Boosting Thresholds

The optimal anti-N boosting threshold for the slope approach, using the unweighted Youden's J method, was ≥0.003 $\log_{10}$(S/CO) per day, and using the weighted Youden's J method was ≥0.006 $\log_{10}$(S/CO) per day. Using unweighted Youden's J method, sensitivity was 87.2% and specificity was 97.0%. Using weighted Youden's J method sensitivity was 78.8% and specificity was 99.4% (Table 1). For the simpler ratio approach, the optimal thresholds were ≥1.43 (95% CI 1.27–1.61) for the unweighted Youden's J method and ≥2.33 (95% CI 2.12–2.56) for specificity-prioritized weighted Youden's J method. For unweighted Youden's J method, associated sensitivity was 87.1% and specificity was 96.0%; for specificity-prioritized weighted Youden's J method, sensitivity was 75.3% and specificity was 99.3% (Table 1).

Seroconversion in Anti-N Negative Prereinfection Samples

Of 2,681 swab-confirmed reinfection cases, 328 (12.2%) did not demonstrate anti-N reactivity above the threshold for positivity (S/CO ≥1) at the immediate prereinfection sample. Of those that did not demonstrate anti-N reactivity, 296 were available for further evaluation; 246 (83.1%) had never seroconverted after the first reported infection and 50 (16.9%) seroreverted before reinfection. All 328 donors with negative prereinfection results seroconverted after reinfection (Figure 1).

Effect of Post–First Infection Anti-N Reactivity on Performance of Anti-N Boosting Thresholds

Using the lower threshold of the ratio method derived from the unweighted Youden's J method, we noted that as prereinfection S/CO increased, sensitivity declined from 93.8% in the S/CO ≤50 group to 88.0% in the S/CO >100–150 group and was lowest at 38.8% in the S/CO >150 group. Specificity was similar across prereinfection reactivity strata (91.7% to 97.0%) (Table 2). Using the higher threshold derived from the weighted Youden's J method, we noted that sensitivity declined from 91.6% in the S/CO ≤50 group to 0.8% in the S/CO >150 group. Specificity was similar across prereinfection reactivity strata (98.9% to 100.0%). Median observed postreinfection to prereinfection S/CO ratios in cases also declined in higher prereinfection reactivity strata, from 15.2 in the lowest reactivity stratum to 1.3 in the highest reactivity stratum (Table 2).

Dilutional Anti-N Testing to Improve Detection of Reinfections

We tested a subset of cases using the anti-N dilutional algorithm (n = 434). When we used the neat testing results only, sensitivities were 85.1% in the group with prereinfection S/CO ≤50 and 38.5% in the S/CO >150 group when using the unweighted ratio threshold

Table 2. Reinfection classification data determined from ratio approach in study of SARS-CoV-2 reinfections detected by nucleocapsid antibody boosting*

	Cases		Controls		Unweighted Youden's J (1.43)		Weighted Youden's J (2.33)	
S/CO	No.	Median ratio	No.	Median ratio	Sensitivity, %	Specificity, %	Sensitivity, %	Specificity, %
Overall	2,681	6.22	5,150	0.55	87.1	96.0	75.3	99.3
0–50	1,661	15.2	2,237	0.49	93.8	97.0	91.6	98.9
50–100	485	3.41	1,042	0.49	89.5	97.3	81.9	99.2
100–150	275	2.15	757	0.56	88.0	91.7	35.6	99.9
>150	260	1.28	1,114	0.76	38.8	95.5	0.8	100.0

*S/CO value is prereinfection. Unweighted and weighted boosting thresholds are ratios of postreinfection to prereinfection S/CO. S/CO, signal-to-cutoff ratio.

Table 3. Reinfection detection data by prereinfection anti-N reactivity level in study of SARS-CoV-2 reinfections detected by nucleocapsid antibody boosting*

S/CO†	No. cases	Median ratio		Sensitivity of unweighted Youden's J (1.43)		Sensitivity of weighted Youden's J (2.33)	
		Neat	Dilution	Neat, %	Dilution, %	Neat, %	Dilution, %
Overall	434	4.50	58.54	79.3	81.6	65.0	80.6
0–50	262	10.94	94.32	85.1	85.1	84.4	84.4
50–100	78	2.82	64.97	78.2	78.5	69.2	78.2
100–150	55	1.90	29.49	81.8	80.0	12.7	80.0
>150	39	1.35	9.20	38.5	66.7	0.0	61.5

*Reactivity was measured with and without expanded dynamic range anti-N testing reinfection cases. S/CO, signal-to-cutoff ratio. Unweighted and weighted boosting thresholds are ratios of postreinfection to prereinfection S/CO.
†S/CO value is prereinfection.

and 84.4% in the S/CO ≤50 and 0.0% in the S/CO >150 group when using the weighted ratio threshold (Table 3). Dilutional testing improved sensitivity in the group with prereinfection S/CO >150 to 66.7% for the unweighted ratio thresholds, and to 61.5% for weighted ratio thresholds. For groups with prereinfection S/CO 100–150, sensitivity remained ≥80% for weighted and unweighted ratio thresholds when we performed dilutional testing (Table 3; Figure 2).

Performance of Anti-N Boosting Thresholds at Different Population Reinfection Rates

When the percentage of population experiencing reinfection was low, NPV was high and declined slowly as the rate of reinfection increased, and PPV was low but increased rapidly as the reinfection rate increased. PPV >80% was achieved when the lower ratio threshold was >15% of the population reinfected (Figure 3, Panel A), and when the higher ratio was >5% of the population reinfected (Figure 3, panel B). The optimal scenario for our thresholds (maximizing PPV and NPV) were 37% reinfected for the lower ratio threshold and 16% reinfected for the for the higher ratio threshold.

Discussion

We evaluated a method for serologic identification of reinfections using anamnestic boosting of anti-N reactivity in longitudinal blood donor samples. Anti-N boosting thresholds optimized to maximize specificity achieved reasonable sensitivity (>75%) and excellent specificity (>99%) for detection of first reinfections. We also derived a lower threshold that achieves sensitivity >87%, but sacrifices some specificity. However, the sensitivity to detect first reinfections was quite low in donors with high anti-N reactivity after first infections; reactivity plateaued near the top of the assay's limited dynamic range and masked anamnestic boosting associated with reinfections. Thus, we developed a dilutional testing algorithm that dramatically expanded the dynamic range, greatly improving sensitivity to detect reinfections in persons with high anti-N reactivity before reinfection. We based the trigger for dilutions (S/CO ≥100) on guidance from the manufacturer, who conducted studies to identify the linear dilutional performance range (P. Contestable, pers. comm., confirmed by email 2025 Apr 7). As multiple reinfections become increasingly common, expanded dynamic range testing will become increasingly important.

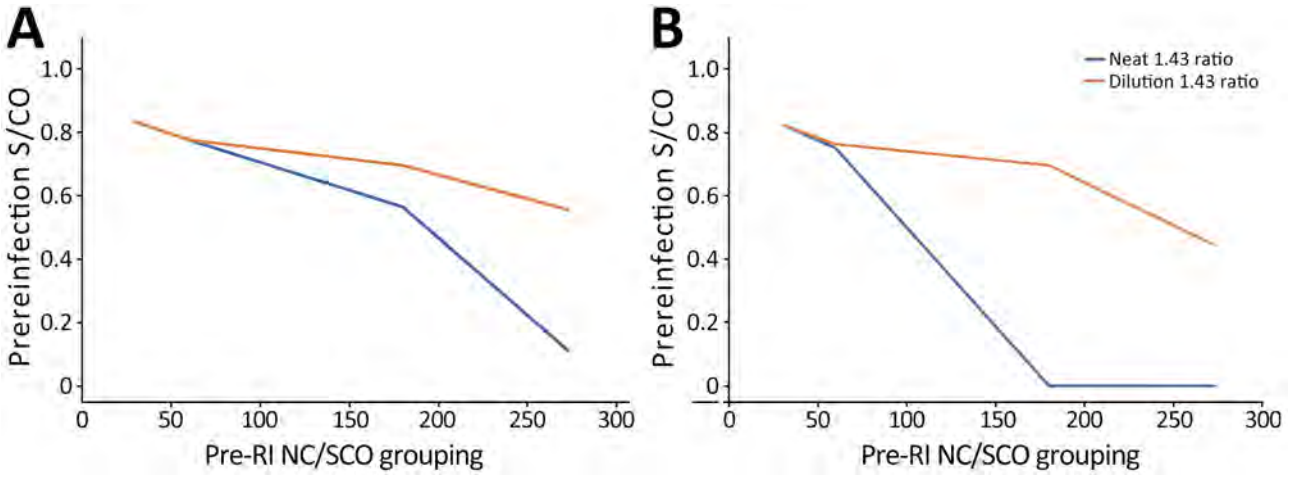

Figure 2. Effect of prereinfection anti-N S/CO on performance of boosting thresholds in study of detection of SARS-CoV-2 reinfections using nucleocapsid antibody boosting. A) Sensitivity by prereinfection anti-N S/CO using neat and dilutional testing for the unweighted threshold (≥1.43); B) sensitivity by prereinfection anti-N S/CO using neat and dilutional testing for the weighted threshold (≥2.33). S/CO, signal-to-cutoff ratio.

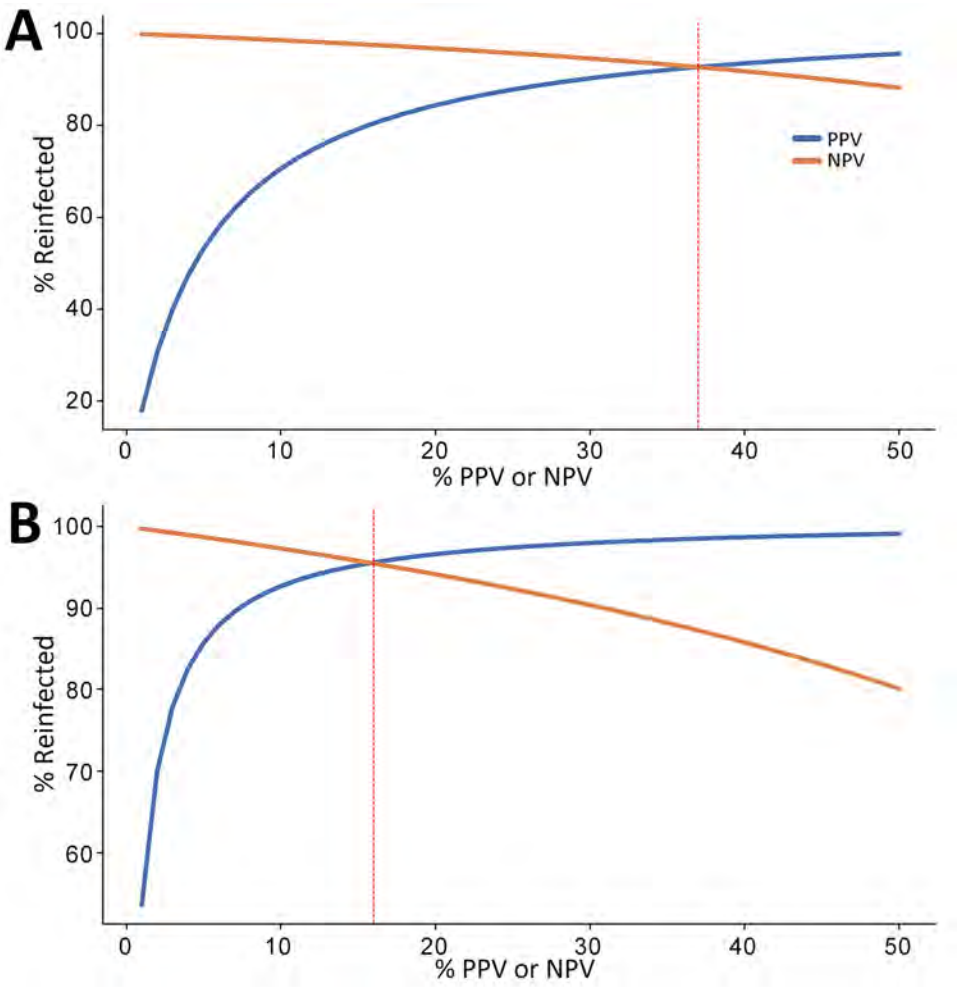

Figure 3. PPV and NPV in a study of detection of SARS-CoV-2 reinfections using nucleocapsid antibody boosting. A) Unweighted threshold ratio ≥1.43. B) Weighted threshold ratio ≥2.33. Predictive values were calculated as a function of percentage of a population of blood donors experiencing SARS-CoV-2 reinfection, at different rates of reinfection. Vertical red lines indicate the proportions reinfected that represent the optimal scenarios for the given threshold ratio, i.e., where PPV and NPV are simultaneously maximized. NPV, negative predictive value; PPV, positive predictive value.

We could not assess the specificity of the dilutional algorithm on the basis of the reflex testing criteria used in this study because we did not perform dilutional testing of controls; the risk for reduced specificity (as demonstrated in neat specimen reactivity ratios) suggests using the higher threshold (ratio ≥2.33) in expanded dynamic range testing. Although sensitivity in the neat testing dropped to 0% using the higher threshold for donors with anti-N S/CO >150 before reinfection, sensitivity was maintained at >60% for this group with dilutional testing.

We considered multiple methods for identifying reinfections based on anti-N boosting. The first and most complex relied on estimating an individual postinfection anti-N reactivity waning rate on the basis of ≥2 observations after first infection. That waning rate would then be used to estimate an expected value of anti-N reactivity at the time of a later donation specimen, and the expected value compared to the observed reactivity. That approach would have enabled us to incorporate uncertainty in expected reactivity arising from assay variability, inconsistent waning patterns, or other factors. We could then compare the observed anti-N reactivity to the expected reactivity; if the former exceeded the latter by a set threshold (e.g., 2 SD), we would classify the IDI as one in which a reinfection occurred. We abandoned that approach because of its complexity, highly variable time to peak and peak level of reactivity time after first infections, relative stability in anti-N reactivity in the Ortho assay, and difficulty in robustly estimating individual waning rates.

Although we did not pursue the originally envisaged method based on estimating average and person-specific anti-N waning rates, that approach could be further explored, especially if an IgG assay is used; IgG assays tend to show more rapid waning than total Ig assays (*2*,*16*). The method and thresholds identified as optimal in this study apply specifically to the Ortho Total Ig anti-N assay. The rapid waning of IgG assays may have advantages for detection of reinfection-associated antibody boosting, although

the length of time intervals between specimens would also be important for interpretation.

We did not expect the finding that 12.2% of prereinfection samples had anti-N S/CO below the threshold for positivity. Possible causes are misreporting of infections or infection dates, seroreversion, or a failure to develop anti-N antibodies after the first infection. We previously reported that 1.9% of samples from unvaccinated donors and 4.4% collected from vaccinated donors after first swab-confirmed infections tested anti-N nonreactive on the Ortho assay (*14*). Petersen et al. (*17*) also reported similar rates of failure to develop antibodies after SARS-CoV-2 infection. All donors seroconverted after the reported reinfection, although serology alone would classify those infections as first infections.

A limitation of our study is that we relied on self-reported infection and vaccination history, supported by our serologic testing. Furthermore, we could not establish with certainty that our (nonreinfected) controls for the ROC curve analysis had not experienced reinfections. However, the contamination of our results by controls who did experience reinfections during the intervals used in the analysis is likely minimal because reinfections were very rare at the time that the donation specimens were collected (*12*). Cases were all swab-confirmed, and because testing is usually triggered by symptomatic disease, cases largely represent symptomatic reinfection cases. Therefore, our thresholds might not be accurate for detection of asymptomatic reinfections; accuracy is further complicated by the possibility of exposures that do not result in substantial viral replication and consequently do not trigger an anamnestic boosting of antibodies (*18*). A further limitation is that no expanded dynamic range testing was available on controls because of limited testing capacity; therefore, we could not identify optimal thresholds for a dilutional testing regime. Second, third, and subsequent reinfections are not included in this study but are the subject of future work. Finally, blood donors are not demographically representative of the general population, and the healthy donor effect means that chronic health conditions are less prevalent in blood donors than in the general population (*19*,*20*).

Despite those limitations, blood donor cohorts have tremendous value for public health research, including enabling serosurveillance of infectious diseases in a healthy population, related focused studies such as correlates of protection and population immunity studies, rapid response to emerging infectious threats, and the ability to address a wide range of general health-related questions in a low-cost manner. The platform established by the NBDC has been leveraged by the Centers for Disease Control and Prevention and its partners to develop a broader respiratory virus surveillance program.

In conclusion, we developed and measured the performance of a method for detecting boosting of N antibodies to identify SARS-CoV-2 reinfections. The method enables detection of total infection incidence by combining detections of first-time infections through anti-N seroconversion with detection of reinfections. Given that most persons have previously been infected with SARS-CoV-2 and public health case reporting has decreased, methods to detect reinfections are needed to estimate the burden of COVID-19 moving forward. Seroepidemiology can provide specific estimates of infections, complementing trends in wastewater surveillance, and COVID-19 test positivity. In addition, antibody testing enables assessment of correlates of protection and vaccine effectiveness against mild or asymptomatic infections.

Acknowledgments

We thank numerous laboratory and data management staff, including Hasan Sulaeman, Brendan Balasko, Jahnavi Bhaskar, Patricia Villaflor, Kaya Duncan, Zhanna Kaidarova, and Anh (Paul) Nguyen at Vitalant Research Institute; Marjorie D. Bravo at Vitalant; Edward P. Notari, James Haynes, Jamel Groves, and Gary Holley at American Red Cross; Rebecca Fink at Westat; Athena Nguyen, Dave Kovach, Chloe Byrne, Daishia Hall, and Tatum Fenner at Creative Testing Solutions; and Melissa Briggs-Hagen at the Centers for Disease Control and Prevention.

All blood donors provided written consent to the use of deidentified, residual specimens for further research purposes. Consistent with the policies and guidance of the University of California–San Francisco Institutional Review Board, Vitalant Research Institute self-certified the use of deidentified donations in this study as not meeting the criteria for human subjects research. Centers for Disease Control and Prevention (CDC) investigators reviewed and relied on this determination as consistent with applicable federal law and CDC policy (45 Code of Federal Regulations [C.F.R.] part 46, 21 C.F.R. part 56; 42 U.S.C. §241[d]; 5 U.S.C. §552a; 44 U.S.C. §3501). The donor surveys conducted by Vitalant and American Red Cross were conducted under protocols supervised and approved by the Advarra and American Red Cross Institutional Review Boards, respectively, and linked to biospecimens in deidentified form.

This work was supported by research contracts from the US Centers for Disease Control and Prevention (contract no. 75D30120C08170).

Vitalant Research Institute receives research funding from QuidelOrtho. V.A.-S. is an employee of Merck Sharp & Dohme LLC., a subsidiary of Merck & Co., Inc., Rahway, NJ, and may own stock or stock options in Merck & Co., Inc., Rahway, NJ, USA. The authors have no other conflicts of interest to declare.

About the Author

Dr. Grebe is a researcher in the epidemiology of infectious diseases and an affiliate investigator at Vitalant Research Institute. His focus areas are HIV incidence estimation, blood donor epidemiology, transfusion safety, and evaluation of laboratory assays.

References

1. Jones JM, Stone M, Sulaeman H, Fink RV, Dave H, Levy ME, et al. Estimated US infection- and vaccine-induced SARS-CoV-2 seroprevalence based on blood donations, July 2020–May 2021. JAMA. 2021;326:1400–9. https://doi.org/10.1001/jama.2021.15161
2. Stone M, Grebe E, Sulaeman H, Di Germanio C, Dave H, Kelly K, et al. Evaluation of commercially available high-throughput SARS-CoV-2 serologic assays for serosurveillance and related applications. Emerg Infect Dis. 2022;28:672–83. https://doi.org/10.3201/eid2803.211885
3. Fink RV, Fisher L, Sulaeman H, Dave H, Levy ME, McCann L, et al. How do we…form and coordinate a national serosurvey of SARS-CoV-2 within the blood collection industry? Transfusion. 2022;62:1321–33. https://doi.org/10.1111/trf.16943
4. Busch MP, Stone M. Serosurveillance for severe acute respiratory syndrome coronavirus 2 (SARS-CoV-2) incidence using global blood donor populations. Clin Infect Dis. 2021;72:254–6. https://doi.org/10.1093/cid/ciaa1116
5. Stone M, Di Germanio C, Wright DJ, Sulaeman H, Dave H, Fink RV, et al.; NHLBI Recipient Epidemiology and Donor Evaluation Study-IV-Pediatric (REDS-IV-P). Use of US blood donors for national serosurveillance of severe acute respiratory syndrome coronavirus 2 antibodies: basis for an expanded national donor serosurveillance program. Clin Infect Dis. 2022;74:871–81. https://doi.org/10.1093/cid/ciab537
6. Jones JM, Opsomer JD, Stone M, Benoit T, Ferg RA, Stramer SL, et al. Updated US infection- and vaccine-induced SARS-CoV-2 seroprevalence estimates based on blood donations, July 2020–December 2021. JAMA. 2022;328:298–301. https://doi.org/10.1001/jama.2022.9745
7. Busch MP, Stramer SL, Stone M, Yu EA, Grebe E, Notari E, et al. Population-weighted seroprevalence from severe acute respiratory syndrome coronavirus 2 (SARS-CoV-2) infection, vaccination, and hybrid immunity among US blood donations from January to December 2021. Clin Infect Dis. 2022;75:S254–63. https://doi.org/10.1093/cid/ciac470
8. Nguyen NN, Houhamdi L, Hoang VT, Delerce J, Delorme L, Colson P, et al. SARS-CoV-2 reinfection and COVID-19 severity. Emerg Microbes Infect. 2022;11:894–901. https://doi.org/10.1080/22221751.2022.2052358
9. Ma KC, Dorabawila V, León TM, Henry H, Johnson AG, Rosenberg E, et al. Trends in laboratory-confirmed SARS-CoV-2 reinfections and associated hospitalizations and deaths among adults aged ≥18 years—18 U.S. jurisdictions, September 2021–December 2022. MMWR Morb Mortal Wkly Rep. 2023;72:683–9. https://doi.org/10.15585/mmwr.mm7225a3
10. Sun K, Tempia S, Kleynhans J, von Gottberg A, McMorrow ML, Wolter N, et al.; PHIRST-C group. Rapidly shifting immunologic landscape and severity of SARS-CoV-2 in the Omicron era in South Africa. Nat Commun. 2023;14:246. https://doi.org/10.1038/s41467-022-35652-0
11. Jones JM, Manrique IM, Stone MS, Grebe E, Saa P, Germanio CD, et al. Estimates of SARS-CoV-2 seroprevalence and incidence of primary SARS-CoV-2 infections among blood donors, by COVID-19 vaccination status—United States, April 2021–September 2022. MMWR Morb Mortal Wkly Rep. 2023;72:601–5. https://doi.org/10.15585/mmwr.mm7222a3
12. León TM, Dorabawila V, Nelson L, Lutterloh E, Bauer UE, Backenson B, et al. COVID-19 cases and hospitalizations by COVID-19 vaccination status and previous COVID-19 diagnosis—California and New York, May–November 2021. MMWR Morb Mortal Wkly Rep. 2022;71:125–31. https://doi.org/10.15585/mmwr.mm7104e1
13. Grebe E, Stone M, Spencer BR, Akinseye A, Wright D, Di Germanio C, et al. Detection of nucleocapsid antibodies associated with primary SARS-CoV-2 infection in unvaccinated and vaccinated blood donors. Emerg Infect Dis. 2024;30:1621–30. https://doi.org/10.3201/eid3008.240659
14. Lau EHY, Tsang OTY, Hui DSC, Kwan MYW, Chan WH, Chiu SS, et al. Neutralizing antibody titres in SARS-CoV-2 infections. Nat Commun. 2021;12:63. https://doi.org/10.1038/s41467-020-20247-4
15. Follmann D, Janes HE, Buhule OD, Zhou H, Girard B, Marks K, et al. Antinucleocapsid antibodies after SARS-CoV-2 infection in the blinded phase of the randomized, placebo-controlled mRNA-1273 COVID-19 vaccine efficacy clinical trial. Ann Intern Med. 2022;175:1258–65. https://doi.org/10.7326/M22-1300
16. Macdonald PJ, Ruan Q, Grieshaber JL, Swift KM, Taylor RE, Prostko JC, et al. Affinity of anti-spike antibodies in SARS-CoV-2 patient plasma and its effect on COVID-19 antibody assays. EBioMedicine. 2022;75:103796. https://doi.org/10.1016/j.ebiom.2021.103796
17. Petersen LR, Sami S, Vuong N, Pathela P, Weiss D, Morgenthau BM, et al. Lack of antibodies to severe acute respiratory syndrome coronavirus 2 (SARS-CoV-2) in a large cohort of previously infected persons. Clin Infect Dis. 2021;73:e3066–73. https://doi.org/10.1093/cid/ciaa1685
18. Le Bert N, Samandari T. Silent battles: immune responses in asymptomatic SARS-CoV-2 infection. Cell Mol Immunol. 2024;21:159–70. https://doi.org/10.1038/s41423-024-01127-z
19. Rahman MM, Karki S, Hayen A. A methods review of the "healthy donor effect" in studies of long-term health outcomes in blood donors. Transfusion. 2022;62:698–712. https://doi.org/10.1111/trf.16791
20. Brodersen T, Rostgaard K, Lau CJ, Juel K, Erikstrup C, Nielsen KR, et al. The healthy donor effect and survey participation, becoming a donor and donor career. Transfusion. 2023;63:143–55. https://doi.org/10.1111/trf.17190

Address for correspondence: Eduard Grebe, Vitalant Research Institute, 270 Masonic Ave, San Francisco, CA 94118 USA; email: egrebe@vitalant.org

Postexposure Antimicrobial Drug Therapy in Goats Infected with *Burkholderia pseudomallei*

Richard A. Bowen, Airn E. Hartwig, Angela M. Bosco-Lauth, Josilene N. Seixas, Jana M. Ritter, Pamela S. Fair, Mindy G. Elrod, Zachary P. Weiner, Robyn A. Stoddard, Antonio R. Vieira, Rachel M. Maison, Elizabeth Lawrence, Hannah Sueper, Mckinzee Barker, William A. Bower

Infection with *Burkholderia pseudomallei*, the causative agent of melioidosis, occurs by exposure to the organism in soil or water. There is concern for *B. pseudomallei* use as a potential bioweapon and as an exposure hazard in diagnostic laboratories processing samples or cultures containing the bacterium. The optimal strategies for treatment and postexposure prophylaxis are inadequately developed. This study used goats to evaluate 3 antimicrobial drug treatment regimens for postexposure therapy because they are a species naturally susceptible to *B. pseudomallei* infection. Goats were infected by percutaneous inoculation, and antimicrobial drug therapies were initiated 48 hours later. Widespread infection with abscess formation in multiple organs developed in untreated goats and goats treated with either amoxicillin/clavulanate or sulfamethoxazole/trimethoprim. In contrast, treatment with the combination of all 4 antimicrobial drugs might have eradicated the infection. Our findings suggest combination therapy with those 4 antimicrobial drugs may be useful for postexposure prophylaxis in humans.

Melioidosis is an infectious disease caused by the soilborne saprophytic gram-negative bacterium *Burkholderia pseudomallei* (*1*–*3*). The organism is endemic in large regions of southeast Asia and northern Australia (*4*) and has been detected in the Caribbean (*5*), South America (*6*), and most recently in the gulf coast region of the United States (*7*,*8*).

B. pseudomallei is a public health concern and has a very broad host range, causing disease in many domestic and wild mammals and even ectothermic vertebrates (*9*–*11*). Although a wide range of animal species are susceptible to infection, melioidosis is not typically considered a zoonotic disease. However, animals can shed *B. pseudomallei* in the environment, and therefore, infected animals are a potential source for human transmission (*12*,*13*).

In addition to the large burden of naturally occurring melioidosis, there are 2 additional causes of concern. First, *B. pseudomallei* is a potential bioweapon and is classified as a tier 1 select agent by the US government because of its low infectious dose by inhalation and resistance to conventional antimicrobial therapy. Second, there are concerns for accidental exposure of clinical or research laboratory personnel by needle stick or aerosol, especially when isolation of *B. pseudomallei* is not expected and biosafety practices are inadequate (*14*–*16*). In contrast to natural disease, where exposure time is likely unknown and could have occurred many weeks if not years earlier, the timing of deliberate or accidental exposures could be known, providing the opportunity for rapid postexposure prophylaxis (PEP). Those scenarios highlight the need to determine the most effective treatment regimen for PEP.

Clinical manifestations of melioidosis are highly variable in both humans and animals and may involve abscess formation in multiple organs, pneumonia, cutaneous lesions, and sepsis (*12*,*17*). Guidelines for therapy in humans are in place and widely used in endemic regions on the basis of long-standing clinical experience (*18*). A major challenge in the treatment of melioidosis is that *B. pseudomallei* is intrinsically resistant to many antimicrobial drugs, and eradication usually involves prolonged therapy, often with >1 antimicrobial agent (*19*,*20*). Melioidosis therapies in animal models are poorly studied and only in the context of acute PEP in mice (*21*–*23*). The common

Author affiliations: Colorado State University College of Veterinary Medicine and Biomedical Sciences, Fort Collins, Colorado, USA (R.A. Bowen, A.E. Hartwig, A.M. Bosco-Lauth, R.M. Maison, E. Lawrence, H. Sueper, M. Barker); Centers for Disease Control and Prevention, Atlanta, Georgia, USA (J.N. Seixas, J.M. Ritter, P.S. Fair, M.G. Elrod, Z.P. Weiner, R.A. Stoddard, A.R. Vieira, W.A. Bower)

DOI: https://doi.org/10.3201/eid3105.241274

finding from those mouse studies is that antimicrobial drug therapy must be initiated rapidly after the inoculation of *B. pseudomallei*, and although critical extension in postinoculation survival can be attained, the organism is not eliminated. The goal of this article was to evaluate 2 commonly used antimicrobial drug treatment regimens, alone and in combination, for postexposure therapy of *B. pseudomallei* infection in goats, a natural host model for melioidosis.

Materials and Methods

We conducted all animal studies in compliance with the Animal Welfare Act and as approved by the Colorado State University Institutional Animal Care and Use Committee, the Institutional Biosafety Committee, and with approval from the Federal Select Agent Program. We conducted all studies under Biosafety Level 3 (BSL-3) or Animal BSL 3 (ABSL-3) containment at Colorado State University. The number of animals per treatment group was determined by available ABSL-3 space.

Bacterial Strain

The strain of *B. pseudomallei* we used to inoculate study goats was an isolate from an infected goat in Australia designated Bp 4176/MSHR 511 (*24*) and was originally provided to us by Dr. Apichai Tuanyok (University of Florida, Gainesville, Florida, USA). We cultured the bacteria for inoculation in Muller-Hinton broth at 37°C in air with constant shaking, harvested at the mid-log phase of growth, and stocks containing 15% glycerol were stored at −80°C.

Culture Methods

For tissues with grossly visible abscesses, we excised the samples collected for bacterial culture away from major gross lesions. For bacterial isolation, we collected ≈100 mg samples from tissues into homogenizing tubes containing 0.9 ml of brain–heart infusion broth supplemented with 10% glycerol. We homogenized those samples and then froze them to −80°C until processing.

We thawed, vortexed, and briefly centrifuged to pellet tissue debris (2,000 × *g* for 10 s) of the frozen tissue homogenates, spread 0.1 mL of each sample onto a 10 cm Ashdown's agar plate, and incubated the plates at 37°C. We examined the plates 48 hours after inoculation and performed colony counts. We sampled representative colonies that appeared to be *B. pseudomallei* on the basis of morphology and color, along with colonies that did not appear to be *B. pseudomallei* and used them to prepare spot slides that were fixed for 15 minutes with 80% acetone. We immunostained those slides along with known positive and negative (*Escherichia coli*) slides by using an antibody to *B. pseudomallei* capsular polysaccharide (*25*) to confirm their identity.

Antimicrobial Drugs

We conducted a preliminary pharmacokinetic study to confirm blood concentrations of 3 of the 4 drugs after oral administration to 2 goats from another project. ELISA kits for trimethoprim, sulfamethoxazole, and amoxicillin were purchased from MyBioSource (https://www.mybiosource.com), and we assayed serum samples according to the manufacturer's instructions. Each kit contained standards that we used to prepare standard curves. We did not assay serum for concentrations of clavulanate.

Animals, Challenge Procedures, and Clinical Observations

We purchased young adult female goats from a private source and clinically evaluated them to ensure baseline health; they were weighed several days before challenge and had an average weight of 70 kg (63–82 kg). We implanted a Biothermo-Lifechip (Destron-Fearing, https://www.destronfearing.com) subcutaneously in each goat for identification and easy monitoring of body temperature. We housed the goats by group (8 animals per 12- × 18-foot room) under ABSL-3 containment for the duration of the study. We fed the goats alfalfa hay supplemented with grain.

We performed percutaneous challenge by a combination of subcutaneous and intradermal injection over the shoulder region, with a target dose of 10^4 CFU in 0.2 mL of solution. We diluted the bacteria in phosphate buffered saline from frozen-thawed stocks. We evaluated the goats clinically 2 times daily for the duration of the study. We recorded the goat's body temperature from their microchip 2 times daily for the first 10 days, then 1 time daily until euthanasia.

We evaluated 4 antimicrobial drug therapies, each in 8 goats: 1, no treatment; 2, amoxicillin/clavulanate; 3, sulfamethoxazole/trimethoprim; and 4, a combination of amoxicillin/clavulanate and sulfamethoxazole/trimethoprim. We initiated drug treatment 48 hours postchallenge; treatment consisted of oral gavage of 25 mL with a dosing syringe. We prepared drugs by dissolving the requisite number of tablets in deionized water within 30 minutes of treatment. Both types of tablets were manufactured by Aurobindo Pharma (https://www.aurobindo.com) and provided in the following formulations:

amoxicillin/clavulanate, 500/125 mg/tablet; sulfamethoxazole/trimethoprim 1,200/240 mg/tablet. On the basis of tablet composition, the goats received the doses and approximate dosages of drugs 2 times daily for 21 days, ceasing on day 23 postchallenge (Table 1).

Serologic Analyses

We assayed serum collected before and after challenge for antibodies by using 2 techniques. The indirect hemagglutination assay was performed as described previously (*26*). For whole cell lysate ELISA, we used a lysate of *B. pseudomallei* Bp82 that we prepared by using techniques similar to those previously described (*27*,*28*). We coated plates with a solution containing 3 μg/mL of lysate, blocked with phosphate-buffered saline containing dried skim milk (blocking buffer), exposed to the test serum diluted 1:100 in blocking buffer, washed again, and then exposed to a horseradish peroxidase-protein A/G conjugate. After a final washing, we added ABTS substrate and, after stopping the reaction, we read absorbance at 450 nm. The cutoff for positivity was set at 3 SDs above the mean value for all preinoculation serum.

Postmortem Analyses and Radiography

We euthanized goats at 14–28 days postinfection (dpi) (Appendix Table 1, https://wwwnc.cdc.gov/EID/article/31/5/24-1274-App1.pdf) by intravenous injection of an overdose of pentobarbital. We then performed collection and gross examination of spleen, lungs, liver, lymph nodes (mandibular, mesenteric, mediastinal, retropharyngeal, prescapular), kidney, and skin. We recorded the occurrence of visible abscesses in those tissues and the extirpated lungs were radiographed. We fixed tissue samples in 10% neutral buffered formalin.

Histopathology and Immunohistochemistry

We processed formalin-fixed tissues by routine paraffin histology. We sent tissue blocks to Center for Disease Control and Prevention's Infectious Diseases Pathology Branch (Division of High-Consequence Pathogens and Pathology, National Center for Emerging and Zoonotic Infectious Diseases), where they were sectioned at 4 μm, mounted on glass slides, and stained with hematoxylin-eosin for histopathologic evaluation. Two veterinary pathologists visually assessed the slides for the presence of inflammatory or other lesions and for *B. pseudomallei* immunoreactivity.

We conducted immunohistochemical (IHC) assays on select tissues on the basis of 2 criteria: the presence of lesions consistent with *B. pseudomallei* infection observed grossly or microscopically; or tissues with positive result for *B. pseudomallei* on bacterial culture. We tested similar types and numbers of tissues from each treatment group. We also examined a subset of tissues from animals without gross or microscopic lesions or with negative cultures. For the detection of bacterial antigen, we used a rabbit polyclonal *B. pseudomallei* antibody at 1:1,000 dilution. We performed colorimetric detection of attached antibodies by using the Mach 4 AP polymer kit (Biocare Medical, https://biocare.net) at room temperature and with heat-induced epitope retrieval. Using EDTA buffer, we conducted heat-induced epitope retrieval by using the NxGen decloaker (Biocare Medical) at 110°C for 15 minutes. We blocked all slides in Background Punisher (Biocare Medical) for 10 minutes and incubated with primary antibody for 30 minutes. We applied Mach 4 Polymer for 30 minutes (Biocare Medical) and visualized the antibody polymer conjugate by applying fast red chromogen dissolved in naphthol phosphate substrate buffer (Sigma Aldrich, https://www.sigmaaldrich.com) to tissue sections for 30 minutes. We ran the negative control serum in parallel. We counterstained slides with Mayer's hematoxylin (Poly Scientific, https://www.statlab.com) and blued in lithium carbonate (Poly Scientific). Positive controls included formalin-fixed, paraffin-embedded human tissue from a patient infected with *B. pseudomallei*.

Statistical Analyses

We evaluated the differences among treatment groups in the number of animals with positive or negative outcomes for different parameters that were evaluated by pairwise contingency tables. We used Fisher exact test by using GraphPad Prism (https://www.graphpad.com) (Appendix Table 2).

Table 1. Antimicrobial drug treatments administered to goats in evaluation of postexposure antimicrobial drug therapy in goats infected with *Burkholderia pseudomallei*

Group	Amoxicillin	Clavulanate	Sulfamethoxazole	Trimethoprim
1	None	None	None	None
2	500 mg, ≈7.1 mg/kg	125 mg, ≈1.8 mg/kg	None	None
3	None	None	1200 mg, ≈17.1 mg/kg	240 mg, ≈3.4 mg/kg
4	500 mg, ≈7.1 mg/kg	125 mg, ≈1.8 mg/kg	1200 mg, ≈17.1 mg/kg	240 mg, ≈3.4 mg/kg

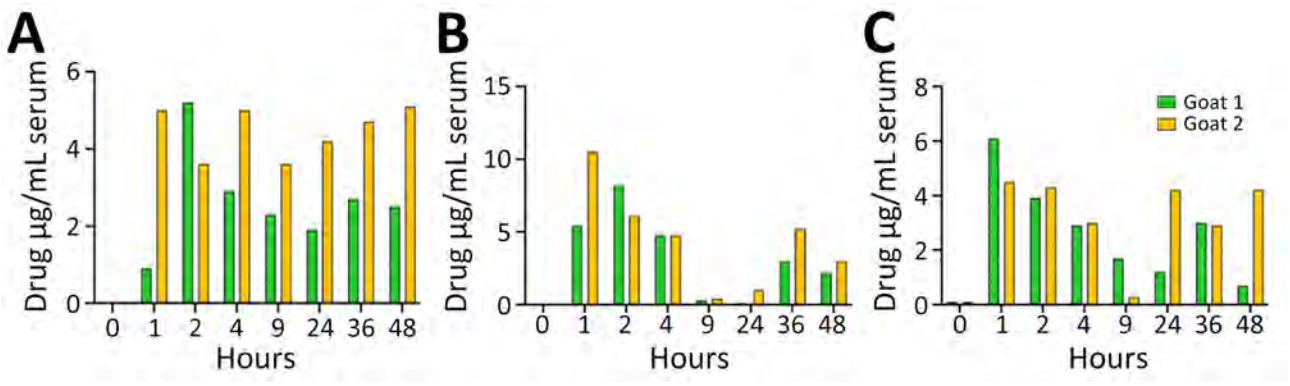

Figure 1. Pharmacokinetic analysis of antibiotics used to study postexposure antimicrobial drug therapy in goats infected with *Burkholderia pseudomallei*. Two female goats received a mixture of 1 capsule containing sulfamethoxazole (800 mg) and trimethoprim (160 mg) plus 1 capsule containing amoxicillin (500 mg) and clavulanate (125 mg) in a total of 25 mL of water. We repeated the treatment 12 hours later and collected blood samples at 1, 2, 4, 9, 24, 36, and 48 hours after the initial treatment. Concentrations of amoxicillin (A), sulfamethoxazole (B), and trimethoprim (C) over the 48-hour period showed acceptable blood levels of the drugs after oral administration.

Results

Preliminary Pharmacokinetic Study

We used 2 female goats for the antibiotic pharmacokinetic study; goat 1 weighed 64 kg and goat 2 weighed 33 kg. We treated the goats by using a dosing syringe with a mixture of 1 capsule containing sulfamethoxazole (800 mg) and trimethoprim (160 mg) plus 1 capsule containing amoxicillin (500 mg) and clavulanate (125 mg) in a total of 25 mL of water. We repeated the treatment 12 hours later. We collected blood samples at 1, 2, 4, 9, 24, 36, and 48 hours after the initial treatment and stored serum frozen until ELISA. We recorded the concentrations of amoxicillin, sulfamethoxazole, and trimethoprim over the 48-hour period (Figure 1). The treatments resulted in acceptable blood levels of the antimicrobial drugs after oral administration.

Clinical Response to Infection

All goats remained clinically unremarkable through 5 dpi and after 3 days of treatment. By 7 days following initiation of treatment, most goats displayed signs of lethargy, anorexia, and diarrhea. This effect was likely because of a combination of infection and adverse influence of the antimicrobial drug therapy on ruminal microbiota. Because of the occurrence of severe disease and for humane considerations, we euthanized groups of goats beginning at 14 dpi. To maintain an ability to compare pathology among groups, we euthanized equal numbers of goats from each group at some of the euthanasia time points (Appendix Table 1).

Gross Pathological Findings and Radiology

The most common gross lesion we observed was splenic abscess, but abscesses were also detected in kidney, liver, and lung (Appendix Table 2; Figure 2). We radiographed extirpated lungs at necropsy to assist in assessing the magnitude of pulmonary abscessation. The number and size of pulmonary lesions varied considerably among goats (Figure 3) and generally corresponded with number of abscesses identified grossly.

Bacterial Culture from Tissues

We individually homogenized and plated 10 tissues from each goat on Ashdown's medium to determine

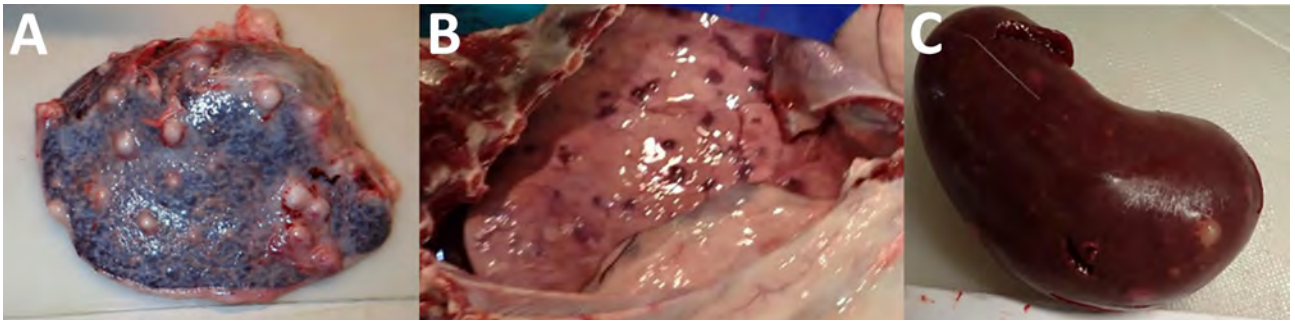

Figure 2. Examples of grossly visible postmortem lesions observed in goats infected with *Burkholderia pseudomallei* in study of postexposure antimicrobial drug therapy. A) Spleen of goat 8429, treated with amoxicillin/clavulanate; B) lung of goat 8549, not treated; C) kidney of goat 8430, treated with amoxicillin/clavulanate.

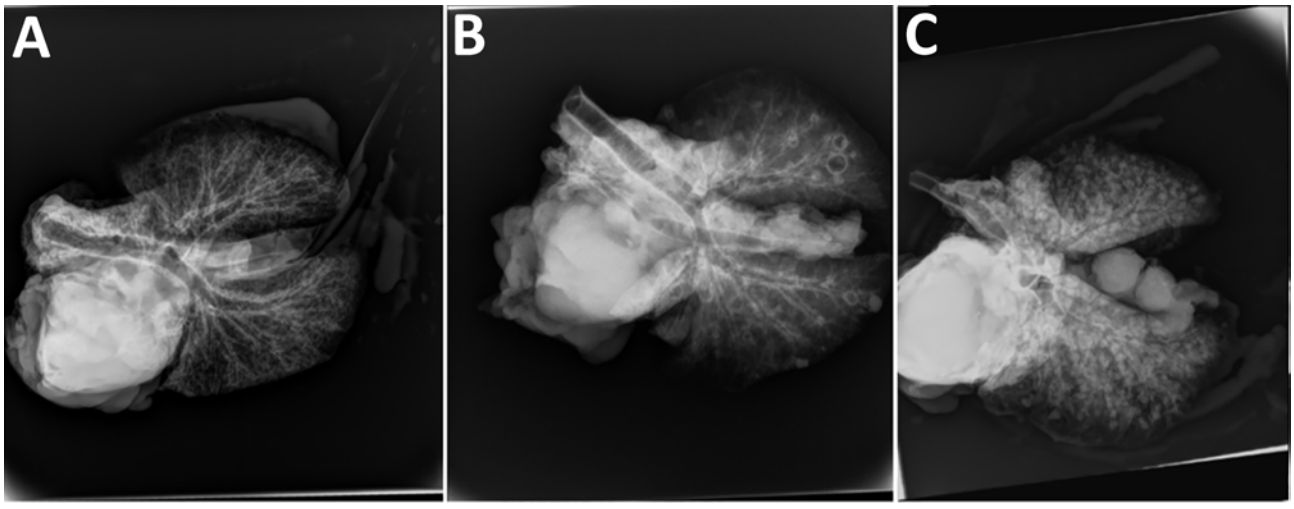

Figure 3. Examples of postmortem pulmonary lesions observed by using radiography in extirpated lungs of goats infected with *Burkholderia pseudomallei* in study of postexposure antimicrobial drug therapy. A) Goat 1197, not treated, showing no visible abscesses; B) goat 8430, treated with amoxicillin/clavulanate, showing moderate abscesses; C) goat 8549, not treated, showing severe abscesses.

whether viable *B. pseudomallei* was present. We compiled results of analyses for individual goats (Appendix Table 3) and by treatment group (Table 2). Treatment with the combination of all 4 antimicrobial drugs had a clear benefit in the number of tissues colonized with bacteria compared with no treatment or treatment with only 2 antimicrobial drugs (Appendix Table 2).

Histopathology and Immunohistochemistry

Abscess or other suppurative inflammation, including occasional pyogranulomas, were consistent histopathologic findings we observed in several organs among all treatment groups except group 4, the goats treated with amoxicillin/clavulanate and sulfamethoxazole/trimethoprim (Table 2). We often observed a typical abscess in experimental infection of *B. pseudomallei*, which is composed by an external fibrotic capsule with epithelioid macrophages within the intermediate layer and with a center containing neutrophils, cellular debris, and fibrin. Lesions were similar at 14 and 28 dpi. Focal or multifocal abscesses were most common in the spleen. We also observed acute and chronic inflammation of variable severity and distribution in a subset of all other examined organs (Table 2; Figure 4).

More acute lesions (14 dpi) had an inflammatory exudate composed of many viable and necrotic neutrophils, whereas more mature abscesses (28 dpi) had more pronounced fibrosis. After 14 dpi, we identified microscopic lesions in fewer animals (n = 4), but lesions were more numerous when found and mainly confined to the spleen; 1 goat at 14 dpi had an abscess in the mediastinal lymph node, and another goat had abscesses in the lungs and liver. We saw few multinucleated giant cells in lymph nodes (mesenteric and retropharyngeal lymph nodes) of 2 animals (from groups 2 and 4); however, we did not find granulomas in any animal.

Table 2. Comparison of bacterial culture and abscesses observed at necropsy or by histologic evaluation of major organs by treatment group in evaluation of postexposure antimicrobial drug therapy in goats infected with *Burkholderia pseudomallei**

	Treatment			
Observation	None	Amoxicillin/ clavulanate	Sulfamethoxazole/ trimethoprim	Sulfamethoxazole/trimethoprim + amoxicillin/clavulanate
No. goats with ≥1 positive *B. pseudomallei* tissue culture	6 of 8	8 of 8	4 of 8	0 of 8
Organs with macroscopic abscesses				
Spleen	8 of 8	8 of 8	5 of 8	0 of 8
Lungs	4 of 16	10 of 16	3 of 15	0 of 16
Liver	0 of 8	3 of 8	0 of 8	0 of 8
Kidney	0 of 8	3 of 8	0 of 8	0 of 8
Organs with microscopic abscesses				
Spleen	6 of 8	8 of 8	5 of 8	0 of 8
Lungs	3 of 16	11 of 16	0 of 15	0 of 16
Liver	1 of 8	3 of 8	0 of 8	0 of 8
Lymph nodes	5 of 8	8 of 8	2 of 8	0 of 8
Kidney	0 of 8	0 of 7	0 of 8	0 of 8

*Statistical analyses of differences between treatment groups are available (Appendix Table 2, https://wwwnc.cdc.gov/EID/article/31/5/24-1274-App1.pdf).

Although abscesses were more numerous at later time points, the distribution and quantity of the immunostaining was similar among groups 1–3. In the group treated with amoxicillin/clavulanate and sulfamethoxazole/trimethoprim, we observed no gross or histopathologic lesions and no immunohistochemical evidence of *B. pseudomallei*. Immunohistochemical staining for *B. pseudomallei* was predominantly in the spleen and lymph nodes, with limited staining in other organs. Of 70 select tested tissues, including those with and without abscesses microscopically, 43 showed multifocal immunoreactivity by IHC at 14–28 dpi, which was strongly correlated with the presence of abscess. Of 40 tissues with histologic evidence

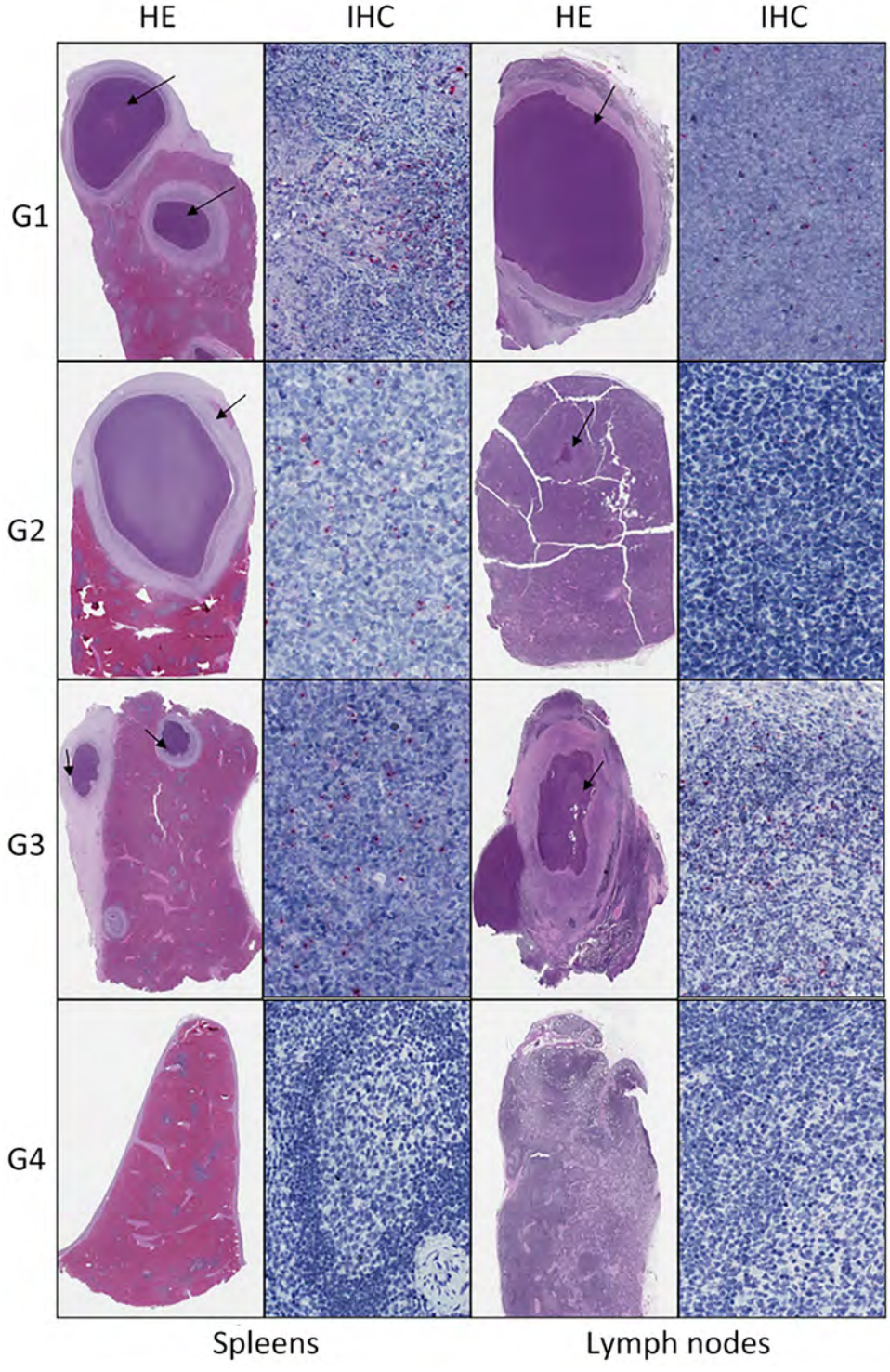

Figure 4. Histopathologic lesions (arrows) and immunocytochemical localization of *Burkholderia pseudomallei* in spleen and lymph nodes of goats infected with *Burkholderia pseudomallei* in study of postexposure antimicrobial drug therapy.

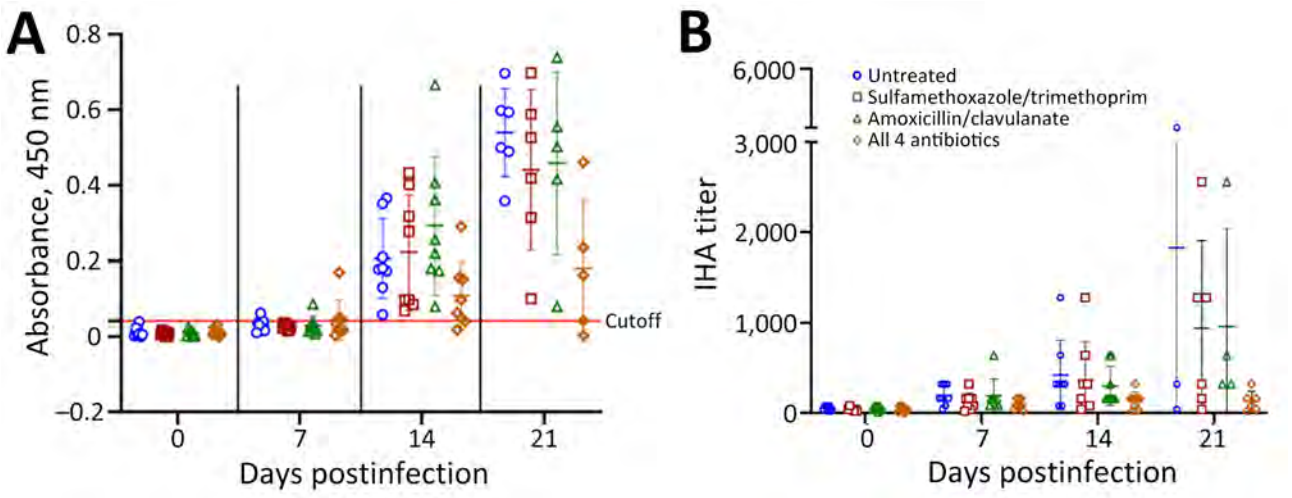

Figure 5. Serologic responses of goats to infection with *Burkholderia pseudomallei* in study of postexposure antimicrobial drug therapy. A) Responses measured by using whole-cell ELISA. Cutoff for positivity was set at 3 SDs above the mean value for all preinoculation serum. B) Responses measured by indirect hemagglutination assays. Horizontal lines indicate means; error bars indicate standard deviation.

of abscess (18 had no reported gross lesions and 15 were negative by culture), 38 showed multifocal immunostaining. No immunostaining was seen in 25 of 30 tissues without microscopic lesions; only 5 were immunoreactive. Of those 5 immunoreactive tissues, 2 had gross lesions and positive culture results, and 3 tissues had no gross lesions and the culture was negative; however, those tissues were from 2 animals (goat 8549, group control; goat 8637, group sulfamethoxazole/trimethoprim) who had abscesses and culture positive in other organs. The distribution of *B. pseudomallei* antigen was typically extracellular, within the necrotic center of the abscesses, and rarely in the cytoplasm of some apparently viable neutrophils (Figure 4).

Besides the abscesses or other neutrophilic infiltrates in different organs, we observed mild changes consisting of moderate-to-severe congestion, lymphoid hyperplasia, sinus histiocytosis, lymphoplasmacytic perivascular, or interstitial inflammation in a few cases. In addition, we observed nonspecific lesions such as hepatic steatosis and hyalinization of the follicular centers of spleens. Vasculitis was evident only in the liver of 1 case (goat 8434), euthanized at 23 dpi. We performed IHC on select tissues without gross or microscopic lesions or with negative cultures; we examined those tissues and observed no immunostaining.

Serology

According to whole-cell ELISA, all but 2 goats (8437 and 8555) had seroconverted by 21 dpi; the 2 goats that failed to seroconvert were in the group treated with the combination of all 4 antimicrobial drugs (Figure 5, panel A). The mean magnitude of antibody response was also significantly lower ($p<0.05$) in the animals receiving the combination of all 4 antimicrobial drugs. The indirect hemagglutination assay demonstrated the same trends as the whole cell lysate ELISA (Figure 5, panel B; Appendix Table 4).

Discussion

The treatment of melioidosis presents substantial challenges because of the intrinsic resistance of *B. pseudomallei* to many antimicrobial drugs, the intracellular nature of the bacteria in infected patients, and the tendency for infections to become latent and recrudesce after treatment is discontinued. Most current recommendations for the treatment of melioidosis involve a biphasic regimen with several weeks of parenteral administration of antimicrobial drugs, followed by months of eradication therapy with orally administered antimicrobial drugs (*18*,*32*). In situations where exposures may have occurred, guidelines have been developed and internationally adopted for PEP, recommending trimethoprim/sulfamethoxazole for 21 days in high-risk exposures and for those with predisposing underlying conditions (diabetes, renal or liver disease, or other immune-suppressing conditions); PEP should be offered even after low-risk exposures (*33*). However, those recommendations are on the basis of limited mouse-model studies that demonstrated efficacy only if PEP was started within 48 hours of exposure, something that is not realistic. Goats are natural hosts for *B. pseudomallei* infection (*9*,*29*) and were shown to be highly susceptible to

both percutaneous and aerosol exposure to *B. pseudomallei* (*30*,*31*).

The objective of this study was to use the goat model to evaluate the efficacy of 3 antimicrobial drug regimens as PEP for *B. pseudomallei* infection induced by percutaneous inoculation. Overt clinical disease manifested in all the goats, including those with minimal lesions at necropsy after treatment with all 4 antimicrobial drugs. However, it was not clear if the observed clinical illness was related to infection with *B. pseudomallei* or adverse events related to therapy. The control animals in group 1 did not receive antimicrobial drugs and had more severe clinical signs and lesions. This increased severity suggests clinical disease in the other groups was likely a result of the infection plus disruptions of ruminal microbiota because of antimicrobial drug therapy, which is a disadvantage to this model and not likely to be a major issue in humans. Another shortcoming of this study is that the pharmacokinetic study we conducted with 2 goats was far from extensive but did indicate the drug treatments we applied provided reasonable blood levels of those antimicrobial drugs. Repeated and more extensive evaluation of blood concentrations over time would be valuable in interpreting future studies. The dosage of amoxicillin we administered might have been suboptimal on the basis of the pharmacokinetics of this antimicrobial drug after oral administration in goats (*34*) and some recent MIC values reported for *B. pseudomallei* (*35*).

A striking observation from this study was that, although treatment with amoxicillin/clavulanate or sulfamethoxazole/trimethoprim had minimal or mild inhibitory effects on abscess formation and the presence of culturable *B. pseudomallei* in tissues, a combination of both treatments appeared highly efficacious. None of the 8 goats treated with all 4 antimicrobial drugs had abscesses visible at necropsy nor had positive organ cultures among the 10 tissues tested. Of interest, antibody titers were lower in goats that received the combination of 4 antimicrobial drugs, suggesting inhibition of infection and a less potent stimulus to the immune system for this treatment group.

In conclusion, our findings indicate PEP with a combination of those 4 antimicrobial drugs might be useful in preventing human cases of melioidosis after exposure to *B. pseudomallei*, and additional studies are justified. In addition, ≥3 additional features of melioidosis will be necessary to address in future studies with similar models. First, it will be critical to delay the onset of treatment for >48 hours to make the model more realistic for initiation of prophylaxis after later identification of exposure. Second, the animals need to be maintained for longer periods of time after cessation of treatment to determine if prophylaxis does indeed eliminate the infection and prevent recrudescence. Finally, more detailed pharmacokinetic studies should be performed in goats to guide antimicrobial drug dosing. Melioidosis after accidental exposure in the clinical or research laboratory is rare, and it would not be possible to utilize these cases to evaluate the efficacy of PEP. Ultimately, clinical observations in humans are necessary to validate this supposition and to determine the efficacy of PEP in exposed humans.

Acknowledgments

We thank Ann Hess for her advice on statistical analyses.

This work was funded by Centers for Disease Control and Prevention (contract no. 75D30121P12136).

About the Author

Dr. Bowen is a professor in the department of biomedical sciences at Colorado State University College of Veterinary Medicine and Biomedical Sciences. His primary field of study is pathogenesis and control of zoonotic diseases.

References

1. Wiersinga WJ, Virk HS, Torres AG, Currie BJ, Peacock SJ, Dance DAB, et al. Melioidosis. Nat Rev Dis Primers. 2018;4:17107. https://doi.org/10.1038/nrdp.2017.107
2. Gassiep I, Armstrong M, Norton R. Human melioidosis. Clin Microbiol Rev. 2020;33:e00006–00019. https://doi.org/10.1128/CMR.00006-19
3. Meumann EM, Limmathurotsakul D, Dunachie SJ, Wiersinga WJ, Currie BJ. *Burkholderia pseudomallei* and melioidosis. Nat Rev Microbiol. 2024;22:155–69. https://doi.org/10.1038/s41579-023-00972-5
4. Limmathurotsakul D, Golding N, Dance D, Messina JP, Pigott DM, Moyes CL, et al. Predicted global distribution of *Burkholderia pseudomallei* and burden of melioidosis. Nat Microbiol. 2016;1:15008. https://doi.org/10.1038/nmicrobiol.2015.8
5. Dance DAB. Editorial commentary: melioidosis in Puerto Rico: the iceberg slowly emerges. Clin Infect Dis. 2015;60:251–3. https://doi.org/10.1093/cid/ciu768
6. Rolim DB, Lima RXR, Ribeiro AKC, Colares RM, Lima LDQ, Rodríguez-Morales AJ, et al. Melioidosis in South America. Trop Med Infect Dis. 2018;3:60. https://doi.org/10.3390/tropicalmed3020060
7. Currie BJ, Meumann EM, Kaestli M. The expanding global footprint of *Burkholderia pseudomallei* and melioidosis. Am J Trop Med Hyg. 2023;108:1081–3. https://doi.org/10.4269/ajtmh.23-0223
8. Petras JK, Elrod MG, Ty MC, Dawson P, O'Laughlin K, Gee JE, et al. Locally acquired melioidosis linked to environment—Mississippi, 2020–2023. N Engl J Med. 2023;389:2355–62. https://doi.org/10.1056/NEJMoa2306448

9. Choy JL, Mayo M, Janmaat A, Currie BJ. Animal melioidosis in Australia. Acta Trop. 2000;74:153–8. https://doi.org/10.1016/S0001-706X(99)00065-0
10. Limmathurotsakul D, Thammasart S, Warrasuth N, Thapanagulsak P, Jatapai A, Pengreungrojanachai V, et al. Melioidosis in animals, Thailand, 2006–2010. Emerg Infect Dis. 2012;18:325–7. https://doi.org/10.3201/eid1802.111347
11. Zehnder AM, Hawkins MG, Koski MA, Lifland B, Byrne BA, Swanson AA, et al. *Burkholderia pseudomallei* isolates in 2 pet iguanas, California, USA. Emerg Infect Dis. 2014;20:304–6. https://doi.org/10.3201/eid2002.131314
12. Birnie E, Virk HS, Savelkoel J, Spijker R, Bertherat E, Dance DAB, et al. Global burden of melioidosis in 2015: a systematic review and data synthesis. Lancet Infect Dis. 2019;19:892–902. https://doi.org/10.1016/S1473-3099(19)30157-4
13. Höger AC, Mayo M, Price EP, Theobald V, Harrington G, Machunter B, et al. The melioidosis agent *Burkholderia pseudomallei* and related opportunistic pathogens detected in faecal matter of wildlife and livestock in northern Australia. Epidemiol Infect. 2016;144:1924–32. https://doi.org/10.1017/S0950268816000285
14. Hemarajata P, Baghdadi JD, Hoffman R, Humphries RM. *Burkholderia pseudomallei*: challenges for the clinical microbiology laboratory. J Clin Microbiol. 2016;54:2866–73. https://doi.org/10.1128/JCM.01636-16
15. Dance DA, Limmathurotsakul D, Currie BJ. *Burkholderia pseudomallei*: challenges for the clinical microbiology laboratory-a response from the front line. J Clin Microbiol. 2017;55:980–2. https://doi.org/10.1128/JCM.02378-16
16. Speiser LJ, Graf EH, Seville MT, Singbartl K, Dalton ML, Harrington D, et al. *Burkholderia pseudomallei* laboratory exposure, Arizona, USA. Emerg Infect Dis. 2023;29:1061–3. https://doi.org/10.3201/eid2905.221865
17. Currie BJ, Fisher DA, Howard DM, Burrow JN, Lo D, Selva-Nayagam S, et al. Endemic melioidosis in tropical northern Australia: a 10-year prospective study and review of the literature. Clin Infect Dis. 2000;31:981–6. https://doi.org/10.1086/318116
18. Sullivan RP, Marshall CS, Anstey NM, Ward L, Currie BJ. 2020 Review and revision of the 2015 Darwin melioidosis treatment guideline; paradigm drift not shift. PLoS Negl Trop Dis. 2020;14:e0008659. https://doi.org/10.1371/journal.pntd.0008659
19. Schweizer HP. Mechanisms of antibiotic resistance in *Burkholderia pseudomallei*: implications for treatment of melioidosis. Future Microbiol. 2012;7:1389–99. https://doi.org/10.2217/fmb.12.116
20. Rhodes KA, Schweizer HP. Antibiotic resistance in *Burkholderia* species. Drug Resist Updat. 2016;28:82–90. https://doi.org/10.1016/j.drup.2016.07.003
21. Steward J, Piercy T, Lever MS, Nelson M, Simpson AJ, Brooks TJ. Comparison of gatifloxacin, moxifloxacin and ciprofloxacin for treatment of experimental *Burkholderia pseudomallei* infection. J Antimicrob Chemother. 2005;55:523–7. https://doi.org/10.1093/jac/dki039
22. Sivalingam SP, Sim SH, Jasper LC, Wang D, Liu Y, Ooi EE. Pre- and post-exposure prophylaxis of experimental *Burkholderia pseudomallei* infection with doxycycline, amoxicillin/clavulanic acid and co-trimoxazole. J Antimicrob Chemother. 2008;61:674–8. https://doi.org/10.1093/jac/dkm527
23. Barnes KB, Steward J, Thwaite JE, Lever MS, Davies CH, Armstrong SJ, et al. Trimethoprim/sulfamethoxazole (co-trimoxazole) prophylaxis is effective against acute murine inhalational melioidosis and glanders. Int J Antimicrob Agents. 2013;41:552–7. https://doi.org/10.1016/j.ijantimicag.2013.02.007
24. Pearson T, Sahl JW, Hepp CM, Handady K, Hornstra H, Vazquez AJ, et al. Pathogen to commensal? Longitudinal within-host population dynamics, evolution, and adaptation during a chronic >16-year *Burkholderia pseudomallei* infection. PLoS Pathog. 2020;16:e1008298. https://doi.org/10.1371/journal.ppat.1008298
25. AuCoin DP, Reed DE, Marlenee NL, Bowen RA, Thorkildson P, Judy BM, et al. Polysaccharide specific monoclonal antibodies provide passive protection against intranasal challenge with *Burkholderia pseudomallei*. PLoS One. 2012;7:e35386. https://doi.org/10.1371/journal.pone.0035386
26. Chaichana P, Jenjaroen K, Amornchai P, Chumseng S, Langla S, Rongkard P, et al. Antibodies in melioidosis: the role of the indirect hemagglutination assay in evaluating patients and exposed populations. Am J Trop Med Hyg. 2018;99:1378–85. https://doi.org/10.4269/ajtmh.17-0998
27. Suttisunhakul V, Wuthiekanun V, Brett PJ, Khusmith S, Day NP, Burtnick MN, et al. Development of rapid enzyme-linked immunosorbent assays for detection of antibodies to *Burkholderia pseudomallei*. J Clin Microbiol. 2016;54:1259–68. https://doi.org/10.1128/JCM.02856-15
28. Yi J, Simpanya MF, Settles EW, Shannon AB, Hernandez K, Pristo L, et al. Caprine humoral response to *Burkholderia pseudomallei* antigens during acute melioidosis from aerosol exposure. PLoS Negl Trop Dis. 2019;13:e0006851. https://doi.org/10.1371/journal.pntd.0006851
29. Pearson T, U'Ren JM, Schupp JM, Allan GJ, Foster PG, Mayo MJ, et al. VNTR analysis of selected outbreaks of *Burkholderia pseudomallei* in Australia. Infect Genet Evol. 2007;7:416–23. https://doi.org/10.1016/j.meegid.2006.12.002
30. Soffler C, Bosco-Lauth AM, Aboellail TA, Marolf AJ, Bowen RA. Development and characterization of a caprine aerosol infection model of melioidosis. PLoS One. 2012;7:e43207. https://doi.org/10.1371/journal.pone.0043207
31. Soffler C, Bosco-Lauth AM, Aboellail TA, Marolf AJ, Bowen RA. Pathogenesis of percutaneous infection of goats with Burkholderia pseudomallei: clinical, pathologic, and immunological responses in chronic melioidosis. Int J Exp Pathol. 2014;95:101–19. https://doi.org/10.1111/iep.12068
32. Lipsitz R, Garges S, Aurigemma R, Baccam P, Blaney DD, Cheng AC, et al. Workshop on treatment of and postexposure prophylaxis for *Burkholderia pseudomallei* and *B. mallei* infection, 2010. Emerg Infect Dis. 2012;18:e2. https://doi.org/10.3201/eid1812.120638
33. Peacock SJ, Schweizer HP, Dance DA, Smith TL, Gee JE, Wuthiekanun V, et al. Management of accidental laboratory exposure to *Burkholderia pseudomallei* and *B. mallei*. Emerg Infect Dis. 2008;14:e2. https://doi.org/10.3201/eid1407.071501
34. Carceles CM, Escudero E, Vicente MS, Serrano JM, Carli S. Pharmacokinetics of amoxicillin/clavulanic acid combination after intravenous and oral administration in goats. Vet Q. 1995;17:134–8. https://doi.org/10.1080/01652176.1995.9694552
35. Dutta S, Haq S, Hasan MR, Haq JA. Antimicrobial susceptibility pattern of clinical isolates of *Burkholderia pseudomallei* in Bangladesh. BMC Res Notes. 2017;10:299. https://doi.org/10.1186/s13104-017-2626-5

Address for correspondence: Richard Bowen, Colorado State University, 3107 Rampart Rd, Fort Collins, CO 80523 USA; email: rbowen@colostate.edu

etymologia

Emayella augustorita [em”-ə-yel’-ə aw-goost’-ō-rē”-tə]

Clyde Partin

In 2024, a novel bacterial genus and species of the Pasteurellaceae family, *Emayella augustorita*, was presented by a team led by Sylvain Meyer from the University of Limoges in Limoges, France. *E. augustorita* is a fermentative, gram-negative organism and a commensal and common inhabitant of feline and canine oral cavities and upper respiratory tracts. This newly identified rod-shaped bacterium was isolated from blood cultures in a woman who had sepsis because of an infected metallic biliary stent.

As a nod to local heritage, in naming their discovery, the authors chose *Emayella*, which translates from Latin as enamel. Limoges is known for its artistic heritage, especially for enamel-painted metalwork dating to the Middle Ages. In the 18th Century, after a kaolin pit was discovered nearby, Limoges became an avatar of exquisite porcelain ware. The species epithet, *augustorita*, in honor of the Emperor Augustus, was the original name given to the town by its Roman founders, in 10 BCE. The Gaulish suffix *-ritum* (*rito* or ford) is a reference to the city’s location on a ford on the Vienne River. The name Limoges itself evolved from a Latin word, Lemovices, referring to a Gaulish tribe who armed themselves with spears fashioned from elm.

Figure. Roundel with a Personification of the Moon, ca. 860–890. This cloisonné-enamel plaque, made of copper alloy with an iron back plate, was created in south-central France, in the area of what is now Limoges. Dimensions: 3 3/8 × 1/4 in (8.6 × 0.6 cm). Public domain image courtesy of The Metropolitan Museum of Art (New York, NY, USA).

Sources

1. Meyer S, Tilloy V, Durand-Fontanier S, Lafon T, Garnier F, Martin C, et al. *Emayella augustorita*, new member of Pasteurellaceae, isolated from blood cultures of septic patient. Emerg Infect Dis. 2024;30(8):1719-1721. https://doi.org/10.3201/eid3008.231651
2. Limoges Boutique. About Limoges, France: world porcelain capitol [cited 2025 March 17]. https://www.limogesboutique.com/pages/about-limoges-france
3. Sinnott-Stutzman V, Sykes JE. Gram-negative bacterial infections. In: Sykes JE, editor. Greene’s infectious diseases of the dog and cat, 5th edition. Amsterdam: W.B. Saunders; 2021. p. 643–54. https://doi.org/10.1016/B978-0-323-50934-3.00053-7
4. Augustoritum lemovicum (Limoges) Haute-Vienne, France. In: Stillwell R, MacDonald WL, McAllister MH, editors. The Princeton encyclopedia of classical sites. Princeton (NJ): Princeton University Press; 1976.
5. Limoges, France [cited 2025 March 17]. https://www.britannica.com/place/Limoges

Author affiliation: Emory University School of Medicine, Atlanta, Georgia, USA

Address for correspondence: Clyde Partin, Emory Clinic, 1365 Clifton Rd NE, Bldg A, 1st Fl, Atlanta, GA 30322, USA; email: wpart01@emory.edu

DOI: https://doi.org/10.3201/eid3105.240723

Exponential Clonal Expansion of 5-Fluorocytosine–Resistant *Candida tropicalis* and New Insights into Underlying Molecular Mechanisms

Nissrine Abou-Chakra, Karen Marie Thyssen Astvad, Jan Martinussen, Amalie Sofie Eilsø Munksgaard, Maiken Cavling Arendrup

In 2022, we initiated systematic 5-fluorocytosine susceptibility testing of *Candida* spp. isolates in Denmark; we observed a bimodal MIC distribution in *C. tropicalis*, with MICs ≥16 mg/L in half the isolates. This study investigates the epidemiology and molecular mechanisms of 5-fluorocytosine resistance in *C. tropicalis*. We analyzed 104 *C. tropicalis* isolates from 3 time periods, alongside 353 *C. albicans* and 227 *C. glabrata* isolates from 2022. We determined MICs using EUCAST E.Def 7.3. Sequencing of *FCY2* (purine-cytosine permease), *FCY1* (cytosine deaminase), *FUR1* (uracil phosphoribosyl transferase), and *URA3* (orotidine-5′-phosphate decarboxylase) genes revealed FCY2 alterations—E49X (30/32), Q7X (1/32), and K6NfsX10 (1/32)—in resistant *C. tropicalis* strains. We found a URA3 alteration, K177E, in both susceptible and resistant strains. Microsatellite genotyping showed that all *C. tropicalis* isolates with E49X were clonally related. The marked increase in resistance, driven by the clonal spread of E49X, necessitates further research into virulence and environmental factors.

Candida tropicalis is a globally distributed opportunistic pathogen that can cause invasive infections in immunocompromised and predisposed patients (*1*,*2*). It ranks among the top 4 *Candida* species responsible for candidemia in Denmark, after the 2 most prevalent species, *C. albicans* and *C. glabrata* (*3*). However, *C. tropicalis* is more prevalent in southern Europe countries and Asia, where clonal spread in hospital settings has been reported (*4*–*6*).

5-fluorocytosine is an antifungal agent that targets nucleic acid and protein synthesis. As a prodrug, it undergoes several chemical modifications to become active (*7*–*9*) (Table 1). 5-fluorocytosine is primarily used for cryptococcal meningitis and difficult-to-treat central nervous system, eye, or bone infections caused by *Candida* species, and in combination with amphotericin B to avoid resistance selection (*7*); it is rarely included in routine susceptibility of *Candida* species.

The European Committee on Antimicrobial Susceptibility Testing (EUCAST) has not set clinical breakpoints for 5-fluorocytosine. To generate MIC data for epidemiologic cutoff (ECOFF) and future breakpoint setting, we included 5-fluorocytosine in our routine EUCAST susceptibility test panels in 2022. The results were somewhat unexpected. All *C. tropicalis* isolates were susceptible to the echinocandins and fluconazole; however, 50% demonstrated high 5-fluorocytosine MICs (≥16 mg/L), whereas the remaining *C. tropicalis* isolates had MICs ≤0.5 mg/L. In comparison, only 0.8% (3/353) of *C. albicans* and 2.2% (5/227) of *C. glabrata* exhibited elevated MICs of 1 to >16 mg/L (Table 2).

Few studies have investigated the prevalence of 5-fluorocytosine resistance in *C. tropicalis* across Europe, where resistance has emerged gradually since the 1990s. In 1996, Law et al. reported a prevalence of 17% for 5-fluorocytosine resistance (defined as MIC >8 mg/L) and 37% for of intermediate susceptibility (defined as MIC 2–8 mg/L) in *C. tropicalis* isolates collected over 4 years in northwestern England (*10*).

Author affiliations: Statens Serum Institut, Copenhagen, Denmark (N. Abou-Chakra, K.M.T. Astvad, A.S.E. Munksgaard, M.C. Arendrup); Technical University of Denmark, Kgs Lyngby, Denmark (J. Martinussen); University of Copenhagen, Copenhagen (A.S.E. Munksgaard, M.C. Arendrup); Rigshospitalet, Copenhagen (M.C. Arendrup)

DOI: https://doi.org/10.3201/eid3105.241910

Table 1. Metabolism and mode of action of 5-fluorocytosine in study of clonal expansion of 5-fluorocytosine–resistant *Candida tropicalis*, Denmark*

Step	Process	Enzyme/mechanism	Outcome
Uptake	5-fluorocytosine is taken up into fungal cells	Transport protein purine-cytosine permease (encoded by *FCY2;* primary uptake mechanism)	Initiates the antifungal activity of the metabolic pathway
Conversion to 5-FU	5-fluorocytosine is metabolized into 5-FU	Cytosine deaminase (encoded by *FCY1*); selective action due to lack of enzyme in mammalian cells	5-fluorocytosine → 5-FU
Formation of 5-FUMP	5-FU is converted into 5-FUMP	Uracil phosphoribosyl transferase (encoded by *FUR1*)	5-FU → 5-FUMP
Phosphorylation to 5-FUDP	5-FUMP is phosphorylated to 5-FUDP	Phosphorylation by specific kinases (e.g., uridine monophosphate kinase)	5-FUMP → 5-FUDP
Formation of 5-FUTP	5-FUDP is further phosphorylated to 5-FUTP	Phosphorylation reactions	5-FUDP → 5-FUTP; integration into RNA leads to dysfunctional RNA and inhibition of RNA synthesis
Formation of 5-FdUDP	5-FUDP is reduced to 5-FdUDP	Ribonucleotide reductase	5-FUDP → 5-FdUDP
Formation of 5-FdUTP	5-FdUDP is phosphorylated to 5-FdUTP	Phosphorylation reactions	5-FdUDP → 5-FdUTP; incorporation into DNA inhibits DNA synthesis and repair
Dephosphorylation to 5-FdUMP	5-FdUTP is dephosphorylated to 5-FdUDP, which is subsequently reduced to 5-FdUMP, inhibiting TS	Dephosphorylation reactions Ribonucleotide reductase	The irreversible inhibition of TS leads to depletion of dTMP and dTTP, disrupting nucleotide pools, leading to DNA damage, potential apoptosis, and "thymine-less death"

*5-FdUMP, 5-fluoro-deoxyuridine monophosphate; 5-FU, 5-fluoro-uracil; 5-FUMP, 5-fluoro-uridine monophosphate; 5-FUDP, 5-fluoro-uridine diphosphate; 5-FUTP, 5-fluoro-uridine triphosphate; 5-FdUDP, 5-fluoro-deoxyuridine diphosphate; 5-FdUTP, 5-fluoro-deoxyuridine triphosphate; dTMP, deoxythymidine monophosphate; dTTP, deoxythymidine triphosphate; TS, thymidylate synthase.

Similarly, Tortorano et al. observed a 30% prevalence of 5-fluorocytosine resistance (MIC ≥32 mg/L) in bloodstream isolates from 11 different institutions in Lombardy, Italy, during 1997–1999, indicating a widespread, non–hospital-specific prevalence of resistance (*11*). More recently, Desnos-Ollivier et al. reported that 35% of *C. tropicalis* strains from blood cultures collected in France (2002–2006) were resistant to 5-fluorocytosine (MIC >8 μg/mL; as defined by authors) (*12*). Although no mutations were identified in key pyrimidine salvage pathway genes involved in 5-fluorocytosine uptake and metabolism, including *FCY2* (purine–cytosine permease), *FCY1* (cytosine deaminase), and *FUR1* (uracil phosphoribosyl transferase), the authors observed evidence of a clonal spread of resistant strains, particularly in the Paris region. In addition, they identified a consistent correlation between 5-fluorocytosine resistance and a missense mutation (K177E) in the *URA3* (orotidine-5′-phosphate decarboxylase) gene, encoding a key enzyme in the later stages of the de novo pyrimidine biosynthesis. The authors proposed that this mutation could alter the structure and function of the URA3 enzyme, potentially modifying its binding affinity for substrates involved in nucleic acid synthesis. They also suggested that increased expression of *URA3* in these strains could contribute to 5-fluorocytosine resistance, possibly by promoting the overproduction of uridine monophosphate (UMP), a precursor for deoxyribonucleotide synthesis. However, direct evidence linking *URA3* upregulation to the observed resistance phenotype was not provided.

In this study, we aimed to investigate the epidemiology of 5-fluorocytosine resistance in *C. tropica-*

Table 2. 5-fluorocytosine susceptibility of *Candida* spp. in study of clonal expansion of 5-fluorocytosine–resistant *Candida tropicalis*, Denmark*

	MIC, mg/L														
Year sampled	≤0.016	0.03	0.06	0.125	0.25	0.5	1	2	4	8	16	>16	Total	Wild-type UL, mg/L	Non–wild-type rate, %
C. tropicalis															
1998–2004	0	1	2	17	4	0	**0**	**0**	**0**	**0**	**0**	**1**	25	0.5	4.0
2011–12	0	0	12	7	0	0	**0**	**0**	**0**	**0**	**0**	**4**	23	0.5	17.4
2022	1	1	9	18	2	1	**0**	**0**	**0**	**0**	**3**	**29**	64	0.5	50.0
C. albicans															
2022	0	2	8	144	154	28	14	**2**	**0**	**0**	**0**	**1**	353	1	0.8
C. glabrata															
2022	1	8	86	122	5	**0**	**1**	**1**	**3**	**0**	**0**	**0**	227	0.25	2.2

*The reference strain, *Candida tropicalis* ATCC 750, had a MIC of 0.06 mg/L. Bold text indicates non–wild-type isolates. UL, upper limit.

lis in Denmark over a 20-year perspective. We also explored the underlying molecular mechanisms of 5-fluorocytosine resistance and investigated the genetic similarity between susceptible and 5-fluorocytosine–resistant *C. tropicalis* isolates.

Materials and Methods

Isolates

Our MIC study included all unique clinical *C. tropicalis* (excluding same patient, same species, same 5-fluorocytosine susceptibility isolates within 30 days) received at Statens Serum Institut (Copenhagen, Denmark) in 3 time periods spanning 2 decades: 25 isolates from 1998–2004, 23 isolates from 2011–2012, and 64 isolates from 2022. We selected the duration of each period to include a minimum of 20 isolates per period. Overall, 78% of the isolates derived from blood cultures. We included the *C. tropicalis* reference strain (ATCC 750) as an external comparator. We performed species identification using morphology on CHROMagar Candida (BD BBL; BD, https://www.bd.com) or cornmeal Tween 80 agar (Dalmau technique), or both, with carbohydrate assimilation profiling with ID32C (bioMérieux, https://www.biomerieux.com) for earlier isolates in some cases. In later periods, we used matrix-assisted laser desorption/ionization time-of-flight mass spectrometry (Bruker, https://www.bruker.com), supplemented with internal transcribed spacer sequence analysis when needed.

Susceptibility Testing and Categorization of Susceptibility

We performed MIC determination in RPMI 1640 medium according to EUCAST E.Def 7.3.2, as previously described (*13*,*14*). We stored 5-fluorocytosine pure substance (Sigma-Aldrich, https://www.sigmaaldrich.com) in aliquots with 5,000 mg/L stock solutions prepared in sterile water at −80°C. The final concentration range was 0.016–16 mg/L. We determined wild-type upper limits (WT-ULs) using the ECOFFinder program with 99.9% of the modeled distributed (https://www.EUCAST.org; accessed 2024 Dec 11) and used to categorize isolates as non–wild-type when MIC >WT-UL (*15*).

DNA Extraction

We transferred colonies to 400 µL of easyMAG Lysis Buffer (bioMérieux) for DNA extraction using the automated eMAG extraction system (bioMérieux). We eluted genomic DNA in 100 µL of Extraction Buffer 3 (bioMérieux) and stored at −20°C until further processing.

Molecular Analysis of 5-Fluorocytosine Resistance Mechanisms in *C. tropicalis*

For the molecular studies, we excluded 8 isolates from 2022 for practical reasons (3 susceptible [MIC≤0.5 mg/L] and 5 non–wild-type [MIC>0.5 mg/L]). We sequenced the genes *FCY2*, *FCY1*, *FUR1*, and *URA3* for the remaining 104 isolates (72 susceptible and 32 non–wild-type isolates) (Appendix Table 1, https://wwwnc.cdc.gov/EID/article/31/5/24-1910-App1.pdf). We validated redesigned and newly designed primers through in silico analysis for specificity and complementarity using the *C. tropicalis* ATCC 750 genome (https://genomes.atcc.org/genomes) as a reference. PCR cycling conditions were initial denaturation at 95°C for 10 minutes, 35 cycles of denaturation at 95°C for 30 seconds, annealing at the specified temperature for 45 seconds, and extension at 72°C for 90 seconds. We included a final extension at 72°C for 7 minutes before cooling to 8°C. We visualized PCR products on agarose gel, then performed Sanger sequencing (Macrogen Europe, https://www.macrogen-europe.com). We analyzed the sequencing data in the CLC Main Workbench software version 23.0.3 (QIAGEN, https://www.qiagen.com) (Appendix Table 1).

Genotyping of *C. tropicalis* and Cluster Analysis

We used the microsatellite-based typing method developed by Wu et al. (*16*). We modified primers for amplifying the microsatellite loci and PCR conditions and ran singleplex assays for some primer sets and duplex assays for others (Appendix Table 2). We assembled PCR reactions in a total volume of 25 µL, containing 2.5 µL genomic DNA, 0.4 µM of each duplex primer or 0.8 µM of each singleplex primer, 6 µL of distilled water for the duplex assay or 8 µL for the singleplex assay, and 12.5 µL of Extract-N-amp-PCR ReadyMix (Sigma Aldrich). We performed all PCR reactions using a SimpliAmp Thermal Cycler (ThermoFisher) under the following conditions: initial denaturation at 95°C for 10 minutes, followed by 35 cycles of denaturation at 95°C for 30 seconds, annealing at 52°C for 30 seconds, elongation at 72°C for 90 seconds, and a final extension at 72°C for 7 minutes. We analyzed PCR products on a 2% agarose gel and visualized after staining with ethidium bromide under UV light.

For fragment sizing, we combined 1 µL of each duplex and corresponding singleplex PCR product with 11.2 µL distilled water and 0.8 µL GeneScan 500 ROX, resulting in a total volume of 14 µL. We heated the mixture at 95°C for 3 minutes, cooled on ice,

and analyzed using the SeqStudio Genetic Analyzer (Thermo Fisher). We analyzed fluorescent peaks with Peak Scanner software (Thermo Fisher) to determine fragment sizes measured in base pairs. We defined a singleton as a genotype found in a single strain, whereas a cluster refers to a genotype shared by ≥2 strains. Finally, we illustrated the genetic relationships among isolates by constructing a minimum-spanning tree using BioNumerics software version 8.1.1 (bioMérieux).

Results

Susceptibility Epidemiology

Adopting the WT-UL values determined using the 2022 dataset and including 99.9% of the modeled MIC distributions, the 5-fluorocytosine proportion of *C. tropicalis* isolates non–wild-type to 5-fluorocytosine increased exponentially from 4.0% to 50.0% over 2 decades (Table 2). In contrast, the non–wild-type rates in *C. albicans* (0.8%) and *C. glabrata* (2.2%) in 2022 remained low. Focusing on the *C. tropicalis* isolates from 2022, we found no pattern regarding 5-fluorocytosine susceptibility and the geographic origin of the isolates (Appendix Table 3). The comparator control strain (ATCC 750) a MIC was 0.06 mg/L.

Molecular Analysis of Genes Contributing to 5-Fluorocytosine Resistance

We detected no mutations resulting in amino acid alterations in the *FCY1* gene in the non–wild-type or susceptible *C. tropicalis* isolates. However, we identified several point mutations that resulted in amino acid substitutions and nonsense mutations (resulting in truncated proteins), in the *FCY2, FUR1*, and *URA3* genes (Table 3). We found 2 nonsense mutations and 1 nucleotide deletion in *FCY2* exclusively in 5-fluorocytosine non–wild-type isolates; the nonsense mutations caused premature translation termination (E49X and Q7X), and the nucleotide deletion caused a frameshift in the protein sequence (K6NfsX10). Of those mutations, E49X was found in 30 of the 32 non–wild-type *C. tropicalis* isolates. In contrast, the *URA3* mutation leading to a K177E alteration was present in both wild-type and non–wild-type isolates. In addition, missense alterations K5Q and A157S in FUR1, along with various heterozygous mutations in *FCY2,* were found exclusively in wild-type isolates (Table 3). The comparator control strain (ATCC 750) exhibited wild-type alleles for all 4 genes analyzed.

Table 3. Overview of target gene mutations found in *Candida tropicalis* isolates in study of clonal expansion of 5-fluorocytosine–resistant *C. tropicalis*, Denmark*

Amino acid alteration	Mutation type	No. strains	Total strains, N = 104	Expected effect on protein	Modal MIC, mg/L (range)†
FCY2					
E49X	Nonsense (homozygous)	30 (R)	32 (R)	Premature termination, loss of function	>16, non–wild-type
Q7X	Nonsense (homozygous)	1 (R)	32 (R)	Premature termination, loss of function	>16, non–wild-type
K6NfsX10	Single-nucleotide deletion (homozygous)	1 (R)	32 (R)	Frameshift leading to premature termination, loss of function	>16, non–wild-type
E49X & M162I	Heterozygous	12 (S)	72 (S)	No significant impact on transporter function	0.125 (0.06–0.5)
H201I	Heterozygous	1 (S)	72 (S)	No significant impact on transporter function	0.125
I473L	Heterozygous	2 (S)	72 (S)	No significant impact on transporter function	(0.06–0.125)
M130T	Heterozygous	1 (S)	72 (S)	No significant impact on transporter function	0.25
M162I	Heterozygous	1 (S)	72 (S)	No significant impact on transporter function	0.125
S108F	Heterozygous	1 (S)	72 (S)	No significant impact on transporter function	0.06
W67X	Heterozygous	1 (S)	72 (S)	Discrete impact on transporter function	0.5
S258X	Heterozygous	1 (S)	72 (S)	No significant impact on transporter function	0.25
FUR1					
K5Q & A157S	Homozygous	1 (S)	72 (S)	No impact on 5-FC conversion	0.125 (0.06–0.5)
URA3					
K177E	Homozygous	30 (R) + 2 (S)	32 (R) + 72 (S)	No impact on protein function	0.125 (0.06–0.5)

*Strains were wild-type except as indicated. *FCY2,* purine-cytosine permease; *FUR1*, uracil phosphoribosyltransferase; R, resistant (non–wild-type); S, susceptible (wild-type); *URA3,* orotidine-5'-phosphate decarboxylase
†Modal MIC value presented for alterations represented by >10 isolates, MIC range in parentheses for alterations represented by <10 isolates, and MIC value for alterations found in a single isolate. For comparison, modal MIC for wild-type population is 0.125 mg/L.

Allelic and Cluster Analysis

We next explored the genetic relationships among *C. tropicalis* strains in Denmark to determine whether 5-fluorocytosine resistance emerged as a result of clonal spread among hospitalized patients. We identified 66 genotypes among the 72 susceptible strains, comprising 84% of the total observed diversity, including 62 unique singletons and 4 small clusters (Figure 1). In contrast, the 32 genotyped non–wild-type strains accounted for 12 genotypes, forming 2 clusters and 10 distinct singletons. One cluster included 15 non–wild-type strains (47% of all non–wild-type isolates), whereas a smaller cluster contained 7 non–wild-type strains (22%). Eight non–wild-type singletons varied by 1 allele, whereas the remaining 2 were completely distinct (Figure 1). We determined the allelic profiles of the 104 clinical *C. tropicalis* strains, including the profile for the comparator control strain (ATCC 750) (Appendix Table 4).

Discussion

In this study, we report a concerning exponential 4-fold increase per decade over a 20-year period in 5-fluorocytosine resistance in clinical *C. tropicalis* isolates in Denmark. The underlying molecular mechanism is primarily associated with an E49X alteration in the purine-cytosine permease enzyme (encoded by *FCY2*), which was found exclusively in non–wild-type strains and results in a severely truncated and likely nonfunctional transporter protein. Furthermore, we show that this genotype has expanded clonally in Denmark. Those findings are both surprising and worrying for several reasons. First, 5-fluorocytosine is rarely used in Denmark (<1–4 patients per year according to the national medicine sales registry [https://medstat.dk]). Second, the non–wild-type strains were unique and epidemiologically unrelated, with no geographic pattern in resistance rates across

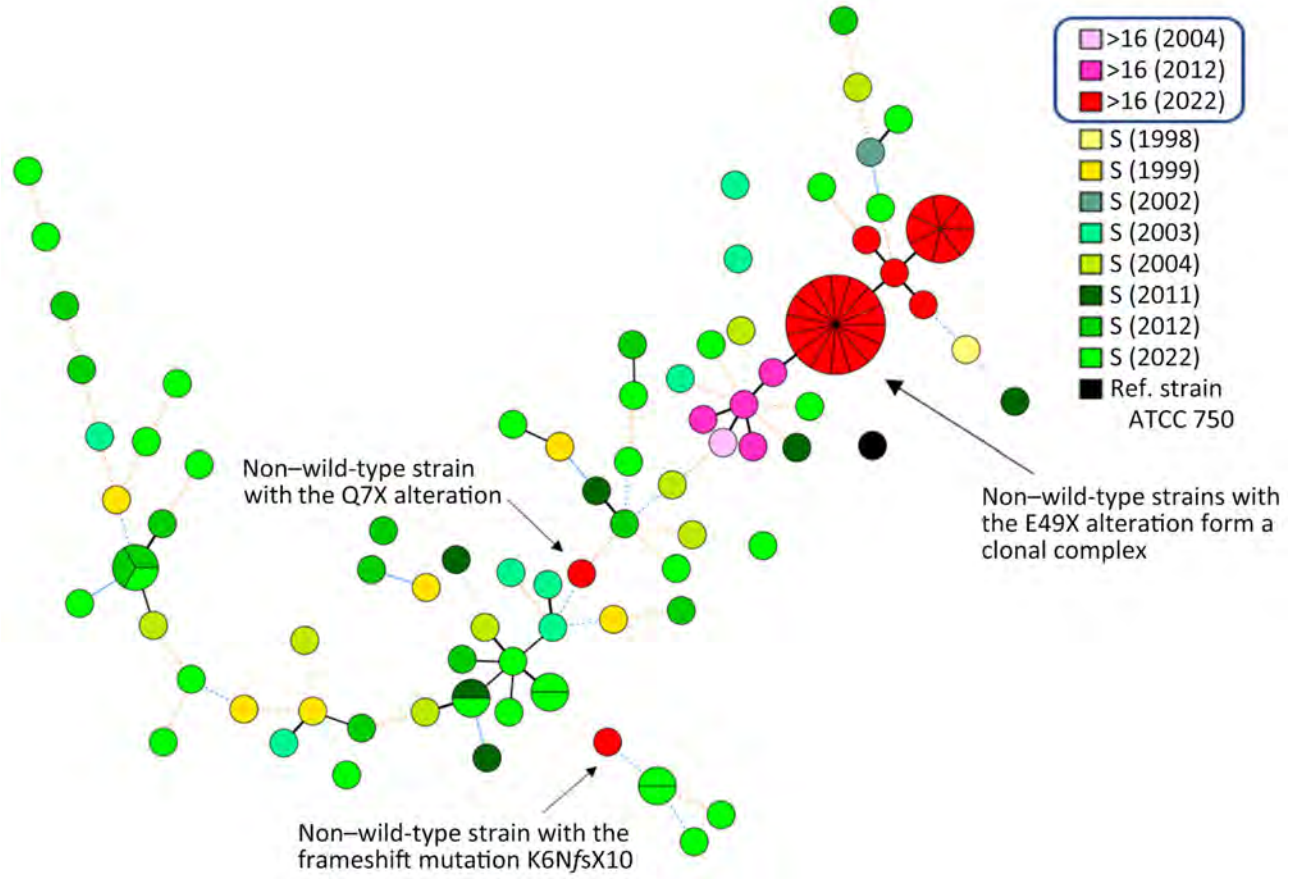

Figure 1. Minimum spanning tree illustrating the genotypic relationships among *Candida tropicalis* isolates, Denmark. Each node represents a distinct genotype; node size is proportional to the number of strains sharing the same allelic profile. Lines connecting nodes indicate genetic differences: thick solid black indicates 1 allele difference; thin solid black, 2 alleles; thin solid blue, 3 alleles; thin dashed blue, 4 alleles; orange dashed, 5 alleles; orange dotted, 6 alleles; and grey dotted, >6 alleles. Node colors represent the year of collection and 5-fluorocytosine resistance status. Non–wild-type strains with the E49X alteration form a clonal complex with minimal genetic variation over a 20-year period. In contrast, isolates carrying the Q7X or K6NfsX10 alterations are genetically unrelated to each other and to other strains, suggesting sporadic acquisition of resistance. Note: Line length does not reflect evolutionary distance. Boxed items at top of key indicate MICs for non–wild-type strains. S, susceptible.

the country, as expected because a previous genotyping study found no evidence of clonal spread of candidemia isolates in Denmark (*17*). This raises the question whether a common source of non–wild-type *C. tropicalis* exists or whether a common selecting factor other than 5-fluorocytosine use in humans has contributed to the observed increase in resistance, either in hospitals or in the environment.

Our sequencing targeted the *FCY2*, *FCY1*, and *FUR1* genes, essential for 5-fluorocytosine uptake and conversion, along with the *URA3* gene involved in UMP biosynthesis. Deleterious mutations were found in *FCY2*-encoding purine-cytosine permease, responsible for the cellular uptake of 5-fluorocytosine and the primary molecular target involved in 5-fluorocytosine resistance. Of note, 92% of non–wild-type strains harbored a G145T nucleotide alteration in both *FCY2* alleles, converting the GAA codon for glutamate (E) to a stop codon (TAA) and resulting in premature termination at position 49 (designated E49X) of the 509-aa sequence. The G145T point mutation has been reported only once, in a study by Chen et al. (2011), where it was observed in 1 resistant isolate among 97 tested clinical strains (*18*). Our data strongly suggest that the G145T point mutation is a key mechanism behind 5-fluorocytosine resistance in *C. tropicalis* isolates in Demark.

Two non–wild-type strains did not contain the E49X alteration. One of those displayed a novel nonsense mutation, termed Q7X, caused by the C19T nucleotide substitution in both *FCY2* alleles. The other non–wild-type strain harbored a novel frameshift mutation caused by the deletion of an adenine (A) at position 18 of the *FCY2* sequence, designated K6NfsX10. This frameshift mutation substitutes a lysine (K) at position 6 to asparagine (N) and results in premature termination of translation after 10 aa. Each of those 3 mutations leads to the early truncation of the FCY2 protein, likely rendering it deficient in critical functional domains essential for proper transporter activity, including substrate binding, cofactor interactions, and cellular localization.

We did not detect amino acid substitutions in cytosine deaminase (FCY1), in either non–wild-type or susceptible *C. tropicalis* isolates. However, 1 susceptible isolate harbored 2 missense mutations in *FUR1*, leading to K5Q and A157S alterations in uracil phosphoribosyl transferase. The absence of mutations in genes (such as *FCY1* and *FUR1*) downstream of 5-fluorouracil, the active metabolite of 5-fluorocytosine, in non–wild-type isolates suggests that 5-fluorouracil, a chemotherapeutic agent (*8*), does not play a significant role in conferring resistance to 5-fluorocytosine in *C. tropicalis*. Furthermore, 5-fluorouracil does not use the same transporter protein (FCY2) as 5-fluorocytosine (*19*). Taken together, those findings indicate that the selection pressure driving 5-fluorocytosine resistance in *C. tropicalis* likely occurred upstream of 5-fluorouracil metabolism. However, other purine analogs that also rely on FCY2 for cellular entry may contribute to resistance emergence. Such agents, whether used as chemotherapies or in other medical or environmental contexts, could impose selective pressure on fungal populations, potentially promoting mutations in the transporter protein that confer 5-fluorocytosine resistance. Those results further suggest the existence of an alternative cytosine salvage pathway in *C. tropicalis*, highlighting its capacity for survival and proliferation in environments with fluctuating drug exposure, both in clinical and environmental contexts.

Desnos-Olivier et al. (*12*) reported a 35% 5-fluorocytosine resistance rate in *C. tropicalis* in the Paris area in 2002–2006, dominated by a clonal population carrying a K177E alteration in orotidine-5′-phosphate decarboxylase (encoded by *URA3*) but no mutations in the *FCY2* gene when compared with the wild-type strain. The authors proposed that increased *URA3* expression, driven by the K177E mutation, could lead to overproduction of UMP by upregulating the pyrimidine biosynthesis pathway, contributing to 5-fluorocytosine resistance. However, considering the high catalytic efficiency of orotidine-5′-phosphate decarboxylase across many organisms and the fact that pyrimidine nucleotide biosynthesis is primarily regulated at earlier steps in the pathway, it seems unlikely that the K177E mutation alone would substantially alter pyrimidine nucleotide pools and drive resistance (*20*–*22*). Although we detected the K177E alteration in all 5-fluorocytosine–non–wild-type isolates from Denmark harboring the nonsense mutation (E49X), the mutation was also present in 2 susceptible isolates, bringing into question its proposed role in resistance. We performed in silico analysis of the *FCY2* forward primer used in the France study and confirmed complementarity to the target gene. However, we noted that the forward primer annealed 126 bp downstream of the open reading frame (Figure 2). This primer positioning likely led to incomplete sequencing of the *FCY2* coding region, missing potential point mutations in the early region of the gene. We speculate that this positioning may be a result of using the *FCY2* reference sequence derived from the genome assembly of *C. tropicalis* MYA 3404 (BioProject no. PRJNA13675). Our in silico analysis indicates a possible mutation or sequencing error in this assembly,

leading to a premature TGA stop codon instead of the TGG tryptophan codon, 199 bp downstream of the open reading frame (Figure 2). Moreover, analysis of the more recent *C. tropicalis* ATCC750 genome assembly (2020) confirmed the presence of the TGG codon with no premature stop codon observed at this position. Finally, our sequencing data of both non–wild-type and susceptible 5-fluorocytosine strains was consistent with the updated reference sequence, supporting our observation. Resequencing of the *FCY2* gene of the strains from France using updated primers and reference sequence would be of interest.

Our sequencing analysis revealed a significant level of heterozygosity across all strains; 12/72 (16.7%) of the 5-fluorocytosine–susceptible population carrying the G145T point mutation (causing E49X in homozygous isolates) in 1 of the 2 *FCY2* alleles. This finding may indicate an increased likelihood of resistance developing through a single genetic rearrangement (*18*,*23*).

In contrast to the broad genetic diversity observed among susceptible strains, the genotyping dataset highlighted the close genetic relatedness among the non–wild-type strains harboring the E49X alteration, with only 1 allele difference between the early 2004 non–wild-type isolate and subsequent strains collected over the next 20 years. This finding supports the hypothesis that this specific non–wild-type genotype, likely introduced or emerged in Denmark 20 years ago, has undergone gradual microevolution and effectively spread among hospitalized patients or in the population in general. In contrast, the 2 remaining non–wild-type isolates (1 carrying Q7X alterations and the other K6Nf*s*X10) were not related to each other or to the remaining non–wild-type and susceptible isolates, suggesting sporadic resistance acquisition. Given that 5-fluorocytosine is rarely used in Denmark and extremely rarely for *C. tropicalis* infections, the drivers of the clonal expansion of the 5-fluorocytosine clone remain unexplained. Those findings call for studies on potential unrecognized selection factors in human medicine, environmental influences, and fungus-specific factors such as virulence, biofilm formation, or surface adherence.

In conclusion, our study provides new knowledge on the molecular mechanisms underlying 5-fluorocytosine resistance in *C. tropicalis* strains and documents a clonal spread along with notable increase

Figure 2. *FCY2* sequence encoding the purine-cytosine permease derived from contig 14 of the *Candida tropicalis* strain ATCC 750 genome assembly, published on the ATCC Genome Portal in 2020. The coding sequence spans positions 2152980–2154500. The ORF is depicted at the top left of the figure; long red arrow illustrates the *FCY2* forward primer designed by Desnos-Ollivier et al. (*12*), and the blue arrow indicates the ORF they used. The green arrow represents the tryptophan codon TGG, which is converted to stop codon TGA in the MYA 3404 genome assembly. CDS, coding sequence; ORF, open reading frame.

in resistance prevalence among *C. tropicalis* isolates in the absence of a recognized selection pressure in Denmark. Our findings present a challenge in healthcare facilities, requiring attention, surveillance, improved infection control measures, and collaborative efforts to clarify drivers of resistance and develop effective prevention strategies.

Acknowledgments

We thank Karin Meinike Jørgensen for her meticulous participation in the daily routine susceptibility testing and Rasmus Krøger Hare for his introduction to the Bionumerics program.

This project has been defended for N.A.-C.'s bachelor degree at the Technical University of Denmark in June 2024.

No external funding was received. The authors have no conflicts of interest related to this study. Outside this study M.C.A. declares the following for the past 36 months: grants or contracts paid to the institution from Scynexis, Pfizer, F2G, Shionogi, Cidara and Mundipharma. She has received an honorarium for one talk from each of the following companies: Shionogi, Gilead, and Mundipharma. She is the current chair of the EUCAST antifungal subcommittee.

Author contributions: N.A.-C., K.M.T.A., and M.C.A. conceptualized the study. N.A.-C. performed the molecular studies, K.M.T.A. conducted the EUCAST MIC determinations. A.S.E.M. conducted susceptibility tests on many of the isolates. N.A.-C. performed the data analysis and prepared the original thesis document, which M.C.A. revised into the journal version. J.M., N.A.-C.'s supervisor, reviewed the original thesis document, provided feedback, and conducted the examination. All authors reviewed and edited the final manuscript.

About the Author

Ms. Abou-Chakra holds a diploma in chemical and bioengineering from the Technical University of Denmark. She is responsible for the molecular work at the mycology unit, Statens Serum Institute, Denmark, and recently defended her bachelor thesis on 5-flourocytosine resistance in *C. tropicalis*.

References

1. Spampinato C, Leonardi D. *Candida* infections, causes, targets, and resistance mechanisms: traditional and alternative antifungal agents. BioMed Res Int. 2013;2013:204237. https://doi.org/10.1155/2013/204237
2. Pappas PG, Lionakis MS, Arendrup MC, Ostrosky-Zeichner L, Kullberg BJ. Invasive candidiasis. Nat Rev Dis Primers. 2018;4:18026. https://doi.org/10.1038/nrdp.2018.26
3. Risum M, Astvad K, Johansen HK, Schønheyder HC, Rosenvinge F, Knudsen JD, et al. Update 2016–2018 of the nationwide Danish fungaemia surveillance study: epidemiologic changes in a 15-year perspective. J Fungi (Basel). 2021;7:491. https://doi.org/10.3390/jof7060491
4. Roilides E, Farmaki E, Evdoridou J, Francesconi A, Kasai M, Filioti J, et al. *Candida tropicalis* in a neonatal intensive care unit: epidemiologic and molecular analysis of an outbreak of infection with an uncommon neonatal pathogen. J Clin Microbiol. 2003;41:735–41. https://doi.org/10.1128/JCM.41.2.735-741.2003
5. Spruijtenburg B, De Carolis E, Magri C, Meis JF, Sanguinetti M, de Groot T, et al. Genotyping of *Candida tropicalis* isolates uncovers nosocomial transmission of two lineages in Italian tertiary-care hospital. J Hosp Infect. 2025;155:115–22. https://doi.org/10.1016/j.jhin.2024.10.003.
6. Wang Q, Tang D, Tang K, Guo J, Huang Y, Li C. Multilocus sequence typing reveals clonality of fluconazole-nonsusceptible *Candida tropicalis*: a study from Wuhan to the global. Front Microbiol. 2020;11:554249. https://doi.org/10.3389/fmicb.2020.554249
7. Sigera LSM, Denning DW. Flucytosine and its clinical usage. Ther Adv Infect Dis. 2023;10:20499361231161387. https://doi.org/10.1177/20499361231161387
8. Longley DB, Harkin DP, Johnston PG. 5-fluorouracil: mechanisms of action and clinical strategies. Nat Rev Cancer. 2003;3:330–8. https://doi.org/10.1038/nrc1074
9. Zhang N, Yin Y, Xu SJ, Chen WS. 5-Fluorouracil: mechanisms of resistance and reversal strategies. Molecules. 2008;13:1551–69. https://doi.org/10.3390/molecules13081551
10. Law D, Moore CB, Joseph LA, Keaney MGL, Denning DW. High incidence of antifungal drug resistance in *Candida tropicalis*. Int J Antimicrob Agents. 1996;7:241–5. https://doi.org/10.1016/S0924-8579(96)00328-7
11. Tortorano AM, Rigoni AL, Biraghi E, Prigitano A, Viviani MA; FIMUA-ECMM Candidaemia Study Group. The European Confederation of Medical Mycology (ECMM) survey of candidaemia in Italy: antifungal susceptibility patterns of 261 non-albicans Candida isolates from blood. J Antimicrob Chemother. 2003;52:679–82. https://doi.org/10.1093/jac/dkg393
12. Desnos-Ollivier M, Bretagne S, Bernède C, Robert V, Raoux D, Chachaty E, et al.; Yeasts Group. Clonal population of flucytosine-resistant *Candida tropicalis* from blood cultures, Paris, France. Emerg Infect Dis. 2008;14:557–65. https://doi.org/10.3201/eid1404.071083
13. Arendrup MC, Arikan-Akdagli S, Jørgensen KM, Barac A, Steinmann J, Toscano C, et al. European candidaemia is characterised by notable differential epidemiology and susceptibility pattern: results from the ECMM Candida III study. J Infect. 2023;87:428–37. https://doi.org/10.1016/j.jinf.2023.08.001
14. European Committee for Antimicrobial Susceptibility Testing (EUCAST). Susceptibility testing of yeasts. version 7.4. October 2023 [cited 2025 Mar 13]. https://www.eucast.org/astoffungi/methodsinantifungalsusceptibilitytesting/susceptibility_testing_of_yeasts
15. Turnidge J, Kahlmeter G, Kronvall G. Statistical characterisation of bacterial wild-type MIC value distributions and the determination of epidemiological cut-off values. Clin Microbiol Infect. 2006;12:418–25. https://doi.org/10.1111/j.1469-0691.2006.01377.x
16. Wu Y, Zhou H-J, Che J, Li W-G, Bian F-N, Yu S-B, et al. Multilocus microsatellite markers for molecular typing of *Candida tropicalis* isolates. BMC Microbiol. 2014;14:245. https://doi.org/10.1186-014-0245-z
17. Guinea J, Arendrup MC, Cantón R, Cantón E, García-Rodríguez J, Gómez A, et al. Genotyping reveals high clonal diversity and widespread genotypes of *Candida*

causing candidemia at distant geographical areas. Front Cell Infect Microbiol. 2020;10:166. https://doi.org/10.3389/fcimb.2020.00166
18. Chen YN, Lo HJ, Wu CC, Ko HC, Chang TP, Yang YL. Loss of heterozygosity of FCY2 leading to the development of flucytosine resistance in *Candida tropicalis*. Antimicrob Agents Chemother. 2011;55:2506–14. https://doi.org/10.1128/AAC.01777-10
19. Chevallier MR, Jund R, Lacroute F. Characterization of cytosine permeation in *Saccharomyces cerevisiae*. J Bacteriol. 1975;122:629–41. https://doi.org/10.1128/jb.122.2.629-641.1975
20. Chan KK, Wood BMK, Fedorov AA, Fedorov EV, Imker HJ, Amyes TL, et al. Mechanism of the orotidine 5′-monophosphate decarboxylase-catalyzed reaction: evidence for substrate destabilization. Biochemistry. 2009;48:5518–31. https://doi.org/10.1021/bi900623r
21. Nygaard P, Saxild HH. Nucleotide metabolism. In: Schaechter M, editor. Encyclopedia of microbiology. 3rd ed. Oxford: Academic Press; 2009. p. 296–307.
22. Li G, Li D, Wang T, He S. Pyrimidine biosynthetic enzyme CAD: its function, regulation, and diagnostic potential. Int J Mol Sci. 2021;22:10253. https://doi.org/10.3390/ijms221910253
23. Xu J. Is natural population of *Candida tropicalis* sexual, parasexual, and/or asexual? Front Cell Infect Microbiol. 2021;11:751676. https://doi.org/10.3389/fcimb.2021.751676

Address for correspondence: Maiken Cavling Arendrup, Unit for Mycology, Bldg 45, Rm 112, Statens Serum Institut, Artillerivej 5, DK-2300 Copenhagen, Denmark; email: maca@ssi.dk

Administration of L-Type Bovine Spongiform Encephalopathy to Macaques to Evaluate Zoonotic Potential

Morikazu Imamura,[1] Ken'ichi Hagiwara, Minoru Tobiume, Minako Ohno, Hiromi Iguchi, Hanae Takatsuki, Tsuyoshi Mori, Ryuichiro Atarashi, Hiroaki Shibata, Fumiko Ono[1]

We administered L-type bovine spongiform encephalopathy prions to macaques to determine their potential for transmission to humans. After 75 months, no clinical symptoms appeared, and prions were undetectable in any tissue by Western blot or immunohistochemistry. Protein misfolding cyclic amplification, however, revealed prions in the nerve and lymphoid tissues.

Worldwide emergence of classical bovine spongiform encephalopathy (C-BSE) is associated with variant Creutzfeldt-Jakob disease in humans (*1*). Two other naturally occurring BSE variants have been identified, L-type (L-BSE) and H-type. Studies using transgenic mice expressing human normal prion protein (PrP^{C}) (*2*) and primates (*3*–*5*) have demonstrated that L-BSE is more virulent than C-BSE. Although L-BSE is orally transmissible to minks (*6*), cattle (*7*), and mouse lemurs (*5*), transmissibility to cynomolgus macaques, a suitable model for investigating human susceptibility to prions, remains unclear. We orally inoculated cynomolgus macaques with L-BSE prions and explored the presence of abnormal prion proteins (PrP^{Sc}) in tissues using protein misfolding cyclic amplification (PMCA) along with Western blot (WB) and immunohistochemistry (IHC). PMCA markedly accelerates prion replication in vitro, and its products retain the biochemical properties and transmissibility of seed prion strains (*8*).

Author affiliations: University of Miyazaki, Miyazaki, Japan (M. Imamura, M. Ohno, H. Iguchi, H. Takatsuki, T. Mori, R. Atarashi); National Institute of Infectious Diseases, Tokyo, Japan (K. Hagiwara, M. Tobiume); The Corporation for Production and Research of Laboratory Primates, Tsukuba, Japan (H. Shibata); Okayama University of Science, Imabari, Japan (F. Ono)

DOI: http://doi.org/10.3201/eid3105.241257

The Study

Two macaques orally inoculated with L-BSE prions remained asymptomatic and healthy but were euthanized and autopsied at 75 months postinoculation. WB showed no PrP^{Sc} accumulation in any tissue (Table), IHC revealed no PrP^{Sc} accumulation, hematoxylin and eosin staining revealed no spongiform changes in brain sections, and pathologic examination revealed no abnormalities.

We next attempted to detect PrP^{Sc} using PMCA, performed as previously described (*9*), with minor modifications (Appendix, https://wwwnc.cdc.gov/EID/article/31/5/24-1257-App1.pdf). First, we evaluated the sensitivity of PMCA. Using serial amplification with 10-fold stepwise dilutions of prion-infected brain homogenates as seeds, we amplified PrP^{Sc}-like proteinase K (PK)–resistant prion protein (PrPres) from a 10^{-7} dilution of 10% brain homogenate (BH) obtained from macaque intracerebrally inoculated with L-BSE prions in the fifth amplification round (Figure 1, panel A). This method also enabled propagation of PrPres from a 10^{-8} dilution of BH from C-BSE–affected cattle during the second amplification round (Figure 1, panel B), suggesting PMCA's higher efficiency and sensitivity for detecting C-BSE prions than macaque L-BSE prions.

We attempted to detect prions in the lymphoid and nervous systems, among other tissues, of the 2 orally inoculated macaques using refined PMCA (Figure 2; Appendix Figure, Table). In lymphoid tissue samples prepared using sodium phosphotungstic acid precipitation (Appendix), we amplified PrPres in the inguinal and mesenteric lymph nodes, ileum, and tonsils of both macaques (Figure 2, panels A, B), as well as in the spleen of 1 macaque (#18) and the thy-

[1]These authors were co–principal investigators.

Table. Detection of PrPres in tissue samples obtained from macaques orally challenged with L-BSE prions in study of oral transmission of L-type bovine spongiform encephalopathy in macaques to evaluate zoonotic potential*

	PMCA, no. positive/no. total					WB, orally challenged animals		IHC, orally challenged animals	
	Orally challenged animals		Negative controls						
Sample location	18	19	9086	1004	9040	18	19	18	19
Nerve tissues									
Cerebral cortex, frontal lobe; PTA, PBS	0/2, 0/2	0/2, 0/2	ND	0/2, 0/2	0/2, 0/2	Neg	Neg	Neg	Neg
Cerebral cortex, temporal lobe	ND	ND	ND	ND	ND	Neg	Neg	Neg	Neg
Cerebral cortex, parietal lobe	ND	ND	ND	ND	ND	Neg	Neg	Neg	Neg
Cerebral cortex, occipital lobe	ND	ND	ND	ND	ND	Neg	Neg	Neg	Neg
Hippocampus	ND	ND	ND	ND	ND	Neg	Neg	Neg	Neg
Thalamus	ND	ND	ND	ND	ND	Neg	Neg	Neg	Neg
Cerebellum	ND	ND	ND	ND	ND	Neg	Neg	Neg	Neg
Cervical cord; EtOH, PBS	0/2, 0/2	0/2, **1/2**	0/2, 0/2	0/2, 0/2	0/2, 0/2	Neg	Neg	Neg	Neg
Thoracic cord; EtOH, PBS	0/2, **1/2**	0/2, **1/2**	0/2, 0/2	0/2, 0/2	0/2, 0/2	Neg	Neg	Neg	Neg
Lumbar cord; EtOH, PBS	0/2, 0/2	0/2, 0/2	0/2, 0/2	0/2, 0/2	0/2, 0/2	Neg	Neg	Neg	Neg
Median nerve, PTA	**2/2**	**1/2**	ND	ND	ND	Neg	Neg	Neg	Neg
Sciatic nerve, PTA	0/2	0/2	ND	ND	ND	Neg	Neg	Neg	Neg
Secondary lymphoid tissues									
Spleen, PTA	**1/2**	0/2	ND	ND	0/2	Neg	Neg	Neg	Neg
Tonsil, PTA	**1/2**	**2/2**	0/2	0/2	0/2	ND	ND	ND	ND
Submandibular lymph node, PTA	0/2	0/2	0/2	ND	0/2	Neg	Neg	Neg	Neg
Inguinal lymph nodes, PTA	**1/2**	**2/2**	ND	ND	ND	ND	ND	ND	ND
Mesenteric lymph node, PTA	**1/2**	**1/2**	0/2	0/2	0/2	ND	ND	ND	ND
Primary lymphoid tissues									
Thymus, PTA	0/2	**2/2**	ND	ND	ND	ND	ND	ND	ND
Others									
Submaxillary gland, PTA	**2/2**	**1/2**	ND	ND	ND	ND	ND	ND	ND
Ileum, PTA	**2/2**	**2/2**	0/2	0/2	0/2	Neg	Neg	Neg	Neg

*Bold indicates positive results. EtOH, ethanol precipitation; IHC, immunohistochemistry; ND, not determined; neg, negative; PBS, suspension in phosphate-buffered saline; PMCA, protein misfolding cyclic amplification; PrPres, PrP^{Sc}-like proteinase K–resistant prion proteins; PTA, sodium phosphotungstic acid precipitation; WB, Western blot.

mus of the other (#19), in the second or third amplification round of PMCA (Figure 2, panel C). We observed no PrPres in the submandibular lymph nodes (Appendix Figure 1). Examining the central nervous system, we observed no PrPres amplification in the cerebral cortex (Figure 2, panel C), whether seeded with phosphate-buffered saline homogenates or phosphotungstic acid precipitates. The spinal cord showed no PrPres amplification upon ethanol precipitation. However, PrPres was amplified in the cervical spinal cord of macaque #19 and in the thoracic spinal cord of both macaques with phosphate-buffered saline homogenates (Figure 2, panel D). We also confirmed PrPres in the median nerve of both

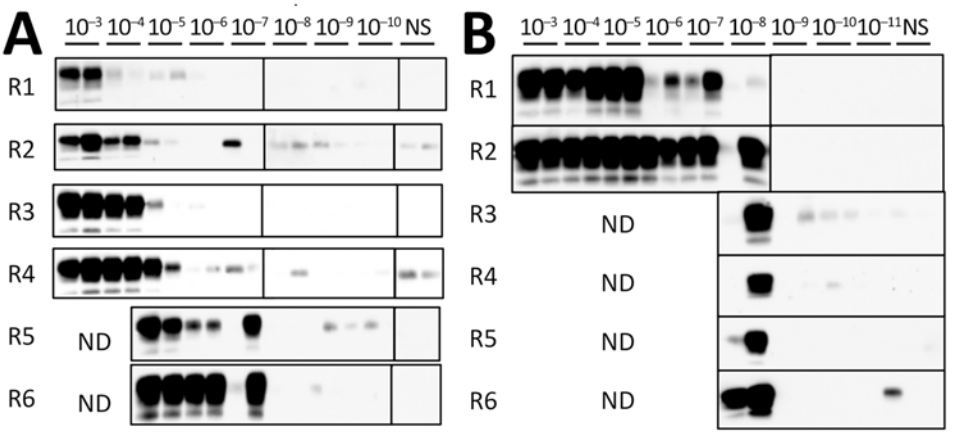

Figure 1. Sensitivity of modified protein misfolding cyclic amplification (PMCA) to detect abnormal prion protein in study of oral transmission of L-type bovine spongiform encephalopathy (L-BSE) in intracerebrally inoculated macaques to evaluate zoonotic potential. We evaluated in macaques intracerebrally inoculated with L-BSE prions (A) and cattle intracerebrally inoculated with classical BSE prions (B) (Appendix, https://wwwnc.cdc.gov/EID/article/31/5/24-1257-App1.pdf). We serially diluted (10^{-3}–10^{-11}) brain homogenates (10% weight by volume) in 50 µL of human normal prion protein (PrP^{C}) substrate and performed PMCA. We further diluted the initial PMCA product to 1:5 with a fresh PrP^{C} substrate for subsequent rounds. We conducted 6 rounds of PMCA in duplicate. In macaques, PMCA propagated PrPSc-like proteinase K–resistant prion protein (PrP^{res}) from a 10^{-7} dilution in the fifth amplification round; in cattle, PMCA propagated PrPres from a 10^{-8} dilution during the second amplification round. We performed Western blot for each PMCA product (2.5 µL) after proteinase K digestion using the T-2 antibody (*10*). ND, assays not done; NS, nonseeded control; R, round.

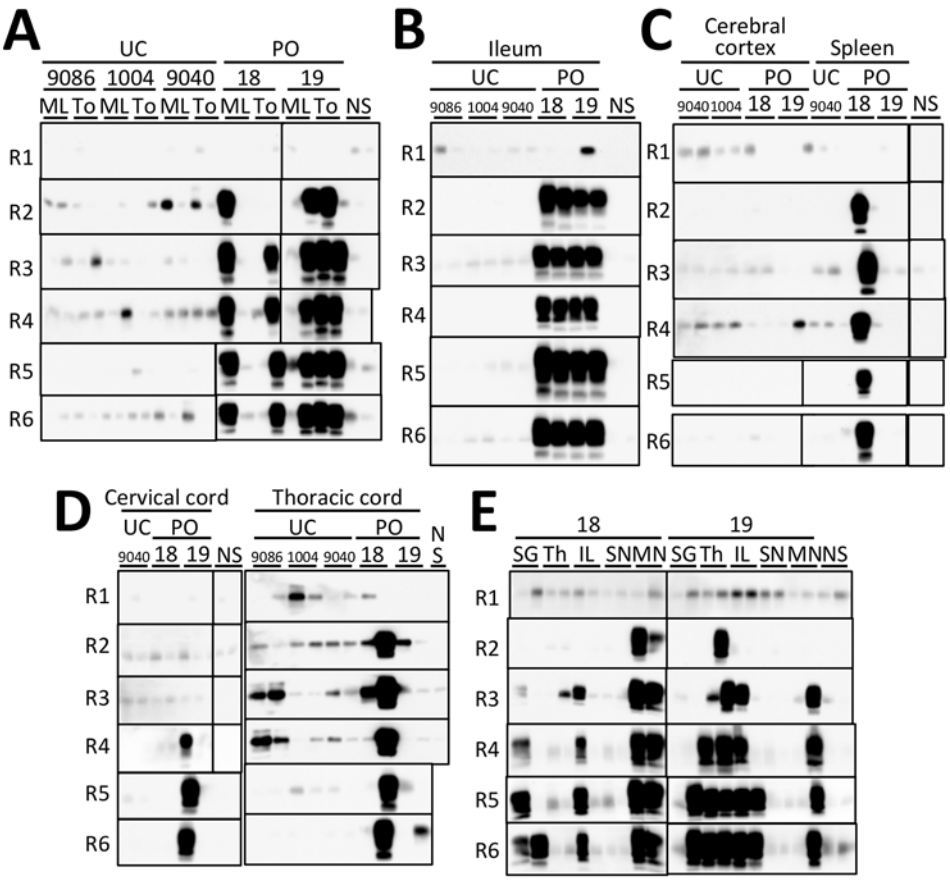

Figure 2. Sensitivity of modified protein misfolding cyclic amplification (PMCA) to detect abnormal prion protein in study of oral transmission of L-type bovine spongiform encephalopathy (L-BSE) in orally inoculated macaques to evaluate zoonotic potential. We performed 6 rounds of PMCA in duplicate in the tissues of 2 macaques (#18 and #19) orally inoculated with L-BSE prions, primarily in the lymphoid and nervous system tissues. A) ML nodes and To tissue; B) ileum; C) cerebral cortex and spleen; D) cervical and thoracic cords; and E) SG, Th, IL nodes, SN, and MN tissues. We prepared PMCA seeds, equivalent to 6.25 mg of tissue, obtained from lymphoid tissues, peripheral nerves, submaxillary glands, and ileum by using a standard sodium phosphotungstic acid precipitation method. For brain tissues, we used 10% homogenates in phosphate-buffered saline (250 µg) and phosphotungstic acid precipitates as seeds. For spinal cords, we used 10% homogenates in phosphate-buffered saline and ethanol precipitates (625 µg equivalent) as seeds. Tissues obtained from 3 uninfected macaques (#9068, #1004, and #9040) served as negative controls and were processed identically to those obtained from inoculated animals. For the thoracic spinal cord of macaque #19, we performed amplification for 7 rounds to determine whether the round 6 signal was positive. IL, inguinal lymph; ML, mesenteric lymph; MN, median nerve; NS, nonseeded control; PMCA, protein misfolding cyclic amplification; PO, L-type bovine spongiform encephalopathy orally inoculated macaques; SG, submaxillary gland; SN, sciatic nerve; TH, thymus; To, tonsil; UC, uninoculated control.

macaques but not in the sciatic nerve (Figure 2, panel E). We noted PrPres signals in the submandibular glands of both animals. In contrast, we found no PrPres amplification in any tissues from uninoculated control macaques.

PrPres obtained from the orally inoculated macaques exhibited diverse banding patterns distinct from those generated by PMCA using L-BSE–affected cattle BH and L-BSE intracerebrally inoculated macaque BH as seeds (Figure 3, panels A–C). Of note, the lowest-molecular-weight PrPres variants from the ileum, spleen, inguinal lymph nodes, thoracic cord, submaxillary gland, and mesenteric lymph nodes of orally inoculated macaques exhibited remarkable PK resistance similarity and banding patterns indistinguishable from those of PrPres generated by PMCA with C-BSE–affected cattle BH as a seed (Figure 3, panel C, Appendix Figures 2 and 3). In contrast, the higher-molecular-weight PrPres variants from the ileum of macaque #18 exhibited a unique banding pattern distinct from those of L-BSE, C-BSE, and H-type BSE prions (Figure 3, panel C). Banding patterns and PK resistance of PrPres amplified from L-BSE–affected cattle BH and L-BSE intracerebrally inoculated macaque BH were notably similar.

This PMCA method was initially designed for the high-sensitivity detection of L-BSE intracerebrally inoculated macaque PrP^{Sc} but was even more efficient and sensitive in detecting bovine C-BSE PrP^{Sc} (Figure 1, panel B). Therefore, we believe that this method enabled the detection of both C-BSE–like PrP^{Sc} and potentially novel PrP^{Sc} variants.

Conclusion

We noted no detectable evidence of PrP^{Sc} by WB or IHC in any tissues of L-BSE orally inoculated macaques. Nevertheless, PMCA successfully amplified PrPres from lymphatic and neural tissues. The PrPres

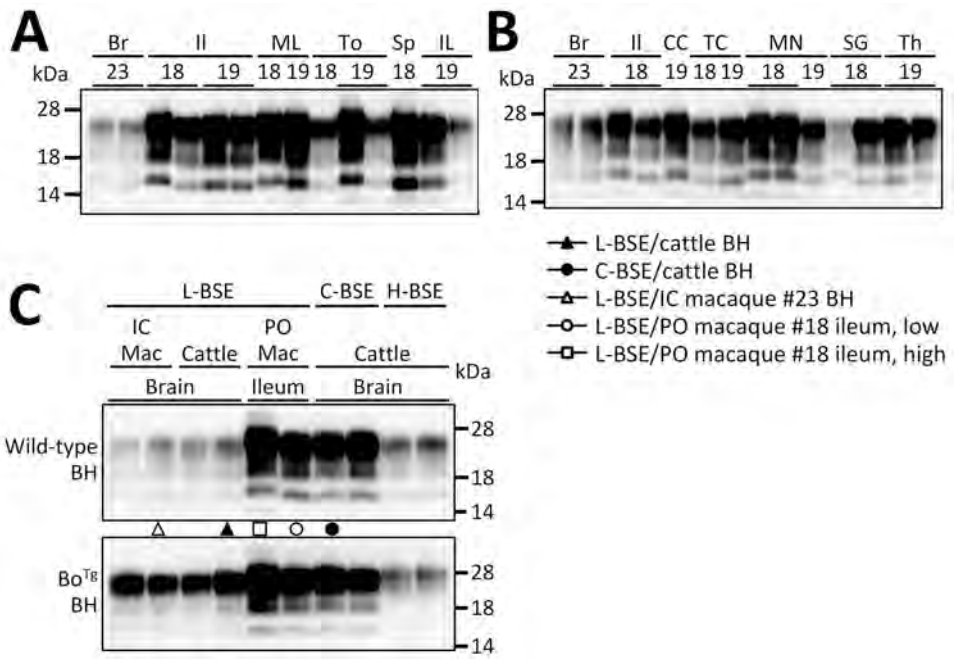

Figure 3. Gel electrophoresis and Western blot testing of tissues obtained from macaques orally inoculated with L-BSE prions in study of oral transmission of L-BSE in macaques to evaluate zoonotic potential. We loaded each 6th-round protein misfolding cyclic amplification (PMCA) product, seeded with tissues obtained from the 2 macaques (#18 and #19), onto 2 gels for sodium dodecyl sulfate-polyacrylamide gel electrophoresis, followed by Western blot. A) PMCA products amplified from ML, To, Sp, and Il; B) PMCA products amplified from CC, TC, MN, SG, and Th; C) Western blot analysis. For comparison, PMCA products amplified using BH obtained from macaque #23, intracerebrally inoculated with L-BSE, were run on both gels together with products amplified from the ileum of macaque #18. Abnormal prion protein (PrP)-like proteinase K–resistant prion proteins (PrPres) from L-BSE orally inoculated macaques exhibited a few distinct banding patterns, which differed from those of PrPres from L-BSE intracerebrally in macaque #23. For Western blot, we compared 6th-round PMCA products, seeded with IL tissue obtained from macaque #18 and Br tissue obtained from macaque #23, L-BSE–affected cattle, C-BSE–affected cattle, and H-BSE–affected cattle. Banding results represent the products of PMCA using the BHs of wild-type mice (upper image) and bovine normal prion protein–expressing transgenic mice (lower image) as substrates, with identical cofactors. Among the PrPres amplified from the ileum of L-BSE/PO macaque #18, the banding pattern of PrPres with a small molecular weight (low) was very similar to that of PrPres amplified from the brain of cattle inoculated intracerebrally with C-BSE. BH, brain homogenate; Bo^{Tg}, bovine normal prion protein–expressing transgenic; Br, brain; C-BSE, classical bovine spongiform encephalopathy; CC, cervical cord; H-BSE, H-type bovine spongiform encephalopathy; IC, inoculated intracerebrally; Il, ileum; IL, inguinal lymph nodes; L-BSE, L-type bovine spongiform encephalopathy; Mac, macaque; ML, mesenteric lymph nodes; MN, median nerve; PO, inoculated orally; SG, submaxillary gland; Sp, spleen; TC, thoracic cord; Th, thymus; To, tonsil.

exhibited electrophoretic patterns distinct from those detected by PMCA using L-BSE–affected cattle BH as the seed (Figure 3, panel C), indicating that the PrP^{Sc} used as the template for PrPres amplification in orally inoculated macaques did not originate from the bovine L-BSE prions used as inoculum. Instead, PrP^{Sc} were newly generated by the conversion of macaque PrP^{C} by bovine L-BSE prions. Our results provide strong evidence that L-BSE can infect macaques via the oral route.

We found no evidence that PrP^{Sc} reached the brain in orally inoculated macaques; however, the macaques euthanized 6 years postinoculation might have been in the preclinical period. At low infection levels, lymph nodes play a vital role in prion spread to the central nervous system (*11*). Therefore, had the macaques been maintained for a longer period, they might have developed prion disease. Retrospective surveillance studies using the appendix and tonsil tissues suggested a considerable number of humans harboring vCJD in a carrier state (*12*). Thus, we cannot exclude that L-BSE orally inoculated macaques could similarly remain in a potentially infectious state.

The brain of L-BSE intracerebrally inoculated macaque accumulated prions with biochemical properties resembling bovine L-BSE prions (Figure 3, panel C; Appendix Figure 2); however, we observed no PrP^{Sc} accumulation in lymphoid tissues by WB or IHC (*4*). In contrast, macaques orally inoculated with C-BSE prions showed PrP^{Sc} accumulation in lymphoid tissues, including the spleen, tonsils, and mesenteric lymph nodes by WB and IHC (*13*). In our study, L-BSE orally inoculated macaques harbored C-BSE–like prions in their lymphoid and neural tissues. Interspecies transmission of L-BSE prions to ovine PrP transgenic mice can result in a shift toward C-BSE–like properties (*14*,*15*). Our data suggest that L-BSE prions may alter biophysical and biochemical properties, depending on interspecies transmission and inoculation route, acquiring traits similar to those of C-BSE prions. This transformation might result from structural changes in the L-BSE prion to C-BSE–like prions and other

lymphotropic prions within lymphoid tissues or from the selective propagation of low-level lymphotropic substrains within the L-BSE prion population.

The first limitation of our study is that the oral inoculation experiment involved only 2 macaques and tissues collected at 6 years postinoculation, before disease onset. Consequently, subsequent progression of prion disease symptoms remains speculative. A larger sample size and extended observation periods are required to conclusively establish infection in orally inoculated macaques. Furthermore, we performed no bioassays for PMCA-positive samples, leaving the relationship between PMCA results and infectious titers undefined. Considering that PrPres amplifications from tissues from the orally inoculated macaque tissues required 2 rounds of PMCA, the PrP^{Sc} levels in positive tissues might have been extremely low and undetectable in the bioassay.

Previous studies have demonstrated that L-BSE can be orally transmitted to cattle (*7*) and might have caused prion disease in farm-raised minks (*6*), indicating that L-BSE could naturally affect various animal species. Our findings suggest that L-BSE can also be orally transmitted to macaques. Therefore, current control measures aimed at preventing primary C-BSE in cattle and humans may also need to consider the potential risk of spontaneous L-BSE transmission.

This study was supported by the Health Labor Sciences Research Grant (H29-Shokuhin-Ippan-004, 20KA1003, and 23KA1004).

About the Author

Dr. Imamura is an associate professor in the Division of Microbiology, Department of Infectious Diseases, Faculty of Medicine, University of Miyazaki, Miyazaki, Japan. His research interests are focused on elucidating the mechanisms underlying prion formation.

References

1. Will RG, Ironside JW, Zeidler M, Cousens SN, Estibeiro K, Alperovitch A, et al. A new variant of Creutzfeldt-Jakob disease in the UK. Lancet. 1996;347:921–5.
2. Béringue V, Herzog L, Reine F, Le Dur A, Casalone C, Vilotte JL, et al. Transmission of atypical bovine prions to mice transgenic for human prion protein. Emerg Infect Dis. 2008;14:1898–901. https://doi.org/10.3201/eid1412.080941
3. Comoy EE, Casalone C, Lescoutra-Etchegaray N, Zanusso G, Freire S, Marcé D, et al. Atypical BSE (BASE) transmitted from asymptomatic aging cattle to a primate. PLoS One. 2008;3:e3017.https://doi.org/10.1371/journal.pone.0003017
4. Ono F, Tase N, Kurosawa A, Hiyaoka A, Ohyama A, Tezuka Y, et al. Atypical L-type bovine spongiform encephalopathy (L-BSE) transmission to cynomolgus macaques, a non-human primate. Jpn J Infect Dis. 2011;64:81–4. https://doi.org/10.7883/yoken.64.81
5. Mestre-Francés N, Nicot S, Rouland S, Biacabe AG, Quadrio I, Perret-Liaudet A, et al. Oral transmission of L-type bovine spongiform encephalopathy in primate model. Emerg Infect Dis. 2012;18:142–5. https://doi.org/10.3201/eid1801.111092
6. Baron T, Bencsik A, Biacabe AG, Morignat E, Bessen RA. Phenotypic similarity of transmissible mink encephalopathy in cattle and L-type bovine spongiform encephalopathy in a mouse model. Emerg Infect Dis. 2007;13:1887–94. https://doi.org/10.3201/eid1312.070635
7. Okada H, Iwamaru Y, Imamura M, Miyazawa K, Matsuura Y, Masujin K, et al. Oral transmission of L-type bovine spongiform encephalopathy agent among cattle. Emerg Infect Dis. 2017;23:284–7.https://doi.org/10.3201/eid2302.161416
8. Castilla J, Morales R, Saá P, Barria M, Gambetti P, Soto C. Cell-free propagation of prion strains. EMBO J. 2008;27:2557–66. https://doi.org/10.1038/emboj.2008.181
9. Murayama Y, Ono F, Shimozaki N, Shibata H. L-Arginine ethylester enhances in vitro amplification of PrP(Sc) in macaques with atypical L-type bovine spongiform encephalopathy and enables presymptomatic detection of PrP(Sc) in the bodily fluids. Biochem Biophys Res Commun. 2016;470:563–8. https://doi.org/10.1016/j.bbrc.2016.01.105
10. Murayama Y, Yoshioka M, Masujin K, Okada H, Iwamaru Y, Imamura M, et al. Sulfated dextrans enhance in vitro amplification of bovine spongiform encephalopathy PrP(Sc) and enable ultrasensitive detection of bovine PrP(Sc). PLoS One. 2010;5:e13152. https://doi.org/10.1371/journal.pone.0013152
11. Kratzel C, Krüger D, Beekes M. Relevance of the regional lymph node in scrapie pathogenesis after peripheral infection of hamsters. BMC Vet Res. 2007;3:22. https://doi.org/10.1186/1746-6148-3-22
12. Hilton DA, Ghani AC, Conyers L, Edwards P, McCardle L, Ritchie D, et al. Prevalence of lymphoreticular prion protein accumulation in UK tissue samples. J Pathol. 2004;203:733–9. https://doi.org/10.1002/path.1580
13. Herzog C, Rivière J, Lescoutra-Etchegaray N, Charbonnier A, Leblanc V, Salès N, et al. PrPTSE distribution in a primate model of variant, sporadic, and iatrogenic Creutzfeldt-Jakob disease. J Virol. 2005;79:14339–45.https://doi.org/10.1128/JVI.79.22.14339-14345.2005
14. Béringue V, Andréoletti O, Le Dur A, Essalmani R, Vilotte JL, Lacroux C, et al. A bovine prion acquires an epidemic bovine spongiform encephalopathy strain-like phenotype on interspecies transmission. J Neurosci. 2007;27:6965–71. https://doi.org/10.1523/JNEUROSCI.0693-07.2007
15. Baron T, Bencsik A, Morignat E. Prions of ruminants show distinct splenotropisms in an ovine transgenic mouse model. PLoS One. 2010;5:e10310. https://doi.org/10.1371/journal.pone.0010310

Address for correspondence: Morikazu Imamura, Division of Microbiology, Department of Infectious Diseases, Faculty of Medicine, University of Miyazaki, 5200 Kihara, Kiyotake, Miyazaki 889-1692, Japan; email: moirkazu_imamura@med.miyazaki-u.ac.jp

Tropheryma whipplei Infections, Mexico, 2019–2021

Jesús Delgado-de la Mora,[1] Peter Grube-Pagola,[1] Christopher D. Paddock, Marlene DeLeon-Carnes, Alvaro C. Laga, Isaac H. Solomon, José María Remes-Troche, Jesús Javier Baquera-Heredia, Gabriel Quintero-Bustos, Juan Carlos León-Contreras, Arturo Ángeles-Ángeles, Braulio Martínez-Benítez

Whipple's disease is rarely diagnosed in Latin America. We describe 2 patients with *Tropheryma whipplei* infection diagnosed in Mexico during 2019–2021. Diagnoses were confirmed by histopathology, electron microscopy, immunohistochemistry, and DNA amplification and sequencing analysis of the 16S rRNA gene. Clinicians should be aware of *T. whipplei* infection and associated syndromes.

Whipple's disease (WD) is an unusual infection with protean manifestations caused by *Tropheryma whipplei*, a fastidious, slow-growing, gram-positive bacterium. Classical WD was originally described in 1907 and is characterized by polyarthritis, diarrhea, and lymphadenopathy (*1*). WD is a rare disease with a prevalence of 9.8 cases/1 million inhabitants in the United States and is most frequently identified in White men >50 years of age (*2*). WD has also been described among patients with various immunosuppressive conditions, including persons with HIV infection (*3*,*4*).

In the appropriate clinical context, WD is suspected when abundant foamy macrophages containing abundant periodic acid–Schiff stain (PAS)–positive and diastase-resistant granules are found in the lamina propria of small bowel biopsy specimens (*5*). However, WD can also be documented as a localized disease in cases of endocarditis, uveitis, isolated lymphadenopathy, encephalitis, or arthritis and negative cultures (*5*).

Classic WD has been reported extensively in western Europe, Canada, and in the United States (*6*). The disease has been described only rarely in countries in Latin America, including a probable case in Mexico (*7*–*10*). The paucity of descriptions of WD from those countries could relate to underrecognition, limited access to confirmatory diagnostic assays, or genetic characteristics of the predominant population in healthcare settings. We report 2 patients with classic WD from the states of Veracruz and Mexico City in Mexico.

The Study

The first patient was a previously healthy 63-year-old man whose signs and symptoms began 2 years earlier and included cough, pneumonia, intermittent diarrhea, and weight loss of 42 kg. Results of serologic tests for celiac disease and stool bacterial cultures and ova and parasite exams were all negative. An echocardiogram revealed moderate aortic valve insufficiency and stenosis, along with severe mitral valve insufficiency, a dilated left ventricle, and mild pulmonary arterial hypertension. Small bowel endoscopy revealed multiple white nodules in the duodenum and ileum. Small bowel biopsies revealed abundant macrophages with foamy, pale, blue-gray cytoplasm in the lamina propria (Figure 1, panel A), which contained numerous globular and falciform inclusions that were strongly PAS-positive and diastase-resistant (Figure 1, panel B). Immunohistochemistry results for *T. whipplei* (*8*) were positive (Figure 1, panel C), and the PCR for gram-positive–specific 16S rRNA V8/V9 gene (*11*) produced

Author affiliations: Weill-Cornell Medicine, New York, New York, USA (J. Delgado-de la Mora); Instituto de Investigaciones Médico Biológicas de la Universidad Veracruzana, Veracruz, Mexico (P. Grube-Pagola, J.M. Remes-Troche); Centers for Disease Control and Prevention, Atlanta, Georgia, USA (C.D. Paddock, M. DeLeon-Carnes); Brigham and Women's Hospital, Boston, Massachusetts, USA (A.C. Laga, I.H. Solomon); Centro Médico ABC, Mexico City, Mexico (J.J. Baquera-Heredia); Laboratorio Flemming, Morelos, Mexico (G. Quintero-Bustos); Instituto Nacional de Ciencias Médicas y Nutrición Salvador Zubirán, Mexico City (J.C. León-Contreras, A. Ángeles-Ángeles, B. Martínez-Benítez).

DOI: https://doi.org/10.3201/eid3105.241046

[1]These authors contributed equally to this article.

a target 350-bp amplicon. After Sanger sequencing, *Tropheryma* spp. was identified through BLAST search (https://blast.ncbi.nlm.nih.gov). The patient initially received ceftriaxone, then received combination doxycycline and hydroxychloroquine therapy. One year after diagnosis, he had another round of duodenum and ileum biopsies, which revealed persistence of macrophages with PAS-positive inclusions; no additional studies were done. Combination therapy with doxycycline and hydroxychloroquine was reinitiated and, 2 years after those biopsies, the patient remained asymptomatic. No further endoscopic procedures were conducted.

The second patient was a 45-year-old man with well-controlled HIV infection. He was receiving raltegravir, darunavir, etravirine, and ritonavir, and his

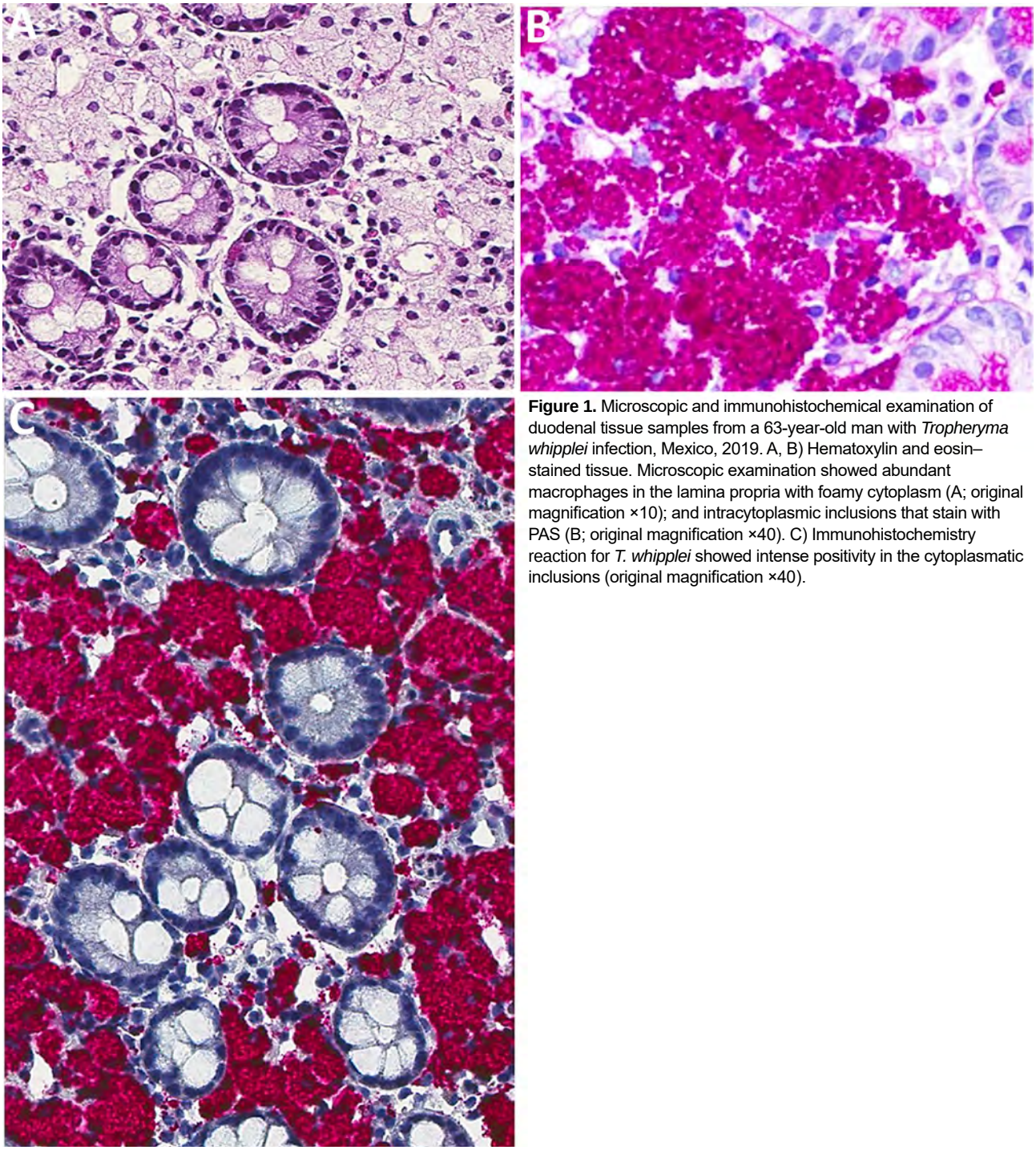

Figure 1. Microscopic and immunohistochemical examination of duodenal tissue samples from a 63-year-old man with *Tropheryma whipplei* infection, Mexico, 2019. A, B) Hematoxylin and eosin–stained tissue. Microscopic examination showed abundant macrophages in the lamina propria with foamy cytoplasm (A; original magnification ×10); and intracytoplasmic inclusions that stain with PAS (B; original magnification ×40). C) Immunohistochemistry reaction for *T. whipplei* showed intense positivity in the cytoplasmatic inclusions (original magnification ×40).

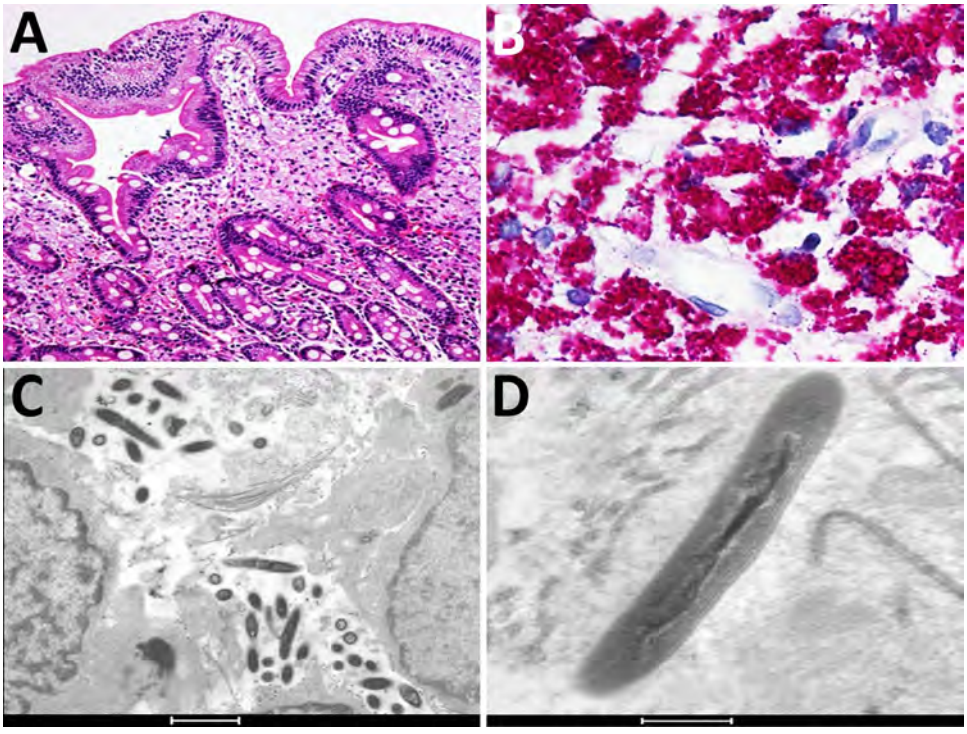

Figure 2. Microscopic and immunohistochemical examination of tissue samples from the ileum in a a 45-year-old man with *Tropheryma whipplei* infection, Mexico, 2021. A, B) Hematoxylin and eosin–stained ileum tissue. Microscopic examination showed abundant macrophages in the lamina propria with foamy cytoplasm (A; original magnification ×4); and intracytoplasmic inclusions that were intensely PAS-positive (B; original magnification ×40). C, D) Electron microscopy showing rod-shaped *T. whipplei* in the lamina propria of ileum (C; scale bar = 1 μm), and trilaminar plasma membranes in macrophages (D; scale bar = 200 nm).

viral load was undetectable. His CD4 count was 439 cells/mm^3. He had a history of 3 months of watery diarrhea. He received ciprofloxacin for 7 days and temporarily improved; however, his diarrhea soon returned after cessation of antibiotic therapy, and then he experienced a 4- kg weight loss. Endoscopy revealed multiple white nodular areas in the mucosa of the duodenum and ileum. Biopsy specimens from both sites revealed expansion of the lamina propria by foamy macrophages with PAS-positive, diastase-resistant inclusions (Figure 2, panels A, B). Electron microscopy performed on formalin-fixed, paraffin-embedded tissue from the small bowel (duodenum and ileum) identified intracellular and extracellular bacilli with a trilaminar plasma membrane (Figure 2, panels C, D). Molecular identification by 16S rRNA V1/V2 sequencing was performed by the Center for Advanced Molecular Diagnostics at the Brigham and Women's Hospital (Boston, MA, USA), as previously described (*12*). A 321-bp contig was assembled and fed into the 16S RipSeq Single database (Pathogenomix, https://www.pathogenomix.com) and matched to *T. whipplei* (GenBank accession no. AF190688). We initiated doxycycline and hydroxychloroquine therapy, and his signs and symptoms resolved.

Conclusions

We document 2 cases of WD in 2 states in Mexico. Both patients were born and raised in the country, had small bowel biopsies histologically compatible with WD, and had *T. whipplei* infection confirmed by immunohistochemical staining and molecular diagnostics.

Identification of *T. whipplei* has epidemiologic implications because of its potential for transmission between humans through saliva or feces (*5*). In addition, from a therapeutic perspective, WD generally has excellent response to antibiotic regimens; however, if such regimens are not provided, WD can result in life-threatening complications (*13*). Because classic WD frequently involves joints, it can be misdiagnosed as autoimmune rheumatologic disease, resulting in immunosuppressive therapies that paradoxically can accelerate the course of WD (*14*).

In conclusion, our findings highlight the need for more specific and widely available diagnostic tests for *T. whipplei* in Mexico and across Latin America, particularly molecular diagnostic assays, to enable characterization of *T. whipplei* in the region. Clinicians should consider *T. whipplei* infection in the differential diagnosis of patients with debilitating, otherwise unexplained, yet treatable conditions such as malabsorption syndromes and localized disease, including culture-negative endocarditis, encephalitis, uveitis, lymphadenopathies, and inflammatory spondyloarthropathies (*5*,*15*).

We dedicate this article to the memory of our beloved friend and colleague, Braulio Martínez-Benítez.

About the Author

Dr. Delgado-de la Mora is a gastrointestinal pathologist currently working as a research assistant at Weill-Cornell Medicine, New York City. His research interests include emerging infectious diseases and viral oncogenesis.

References

1. Whipple GH. A hitherto undescribed disease characterized anatomically by deposits of fat and fatty acids in the intestinal and mesenteric lymphatic tissues. Bull Johns Hopkins Hosp. 1907;18:382–93.
2. Elchert JA, Mansoor E, Abou-Saleh M, Cooper GS. Epidemiology of Whipple's disease in the USA between 2012 and 2017: a population-based national study. Dig Dis Sci. 2019;64:1305–11. https://doi.org/10.1007/s10620-018-5393-9
3. Lozupone C, Cota-Gomez A, Palmer BE, Linderman DJ, Charlson ES, Sodergren E, et al.; Lung HIV Microbiome Project. Widespread colonization of the lung by *Tropheryma whipplei* in HIV infection. Am J Respir Crit Care Med. 2013; 187:1110–7. https://doi.org/10.1164/rccm.201211-2145OC
4. Guérin A, Kerner G, Marr N, Markle JG, Fenollar F, Wong N, et al. IRF4 haploinsufficiency in a family with Whipple's disease. eLife. 2018;7:e32340. https://doi.org/10.7554/eLife.32340
5. Paddock CD, Fenollar F, Lagier JC, Raoult DA. 21st Century appraisal of Whipple's disease and *Tropheryma whipplei*. Clin Microbiol Newsl. 2022;44:123–29. https://doi.org/10.1016/j.clinmicnews.2022.07.001
6. Dolmans RA, Boel CH, Lacle MM, Kusters JG. Clinical manifestations, treatment, and diagnosis of *Tropheryma whipplei* infections. Clin Microbiol Rev. 2017;30:529–55. https://doi.org/10.1128/CMR.00033-16
7. Vega-López CA, Carrillo-Ocampo JL, Castillo-García J, González-de la Mora JJ, Alemán-Ortiz G, Romo-Aguirre C. Whipple's disease: a case report and review of the literature [in Spanish]. Rev Gastroenterol Mex. 2010;75:517–21.
8. Renon VP, Appel-da-Silva MC, D'Incao RB, Lul RM, Kirschnick LS, Galperim B. Whipple's disease: rare disorder and late diagnosis. Rev Inst Med Trop São Paulo. 2012;54:293–7. https://doi.org/10.1590/S0036-46652012000500010
9. Rollin DC, Paddock CD, Pritt BS, Cunningham SA, Denison AM. Genotypic analysis of *Tropheryma whipplei* from patients with Whipple disease in the Americas. J Clin Pathol. 2017;70:891–5. https://doi.org/10.1136/jclinpath-2017-204382
10. Rey R M, Orozco LA, Marrugo K, López R, Pérez-Riveros ED, De la Hoz-Valle J, et al. Whipple disease diagnosed by enteroscopy: first case report in Colombia of an underdiagnosed disease and literature review. BMC Gastroenterol. 2020;20:197. https://doi.org/10.1186/s12876-020-01302-2
11. Klausegger A, Hell M, Berger A, Zinober K, Baier S, Jones N, et al. Gram type-specific broad-range PCR amplification for rapid detection of 62 pathogenic bacteria. J Clin Microbiol. 1999;37:464–6. https://doi.org/10.1128/JCM.37.2.464-466.1999
12. Solomon IH, Lin C, Horback KL, Kanjilal S, Rojas-Rudilla V, Brigl M, et al. Utility of histologic and histochemical screening for 16S ribosomal RNA gene sequencing of formalin-fixed, paraffin-embedded tissue for bacterial endocarditis. Am J Clin Pathol. 2019;152:431–7. https://doi.org/10.1093/ajcp/aqz055
13. Moos V, Schneider T. Changing paradigms in Whipple's disease and infection with *Tropheryma whipplei*. Eur J Clin Microbiol Infect Dis. 2011;30:1151–8. https://doi.org/10.1007/s10096-011-1209-y
14. Lagier JC, Lepidi H, Raoult D, Fenollar F. Systemic *Tropheryma whipplei*: clinical presentation of 142 patients with infections diagnosed or confirmed in a reference center. Medicine (Baltimore). 2010;89:337–45. https://doi.org/10.1097/MD.0b013e3181f204a8
15. Fenollar F, Lagier JC, Raoult D. *Tropheryma whipplei* and Whipple's disease. J Infect. 2014;69:103–12. https://doi.org/10.1016/j.jinf.2014.05.008

Address for correspondence: Jesus Delgado-de la Mora, Weill Cornell Medicine Ringgold Standard Institution, Department of Pathology and Laboratory Medicine, 1300 York Ave, New York, NY 10065, USA; email: jdelgadom1992@gmail.com

Venezuelan Equine Encephalitis, Peruvian Amazon, 2020

Marta Piche-Ovares, Maria Paquita García Mendoza, Andres Moreira-Soto, Carlo Fischer, Sebastian Brünink, Maribel Dana Figueroa-Romero, Nancy Susy Merino-Sarmiento, Adolfo Ismael Marcelo-Ñique, Edward Málaga-Trillo, Miladi Gatty-Nogueira, César Augusto Cabezas Sanchez, Jan Felix Drexler

We screened 1,972 febrile patients from the Peruvian Amazon in 2020–2021 for Venezuelan equine encephalitis virus (VEEV). Neutralizing antibody detection rate was 3.9%; 2 patients were PCR positive. Genome identity compared to Peru VEEV subtype ID strains was 97.6%–98.1%. Evidence for purifying selection and ancestry ≈54 years ago corroborated VEEV endemicity.

The Venezuelan equine encephalitis antigenic complex of alphaviruses encompasses 6 subtypes (I–VI), originally designated according to antigenic properties (*1*); those 6 subtypes are further divided into antigenic varieties. Venezuelan equine encephalitis virus (VEEV) consists of 4 varieties (AB, C, D, and E); subtype ID is enzootic in Central and South America (*2*). The VEEV ID transmission cycle involves mosquitoes of the genus *Culex* (subgenus *Melanoconion*); however, knowledge of vertebrate sylvatic hosts is scarce (*3*). A prior study from the Peruvian Amazon conducted in 2001–2007 using molecular and serologic techniques indicated that up to 7% of febrile cases are potentially caused by VEEV, making it one of the most relevant arthropodborne viruses regionally (*4*).

VEEV has been detected continuously in humans in the Peruvian Amazon since 1993 (*4*,*5*). In 2006, a reported outbreak of VEEV resulted in a 5-fold increase in cases (63 cases) compared with previous years (10–14 cases/year) and 2 human deaths (*6*,*7*). All samples sequenced in the 2006 outbreak belonged to subtype ID (*8*). Since 2013, no data have become available on VEEV from Peru, so it is possible that the epidemiology of VEEV might have changed. We thus investigated VEEV in the Peruvian Amazon during 2020–2021 by using molecular, serologic, and bioinformatic methods.

The Study

We screened 1,972 serum samples from febrile humans sampled in the Peruvian Amazon as part of routine acute febrile illness surveillance in 2020–2021 during overlapping dengue virus and SARS-CoV-2 outbreaks (*9*). We tested samples for alphavirus RNA by a genuswide, nested reverse transcription PCR (RT-PCR) (*10*). Two serum samples (0.1%, 95% CI 0.001%–0.4%) tested positive for the presence of VEEV RNA. We obtained the first sample (Peru_2020) from a 74-year-old man from the district of Nauta in February 2020 (Figure 1). The patient sought treatment for headache, fever, muscle pain, and respiratory symptoms 4 days before sampling. The patient's viral load was 8.1×10^5 copies/mL, as determined by a strain-specific real-time RT-PCR (*6*), consistent with the time elapsed since the onset of symptoms. We obtained the second sample (Peru_2021) from a 12-year-old girl in January 2021. Her viral load was 1.2×10^3 copies/mL, but no additional information was available. Isolation of both samples on Vero cells enabled the viral genomes to be characterized by high-throughput sequencing (Illumina, https://www.illumina.com) (Appendix, https://wwwnc.cdc.gov/EID/article/31/5/24-1694-App1.pdf).

In a Bayesian whole genome–based phylogeny, the 2 newly generated sequences (GenBank accession

Author affiliations: Charité Universitätsmedizin Berlin, Berlin, Germany (M. Piche-Ovares, A. Moreira-Soto, C. Fischer, S. Brünink, J.F. Drexler); Instituto Nacional de Salud, Lima, Peru (M.P. García Mendoza, M.D. Figueroa-Romero, N.S. Merino-Sarmiento, A.I. Marcelo-Ñique, C.A. Cabezas Sanchez); Universidad Nacional de Costa Rica, Heredia, Costa Rica (A. Moreira-Soto); Universidad Peruana Cayetano Heredia, Lima (E. Málaga-Trillo); Laboratorio de Refencia Regional en Salud Publica, Loreto, Peru (M. Gatty-Nogueira); German Centre for Infection Research, associated partner Charité-Universitätsmedizin Berlin, Berlin (J.F. Drexler)

DOI: http://doi.org/10.3201/eid3105.241694

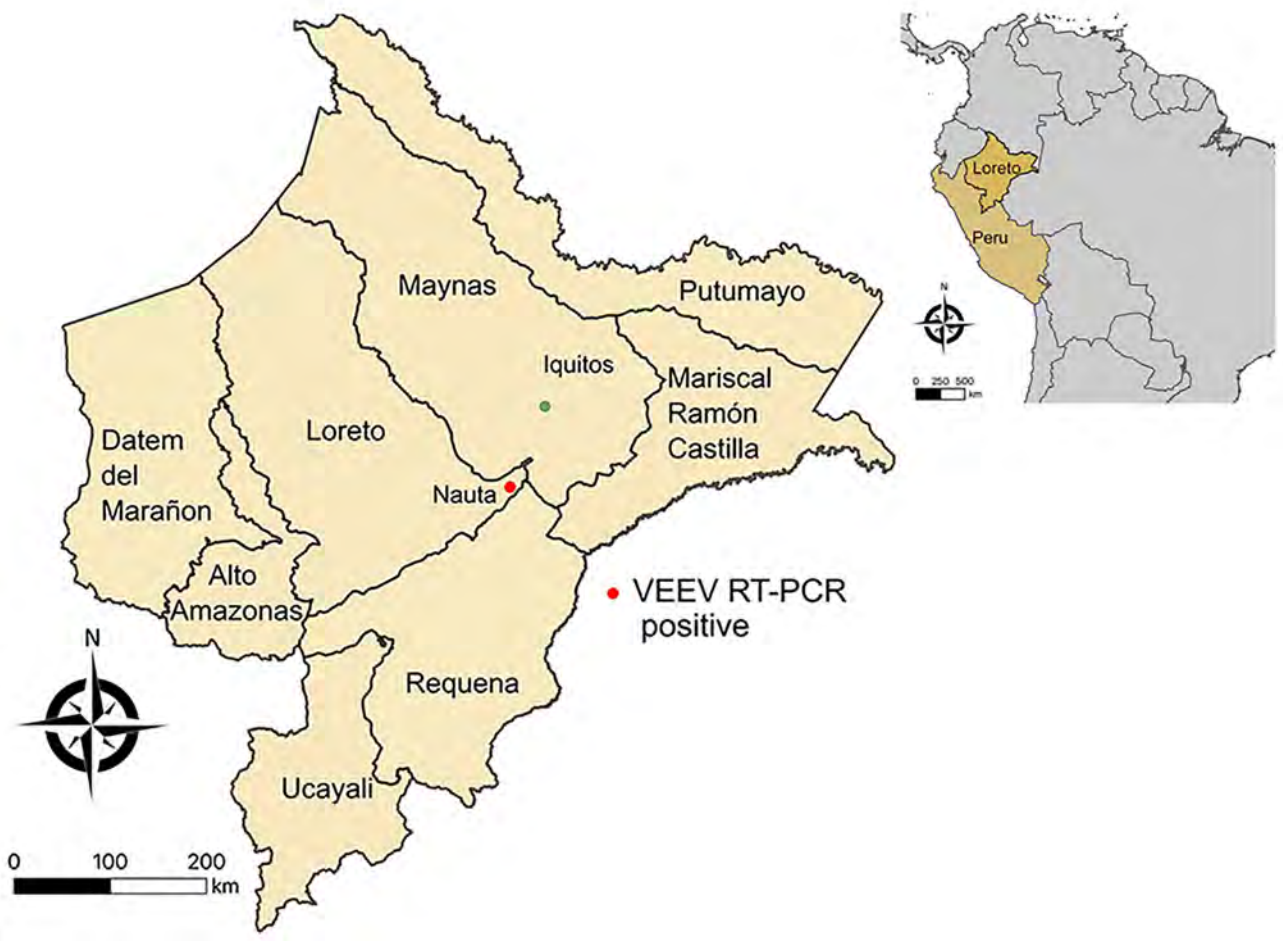

Figure 1. Geographic location of Venezuelan equine encephalitis virus–positive case from study of Venezuelan equine encephalitis, Peruvian Amazon, 2020. Red dot shows location of case for which metadata were available; green dot represents Iquitos, capital of the department of Loreto. Inset map shows location of Peru in South America and of Loreto department. All maps were created using QGIS 3.36.0 based on freely available maps from Bucknell University (https://hub.arcgis.com) and Instituto Nacional de Estadística e Informática, Peru (https://ide.inei.gob.pe/#capas).

nos. PP700505 and PQ513527) clustered with the ID subtype (Figure 2, panel A). We also observed clustering within ID in phylogenies based on all publicly available envelope glycoprotein precursor genomic sequences of the ID Panama/Peru lineage (Figure 2, panel B). Sequence comparisons indicated that both VEEV strains from our study were closely related (sequence identity 97.6%–98.1%) to other Peruvian strains belonging to the ID lineage but not were monophyletic, highlighting the cocirculation of different strains and suggesting maintenance of that VEEV clade in the region. We estimated the time to most recent common ancestor at ≈54 years ago (95% highest posterior density 38–66 years ago) (Figure 2, panel C) and noted evidence for purifying selection that suggested a regionally stable VEEV transmission cycle (*11*) (Appendix).

To determine past VEEV infections in Peru's Loreto department, we selected a subset of 463 samples collected during January–April 2020 and September 2020–January 2021, corresponding to rainy seasons, when vector presence is highest and transmission is most likely. Samples were also selected to be negative for dengue virus by RT-PCR and of sufficient volume to enable serologic testing. We tested serum samples first by plaque reduction neutralization test (PRNT) in a 96-well plate format at 1:40 serum dilution to neutralize ≈50% ($PRNT_{50}$) of the plaque-forming units of a VEEV isolate from this study. We retested positive samples (53/463) by $PRNT_{50}$ in a 12-well plate format, which enables better count of plaque-forming units, in 2-fold dilutions ranging from 1:40 to 1:320 (Appendix). The titration showed that 18 of the 463 samples (3.9%, 95% CI 2.4%–6.1%) robustly demonstrated neutralizing antibodies (Table 1). Of note, a 2006 study reported a VEEV seroprevalence of 23%, which differed from our results for unknown reasons, potentially including

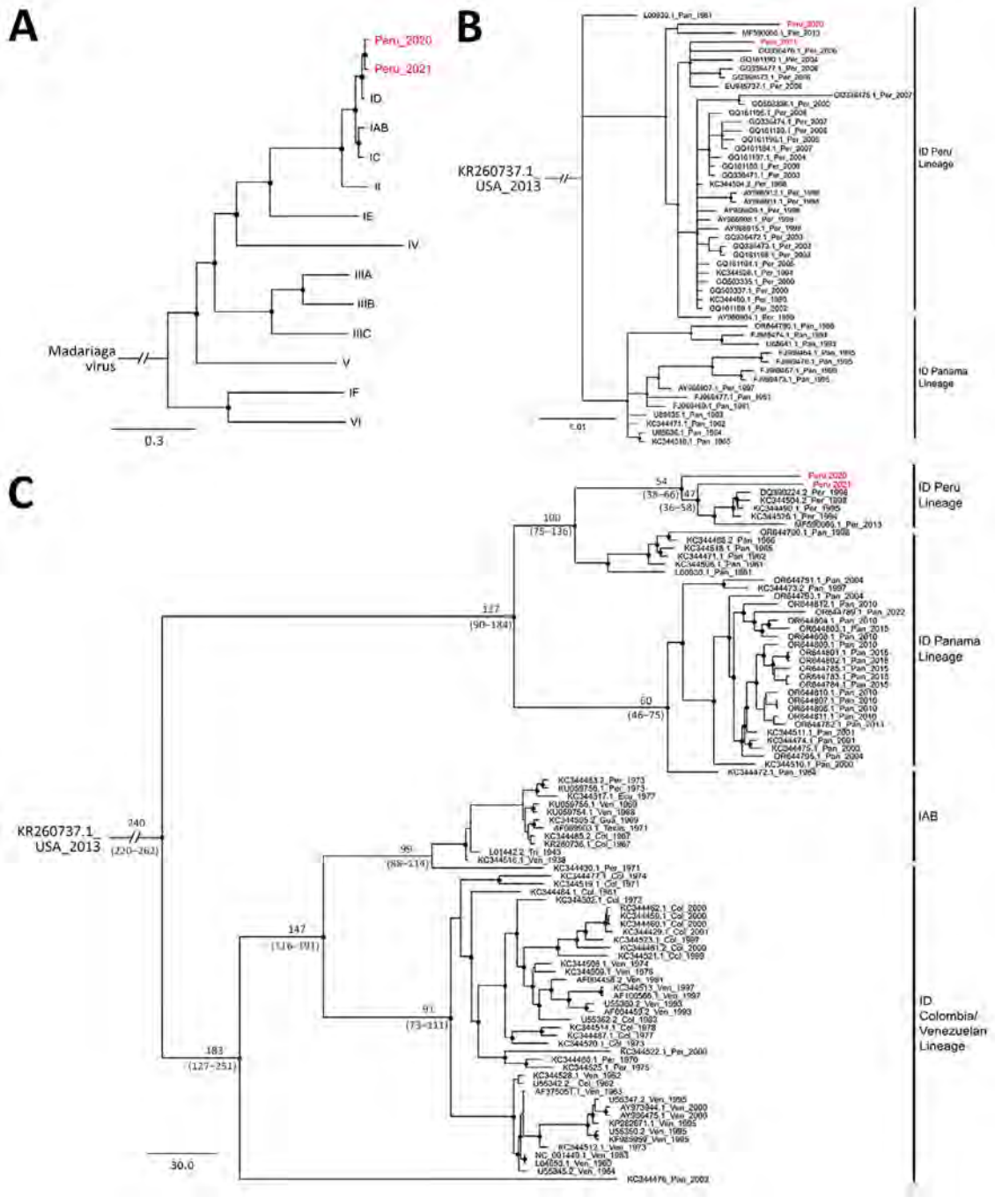

Figure 2. Phylogenetic relationships of Venezuelan equine encephalitis virus (VEEV) from study of Venezuelan equine encephalitis, Peruvian Amazon, 2020. A) Relationships of VEEV from Peru (Peru 2020 and Peru 2021, depicted in red) and members of the Venezuelan equine encephalitis antigenic complex, based on the concatenated coding sequence (11,629 nt). Madariaga virus was included as an outgroup. B) Phylogenetic relationships of Peru 2020 and Peru 2021 (shown in red) and members of VEEV subtype ID Panama/Peru lineage, based on a partial sequence of the envelope glycoprotein precursor (PE2, 817 nt). Phylogenetic trees were constructed using MrBayes 3.2.6 (https://github.com/NBISweden/MrBayes/releases/tag/v3.2.6). GenBank accession number, country, and collection year are indicated for each sequence. Posterior probability ≥0.80 is indicated as a black circle in the node. C) Time to most recent common ancestor of VEEV identified in this study (Peru 2020 and Peru 2021, shown in red) and members of the ID and IAB subtypes, by number of years ago, calculated using BEAST 1.7.1 (https://beast.community), based on the concatenated coding sequence (11,629 nt). Tip dates were obtained from the sampling year following a previous phylogenetic analysis of VEEV subtype ID and IAB; no further calibration of node ages was performed to construct the tree. Times are identified at each branch by number of years ago; numbers in parentheses indicate 95% highest posterior density values in years (*11*). Col, Colombia; Ecu, Ecuador; Gua, Guatemala; Pan, Panama; Per, Peru; Ven, Venezuela.

Table 1. Alphavirus serologic reactivity patterns in VEEV IgG-positive serum samples from Loreto, Peru, in study of Venezuelan equine encephalitis, Peruvian Amazon, 2020*

Sample	VEEV $PRNT_{50}$ titer	IgG indirect immunofluorescent assay result									
		CHIKV	ONNV	RRV	BFV	SINV	WEEV	EEEV	VEEV	CHIKV vlp	MAYV vlp
3216	>1:320	+	+	+	–	–	+	–	+	+	+
3270	1:40	+	+	+	+	+	+	+	+	+	+
3393	1:40	–	–	–	–	–	–	–	+	–	–
3399	1:160	–	–	–	–	–	–	–	+	–	–
3624	1:40	–	–	–	–	–	–	–	+	–	–
3634	1:40	+	+	+	–	–	+	–	+	+	+
3876	1:40	–	–	–	–	–	–	–	+	–	–
3927	1:80	–	–	–	–	–	–	–	+	–	–
3940	1:40	–	–	–	–	–	–	–	+	–	–
4140	>1:320	+	–	+	–	–	+	–	+	–	–
4294	1:160	+	+	+	–	–	–	–	+	+	+
4321	1:80	+	–	+	–	–	+	+	+	–	–
4420	1:80	–	–	–	–	–	–	–	+	–	+
4590	1:40	–	–	–	–	–	–	–	+	–	–
4669	1:80	–	–	–	–	–	–	–	+	–	–
4747	1:160	–	–	–	–	–	–	–	+	–	–
4768	1:40	+	–	–	–	–	–	–	+	+	+
4797	1:160	+	–	–	–	–	+	–	+	–	+

*Bold indicates monotypic reactions. BFV, Barmah Forest virus; CHIKV, chikungunya virus; EEEV, Eastern equine encephalitis virus; MAYV, Mayaro virus; ONNV, o'nyong-nyong virus; $PRNT_{50}$, plaque reduction neutralization test with ≥50% plaque reduction considered positive; RRV, Ross River virus; SINV, Sindbis virus; VEEV, Venezuelan equine encephalitis virus; vlp, virus-like particle; WEEV, Western equine encephalitis virus.

sampling focused on urban areas and the VEEV outbreak reported during that year (*7*).

Considering the potential for cross-reaction with other alphaviruses, we tested $PRNT_{50}$–positive samples by using a commercially available indirect immunofluorescent assay (IFA) (EUROIMMUN, https://www.euroimmun.com). The assay was based on cells infected with VEEV along with chikungunya, o'nyong-nyong, Ross River, Western equine encephalitis, Sindbis, Barmah Forest, and Eastern equine encephalitis viruses, as well as virus-like particles for Mayaro and chikungunya viruses (Appendix). Serum samples were tested at 1:100 for IgG and at 1:10 for IgM, which is the serum dilution recommended by the manufacturer. All $PRNT_{50}$–positive serum samples tested positive for VEEV in the IgG IFA, and we observed monotypic VEEV reactivity in 9 of 18 samples (50%, 95% CI 29.0%–71%) (Appendix Figure 1). All other samples reacted with ≥2 viruses, results expected in tropical areas where several alphaviruses cocirculate (*12*). Cross-reactivity might have affected IFA patterns, since reactivity was observed with viruses not previously reported in Latin America, such as o'nyong-nyong, Ross River, Sindbis, and Barmah Forest viruses (*13*) (Table 1). Reactivity patterns suggested a predominance of Mayaro (n = 7) over chikungunya (n = 5) virus and of Western equine encephalitis (n = 6) over Eastern equine encephalitis (n = 2) virus, highlighting the relevance of targeting Mayaro and Western equine encephalitis virus in regional diagnostic testing and targeted epidemiologic studies.

IgG detection rates did not vary significantly by sex (p = 1.0 by Fisher exact test) but were higher in adults ≥30 years of age (p = 0.0001 by Fisher exact test), potentially a consequence of the 2006 VEEV outbreak (Table 2) (*7*). Adapting the IFA for IgM yielded entirely negative results, which is consistent with low levels of VEEV-specific IgM in the serum of acutely infected patients (*14*) and predominant detection of nonrecent infections in this study (Appendix Figure 2).

Table 2. Seropositive patients and demographic variables from study of Venezuelan equine encephalitis, Peruvian Amazon, 2020*

Category	VEEV IgG IFA positive, no. (%)	Total no. (%)
Sex†		
F	9 (3.9)	234 (50.4)
M	9 (4.0)	229 (49.5)
Age, y‡		
<15	0 (0.0)	202 (43.6)
15–29	4 (3.3)	121 (26.1)
30–44	7 (9.9)	71 (15.3)
≥45	7 (10.1)	69 (14.9)

*Statistical analyses were performed using R version 2024.04.2 (The R Project for Statistical Computing, https://www.r-project.org). VEEV, Venezuelan equine encephalitis virus.
†p = 1.0 by Fisher exact test.
‡Compared in 2 age groups: 0–29 and ≥30 years; p = 0.0001 by Fisher exact test.

Conclusion

Despite evidence for the medical relevance of VEEV ID in the Peruvian Amazon from a prior study (*5*) and our study, the diagnosis of VEEV is not included in the routine arbovirus surveillance panel of Peru (N°125-MINSA/2016/CDC-INS). Our study demonstrates that the lack of surveillance and diagnosis is making the infection go unnoticed.

In tropical regions, factors such as the proximity of the rainforest to urban areas, agricultural activities, and deforestation may increase the likelihood of

human contact with vectors, leading to virus transmission (*14*). These factors are of particular significance in the Peruvian Amazon, where ≤96.7% of households engage in activities related to agriculture or aquaculture (https://data-peru.itp.gob.pe). This information could explain why adults are more likely to be in contact with the virus and why nonpharmaceutical interventions to combat the spread of SARS-CoV-2 do not appear to affect the transmission of VEEV (*15*).

Beyond increased diagnostics, future research should prioritize investigating transmission cycles of different VEEV subtypes to identify populations at risk and focus on potential prevention strategies, such as targeted control of vectors and identifying potential amplifying vertebrate hosts (*1*). Arboviral surveillance, including of VEEV, should be generally strengthened with a syndromic diagnostic approach, particularly during periods of increased rainfall and harvest season, when the risk of arboviral infection may be increased (*14*).

Acknowledgments

We thank José Encinas for support.

Scientific investigation of samples collected within routine public health surveillance by the Instituto Nacional de Salud reference laboratory for viral zoonoses was approved by the institutional bioethics committees VIA LIBRE (protocol no. 6528) and Charité Universitätsmedizin Berlin (protocol no. EA2/031/22).

This work was supported by the Deutsche Gesellschaft für Internationale Zusammenarbeit GmbH (project no. 81262528) and a doctoral program scholarship (no. 91609043) from the German academic exchange service.

About the Author

Ms. Piche is a PhD student at the Institute of Virology at Charité-Universitätsmedizin, Berlin, and the Institute for the History of Medicine at Justus Liebig University of Giessen. Her research is focused on the epidemiology of arthropodborne viruses.

References

1. Weaver SC, Barrett AD. Transmission cycles, host range, evolution and emergence of arboviral disease. Nat Rev Microbiol. 2004;2:789–801. https://doi.org/10.1038/nrmicro1006
2. Aguilar PV, Estrada-Franco JG, Navarro-Lopez R, Ferro C, Haddow AD, Weaver SC. Endemic Venezuelan equine encephalitis in the Americas: hidden under the dengue umbrella. Future Virol. 2011;6:721–40. https://doi.org/10.2217/fvl.11.50
3. Aguilar PV, Greene IP, Coffey LL, Medina G, Moncayo AC, Anishchenko M, et al. Endemic Venezuelan equine encephalitis in northern Peru. Emerg Infect Dis. 2004;10:880–8. https://doi.org/10.3201/eid1005.030634
4. Forshey BM, Guevara C, Laguna-Torres VA, Cespedes M, Vargas J, Gianella A, et al.; NMRCD Febrile Surveillance Working Group. Arboviral etiologies of acute febrile illnesses in western South America, 2000-2007. PLoS Negl Trop Dis. 2010;4:e787. https://doi.org/10.1371/journal.pntd.0000787
5. Watts DM, Russell KL, Wooster MT, Sharp TW, Morrison AC, Kochel TJ, et al. Etiologies of acute undifferentiated febrile illnesses in and near Iquitos from 1993 to 1999 in the Amazon River Basin of Peru. Am J Trop Med Hyg. 2022;107:1114–28. https://doi.org/10.4269/ajtmh.22-0259
6. Vilcarromero S, Aguilar PV, Halsey ES, Laguna-Torres VA, Razuri H, Perez J, et al. Venezuelan equine encephalitis and 2 human deaths, Peru. Emerg Infect Dis. 2010;16:553–6. https://doi.org/10.3201/eid1603.090970
7. Morrison AC, Forshey BM, Notyce D, Astete H, Lopez V, Rocha C, et al. Venezuelan equine encephalitis virus in Iquitos, Peru: urban transmission of a sylvatic strain. PLoS Negl Trop Dis. 2008;2:e349. https://doi.org/10.1371/journal.pntd.0000349
8. Aguilar PV, Adams AP, Suárez V, Beingolea L, Vargas J, Manock S, et al. Genetic characterization of Venezuelan equine encephalitis virus from Bolivia, Ecuador and Peru: identification of a new subtype ID lineage. PLoS Negl Trop Dis. 2009;3:e514. https://doi.org/10.1371/journal.pntd.0000514
9. Plasencia-Dueñas R, Failoc-Rojas VE, Rodriguez-Morales AJ. Impact of the COVID-19 pandemic on the incidence of dengue fever in Peru. J Med Virol. 2022;94:393–8. https://doi.org/10.1002/jmv.27298
10. Grywna K, Kupfer B, Panning M, Drexler JF, Emmerich P, Drosten C, et al. Detection of all species of the genus Alphavirus by reverse transcription-PCR with diagnostic sensitivity. J Clin Microbiol. 2010;48:3386–7. https://doi.org/10.1128/JCM.00317-10
11. Forrester NL, Wertheim JO, Dugan VG, Auguste AJ, Lin D, Adams AP, et al. Evolution and spread of Venezuelan equine encephalitis complex alphavirus in the Americas. PLoS Negl Trop Dis. 2017;11:e0005693. https://doi.org/10.1371/journal.pntd.0005693
12. Fischer C, Jo WK, Haage V, Moreira-Soto A, de Oliveira Filho EF, Drexler JF. Challenges towards serologic diagnostics of emerging arboviruses. Clin Microbiol Infect. 2021;27:1221–9. https://doi.org/10.1016/j.cmi.2021.05.047
13. Postigo-Hidalgo I, Jo WK, Pedroso C, Brites C, Drexler JF. Introduction of chikungunya virus in coastal northeast Brazil. Lancet Microbe. 2023;4:e764. https://doi.org/10.1016/S2666-5247(23)00176-3
14. Carrera JP, Forrester N, Wang E, Vittor AY, Haddow AD, López-Vergès S, et al. Eastern equine encephalitis in Latin America. N Engl J Med. 2013;369:732–44. https://doi.org/10.1056/NEJMoa1212628
15. Moreira-Soto A, Bruno A, de Mora D, Paez M, Garces J, Wulf B, et al. Virological evidence of the impact of non-pharmaceutical interventions against COVID-19 in Ecuador, a resource-limited setting. Emerg Microbes Infect. 2023;12:2259001. https://doi.org/10.1080/22221751.2023.2259001

Address for correspondence: Jan Felix Drexler, Institute of Virology, Charitéplatz 1, 10117 Berlin, Germany; email: felix.drexler@charite.de

Rapid Transmission and Divergence of Vancomycin-Resistant *Enterococcus faecium* Sequence Type 80, China

Liqiang Li,[1] Xingwei Wang,[1] Yanyu Xiao, Bing Fan, Jiehong Wei, Jie Zhou, Zetian Lai, Yanpeng Zhang, Hongmei Mo, Li Zhang, Dixian Luo, Dayong Gu, Shucai Yang, Yidi Wang, Jiuxin Qu; Shenzhen Pathogen Infection Research Alliance (SPIRA)

We investigated genomic evolution of vancomycin-resistant *Enterococcus faecium* (VREF) during an outbreak in Shenzhen, China. Whole-genome sequencing revealed 2 sequence type 80 VREF subpopulations diverging through insertion sequence–mediated recombination. One subpopulation acquired more antimicrobial resistance and carbohydrate metabolism genes. Persistent VREF transmission underscores the need for genomic surveillance to curb spread.

Vancomycin-resistant *Enterococcus faecium* (VREF) causes hospital-acquired infections worldwide and poses a threat to public health (*1*). Whole-genome sequencing (WGS) has demonstrated that new healthcare-associated *E. faecium* clones rapidly emerge, evolve, and adapt through intragenus recombination, displacing existing clones (*2*,*3*).

During the past decade, clonal complex 17 sequence type (ST) 80 rapidly became the predominant VREF lineage in Denmark (*4*), Australia (*5*), Ireland (*6*), Spain (*7*), and Sweden (*8*) and accounted for 40%–67.1% of VREF isolates disseminated in hospital settings. Few ST80 cases were reported in Asia countries, including China, until an independent lineage of ST80, sequence cluster (SC)11, emerged in January 2021 as the predominant cause of an ongoing VREF outbreak in Guangdong Province (*9*) and posed a risk of spreading to other areas. However, the pangenomic features and adaptation potential of the emerging SC11 remain unknown.

VREF isolation rates also substantially increased in the metropolitan city of Shenzhen, Guangdong Province, China, during 2021–2024. VREF isolation rates before 2021 remained <6% (predominantly ≤5%) but rose to an average of 11.53% in 2024 (Appendix 1 Figure 1, panel A, https://wwwnc.cdc.gov/EID/article/31/5/24-1649-App1.pdf). To trace the source and characterize genomic features that potentially contributed to outbreaks, we conducted a multicenter genomic epidemiology study and integrated pangenomic variation analysis.

The Study

We performed WGS analysis (Appendix 1) on 42 VREF isolates (primarily collected after April 2022) from 39 patients across 7 hospitals, designated SZ_A through SZ_F, including 2 affiliated hospitals, SZ_C1 and SZ_C2, grouped as SZ_C. We used WGS to identify STs and used phylogenetic analysis to determine ST sources in a global context. We assessed genetic diversity, indicating mutation rates during circulation, using pairwise core genome single-nucleotide

Author affiliations: Shenzhen Third People's Hospital Department of Clinical Laboratory, National Clinical Research Center for Infectious Diseases, Second Affiliated Hospital of Southern University of Science and Technology, Shenzhen, China (L. Li, X. Wang, Y. Xiao, Y. Wang, J. Qu); Shenzhen Institute of Translational Medicine, First Affiliated Hospital of Shenzhen University, Shenzhen Second People's Hospital, Shenzhen (B. Fan, Y. Zhang, D. Gu); Medical Laboratory of the Third Affiliated Hospital of Shenzhen University, Shenzhen (J. Wei, H. Mo); Pingshan Hospital, Southern Medical University, Pingshan District People's Hospital of Shenzhen, Shenzhen (J. Zhou, L. Zhang, S. Yang); Shenzhen Nanshan People's Hospital, Shenzhen (Z. Lai, D. Luo); Shenzhen University Medical School, Shenzhen (Z. Lai, D. Luo)

DOI: https://doi.org/10.3201/eid3105.241649

[1]These authors contributed equally to this article.

polymorphism (cgSNP) distance. We characterized population structure to show divergence and emergence of novel variant populations.

Among the 42 isolates, 34 (81%) were ST80 isolates, 7 (17%) were ST80 variant isolates (ST80_GDvariant1) with *ddl* loci mutated from 1 to 194, and 1 (2%) was an ST78 isolate that was collected in 2023 (Appendix 1 Figure 1, panel B; Appendix 2, https://wwwnc.cdc.gov/EID/article/31/5/24-1649-App2.xlsx). Unexpectedly, ST80_GDvariant1 isolates independently emerged in 5 branches and did not originate from a single mutation event (Figure 1; Appendix 1 Figure 2, panel A).

Phylogenetic analysis inferred from cgSNP of the 41 isolates (ST80 and variants) and 703 other publicly available ST80 isolates revealed that the 41 isolates from the ongoing outbreak in Guangdong are affiliated with SC11 (Appendix 1 Table 2, Figure 2, panel A) (*9*). Within SC11, two 2022 strains from Guangzhou, SZYSC_ZDYVRE007 and SZYSC_ZDYVRE008G, with a 5-SNP divergence, clustered adjacent to the lineage root (Figure 1; Appendix 1 Figure 2, panel A) and formed a distinct VREF sublineage (SC11-root sublineage) with a 37-SNP average divergence from other SC11 strains (bootstrap = 72) (Figure 1). In contrast, the remaining SC11 strains exhibited tight clustering (pairwise distances of ≤5 SNPs [36.5%] and 5–10 SNPs [49.8%]) and formed a dominant clade (SC11-outbreak sublineage) (Figure 1). Those findings suggest that the SC11-outbreak

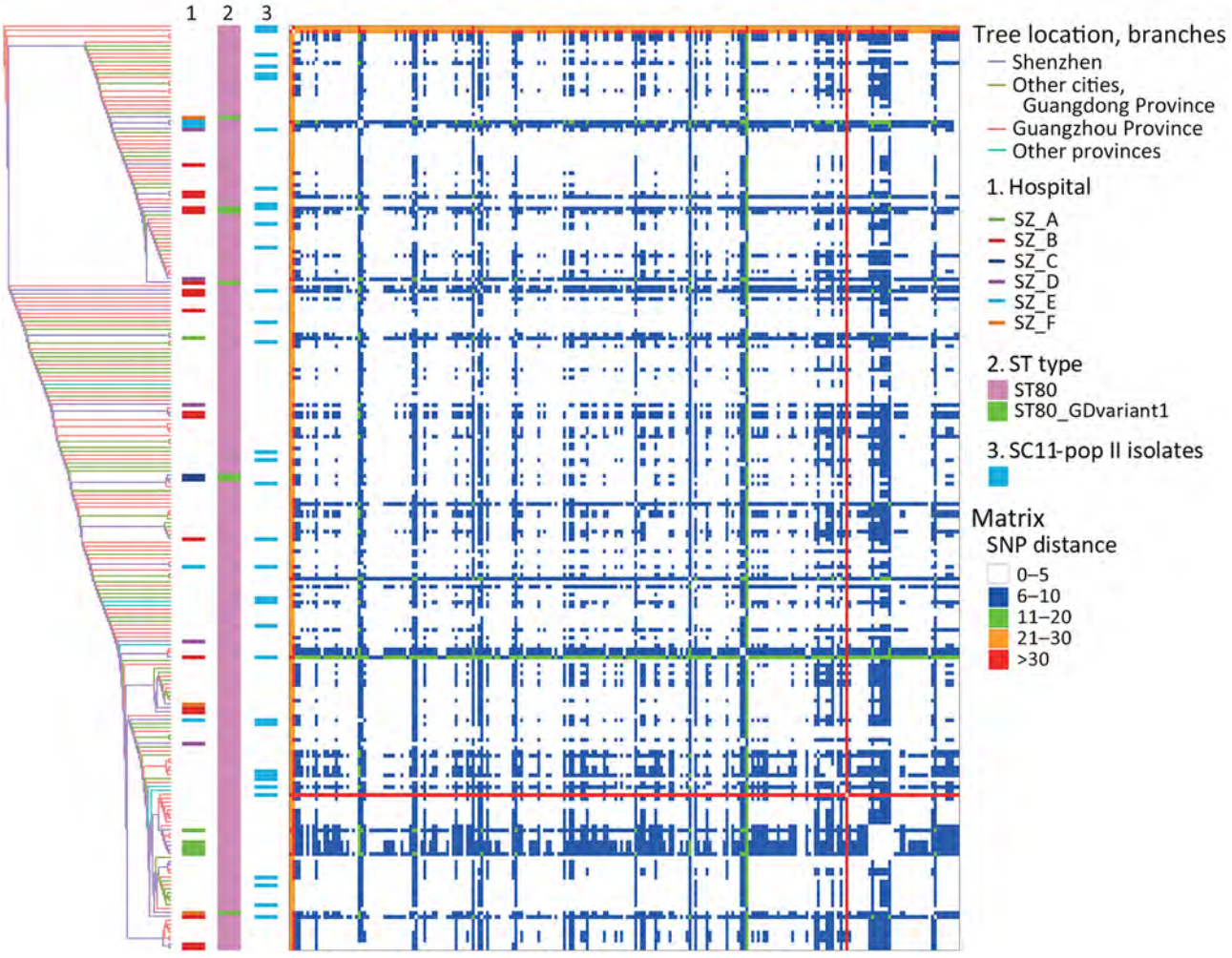

Figure 1. Evolution and variation of SC11 inferred from core genome SNPs during rapid transmission and divergence of vancomycin-resistant *Enterococcus faecium* ST80, China. Graphs shows reconstructed tree from core genome SNPs (left) among all SC11 isolates (n = 235) using strain SZYSC_GYSVRE003 (GenBank accession no. GCA_037475005.1) as reference. Hospital sources of isolates from Shenzhen ST80 and its variant, and SC11-pop II isolates are indicated (1, 2, and 3) next to the tree. The heatmap (right) shows pairwise SNP distance matrix indicating diversity of SC11 lineage presented in the form of symmetry in the bottom left and top right. Cells in the heatmap are colored to show SNP distance in a graded gradient. Red lines indicate large SNP distances and correspond to SZYSC_23VRE019 in the tree. pop, population; SC, sequence cluster; SNP, single-nucleotide polymorphism; ST, sequence type.

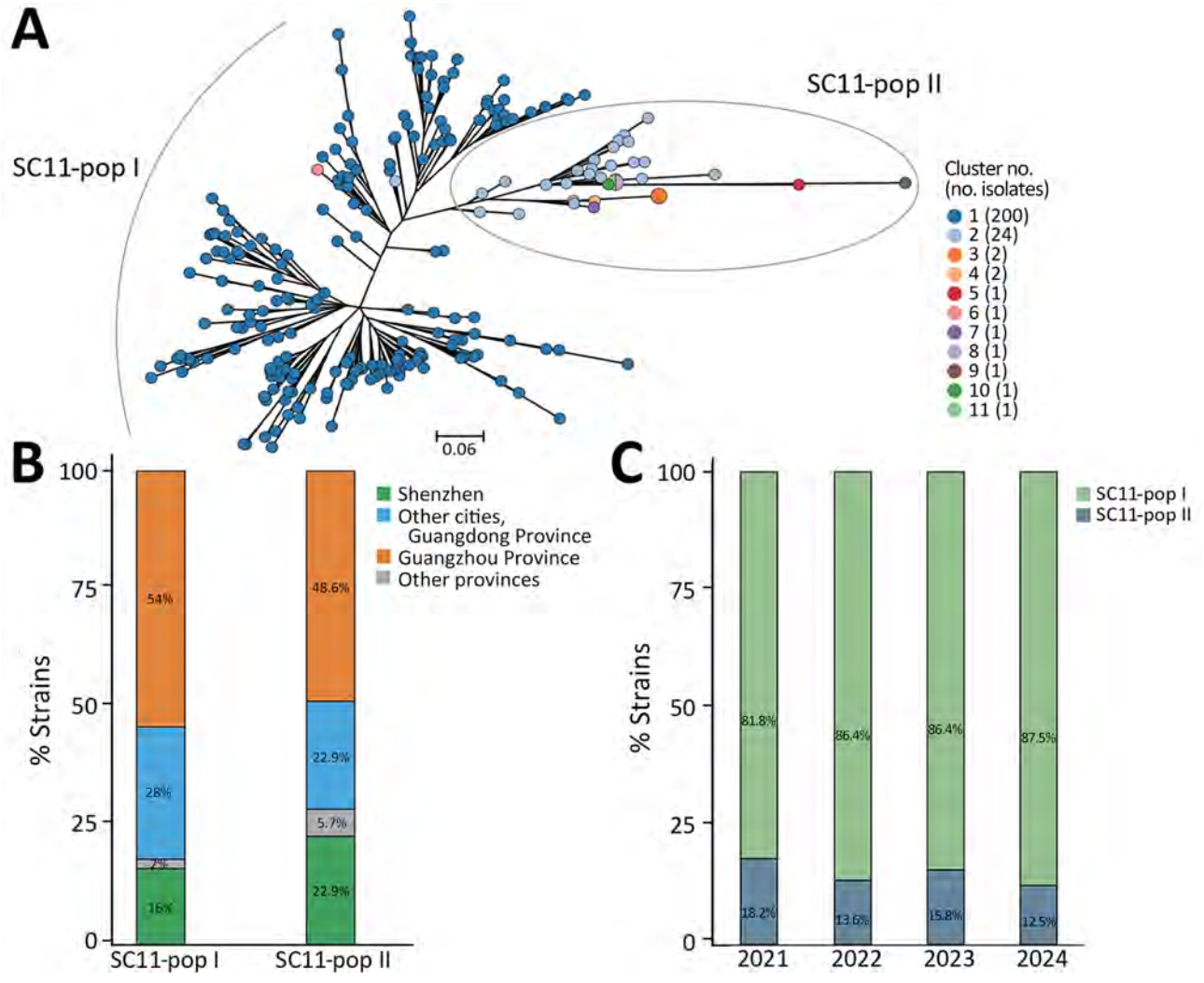

Figure 2. Lineages detected in a study of rapid transmission and divergence of vancomycin-resistant *Enterococcus faecium* ST80, China, showing 2 lineages circulating in parallel. A) SC11 subpopulations labeled on pangenomic tree inferred from gene presence and absence matrix. Eleven clusters were delineated in PopPUNK, labeled in different colors. Clusters 1 and 2 are the 2 major populations. Cluster 6 (1 strain) is nested in cluster 1 (200 strains) on the pangenomic tree and thus are denoted together as SC11-pop I, whereas strains from clusters 3–11 (except cluster 6, 10 strains together) are nested in cluster 2 (24 strains) and are denoted as SC11-pop I. Scale bar is unit of tree branch length, indicating the genetic distance stimulated from gene presence and absence matrix using roary (https://sanger-pathogens.github.io/Roary). B) Parallel circulation of SC11-pop I and SC11-pop II strains from 2021 to 2024. C) Geographic distribution of SC11-pop I (n = 200) and SC11-pop II (n = 35) strains. Prevalence is displayed in percentage. pop, population; SC, sequence cluster; ST, sequence type.

lineage originated from a single progenitor or highly related lineage, enabling rapid transmission.

To resolve strain differentiation, we analyzed SC11-outbreak_lineage population structure by using PopPUNK (https://github.com/bacpop/PopPUNK), which integrates core and accessory genomic variation (*10*). We delineated 2 subpopulations, SC11-pop I and SC11-pop II (Figure 2, panel A; Appendix 1 Figure 4). SC11-pop II isolates formed tight clusters in the pangenome-based tree (Figure 2, panel A) but dispersed in the cgSNP phylogeny (Figure 1), suggesting subpopulation divergence was primarily driven by gene gain or loss.

SC11-pop I and SC11-pop II circulated in parallel for ≥3 years (2021–2024), and SC11-pop II showed broader transmission (Figure 2, panel B) and maintained ≈15% prevalence (Figure 2, panel C). SC11-pop II showed higher prevalence than SC11-pop I in Shenzhen and other provinces (Figure 2, panel B). Genetically, SC11-pop II exhibited enhanced horizontal gene transfer activity, carrying more insertion sequences (ISs) (Appendix 1 Figure 5), plasmid-like elements (Appendix 1 Figure 6), and diverse antimicrobial resistance genes (Figure 3). Although all SC11 isolates harbored the *VanA* operon, 8 SC11-pop II strains uniquely acquired *VanM* operon

(Figure 3). SC11-pop II cases showed trends of increased hospitalization and underlying conditions, including hypertension and cardiovascular, respiratory, and kidney diseases, but statistical significance was limited by the sample size (Appendix 1 Table 5). Expanded surveillance is required to clarify clinical distinctions between SC11-pop I and SC11-pop II.

To identify divergence drivers, we compared core genomic mutations and accessory gene variations between SC11-pop I and SC11-pop II. Unexpectedly, no substantial cgSNP differences emerged (Appendix 3, https://wwwnc.cdc.gov/EID/article/31 /5/24-1649-App3.xlsx), indicating divergence was not driven by core genome mutations. The SC11 lineage pangenome (n = 235) comprised 3,674 genes, including 2,367 core genes and 1,307 accessory genes, an accessory-to-core gene ratio of 0.55. Concerning gene gain or loss, SC11-pop II specifically acquired 152 genes

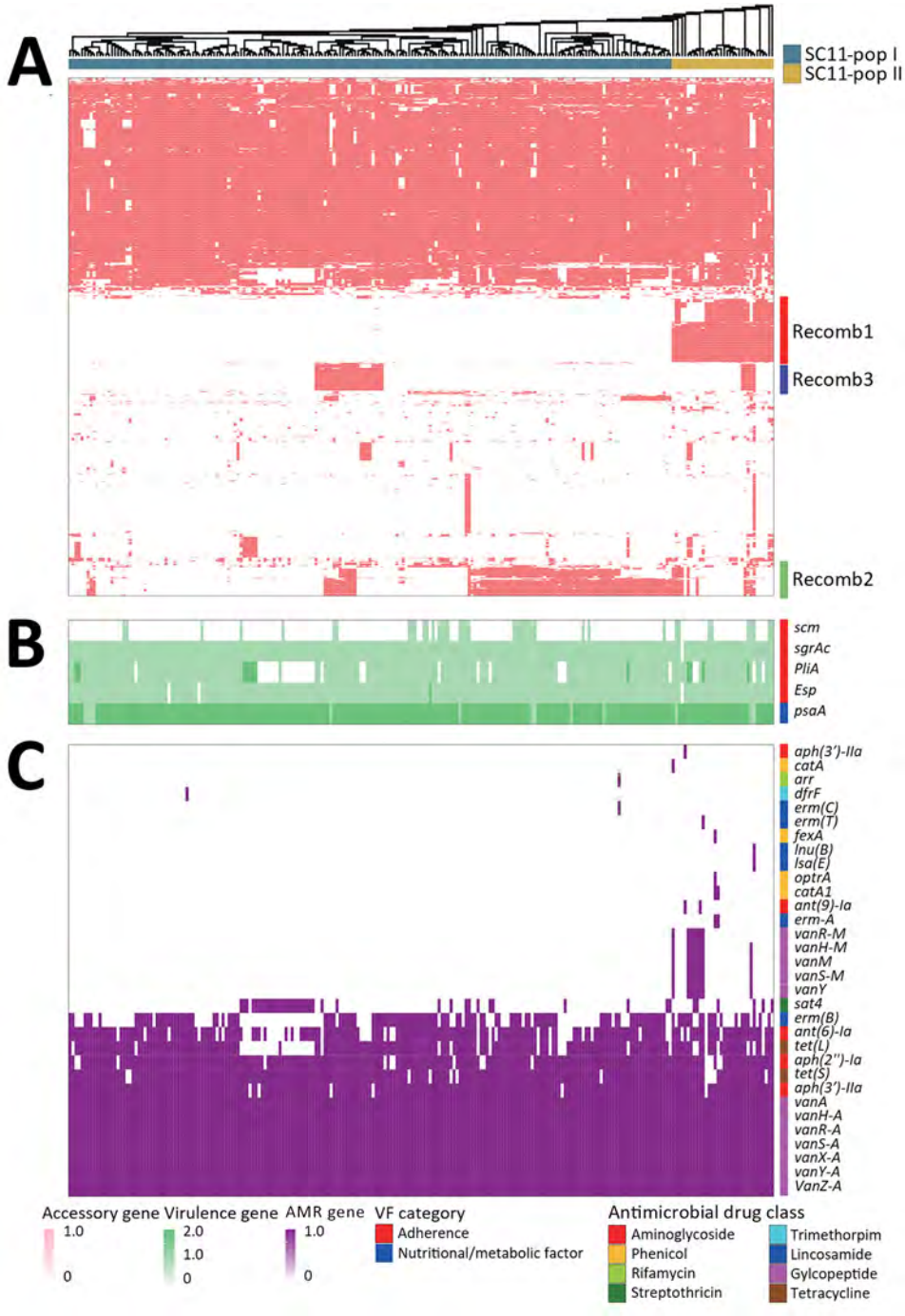

Figure 3. Alignment of SC11 to determine divergence during rapid transmission and divergence of vancomycin-resistant *Enterococcus faecium* ST80, China. To determine the genes associated with the divergence of SC11 we aligned various SC11 genes to pangenomic phylogeny. A) Accessory genes; B) virulence genes; C) AMR genes. Gene copy numbers are displayed in a color grade. We identified 17 total virulence genes; 12 are conserved in all SC11 isolates, and thus only 5 variable virulence genes are shown. Functional categories are indicated by color on the top of the virulence gene heatmap, and drug class corresponding to each AMR gene is shown on the top of AMR gene heatmap. Compared with SC11-pop I, SC11-pop II was more active in acquiring AMR genes against various antibiotic drugs, including sporadic acquisition of aminoglycoside resistance genes *ant9Ia* and *aph3IIIa*; rifamycin resistance gene *arr*; trimethoprim resistance gene *dfrF*; lincosamide resistance genes *ermA*, *ermC*, *ermT*, *lnuB*, and *lsaE*; and phenicol resistance genes *fexA*, *optrA*, *catA1*, and *catA*. AMR, antimicrobial resistance; pop, population; ARG, antimicrobial resistance gene; SC, sequence cluster; ST, sequence type.

Table. Distribution of insertion sequences associated with 3 recombination regions during rapid transmission and divergence of vancomycin-resistant *Enterococcus faecium* sequence type 80, China*

Region	SC11	IS+ sample	IS91	ISL3	IS1182	IS200/IS605	IS256	IS3	IS66	IS982	IS30
Recomb1	SC11-pop I	0	0	0	0	0	0	0	0	0	0
	SC11-pop II	31	24†	23	1	3	11	0	0	0	0
	Proportion of SC11-pop II‡	31/35	24/35‡	23/35	1/35	3/35	11/35	0	0	0	0
Recomb2	SC11-pop I	80	0	4	0	0	1	81	3	2	1
	SC11-pop II	8	0	0	0	0	0	8	0	0	0
	Proportion of SC11-pop I	80/200	0	2/200	0	0	1/200	78/200	3/200	2/200	1/200
	Proportion of SC11-pop II	8/35	0	0/35	0	0	0/35	8/35	0/35	0/35	0/35
Recomb3	SC11-pop I	0	0	0	0	0	0	0	0	0	0
	SC11-pop II	7	0	0	0	0	0	7	0	0	0
	Proportion of SC11-pop II	7/35	0	0	0	0	0	7/35	0	0	0

*SC11-pop I, n = 200 strains; SC11-pop II, n = 35 strains. For identifying the associated IS, in certain Recomb modulars, the upstream (5 kb) and downstream (5 kb) of each Recomb component gene were searched using ISEscan v1.7.2.3 (*14*). IS, insertion sequence; pop, population; SC11, sequence cluster 11; +, positive.
†Total IS number can be identified.
‡The frequency of isolates carrying the corresponding IS.

(forming Recomb1 modular) and showed higher frequency of 13 other functional unknown genes (except endoribonuclease *Pem*K) and lower frequency of 9 genes versus SC11-pop I ($p<0.05$) (Appendix 1 Table 6), indicating greater exogenous gene acquisition. As was observed in the hierarchical clustering of accessory genes on the pangenomic phylogeny, we identified 3 recombination gene modules (Recomb1–3) that were frequently acquired in SC11 (Figure 3, panel A). Recomb1 was exclusive to SC11-pop II (31/35 strains; 1 strain carries more than half of Recomb1 genes and is recognized as Recomb1 positive, similar to the standard for recognizing positivity in Recomb2 and Recomb3), whereas Recomb2 (68 strains) and Recomb3 (23 strains) occurred in both populations (Figure 3, panel A). The fixation of Recomb1–3 suggested their roles in emergence and adaptation of novel variants in SC11. Of note, Recomb1 contained 11 carbohydrate metabolism genes (Appendix 1 Table 4), which are known factors in *E. faecium* that contribute to clinical adaption and epidemics of *E. faecium* (*12*). The stable 3-year persistence of Recomb1 in SC11-pop II across regions suggests a functional importance in host adaptation and potential virulence.

Recombination surpasses mutation as the primary driver of *E. faecium* genetic diversity (*11*), and IS-mediated events occur within days during infection (*13*). Ten families of IS elements were found in all SC11 isolates (Appendix 1 Figure 5**)**. Enhanced IS transposition was associated with rapid core gene mutation (Appendix 1). Recomb1–3 acquisitions were linked to IS-mediated recombination, primarily involving genes related to DNA transposition, replication, or recombination (Appendix 1 Table 4). Recomb1 contained more ISs than Recomb2 or Recomb3, and IS91 was exclusively acquired by SC11-pop II. High-frequency modular recombination in Recomb1 involved IS91, ISL3, and IS256 (specific to SC11-pop II), whereas IS200/IS605 and IS1182 occurred at lower frequencies (Table; Appendix 1 Figure 5). Recomb2 in SC11-pop I occasionally incorporated IS3 alongside ISL3, IS66, IS982, IS256, or IS30 (Table). Recomb3 exclusively associated with IS3 in all 7 SC11-pop II isolates but was absent in SC11-pop I (Table). No plasmid marker genes co-occurred with Recomb1–3, except 9 Recomb1 genes colocalized with MOBT (plasmid relaxase) on contig AXARS010000069.1 (strain SZYSC_22VRE31), suggesting that plasmids did not directly transmit Recomb1–3.

Conclusions

Identifying SC11's most recent ancestor is crucial for elucidating its evolutionary mechanism and mitigating emergent threats. We hypothesize a shared ancestry between SC11-root and SC11-outbreak sublineages. Expanded surveillance of outbreak-associated hospitals and retrospective analysis of pre-2021 VREF isolates are needed to trace the origin.

In summary, we showed that increasing VREF prevalence in Shenzhen, China, constitutes part of the ongoing SC11 outbreak, likely originating from Guangzhou. Population structure analysis revealed 2 stable, circulating SC11 subpopulations, emergence of which was driven by IS-mediated recombination. Sustained surveillance of those subpopulations is essential to prevent the emergence of high-risk clones with increased transmissibility and virulence.

The whole-genome assemblies produced in this study are deposited in GenBank (BioProject accession no. PRJNA1221312).

This study was approved by the Bioethics Committee of Shenzhen Third People's Hospital (ref. no. 2024-009-02). All methods were performed in accordance with the relevant guidelines and regulations.

This work was funded by the Guangdong Basic and Applied Basic Research Foundation (grant no. 2024A1515010319), the Science and Technology Program of Shenzhen (grant nos. KCXFZ20230731100901003 and KJZD20230923115116032), the Shenzhen Key Laboratory of Biochip (grant no. ZDSYS201504301534057), and the Shenzhen High-Level Hospital Construction Fund.

Author contributions: J.Q. and L.L. were involved in the conceptualization. Y.X., B.F., J.W., J.Z., Z.L., Y.Z., H.M., L.Z., D.L., D.G., S.Y., and L.L. were involved in laboratory experiments and data collection. L.L., X.W., and Y.W. were involved in data curation. X.W., L.L., and Y.W. were involved in data analysis and results visualization. J.Q. acquired the funding acquisition. L.L. and X.W. were involved in writing the original draft. J.Q. and L.L. were involved in revising and editing the manuscript. All authors contributed to the article and approved the submitted version.

About the Author

Dr. Li is a research scientist at the National Clinical Research Center for Infectious Diseases, Shenzhen, China. His research interests include genomic epidemiology and the mechanisms underlying epidemic spread of pathogens.

References

1. Van Tyne D, Gilmore MS. Friend turned foe: evolution of enterococcal virulence and antibiotic resistance. Annu Rev. Microbiol. 2014;68:337–56. https://doi.org/10.1146/annurev-micro-091213-113003
2. Gao W, Howden BP, Stinear TP. Evolution of virulence in *Enterococcus faecium*, a hospital-adapted opportunistic pathogen. Curr Opin Microbiol. 2018;41:76–82. https://doi.org/10.1016/j.mib.2017.11.030
3. Gorrie C, Higgs C, Carter G, Stinear TP, Howden B. Genomics of vancomycin-resistant *Enterococcus faecium*. Microb Genom. 2019;5:e000283. https://doi.org/10.1099/mgen.0.000283
4. Pinholt M, Bayliss SC, Gumpert H, Worning P, Jensen VVS, Pedersen M, et al. WGS of 1058 *Enterococcus faecium* from Copenhagen, Denmark, reveals rapid clonal expansion of vancomycin-resistant clone ST80 combined with widespread dissemination of a *vanA*-containing plasmid and acquisition of a heterogeneous accessory genome. J Antimicrob Chemother. 2019;74:1776–85. https://doi.org/10.1093/jac/dkz118
5. Pratama R, Beukers AG, McIver CJ, Keighley CL, Taylor PC, van Hal SJ. A *vanA* vancomycin-resistant *Enterococcus faecium* ST80 outbreak resulting from a single importation event. J Antimicrob Chemother. 2021;77:31–7. https://doi.org/10.1093/jac/dkab379
6. Egan SA, Kavanagh NL, Shore AC, Mollerup S, Samaniego Castruita JA, O'Connell B, et al. Genomic analysis of 600 vancomycin-resistant *Enterococcus faecium* reveals a high prevalence of ST80 and spread of similar *vanA* regions via IS1216E and plasmid transfer in diverse genetic lineages in Ireland. J Antimicrob Chemother. 2022;77:320–30. https://doi.org/10.1093/jac/dkab393
7. Rodríguez-Lucas C, Fernández J, Raya C, Bahamonde A, Quiroga A, Muñoz R, et al. Establishment and persistence of glycopeptide-resistant *Enterococcus faecium* ST80 and ST117 clones within a health care facility located in a low-prevalence geographical region. Microb Drug Resist. 2022;28:217–21. https://doi.org/10.1089/mdr.2021.0171
8. Fang H, Fröding I, Ullberg M, Giske CG. Genomic analysis revealed distinct transmission clusters of vancomycin-resistant *Enterococcus faecium* ST80 in Stockholm, Sweden. J Hosp Infect. 2021;107:12–5. https://doi.org/10.1016/j.jhin.2020.10.019
9. Shen C, Luo L, Zhou H, Xiao Y, Zeng J, Zhang L, et al. Emergence and ongoing outbreak of ST80 vancomycin-resistant *Enterococcus faecium* in Guangdong province, China from 2021 to 2023: a multicenter, time-series and genomic epidemiological study. Emerg Microbes Infect. 2024;13:2361030. https://doi.org/10.1080/22221751.2024.2361030
10. Lees JA, Harris SR, Tonkin-Hill G, Gladstone RA, Lo SW, Weiser JN, et al. Fast and flexible bacterial genomic epidemiology with PopPUNK. Genome Res. 2019;29:304–16. https://doi.org/10.1101/gr.241455.118
11. Palmer KL, Schaik WV, Willems RJL, Gilmore MS. Enterococcal genomics. In: Gilmore MS, Clewell DB, Ike Y, Shankar N, editors. Enterococci: from commensals to leading causes of drug resistant infection. Boston: Massachusetts Eye and Ear Infirmary; 2014. p. 193–230.
12. Chilambi GS, Nordstrom HR, Evans DR, Ferrolino JA, Hayden RT, Marón GM, et al. Evolution of vancomycin-resistant *Enterococcus faecium* during colonization and infection in immunocompromised pediatric patients. Proc Natl Acad Sci U S A. 2020;117:11703–14. https://doi.org/10.1073/pnas.1917130117
13. Udaondo Z, Abram KZ, Kothari A, Jun SR. Insertion sequences and other mobile elements associated with antibiotic resistance genes in *Enterococcus* isolates from an inpatient with prolonged bacteraemia. Microb Genom. 2022;8:mgen000855. https://doi.org/10.1099/mgen.0.000855
14. Xie Z, Tang H. ISEScan: automated identification of insertion sequence elements in prokaryotic genomes. Bioinformatics. 2017;33:3340–7. https://doi.org/10.1093/bioinformatics/btx433

Address for correspondence: Jiuxin Qu, Department of Clinical Laboratory, Shenzhen Third People's Hospital, National Clinical Research Center for Infectious Diseases, Second Affiliated Hospital of Southern University of Science and Technology, No. 29 Bulan Rd, Longgang District, Shenzhen 518000, China; email: qujiuxin@mail.sustech.edu.cn

Self-Reported SARS-CoV-2 Infections among National Blood Donor Cohort, United States, 2020–2022

Bryan R. Spencer, Akintunde Akinseye, Eduard Grebe, Mars Stone, Karla G. Zurita, David J. Wright, James M. Haynes, Susan L. Stramer, Michael P. Busch

SARS-CoV-2 case surveillance in the United States did not distinguish first infections from reinfections. In a large blood donor cohort, self-reported first infections and reinfections during 2020–2022 mirrored public health case count surveillance, and reinfection incidence peaked in 2022. Blood donor data could aid in SARS-CoV-2 and emerging infectious disease surveillance.

During the COVID-19 pandemic in the United States, case counts, test positivity rates, hospitalizations, number of deaths, wastewater surveillance, genomic surveillance, and serologic testing from blood donor populations and commercial laboratories provided surveillance information for SARS-CoV-2, but none of those methods distinguished reinfection from first infection (*1*–*6*). A further challenge to public health surveillance was widespread adoption of rapid antigen tests conducted at home; infections detected outside laboratory or healthcare settings remained outside the national surveillance system (*7*). We leveraged self-reports from a large blood donor cohort to estimate first infection and reinfection incidence during 2020–2022.

The Study

Two large US blood collectors, American Red Cross (https://www.redcross.org) and Vitalant (https://www.vitalant.org), established a prospective cohort of 142,599 repeat blood donors to support serosurveillance of SARS-CoV-2 transmission during 2022 and to assess serologic correlates of protection against infection and illness. We used serologic status and reported COVID-19 vaccine history as of July 2021 to classify blood donors after blood center testing for spike and nucleocapsid (N) antibodies of all blood donations during June 2020–June 2021. Together, American Red Cross and Vitalant collect blood in >40 states and account for ≈45% of the US blood supply. The Advarra (https://www.advarra.com, approval no. Pro00056783) and American Red Cross (approval no. 2021-033) institutional review boards approved the study activities.

Both blood centers electronically distributed an index survey to cohort members whose donor record confirmed acceptance of email contact. Vitalant also reached out to cohort members accepting postal mail contact. Harmonized survey content captured self-reported SARS-CoV-2 infections at time of donor response that had been swab confirmed or diagnosed by a healthcare provider, date of diagnosis, attendant symptoms, and hospitalization (Appendix, https://wwwnc.cdc.gov/EID/article/31/5/24-1953-App1.pdf). We distributed index surveys and automated reminders to encourage survey completion during December 2021–December 2022. We distributed follow-up surveys capturing new infections at quarterly intervals through January 2023.

The principal outcomes of interest were survey-reported first or second infections (i.e., first reinfection) that were swab-confirmed or diagnosed by a healthcare provider. Second infections were counted only if reported ≥90 days after the first infection. First and second infection rates were tabulated on a quarterly basis and estimated as the infection count divided

Author affiliations: American Red Cross, Dedham, Massachusetts, USA (B.R. Spencer, J.M. Haynes); Westat, Rockville, Maryland, USA (A. Akinseye, D.J. Wright); Vitalant Research Institute, San Francisco, California, USA (E. Grebe, M. Stone, K.G. Zurita, M.P. Busch); Infectious Disease Consultant, North Potomac, Maryland, USA (S.L. Stramer)

DOI: https://doi.org/10.3201/eid3105.241953

by the population at risk. We defined the population at risk for first infection for a given quarter as the participants who completed a survey during or after that quarter and who had not reported any infection before that quarter. We similarly calculated the population at risk for second infection, and participants counted toward the population at risk in the quarters after the first infection if they completed a survey during or after those quarters. We only tabulated the first reinfection for that effort; donors were censored for any quarter after their second infection or their last survey completion. Hence, donors completing at least an index survey might have been informative for population at risk for 8–12 quarters starting in January 2020.

We did not conduct modeling; we only described counts and rates estimated and plotted to show temporal trends in reported infections from the first quarter of 2020 through the fourth quarter of 2022. We combined data across the 2 blood centers and reported without weighting after observing comparable trends in both centers. We compared survey respondents with the underlying cohort in qualitative terms for assessment of the representativeness of data reported here. Comparisons to public health case surveillance were also qualitative in nature; we did not conduct statistical tests.

Our cohort included 66,274 donors (46.5% of the cohort) who completed an index survey (Table 1); of those, 46,292 (70%) completed a survey during or after the fourth quarter of 2022. Among survey respondents, 55% were women and 45% were men, and most (74%) were ≥50 years of age, self-reported race as non-Hispanic White (>90%), and were donors to the American Red Cross (79%). Based on self-reported vaccine status and serologic testing in mid-2021, 72% of those who completed an index survey had received a COVID-19 vaccine, 25% had N antibodies indicating prior infection, 16% were both previously infected and vaccinated, and 18% were neither vaccinated nor previously infected at cohort formation. Among survey nonrespondents, the corresponding percentages were as follows: 50% had received a vaccine, 21% had N antibodies, 12.5% had hybrid immunity, and 41.5% were unexposed at cohort formation. Compared with the full cohort, younger donors (age groups 16–29 and 30–49 years) were underrepresented and older donors (age ≥65 years) were overrepresented among survey respondents. Survey respondents showed modest variation relative to the underlying cohort in terms of sex, race, and ethnicity distribution, but participation varied by infection and vaccine history. Among donors with previous SARS-CoV-2 infection at time of cohort formation, vaccine history was similar in survey respondents compared with the full cohort. In contrast, among those who had not been infected by mid-2021, unvaccinated donors were less likely and vaccinated donors were more likely to complete surveys.

Table 1. Demographic description of underlying national blood donor cohort and survey responders for self-reported SARS-CoV-2 infections among national blood donor cohort, United States, 2020–2022

Demographic data	Full cohort, no. (%)	Completed index survey, no. (%)
All	142,599 (100%)	66,274 (46.5%)
Sex		
F	74,561 (52.3)	36,659 (55.3)
M	68,038 (47.7)	29,615 (44.7)
Age group, y		
16–29	12,357 (8.7)	2,468 (3.7)
30–49	39,054 (27.4)	14,733 (22.2)
50–64	52,507 (36.8)	26,061 (39.3)
≥65	38,681 (27.1)	23,012 (34.7)
Race/ethnicity		
Native American/Alaskan, non-Hispanic	795 (0.6)	210 (0.3)
Asian/Pacific Islander, non-Hispanic	3,816 (2.7)	1,308 (2.0)
Black, non-Hispanic	2,339 (1.6)	797 (1.2)
Hispanic	12,983 (9.1)	3,004 (4.5)
Other/mixed, non-Hispanic	1,518 (1.1)	511 (0.8)
Missing/unknown/refused	2,458 (1.7)	554 (0.8)
White, non-Hispanic	118,690 (83.2)	59,890 (90.4)
Cohort assignment, July 2021		
Infected, not vaccinated	12,751 (8.9)	6,318 (9.5)
Infected, vaccinated	19,969 (14.0)	10,440 (15.8)
Not infected, not vaccinated	43,887 (30.8)	12,196 (18.4)
Not infected, vaccinated	65,992 (46.3)	37,320 (56.3)
Blood collection organization		
American Red Cross	77,075 (54.1)	52,439 (79.1)
Vitalant	65,524 (45.9)	13,835 (20.9)

Table 2. Self-reported SARS-CoV-2 first and second infections by quarter among national blood donor cohort, United States, 2020–2022*

	2020				2021				2022			
Infection measure	Q1	Q2	Q3	Q4	Q1	Q2	Q3	Q4	Q1	Q2	Q3	Q4
First infection count	549	432	1,043	4,684	1,242	170	1,494	3,102	3,822	3,807	3,672	1,956
At-risk population	66,274	65,725	65,293	64,250	59,566	58,324	58,154	56,660	52,913	43,587	38,995	30,133
First infection per 1,000 population at risk, rate	8.3	6.6	16.0	72.9	20.9	2.9	25.7	54.8	72.2	87.3	94.2	64.9
Second infection count	0	1	6	33	50	29	68	322	841	545	717	476
At-risk population	0	549	980	2,017	6,668	7,860	8,001	9,427	12,050	13,022	15,935	16,159
Second infection per 1,000 population at risk, rate	0	1.8	6.1	16.4	7.5	3.7	8.5	34.2	69.8	41.9	45.0	29.5

*Q, quarter.

Donors reported 25,973 first and 3,088 second infections during 2020–2022 (Table 2). Peak rates of first infections were observed in the fourth quarter of 2020 (4,684 cases; 72.9 cases/1,000 population at risk) and in the third quarter of 2022 (3,672 cases; 94.2 cases/1,000 at risk) and had a nadir of 170 cases (2.9 cases/1,000 population at risk) during the second quarter of 2021 (Table 2; Figure, panel A). Second infections represented 10.6% of the 29,061 combined first and second infections in aggregate, and the percentages of reported infections that were second infections varied from 0% to 1% during 2020 and from 13% to 20% during 2022 (Figure, panel B). Adjusting for population at risk, rates of second infection remained low (<2% per quarter) during the pre-Delta period (through June 2021) but surged in the second half of 2021 and almost reached parity with first infection rates during the Omicron wave in quarter 1 of 2022 (72.2 vs. 69.8 cases/1,000 population at risk) (Figure, panel A). Temporal increases and decreases in second infection rates largely mirrored the trends in first infection rates until 2022, diverged during the second and third quarters, and decreased in parallel during the fourth quarter. Combined first and second infection rates (Figure, panel C) yielded a curve that largely mirrored Centers for Disease Control and Prevention case counts grouped into quarterly bins (Figure, panel D): peak in late 2020, nadir in

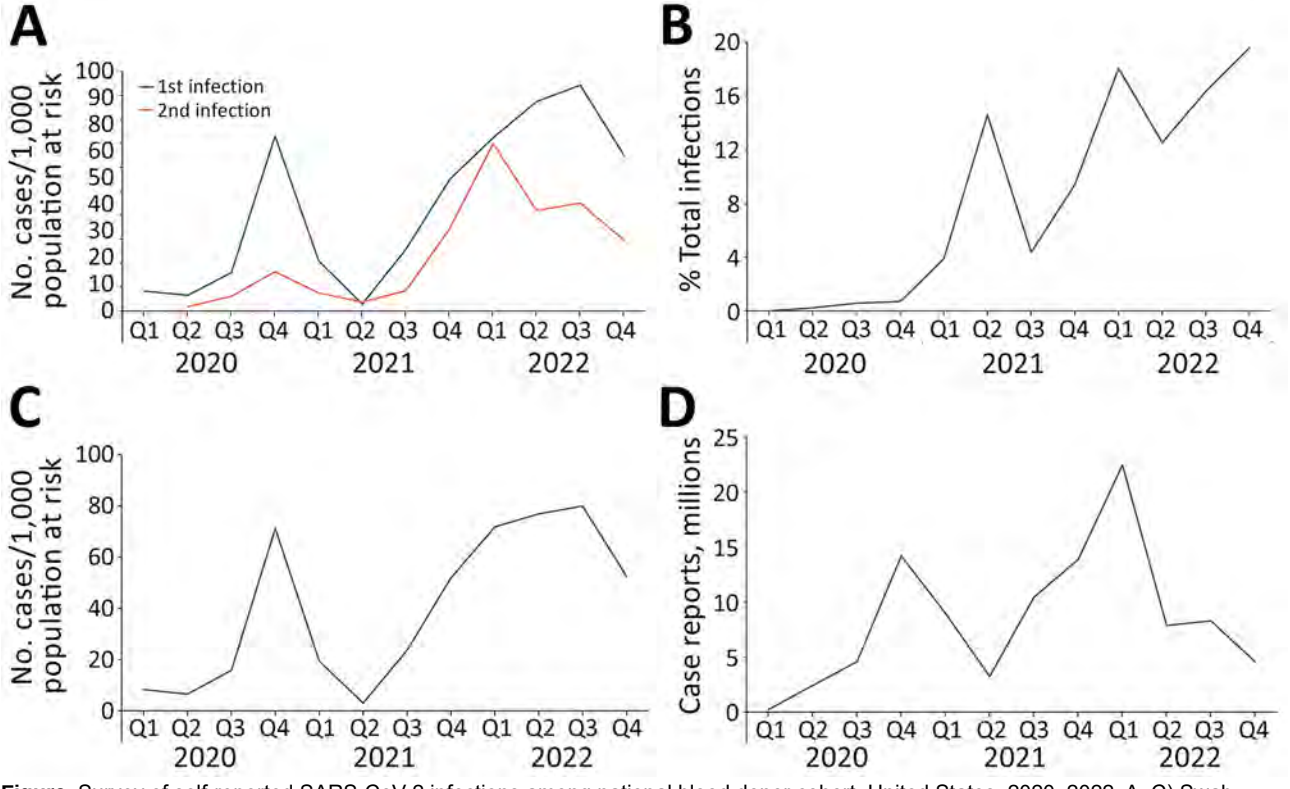

Figure. Survey of self-reported SARS-CoV-2 infections among national blood donor cohort, United States, 2020–2022. A–C) Swab-confirmed or healthcare provider–diagnosed infections grouped into quarterly bins: US blood donor survey-reported first and second COVID-19 infection incidence (A); reinfections as percentage of total infections (B); and total infection incidence (C). D) Quarterly counts of case reports through the US surveillance system.

mid-2021, and surge in second half of 2021 during emergence of Delta that continued with the Omicron period. We saw the most notable difference in 2022, where our donor population reported a continuing increase in infections that peaked only in the third quarter, whereas public health surveillance showed a sharp decrease between the first and second quarters of 2022.

Conclusions

Despite the limitation that our analysis excludes infections not confirmed by a swab test or healthcare provider diagnosis (i.e., asymptomatic or mild infections for which testing was not performed), the temporal trends and rates of SARS-CoV-2 infection reported by a cohort of US blood donors are broadly consistent with public health surveillance case counts during the first 3 years of the COVID-19 pandemic, reinforcing a 2024 survey-based report (*8*). The ability to distinguish first infections from reinfections provides utility in the context of ongoing transmission, when rates of severe illness, hospitalization, and death are lower than initial waves. Although known to be healthier on average than the general population, blood donors nonetheless represent an informative population for monitoring SARS-CoV-2 and potentially other emerging infectious diseases. Blood donor data could aid in SARS-CoV-2 and emerging infectious disease surveillance.

Acknowledgments

The authors thank the blood donors for completion of surveys and the blood center, coordinating center, and Centers for Disease Control and Prevention staff, including Roberta Bruhn, Marjorie D. Bravo, Edward P. Notari, and Jamel Groves for data collection and Paula Saá, Rebecca Fink, Jefferson Jones, and Melissa Briggs-Hagen for program oversight and coordination.

This work was supported by a research contract from the Centers for Disease Control and Prevention (contract no. 75D30120C08170).

About the Author

Dr. Spencer is an epidemiologist and director of data science at the American Red Cross. His research interests include infectious risks of transfusion, iron status of blood donors, and risk analysis modeling related to blood safety and availability.

References

1. Centers for Disease Control and Prevention. COVID data tracker [cited 2024 Nov 21]. https://covid.cdc.gov/covid-data-tracker/#datatracker-home
2. Bajema KL, Wiegand RE, Cuffe K, Patel SV, Iachan R, Lim T, et al. Estimated SARS-CoV-2 seroprevalence in the US as of September 2020. JAMA Intern Med. 2021;181:450–60. https://doi.org/10.1001/jamainternmed.2020.7976
3. Jones JM, Stone M, Sulaeman H, Fink RV, Dave H, Levy ME, et al. Estimated US infection- and vaccine-induced SARS-CoV-2 seroprevalence based on blood donations, July 2020–May 2021. JAMA. 2021;326:1400–9. https://doi.org/10.1001/jama.2021.15161
4. Paul P, France AM, Aoki Y, Batra D, Biggerstaff M, Dugan V, et al. Genomic surveillance for SARS-CoV-2 variants circulating in the United States, December 2020–May 2021. MMWR Morb Mortal Wkly Rep. 2021;70:846–50. https://doi.org/10.15585/mmwr.mm7023a3
5. Yu AT, Hughes B, Wolfe MK, Leon T, Duong D, Rabe A, et al. Estimating relative abundance of 2 SARS-CoV-2 variants through wastewater surveillance at 2 large metropolitan sites, United States. Emerg Infect Dis. 2022;28:940–7. https://doi.org/10.3201/eid2805.212488
6. Ma KC, Dorabawila V, León TM, Henry H, Johnson AG, Rosenberg E, et al. Trends in laboratory-confirmed SARS-CoV-2 reinfections and associated hospitalizations and deaths among adults aged ≥18 years—18 U.S. jurisdictions, September 2021–December 2022. MMWR Morb Mortal Wkly Rep. 2023;72:683–9. https://doi.org/10.15585/mmwr.mm7225a3
7. Rader B, Gertz A, Iuliano AD, Gilmer M, Wronski L, Astley CM, et al. Use of at-home COVID-19 tests—United States, August 23, 2021–March 12, 2022. MMWR Morb Mortal Wkly Rep. 2022;71:489–94. https://doi.org/10.15585/mmwr.mm7113e1
8. Santillana M, Uslu AA, Urmi T, Quintana-Mathe A, Druckman JN, Ognyanova K, et al. Tracking COVID-19 infections using survey data on rapid at-home tests. JAMA Netw Open. 2024;7:e2435442. https://doi.org/10.1001/jamanetworkopen.2024.35442

Address for correspondence: Bryan R. Spencer, American Red Cross, 180 Rustcraft Rd, Dedham, MA 02026, USA; email: bryan.spencer@redcross.org

Molecular Detection of *Histoplasma* in Bat-Inhabited Tunnels of Camino de Hierro Tourist Route, Spain

Joaquina María García-Martín,[1] Julio David Soto López,[1]
Diego Lizana-Ciudad, Pedro Fernández-Soto, Antonio Muro

We detected *Histoplasma capsulatum* in 2 bat-inhabited tunnels of a tourist route in northern Spain. This finding confirms that the geographic distribution of this fungal pathogen is wider than previously thought. Our results highlight the need for surveillance and assessment of the potential infection risk for workers and visitors.

Histoplasmosis is a primary pulmonary infection caused by inhalation of aerosolized spores of *Histoplasma* fungi, naturally present in soils, after disruption of soil aggregates (*1*). This fungal disease is endemic to tropical, subtropical, and temperate regions, and most cases occur in Latin America (e.g., Brazil, Guyanas), North America (mainly in the Ohio and Mississippi River Valleys), and Western and Central Africa. Most cases occurring in Latin America are attributed to *H. capsulatum* sensu stricto (formerly *H. capsulatum* Panama or H81 lineage) and *H. suramericanum* (formerly *H. capsulatum* LAm A lineage). In North America, *H. mississippiense* (formerly *H. capsulatum* NAm 1) and *H. ohiense* (formerly *H. capsulatum* NAm 2) are the predominant etiologic agents of chronic pulmonary histoplasmosis; *H. ohiense* is more virulent (*2*). Cases in Africa, often with skin and bone involvement, are associated with *Histoplasma* varietas *duboisii*, also referred to as *H. duboisii* or *H. capsulatum* H88 lineage (*2*).

Different species of the genus *Histoplasma* are found in soils enriched with bird and bat guano, which contribute to the accumulation of nitrogen and phosphorus in soils, favoring fungal growth. In particular, bats (order Chiroptera) act as natural reservoirs and dispersers of *Histoplasma*, which is often isolated from their organs and guano collected from natural and artificial roosts, including abandoned caves and tunnels, mines, cellars, or basements (*3*). In addition, numerous histoplasmosis outbreaks linked to bat guano exposure have been reported; for example, a severe histoplasmosis outbreak with fatal outcomes occurred among workers in abandoned tunnels contaminated with spore-bearing dust in the Dominican Republic (*4*).

In nonendemic regions, such as Europe, few imported cases of histoplasmosis and even fewer apparently autochthonous cases have been reported (*5*). Regarding the presence of *Histoplasma* spp. in the environment, reports are related to isolations by traditional culture methods from guano and soil samples collected in caves inhabited by bats in Romania and in a chicken farm in Italy (*6*,*7*). In addition, in northern Italy, some persons tested positive for histoplasmin skin tests, suggesting that environmental conditions may have enabled establishment and spread of *Histoplasma* in certain areas of Europe (*8*). In Spain, *Histoplasma* has not been isolated from bat organs or guano, and most clinical cases of histoplasmosis have been considered imported, resulting from international travel and migration (*9*). Numerous cases of histoplasmosis related to bat exposure have been reported in Africa (*10*), Central America (*4*), South America (*11*), and North America (*12*). We describe detection of *H. capsulatum* in 2 bat-inhabited tunnels of a tourist route in northern Spain.

The Study

To shed light on the distribution of *Histoplasma* beyond traditional known endemic areas, we conducted a study in 2 bat-inhabited tunnels of the Camino de Hierro in Salamanca, northern Spain, a pedestrian

Author affiliations: Universidad de Salamanca, Salamanca, Spain (J.M. García-Martín, J.D. Soto López, D. Lizana-Ciudad, P. Fernández-Soto, A. Muro); Instituto de Investigación Biomédica de Salamanca, Salamanca (J.M. García-Martín, J.D. Soto López, P. Fernández-Soto, A. Muro); Centro de Estudios Ambientales y Dinamización Rural, Salamanca (D. Lizana-Ciudad)

DOI: https://doi.org/10.3201/eid3105.241117

[1]These first authors contributed equally to this article.

route receiving >60,000 visitors since its opening as an ecotourism attraction in 2021 (Appendix, https://wwwnc.cdc.gov/EID/article/31/5/24-1117-App1.pdf). We collected 101 guano samples in the tunnels (Appendix Table 1) and found almost 42% were positive for *Histoplasma* by nested PCR, using previously published primers (Appendix Table 2). Specifically, the *Hcp100* gene sequences we isolated (submitted to GenBank under accession nos. PP887829–78) (Table) shared high homology with GenBank sequences corresponding to *H. capsulatum* s.s., *H. suramericanum*, *H. capsulatum* LAm B2, and *H. capsulatum* var. *duboisii*. Moreover, our phylogenetic analyses (Appendix) indicated that the newly obtained sequences form a fully supported monophyletic group with multiple GenBank sequences of *Histoplasma* (posterior probability = 1; bootstrap support = 100%), without a clear geographic or host-related pattern (Figure).

To determine species of bats roosting in this area, we used BLAST (https://blast.ncbi.nlm.nih.gov) to identify cytochrome c oxidase subunit I sequences obtained from *Histoplasma*-positive samples. Results corresponded to different species that are mainly distributed in Europe: *Myotis blythii* was

Table. Identities of *Histoplasma* isolates obtained from guano samples collected in the tunnels of the Camino de Hierro tourist route in study of molecular detection of *Histoplasma*, Spain*

Isolate code	Isolate BLAST identity (sublineage)†	Isolate accession no.	Source species for guano samples	Source accession no.
H1	*H. suramericanum* (LAm A1)	PP887829	*Rhinolophus ferrumequinum*	PP919660
H2	*H. suramericanum* (LAm A1)	PP887830	*Myotis blythii*	PP919661
H3	*H. suramericanum* (LAm A1)	PP887831	*Myotis* sp.	PP919662
H4	*H. capsulatum* variant *duboisii*/*H. capsulatum* sensu lato (LAm B2)	PP887832	*M. blythii*	PP919663
H5	*H. suramericanum* (LAm A1)	PP887833	*Myotis* sp.	PP919664
H6	*H. capsulatum* var. *duboisii*/*H. capsulatum* s.l. (LAm B2)	PP887834	*M. blythii*	PP919665
H7	*H. capsulatum* var. *duboisii*/*H. capsulatum* s.l. (LAm B2)	PP887835	*M. blythii*	PP919666
H8	*H. capsulatum* var. *duboisii*/*H. capsulatum* s.l. (LAm B2)	PP887836	*Myotis* sp.	PP919667
H9	*H. suramericanum* (LAm A1)	PP887837	*M. blythii*	PP919668
H10	*H. suramericanum* (LAm A1)	PP887838	NA	NA
H11	*H. capsulatum* var. *duboisii*/*H. capsulatum* s.l. (LAm B2)	PP887839	*Miniopterus schreibersii*	PP919669
H12	*H. suramericanum* (LAm A1)	PP887840	*M. blythii*	PP919670
H13	*H. suramericanum* (LAm A1)	PP887841	*M. blythii*	PP919671
H14	*H. suramericanum* (LAm A1)	PP887842	*M. blythii*	PP919672
H15	*H. suramericanum* (LAm A1)	PP887843	*M. blythii*	PP919673
H16	*H. suramericanum* (LAm A1)	PP887844	*M. blythii*	PP919674
H17	*H. capsulatum* var. *duboisii*/*H. capsulatum* s.l. (LAm B2)	PP887845	*Myotis* sp.	PP919675
H18	*H. suramericanum* (LAm A1)	PP887846	*M. blythii*	PP919676
H19	*H. suramericanum* (LAm A1)	PP887847	*M. blythii*	PP919677
H21	*H. suramericanum* (LAm A1)	PP887849	*Myotis* sp.	PP919679
H22	*H. suramericanum* (LAm A1)	PP887850	*Myotis* sp.	PP919680
H23	*H. suramericanum* (LAm A1)	PP887851	*M. blythii*	PP919681
H26	*H. suramericanum* (LAm A1)	PP887854	*Myotis* sp.	PP919684
H27	*H. suramericanum* (LAm A1)	PP887855	*M. blythii*	PP919685
H28	*H. suramericanum* (LAm A1)	PP887856	*M. blythii*	PP919686
H29	*H. suramericanum* (LAm A1)	PP887857	*R. ferrumequinum*	PP919687
H30	*H. capsulatum* var. *duboisii*/*H. capsulatum* s.l. (LAm B2)	PP887858	*M. blythii*	PP919688
H31	*H. suramericanum* (LAm A1)	PP887859	NA	NA
H32	*H. suramericanum* (LAm A1)	PP887860	*M. blythii*	PP919689
H33	*H. suramericanum* (LAm A1)	PP887861	*M. blythii*	PP919690
H34	*H. capsulatum* var. *duboisii*/*H. capsulatum* s.l. (LAm B2)	PP887862	*Myotis* sp.	PP919691
H35	*H. capsulatum* var. *duboisii*/*H. capsulatum* s.l. (LAm B2)	PP887863	*R. ferrumequinum*	PP919692
H36	*H. suramericanum* (LAm A1)	PP887864	*Myotis* sp.	PP919693
H37	*H. capsulatum* sensu stricto	PP887865	*M. blythii*	PP919694
H38	*H. capsulatum* var. *duboisii*/*H. capsulatum* s.l. (LAm B2)	PP887866	*Myotis* sp.	PP919695
H39	*H. capsulatum* var. *duboisii*/*H. capsulatum* s.l. (LAm B2)	PP887867	*M. blythii*	PP919696
H40	*H. capsulatum* var. *duboisii*/*H. capsulatum* s.l. (LAm B2)	PP887868	*M. schreibersii*	PP919697
H41	*H. suramericanum* (LAm A1)	PP887869	*M. blythii*	PP919698
H42	*H. capsulatum* var. *duboisii*/*H. capsulatum* s.l. (LAm B2)	PP887870	*M. blythii*	PP919699
H43	*H. capsulatum* s.s.	PP887871	*M. blythii*	PP919700
H49	*H. suramericanum* (LAm A1)	PP887877	*M. blythii*	PP919706
H50	*H. suramericanum* (LAm A1)	PP887878	*M. blythii*	PP919707

*GenBank accession numbers are shown; further details are provided in Appendix Table 4 (https://wwwnc.cdc.gov/EID/article/31/5/24-1117-App1.pdf). NA, not available.

†Species names, according to (*2*), followed by sublineage when applicable. *H. capsulatum* s.s. = *H. capsulatum* Panama or H81 lineage; *H. capsulatum* var. *duboisii* = *H. capsulatum* African lineage or *H. duboisii*; *H. suramericanum* = *H. capsulatum* LAm A. Note that the identity of some isolates could not be determined at species level because the corresponding Hcp100 sequences shared high similarity values with several GenBank isolates representing different *Histoplasma* species or lineages (separated by a slash).

the most common, followed by *Rhinolophus ferrumequinum* and *Miniopterus schreibersii* (all sequences were submitted to GenBank under accession nos. PP919660–707) (Table). That finding increases the number of possible hosts and dispersers associated with this human pathogen.

The degree of positivity we observed suggests a substantial presence of *Histoplasma* in the tunnels

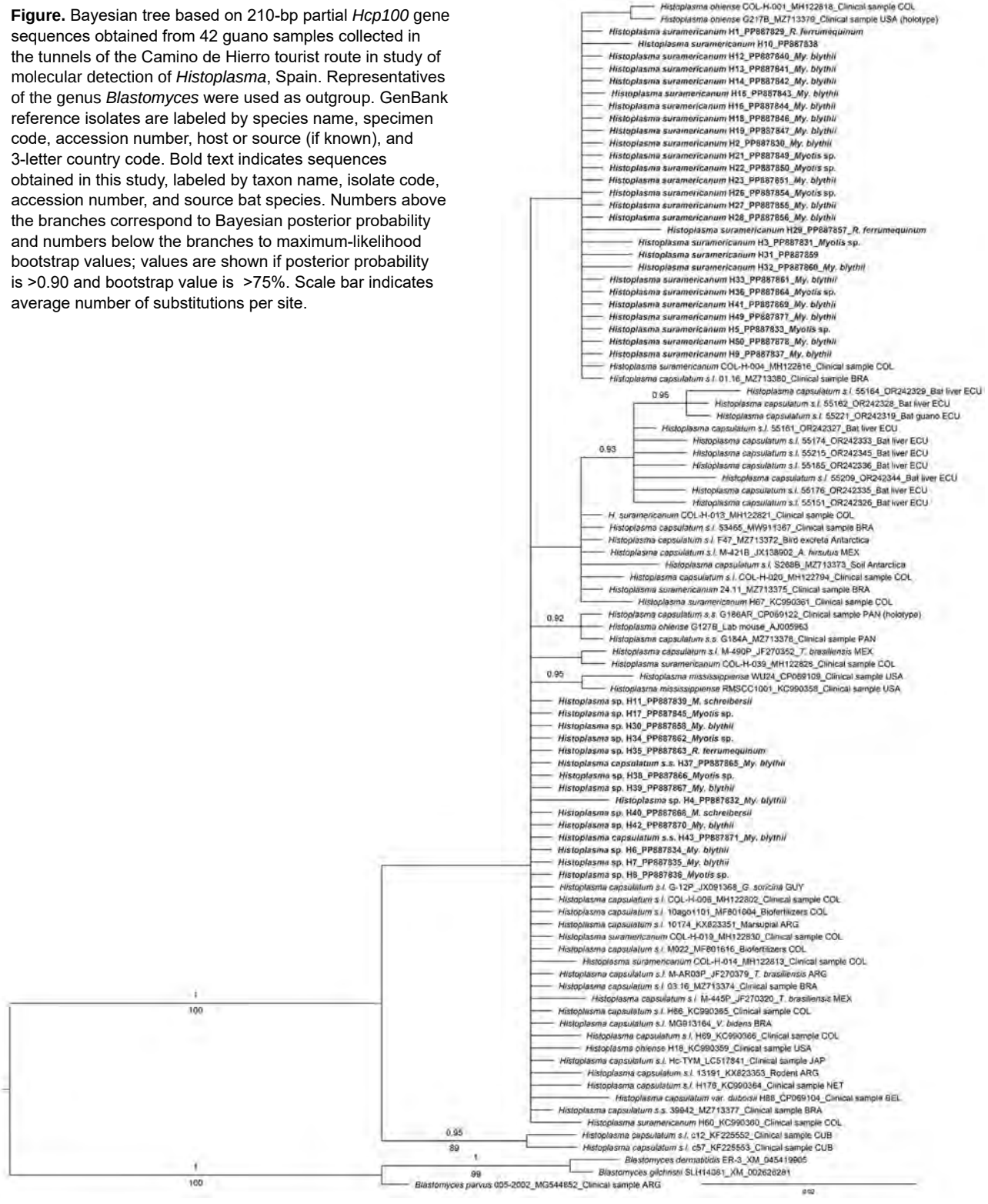

Figure. Bayesian tree based on 210-bp partial *Hcp100* gene sequences obtained from 42 guano samples collected in the tunnels of the Camino de Hierro tourist route in study of molecular detection of *Histoplasma*, Spain. Representatives of the genus *Blastomyces* were used as outgroup. GenBank reference isolates are labeled by species name, specimen code, accession number, host or source (if known), and 3-letter country code. Bold text indicates sequences obtained in this study, labeled by taxon name, isolate code, accession number, and source bat species. Numbers above the branches correspond to Bayesian posterior probability and numbers below the branches to maximum-likelihood bootstrap values; values are shown if posterior probability is >0.90 and bootstrap value is >75%. Scale bar indicates average number of substitutions per site.

studied, which seems reasonable because the moderate temperature, constant humidity, and darkness of both tunnels investigated are suitable environmental conditions for fungal growth. Of note, outside known areas of endemicity, *Histoplasma* has been isolated from soils contaminated with bat guano in Romania (*6*).

A total of 728 cases of human histoplasmosis have been diagnosed in 17 countries in Europe, of which Spain accounts for up to 60% (*5*). Most cases were imported from Central and South America (*9*), except 4 cases: 1 autochthonous laboratory-acquired case and 3 cases with no epidemiologic history in patients who had never visited endemic areas. One case was in a drug user with HIV/AIDS, another was in a patient who had disseminated histoplasmosis develop after renal transplantation, and the third was in a patient who had occasionally traveled to France, Italy, and the United Kingdom and had previously been treated with an immunosuppressant, suggesting reactivation of a latent infection (*13*). However, to date, *Histoplasma* has not been isolated from environmental samples in Spain, and no autochthonous clinical case of histoplasmosis has been associated with exposure to bats.

Conclusions

The results of this study indicate that *Histoplasma* is present in bat-inhabited tunnels at Camino de Hierro in northern Spain. That finding evidences that the geographic distribution of this genus is wider than previously thought and also reinforces the known association between *Histoplasma* and bats.

The risk for histoplasmosis increases with contact with guano deposited in bat roosts. Exploring caves and similar environments is a well-documented source of *Histoplasma* exposure; the first outbreaks of histoplasmosis were related to bat-inhabited locations dating back to the 1930s (*14*). For that reason, the need to assess the presence of *Histoplasma* in bat-inhabited places before opening them to public access has been emphasized (*11*). Therefore, even though no autochthonous cases of histoplasmosis have been reported in Spain, the detection of *Histoplasma* in such a popular tourist attraction as Camino de Hierro makes it advisable to alert local clinicians about the importance of considering histoplasmosis in the differential diagnosis of patients with community-acquired pneumonia. Clinicians can refer to available clinical diagnostic algorithms for histoplasmosis for evidenced-based testing guidance (*15*).

Our results provide a warning about the presence of *Histoplasma* in Camino de Hierro but also could stimulate further research on bat populations in Spain, opening lines of research into their role in the transmission of histoplasmosis and other airborne infectious diseases. Research on the effects *Histoplasma* and other pathogens on the health of bats should also be considered, and we advise carrying out a serologic study to assess possible exposure to *Histoplasma* among workers and susceptible persons who have visited the tunnels. Given the tourism value and high number of visitors to Camino de Hierro, health authorities should consider our findings and implement measures to prevent potential cases of histoplasmosis, in both visitors and workers of this tourist route.

Acknowledgments

We are deeply grateful to Luis Hernández Tabernero and Miguel Lizana Avia for their advice on bats, logistical support, and field sampling. We would also like to thank Carmen Vieria Lista, Laura Noelly Niño Puerto, and other e-INTRO group members for their collaboration in fieldwork and photo report.

This work was funded by the Instituto de Salud Carlos III (ISCIII) through project no. PI22/01721 and co-funded by the European Union. We also acknowledge support of Ministry of Universities of the Spanish Government, financed by The European Next Generation Funds, through a Margarita Salas postdoctoral contract awarded to J.M.G.-M. The funders had no role in study design, data collection, analysis or interpretation, in writing the manuscript or the decision to publish the results.

Author contributions: conceptualization: J.M.G.-M., J.D.S.L., P.F.-S., and A.M.; field sampling: D.L.-C., J.M.G.-M., and J.D.S.L.; wet lab: J.M.G.-M. and J.D.S.L.; phylogenetic analyses: J.M.G.-M.; investigation and data curation: J.M.G.-M.; writing—original draft preparation: J.M.G.-M.; writing—review and editing: J.M.G.-M., J.D.S.L., P.F.-S., and A.M.; supervision: P.F.-S. and A.M.; funding: P.F.-S; project administration: P.F.-S., and A.M. All authors have read and agreed to the published version of the manuscript.

About the Author

Dr. García-Martín works in the Department of Parasitology of the Universidad de Salamanca. Her research interests include taxonomy, phylogeny, and diagnosis of invasive fungal infections.

References

1. Emmons CW. Isolation of *Histoplasma capsulatum* from soil. Public Health Rep. 1949;64:892–6. https://doi.org/10.2307/4587021
2. Sepúlveda VE, Márquez R, Turissini DA, Goldman WE, Matute DR. Genome sequences reveal cryptic speciation

in the human pathogen *Histoplasma capsulatum*. MBio. 2017;8:e01339–17. https://doi.org/10.1128/mBio.01339-17
3. Gugnani HC, Denning DW. Infection of bats with *Histoplasma* species. Med Mycol. 2023;61:myad080. https://doi.org/10.1093/mmy/myad080
4. Armstrong PA, Beard JD, Bonilla L, Arboleda N, Lindsley MD, Chae S-R, et al. Outbreak of severe histoplasmosis among tunnel workers—Dominican Republic, 2015. Clin Infect Dis. 2018;66:1550–7. https://doi.org/10.1093/cid/cix1067
5. Antinori S, Giacomelli A, Corbellino M, Torre A, Schiuma M, Casalini G, et al. Histoplasmosis diagnosed in Europe and Israel: a case report and systematic review of the literature from 2005 to 2020. J Fungi (Basel). 2021;7:481. https://doi.org/10.3390/jof7060481
6. Alteras I. First Romanian isolation of *Histoplasma capsulatum* from the soil. Dermatol Int. 1966;5:69–71. https://doi.org/10.1111/j.1365-4362.1966.tb05188.x
7. Sotgiu G, Mazzoni A, Mantovani A, Ajello L, Palmer J. *Histoplasma capsulatum*: occurrence in soil from the Emilia-Romagna region of Italy. Science. 1965;147:624.
8. Taylor ML, Reyes-Montes MDR, Estrada-Bárcenas DA, Zancopé-Oliveira RM, Rodríguez-Arellanes G, Ramírez JA. Considerations about the geographic distribution of *Histoplasma* species. Appl Environ Microbiol. 2022;88:e0201021. https://doi.org/10.1128/aem.02010-21
9. Molina-Morant D, Sánchez-Montalvá A, Salvador F, Sao-Avilés A, Molina I. Imported endemic mycoses in Spain: evolution of hospitalized cases, clinical characteristics and correlation with migratory movements, 1997–2014. PLoS Negl Trop Dis. 2018;12:e0006245. https://doi.org/10.1371/journal.pntd.0006245
10. Pakasa N, Biber A, Nsiangana S, Imposo D, Sumaili E, Muhindo H, et al. African histoplasmosis in HIV-negative patients, Kimpese, Democratic Republic of the Congo. Emerg Infect Dis. 2018;24:2068–70.
11. Rocha-Silva F, Figueiredo SM, Silveira TT, Assunção CB, Campolina SS, Pena-Barbosa JP, et al. Histoplasmosis outbreak in Tamboril cave—Minas Gerais state, Brazil. Med Mycol Case Rep. 2013;4:1–4.
12. Velasco-Castrejón O, González-Ochoa A. Primary pulmonary epidemic histoplasmosis in an abandoned mine. Mykosen. 1977;20:393–9.
13. Buitrago MJ, Cuenca-Estrella M. Current epidemiology and laboratory diagnosis of endemic mycoses in Spain [in Spanish]. Enferm Infecc Microbiol Clin. 2012;30:407–13.
14. Benedict K, Mody RK. Epidemiology of histoplasmosis outbreaks, United States, 1938–2013. Emerg Infect Dis. 2016;22:370–8. https://doi.org/10.3201/eid2203.151117
15. Smith DJ, Free RJ, Thompson GR III, Baddley JW, Pappas PG, Benedict K, et al.; Endemic Mycoses Diagnostic Algorithm Subject Matter Expert Group. Clinical testing guidance for coccidioidomycosis, histoplasmosis, and blastomycosis in patients with community-acquired pneumonia for primary and urgent care providers. Clin Infect Dis. 2024;78:1559–63. https://doi.org/10.1093/cid/ciad619

Address for correspondence: Pedro Fernández-Soto, Facultad de Farmacia, Universidad de Salamanca. Avda. Licenciado Méndez Nieto s/n, Salamanca, 37007, Spain; email: pfsoto@usal.es

etymologia revisited

Originally published in March 2019

Streptomycin

strep'to-mi'sin

In the late 1930s, Selman Waksman, a soil microbiologist working at the New Jersey Agricultural Station of Rutgers University, began a large-scale program to screen soil bacteria for antimicrobial activity. By 1943, Albert Schatz, a PhD student working in Waksman's laboratory, had isolated streptomycin from *Streptomyces griseus* (from the Greek *strepto-* ["twisted"] + *mykēs* ["fungus"] and the Latin *griseus*, "gray").

In 1944, Willam H. Feldman and H. Corwin Hinshaw at the Mayo Clinic showed its efficacy against *Mycobacterium tuberculosis*. Waksman was awarded a Nobel Prize in 1952 for his discovery of streptomycin, although much of the credit for the discovery has since been ascribed to Schatz. Schatz later successfully sued to be legally recognized as a co-discoverer of streptomycin.

References:

1. Comroe JH Jr. Pay dirt: the story of streptomycin. Part I. From Waksman to Waksman. Am Rev Respir Dis. 1978;117:773–81.
2. Wainwright M. Streptomycin: discovery and resultant controversy. Hist Philos Life Sci. 1991;13:97–124.

https://wwwnc.cdc.gov/eid/article/25/3/et-2503_article

Co-Infections with Orthomarburgviruses, Paramyxoviruses, and Orthonairoviruses in Egyptian Rousette Bats, Uganda and Sierra Leone

Brian R. Amman, Amy J. Schuh, Tara K. Sealy, Immah Conteh, Gloria G. Akurut, Alusine H. Koroma, Kilama Kamugisha, James C. Graziano, Emmanuel Saidu, Doris F. Bangura, Emmanuel S. Kamanda, Ibrahim A. Bakarr, Jonathan Johnny, Eric M. Enyel, Jonathan A. Musa, Augustus Osborne, Ibrahim K. Foday, Camilla Bangura, Christian Sumaila, Samuel M.T. Williams, George M. Fefegula, Patrick Atimnedi, Aiah Lebbie, Jonathan S. Towner

We report 1.3% (19/1,511) of Egyptian rousette bats (ERBs) in Uganda and Sierra Leone were co-infected with different combinations of Marburg, Sosuga, Kasokero, or Yogue viruses. To prevent infection by those viruses, we recommend avoiding ERB-populated areas, avoiding ERBs and ERB-contaminated objects, and thoroughly washing harvested fruits before consumption.

Zoonotic co-infections occur when ≥2 genetically distinct infectious agents are detected in a single host (*1*) and are common in wildlife (*2*–*4*). Compared with infection by a single pathogen, co-infections can alter host susceptibility to other agents, disease transmission dynamics, and duration of illness (*4*), as well as replication and shedding of infectious agents (*5*).

Bats belong to the second largest order of mammals (order Chiroptera), representing 20% of known mammal species. Bats are also associated with >4,100 distinct animal viruses (*6*). Egyptian rousette bats (ERBs; *Rousettus aegyptiacus*) have been well studied as vertebrate hosts for zoonotic viruses. ERBs are the known reservoir for Marburg virus (MARV) and Ravn virus (family Filoviridae, genus Orthomarburgvirus) (*7*), a putative reservoir for Sosuga virus (SOSV; family Paramyxoviridae, genus *Pararubulavirus*) (*8*), and the only known vertebrate reservoir for Kasokero virus (KASV) in East Africa and Yogue virus (YOGV; family Nairoviridae, genus *Orthonairovirus*) in West Africa (*9*). Virus co-infections are also frequently observed in bats; many virus-positive bats in China are co-infected with ≥2 viruses (*10*). Simultaneous shedding of multiple distinct paramyxoviruses has been reported in flying fox bats (*Pteropus* spp.) in Australia (*11*). Co-infections with multiple rubulavirus-related viruses and other unclassified paramyxoviruses have been reported in ERBs in South Africa (*12*). Virus co-infection in bats has been described as an underappreciated phenomenon in disease ecology and surveillance data reporting (*2*). Here, we investigated zoonotic virus co-infections in ERBs from Uganda and Sierra Leone.

The Study

During filovirus ecology research efforts in Uganda and Sierra Leone, we captured ERBs by using mist nets and harp traps (Table). We collected visceral

Author affiliations: Centers for Disease Control and Prevention, Atlanta, Georgia, USA (B.R. Amman, A.J. Schuh, T.K. Sealy, J.C. Graziano, J.S. Towner); Njala University, Bo, Sierra Leone (I. Conteh, A.H. Koroma, E. Saidu, D.F. Bangura, E.S. Kamanda, I.A. Bakarr, J. Johnny, J.A. Musa, A. Osborne, I.K. Foday, C. Bangura, C. Sumaila, S.M.T. Williams, G.M. Fefegula, A. Lebbie); Uganda Wildlife Authority, Kampala, Uganda (G.G. Akarut, K. Kamugisha, E.M. Enyel, P. Atimnedi); University of Sierra Leone, Freetown, Sierra Leone (A. Lebbie)

DOI: https://doi.org/10.3201/eid3105.241669

Table. Numbers of Egyptian rousette bats (*Rousettus aegyptiacus*) captured according to site in study of co-infections with orthomarburgviruses, paramyxoviruses, and orthonairoviruses, Uganda and Sierra Leone

Captured bats	Uganda				Sierra Leone			Grand total
	Python Cave*	Kasungwa Cave*	Kitaka Mine†	Total no.	Tailu Village‡	Kasewe Cave§	Total no.	
Female	256	53	202	511	2	183	185	696
Adult	140	36	105	281	2	65	67	348
Juvenile	116	17	97	230	0	118	118	348
Male	381	43	197	621	5	189	194	815
Adult	219	41	128	388	2	86	88	476
Juvenile	162	2	69	233	3	103	106	339
Total no.	637	96	399	1,132	7	372	379	1,511

*Stable populations.
†Depopulated, undergoing repopulation.
‡Forest caught, population unknown.
§Transient population, possible maternal colony.

samples, including liver, spleen, heart, lung, kidney, axillary lymph node, salivary gland, colon, and blood, for virologic testing. We tested the samples for the known zoonotic viruses SOSV, KASV (Uganda; blood samples only), and YOGV (Sierra Leone; blood samples only). We additionally tested samples from 1,511 bats captured during November 2009–February 2022 in Uganda and Sierra Leone (Appendix Table 1, https://wwwnc.cdc.gov/EID/article/29/1/22-0154-App1.pdf) for MARV (nucleoprotein and viral protein 35 genes), SOSV (nucleoprotein, hemagglutinin, and neuraminidase genes) and KASV and YOGV (nucleoprotein genes) by quantitative reverse transcription PCR.

In ERB samples, we detected individual infections and multiple co-infections with MARV and SOSV (n = 1,132 samples from Uganda; n = 379 from Sierra Leone), KASV (n = 942 from Uganda), and YOGV (n = 275 from Sierra Leone) (Appendix Table 1). For 1,511 bats sampled in both Uganda and Sierra Leone, 6.0% (90/1,511) had detectable MARV RNA and 10.7% (162/1,511) had detectable SOSV RNA; 3.1% (29/942) of ERBs from Uganda only had detectable KASV RNA, and 0.4% (1/275) from Sierra Leone only had detectable YOGV RNA.

In Uganda and Sierra Leone, we detected 23 co-infections with ≥2 viruses: 10 (43.5%) co-infections in Uganda and 13 (56.5%) in Sierra Leone. Co-infections with MARV and SOSV (1.3% [19/1,511]) were most prevalent in both Uganda (0.8% [9/1,132]) and Sierra Leone (2.6% [10/379]). We did not detect MARV and KASV co-infections in Uganda; we detected only 1 (0.4%) of 275 tested samples co-infected with MARV and YOGV in Sierra Leone. We also detected co-infection with SOSV and KASV in Uganda (0.1% [1/942]) and SOSV and YOGV co-infection in Sierra Leone (0.4% [1/275]). A single ERB from Sierra Leone had detectable RNA for MARV, SOSV, and YOGV (0.4% [1/275]) (Appendix Table 1).

Among the 19 ERBs co-infected with MARV and SOSV, 9 (47.4%) were female and 10 (52.6%) male. Eight (42.1% [8/19]) of the bats were adults (forearm ≥89 mm length) and 11 (57.9% [11/19]) were juveniles (forearm <89 mm length).

We detected co-infections with MARV, SOSV, KASV (Uganda only), and YOGV (Sierra Leone only) in ERBs from Uganda and Sierra Leone; most bats were co-infected with MARV and SOSV and primarily at only 1 site in each country. Most MARV/SOSV co-infections in Uganda were observed in bats from the Kitaka Mine sampling during November 2012. The mine was undergoing a resurgence of MARV infections after a depopulation and repopulation event, as previously reported (*13*); MARV active infection rates in ERBs had more than doubled at the mine since 2007 (*7*). The SOSV active infection rates were also much higher at Kitaka Mine than at the undisturbed and permanent ERB colonies at Kasungwa Cave and Python Cave sites (*8*). It is possible that a newly formed naive ERB population occupied the recently re-opened mine, providing an excess of bats not previously exposed to MARV or SOSV.

A comparable SOSV rate of active infection was identified at Kasewe Cave in Sierra Leone. One possible explanation for high SOSV infections at Kasewe Cave could be that the ERB population there appeared to be migratory, and the cave was mostly devoid of ERBs at certain times of the year (February–April). The ERB population at Kasewe Cave might be an amalgamation of many smaller populations that return annually to the cave site to use area resources and then disperse into smaller populations to return to other, smaller roosting sites. Subsequent reoccupations by smaller ERB populations year after year at Kasewe Cave bring new, virus naive bats together in larger numbers, similar to the repopulation of Kitaka Mine, causing higher numbers of SOSV infections in the population and, subsequently, higher rates of co-infection with MARV. Moreover, the limited data collected at the Kasewe Cave suggest the site could be a maternity roost, but because of that limitation, a definitive designation cannot be made.

The ratio of juveniles to adults was higher at Kasewe Cave (59.4% [221/372]) than at Kitaka Mine (41.6% [166/399]), which could also explain the high SOSV prevalence at the cave site given recent findings of an age-related bias in SOSV prevalence at Kasewe Cave (*14*). More surveillance will be needed to determine normal rates of SOSV infection in ERB populations across Sierra Leone.

Conclusions

It remains unknown why levels of active MARV infection at Kasewe Cave are not following the same repopulation patterns as those at Kitaka Mine or following the rates of SOSV in Kasewe Cave. One possibility involves timing of collection efforts, which might have missed the peak of active MARV infections. Another potential explanation could be that SOSV, and paramyxoviruses in general, are more easily transmitted within ERB populations than MARV, when considering possible SOSV recrudescence and vertical transmission has been seen for other paramyxoviruses, such as Nipah virus (Appendix reference *16*). Increases in rubulavirus-like paramyxovirus transmission during female aggregation and reproduction have been identified in a population of ERBs in South Africa, which showed seasonal population fluctuations similar to those in Sierra Leone (*12*). The high active SOSV infection rate, in addition to the high infection risk associated with MARV co-infection of ERBs in Kasewe Cave, indicates a substantial public health risk because of public harvests of bats for food, as well as guano mining to produce crop fertilizer. SOSV and other rubula-like paramyxoviruses have been reported to be shed in both urine and feces (guano) from infected bats (*12*,*15*). Our public health recommendations to prevent human infection by ERB-borne zoonotic viruses are to avoid entering areas where ERBs are known to roost, avoid contact with ERBs, avoid objects obviously contaminated by ERBs (including guano mining within known ERB roosts), and thoroughly wash all harvested vegetable and fruit produce from those areas before consumption.

Acknowledgments

We thank the Uganda Virus Research Institute and the Uganda Wildlife Authority park rangers for their assistance during this work, the Sierra Leone government for permission to conduct this work, the Sierra Leone district and community stakeholders for support and for allowing us to perform sampling in their districts and community, and the residents and community leaders of both Tailu Village (Kailahun District) and Kasewe (Moyamba District) for their support during the field work.

All animal work was approved by the Centers for Disease Control and Prevention's Institutional Animal Care and Use Committee (protocol no. 3063AMMBATX-A2) and had permissions from the governments of Sierra Leone and Uganda. All personnel wore appropriate personal protective equipment, including disposable gowns or Tyvek coveralls, double latex gloves or bite resistant gloves (if necessary), face shields, and respiratory protection, when handling bats and bat samples.

All data supporting the findings of this study are available within the article or from the authors upon request.

This work was funded by the US Defense Threat Reduction Agency (grant no. HDTRA1033036) and core funding from the Centers for Disease Control and Prevention.

Contributions: B.R.A, A.J.S., T.K.S., and J.S.T. conceptualized the research. B.R.A, A.J.S., T.K.S, I.C., G.G.A., A.H.K., J.C.G., K.K., and I.K.F. performed the formal analysis. B.R.A., A.J.S., T.K.S., G.G.A., K.K., J.C.G., E.S., D.F.B., E.K., I.A.B., J.J., E.M.E., J.A.M., A.O., C.B., C.S., S.M.T.W., G.M.F., A.L., P.A., and J.S.T. conducted the investigations. B.R.A, A.L., P.A., and J.S.T. were responsible for logistics. B.R.A, A.J.S., and T.K.S. determined methodology. B.R.A., A.J.S., T.K.S., I.C., G.G.A., A.H.K., K.K., J.C.G., E.S., D.F.B., E.K., I.A.B., J.J., E.M.E., J.A.M., A.O., I.K.F., C.B., C.S., S.M.T.W., G.M.F., A.L., P.A., and J.S.T. performed data collection and curation. B.R.A., A.J.S., and J.S.T. wrote and prepared the original manuscript draft. B.R.A., A.J.S., A.L., and J.S.T. reviewed and edited the manuscript. All authors have read and agreed to the published version of this manuscript.

About the Author

Dr. Amman is a disease ecologist in the Virus Host Ecology Unit, Viral Special Pathogens Branch, National Center for Emerging and Zoonotic Infectious Diseases, Centers for Disease Control and Prevention, Atlanta, Georgia, USA. His primary research interests focus on investigating the ecology of and relationships between emerging zoonotic viruses and their reservoirs.

References

1. Hoarau AOG, Mavingui P, Lebarbenchon C. Coinfections in wildlife: focus on a neglected aspect of infectious disease epidemiology. PLoS Pathog. 2020;16:e1008790. https://doi.org/10.1371/journal.ppat.1008790
2. Jones BD, Kaufman EJ, Peel AJ. Viral co-infection in bats: a systematic review. Viruses. 2023;15:1860. https://doi.org/10.3390/v15091860
3. Petney TN, Andrews RH. Multiparasite communities in animals and humans: frequency, structure and pathogenic significance. Int J Parasitol. 1998;28:377–93. https://doi.org/10.1016/S0020-7519(97)00189-6

4. Vaumourin E, Vourc'h G, Gasqui P, Vayssier-Taussat M. The importance of multiparasitism: examining the consequences of co-infections for human and animal health. Parasit Vectors. 2015;8:545. https://doi.org/10.1186/s13071-015-1167-9
5. Davy CM, Donaldson ME, Subudhi S, Rapin N, Warnecke L, Turner JM, et al. White-nose syndrome is associated with increased replication of a naturally persisting coronaviruses in bats. Sci Rep. 2018;8:15508. https://doi.org/10.1038/s41598-018-33975-x
6. Chen L, Liu B, Yang J, Jin Q. DBatVir: the database of bat-associated viruses. Database (Oxford). 2014;2014:bau021. https://doi.org/10.1093/database/bau021
7. Towner JS, Amman BR, Sealy TK, Carroll SA, Comer JA, Kemp A, et al. Isolation of genetically diverse Marburg viruses from Egyptian fruit bats. PLoS Pathog. 2009;5:e1000536. PubMed https://doi.org/10.1371/journal.ppat.1000536
8. Amman BR, Albariño CG, Bird BH, Nyakarahuka L, Sealy TK, Balinandi S, et al. A recently discovered pathogenic paramyxovirus, Sosuga virus, is present in *Rousettus aegyptiacus* fruit bats at multiple locations in Uganda. J Wildl Dis. 2015;51:774–9. https://doi.org/10.7589/2015-02-044
9. Walker PJ, Widen SG, Firth C, Blasdell KR, Wood TG, Travassos da Rosa AP, et al. Genomic characterization of Yogue, Kasokero, Issyk-Kul, Keterah, Gossas, and Thiafora viruses: nairoviruses naturally infecting bats, shrews, and ticks. Am J Trop Med Hyg. 2015;93:1041–51. PubMed https://doi.org/10.4269/ajtmh.15-0344
10. Wang J, Pan YF, Yang LF, Yang WH, Lv K, Luo CM, et al. Individual bat virome analysis reveals co-infection and spillover among bats and virus zoonotic potential. Nat Commun. 2023;14:4079. https://doi.org/10.1038/s41467-023-39835-1
11. Peel AJ, Wells K, Giles J, Boyd V, Burroughs A, Edson D, et al. Synchronous shedding of multiple bat paramyxoviruses coincides with peak periods of Hendra virus spillover. Emerg Microbes Infect. 2019;8:1314–23. https://doi.org/10.1080/22221751.2019.1661217
12. Mortlock M, Dietrich M, Weyer J, Paweska JT, Markotter W. Co-circulation and excretion dynamics of diverse *Rubula*- and related viruses in Egyptian rousette bats from South Africa. Viruses. 2019;11:37. https://doi.org/10.3390/v11010037
13. Amman BR, Nyakarahuka L, McElroy AK, Dodd KA, Sealy TK, Schuh AJ, et al. Marburgvirus resurgence in Kitaka Mine bat population after extermination attempts, Uganda. Emerg Infect Dis. 2014;20:1761–4. https://doi.org/10.3201/eid2010.140696
14. Amman BR, Koroma AH, Schuh AJ, Conteh I, Sealy TK, Foday I, et al. Sosuga virus detected in Egyptian rousette bats (*Rousettus aegyptiacus*) in Sierra Leone. Viruses. 2024;16:648. https://doi.org/10.3390/v16040648
15. Amman BR, Schuh AJ, Sealy TK, Spengler JR, Welch SR, Kirejczyk SGM, et al. Experimental infection of Egyptian rousette bats (*Rousettus aegyptiacus*) with Sosuga virus demonstrates potential transmission routes for a bat-borne human pathogenic paramyxovirus. PLoS Negl Trop Dis. 2020;14:e0008092. https://doi.org/10.1371/journal.pntd.0008092

Addresses for correspondence: Brian R. Amman or Jonathan S. Towner, Centers for Disease Control and Prevention, 1600 Clifton Rd NE, Mailstop H18-B, Atlanta, GA 30329-4018, USA; email: cxx1@cdc.gov or email: jit8@cdc.gov

Influenza A(H1N1)pdm09 Virus with Reduced Susceptibility to Baloxavir, Japan, 2024

Emi Takashita, Hiroko Morita, Shiho Nagata, Seiichiro Fujisaki, Hideka Miura, Tatsuya Ikeda, Kenichi Komabayashi, Mika Sasaki, Yohei Matoba, Tomoko Takahashi, Naomi Ogawa, Katsumi Mizuta, Sueshi Ito, Noriko Kishida, Kazuya Nakamura, Masayuki Shirakura, Shinji Watanabe, Hideki Hasegawa

Influenza A(H1N1)pdm09 virus carrying an I38N substitution was detected in an untreated teenager in Japan. The I38N mutant virus exhibited reduced susceptibility to baloxavir but remained susceptible to neuraminidase inhibitors and showed reduced growth capability. Monitoring antiviral drug susceptibility of influenza viruses is necessary to aid public health planning and clinical recommendations.

The cap-dependent endonuclease inhibitor baloxavir marboxil is approved in Japan for the treatment and prophylaxis of influenza virus infection in young patients. For patients ≥12 years of age, the approved doses are 80 mg for those weighing ≥80 kg and 40 mg for those weighing <80 kg. For patients <12 years of age, the approved doses are 40 mg for those weighing ≥40 kg, 20 mg for those weighing 20 to <40 kg, and 10 mg for those weighing 10 to <20 kg. The Japan Pediatric Society did not recommend use of baloxavir in children <5 years of age during the 2023–24 influenza season (https://www.jpeds.or.jp/uploads/files/20231122_influenza.pdf). Baloxavir acid, an active form of baloxavir marboxil, binds to the polymerase acidic (PA) protein endonuclease domain and inhibits RNA cleavage by the PA cap-dependent endonuclease (*1*). Amino acid substitutions at position 38 in the PA protein are recognized as treatment-emergent mutations associated with reduced susceptibility to baloxavir (*2*,*3*) and are considered the primary pathway for the emergence of baloxavir resistance (*4*). The PA I38T substitution is the most frequent substitution and has the greatest effect on baloxavir susceptibility (*5*). Influenza A(H1N1)pdm09 (pH1N1) and A(H3N2) viruses with the PA I38T substitution isolated from baloxavir-treated patients show similar replication fitness and pathogenicity to wild-type isolates tested in hamsters and efficiently transmit between ferrets by respiratory droplets (*6*). We have monitored baloxavir susceptibility of seasonal influenza viruses in Japan since the 2017–18 season and reported human-to-human transmission of PA I38T mutant H3N2 viruses in children ≤10 years of age (*7*,*8*).

Researchers detected a PA I38N substitution in a pH1N1 virus isolated from a patient during a phase 3 clinical trial of baloxavir. That substitution conferred a 24-fold reduction in baloxavir susceptibility in recombinant A/WSN/33(H1N1) and a 10-fold reduction in recombinant A/Victoria/3/75(H3N2) and reduced growth capability in both viruses (*3*,*9*). However, its effect on pH1N1 virus has not been reported. During our 2023–24 surveillance, we detected a PA I38N mutant pH1N1 virus in a 14-year-old patient not treated with baloxavir. Here, we report the in vitro characterization of the PA I38N mutant pH1N1 virus.

The Study

In March 2024, we detected a pH1N1 virus with the PA I38N substitution (A/Yamagata/103/2024) in Yamagata, Japan. During the 2023–24 season, H3N2 viruses predominated in Japan, followed by pH1N1 and B/Victoria-lineage viruses. In Yamagata, we collected 137 pH1N1, 206 H3N2, and 135 B/Victoria-lineage viruses during the 2023–24 season (Figure 1).

A 14-year-old patient experienced influenza symptom onset on March 12, 2024, including a high

Author affiliations: National Institute of Infectious Diseases, Tokyo, Japan (E. Takashita, H. Morita, S. Nagata, S. Fujisaki, H. Miura, N. Kishida, K. Nakamura, M. Shirakura, S. Watanabe, H. Hasegawa); Yamagata Prefectural Institute of Public Health, Yamagata, Japan (T. Ikeda, K. Komabayashi, M. Sasaki, Y. Matoba, T. Takahashi, N. Ogawa, K. Mizuta); Ito Clinic, Yamagata (S. Ito)

DOI: https://doi.org/10.3201/eid3105.241123

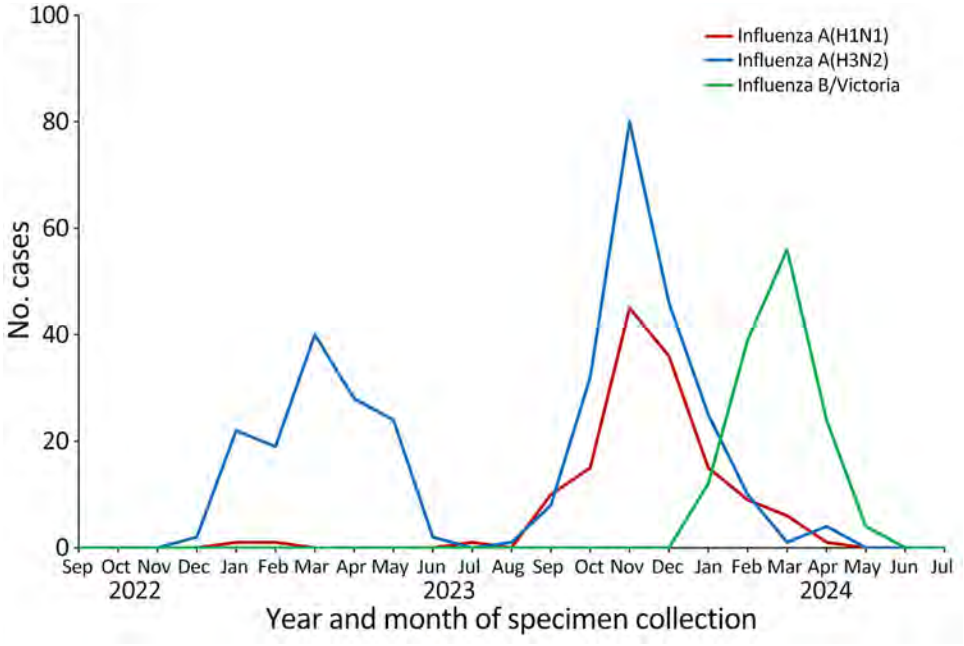

Figure 1. Detection of influenza viruses in Yamagata, Japan, during the 2022–23 and 2023–24 influenza seasons (n = 619). Monthly reports of influenza virus detection by the National Epidemiologic Surveillance of Infectious Diseases (https://www.niid.go.jp/niid/en/survaillance-data-table-english.html) were used for study of influenza A(H1N1)pdm09 virus with reduced susceptibility to baloxavir. Clinical specimens were collected from outpatients who had influenza or influenza-like illness diagnosed.

fever and upper respiratory tract infection. A nasal swab specimen was collected on the day of symptom onset. The patient had not received any influenza antiviral drugs before specimen collection. An influenza outbreak occurred at the school attended by the patient, and a class in a different grade was closed on March 13, 2024. No other specimens from the outbreak were available. Ethical approval was not required because this study used data obtained through routine surveillance.

Deep sequencing analysis performed by using MiSeq (Illumina, https://www.illumina.com) showed that the PA I38N substitution was present at 100% frequency in both the specimen from the patient and the virus isolate. We did not detect any amino acid substitutions associated with reduced inhibition by neuraminidase (NA) inhibitors.

We assessed the susceptibility of the PA I38N mutant and representative pH1N1 viruses, including a PA I38T mutant virus isolated in Yamagata, to baloxavir acid (Funakoshi Co., Ltd., https://www.funakoshi.co.jp) and 4 NA inhibitors approved in Japan: oseltamivir acid (active metabolite of oseltamivir), peramivir, zanamivir, and laninamivir (MedChemExpress, https://www.medchemexpress.com). We determined antiviral drug susceptibilities by using a focus reduction assay (*10*) and a fluorescence-based NA inhibition assay (NA-Fluor Influenza Neuraminidase Assay Kit; Invitrogen, https://www.thermofisher.com/us/en/home/brands/invitrogen.html) and calculated 50% effective concentration (EC_{50}) and 50% inhibitory concentration (IC_{50}) values by using GraphPad Prism (GraphPad Software, https://www.graphpad.com). To interpret the antiviral drug

Table 1. Antiviral drug susceptibilities of influenza A(H1N1)pdm09 viruses, Japan, 2024*

Influenza virus	GISAID isolate ID	PA substitution	Specimen collection	Baloxavir† (fold-change)	NA inhibitors‡ (fold-change)			
					Oseltamivir	Peramivir	Zanamivir	Laninamivir
A/Yamagata/103/2024	19183931	I38N	2024 Mar 12	388.20 (90)	0.21 (0.9)	0.11 (1.4)	0.43 (1.1)	0.52 (0.9)
A/Yamagata/333/2023	19045749	I38T	2023 Dec 15	929.18 (216)	0.26 (1.1)	0.08 (1.0)	0.32 (0.8)	0.44 (0.8)
A/Yamagata/122/2023	18744526	None	2023 Sep 21	4.05 (0.9)	0.23 (1.0)	0.08 (1.0)	0.46 (1.2)	0.70 (1.2)
A/Yamagata/127/2023	18744528	None	2023 Oct 2	5.38 (1.3)	0.22 (1.0)	0.08 (1.0)	0.44 (1.2)	0.70 (1.2)
A/Yamagata/135/2023	18799184	None	2023 Oct 15	6.08 (1.4)	0.24 (1.0)	0.08 (1.0)	0.43 (1.1)	0.71 (1.3)
A/Yamagata/177/2023	18853702	None	2023 Nov 4	6.69 (1.6)	0.22 (1.0)	0.06 (0.8)	0.25 (0.7)	0.36 (0.6)
A/Yamagata/292/2023	18987233	None	2023 Dec 4	5.15 (1.2)	0.22 (1.0)	0.09 (1.1)	0.35 (0.9)	0.52 (0.9)
A/Yamagata/312/2023	18987234	None	2023 Dec 11	5.05 (1.2)	0.22 (1.0)	0.11 (1.4)	0.38 (1.0)	0.49 (0.9)
A/Yamagata/336/2023	19045750	None	2023 Dec 15	6.47 (1.5)	0.23 (1.0)	0.09 (1.1)	0.30 (0.8)	0.42 (0.7)
A/Yamagata/104/2024	19201115	None	2024 Mar 27	4.32 (1.0)	0.28 (1.2)	0.09 (1.1)	0.33 (0.9)	0.50 (0.9)

*Influenza A(H1N1)pdm09 for 2023–24 was 4.30 ± 2.38 (n = 214) for baloxavir and 0.23 ± 0.06 (n = 208) for oseltamivir, 0.08 ± 0.02 (n = 208) for peramivir, 0.38 ± 0.12 (n = 208) for zanamivir, and 0.56 ± 0.14 (n = 208) for laninamivir. EC_{50}, 50% effective concentration; fold-change, fold-change in EC_{50} and IC_{50} values compared with the median values of 2023–24 seasonal pH1N1 viruses isolated in Japan; GISAID, GISAID EpiFlu database (http://www.gisaid.org); IC_{50}, 50% inhibitory concentration; NA, neuraminidase; PA, polymerase acidic protein.
†Mean EC_{50}, nmol/L. Mean EC_{50} values of triplicate reactions in a single run were determined by using a focus reduction assay.
‡Mean IC_{50}, nmol/L. Mean IC_{50} values of duplicate reactions in a single run were determined by using a fluorescence-based NA inhibition assay.

susceptibility, we applied the criteria proposed by the World Health Organization Expert Working Group on Surveillance of Influenza Antiviral Susceptibility for the Global Influenza Surveillance and Response System (*11*,*12*) by using EC_{50} and IC_{50} fold-change values compared with the median values of pH1N1 viruses isolated during the 2023–24 season in Japan. The criteria for NA inhibitor susceptibility define inhibition of NA activity of influenza A virus as normal (<10-fold increase), reduced (10- to 100-fold increase), or highly reduced (>100-fold increase) (*11*). For baloxavir susceptibility, the provisional criteria define influenza virus susceptibility as normal (≤3-fold increase) or reduced (>3-fold increase) (*12*). The PA I38N and PA I38T mutant viruses showed normal inhibition by all 4 NA inhibitors, but PA I38N exhibited 90-fold higher EC_{50} values and PA I38T exhibited 216-fold higher EC_{50} values to baloxavir compared with the median EC_{50} value of 2023–24 seasonal pH1N1 viruses isolated in Japan (Table 1). Those results indicate that the PA I38N and PA I38T substitutions reduce the susceptibility of pH1N1 virus to baloxavir in vitro.

We then evaluated the effect of the PA I38N substitution on pH1N1 virus growth in vitro (Figure 2) by infecting humanized MDCK cells with the PA I38N mutant or its corresponding wild-type virus at a multiplicity of infection of 0.001 focus-forming units per cell. The wild-type A/Yamagata/336/2023 virus had the most closely related sequences to the PA I38N mutant A/Yamagata/103/2024 virus (Table 2). However, no reports have indicated that those substitutions affect viral replication. The PA I38N mutant virus grew less efficiently than the wild-type virus and showed substantially lower virus titers at all time points. Those results indicated that the PA I38N substitution may negatively affect pH1N1 virus growth in vitro.

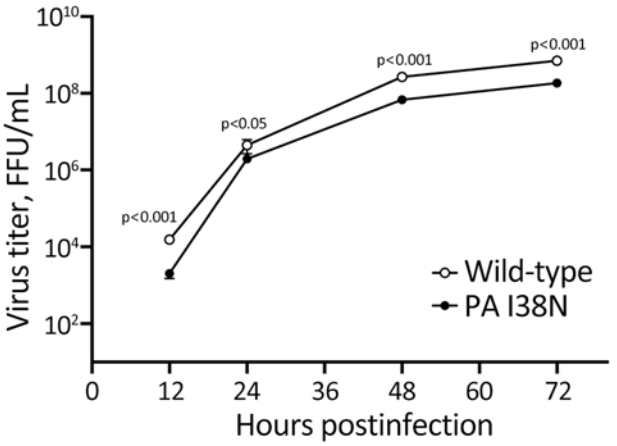

Figure 2. In vitro growth kinetics of the polymerase acidic I38N mutation from study of influenza A(H1N1)pdm09 virus with reduced susceptibility to baloxavir, Japan, 2024. Humanized MDCK cells were infected with the polymerase acidic I38N mutant virus (A/Yamagata/103/2024) or its corresponding wild-type virus (A/Yamagata/336/2023) at a multiplicity of infection of 0.001 focus-forming units per cell. The supernatants were harvested at the indicated times and virus was titrated by using a focus assay. Means (circles) and SDs (error bars) of 4 experiments are shown. p values were calculated by using a *t*-test and fitting a mixed-effects model. FFU, focus-forming units; PA, polymerase acidic.

Conclusions

In this study, we showed that the PA I38N mutant pH1N1 virus had reduced susceptibility to baloxavir but remained susceptible to NA inhibitors. Our results indicate that the PA I38N substitution in the pH1N1 virus contributed to a reduction in baloxavir susceptibility, but the reduction in susceptibility was less than that caused by the PA I38T substitution (*3*,*9*).

PA I38 is highly conserved in influenza A and B viruses (*1*). During October 2023–March 2024, medical institutions that serve ≈3.7 million persons in Japan received baloxavir to use for antiviral treatment. The PA I38N substitution may negatively affect the growth capability of the virus in vitro; however, our findings suggest possible transmission of the PA I38N mutant pH1N1 virus from another host harboring the mutant virus, which may have emerged under the selective pressure of baloxavir or as a result of a rare spontaneous mutation.

In Japan, influenza activity was low throughout the COVID-19 pandemic; the first influenza outbreak occurred in the 2022–23 season (*13*). The influenza outbreak in the 2023–24 season was larger than that of 2022–23 (Figure 1). Influenza pH1N1 virus activity peaked in November 2023 and then declined. The PA I38N mutant pH1N1 virus in this study was detected in March 2024. By March, the pH1N1 outbreak was almost over, and no regional spread of the PA I38N mutant pH1N1 virus was observed.

Table 2. Amino acid differences in influenza A(H1N1)pdm09 viruses with reduced susceptibility to baloxavir, Japan, 2024*

	PA			PB1			PB2			HA		NA		NS1
Influenza virus	38	258	531	617	622	661	152	308	649	6	274	51	383	178
A/Yamagata/103/2024	N	E	K	D	G	T	S	I	I	V	V	E	T	I
A/Yamagata/333/2023	T	E	R	N	G	A	A	V	V	I	M	K	T	V
A/Yamagata/336/2023	I	K	R	D	R	A	A	V	V	V	M	K	I	V

*HA, hemagglutinin; NA, neuraminidase; NS1, nonstructural protein 1; PA, polymerase acidic protein; PB1, polymerase basic protein 1; PB2, polymerase basic protein 2.

We reported a community cluster of influenza A(H3N2) viruses with reduced susceptibility to baloxavir caused by a PA E199G substitution in Japan in February–March 2023 (*13*). In addition, researchers reported widespread community clusters of pH1N1 viruses with cross-resistance to oseltamivir and peramivir in Australia and Japan (*14*,*15*). Monitoring of antiviral drug susceptibility of influenza viruses is necessary to aid public health planning and clinical recommendations for antiviral drug use.

Acknowledgments

We thank members of the Influenza Virus Surveillance Group of Japan for virus isolation and identification. We also thank Aya Sato, Miki Akimoto, and Hiromi Sugawara for technical assistance and Susan Watson for scientific editing.

This work was supported by grants-in-aid for emerging and reemerging infectious diseases from the Ministry of Health, Labour and Welfare, Tokyo, Japan (grant nos. 21HA2003 and 24HA2005).

About the Author

Dr. Takashita is a virologist with the National Institute of Infectious Diseases, Tokyo, Japan. Her research interests include antiviral drug susceptibilities of influenza viruses.

References

1. Omoto S, Speranzini V, Hashimoto T, Noshi T, Yamaguchi H, Kawai M, et al. Characterization of influenza virus variants induced by treatment with the endonuclease inhibitor baloxavir marboxil. Sci Rep. 2018;8:9633. https://doi.org/10.1038/s41598-018-27890-4
2. Uehara T, Hayden FG, Kawaguchi K, Omoto S, Hurt AC, De Jong MD, et al. Treatment-emergent influenza variant viruses with reduced baloxavir susceptibility: impact on clinical and virologic outcomes in uncomplicated influenza. J Infect Dis. 2020;221:346–55. https://doi.org/10.1093/infdis/jiz244
3. Ince WL, Smith FB, O'Rear JJ, Thomson M. Treatment-emergent influenza virus polymerase acidic substitutions independent of those at I38 associated with reduced baloxavir susceptibility and virus rebound in trials of baloxavir marboxil. J Infect Dis. 2020;222:957–61. https://doi.org/10.1093/infdis/jiaa164
4. Ison MG, Hayden FG, Hay AJ, Gubareva LV, Govorkova EA, Takashita E, et al. Influenza polymerase inhibitor resistance: assessment of the current state of the art—a report of the ISIRV antiviral group. Antiviral Res. 2021;194:105158. https://doi.org/10.1016/j.antiviral.2021.105158
5. Takashita E. Influenza polymerase inhibitors: mechanisms of action and resistance. Cold Spring Harb Perspect Med. 2021;11:a038687. https://doi.org/10.1101/cshperspect.a038687
6. Imai M, Yamashita M, Sakai-Tagawa Y, Iwatsuki-Horimoto K, Kiso M, Murakami J, et al. Influenza A variants with reduced susceptibility to baloxavir isolated from Japanese patients are fit and transmit through respiratory droplets. Nat Microbiol. 2020;5:27–33. https://doi.org/10.1038/s41564-019-0609-0
7. Takashita E, Ichikawa M, Morita H, Ogawa R, Fujisaki S, Shirakura M, et al. Human-to-human transmission of influenza A(H3N2) virus with reduced susceptibility to baloxavir, Japan, February 2019. Emerg Infect Dis. 2019;25:2108–11. https://doi.org/10.3201/eid2511.190757
8. Takashita E, Kawakami C, Ogawa R, Morita H, Fujisaki S, Shirakura M, et al. Influenza A(H3N2) virus exhibiting reduced susceptibility to baloxavir due to a polymerase acidic subunit I38T substitution detected from a hospitalised child without prior baloxavir treatment, Japan, January 2019. Euro Surveill. 2019;24:1900170. https://doi.org/10.2807/1560-7917.ES.2019.24.12.1900170
9. Hashimoto T, Baba K, Inoue K, Okane M, Hata S, Shishido T, et al. Comprehensive assessment of amino acid substitutions in the trimeric RNA polymerase complex of influenza A virus detected in clinical trials of baloxavir marboxil. Influenza Other Respir Viruses. 2021;15:389–95. https://doi.org/10.1111/irv.12821
10. Takashita E, Morita H, Ogawa R, Nakamura K, Fujisaki S, Shirakura M, et al. Susceptibility of influenza viruses to the novel cap-dependent endonuclease inhibitor baloxavir marboxil. Front Microbiol. 2018;9:3026. https://doi.org/10.3389/fmicb.2018.03026
11. World Health Organization. Meetings of the WHO working group on surveillance of influenza antiviral susceptibility—Geneva, November 2011 and June 2012. Wkly Epidemiol Rec. 2012;87:369–74.
12. Govorkova EA, Takashita E, Daniels RS, Fujisaki S, Presser LD, Patel MC, et al. Global update on the susceptibilities of human influenza viruses to neuraminidase inhibitors and the cap-dependent endonuclease inhibitor baloxavir, 2018–2020. Antiviral Res. 2022;200:105281. https://doi.org/10.1016/j.antiviral.2022.105281
13. Takashita E, Fujisaki S, Morita H, Nagata S, Miura H, Matsuura Y, et al. A community cluster of influenza A(H3N2) virus infection with reduced susceptibility to baloxavir due to a PA E199G substitution in Japan, February to March 2023. Euro Surveill. 2023;28:2300501. https://doi.org/10.2807/1560-7917.ES.2023.28.39.2300501
14. Hurt AC, Hardie K, Wilson NJ, Deng YM, Osbourn M, Leang SK, et al. Characteristics of a widespread community cluster of H275Y oseltamivir-resistant A(H1N1)pdm090 influenza in Australia. J Infect Dis. 2012;206:148–57. https://doi.org/10.1093/infdis/jis337
15. Takashita E, Kiso M, Fujisaki S, Yokoyama M, Nakamura K, Shirakura M, et al. Characterization of a large cluster of influenza A(H1N1)pdm09 viruses cross-resistant to oseltamivir and peramivir during the 2013–2014 influenza season in Japan. Antimicrob Agents Chemother. 2015;59:2607–17. https://doi.org/10.1128/AAC.04836-14

Address for correspondence: Emi Takashita, National Institute of Infectious Diseases, Gakuen 4-7-1, Musashimurayama, Tokyo 208-0011, Japan; email: emitaka@niid.go.jp

High Prevalence of Influenza D Virus Infection in Swine, Northern Ireland

Paula Lagan, Ken Lemon

We detected influenza D virus in multiple swine herds in Northern Ireland. Whole-genome sequencing showed several circulating genotypes and novel mutations in the receptor-binding site and esterase domains of the hemagglutinin-esterase fusion protein. Transmission routes of influenza D virus to swine remain to be clarified but could be direct or indirect.

Cattle are the main reservoir of influenza D virus (IDV) worldwide, although the virus is occasionally detected in other species, including swine (*1*). In Europe, surveillance for IDV in swine has either failed to detect the virus by molecular methods or detected the virus at low prevalence, at ≤5.6% at the herd level (*2*). Cattle in Northern Ireland have previously tested positive for IDV (*3*). Here, we describe detection of IDV in multiple swine herds from Northern Ireland and report on the genetic characterization of the swine-origin IDV strains.

The Study

Veterinarians visited 17 swine breeding units, composed of a mixture of farrow-to-wean and farrow-to-finish operations, during January–May 2023. The farms were involved in an ongoing regional control program for porcine reproductive and respiratory syndrome virus (PRRSV) that targeted 10- to 12-week-old pigs according to the PRRSV testing algorithm (https://www.cafre.ac.uk/wp-content/uploads/2023/10/Area-Regional-Control-Final-Report.pdf) for growing pigs. In addition to serum samples for PRRSV testing, 30 nasal swab samples per unit were obtained from the same cohort of growing pigs and tested for the presence of influenza A virus (IAV) and IDV by real-time reverse transcription PCR (rRT-PCR), as previously described (*4*,*5*). Serum samples were sent to a commercial diagnostics company (aCare Lab, https://acarelab.com) for determination of PRRSV status by rRT-PCR and open reading frame 5 gene sequencing. Farms were sampled on 1 occasion, except for farm 2170, which was originally sampled in February and resampled in May at the request of the farmer because of a deteriorating clinical situation.

Samples from 7 units (41.2% of herds) tested positive for IDV and had sample positivity of 10%–93% (Figure 1, panel A). Farm 2170 tested positive for IDV at both timepoints. Associated rRT-PCR cycle thresholds ranged from 17.4 to 36.9 (median 28.0) (Figure 1, panel B). The highest rates of sample positivity were 93% for farm 2163 and 50% for farm 2170; the lowest average cycle thresholds were 28.4 for farm 2163 and 25.1 for farm 2170. Four of 7 IDV-positive farms were also positive for IAV, and 3 of 7 were positive for a field strain of PRRSV (Table). Although clinical signs such as coughing and fever were not recorded at the time of sampling, we retrospectively asked producers whose farms tested positive for IDV about the clinical situation on the farm. Three farms (2160, 2163, 2170) reported increased death and slow growth, 3 (2155, 2156, 2166) reported no overt clinical signs, and no response was received from 1 farm (2179) (Table). A follow-up investigation with the attending veterinarians revealed that 5 of the positive farms (2160, 2163, 2168, 2170, 2179) also kept cattle, whereas 2 farms (2155, 2156) were swine-only farms. Cattle grazed in pastures adjacent to the IDV-positive swine-only units, and ≥1 worker on each swine unit also worked on the nearby cattle farms. Five of the IDV-positive units were located in a swine-dense region, within a 5.5-km radius (2160, 2163, 2168, 2156, 2170), whereas 2 farms were outside that region: 29

Author affiliation: Veterinary Sciences Division, Agri-Food and Biosciences Institute, Belfast, Northern Ireland

DOI: https://doi.org/10.3201/eid3105.241948

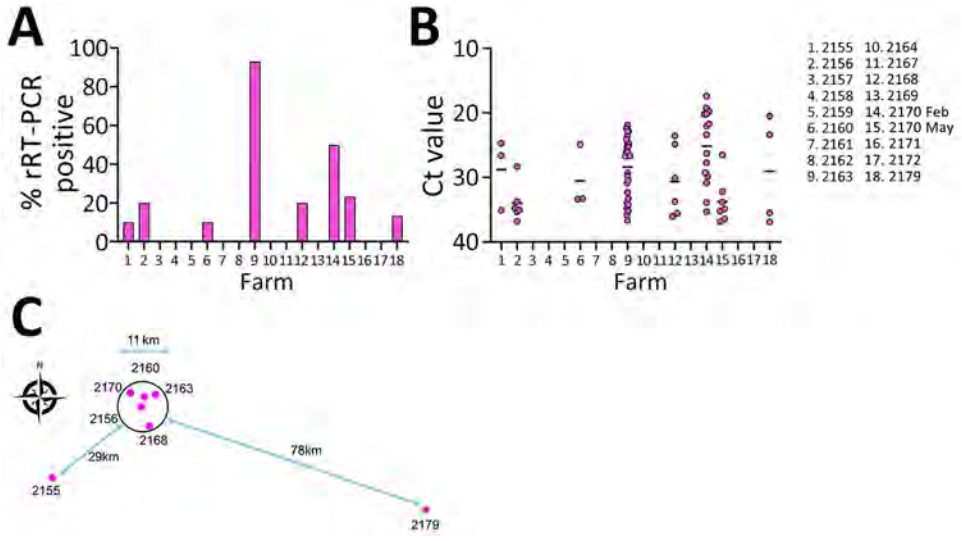

Figure 1. Molecular detection of influenza D virus (IDV) infection in swine, Northern Ireland. A) Percentage of nasal swab samples (n = 30) collected from 10- to 12-week-old growing pigs testing positive for IDV RNA by rRT-PCR. B) Plot of Ct values for IDV-positive rRT-PCR nasal swab samples per farm. Horizonal lines indicate mean Ct values. C) Locations and proximity of IDV-positive swine units. Ct, cycle threshold; rRT-PCR, real-time reverse transcription PCR.

km to the southwest (farm 2155) and 78 km to the southeast (farm 2179) (Figure 1, panel C; Appendix, https://wwwnc.cdc.gov/EID/article/31/5/24-1948-App1.pdf).

We compared hemagglutinin-esterase fusion (HEF) amino acid sequences from swine-origin IDV from Northern Ireland with cattle isolate D/bovine/Northern_Ireland/24280/2017 and noted the substitutions (Figure 2). We used amino acid numbering, as previously described, after removal of the first 16 N-terminal residues (*6*). We determined the degree of conservation at each substituted position by alignment of all 169 publicly available sequences (Appendix).

We mapped the location of the amino acid substitutions in the HEF protein structure onto a homology model of D/bovine/Northern_Ireland/24280/2017 HEF (Figure 3). Swine-origin strains differed from the bovine sequence at 5 positions around the receptor binding site. Of those positions, 3 were at highly conserved positions: G194R/K, I270M, and K276R. We only detected substitutions at 270 and 276 in samples from farm 2160, whereas we detected G194R/K in samples from 3 farms (2156, 2163, 2170).

Table. Co-infection status, clinical signs, and links to cattle of sampled farms showing high prevalence of influenza D virus infection in swine, Northern Ireland*

Farm no.	Farm type	IAV status (type)	IDV status	PRRSV status (strain)	Clinical signs	Multispecies farm
2155	Farrow-to-finish	Negative	Positive	Negative	None	Cattle graze beside unit, and 1 worker works on cattle farm
2156	Farrow-to-finish	Positive (untyped)	Positive	Negative	None	Cattle graze beside unit, and 1 worker works on cattle farm
2157	Farrow-to-finish	Inconclusive	Negative	Negative	Unknown	No cattle
2158	Farrow-to-wean	Negative	Negative	Negative	Unknown	Extended family keeps cattle
2159	Farrow-to-finish	Negative	Negative	Inconclusive	Unknown	Dairy cattle on farm
2160	Farrow-to-finish	Positive (H1N2)	Positive	Positive (field strain)	Death and slow growth	Unspecified cattle on farm
2161	Farrow-to-finish	Negative	Negative	Positive (field strain)	Unknown	Extended family keeps cattle
2162	Farrow-to-finish	Positive (pH1N1)	Negative	Negative	Unknown	Dairy cattle on farm
2163	Farrow-to-wean	Negative	Positive	Positive (field strain)	Death and slow growth	Unspecified cattle on farm
2164	Farrow-to-finish	Inconclusive	Negative	Positive (field strain)	Unknown	No cattle
2167	Farrow-to-finish	Positive (untyped)	Negative	Positive (field strain)	Unknown	Beef cattle on farm
2168	Farrow-to-finish	Negative	Positive	Negative	None	Unspecified cattle on farm
2169	Farrow-to-finish	Negative	Negative	Negative	Unknown	Beef cattle on farm
2170	Farrow-to-wean	Positive (H1N2)	Positive	Positive (field strain)	Death and slow growth	Unspecified cattle on farm
2171	Farrow-to-finish	Negative	Negative	Negative	Unknown	Dairy cattle on farm
2172	Farrow-to-finish	Negative	Negative	Negative	Unknown	Beef cattle on farm
2179	Farrow-to-finish	Positive (untyped)	Positive	Negative	Unknown	Unspecified cattle on farm

*IAV, influenza A virus; IDV, influenza D virus; PRRSV, porcine reproductive and respiratory syndrome virus.

Swine-origin strains also differed from the bovine sequence at 2 positions around the esterase domain at the highly conserved positions A68V and A324S. We only detected substitutions at 68 in samples from farm 2163, whereas we detected A324S in samples from 3 farms (2160, 2168, 2179).

Conclusions

Interspecies transmission from cattle, followed by some host adaptation and intraspecies spread, most likely initiates swine infection by IDV (*7*,*8*). Previous detection of IDV in swine have been associated with sample positivity rates mostly <1% (*2*). Combined with the low prevalence of IDV at the herd level, that positivity rate suggests intraspecies transmission is limited in swine.

The organization of the agricultural sector in Northern Ireland may partly explain the high prevalence of IDV shown in our study. Multispecies farms containing both cattle and pigs are common and increase the likelihood of multiple IDV spillover events from cattle reservoirs. Indeed, phylogenetic analysis of swine-origin IDV in Northern Ireland identified several distinct genotypes, supporting the idea of repeated introductions from cattle (Appendix). However, the high rate of sample positivity observed on some farms is indicative of efficient pig-to-pig transmission. Furthermore, the continued detection of IDV on 1 farm (2170), 3 months after the initial detection, may represent continuous circulation of the virus within the herd. Those findings provide preliminary evidence for efficient adaptation of IDV to swine hosts and establishment within those populations. In addition, our data suggest that spread between farms might be a factor contributing to the high herd-level prevalence observed. The close genetic relatedness of some IDV strains isolated from both neighboring and geographically distant farms may indicate both local (direct) and long-distance (indirect) spread. Although common sources of indirect spread such as contaminated service vehicles should be considered, we must also consider cattle movements as a possible source of spread between swine units.

The molecular basis of IDV host adaptation has yet to be determined but likely includes changes that affect receptor binding. The receptor binding site in the IDV HEF protein is in a shallow cavity surrounded by secondary structure elements from the 170, 190, and 270 loops and the 230 helix (*6*). Substitutions in those secondary structure elements have the potential

Isolate name	HEF amino acid position																	
	31	40	68	147	165	172	194	212	220	260	270	273	276	292	324	369	393	394
D/bovine/NI/24280/2017	E	T	A	R	T	A	G	T	N	M	I	V	K	R	A	S	K	D
D/swine/NI/2168-27/2023										I					S		R	N
D/swine/NI/2168-29/2023										I					S		R	N
D/swine/NI/2179-26/2023					K					I					S		R	N
D/swine/NI/2179-28/2023					K					I					S		R	N
D/swine/NI/2160-28/2023										I	M		R		S		R	N
D/swine/NI/2160-29/2023										I	M		R		S		R	N
D/swine/NI/2155-15/2023						T			S			A				N	R	
D/swine/NI/2155-27/2023						T			S			A				N	R	
D/swine/NI/2163-09/2023		I	V			T	R							K			R	
D/swine/NI/2163-17/2023		I	V			T	R							K			R	
D/swine/NI/2156-02/2023				K	K	T	R	K									R	
D/swine/NI/2156-07/2023				K	K	T	R	K									R	
D/swine/NI/2170-22/2023	K			K	K	T	K	K									R	
D/swine/NI/2170-23/2023	K			K	K	T	K	K									R	

Figure 2. Amino acid substitutions in swine-origin influenza D virus HEF protein relative to bovine-origin influenza D virus, Northern Ireland. Changes relative to the bovine-origin sequence are displayed. Amino acid numbering is according to Song et al. (*6*). Substitutions occurring at the receptor-binding site and esterase are highlighted with red text on a blue background. Sequence conservation at each position is indicated by logo generated at WebLogo (https://weblogo.berkeley.edu/logo.cgi) (bottom) on the basis of alignment of 169 influenza D virus sequences. HEF, hemagglutinin-esterase fusion; NI, Northern Ireland.

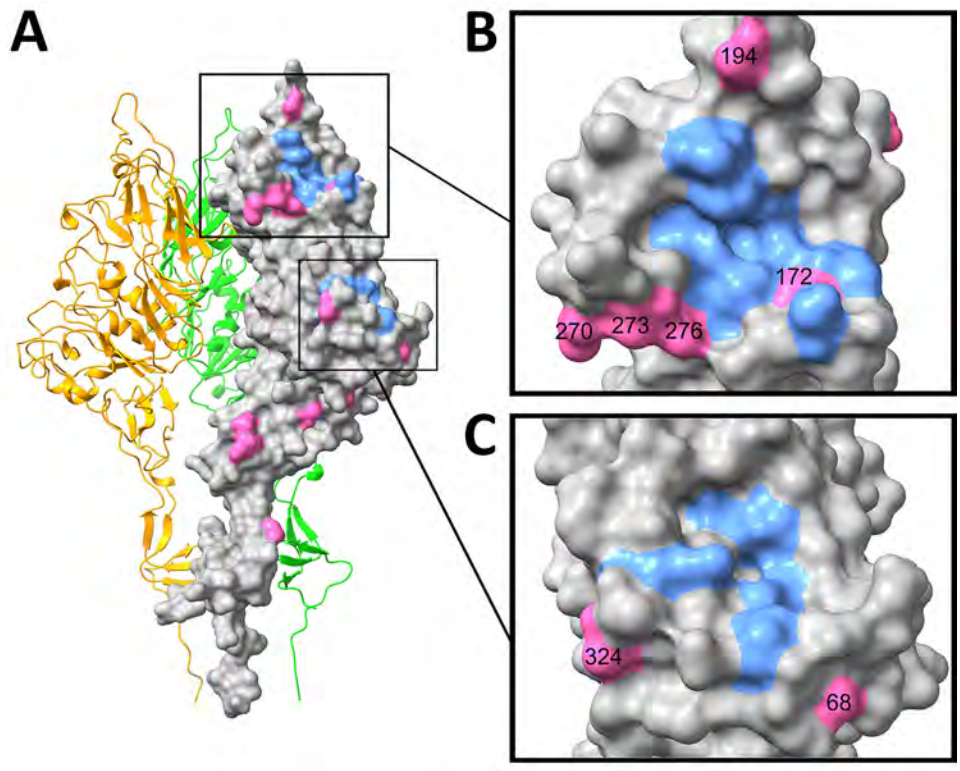

Figure 3. Locations of amino acid substitutions in swine-origin influenza D virus HEF protein structure, for high prevalence of influenza D virus infection in swine, Northern Ireland. A) Homology model of D/bovine/Northern_Ireland/24280/2017 hemagglutinin-esterase fusion protein generated with Swiss-Model (https://swissmodel.expasy.org) by using the structure of D/swine/Oklahoma/1334/2011 (https://doi.org/10.2210/pdb5e64/pdb) as a template. B) Close-up of receptor-binding site. C) Close-up of esterase. Homology model was annotated in ChimeraX version 1.8 (https://www.cgl.ucsf.edu/chimerax). Blue indicates receptor-binding site (F127, T171, A172, S173, W185, F229, Y231, T239, F240, V273, V275, F297) and esterase (S57, G85, N117, R326, D356, H359) residues. Pink indicates residues substituted in swine-origin isolates.

to modify receptor binding activity. For example, the open channel between the 230 helix and 270 loop is thought to enable broad cell tropism of IDV. Substitutions in those elements in the related influenza C virus HEF close that channel and restrict broad cell tropism (*6*). Candidate swine adaptations A236V and R268K have been previously identified after likely cattle-to-pig transmission (*7*), and L100F was observed after experimental infection of swine with a bovine-origin IDV isolate (*9*). In our study, we identified several additional candidates in both the receptor binding site and esterase. Of particular interest is mutation of G194 to a basic residue (R or K). Sequences from farms with the highest sample positivity rates (2163 and 2170) contained that mutation, and phylogenetic analysis indicated that strains from those farms were only distantly related and therefore seem to have independently converged on that adaptation. However, multiple routes to swine adaptation for IDV are likely, and alternative substitutions, such as the 270–273–276 triplet and the esterase changes at positions 68 and 324, should be examined further. Researchers should validate the proposed swine adaptive mutations, including receptor binding analysis and experimental transmission studies. Transmission routes of IDV to swine remain to be clarified but could be direct (e.g., contact with infected cattle) or indirect (e.g., contaminated vehicles).

Acknowledgments

We thank the swine producers and veterinarians from Northern Ireland for their support.

About the Author

Dr. Lemon is a researcher in the Mammalian Virology Unit at the Agri-Food and Bioscience Institute in Northern Ireland. His research interests include the molecular epidemiology of animal influenza viruses.

References

1. Kwasnik M, Rola J, Rozek W. Influenza D in domestic and wild animals. Viruses. 2023;15:2433. https://doi.org/10.3390/v15122433
2. Gaudino M, Chiapponi C, Moreno A, Zohari S, O'Donovan T, Quinless E, et al. Evolutionary and temporal dynamics of emerging influenza D virus in Europe (2009–22). Virus Evol. 2022;8:veac081. https://doi.org/10.1093/ve/veac081
3. Dane H, Duffy C, Guelbenzu M, Hause B, Fee S, Forster F, et al. Detection of influenza D virus in bovine respiratory disease samples, UK. Transbound Emerg Dis. 2019;66:2184–7. https://doi.org/10.1111/tbed.13273
4. Hause BM, Ducatez M, Collin EA, Ran Z, Liu R, Sheng Z, et al. Isolation of a novel swine influenza virus from Oklahoma in 2011 which is distantly related to human influenza C viruses. PLoS Pathog. 2013;9:e1003176. https://doi.org/10.1371/journal.ppat.1003176
5. Lagan P, Hamil M, Cull S, Hanrahan A, Wregor RM, Lemon K. Swine influenza A virus infection dynamics and

evolution in intensive pig production systems. Virus Evol. 2024;10:veae017. https://doi.org/10.1093/ve/veae017
6. Song H, Qi J, Khedri Z, Diaz S, Yu H, Chen X, et al. An open receptor-binding cavity of hemagglutinin-esterase-fusion glycoprotein from newly identified influenza D virus: basis for its broad cell tropism. PLoS Pathog. 2016;12:e1005411. https://doi.org/10.1371/journal.ppat.1005411
7. Gorin S, Richard G, Hervé S, Eveno E, Blanchard Y, Jardin A, et al. Characterization of influenza D virus reassortant strain in swine from mixed pig and beef farm, France. Emerg Infect Dis. 2024;30:1672–6. https://doi.org/10.3201/eid3008.240089
8. Kaplan BS, Falkenberg S, Dassanayake R, Neill J, Velayudhan B, Li F, et al. Virus strain influenced the interspecies transmission of influenza D virus between calves and pigs. Transbound Emerg Dis. 2021;68:3396–404. https://doi.org/10.1111/tbed.13943
9. Gorin S, Richard G, Quéguiner S, Chastagner A, Barbier N, Deblanc C, et al. Pathogenesis, transmission, and within-host evolution of bovine-origin influenza D virus in pigs. Transbound Emerg Dis. 2024;2024:9009051. https://doi.org/10.1155/2024/9009051

Address for correspondence: Ken Lemon, Veterinary Sciences Division, Agri-Food and Biosciences Institute, Stormont Stoney Road, Belfast BT4 3SD, Northern Ireland; email: kenneth.lemon@afbini.gov.uk

Recent and Forecasted Increases in Coccidioidomycosis Incidence Linked to Hydroclimatic Swings, California, USA

Simon K. Camponuri,[1] Alexandra K. Heaney,[1] Gail Sondermeyer Cooksey, Duc J. Vugia, Seema Jain, Daniel L. Swain, John Balmes, Justin V. Remais, Jennifer R. Head

In 2023, California reported near–record high coccidioidomycosis cases after a dramatic transition from drought to heavy precipitation. Using an ensemble model, we forecasted 12,244 cases statewide during April 1, 2024–March 31, 2025, a 62% increase over cases reported 2 years before and on par with cases reported during April 2023–March 2024.

Incidence of coccidioidomycosis, an emerging infectious disease caused by *Coccidioides* spp. fungi, has increased dramatically since 2000 (*1*). In 2023, California, USA, reported a near-record 9,054 coccidioidomycosis cases (only surpassed by 9,093 cases in 2019). During April 2023–March 2024, a period capturing the full seasonal rise and fall in incidence, California reported 10,519 cases, 39% higher than the same period the previous year (*2*).

The 2023 spike in incidence might be attributable, in part, to a swing from extreme drought to heavy precipitation during winter 2022–2023. Transitions from dry to wet years have been linked to increased coccidioidomycosis incidence (*3*,*4*). Soil moisture during wet winters is hypothesized to support fungal growth, contributing to an abundance of spores available for airborne dispersal during hot, dry conditions characteristic of summer and early fall (*3*). Drought preceding rainy seasons might enhance fungal growth by eliminating microbial competitors from soils (*5*) or by affecting rodent populations, a putative reservoir host and nutrient source for the fungus (*6*). During 2020–2022, California experienced severe drought (*7*). An unusually wet winter followed in 2022–2023; statewide precipitation exceeded 150% of average, among the top 10 wettest seasons in the past century (*7*). Statewide precipitation during the 2023–2024 wet season was 115% of the long-term average, marking the second consecutive wetter-than-average season after a severe drought (*7*). That pattern suggested high coccidioidomycosis incidence might continue throughout the 2024 transmission year. We developed a disease forecast to guide public health alerts and messages by pinpointing when and where disease risk is expected to be highest. Such targeted messaging can raise awareness about disease risk, leading to earlier diagnosis and more effective disease management (*8*).

The Study

We adapted our previously published ensemble prediction model relating monthly reported cases per census tract to climatologic or environmental predictors (Appendix Table 1, https://wwwnc.cdc.gov/EID/article/31/5/24-1338-App1.pdf) (*3*). Using a progressive time-series cross validation approach (Appendix Figure 1), we examined how each of 5 candidate algorithms performed when forecasting future out-of-sample cases and calculated an ensemble weight for each candidate model as proportional to the inverse of each model's mean out-of-sample prediction error (Appendix Table 2) (*9*). We fit separate models

Author affiliations: University of California, Berkeley, California, USA (S.K. Camponuri, J. Balmes, J.V. Remais); University of California, San Diego, California, USA (A. K. Heaney); California Department of Public Health, Richmond, California, USA (G.S. Cooksey, D.J. Vugia); San Francisco Department of Public Health, San Francisco, California, USA (S. Jain); University of California Agriculture and Natural Resources, Davis, California, USA (D.L. Swain); University of California, Los Angeles, California, USA (D.L. Swain); NSF National Center for Atmospheric Research, Boulder, Colorado, USA (D.L. Swain); University of California, San Francisco (J. Balmes); University of Michigan, Ann Arbor, Michigan, USA (J.R. Head)

DOI: https://doi.org/10.3201/eid3105.241338

[1]These authors contributed equally to this article.

for each county (for highly endemic regions) or region (for low to moderately endemic regions) to account for spatial differences in the effects of precipitation and temperature on coccidioidomycosis incidence (Appendix Figure 2). Within random forest models, temperature had high variable importance in forecasting cases in wetter, coastal regions, whereas precipitation had high importance in the drier Central Valley (Appendix Figure 3). Those results align with previous findings and emphasize the role of wet periods for fungal growth and hot, dry periods for spore dispersal (*3*).

To forecast coccidioidomycosis cases, we applied each model to temperature and precipitation data from January 2023–March 2024 and extrapolated temperature and precipitation data through March 2025 (*10*). We generated future temperature and precipitation estimates beyond April 2024 (the date of analysis) by extrapolating historical monthly temperature averages in each census tract using a 42-year linear trend (1981–2023) and by setting precipitation to the 50th percentile of the 42-year precipitation distribution (*10*). Because future climate is unknown, we examined the sensitivity of forecasts to 2 alternative precipitation scenarios, drier-than-average (20th percentile) and wetter-than-average (80th percentile), and 2 temperature scenarios, warmer-than-average (+3°F) and cooler-than-average (−3°F). We fit each model to data from January 1, 2000–December 31, 2022, and created an ensemble forecast of cases for each month during January 1, 2023–March 31, 2025, by taking the weighted average of each model's forecast. We summed cases across calendar years and the coccidioidomycosis transmission year (*2*), which spans April 1 of 1 year to March 31 of the next. To quantify uncertainty in our forecasts, we generated 90% prediction intervals (PIs) using a 2-step bootstrapping process (Appendix Figure 4). All analyses were conducted in R v.4.3.2 (The R Project for Statistical Computing, https://www.r-project.org).

Our ensemble forecast model predicted 11,846 cases (90% PI 11,261–12,505) in California during April 1, 2023–March 31, 2024, closely matching the preliminary state report of 10,519 (Figure 1) (*2*). The reported number of monthly cases in California in 2023 peaked at 1,462, aligning with our model forecast of 1,619 (90% PI 1,410–1,745). Our forecast model predicted the highest case counts in the Southern San Joaquin Valley, Southern Coast, and Central Coast (Table, Figure 2). Although our model slightly overpredicted cases in these regions, our predictions aligned with the relative magnitude of cases across regions (Appendix Table 3).

Our model forecasted 12,244 cases (90% PI 11,579–12,964) statewide during April 1, 2024–March 31, 2025, a 62% increase over the transmission year 2 years before. The Southern San Joaquin Valley (5,399 [90% PI 4,993–5,902] cases), Southern Coast (3,322 [90% PI 3,172–3,494] cases), and Central Coast (1,207 [90% PI 1,071–1,378] cases) were expected to have the largest number of

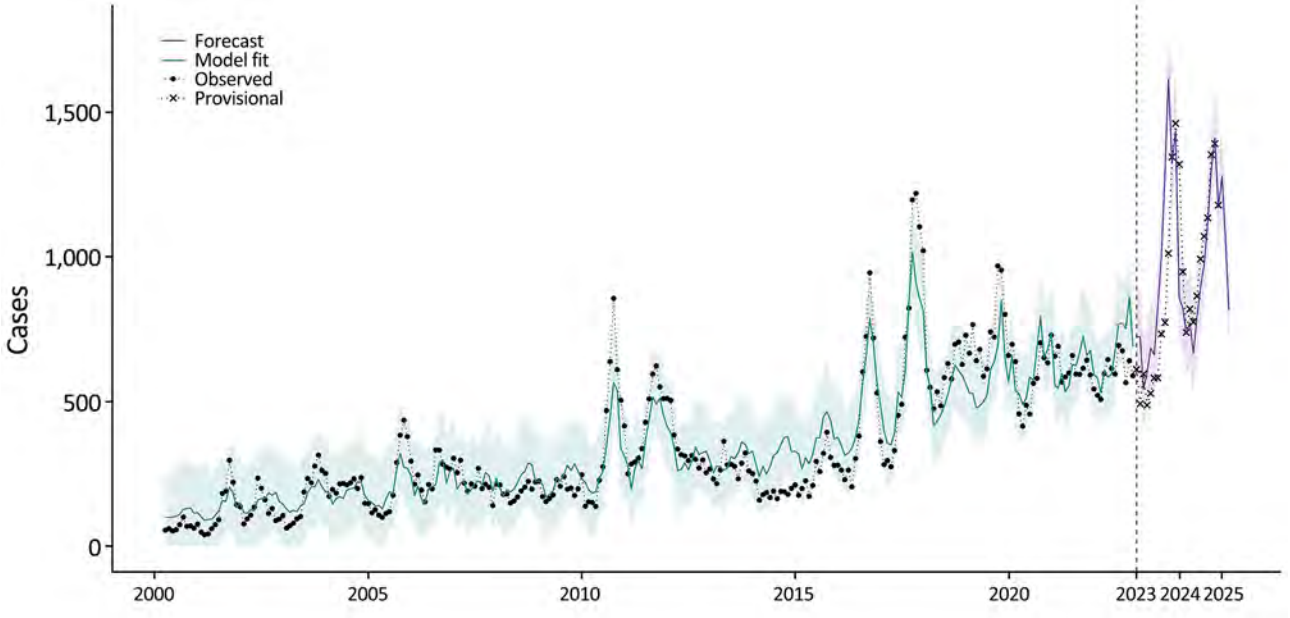

Figure 1. Statewide monthly coccidioidomycosis cases, January 1, 2000–March 31, 2025, in study of recent and forecasted increases in coccidioidomycosis incidence linked to hydroclimatic swings, California, USA. Black dots indicate confirmed cases reported during 2000–2022, times symbols indicate the provisional cases reported during January 1, 2023–December 31, 2024, the green line represents the ensemble model fit to the observed case data (R^2 = 0.87), and the purple line indicates the ensemble model predicted (April 1, 2023–March 31, 2024) and forecasted (April 1, 2024–March 31, 2025) cases. Shading represents 90% prediction intervals.

Table. Region-level forecasted incident cases for the 2023 (April 2023–March 2024) and 2024 (April 2024–March 2025) transmission years in study of recent and forecasted increases in coccidioidomycosis incidence linked to hydroclimatic swings, California, USA*

Region	2023 forecasted (90% PI)	2024 forecasted (90% PI)
Bay Area	529 (482–589)	558 (512–610)
Central Coast	1,189 (1,025–1,400)	1,207 (1,071–1,378)
Eastern California	42 (30–76)	49 (32–82)
Northern California	32 (22–43)	28 (19–38)
Northern San Joaquin Valley	605 (515–703)	811 (696–924)
Southern Coast	3,049 (2,875–3,269)	3,322 (3,172–3,494)
Southern Inland	694 (625–770)	725 (658–797)
Southern San Joaquin Valley	5,557 (5,084–6,182)	5,399 (4,993–5,902)
Southern Sacramento Valley	149 (120–542)	147 (120–255)
Statewide	11,846 (11,224–12,456)	12,244 (11,638–12,917)

*PI, prediction interval.

infections (Table; Figure 2). Our model forecasted pronounced seasonality in disease incidence (Figure 2), with incidence beginning to rise in June and peaking in November at 1,411 (90% PI 1,267–1,587) cases statewide, 98% higher than the 2022 peak (714) and nearly as high as the 2023 peak (1,462). Forecasts were similar under alternative climate scenarios in the forecasted period (Figure 3), suggesting that previous climate conditions are a larger driver of incidence than concurrent climate. Forecasts were robust to model specifications that modeled year as a natural spline and removed collinear predictors (Appendix Table 4).

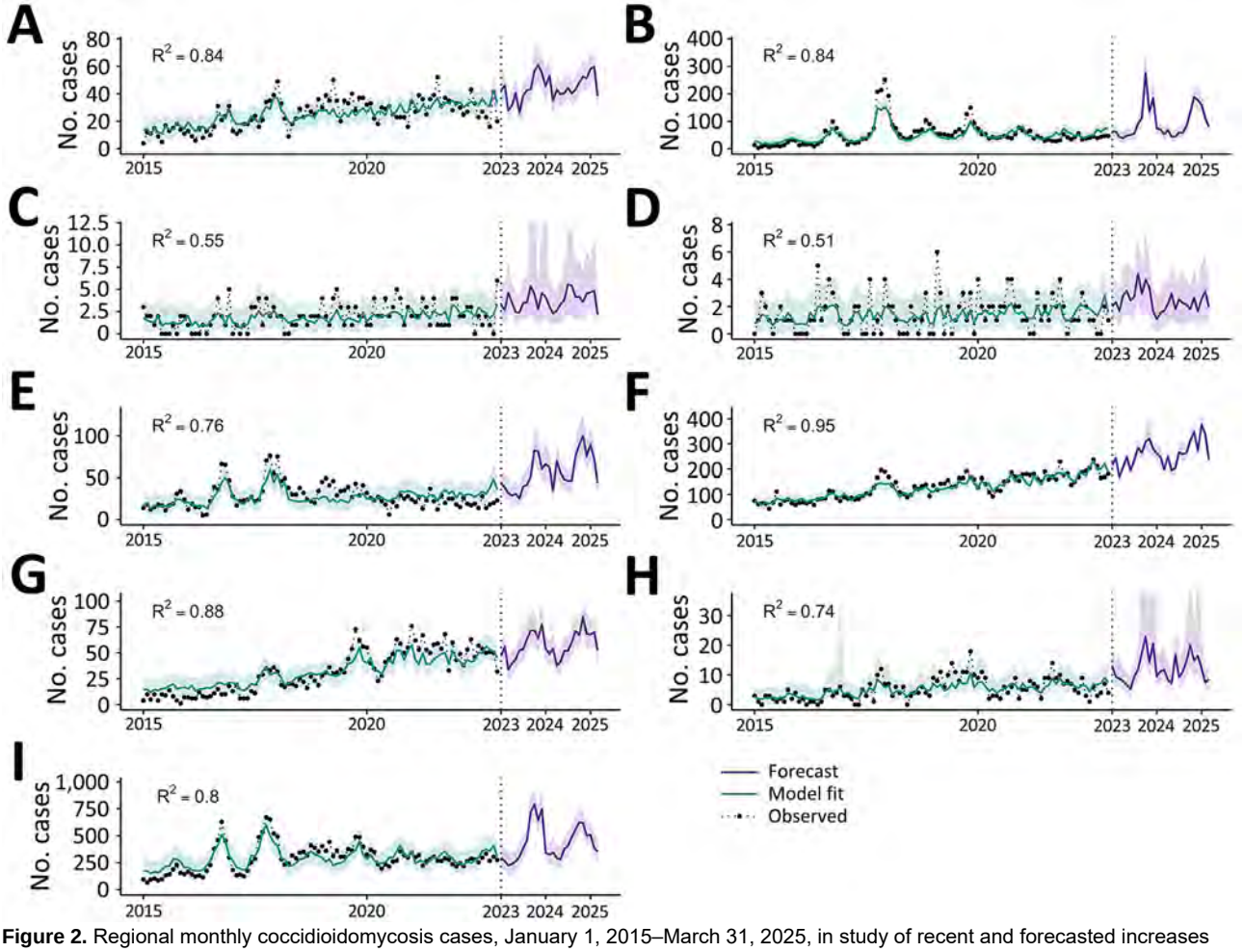

Figure 2. Regional monthly coccidioidomycosis cases, January 1, 2015–March 31, 2025, in study of recent and forecasted increases in coccidioidomycosis incidence linked to hydroclimatic swings, California, USA. A) Bay Area; B) Central Coast; C) Eastern California; D) Northern California; E) Northern San Joaquin Valley; F) Southern Coast; G) Southern Inland; H) Southern Sacramento Valley; I) Southern San Joaquin Valley. Black dots indicate confirmed cases reported during 2015–2022, green line represents the ensemble model fit to the observed case data, and the purple line indicates the ensemble model predicted (April 1, 2023–March 31, 2024) and forecasted (April 1, 2024–March 31, 2025) cases during April 1, 2023–March 31, 2025. Shading represents 90% prediction intervals.

Conclusions

Predictive models that forecast disease risk can provide public health officials and healthcare providers with information about timing, location, and magnitude of future disease risk (*8*). Our forecast of high incidence after a swing from extreme drought to heavy precipitation aligns with previous work showing an association between coccidioidomycosis incidence and transitions from anomalously dry to wet years (*3*). Climate change is altering the hydroclimate of California and adjacent regions, with implications for coccidioidomycosis (*11*,*12*). Although changes in average precipitation in California are likely to be modest (*13*), precipitation variability will likely increase considerably (*14*), including increasingly large and frequent swings between high and low precipitation conditions from season to season and between years, a phenomenon known as precipitation whiplash (*12*).

Risk for *Coccidioides* exposure is likely to be highest in the dry summer and fall months; drier soil leads to more dust and the release of *Coccidioides* spores. Reported cases typically lag pathogen exposure by 1–2 months, aligning with the observed peak of cases around November (*15*). However, risk for infection persists year-round. To prevent exposure, persons in regions where coccidioidomycosis is endemic and emerging should avoid dust where possible, practice dust suppression, and consider using N95 masks

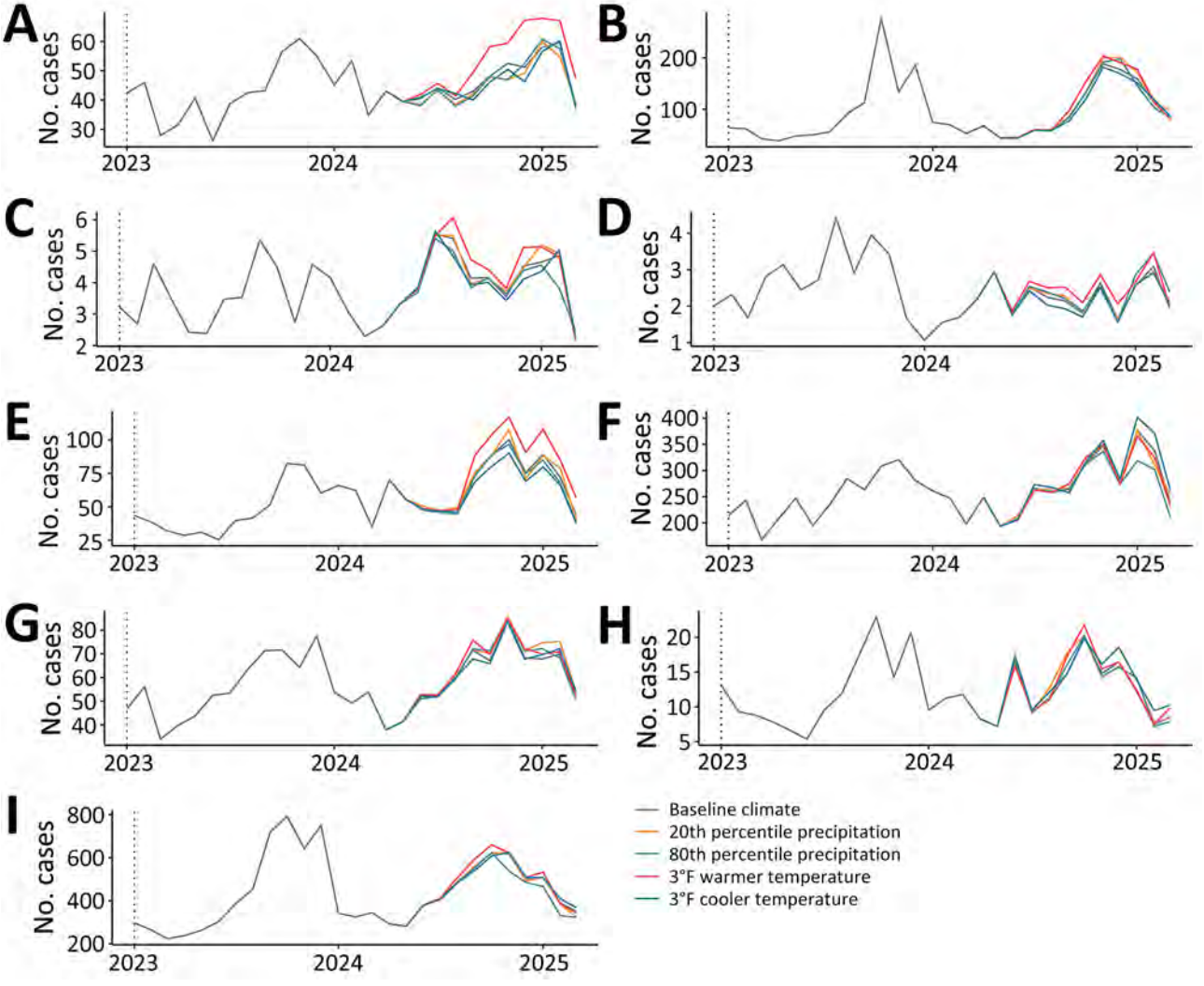

Figure 3. Forecasted regional monthly coccidioidomycosis cases during January 1, 2023–March 31, 2025, under varying future climates in 2024–2025 in study of recent and forecasted increases in coccidioidomycosis incidence linked to hydroclimatic swings, California, USA. A) Bay Area; B) Central Coast; C) Eastern California; D) Northern California; E) Northern San Joaquin Valley; F) Southern Coast; G) Southern Inland; H) Southern Sacramento Valley; I) Southern San Joaquin Valley. The baseline climate scenario represents the 50th percentile of precipitation during 1981–2023 and extrapolated monthly average temperatures assuming a 42-year linear trend. The 20th and 80th percentile precipitation scenarios assume the baseline temperature scenario, and the 3°F warmer or cooler temperature scenarios assume the baseline precipitation scenario (i.e., 50th percentile).

when disturbing soil. Clinicians should consider coccidioidomycosis when evaluating a patient with respiratory illness who has spent time in an endemic or emerging region, particularly those who are unresponsive to antibiotics, who had exposure to dust or dirt, or whose symptoms last >1–2 weeks.

This analysis is subject to exposure misclassification because case data were aggregated to disease onset, which lags exposure, and census tract of patient residence, which might not represent exposure location. Climate conditions in the forecasted period are uncertain; however, forecasts were similar under the alternate climate scenarios examined. Future work might consider using seasonal climate predictions from large ensemble climate models. Our forecasts cannot account for stochastic point source outbreaks that might lead to anomalously high case counts in certain regions. Continued collaborative work might focus on developing an accurate coccidioidomycosis forecasting system that can be integrated into public health practice in California and other endemic regions.

This article was originally published as a preprint at https://www.medrxiv.org/content/10.1101/2024.08.30.24312858v1.

Research reported in this manuscript was supported by the National Institute of Allergy and Infectious Diseases (NIAID) of the National Institutes of Health under award numbers R01AI148336, R01AI176770, and K01AI173529. The content is solely the responsibility of the authors and does not necessarily represent the official views of the National Institutes of Health.

The findings and conclusions in this article are those of the authors and do not necessarily represent the views or opinion of the California Department of Public Health or the California Health and Human Services Agency.

About the Author

Mr. Camponuri is a PhD candidate in environmental health sciences at the University of California, Berkeley, School of Public Health. His research focuses on how environmental change influences the dynamics of coccidioidomycosis in California. Dr. Heaney is an assistant professor at the Herbert Wertheim School of Public Health at the University of California, San Diego. Her research combines epidemiology and computational sciences to understand the relationships between climate variability and human disease.

References

1. Sondermeyer Cooksey GL, Nguyen A, Vugia D, Jain S. Regional analysis of coccidioidomycosis incidence—California, 2000–2018. MMWR Morb Mortal Wkly Rep. 2020;69:1817–21. https://doi.org/10.15585/mmwr.mm6948a4
2. Nguyen A, Sondermeyer Cooksey G, Djamba Y. Coccidioidomycosis. California provisional monthly report, January–July 2024. Sacramento (California): California Department of Public Health; 2024.
3. Head JR, Sondermeyer-Cooksey G, Heaney AK, Yu AT, Jones I, Bhattachan A, et al. Effects of precipitation, heat, and drought on incidence and expansion of coccidioidomycosis in western USA: a longitudinal surveillance study. Lancet Planet Health. 2022;6:e793–803. https://doi.org/10.1016/S2542-5196(22)00202-9
4. Heaney AK, Camponuri SK, Head JR, Collender P, Weaver A, Sondermeyer Cooksey G, et al. Coccidioidomycosis seasonality in California: a longitudinal surveillance study of the climate determinants and spatiotemporal variability of seasonal dynamics, 2000–2021. Lancet Reg Health Am. 2024;38:100864. https://doi.org/10.1016/j.lana.2024.100864
5. Greene DR, Koenig G, Fisher MC, Taylor JW. Soil isolation and molecular identification of *Coccidioides immitis*. Mycologia. 2000;92:406–10. https://doi.org/10.1080/00275514.2000.12061175
6. Taylor JW, Barker BM. The endozoan, small-mammal reservoir hypothesis and the life cycle of Coccidioides species. Med Mycol. 2019;57(Supplement_1):S16–20. https://doi.org/10.1093/mmy/myy039
7. National Centers for Environmental Information, National Oceanic and Atmospheric Administration. Climate at a glance [cited 2024 May 15]. https://www.ncei.noaa.gov/access/monitoring/climate-at-a-glance/statewide
8. California Department of Public Health. Potential increased risk for Valley fever expected [press release]. August 1, 2023 [cited 2024 Jul 1]. https://www.cdph.ca.gov/Programs/OPA/Pages/NR23-023.aspx
9. Bergmeir C, Benítez JM. On the use of cross-validation for time series predictor evaluation. Information Sciences. 2012;191:192–213. https://doi.org10.1016/j.ins.2011.12.028
10. PRISM Climate Group. PRISM climate data [cited 2024 Apr 10]. https://prism.oregonstate.edu
11. Diffenbaugh NS, Swain DL, Touma D. Anthropogenic warming has increased drought risk in California. Proc Natl Acad Sci U S A. 2015;112:3931–6. https://doi.org/10.1073/pnas.1422385112
12. Swain DL, Langenbrunner B, Neelin JD, Hall A. Increasing precipitation volatility in twenty-first-century California. Nature Clim Change. 2018;8:427–33. https://doi.org/10.1038/s41558-018-0140-y
13. Persad GG, Swain DL, Kouba C, Ortiz-Partida JP. Inter-model agreement on projected shifts in California hydroclimate characteristics critical to water management. Climatic Change. 2020;162:1493–513. https://doi.org/10.1007/s10584-020-02882-4
14. Wood RR, Lehner F, Pendergrass AG, Schlunegger S. Changes in precipitation variability across time scales in multiple global climate model large ensembles. Environmental Research Letters. 2021;16:084022.
15. Benedict K, Ireland M, Weinberg MP, Gruninger RJ, Weigand J, Chen L, et al. Enhanced surveillance for coccidioidomycosis, 14 US States, 2016. Emerg Infect Dis. 2018;24:1444–52. https://doi.org/10.3201/eid2408.171595

Address for correspondence: Jennifer R. Head, Department of Epidemiology, School of Public Health, University of Michigan, 1415 Washington Heights, Ann Arbor, MI 48109-2029, USA; email: jrhead@umich.edu

Clade Ia Monkeypox Virus Linked to Sexual Transmission, Democratic Republic of the Congo, August 2024

Jean-Claude Makangara-Cigolo,[1] Kelly-Michel Kenye,[1] Lygie Lunyanga, Daan Jansen, Eddy Kinganda-Lusamaki, Sifa Kavira, Adrienne Amuri-Aziza, Emile Malembi, Yvon Anta, Prince Akil-Bandali, Emmanuel Lokilo-Lofiko, Emmanuel Hasivirwe Vakaniaki, Sabin Sabiti Nundu, Elisabeth Pukuta-Simbu, Princesse Paku-Tshambu, Rilia Ola-Mpumbe, Raphael Lumembe-Numbi, Gabriel Kabamba-Lungenyi, Gradi Luakanda, Cris Kacita, Robert Shongo-Lushima, Dieudonné Mwamba, Áine O'Toole, Sydney Merritt, Megan Halbrook, Daniel Mukadi-Bamuleka, Nicole A. Hoff, Nicola Low, Isaac Bogoch, Muge Cevik, Gregg Gonsalves, Souradet Shaw, Lorenzo Subissi, Laurens Liesenborghs, Ahidjo Ayouba, Martine Peeters, Eric Delaporte, Sofonias Tessema, Anne W. Rimoin, Jean-Jacques Muyembe-Tamfum, Andrew Rambaut, Koen Vercauteren, Steve Ahuka-Mundeke, Jason Kindrachuk,[2] Tony Wawina-Bokalanga,[2] Placide Mbala-Kingebeni[2]

Several concurrent mpox outbreaks are ongoing in the Democratic Republic of the Congo. We report a case of severe clade Ia mpox in an adult woman with indeterminate HIV status who died 16 days after symptom onset. She self-identified as a sex worker and had spent time in the capital city, Kinshasa.

Mpox, a zoonotic viral disease caused by monkeypox virus (MPXV), is endemic in forested regions of central and western Africa. In recent years, disease burden has increased notably in mpox-endemic areas, alongside rapid geographic spread to nonendemic regions worldwide (*1*).

Historically, clade I mpox outbreaks have been predominantly driven by zoonotic transmission (*2*). In 2024, we reported a cluster of clade I mpox cases associated with sexual contact in Kwango Province, Democratic Republic of the Congo (DRC) (*3*). Although this outbreak subsided spontaneously, the emergence of clade Ib in eastern DRC has been

Author affiliations: Institut National de Recherche Biomédicale, Kinshasa, Democratic Republic of the Congo (J.-C. Makangara-Cigolo, K.-M. Kenye, L. Lunyanga, E. Kinganda-Lusamaki, S. Kavira, A. Amuri-Aziza, Y. Anta, P. Akil-Bandali, E. Lokilo-Lofiko, E. Hasivirwe Vakaniaki, S. Sabiti Nundu, E. Pukuta-Simbu, P. Paku-Tshambu, R. Ola-Mpumbe, R. Lumembe-Numbi, G. Kabamba-Lungenyi, G. Luakanda, D. Mukadi-Bamuleka, J.-J. Muyembe-Tamfum, S. Ahuka-Mundeke, T. Wawina-Bokalanga, P. Mbala-Kingebeni); Cliniques Universitaires de Kinshasa, Université de Kinshasa, Kinshasa (J.-C. Makangara-Cigolo, K.-M. Kenye, E. Kinganda-Lusamaki, R. Lumembe-Numbi, G. Kabamba-Lungenyi, D. Mukadi-Bamuleka, J.-J. Muyembe-Tamfum, S. Ahuka-Mundeke, T. Wawina-Bokalanga, P. Mbala-Kingebeni); University of Bern, Bern, Switzerland (J.-C. Makangara-Cigolo, N. Low); Institute of Tropical Medicine, Antwerp, Belgium (D. Jansen, E. Hasivirwe Vakaniaki, L. Liesenborghs, K. Vercauteren, T. Wawina-Bokalanga); TransVIHMI, Université de Montpellier, INSERM, IRD, Montpellier, France (E. Kinganda-Lusamaki, A. Ayouba, M. Peeters, E. Delaporte); Hemorrhagic Fever and Monkeypox Program, Ministry of Health, Kinshasa (E. Malembi, R. Shongo-Lushima); Institut National de Santé Publique (INSP), Kinshasa (C. Kacita, D. Mwamba); Institute of Ecology and Evolution, University of Edinburgh, Edinburgh, Scotland, UK (A. O'Toole, A. Rambaut); Jonathan and Karin Fielding School of Public Health, University of California, Los Angeles, CA, USA (S. Merritt, M. Halbrook, N.A. Hoff, A.W. Rimoin); Toronto General Hospital, University Health Network, Toronto, Ontario, Canada (I. Bogoch); University of St. Andrews, St. Andrews, Scotland, UK (M. Cevik); Yale School of Public Health, New Haven, Connecticut, USA (G. Gonsalves); University of Manitoba, Winnipeg, Manitoba, Canada (S. Shaw, J. Kindrachuk); World Health Organization, Geneva, Switzerland (L. Subissi); KU Leuven, Leuven, Belgium (L. Liesenborghs); Africa Centers for Disease Control and Prevention, Addis Ababa, Ethiopia (S. Tessema)

DOI: https://doi.org/10.3201/eid3105.241690

[1]These authors contributed equally to this article.

[2]These authors jointly supervised this study.

Table. Laboratory results for patient with clade Ia monkeypox virus linked to sexual transmission, Democratic Republic of the Congo, August 2024

Laboratory test	Result (reference range)	Interpretation
Peripheral blood smear	1 to 10 trophozoites in 100 microscopic fields	Positive for malaria
Hemoglobin level	12 g/dL (10.5–13.5 g/dL)	Normal
Leukocytes	17,000 cells/μL (4,000–12,000 cells/μL)	Abnormal
Erythrocyte sedimentation	30 mm/h (<20 mm/h)	Abnormal

associated with sustained human-to-human transmission (*4*,*5*). In parallel, clade Ia MPXV, associated primarily with zoonotic transmission, has been responsible for most mpox cases in DRC during the current public health emergency and has spread rapidly across the country.

Genomic investigations of mpox cases in 2024 found clades Ia and Ib in Kinshasa Province, a large urban center with international connectivity (*6*). This situation raises concerns about the potential public health effects on zoonotic and nonzoonotic transmission of clade Ia. In this study, we describe a fatal case of mpox caused by clade Ia, suspected to have been acquired through sexual contact, in a woman returning to Kwango from Kinshasa. Samples were collected under routine mpox surveillance, exempt from ethical approval. The Ethics Committee of Kinshasa School of Public Health (ESP-UNIKIN, nos. ESP/CE/05/2023 and ESP/CE/47/2023) and the Health Research Ethics Board at the University of Manitoba (HS25837) approved data use for this publication.

The Study

A woman (>20 years of age) with no noteworthy known medical history was transferred from a local health center to a reference hospital because of generalized cutaneous pustule-like lesions that appeared in mid-2024. She had no history of smallpox vaccination. The patient self-identified as a sex worker and had recently returned from a 6-month stay in Kinshasa, where she had multiple casual sexual partners. She reported no recent contact with persons with confirmed or suspected mpox and no recent contact with wildlife. Her first symptom was fever, followed by vulval rash and itching, which began in Kinshasa. Acetaminophen, amoxicillin, and clotrimazole vaginal pessaries were given, but no diagnostic tests were performed. Observing no improvement 4 days after symptoms started, she returned home from Kinshasa by bus. She consulted a local health center 2 days later for fever, joint pain, and generalized cutaneous and genital lesions. She was admitted and treated with ceftriaxone, vitamin C, and cetirizine before transfer 3 days later by motorcycle to the reference hospital.

At admission, clinical examination revealed fever, joint tenderness, and generalized and genital pustular lesions. Suspecting mpox, the physician placed the patient in isolation. HIV rapid diagnostic test results in 2 different health facilities were discordant. The first test at the health center was negative using the Determine HIV-1/2 kit (Abbott, https://www.abbott.com). The second test, performed 3 days later at the hospital using Uni-Gold kit (Trinity Biotech, https://www.trintybiotech.com), returned a positive result. A PCR test for HIV was not performed (Table). She was treated with artemisinin-based combination therapy for malaria and antibiotic drugs (ceftriaxone followed by lincocin) and topical antiseptic solutions to prevent secondary bacterial infections arising from skin lesions. She also received oxygen therapy for signs of respiratory distress, acetaminophen for fever, and intravenous fluids for dehydration. Despite those interventions, the patient died 16 days after symptom onset.

A case investigation team from INRB (Institut National de Recherche Biomédicale) was mobilized during a monitoring and surveillance visit on the day the patient died. The patient was in respiratory distress and had lesions at varying stages of development, some with crusting, leading to a diagnosis of mpox complicated by acute respiratory distress syndrome. Counting lesions manually was not possible because of the generalized distribution and high number. Crust and vesicle swab samples were collected and sent to INRB for diagnosis. Mpox was confirmed by PCR using pan-orthopoxvirus and MPXV-generic primers (*7*,*8*). PCR results indicated amplification cycle threshold values of 16.08 in crust samples and 15.89 in vesicle samples for the pan-orthopoxvirus primers and cycle threshold values of 14.45 in crust samples and 15.80 in vesicle samples for the MPXV-generic primers (using the same samples).

After PCR confirmation, we performed whole-viral genome sequencing using the clade IIb tiling sequencing protocol (https://www.protocols.io/view/monkeypox-virus-multiplexed-pcr-amplicon-sequencin-5qpvob1nbl4o/v2) and prepared the library on the basis of the Illumina DNA Prep protocol. We loaded the final enriched libraries onto an Illumina iSeq100 (https:/www.illumina.com). We generated MPXV consensus genomes by processing FASTQ files using CZid pipeline (https://czid.org);

we used clade I MPXV genome (GenBank accession no. NC_003310.1) as reference. We used the Nextclade online tool (https://clades.nextstrain.org) to assign the clade of MPXV genomes. In addition, we used SQUIRREL to align sequences (https://github.com/aineniamh/squirrel) and inferred a maximum-likelihood phylogeny using IQ-TREE version 2.1.4 (https://github.com/Cibiv/IQ-TREE) with the Kimura 3-substitition plus empirical base frequencies plus invariant sites model as the best fit. Branch support was estimated by the ultrafast bootstrap approximation with 10,000 replicates (*9*). The phylogenetic tree showed that both sequences from the patient were closely related and cluster with clade Ia MPXV sequences from the ongoing outbreak in Kinshasa (Figure). This finding is consistent with severe mpox caused by clade Ia MPXV acquired during the patient's stay in Kinshasa.

As part of routine contact tracing, 37 contacts were identified: 10 family members, 4 healthcare workers, 20 friends, and 3 sexual partners; 19 were high-risk contacts. No clinical symptoms of mpox were identified among contacts after 21 days of follow-up.

Conclusions

This case report describes fatal mpox caused by clade Ia MPXV in a woman with indeterminate HIV test results and early onset of genital symptoms. This finding could represent HIV seroconversion syndrome in the context of mpox infection, given the history of sexual contacts, clinical symptoms, location of lesions, and discordant HIV test results. In this resource-limited setting, details from clinical examination and laboratory investigations were insufficient to exclude other comorbidities. A false-positive HIV test result is also possible, given the low prevalence of HIV in the general population (15–49 years of age) in the DRC (0.5%–0.7%) (*10*). HIV prevalence of 7.5% was estimated among the key population of sex workers in 2023 (*10*). Given that the sex worker population might

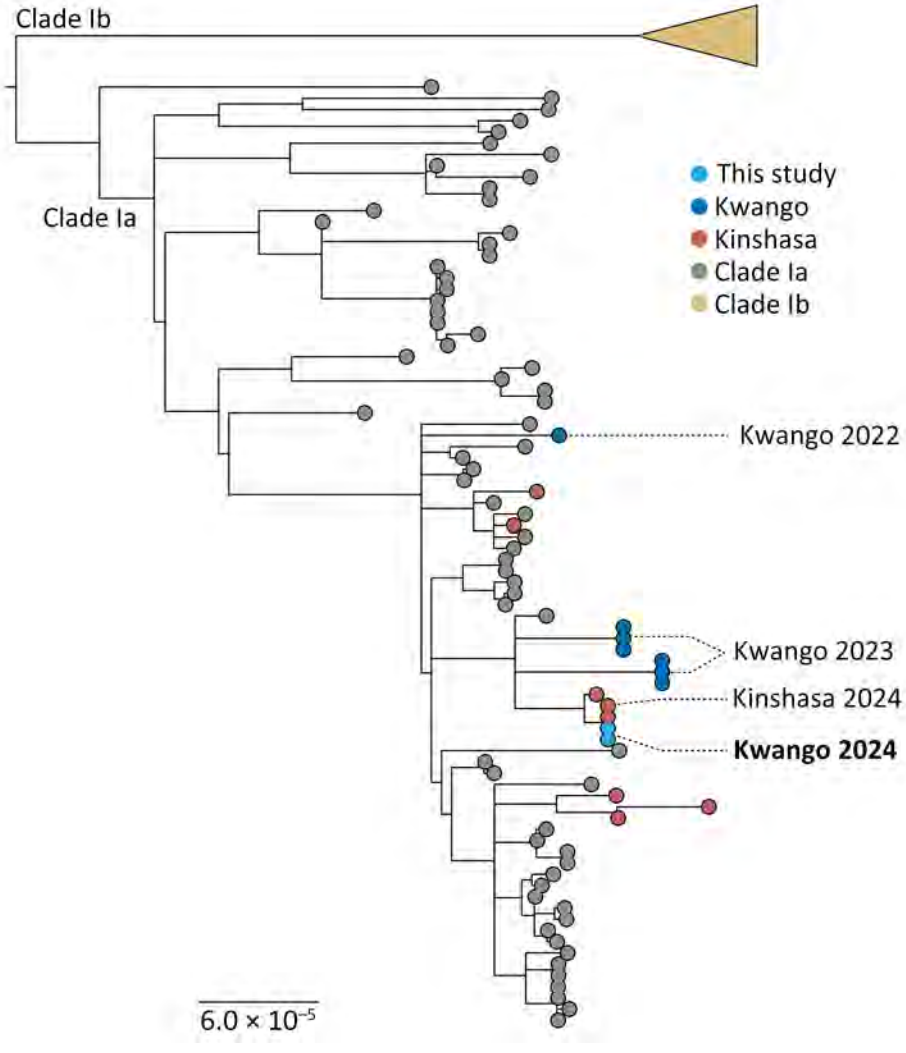

Figure. Phylogenetic tree of mpox virus sequences from patient with clade Ia mpox virus linked to sexual transmission and reference sequences, Democratic Republic of the Congo, August 2024.

be ≈1% in DRC (*11*), this group might be at risk for poor outcomes from mpox, especially if HIV testing rates are low (*12*). PCR testing confirmed the mpox diagnosis, and whole-viral genome sequencing identified clade Ia MPXV.

This report highlights the potential severity of mpox in DRC and the need to mobilize the community to mitigate spread. The patient was a sex worker and had lived in Kinshasa, from where we reported co-circulation of clades Ia and Ib MPXV during July–August 2024 (*6*). This fact underscores increasing concerns about the expansion of MPXV in DRC, including to a large urban center with extensive regional and international connections, and the changing epidemiology for clade I MPXV. Although MPXV transmission through sexual contact has been predominantly associated with clade Ib (*4*), this case of clade Ia MPXV infection might have been linked to sexual contact, as evidenced by presence of genital lesions. The findings are consistent with our previous report of a cluster of mpox cases associated with sexual contacts in Kwango Province, which also involved clade Ia (*3*).

In summary, this report highlights the importance of prompt diagnosis and public health intervention, specifically among high-risk groups, to prevent the spread of mpox, as well as early diagnosis and management of HIV infection. In regions where mpox is emerging, healthcare providers must maintain a high index of suspicion, particularly in patients with vesiculopustular rash and systemic symptoms.

Acknowledgments

We thank the Provincial Health Division of Kwango and the local team supporting the International Mpox Research Consortium activities, including Tshotsho Tshonaka Dixon, Seraphin Tseke, Lucien Lufutu, Judith Mayamba, Guillaume Nduka, and Mundos Mwayi. We also acknowledge all the staff of INRB, particularly those from the Virology Department and the Epidemiology and Global Health Department. We also gratefully acknowledge the support provided by the US Centers for Disease Control and Prevention Poxvirus and Rabies Branch (Division of High-Consequence Pathogens and Pathology, National Center for Emerging and Zoonotic Infectious Diseases) during the ongoing mpox public health emergency of international concern, as well as their historic support for mpox surveillance in the region.

The project or effort depicted is sponsored by the International Mpox Research Consortium through funding from the Canadian Institutes of Health Research and International Development Research Centre (grant no. 202209MRR-489062-MPX-CDAA-168421). Additional support was provided in part by the Department of Defense Threat Reduction Agency (HDTRA1-21-1-0040). This work is also supported by the US Department of Agriculture (Agriculture Research Service (Non-Assistance Cooperative Agreement no. 20230048, grant no. 58-3022-2-020). The content of the information does not necessarily reflect the position or the policy of the United States or Canada governments, and no official endorsement should be inferred. The Africa Pathogen Genomics Initiative helped acquiring and maintaining the sequencer; Agence Française de Développement through the AFROSCREEN project (grant agreement CZZ3209, coordinated by ANRS Maladies infectieuses émergentes in partnership with Institut de Recherche pour le Développement and Pasteur Institute) for laboratory support and PANAFPOX project funded by ANRS Maladies infectieuses émergentes; Belgian Directorate-general for Development Cooperation and Humanitarian Aid, the Department of Economy, Science, and Innovation of the Flemish government, the Research Foundation–Flanders (FWO, grant no. G096222 N to L.L.), and EDCTP grant no. 101195465 (MBOTE-SK); and US National Institute of Allergy and Infectious Diseases/National Institutes of Health grant no. U01AI151799 through Center for Research in Emerging Infectious Disease-East and Central Africa. We acknowledge the support of the Wellcome Trust (Collaborators Award 206298/Z/17/Z, ARTIC network) and the CIZD group. T.W.B. acknowledges funding from the European Union (FORTIFIEDx project under the Horizon Europe research and innovation programme and grant agreement no. 101092049). Views and opinions expressed are those of the author(s) only and do not necessarily reflect those of the European Union or the granting authority European Union's Horizon Europe research and innovation programme. Neither the European Union nor the granting authority can be held responsible for them.

J.K., T.W.B., and P.M.K. conceived, designed, and supervised the study. J.-C.M.-C., K.M.K., L.L., Y.A., S.K., D.J., E.K.L., A.A.A., E.M., P.A.B., E.L.L., R.L.N., G.K.L., G.L., J.J.M.T., S.A.M., T.W.B., and P.M.K. acquired the data. J.-C.M.-C., K.M.K., L.L., Y.A., S.K., D.J., E.K.L., S.K., A.A.A., E.M., P.A.B., E.L.L., E.H.V., S.S.N., E.P.S., P.P.T., R.O.M., R.L.N., G.K.L., G.L., Á.O., D.M.B., N.A.H., N.L., A.W.R., J.J.M.T., A.R., K.V., S.A.M., J.K., T.W.B., and P.M.K. analyzed and interpreted data. J.C.M.C. and K.M.K. wrote the first draft, and J.K., T.W.B., and P.M.K. reviewed that draft. J.C.M.C., K.M.K., L.L., S.K., D.J., E.K.L., S.K., A.A.A., E.M., Y.A., P.A.B., E.L.L., E.H.V., S.S.N., E.P.S., P.P.T., R.O.M., R.L.N., G.K.L., G.L., C.K., R.S.L., D.M., Á.O., S.M., M.H., D.M.B., N.A.H., N.L., L.S., L.L., A.A., M.P., E.D., S.T., A.W.R., J.J.M.T., A.R., K.V., S.A.M., J.K., T.W.B., and P.M.K. revised the submitted article.

About the Author

Dr. Makangara-Cigolo is a doctoral student at Graduate School of Cellular and Biomedical Sciences, University of Bern, Switzerland. His research interests include emerging and reemerging viral diseases with a focus on genome sequencing, bioinformatics, and public health interventions.

References

1. Alakunle E, Kolawole D, Diaz-Cánova D, Alele F, Adegboye O, Moens U, et al. A comprehensive review of monkeypox virus and mpox characteristics. Front Cell Infect Microbiol. 2024;14:1360586. https://doi.org/10.3389/fcimb.2024.1360586
2. Van Dijck C, Hoff NA, Mbala-Kingebeni P, Low N, Cevik M, Rimoin AW, et al. Emergence of mpox in the post-smallpox era—a narrative review on mpox epidemiology. Clin Microbiol Infect. 2023;29:1487–92.
3. Kibungu EM, Vakaniaki EH, Kinganda-Lusamaki E, Kalonji-Mukendi T, Pukuta E, Hoff NA, et al.; International Mpox Research Consortium. Clade I–associated mpox cases associated with sexual contact, the Democratic Republic of the Congo. Emerg Infect Dis. 2024;30:172–6. https://doi.org/10.3201/eid3001.231164
4. Vakaniaki EH, Kacita C, Kinganda-Lusamaki E, O'Toole Á, Wawina-Bokalanga T, Mukadi-Bamuleka D, et al. Sustained human outbreak of a new MPXV clade I lineage in eastern Democratic Republic of the Congo. Nat Med. 2024;30:2791–5.
5. Hoffmann C. Mpox-is there a more dangerous new clade? Lancet Infect Dis. 2024;24:e667.
6. Wawina-Bokalanga T, Akil-Bandali P, Kinganda-Lusamaki E, Lokilo E, Jansen D, Amuri-Aziza A, et al. Co-circulation of monkeypox virus subclades Ia and Ib in Kinshasa Province, Democratic Republic of the Congo, July to August 2024. Euro Surveill. 2024;29:2400592. https://doi.org/10.2807/1560-7917.ES.2024.29.38.2400592
7. Schroeder K, Nitsche A. Multicolour, multiplex real-time PCR assay for the detection of human-pathogenic poxviruses. Mol Cell Probes. 2010;24:110–3. https://doi.org/10.1016/j.mcp.2009.10.008
8. Li Y, Zhao H, Wilkins K, Hughes C, Damon IK. Real-time PCR assays for the specific detection of monkeypox virus West African and Congo Basin strain DNA. J Virol Methods. 2010;169:223–7. https://doi.org/10.1016/j.jviromet.2010.07.012
9. Hoang DT, Chernomor O, von Haeseler A, Minh BQ, Vinh LS. UFBoot2: improving the ultrafast bootstrap approximation. Mol Biol Evol. 2018;35:518–22. https://doi.org/10.1093/molbev/msx281
10. World Health Organization. Democratic Republic of the Congo HIV country profile 2023 [cited 2024 Oct 10]. https://cfs.hivci.org
11. UNAIDS. UNAIDS data 2022 [cited 2024 Oct 10]. https://www.unaids.org/en/resources/documents/2023/2022_unaids_data
12. Migaud P, Naidenow J, Ghaeni L, Hosmann K, Kaghoma J, Kowomba J, et al. Indicator-condition-guided HIV testing in rural DRC. Infection. 2024;52:1171–4.

Address for correspondence: Placide Mbala-Kingebeni, Institut National de Recherche Biomédicale, Department of Epidemiology and Global Health, Avenue de la Démocratie, Kinshasa/Gombe, B.P. 1197 Kinshasa 1, Democratic Republic of the Congo; email: mbalaplacide@gmail.com; Jason Kindrachuk, Department of Medical Microbiology & Infectious Diseases, Max Rady College of Medicine, 523-745 Bannatyne Ave, Winnipeg, MB R3E 0J9, Canada; email: jason.kindrachuk@umanitoba.ca

Napoleon Bonaparte—A Possible Case of Trench Fever

Éric Faure

Author affiliation: I2M–CNRS UMR 7373, Aix-Marseille University, Marseilles, France

DOI: http://doi.org/10.3201/eid3105.240970

In 1789, Napoleon Bonaparte reported having a recurrent febrile illness that initially subsided for 4 days and then had multiple relapses of similar duration. A speculative diagnosis of trench fever would be supported by poor hygiene conditions, prolonged exposure to cold, and the presence of lice in Napoleon's barracks environment.

Napoleon Bonaparte's health has been the subject of numerous retrospective studies. He has been thought to have had ≈40 individual diseases (*1*), and an additional disease should be added to that list. In January 1789, Bonaparte, who served at the Artillery School of Auxonne, France, wrote to his mother: "I have had attacks of persistent fever from time to time. The fever subsides for some four days and then relapses, lasting for about the same time again" (*2*).

Auxonne was notoriously malarious, and Bonaparte, who had already had intermittent fevers, attributed his illness to miasmas, noxious forms of "bad air" (*2*,*3*). However, the periodicity of his fevers would rather suggest a more likely diagnosis of trench fever, a disease caused by *Bartonella quintana*, a bacteria transmitted by infected human body lice. The fever pattern of trench fever is frequently characterized by episodes of fever lasting 4–5 days, with apyretic intervals of 4–5 days between each episode (*4*). The major predisposing risk factors for trench fever are poor hygiene, louse infestation, immune system compromise, and prolonged exposure to cold (*5*), all factors likely present at the time of Napoleon's correspondence. The winter of 1788–89 was extreme. Bonaparte had been ill during the summer of 1788 (*3*,*6*). In March 1789, Bonaparte wrote that he rarely changed his clothes, which was a habit he had practiced in the past (*3*). The presence of lice at the School of Auxonne was likely (*3*).

Trench fever was not recognized as a distinct clinical entity until 1915 (*7*). Nonetheless, analysis of DNA extracted from gravesites has provided evidence of human infection with *B. quintana* since at least 4,000 years ago (*8*). Researchers have identified *B. quintana* frequently in both barrack and field environments and have detected its DNA in mass graves of soldiers from the Napoleonic era in Vilnius, Lithuania, and in Kassel, Germany (*8*).

Retrospective diagnosis is always a precarious endeavor, particularly without DNA evidence. However, I believe that trench fever should be recognized as among the many ailments that befell Napoleon Bonaparte.

Acknowledgments

The author extends sincere thanks to the 2 anonymous reviewers whose comments and suggestions helped improve and clarify this Research Letter.

About the Author

Prof. Faure is a professor at the University of Aix-Marseille. He is an interdisciplinary biologist who researches, among other things, the conditions surrounding the appearance and decline of past epidemics in Europe. He also works on establishing the timeline for the emergence of malaria in various regions of Europe.

References

1. Murray JF. Napoleon—of what did he die? S Afr Med J. 1971;45:1005–9.
2. Kemble J. Napoleon immortal, The medical history and private life of Napoleon Bonaparte. Br J Surgery. 1960;47:454. https://doi.org/10.1002/bjs.18004720444
3. Cabanès A. At the emperor's bedside [in French]. Paris: Albin Michel; 1958.
4. Relman DA. Has trench fever returned? N Engl J Med. 1995;332:463–4. https://doi.org/10.1056/NEJM199502163320710
5. Minnick MF, Anderson BE. *Bartonella*. In: Tang YW, Sussman M, Liu D, Poxton I, Schwartzman J, editors. Molecular medical microbiology, second edition. London: Academic Press; 2015. p. 1911–39. https://doi.org/10.1016/C2010-1-67744-9
6. Bizouard JT. History of Auxonne's hospital (1374–1884) [in French]. Dijon, Frnace: H. Grigne; 1884. p. 158–63.
7. Anstead GM. The centenary of the discovery of trench fever, an emerging infectious disease of World War 1. Lancet Infect Dis. 2016;16:e164–72. https://doi.org/10.1016/S1473-3099(16)30003-2
8. Mai BHA, Barbieri R, Chenal T, Castex D, Jonvel R, Tanasi D, et al. Five millennia of *Bartonella quintana* bacteraemia. PLoS One. 2020;15:e0239526. https://doi.org/10.1371/journal.pone.0239526

Address for correspondence: Eric Faure, Aix-Marseille University, CNRS UMR 7373, I2M, 3 Place Victor Hugo, 13331 CEDEX 3, Marseilles, France; email: eric.faure@univ-amu.fr

Autochthonous *Leishmania* (*Viannia*) *lainsoni* in Dog, Rio de Janeiro State, Brazil, 2023

Isabela Cordeiro da Silva Santos, Daniel Moreira de Avelar, Luciana de Freitas Campos Miranda, Artur Augusto Velho Mendes Júnior, Lucas Keidel Oliveira, Luanna da Silva Ventura, Aline Fagundes da Silva, Fernanda Nunes Santos, Liliane de Fátima Antônio Oliveira, Rodrigo Caldas Menezes,[1] Andreza Pain Marcelino[1]

Author affiliations: Fundação Oswaldo Cruz, Rio de Janeiro, Brazil (I.C.d.S. Santos, L.d.F.C. Miranda, L.K. Oliveira, L.d.S. Ventura, A.F. da Silva, F.N. Santos, L.d.F.A. Oliveira, R.C. Menezes, A.P. Marcelino); Fundação Oswaldo Cruz, Belo Horizonte, Brazil (D.M. de Avelar); Instituto Carlos Chagas, Curitiba, Brazil (A.A.V.M. Júnior)

DOI: https://doi.org/10.3201/eid3105.241058

In Brazil, *Leishmania* (*Leishmania*) *infantum* causes canine visceral leishmaniasis; the primary vector is the *Lutzomyia longipalpis* sand fly. We describe a case of canine visceral leishmaniasis caused by *Leishmania (Viannia) lainsoni* in a dog from Barra Mansa municipality, Rio de Janeiro state. Better specificity of serologic diagnostic techniques is needed for diagnoses.

Protozoa transmitted by sand flies cause leishmaniasis, and several pathogenic species affect humans. Various clinical forms of the disease have been described, including visceral, cutaneous, and mucocutaneous leishmaniasis (*1*). *Leishmania* (*Viannia*) *lainsoni* was described in Brazil in 1987 as the causative agent of human cases of cutaneous leishmaniasis. Its vector is the *Lutzomyia ubiquitalis* sand fly (*2*). Other countries in Latin America have reported human cases of *L.* (*V.*) *lainsoni* infection. Researchers isolated the parasite from the rodent species *Cuniculus paca*, the lowland paca, in the state of Pará, Brazil, suggesting a potential wild reservoir (*3*,*4*).

This study reports the case of a dog (*Canis familiaris*) infected with *L.* (*V.*) *lainsoni* that was from the municipality of Barra Mansa, an urban area in Rio de Janeiro state with widespread visceral leishmaniasis (VL) (Appendix, https://wwwnc.cdc.gov/EID/article/31/5/24-1058-App1.pdf). The Ethics Committee on the Use of Animals–Fiocruz approved this work (license no. LW 19/20; https://www.ceua.fiocruz.br/ceuaw000.aspx).

A 5-year-old male dog of mixed breed domiciled in Barra Mansa tested positive for VL by both rapid immunochromatographic testing and enzyme immunoassay (Bio-Manguinhos, https://portal.fiocruz.br/en/unidade/immunobiological-technology-institute-biomanguinhos) during epidemiologic surveillance in 2023 and was euthanized using the recommendations of the Brazilian Ministry of Health (https://www.gov.br). The dog had not moved to other regions and had localized alopecia, crusted skin ulcers, onychogryphosis, keratoconjunctivitis, normocytic normochromic anemia, hyperproteinemia, hyperglobulinemia, hypoalbuminemia, and a low albumin:globulin ratio (Appendix). Histopathologic changes included skin with hyperkeratosis and multifocal and moderate granulomatous dermatitis, as well as lymphoid hyperplasia of the spleen. Immunohistochemistry was positive for amastigote forms of *Leishmania* in skin and spleen (Figure 1).

We performed parasitologic and PCR tests (Appendix Table 2). We used multilocus enzyme electrophoresis with 5 enzyme profiles (phosphoglucomutase, glucose-6-phosphate dehydrogenase, nucleoside hydrolase, 6-phosphogluconate dehydrogenase, and phosphoglucose isomerase) (*5*). We extracted DNA from the isolated parasite and used it for PCR restriction fragment length polymorphism analysis (*Hae*III and *Bst*UI). We sequenced the 70-kDa heat shock protein products with the same primers by Sanger sequencing (primers: BankIt2825220 and Seq1PP760383) (*6*). Those techniques identified the parasite as *L.* (*V.*) *lainsoni* in all profiles studied in the bone marrow sample (Figure 2).

Like other species of the subgenus *Viannia*, *L.* (*V.*) *lainsoni* can cause ulcerative or nodular dermal lesions in humans (*4*). The clinical signs found in this infected dog included onychogryphosis and skin alterations. Development of skin lesions can lead to hematogenous dissemination and parasitemia of internal organs, as observed in this case, and visceral involvement of lymph nodes and spleen (*7*). The positive results of serologic tests show flaws in the specificity of the techniques because those tests were validated for detecting dogs with canine VL caused by *L.* (*Leishmania*) *infantum*. Hematocrit values less than the reference range, along with a slight increase in total protein, are expected in chronic diseases. We observed no changes in renal function markers. The host–parasite interaction has been extensively studied in dogs infected with *L.* (*L.*) *infantum*; however,

[1]These authors contributed equally to this article.

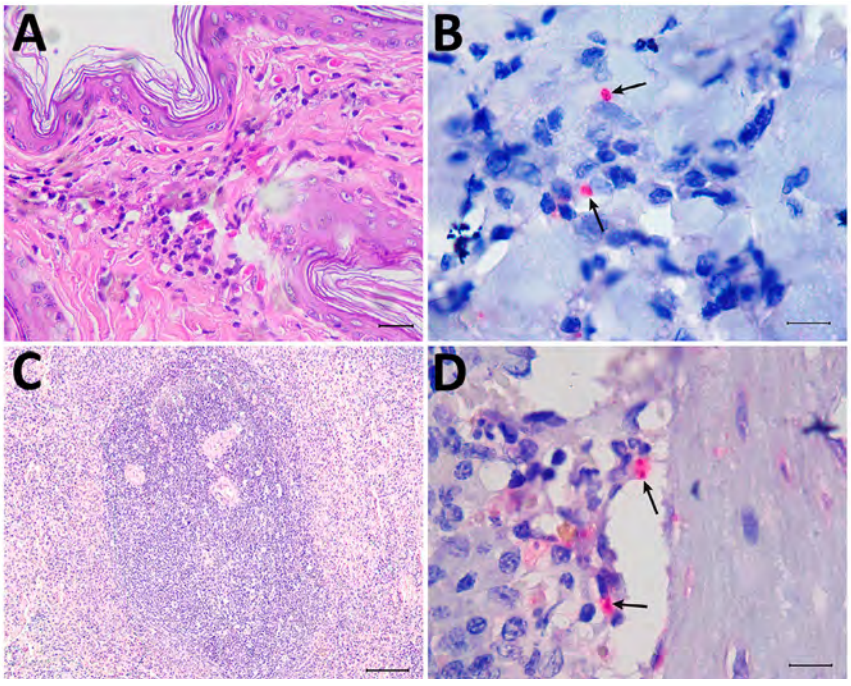

Figure 1. Histologic sections from autochthonous *Leishmania* (*Viannia*) *lainsoni* in dog (*Canis familiaris*), Rio de Janeiro state, Brazil, 2023. A, B) Skin of the examined dog: hyperkeratosis and moderate granulomatous infiltrate in the dermis are composed mainly of macrophages, with a smaller number of plasma cells and lymphocytes (A) and red-stained amastigotes in the cytoplasm of macrophages (arrows) (B). C, D) Spleen of the examined dog: lymphoid hyperplasia (C) and red-stained amastigotes in the cytoplasm of macrophages in the parenchyma (arrows) (D). A, C) Hematoxylin-eosin stain; B, D) immunohistochemistry. Scale bars indicate 10 μm.

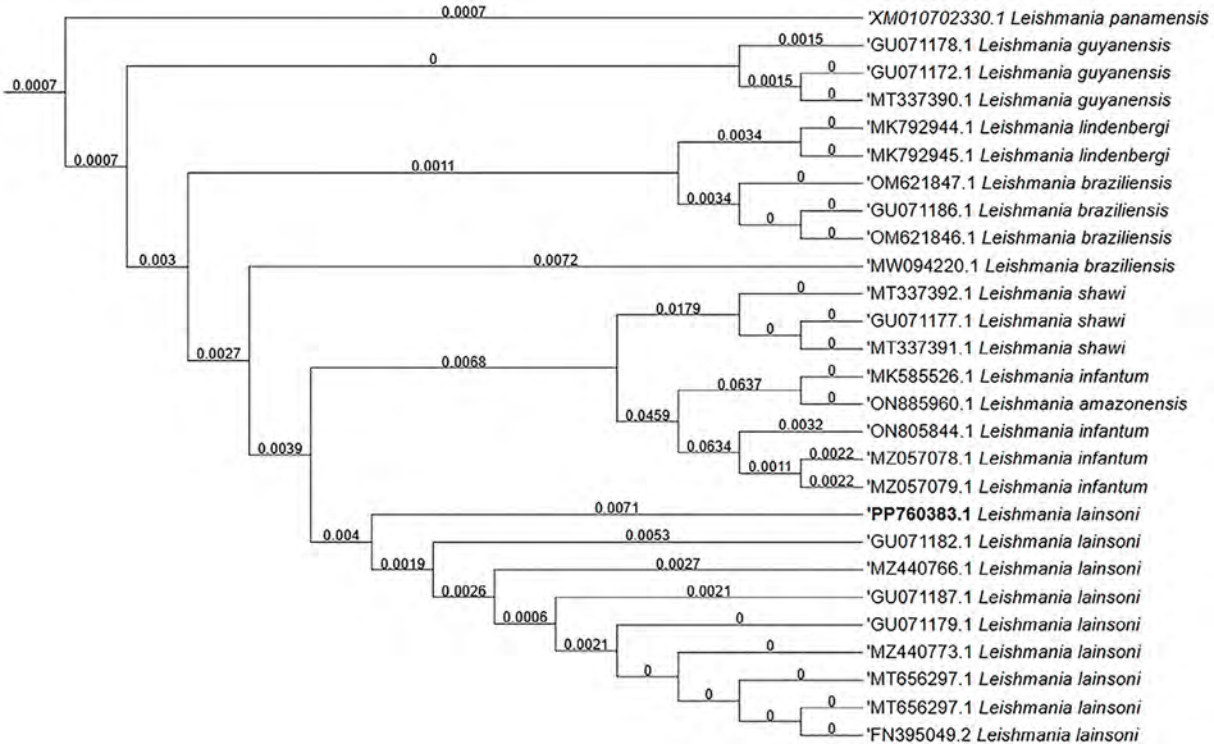

Figure 2. Evolutionary analysis of autochthonous *Leishmania* (*Viannia*) *lainsoni* in dog (*Canis familiaris*), Rio de Janeiro state, Brazil, 2023. Bold text indicates isolate from this study. Evolutionary history was inferred by using the maximum-likelihood method and Kimura 2-parameter model. The bootstrap consensus tree inferred from 1,000 replicates represents evolutionary history of the taxa analyzed. Branches corresponding to partitions reproduced in <50% bootstrap replicates are collapsed. The percentage of replicate trees in which the associated taxa clustered together in the bootstrap test (1,000 replicates) are shown next to the branches. Initial tree(s) for the heuristic search were obtained by applying the BioNJ (https://bionj.org) method to a matrix of pairwise distances estimated by using the maximum composite likelihood approach. This analysis involved 33 nucleotide sequences. There were a total of 463 positions in the final dataset. Evolutionary analyses were conducted in MEGA11 (https://www.megasoftware.net). MEGA used the first position for each codon in the construction of the phylogenetic tree. GenBank accession numbers are shown.

little is known about that interaction in dogs infected with other *Leishmania* species.

In Latin America, *L.* (*V.*) *lainsoni* is found in tropical and sub-Andean regions with different climatic conditions. Its presence in other countries highlights the high dispersal capacity of the parasite and potential involvement of unidentified mammalian host vectors. Barra Mansa has a crucial migratory flow because it is located on the banks of the Paraíba do Sul River and influences the Médio Paraíba region and southern part of the south-central region of Rio de Janeiro State.

The dog lived in an area surrounded by natural and abundantly wooded areas. A large portion of the Hemlock Forest is located in Barra Mansa, and *C. paca* rodents are part of the local fauna and could serve as reservoirs of *L.* (*V.*) *lainsoni* in that area (*8*).

Few entomologic surveys have been conducted in Barra Mansa, and only *Lu. sallesi* and *Lu. longipalpis* sand flies were confirmed, limiting the conclusions of this study (*9*). Although the *Lu. ubiquitalis* sand fly is considered the primary vector of *L.* (*V.*) *lainsoni* in Brazil, other species such as *Lu. nuneztovari anglesi* and *Lu. velascoi* sand flies in Bolivia have been reported (*10*). Therefore, identification of a dog infected with *L.* (*V.*) *lainsoni* in Barra Mansa may be linked to transmission by other yet undocumented sand fly species in that municipality. The dog did not have a history of moving to other locations. We consider environmental changes caused by humans in the region, as well as local wildlife and migratory flows, as possible causes of infection. This study raises several questions. Is a new and yet unknown disease cycle being established locally? What is the risk for the disease becoming endemic in the population? Will the cycle persist? Also, could other regions in Brazil or elsewhere face similar risks of emerging *Leishmania* species infecting dogs? Further epidemiologic investigations and taxonomic characterization studies are essential and should be continuously supported. Efforts to create clearer specificity in serologic diagnostic techniques are also needed.

Acknowledgments

We thank the Municipal Health Department of Barra Mansa and the Central Laboratory of Public Health for collaboration and Adilson Benedito de Almeida and Ricardo Baptista Schmidt for processing the figures.

This study was supported by Fundação Carlos Chagas Filho de Amparo à Pesquisa do Estado do Rio de Janeiro (grant no. CNE-E-26/201.032/2021) and Coordenação de Aperfeiçoamento de Pessoal de Nível Superior, Brazil (finance code 001). R.C. Menezes is a recipient of productivity fellowships from Conselho Nacional de Desenvolvimento Cientifico e Tecnológico, Brazil (grant no. 305956/2021-3).

A.P.M., D.M.d.A., and R.C.M. conceptualized the study. I.C.d.S.S., D.M.d.A, L.d.F.C.M., A.A.V.M.J., L.K.O., L.d.S.V., A.F.d.S., F.N.S., L.d.F.A.O., R.C.M., and A.P.M. constructed the methodology. I.C.d.S.S., D.M.d.A, L.F.C.M., A.A.V.M.J., L.K.O., L.d.S.V., and F.N.S. carried out the investigation. R.C.M., A.F.d.S., L.d.F.A.O., and A.P.M. performed data analysis. A.P.M. and R.C.M. acquired funding. A.P.M. was the study administrator. R.C.M. supervised the study. I.C.d.S.S. and A.P.M. wrote the original draft. All authors contributed to the review and editing of the final manuscript.

About the Author

Ms. Santos is a PhD student at the Instituto Nacional de Infectologia Evandro Chagas, Fundação Oswaldo Cruz, Rio de Janeiro, Brazil. Her research interests include the evaluation of diagnostic techniques for dogs suspected of having canine visceral leishmaniasis, using molecular techniques such as conventional PCR, quantitative PCR, and loop-mediated isothermal amplification.

References

1. World Health Organization. Leishmaniasis [cited 2024 Jul 2]. https://www.who.int/news-room/fact-sheets/detail/leishmaniasis
2. Silveira FT, Shaw JJ, Braga RR, Ishikawa E. Dermal leishmaniasis in the Amazon region of Brazil: *Leishmania (Viannaia) lainsoni* sp.n., a new parasite from the State of Pará. Mem Inst Oswaldo Cruz. 1987;82:289–91. https://doi.org/10.1590/S0074-02761987000200018
3. Silveira FT, Lainson R, Shaw JJ, Braga RR, Ishikawa EE, Souza AA. Cutaneous leishmaniasis in Amazonia: isolation of *Leishmania* (*Viannia*) *lainsoni* from the rodent *Agouti paca* (Rodentia: Dasyproctidae), in the state of Pará, Brazil [in Portuguese]. Rev Inst Med Trop São Paulo. 1991;33:18–22. https://doi.org/10.1590/S0036-46651991000100004
4. Corrêa JR, Brazil RP, Soares J. *Leishmania* (*Viannia*) *lainsoni* (Kinetoplastida: Trypanosomatidae), a divergent *Leishmania* of the *Viannia* subgenus: a mini review. Mem Inst Oswaldo Cruz. 2005;100:587–92. 10.1590/s0074-02762005000600014
5. Cupolillo E, Grimaldi G Jr, Momen H. A general classification of New World *Leishmania* using numerical zymotaxonomy. Am J Trop Med Hyg. 1994;50:296–311. https://doi.org/10.4269/ajtmh.1994.50.296
6. Graça GC, Volpini AC, Romero GAS, Oliveira Neto MP, Hueb M, Porrozzi R, et al. Development and validation of PCR-based assays for diagnosis of American cutaneous leishmaniasis and identification of the parasite species. Mem Inst Oswaldo Cruz. 2012;107:664–74. https://doi.org/10.1590/S0074-02762012000500014
7. Marquez ES, de Castro EA, Nabut LB, da Costa-Ribeiro MCV, Dela Coletta Troiano Araújo L, Poubel SB, et al. Cutaneous leishmaniosis in naturally infected dogs in Paraná, Brazil,

and the epidemiological implications of *Leishmania* (*Viannia*) *braziliensis* detection in internal organs and intact skin. Vet Parasitol. 2017;243:219–25. https://doi.org/10.1016/j.vetpar.2017.07.003
8. Brasil, Ministério do Meio Ambiente. Plano de manejo ARIE floresta da cicuta [cited 2024 Jul 16]. https://www.gov.br/icmbio/pt-br/assuntos/biodiversidade/unidade-de-conservacao/unidades-de-biomas/mata-atlantica/lista-de-ucs/arie-floresta-da-cicuta/arquivos/plano-de-manejo-arie-cicuta-oficial.pdf
9. Carvalho BM, Dias CMG, Rangel EF. Phlebotomine sand flies (Diptera, Psychodidae) from Rio de Janeiro state, Brazil: species distribution and potential vectors of leishmaniasis. Rev Bras Entomol. 2014;58:77–87. https://doi.org/10.1590/S0085-56262014000100013
10. Kato H, Cáceres AG, Mimori T, Ishimaru Y, Sayed ASM, Fujita M, et al. Use of FTA cards for direct sampling of patients' lesions in the ecological study of cutaneous leishmaniasis. J Clin Microbiol. 2010;48:3661–5. https://doi.org/10.1128/JCM.00498-10

Address for correspondence: Andreza Pain Marcelino, Laboratório de Pesquisa Clínica e Vigilância em leishmanioses, Instituto Nacional de Infectologia Evandro Chagas, Fundação Oswaldo Cruz, 4365 Brasil Ave, Manguinhos, Rio de Janeiro 21040-900, Brazil; email: andreza.marcelino@ini.fiocruz.br

Unexpected Zoonotic and Hybrid Schistosome Egg Excretion Patterns, Malawi, 2024

Angus M. O'Ferrall, Sekeleghe A. Kayuni, Lucas J. Cunningham, Peter Makaula, John Archer, Adam P. Roberts, Janelisa Musaya,[1] J. Russell Stothard[1]

Author affiliations: Liverpool School of Tropical Medicine, Liverpool, UK (A.M. O'Ferrall, S.A. Kayuni, L.J. Cunningham, J. Archer, A.P. Roberts, J.R. Stothard); Malawi-Liverpool-Wellcome Trust Clinical Research Programme, Queen Elizabeth Central Hospital, Blantyre, Malawi (S.A. Kayuni, P. Makaula, J. Musaya); School of Medicine and Oral Health, Kamuzu University of Health Sciences, Blantyre (S.A. Kayuni, J. Musaya); Wolfson Wellcome Biomedical Laboratories, Natural History Museum, London, UK (J. Archer)

DOI: https://doi.org/10.3201/eid3105.241757

[1]These senior authors contributed equally to this article.

Two exemplary cases of mixed urogenital and intestinal schistosomiasis in Malawi show hybridizations of *Schistosoma mattheei* with *S. haematobium* and *S. mansoni*, indicating newly emerging genetic diversity. Complex egg excretion patterns in feces expose current diagnostic gaps and alert to future sampling needs for effective surveillance of zoonotic schistosomiasis.

Schistosomiasis is a waterborne, parasitic disease transmitted by several species of *Bulinus* and *Biomphalaria*, two distinct freshwater snail genera common across sub-Saharan Africa (*1*). In sub-Saharan Africa, *Schistosoma haematobium* is the predominant cause of urogenital schistosomiasis, and *S. mansoni* is the predominant cause of intestinal schistosomiasis (*1*). *S. haematobium* is endemic in Malawi, where infections with zoonotic and hybrid species from the *S. haematobium* group (*S. mattheei* and *S. haematobium* × *S. mattheei*) have also been detected in humans (*2*,*3*). *S. mattheei* is considered a livestock-infecting schistosome that causes intestinal disease (*4*); however, excretion of ova from humans infected with *S. mattheei* and associated *S. haematobium* group hybrids reportedly has occurred through the urogenital tract (*2*,*3*). Meanwhile, *Biomphalaria* freshwater snails were first detected along the southern shores of Lake Malawi in 2017 (*5*). Since then, autochthonous *S. mansoni* transmission and intestinal schistosomiasis outbreaks have been confirmed in Mangochi District, Malawi (*5*,*6*).

To clarify *S. haematobium* group hybridization dynamics, we conducted a longitudinal cohort study in southern Malawi. The College of Medicine Research Ethics Committee, Malawi (approval no. P.08/21/3381, https://www.ncst.mw) and the Liverpool School of Tropical Medicine Research Ethics Committee, United Kingdom (approval no. 22-028, https://www.lstmed.ac.uk/research/research-integrity/research-ethics-committee) provided ethics approval. This study also tracked *S. mansoni* prevalence in a community cohort recruited from Samama Village, Mangochi District (Appendix Figure 1, https://wwwnc.cdc.gov/EID/article/31/5/24-1757-App1.pdf), where the outbreak of intestinal schistosomiasis was initially reported (*5*,*6*).

In June 2024, we determined *S. mansoni* prevalence in Mangochi District to be 14.8% (165/1,116) using point-of-care urine circulating cathodic antigen cassette tests (POC-CCA; ICT International, https://ictinternational.com), and considered trace results positive. Those results represented the lowest reported *S. mansoni* prevalence in Samama Village since it emerged in 2017 (*5*–*7*). However, we observed numer-

ous atypical schistosome ova within feces provided by 2 POC-CCA–positive participants upon Kato-Katz examination (https://microbeonline.com/kato-katz-technique-principle-procedure-results) (Figure). Patient X, a 10-year-old girl, and patient Y, a 19-year-old man (Table), both received treatment with praziquantel from a study-affiliated clinician. The unexpected morphologic diversity raised concerns about underreporting of intestinal schistosomiasis being caused by species other than *S. mansoni*, prompting closer molecular analysis for robust speciation that cannot be achieved by microscopy.

We obtained hatched miracidia from the urine and feces of patients X and Y by using Pitchford-Visser filtration and collected and preserved individual miracidia on Whatman Flinders Technology Associates cards (GE Healthcare Life Sciences, https://www.gehealthcare.com/products/life-sciences), according to standard protocols (*8*). To identify the schistosome larvae, we used a newly described 2-tube high-resolution melt real-time PCR assay on DNA extracted from individual preserved miracidia (*9*). To detect evidence of mixed ancestry or putative genetic introgression, we targeted both the nuclear DNA ribosomal internal transcribed spacer 2 locus and species-specific mitochondrial DNA (mtDNA) loci of 6 *Schistosoma* species: *S. bovis*, *S. curassoni*, *S. haematobium*, *S. mansoni*, *S. margrebowiei*, and *S. mattheei*. For *S. bovis*, *S. curassoni*, *S. haematobium*, and *S. mansoni* we targeted the tRNA lysine region; for *S. margrebowiei* the NADH dehydrogenase subunit 4 region; and for *S. mattheei*, the NADH dehydrogenase subunit 6 region.

Miracidia hatched from ova in the feces of patient X mostly typed as *S. haematobium* × *S. mattheei* hybrids (93.3%), whereas most miracidia hatched from the paired urine sample typed as pure *S. haematobium* (95.8%). Similarly, atypical zoonotic and hybrid schistosome species ova from patient Y were predominantly in feces (Appendix Figure 2). Of the 59 *S. haematobium* × *S. mattheei* hybrid miracidia typed from feces, high-resolution melt profiles indicated that mtDNA (maternal) was inherited from *S. mattheei* in 58 miracidia, although *S. haematobium*

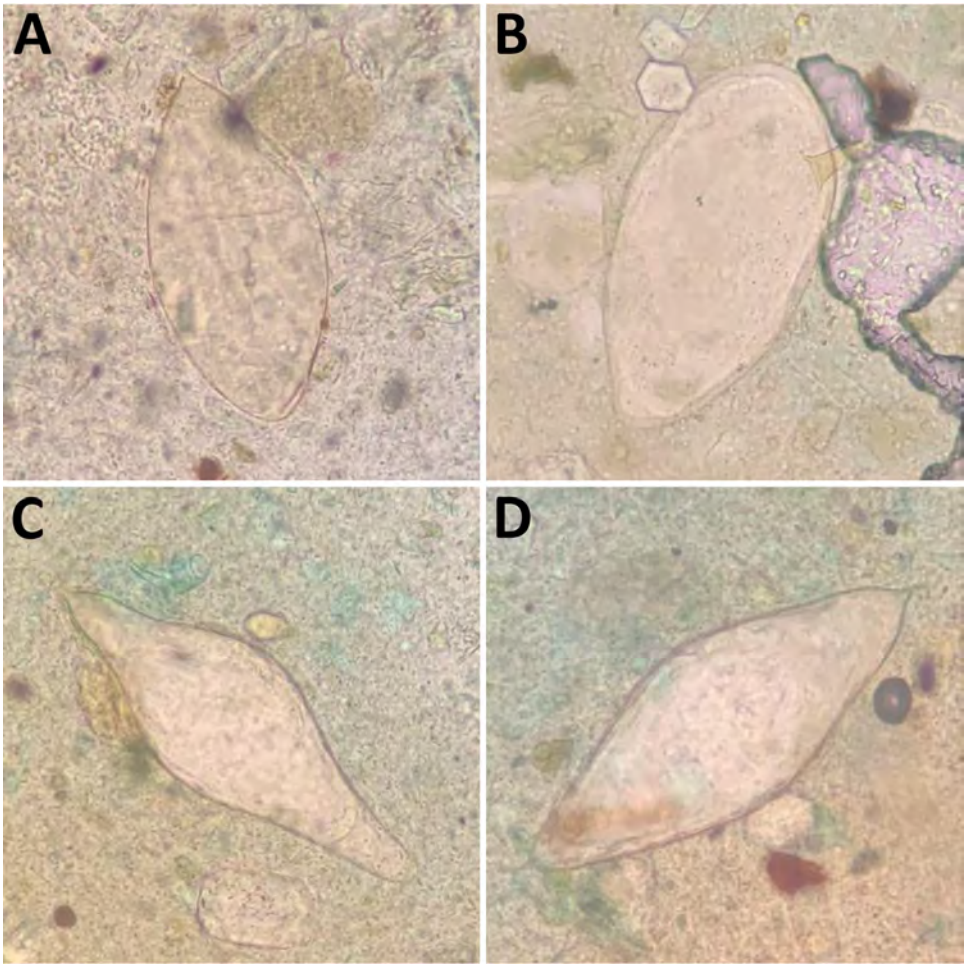

Figure. Morphologic *Schistosoma* spp. identification from 2 patient's feces samples in an investigation of unexpected zoonotic and hybrid schistosome egg excretion patterns, Malawi, 2024. A) Typical *S. haematobium* (length 130 μm); B) typical *S. mansoni* (length 150 μm); C) atypical terminal-spined egg (length 188 μm); D) atypical terminal-spined egg (length 154 μm). Samples were stained with methylene blue glycerol solution using the Kato-Katz method (https://microbeonline.com/kato-katz-technique-principle-procedure-results). Atypical morphology (C,D) prompted closer molecular analysis for speciation, which revealed *S. haematobium* × *S. mattheei* hybrids.

Table. Summary of diagnostic information for patient X and patient Y from unexpected zoonotic and hybrid schistosome egg excretion patterns, Malawi, 2024*

Diagnostic test	Patient X	Patient Y
Urinary diagnostics		
Eggs/10 mL urine (no. typed)†	>50 (71)	30 (50)
Microhematuria	Large	Large
Visible hematuria	Yes	Yes
Proteinuria	≥2,000 mg/dL	≥2,000 mg/dL
Turbid urine	Yes	Yes
POC-CCA	Positive	Positive
Fecal diagnostics		
Eggs/g feces (no. typed)†	84 (60)	240 (34)
Fecal occult blood	Negative	Positive

*POC-CCA, point-of-care urine circulating cathodic antigen cassette tests.
†Miracidia typing.

mtDNA was detected in the remaining *S. haematobium* × *S. mattheei* miracidia. From patient Y, 1 miracidium showed mixed ancestry between *S. mansoni* and *S. mattheei*, with discordance between mtDNA and nuclear DNA profiles (Appendix Figure 3). Although adult worm pairings between distantly related species usually result in the production of parthenogenetic eggs, previous experimental pairings of *S. mansoni* and *S. mattheei* resulted in the production of eggs viable to the third generation (*10*).

Our findings not only provide evidence of complex hybridization events in the natural setting among *S. haematobium*, *S. mansoni*, and *S. mattheei* but also highlight the greater relative abundance of zoonotic and hybrid schistosome species ova in feces compared with paired urine samples. That observation suggests that *S. mattheei* and associated hybrids, previously linked to urogenital schistosomiasis in humans, may dominate in intestinal infections by migrating to the intestinal mesenteries, just as *S. mattheei* likely does in other mammalian hosts where it causes rectal schistosomiasis (*4*). POC-CCA tests were not designed to detect zoonotic schistosomiasis; although we acknowledge that patients X and Y were both POC-CCA positive, those results do not assure the ability of POC-CCA tests to detect *S. haematobium* group intestinal infections because we did not perform detailed inspection of feces from POC-CCA–negative participants in the field.

In summary, we detected *S. haematobium* × *S. mattheei* hybrid ova from 2 patients in Malawi. Further fecal sampling and molecular testing with species-specific TaqMan probe assays will be essential for monitoring intestinal schistosomiasis in coendemic areas where zoonotic transmission could occur.

Acknowledgments

We thank all participants in our study, particularly the 2 participants providing samples that enabled this analysis. We are grateful to staff and students at the Liverpool School of Tropical Medicine, Malawi-Liverpool Wellcome Programme, and Mangochi District Hospital for their valuable support and expertise in the study, including Alexandra Juhász, Sam Jones, Gladys Namacha, David Lally Jr., Priscilla Chammudzi, Donales R. Kapira, Bright Mainga, Clinton Nkolokosa, Ruth Cowlishaw, Sarah Rollason, and James E. LaCourse.

This research was funded by the National Institute for Health Research and Wellcome Trust through a Joint Investigator Award (grant no. WT 220818/Z/20/Z). A.M. O'Ferrall is supported by the Medical Research Council via the Liverpool School of Tropical Medicine-Lancaster University doctoral training partnership (grant no. MR/W007037/1).

About the Author

Dr. O'Ferrall is a clinician-scientist and PhD researcher in the Department of Tropical Disease Biology at the Liverpool School of Tropical Medicine, UK. His research focuses on the genomic epidemiology of pathogens in tropical settings, including drug-resistant bacteria and schistosomes.

References

1. Buonfrate D, Ferrari TCA, Akim Adegnika A, Stothard JR, Gobbi FG. Human schistosomiasis. Lancet. 2025;405:658–70. https://doi.org/10.1016/S0140-6736(24)02814-9
2. Webster BL, Alharbi MH, Kayuni S, Makaula P, Halstead F, Christiansen R, et al. Schistosome interactions within the *Schistosoma haematobium* group, Malawi. Emerg Infect Dis. 2019;25:1245–7. https://doi.org/10.3201/eid2506.190020
3. Kayuni S, Cunningham L, Mainga B, Kumwenda D, Lally D Jr, Chammudzi P, et al. Detection of male genital schistosomiasis (MGS) associated with human, zoonotic and hybrid schistosomes in Southern Malawi. BMC Infect Dis. 2024;24:839. https://doi.org/10.1186/s12879-024-09732-z
4. Juhász A, Makaula P, Cunningham LJ, Jones S, Archer J, Lally D Jr, et al. Revealing bovine schistosomiasis in Malawi: connecting human and hybrid schistosomes within cattle. One Health. 2024;19:100761. https://doi.org/10.1016/j.onehlt.2024.100761
5. Alharbi MH, Condemine C, Christiansen R, LaCourse EJ, Makaula P, Stanton MC, et al. *Biomphalaria pfeifferi* snails and intestinal schistosomiasis, Lake Malawi, Africa, 2017–2018. Emerg Infect Dis. 2019;25:613–5. https://doi.org/10.3201/eid2503.181601
6. Kayuni SA, O'Ferrall AM, Baxter H, Hesketh J, Mainga B, Lally D Jr, et al. An outbreak of intestinal schistosomiasis, alongside increasing urogenital schistosomiasis prevalence, in primary school children on the shoreline of Lake Malawi, Mangochi District, Malawi. Infect Dis Poverty. 2020;9:121. https://doi.org/10.1186/s40249-020-00736-w
7. Archer J, Cunningham LJ, Juhász A, Jones S, O'Ferrall AM, Rollason S, et al. Molecular epidemiology and population genetics of *Schistosoma mansoni* infecting school-aged children situated along the southern shoreline of Lake

Malawi, Malawi. PLoS Negl Trop Dis. 2024;18:e0012504. https://doi.org/10.1371/journal.pntd.0012504
8. Stothard JR, Webster BL, Weber T, Nyakaana S, Webster JP, Kazibwe F, et al. Molecular epidemiology of *Schistosoma mansoni* in Uganda: DNA barcoding reveals substantial genetic diversity within Lake Albert and Lake Victoria populations. Parasitology. 2009;136:1813–24. https://doi.org/10.1017/S003118200999031X
9. Cunningham LJ, Kayuni S, Juhász A, Makaula P, Lally D Jr, Namacha G, et al. A rapid DNA screening method using high-resolution melt analysis to detect putative *Schistosoma haematobium* and *Schistosoma mattheei* hybrids alongside other introgressing schistosomes. Front Trop Dis. 2024;5:1350680. https://doi.org/10.3389/fitd.2024.1350680
10. Leger E, Webster JP. Hybridizations within the genus *Schistosoma*: implications for evolution, epidemiology and control. Parasitology. 2017;144:65–80. https://doi.org/10.1017/S0031182016001190

Address for correspondence: Russell Stothard, Department of Tropical Disease Biology, Liverpool School of Tropical Medicine, Pembroke Place, Liverpool L3 5QA, UK; email: russell.stothard@lstmed.ac.uk

Emergence of Feline Sporotrichosis near Brazil Border, Argentina, 2023–2024

Katherina Alicia Vizcaychipi, María Cecilia López-Joffre, Mónica Martínez, Jerson Andrés Cuéllar-Sáenz, Marina Ramos, Celeste Agüero, Natalia Olsina, Emanuel Grassi, Esteban Couto, Jorge Mendoza, Carolina Melchior do Prado, Jorge Pablo Castillo, Mabel D. Giménez, Karen E. DeMatteo, Álvaro A. Faccini-Martínez, Mariana Viale, Adriana Toranzo, Cristina Elena Canteros

Author affiliations: Instituto Misionero de Biodiversidad, Puerto Iguazú, Argentina (K.A. Vizcaychipi, M. Martínez, E. Grassi); Universidad del Salvador, Virasoro, Argentina (K.A. Vizcaychipi, J. Mendoza, J.P. Castillo); Instituto Nacional de Medicina Tropical Administración Nacional de Laboratorios e Institutos de Salud–"Carlos G. Malbrán," Puerto Iguazú (K.A. Vizcaychipi, E. Couto); Instituto Nacional de Enfermedades Infecciosas, Administración Nacional de Laboratorios e Institutos de Salud–"Carlos G. Malbrán," Buenos Aires, Argentina (M.C. López-Joffré, M. Viale, A. Toranzo, C.E. Canteros); Universidad Nacional de Colombia, Bogota, Colombia (J.A. Cuéllar-Sáenz); Dirección Municipal de Zoonosis, Puerto Iguazú (M. Ramos, C. Agüero); Clínica Veterinaria, Puerto Iguazú (N. Olsina); Universidad Federal de Paraná, Curitiba, Brazil (C. Melchior do Prado); Instituto de Genética Humana de Misiones, Consejo Nacional de Investigaciones Científicas y Técnicas, Posadas, Argentina (M.D. Giménez); Universidad Nacional de Misiones, Posadas (M.D. Giménez); Washington University in St. Louis, St. Louis, Missouri, USA (K.E. DeMatteo), WildCare Institute at the Saint Louis Zoo, St. Louis (K.E. DeMatteo); Hospital Militar Central, Bogota (Á.A. Faccini-Martínez); Universidad Militar Nueva Granada, Bogota (Á.A. Faccini-Martínez)

DOI: https://doi.org/10.3201/eid3105.241882

We describe a large urban outbreak of feline sporotrichosis caused by *Sporothrix brasiliensis* fungi in Argentina. Over a 7-month period in Puerto Iguazú, which borders Brazil, we identified culture-proven sporotrichosis in 9 cases across 7 households. Public health officials should coordinate cross-border One Health actions and institute context-specific interventions.

Sporotrichosis is an implantation mycosis caused by thermal-dimorphic fungi belonging to the *Sporothrix schenckii* complex (*1*). Among pathogenic species, *S. brasiliensis* has high virulence, epidemic potential, and zoonotic/enzootic transmission that occurs through bites, scratches, or contact with exudates from infected animals, particularly domestic cats (*2*–*4*).

In South America, *S. brasiliensis* was first identified in Brazil and has since been reported in other Latin America countries (*1*–*8*). Over recent decades, sporotrichosis in Brazil has seen a substantial epidemiologic shift, marked by intense, widespread urban zoonotic outbreaks, initially concentrated in Rio de Janeiro, affecting cats, dogs, and humans (*2*,*9*). Those outbreaks have spread to several cities in the southern and southeastern states, including Foz do Iguaçu, located on the Triple Frontier (Argentina, Brazil, and Parguay) between Argentina and Paraguay (*2*,*3*,*5*,*7*,*10*). Recently, a cat (*Felis catus*) infection by *S. brasiliensis* was reported in Ciudad del Este in Paraguay (*8*). In Argentina, the first human isolation of *S. brasiliensis* was documented in 1986 in the south of province of Misiones with no identified source of infection (*4*). Since then, zoonotic sporotrichosis cases have increased, and the central and southern regions of the country report most occurrences (*1*,*4*).

This study reports the emergence of urban transmission of feline sporotrichosis in Puerto Iguazú, Misiones, Argentina (25°36′39″S, 54°34′49″W). Located in the extreme northeast of Argentina, on the border of

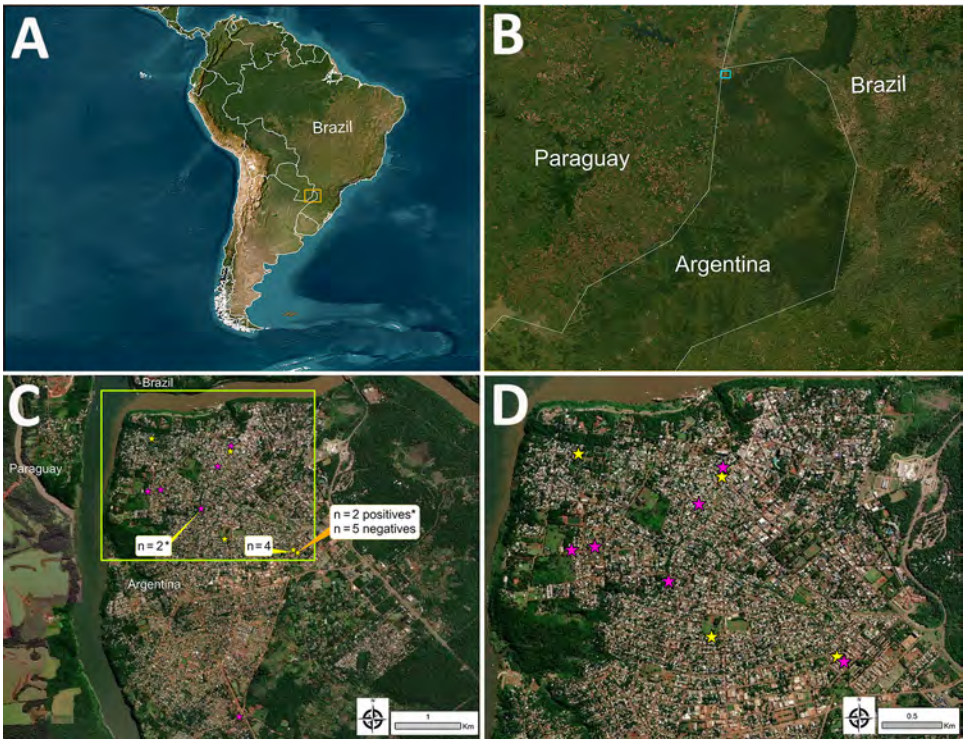

Figure. Spatial distribution of feline sporotrichosis near Brazil border, Argentina, 2023–2024. A, B) Relative position in South America showing the location of the Triple Frontier (A) and province of Misiones, Argentina (B). C) Puerto Iguazú within Argentina, showing positive confirmed feline sporotrichosis cases (n = 9; pink stars) and ruled-out cases (n = 12; yellow stars). D) Enlarged image of yellow box in panel C. For those areas where multiple cases (positive and negative) overlap in location, the number of individual cases is indicated. *Cases where intrahousehold transmission occurred between 2 cats (FSCMi24–FSCMi25 and FSCMi41–FSCMi43). In the spatial analysis, the distance between households with feline sporotrichosis cases was measured by using nearest-neighbor calculation in ArcGIS Pro (https://pro.arcgis.com), which calculates the shortest distance between 2 points.

the Triple Frontier, the city has a population of ≈54,675 people and is 1,278 km from Buenos Aires. Puerto Iguazú is a major tourist destination because of the Iguazú Falls and is characterized by substantial cross-border dynamics, including high population and commercial movement.

During August 2023–February 2024, we conducted an intensified passive surveillance on 21 domestic cats (*F. catus*) from 12 households in the urban area of Puerto Iguazú (Figure). We included cats with lesions consistent with feline sporotrichosis (ulcers, scabs, soft nodules, and ulcerated subcutaneous nodules with exudate) and other cats without lesions but in contact with affected cats or living in areas with documented cases. No cats received treatment before sample collection. Pet owners provided written consent, and we recorded clinical, epidemiologic, and demographic data. Veterinarians evaluated all suspected cases and unaffected cats in contact with affected cats, and ongoing prevention and awareness campaigns provided information to owners and the community.

We collected nasal and lesion swab specimens from cats with skin lesions and nasal swabs from cats without lesions. We conducted diagnosis and species identification of *Sporothrix* by using phenotypic (Giemsa stain and culture) and genotypic methods (sequencing internal transcribed spacer region and partial sequencing of the calmodulin gene) (*1*,*4*,*10*).

We studied 21 cases. Nine (42.9%) were suspected cases, and 12 (57.1%) were unaffected cats. We confirmed feline sporotrichosis by culture in 77.8% (7/9) of the suspected cases and 16.7% (2/12) of the unaffected cats (Appendix Figure, https://wwwnc.cdc.gov/EID/article/31/5/24-1882-App1.pdf). We confirmed *S. brasiliensis* in 77.8% (7/9) cases by using molecular analysis. Two samples were inconclusive because of mold and bacterial contamination, which hindered identification of *Sporothrix* species (Table). Among the 2 confirmed cases in unaffected cats, we identified sneezing as the sole symptom in 1 case, and we ruled out 2 suspected cases because of differential diagnosis (dog bite and dermatophytosis) (Table). We reported all cases to health authorities.

We identified feline sporotrichosis cases in 58.3% (7/12) of the households. In 2 households, we detected multiple cases, suggesting intradomestic transmission. However, in 5 households, we found only 1 cat with sporotrichosis. Most of the cats had free access to streets, neighboring properties, and vacant lots. The average distance between the nearest households with feline sporotrichosis cases was 1.84 ± 1.22 km (range 0–4.54 km) (Table; Figure).

Table. Features of domestic cats (*Felis catus*) suspected of feline sporotrichosis near Brazil Border, Argentina, 2023–2024*

HH no.	Cat ID	Date	Age/sex	Altered	Habitation†	Type, location of lesion	Collected material	DE, culture	Species, strain no.
1	FSCMi-011‡	2023 Aug 1	Adult/M	No	Feral	Multiple dog bites	NS, LS, C	N/N	NA
2	FSCMi-017	2023 Nov 13	Adult/M	Yes	Outdoor	NI	NS, C	N/N	NA
	FSCMi-024	2023 Nov 24	Adult/M	Yes	Outdoor	NI	NS	ND, *Sporothrix* sp.	*S. brasiliensis*, 247479
	FSCMi-025§	2023 Nov 13	Adult/M	Yes	Outdoor	NI	NS	N, *Sporothrix* sp.	*S. brasiliensis*, 247478
	FSCMi-019	2023 Nov 13	Adult/F	Yes	Outdoor	NI	NS	N/N	
3	FSCMi-021	2023 Nov 16	Adult/F	No	Indoor	Localized, head	NS, LS	Yeast, *Sporothrix* sp.	NC
4	FSCMi-023	2023 Nov 24	Adult/M	Yes	Outdoor	Multiple, head, dorsum, and extremities	NS, LS	ND, *Sporothrix sp*.	*S. brasiliensis*, 247481
5	FSCMi-026	2023 Nov 24	Adult/M	Yes	Feral	Localized, head	NS, LS	ND, *Sporothrix* sp.	*S. brasiliensis,* 247480
6	FSCMi-031	2023 Dec 20	Kitten/M	No	Outdoor	NI	NS	N/N	NA
	FSCMi-032	2023 Dec 20	Juvenile/?	No	Outdoor	NI	NS	N/N	NA
	FSCMi-033	2023 Dec 20	Kitten/M	No	Outdoor	NI	NS	N/N	NA
7	FSCMi-034	2023 Dec 20	Adult/M	Yes	Outdoor	NI	NS	N/N	NA
	FSCMi-035	2023 Dec 20	Adult/M	Yes	Outdoor	NI	NS	N/N	NA
	FSCMi-036	2023 Dec 20	Adult/M	Yes	Outdoor	NI	NS	N/N	NA
	FSCMi-037	2023 Dec 20	Adult/F	Yes	Outdoor	NI	NS	N/N	NA
8	FSCMi-038	2023 Dec 20	Juvenile/F	Yes	Outdoor	NI	NS	N/N	NA
9	FSCMi-040	2024 Jan 10	Juvenile/F	No	Feral	Multiple, head and extremities	NS, LS	Yeast, *Sporothrix* sp.	NC
10	FSCMi-041	2024 Jan 15	Adult/M	Yes	Outdoor	Multiple, head, dorsum, and extremities	NS, LS	Yeast, *Sporothrix* sp.	*S. brasiliensis*, 247599
	FSCMi-043	2024 Jan 22	Adult/M	Yes	Outdoor	Multiple, head and extremities	NS, LS	Yeast, *Sporothrix* sp.	*S. brasiliensis*, 247600
11	FSCMi-042‡	2024 Jan 15	Juvenile/F	No	Outdoor	Alopecia	NS, LS	ND, *Microsporum canis*	NA
12	FSCMi-049	2024 Feb 28	Senior/M	Yes	Outdoor	Multiple, head, dorsum, and extremities	NS, LS	Yeast, *Sporothrix* sp.	*S. brasiliensis*, 247735

*C, claw; DE, direct examination of the sample with Giemsa staining; HH, household; LS, lesion swab; N, negative; NA, not applicable; NC, inconclusive because of mold and bacterial contamination; ND, not determined; NI, no injuries; NS, nasal swab specimen; ?, unknown.
†Habitation: indoor, cats kept exclusively indoors or in enclosed spaces without outdoor access; outdoor, cats with free access to roam outdoors, including streets, neighboring properties, or vacant lots; feral, cats living in the wild with minimal or no human interaction.
‡Dog bites and diagnosis of dermatophytosis.
§The cat had frequent sneezing.

Our results describe a large outbreak of *S. brasiliensis* in Argentina. We identified 9 proven cases of feline sporotrichosis in 7 months in Puerto Iguazú, in the province of Misiones, which is more than reported for the whole country (*1*). The outbreak reflects transmission dynamics similar to the epidemic in Brazil. Evidence shows multiple foci of transmission and asymptomatic carriers spreading the *S. brasiliensis* fungus (*2*,*5*,*7*,*10*). In addition, the nearest epidemic focus is on the Brazil side of the Triple Frontier (*7*), and to our knowledge, Buenos Aires and Santa Cruz reported the latest cases of feline sporotrichosis in Argentina (*1*).

Asymptomatic carriers hinder sporotrichosis control efforts by delaying diagnosis and treatment. Screening all contacts of confirmed cases is essential to minimize the risk for transmission (*1*,*10*). Addressing those challenges requires mandatory case reporting and public health measures. The detection and control of the expansion of feline sporotrichosis outside Brazil in contiguous countries requires coordinated cross-border One Health actions and context-specific interventions, which will be crucial to safeguard local communities and tourists (*1*,*5*).

Acknowledgments

We thank the Ministerio de Salud Pública (Misiones) and Instituto Misionero de Biodiversidad for support and collaboration, as well as Consejo de Veterinarios de Misiones, Zoonosis Iguazú, private veterinary clinics in Puerto Iguazú, the Sociedad Rural de Ganado Menor (Misiones), and all pet owners involved in the study for their trust and cooperation.

This study adhered to established ethical standards for veterinary research, ensuring the welfare and humane treatment of all animals involved. Sample collection was performed by qualified veterinarians using minimally invasive methods to reduce discomfort and stress. Procedures followed veterinary best practices and complied with international guidelines. Informed consent was obtained from all pet owners, who were briefed on the study objectives, methods, and potential benefits. The study protocol was reviewed and approved by the Institutional Ethics Committee and Institutional Commission for the Care and Use of Experimental Animals of the Faculty of Agricultural and Veterinary Sciences, Universidad del Salvador, Pilar, Provincia de Buenos Aires, Argentina (ICCUEA06-2021), with permits for the collection of natural resources and/or genetic material granted by the Instituto Misionero de Biodiversidad, Puerto Iguazú, Misiones, Argentina, and the Ministerio de Ecología y Recursos Naturales (Misiones) Argentina (Expte. 9950-70-2023-1).

The strains were deposited in the culture collection of the Mycology Department at Instituto Nacional de Enfermedades Infecciosas, Administración Nacional de Laboratorios e Institutos de Salud, Buenos Aires, Argentina and in the Biobank of the Instituto Misionero de Biodiversidad, Puerto Iguazú, Misiones, Argentina (https://imibio.misiones.gob.ar/es). The data presented are part of a broader ongoing project, Proyecto SIGEVA-USAL 2022-2025, entitled Estudio eco-epidemiológico y sanitario de *Sporothrix brasiliensis* en localidades correntinas y misioneras del Corredor Jesuítico Guaraní Argentino.

About the Author

Dr. Vizcaychipi is a professor of microbiology at Universidad del Salvador and a researcher at the Instituto Misionero de Biodiversidad and the Instituto Nacional de Medicina Tropical, Administración Nacional de Laboratorios e Institutos de Salud–"Carlos G. Malbrán," Puerto Iguazú, Misiones, Argentina. Her research interests focus on emerging tropical zoonoses, including parasites and fungi, approached through a One Health framework.

References

1. Etchecopaz A, Toscanini MA, Gisbert A, Mas J, Scarpa M, Iovannitti CA, et al. *Sporothrix brasiliensis*: a review of an emerging South American fungal pathogen, its related disease, presentation and spread in Argentina. J Fungi (Basel). 2021;7:170. https://doi.org/10.3390/jof7030170
2. Rodrigues AM, de Hoog GS, de Camargo ZP. *Sporothrix* species causing outbreaks in animals and humans driven by animal–animal transmission. PLoS Pathog. 2016;12:e1005638. https://doi.org/10.1371/journal.ppat.1005638
3. Rabello VBS, Almeida MA, Bernardes-Engemann AR, Almeida-Paes R, de Macedo PM, Zancopé-Oliveira RM. The historical burden of sporotrichosis in Brazil: a systematic review of cases reported from 1907 to 2020. Braz J Microbiol. 2022;53:231–44. https://doi.org/10.1007/s42770-021-00658-1
4. Córdoba S, Isla G, Szusz W, Vivot W, Hevia A, Davel G, et al. Molecular identification and susceptibility profile of *Sporothrix schenckii* sensu lato isolated in Argentina. Mycoses. 2018;61:441–8. https://doi.org/10.1111/myc.12760
5. Rossow JA, Queiroz-Telles F, Caceres DH, Beer KD, Jackson BR, Pereira JG, et al. A One Health approach to combatting *Sporothrix brasiliensis*: narrative review of an emerging zoonotic fungal pathogen in South America. J Fungi (Basel). 2020;6:247. https://doi.org/10.3390/jof6040247
6. Thomson P, González C, Blank O, Ramírez V, Río CD, Santibáñez S, et al. Sporotrichosis outbreak due to *Sporothrix brasiliensis* in domestic cats in Magallanes, Chile: a One-Health-approach study. J Fungi (Basel). 2023;9:226. https://doi.org/10.3390/jof9020226
7. Prado C, Chiyo L, Santi C, Cognialli R, Reis G, Geraldo M, et al. P464 feline sporotrichosis: an emerging disease in the Brazilian side of the Southern Triple Border. Med Mycol. 2022;60(suppl 1):myac072P464.
8. do Prado CM, Razzolini E, Santacruz G, Ojeda L, Geraldo MR, Segovia N, et al. First cases of feline sporotrichosis caused by *Sporothrix brasiliensis* in Paraguay. J Fungi (Basel). 2023;9:972. https://doi.org/10.3390/jof9100972
9. Ribeiro Dos Santos A, Misas E, Min B, Le N, Bagal UR, Parnell LA, et al. Emergence of zoonotic sporotrichosis in Brazil: a genomic epidemiology study. Lancet Microbe. 2024;5:e282–90. https://doi.org/10.1016/S2666-5247(23)00364-6
10. Cognialli RCR, Cáceres DH, Bastos FAGD, Cavassin FB, Lustosa BPR, Vicente VA, et al. Rising incidence of *Sporothrix brasiliensis* infections, Curitiba, Brazil, 2011–2022. Emerg Infect Dis. 2023;29:1330–9. https://doi.org/10.3201/eid2907.230155

Address for correspondence: Katherina A. Vizcaychipi, Rucci No. 56, N3370 Puerto Iguazú, Misiones, Argentina; email: kvizcaychipi@gmail.com

Trichophyton indotineae Infection, São Paulo, Brazil, 2024

João Nobrega de Almeida Jr, Amanda R. dos Santos, Mario Roberto de S. Trindade, Jeremy A.W. Gold, Fernanda P.M. Razo, Sarah S. Gonçalves, Erick G. Dorlass, Renato de Mello Ruiz, Jacyr Pasternak, Cristovão L.P. Mangueira, Silke Uhrlaß, Pietro Nenoff, Shyam B. Verma, André M. Doi, Marines D.V. Martino

Author affiliations: Federal University of São Paulo, São Paulo, Brazil (J. Nobrega de Almeida Jr); Antimicrobial Resistance Institute of São Paulo, São Paulo (J. Nobrega de Almeida Jr); Hospital Israelita Albert Einstein, São Paulo (J. Nobrega de Almeida Jr, M.R. de S. Trindade, E.G. Dorlass, R. de Mello Ruiz, J. Pasternak, C.L.P. Mangueira, A.M. Doi, M.D.V. Martino); Centers for Disease Control and Prevention, Atlanta, Georgia, USA (A.R. dos Santos, J.A.W. Gold); Policlínica Lincoln de Freitas Filho, Rio de Janeiro, Brazil (F.P.M. Razo); Federal University of Espírito Santo, Vitoria, Brazil (S.S. Gonçalves); Labopart Medical Laboratories, Roetha OT Moelbis, Germany (S. Uhrlaß, P. Nenoff); Nirvan and In Skin Clinics, Vadodara, Gujarat, India (S.B. Verma)

DOI: https://doi.org/10.3201/eid3105.250048

We report an extensive, terbinafine-resistant (squalene epoxidase F397L mutation) *Trichophyton indotineae* infection in a previously healthy businessman from São Paulo, Brazil. The patient had previously traveled to France, Spain, and the United States. Clinician awareness, laboratory testing capacity, and surveillance are essential to prevent *T. indotineae* spread and inform healthcare practices.

Trichophyton indotineae is an anthropophilic, frequently terbinafine-resistant fungus causing recalcitrant dermatophytosis. It has become endemic in South Asia; cases are documented across 6 continents, and possible local US transmission has been reported (*1*,*2*). São Paulo, Brazil, South America's largest city, is known for its global business connections and frequent international travelers.

In September 2024, a previously healthy São Paulo man in his 40s sought treatment for difficult-to-treat tinea cruris. In October 2023, he traveled to Paris and Barcelona, and 30 days later, he traveled to Boston, Massachusetts, USA. He had not traveled to Asia. Six weeks after he returned home, he noticed pruritic, erythematous, bilateral groin lesions. He treated the lesions with topical betamethasone and ketoconazole, but they worsened. After consulting multiple dermatologists, he was prescribed oral terbinafine (9 weeks), with no improvement.

Subsequently, another dermatologist, accessed by telemedicine, performed a full-body examination and identified additional lesions at the dorsal region of the left foot. Groin lesions had irregular borders, erythematous inflammatory areas, and reddish scaly plaques (Figure 1); the dorsal region of the left foot had small scaly erythematous plaques. Direct microscopy from groin and foot skin scrapings was positive, and a culture of groin scrapings showed dermatophyte mold.

Initial matrix-assisted laser desorption/ionization time-of-flight mass spectrometry analysis using the Biotyper 3.0 database (Bruker Daltonics, https://www.bruker.com) identified the organism as part of the *Trichophyton mentagrophytes* group. Additional analysis using the MSI-2 database (Université Paris VI, https://msi.happy-dev.fr) identified *T. indotineae* with high confidence (*3*). The physician switched the patient's treatment to itraconazole (200 mg/d), with substantial improvement noted after 8 weeks.

We confirmed the identification of *T. indotineae* by using internal transcribed spacer ribosomal DNA sequencing analysis (GenBank accession no. PQ726960). Antifungal susceptibility testing (Appendix, https://wwwnc.cdc.gov/EID/article/31/5/25-0048-App1.pdf) for the isolate using broth microdilution showed high MICs against terbinafine (>4 mg/L) and fluconazole (32 mg/L) and strong in vitro activity against itraconazole (0.016 mg/L) and voriconazole (0.125 mg/L) (*4*). Currently, clinical breakpoints for interpreting antifungal susceptibility testing of *T. indotineae* do not exist.

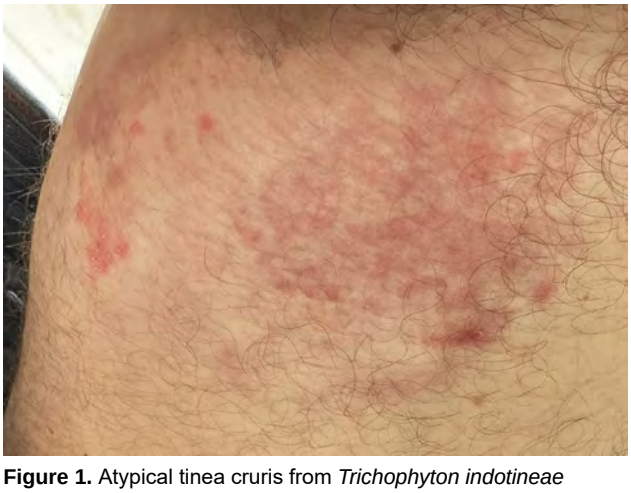

Figure 1. Atypical tinea cruris from *Trichophyton indotineae* infection, São Paulo, Brazil, 2024. A photograph of the left groin (provided by the patient) shows lesions characterized by poorly defined margins, hyperemic scaly plaques in the medial region, and an inflammatory infiltrate in the central-lateral area.

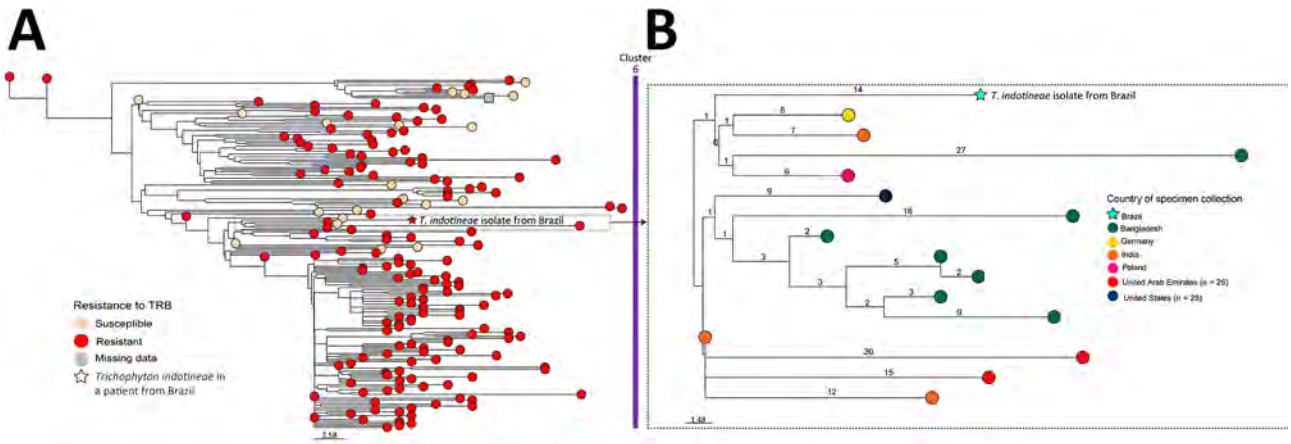

Figure 2. *Trichophyton indotineae* phylogenetic tree analysis by terbinafine susceptibility profile and country of origin for *T. indotineae* infection, São Paulo, Brazil, 2024. A) Neighbor-joining phylogenetic tree, which includes terbinafine-resistant and -susceptible *T. indotineae* isolates belonging to cluster 6. Isolates were considered terbinafine resistant if they had a missense point mutation in the squalene epoxidase (*SQLE*) gene for *Trichophyton* spp. linked to terbinafine resistance (*5*,*6*). B) Subcluster containing the isolate from the patient in Brazil. Among the 12 isolates in that subcluster, 5 resistant isolates, including an isolate from Germany, had the *SQLE* substitution F397L. Branch lengths represent the single-nucleotide polymorphism distance between isolates, and leaf colors correspond to the different countries in which each specimen was collected. The neighbor-joining tree and map were visualized together with each sample's metadata using Microreact version 252 (https://docs.microreact.org). Scale bar represents number of single-nucleotide polymorphisms. TRB, terbinafine.

We performed genomic analyses to assess the isolate's possible origins and to detect the presence of squalene epoxidase (*SQLE*) gene mutations associated with terbinafine resistance (*5*,*6*). We performed whole-genome sequencing by using the NextSeq 550 system (Illumina, https://www.illumina.com). We deposited read data into National Center for Biotechnology Institute Sequence Read Archive database (https://www.ncbi.nlm.nih.gov/sra; BioProject no. PRJNA1196410). We downloaded an additional 347 *T. indotineae* sequences from isolates collected in 14 countries from the Sequence Read Archive database (Appendix Table 2) and included them in the genomic analysis (A.R. dos Santos et al., unpub. data). We performed single-nucleotide polymorphism (SNP) identification and phylogenetic analysis using MycoSNP version 1.5 (https://github.com/CDCgov/mycosnp-nf), with *T. indotineae* strain TIMM20114 as the reference genome. We performed SNP identification in the *SQLE* gene by mapping filtered reads to a reference sequence (OM313310.1) by using the Burrows-Wheeler Aligner (https://bio-bwa.sourceforge.net), followed by variant calling with freebayes (https://github.com/freebayes/freebayes). Genomic analysis showed that the isolate from the patient from Brazil was closely related to other terbinafine-resistant *T. indotineae* isolates from 13 countries (Figure 2). Among isolates analyzed, the isolate from the patient from Brazil was most genetically similar to one from Lower Saxony, Germany (21 SNPs distance). The isolate was collected from a patient with terbinafine-resistant *T. indotineae* in June 2022, and, like the isolate from the patient in Brazil, it had a terbinafine resistance–conferring *SQLE* gene mutation (F397L).

We report a case of tinea caused by terbinafine-resistant *T. indotineae* in a businessman from Brazil who traveled to Europe and the United States. Genomic analysis revealed that the patient's isolate contained a terbinafine resistance–conferring *SQLE* mutation, F397L, and fit within a predominantly terbinafine-resistant cluster of isolates collected from countries across North America, Europe, and Asia. Although it is uncertain where the patient acquired infection, his isolate's close relatedness to one from Germany suggests possible acquisition in Europe. However, additional analysis, including of isolates from Barcelona, Paris, and Boston, is essential to confirm where the infection was acquired.

Clinicians should be vigilant for possible *T. indotineae* infection in persons who have traveled abroad or seek treatment for difficult-to-treat tinea because local transmission may occur. Clinicians should advise those patients about strategies to prevent transmission (*7*), need for prolonged therapy (e.g., ≥6 weeks) with itraconazole (*8*), and importance of avoiding topical corticosteroids and antifungal corticosteroid products, which can worsen tinea infections (*8*).

In Brazil and other resource-limited settings, lack of specialized and well-equipped microbiology laboratories could enable unrecognized introduction and local spread (*9*). Increasing laboratory capacity

for dermatophyte species identification, antifungal susceptibility testing, and genomic epidemiology studies is essential for monitoring transmission patterns and guiding effective treatment strategies (*10*). Combining matrix-assisted laser desorption/ionization time-of-flight mass spectrometry with the improved MSI-2 database might help overcome challenges of identifying *T. indotineae* in skin scraping cultures in clinical laboratories. That approach might also enhance epidemiologic understanding of global spread of that species and contribute to improved patient care (*3*). In conclusion, this case highlights the importance of integrating clinical, microbiological, and genomic data to address spread of antimicrobial-resistant pathogens in an increasingly interconnected world.

Acknowledgments

We thank the whole Mycology and Molecular Biology Teams from the Clinical Laboratory of Hospital Albert Einstein, including Wendy Colalto Rodrigues da Silva, Kornelia Bogner, Lidiane de Oliveria, Fabiane Camargo Gomes Nunes, Cristiani da Silva Calo, Nair Hideko Muto, and Rubia Anita Ferraz Santana, for invaluable support in sample processing, data analysis, and expertise in molecular techniques that contributed to the success of this study.

This report was approved by the institutional review board from Hospital Albert Einstein (no. CAAE 85377824.2.0000.0071). J.N.d.A. has a research grant from Fundação de Amparo à Pesquisa do Estado de São Paulo (grant no. 2024/12605-9).

About the Author

Dr. Nobrega de Almeida Jr is a physician specializing in infectious diseases and clinical pathology. He serves as a medical assistant at the Clinical Laboratory of Hospital Albert Einstein in São Paulo and is an assistant professor of infectious diseases at the Federal University of São Paulo. His primary research interest is in medical mycology.

References

1. Uhrlaß S, Verma SB, Gräser Y, Rezaei-Matehkolaei A, Hatami M, Schaller M, et al. *Trichophyton indotineae*—an emerging pathogen causing recalcitrant dermatophytoses in India and worldwide—a multidimensional perspective. J Fungi (Basel). 2022;8:757. https://doi.org/10.3390/jof8070757
2. Caplan AS, Todd GC, Zhu Y, Sikora M, Akoh CC, Jakus J, et al. Clinical course, antifungal susceptibility, and genomic sequencing of *Trichophyton indotineae*. JAMA Dermatol. 2024;160:701–9. https://doi.org/10.1001/jamadermatol.2024.1126
3. Normand AC, Moreno-Sabater A, Jabet A, Hamane S, Cremer G, Foulet F, et al. MALDI-TOF mass spectrometry online identification of *Trichophyton indotineae* using the MSI-2 application. J Fungi (Basel). 2022;8:1103. https://doi.org/10.3390/jof8101103
4. Arendrup MC, Kahlmeter G, Guinea J, Meletiadis J; Subcommittee on Antifungal Susceptibility Testing (AFST) of the ESCMID European Committee for Antimicrobial Susceptibility Testing (EUCAST). How to: perform antifungal susceptibility testing of microconidia-forming dermatophytes following the new reference EUCAST method E.Def 11.0, exemplified by Trichophyton. Clin Microbiol Infect. 2021;27:55–60. https://doi.org/10.1016/j.cmi.2020.08.042
5. De Paepe R, Normand AC, Uhrlaß S, Nenoff P, Piarroux R, Packeu A. Resistance profile, terbinafine resistance screening and MALDI-TOF MS identification of the emerging pathogen *Trichophyton indotineae*. Mycopathologia. 2024;189:29. https://doi.org/10.1007/s11046-024-00835-4
6. Saunte DML, Hare RK, Jørgensen KM, Jørgensen R, Deleuran M, Zachariae CO, et al. Emerging terbinafine resistance in *Trichophyton*: clinical characteristics, squalene epoxidase gene mutations, and a reliable EUCAST method for detection. Antimicrob Agents Chemother. 2019;63:e01126–219. https://doi.org/10.1128/AAC.01126-19
7. American Academy of Dermatology Association. Preventing and treating *Trichophyton indotineae* [cited 2024 Dec 17]. https://www.aad.org/member/clinical-quality/clinical-care/emerging-diseases/dermatophytes/preventing-treating-trichophyton-indotineae
8. Khurana A, Sharath S, Sardana K, Chowdhary A. Clinico-mycological and therapeutic updates on cutaneous dermatophytic infections in the era of *Trichophyton indotineae*. J Am Acad Dermatol. 2024;91:315–23. https://doi.org/10.1016/j.jaad.2024.03.024
9. Falci DR, Pasqualotto AC. Clinical mycology in Latin America and the Caribbean: a snapshot of diagnostic and therapeutic capabilities. Mycoses. 2019;62:368–73. https://doi.org/10.1111/myc.12890
10. Lockhart SR, Smith DJ, Gold JAW. *Trichophyton indotineae* and other terbinafine-resistant dermatophytes in North America. J Clin Microbiol. 2023;61:e0090323. https://doi.org/10.1128/jcm.00903-23

Address for correspondence: João Nobrega de Almeida Jr, Hospital Israelita Albert Einstein, Av Albert Einstein, 627/701 Morumbi, São Paulo SP 05652–900, Brazil; email: joao.nobregaa@einstein.br

Molecular Epidemiology of St. Louis Encephalitis Virus, São Paulo State, Brazil, 2016–2018

Giovana Santos Caleiro,[1] Ingra M. Claro,[1] Xinyi Hua, Giovana V. Basile, Karolina M.B. Nuevo, Charlys A. da Costa, Rosa M. Tubaki, Regiane M.T. de Menezes, Sirle A.S. Scandar, Lilian A.R. Colebrusco, Emerson L.L. Araújo, William M. de Souza, Ester C. Sabino, Nuno R. Faria, Mariana Sequetin Cunha

Author affiliations: University of São Paulo, São Paulo, Brazil (G.S. Caleiro, I.M. Claro, C.A. da Costa, E.C. Sabino, N.R. Faria); Instituto Adolfo Lutz, São Paulo (G.S. Caleiro, G.V. Basile, K.M.B. Nuevo, M.S. Cunha); University of Kentucky, Lexington, Kentucky, USA (I.M. Claro, X. Hua, W.M. de Souza); Pasteur Institute, São Paulo, São Paulo (R.M. Tubaki, R.M.T. de Menezes, S.A.S. Scandar, L.A.R. Colebrusco); Ministry of Health, Brasília, Brazil (E.L.L. Araújo); Imperial College London, London, UK (N.R. Faria)

DOI: https://doi.org/10.3201/eid3105.250158

We detected St. Louis encephalitis virus (SLEV) in 0.16% (3/3,375) of *Aedes* and *Sabethes* spp. mosquitoes captured during 2016–2018 in São Paulo State, Brazil. We also isolated and confirmed that the SLEV strains belong to genotype III. Continued surveillance is required to clarify the burden of SLEV in Brazil.

St. Louis encephalitis virus (SLEV; species *Orthoflavivirus louisense*) is an endemic mosquitoborne orthoflavivirus in the Americas that can cause febrile and central nervous system diseases in humans, neurologic illnesses in equids, and fatal outcomes in both (*1*,*2*). SLEV is transmitted in enzootic and epizootic transmission cycles mainly by *Culex* and related genera of mosquitoes; humans and equids are incidental and dead-end hosts (*1*). In South America, sporadic SLEV human cases have been reported since 1953, and numerous serosurveys indicated SLEV circulation (*1*,*3*–*5*). However, reports of active SLEV circulation remain scarce in South America. Here, we conducted a molecular epidemiology study in mosquitoes collected during 2016–2018 in São Paulo state, Brazil.

During November 2016–June 2019, we captured Culicinae mosquitoes across 9 genera and combined the samples into 3,375 pools for analysis. The most abundant species were *Aedes scapularis* (26.5%, 893/3,375) and *Ae. albopictus* (21.7%, 731/3,375) (Appendix, https://wwwnc.cdc.gov/EID/article/31/5/25-0158-App1.pdf). Next, we extracted RNA from all homogenized mosquito pools and performed real-time reverse transcription PCR (RT-PCR) to detect flavivirus RNA (*6*). We detected flavivirus RNA in 0.16% (3/3,375) of the mosquito pools. Positive mosquito pools were *Ae. albopictus* (strain no. MO239, n = 3 specimens), *Ae. aegypti* (strain no. MO1424, n = 1 specimen), and *Sabethes chloropterus* (strain no. MO730, n = 1 specimen), which were collected during November 24, 2016–February 16, 2017, in São José do Rio Preto and Araçatuba municipalities (Appendix). Subsequently, we conducted viral isolation in *Ae. albopictus* clone C6/36 cells from positive samples. We isolated all 3 positive strains in C6/36 cells and confirmed by immunofluorescent staining and real-time RT-PCR. Then, we used nanopore sequencing (*7*) to obtain nearly complete coding sequences (≥99%) for 6 SLEV strains, at an average coverage >20-fold/nucleotide. We submitted all sequences to GenBank (accession nos. PP855630–4 and PP871388).

To contextualize SLEV circulation in São Paulo state, we sequenced 3 SLEV isolates identified in São Paulo state during 1993–2004 that had been either partially sequenced or never sequenced (Appendix). Next, we conducted a maximum-likelihood phylogenetic analysis that showed that the SLEV strains MO239, MO1424, and MO730 from this study, and historical strain SPH253157 clustered in a well-supported clade (100% bootstrap) at the basal of genotype III (Figure). In addition, historical SLEV strains SPAR149623 and SPAR147631 clustered within genotype V, along with strains identified in Brazil and Peru during 1973–2006 and in the United States in 2003 (Figure). The SLEV strains we sequenced shared 98.6%–98.9% nucleotide identity with other genotype III strains and 99.8%–99.9% nucleotide identity among themselves. The newly sequenced genotype V strains showed a 93.3% nucleotide divergence from the genotype III strains. We identified 75 aa substitutions across the sequenced SLEV strains; most substitutions were in the envelope and nonstructural 4B proteins (16.0%, 12/75 in each) and the nonstructural 5 protein (38.7%, 29/75) (Appendix).

This study reports the active circulation of SLEV during 2016–2018 in São Paulo state, Brazil. We found that SLEV genotype III continues to circulate in Brazil in *Aedes* and *Sabethes* spp. mosquitoes since the human case that was reported in 2004 (*8*). SLEV genotype III has caused sporadic outbreaks in Argentina since 1979 (*6*). In 2014, SLEV genotype III was identified in the western United States, presumably intro-

[1]These authors contributed equally to this article.

duced from South America by migratory birds (*9*). We detected SLEV in *Ae. albopictus*, *Ae. aegypti*, and *Sa. chloropterus* mosquitoes, but the role of those mosquito species in SLEV transmission requires further field and experimental entomological studies. Also, the *Sa. chloropterus* mosquito is a vector of yellow fever virus in Brazil, but its role in SLEV transmission remains to be determined.

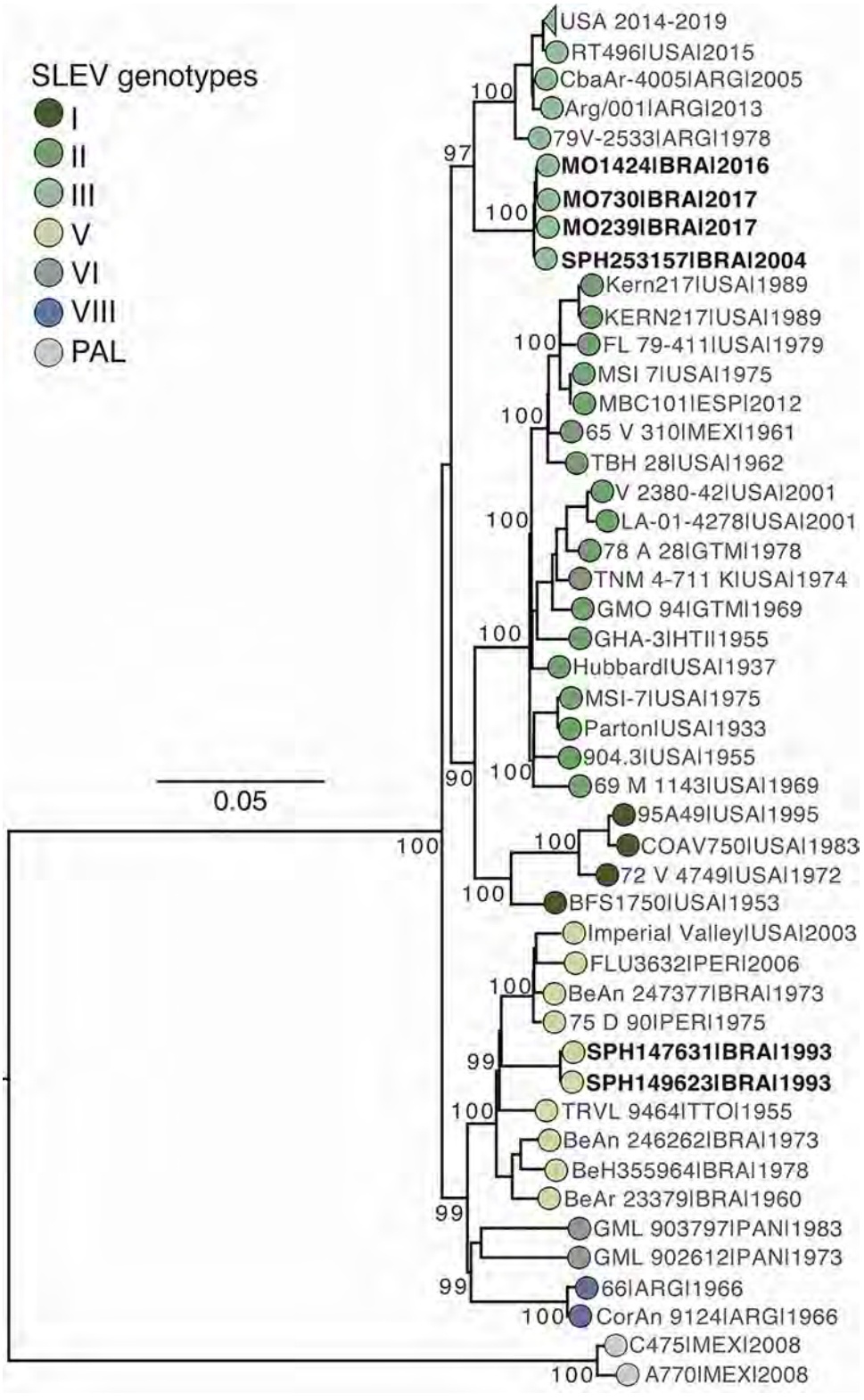

Figure. Maximum-likelihood phylogenetic tree in a study of molecular epidemiology of St. Louis encephalitis virus in São Paulo State, Brazil, 2016–2018. Tree shows 219 representative SLEV complete coding sequence genomes, including 3 new genomes generated in this study from *Aedes albopictus* (MO239), *Ae. aegypti* (MO1424), and *Sabethes chloropterus* (MO730) mosquitoes. The tree also includes 3 historical partially sequenced or unsequenced SLEV isolates from São Paulo state: SPAR149623 (*Culex* sp. mosquito, Santo Antônio de Aracanguá, May 12, 1993), SPAR147631 (*Anopheles triannulatus* mosquito, Pereira Barreto, March 11, 1993), and SPH253157 (human, São Pedro, January 1, 2004). Tree tips are colored by genotype. Phylogenies are midpoint-rooted for clarity; bootstrap values (1,000 replicates) are shown on major nodes. Scale bar represents nucleotide substitutions per site. GenBank accession numbers for the sequences and detailed information on the collapsed USA clade (genotype III, circulating during 2014–2019) is provided in the Appendix (https://wwwnc.cdc.gov/EID/article/31/5/25-0158-App1.pdf). SLEV, St. Louis encephalitis virus.

The first limitation of our study is that we focused on the molecular detection of SLEV in mosquitoes, which provides insight into active infections, but further investigations are required to assess SLEV circulation in vertebrates, including humans, through molecular and serologic methods. Serologic methods in areas with cocirculating flaviviruses present challenges because of potential cross-reactivity (*10*); however, this approach can substantially contribute to our understanding of the extent of both current and past SLEV infections in the region. Second, our mosquito sampling was predominately *Aedes* spp., but because *Culex* spp. mosquitoes are the primary vector for SLEV, more research is needed to determine the dynamic transmission of SLEV in Brazil. Finally, the lack of blood meal analysis in our study prevents the identification of potential amplifying hosts for SLEV in the region and the determining vector feeding preferences.

In conclusion, our study demonstrates active SLEV circulation in mosquitoes in São Paulo state, Brazil. These findings emphasize the need for continued surveillance efforts using a One Health concept to understand the transmission dynamics and ecologic drivers of SLEV.

Acknowledgments

We thank the Superintendence for Control of Endemic Diseases, State of São Paulo (Sucen), team for mosquito capture and Viviana Menezes for mosquito RNA extraction. We also thank Vector-borne Diseases laboratory staff for field surveillance studies and virus isolation.

We dedicate this article in memory of Akemi Suzuki.

This study was supported by CNPq (grant no. 305628/2020-8) and the Medical Research Council (MRC) and São Paulo Research Foundation (FAPESP) (grant nos. MR/S0195/1, 2018/14389-0, and 2022/05637-6).

G.S.C. was sponsored by Fesima project (grant no. GAPS/NATO 479/2020). I.M.C. was supported by São Paulo Research Foundation (grant nos. 2018/17176-8 and 2023/11521-3), and the Bill and Melinda Gates Foundation (INV-034540). G.V.B. was sponsored by São Paulo Research Foundation (grant no. 2021/09103-3). W.M.d.S was supported by a Global Virus Network fellowship, Burroughs Wellcome Fund (grant no. 1022448), and Wellcome Trust–Digital Technology Development award (Climate Sensitive Infectious Disease Modelling; grant no. 226075/Z/22/Z).

About the Author

Dr. Caleiro is a postdoctoral researcher at the Institute of Biological Sciences, University of São Paulo, Brazil. Her research interests include epidemiological surveillance of emerging viruses with a focus on arboviruses and respiratory viruses.

References

1. Diaz A, Coffey LL, Burkett-Cadena N, Day JF. Reemergence of St. Louis encephalitis virus in the Americas. Emerg Infect Dis. 2018;24:2150–7. https://doi.org/10.3201/eid2412.180372
2. Rosa R, Costa EA, Marques RE, Oliveira TS, Furtini R, Bomfim MR, et al. Isolation of Saint Louis encephalitis virus from a horse with neurological disease in Brazil. PLoS Negl Trop Dis. 2013;7:e2537. https://doi.org/10.1371/journal.pntd.0002537
3. Rodrigues SG, Nunes MR, Casseb SM, Prazeres AS, Rodrigues DS, Silva MO, et al. Molecular epidemiology of Saint Louis encephalitis virus in the Brazilian Amazon: genetic divergence and dispersal. J Gen Virol. 2010;91:2420–7. https://doi.org/10.1099/vir.0.019117-0
4. Diaz LA, Ré V, Almirón WR, Farías A, Vázquez A, Sanchez-Seco MP, et al. Genotype III Saint Louis encephalitis virus outbreak, Argentina, 2005. Emerg Infect Dis. 2006;12:1752–4. https://doi.org/10.3201/eid1211.060486
5. Silva JR, Romeiro MF, Souza WM, Munhoz TD, Borges GP, Soares OA, et al. A Saint Louis encephalitis and Rocio virus serosurvey in Brazilian horses. Rev Soc Bras Med Trop. 2014;47:414–7. https://doi.org/10.1590/0037-8682-0117-2014
6. Cunha MS, Luchs A, Dos Santos FCP, Caleiro GS, Nogueira ML, Maiorka PC. Applying a pan-flavivirus RT-qPCR assay in Brazilian public health surveillance. Arch Virol. 2020;165:1863–8. https://doi.org/10.1007/s00705-020-04680-w
7. Claro IM, Ramundo MS, Coletti TM, da Silva CAM, Valenca IN, Candido DS, et al. Rapid viral metagenomics using SMART-9N amplification and nanopore sequencing. Wellcome Open Res. 2023;6:241. https://doi.org/10.12688/wellcomeopenres.17170.2
8. Santos CL, Sallum MA, Franco HM, Oshiro FM, Rocco IM. Genetic characterization of St. Louis encephalitis virus isolated from human in São Paulo, Brazil. Mem Inst Oswaldo Cruz. 2006;101:57–63. https://doi.org/10.1590/S0074-02762006000100011
9. Swetnam DM, Stuart JB, Young K, Maharaj PD, Fang Y, Garcia S, et al. Movement of St. Louis encephalitis virus in the western United States, 2014–2018. PLoS Negl Trop Dis. 2020;14:e0008343. https://doi.org/10.1371/journal.pntd.0008343
10. Fischer C, Jo WK, Haage V, Moreira-Soto A, de Oliveira Filho EF, Drexler JF. Challenges towards serologic diagnostics of emerging arboviruses. Clin Microbiol Infect. 2021;27:1221–9. https://doi.org/10.1016/j.cmi.2021.05.047

Address for correspondence: Mariana Sequetin Cunha, Instituto Adolfo Lutz, São Paulo, São Paulo, Brazil; email: masequetin@gmail.com

Case Report of *Aerococcus urinae* Tricuspid Valve Endocarditis, New York, USA

Tasfia Siam, Tyler Stephen, Sonal Munsiff

Author affiliations: Shaheed Tajuddin Medical College, Gazipur, Bangladesh (T. Siam); University of Rochester Medical Center, Rochester, New York, USA (T. Stephen, S. Munsiff)

DOI: https://doi.org/10.3201/eid3105.250013

We report a case of a 61-year-old man in New York, USA, who had recurrent *Aerococcus urinae* endocarditis that first involved his native and then his bioprosthetic tricuspid valve. We demonstrate that a complicated *A. urinae* endocarditis case can be successfully treated with single-agent antimicrobial drug therapy and surgery.

Aerococcus urinae is a gram-positive, catalase-negative, α-hemolytic coccal bacterium predominantly found in the urinary tract. Historically, *A. urinae* has been frequently misidentified because of limitations in biochemical testing. However, advances in microbiology have enabled more reliable identification (*1*). Infective endocarditis caused by *A. urinae* is rarely reported (*2*). We report a case of *A. urinae* endocarditis in a patient who had a previous bioprosthetic valve replacement because of endocarditis caused by this organism. Written consent was obtained from the patient for publication of clinical information and photographs.

A 61-year-old man sought care at an emergency department in New York, USA, after a fall at home. Three weeks before seeking care, he had stopped taking torsemide, metformin, and lisinopril at his home and had switched to a carnivore diet consisting of only meat. Two weeks before seeking care, he experienced recurrent falls, progressive general weakness, fatigue, dyspnea on exertion, and decreased oral intake; painful hand and foot lesions also developed. He denied having fevers, chills, chest pain, or urinary symptoms before hospital admission. His medical history included chronic kidney disease, bulbar urethral stricture with prior perineal urethrostomy 8 years before, type 2 diabetes mellitus, and coronary artery disease. In addition, he had been admitted 14 months before for native tricuspid valve endocarditis caused by *A. urinae* and for L2–L3 lumbar discitis. He was treated for 6 weeks with intravenous ceftriaxone for endocarditis and osteomyelitis. Two weeks into therapy, he underwent bioprosthetic tricuspid valve replacement and coronary artery bypass graft surgery. Pathologic examination indicated acute endocarditis with fibrinosuppurative vegetations; however, Gram stain results were negative, and no organisms were isolated.

At emergency department admission, the patient was afebrile. Physical examination revealed a new III/VI systolic murmur and reddish/purple papular, nonblanching rashes on all 4 distal extremities (Figure 1). The patient's serum creatinine level was 4.13 mg/dL, glomerular filtration rate was 16 mL/min/1.73 m^2, and blood hemoglobin A1C was 10.0%. Urinalysis showed 3+ blood, 2+ leukocyte esterase, 6–10 leukocytes/high-power field, and no bacteria. No sample was sent for culture because of minimal pyuria. Blood cultures grew *A. urinae* (penicillin MIC <0.03 μg/mL, ceftriaxone MIC <0.12 μg/mL). A transthoracic echocardiogram showed large masses involving all bioprosthetic tricuspid valve leaflets, leading to reduced excursion and severe valve stenosis (Figure 2). Magnetic resonance imaging of the lumbar spine showed no evidence of active osteomyelitis or discitis. Bladder examination showed postvoid residual volumes within reference ranges, and prostate ultrasound results were unremarkable. Biopsies of skin lesions indicated leukocytoclastic vasculitis.

We diagnosed infective endocarditis associated with vasculitis and immune complex–mediated glomerulonephritis. We considered the infection to be recurrent rather than relapsed. He underwent intravenous ceftriaxone (2 g/d) treatment while awaiting drug susceptibility testing, and his blood cultures cleared within 24 hours. After MIC testing indicated antimicrobial drug susceptibility, we switched his treatment to renally dosed, continuous infusion penicillin G (12 million units/d). Because of large vegetations and valvular dysfunction, he underwent a repeat tricuspid valve replacement 4 weeks into therapy; tissue cultures were negative, and pathologic examination showed inflammatory cells and fibrin without

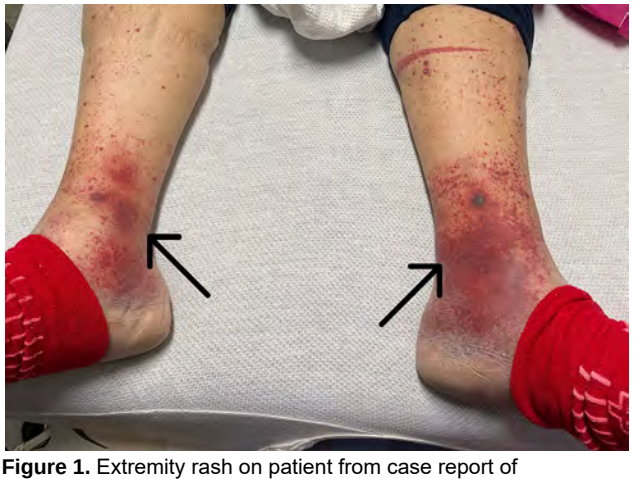

Figure 1. Extremity rash on patient from case report of *Aerococcus urinae* tricuspid valve endocarditis. Rash (arrows) was documented at the time the patient sought care.

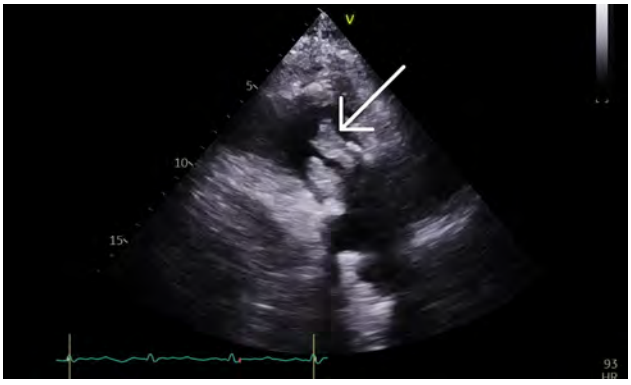

Figure 2. Echocardiogram of patient from case report of *Aerococcus urinae* tricuspid valve endocarditis. Arrow indicates tricuspid mass. V at top of image indicates positive inflection. Numbers on the left side indicate depth from the ultrasound probe (in cm). Electrical signal profile is indicated at the bottom of the image.

organisms. He completed 6 weeks of parenteral antimicrobial drug therapy without adverse drug effects. Nine months after completion of antimicrobial drug therapy, he had no residual or recurrent symptoms.

A. urinae and other aerococci are more common as uropathogens. Although the urinary tract is believed to be the initial source of bacteremia and endocarditis in many reports, aerococcal infections might remain unidentified in urinary cultures because of the lack of optimal (5%) carbon dioxide exposure during laboratory incubation (*2*,*3*). Risk factors for aerococcal endocarditis include older age, male sex, urinary tract infection, prostate hyperplasia, urethral strictures, urinary tract surgery, and urinary catheter usage (*4*,*5*). Our patient's previous urethral stricture had been addressed by perineal urethrostomy years before this case, and he was functioning without urinary symptoms, although that history appears to be his strongest predisposing factor. It is unclear whether his dietary change and discontinuation of cardiac and diabetes medications directly contributed to his more recent illness.

A review of 58 cases of *Aerococcus* endocarditis revealed that mitral and aortic valve involvement was predominant; only 2 cases implicated the tricuspid valve, and only 2 cases involved prosthetic valves (*6*). Additional cases showed endocarditis affected a native tricuspid valve and a prosthetic aortic valve (*7*,*8*). This case showed a less commonly reported prosthetic tricuspid valve endocarditis.

Case-fatality rates of 14%–27% have been reported for *Aerococcus* endocarditis in case series, underscoring an opportunity and need for improved care (*7*,*9*). Clinical studies to determine optimal doses and duration of therapy against aerococcal infections have not been performed. *Aerococcus* spp. consistently show susceptibility to vancomycin, but some species show decreased susceptibility to penicillin and sulfamethoxazole. In vitro bactericidal synergism with β-lactams and daptomycin or an aminoglycoside has also been reported (*2*,*10*). Surgical intervention is not always required because many cases respond well to antimicrobial drug therapies (*1*). However, this case demonstrates successful treatment of a complicated case by using single-agent antimicrobial drug therapy and surgery.

About the Author

Dr. Siam is a graduate of Shaheed Tajuddin Ahmad Medical College, Bangladesh, and is currently volunteering on a research project focusing on antibiotic stewardship interventions and rare bacterial infections. Her interests include clinical training and research in internal medicine, particularly infectious diseases.

References

1. Feghaly J, Rivas Rios J, Ravi M, Sattiraju S, Missov E. Aerococcus urinae infective endocarditis. Cureus. 2022;14:e23947. https://doi.org/10.7759/cureus.23947
2. Rasmussen M. Aerococcus: an increasingly acknowledged human pathogen. Clin Microbiol Infect. 2016;22:22–7. https://doi.org/10.1016/j.cmi.2015.09.026
3. Senneby E, Petersson AC, Rasmussen M. Clinical and microbiological features of bacteraemia with Aerococcus urinae. Clin Microbiol Infect. 2012;18:546–50. https://doi.org/10.1111/j.1469-0691.2011.03609.x
4. Varughese R, Mathew A, Chadha R, Kostka J, Regelmann D. Prosthetic valve endocarditis caused by Aerococcus urinae. IDCases. 2020;21:e00912. https://doi.org/10.1016/j.idcr.2020.e00912
5. Yabes JM, Perdikis S, Graham DB, Markelz A. A rare case of Aerococcus urinae infective endocarditis in an atypically young male: case report and review of the literature. BMC Infect Dis. 2018;18:522. https://doi.org/10.1186/s12879-018-3414-0
6. Saeed Al-Asad K, Mazhar N, Srivastava S, Quadri S, Mitra S. Aerococcus urinae endocarditis: a case report and literature review. Cureus. 2022;14:e29853. https://doi.org/10.7759/cureus.29853
7. Adeel M, Tariq S, Akthar H, Zaghloul A, Iorgoveanu C, Dehner C. Case report: a rare case of prosthetic valve infective endocarditis caused by Aerococcus urinae. F1000Res. 2017;6:1998. https://doi.org/10.12688/f1000research.12776.1
8. Banerjee S, Murali S, Azhar A, Pathmanathan A, Chaudhuri D. Aerococcus urinae tricuspid valve infective endocarditis. Proc (Bayl Univ Med Cent). 2022;35:522–3. https://doi.org/10.1080/08998280.2022.2054042
9. Tai DBG, Go JR, Fida M, Saleh OA. Management and treatment of Aerococcus bacteremia and endocarditis. Int J Infect Dis. 2021;102:584–9. https://doi.org/10.1016/j.ijid.2020.10.096
10. Hirzel C, Hirzberger L, Furrer H, Endimiani A. Bactericidal activity of penicillin, ceftriaxone, gentamicin and daptomycin alone and in combination against Aerococcus urinae. Int J Antimicrob Agents. 2016;48:271–6. https://doi.org/10.1016/j.ijantimicag.2016.05.007

Address for correspondence: Tyler Stephen, University of Rochester Medical Center, 601 Elmwood Ave, Box 689, Rochester, NY 14627, USA; email: tyler_stephen@urmc.rochester.edu

Increased Pneumonia-Related Emergency Department Visits, Northern Italy

Simone Villa, Manuel Maffeo, Mauro Maistrello, Giorgio Bagarella, Vincenzo Navobi Porrello, Federica Morani, Francesco Scovenna, Fausto Baldanti, Paolo Bonfanti, Elena Pariani, Andrea Gori, Luigi Vezzosi, Gabriele Del Castillo, Sabrina Buoro, Danilo Cereda

Author affiliations: University of Milan, Milan, Italy (S. Villa, F. Scovenna, E. Pariani, A. Gori); Directorate General for Health of the Lombardy Region, Milan (M. Maffeo, M. Maistrello, G. Bagarella, L. Vezzosi, G. Del Castillo, S. Buoro, D. Cereda); University of Pavia, Pavia, Italy (V.N. Porrello, F. Baldanti); Istituto di Ricovero e Cura a Carattere Scientifico San Raffaele Scientific Institute, Milan (F. Morani); Fondazione Istituto di Ricovero e Cura a Carattere Scientifico Policlinico San Matteo, Pavia, (F. Baldanti); University of Milano Bicocca, Monza, Italy (P. Bonfanti)

DOI: https://doi.org/10.3201/eid3105.241790

An increase in pneumonia-related emergency department visits was observed in Lombardy, northern Italy, during June–October 2024. Viral causes appear insufficient to explain the increase, suggesting a bacterial cause. *Mycoplasma pneumoniae* and *Bordetella pertussis* emerged as possible causes when other surveillance systems were consulted, but the reasons behind this trend remain unknown.

The Emergency Department (ED) Syndromic Surveillance (EDSyS) system has been implemented in various settings and has proven to be useful for detecting early signs of infectious disease outbreaks (*1*). In preparation for the 2024–25 influenza season and to enhance pandemic preparedness, EDSyS was implemented across the Lombardy region (≈10 million population) in northern Italy, covering all 103 EDs. This system can provide early warnings of public health issues and to adapt health care capacity in response to seasonal public health challenges such as influenza and emergent or unknown threats. Visits are classified by diagnosis and coded by using the International Classification of Diseases, 9th Revision. Visits were coded according to Centers for Disease Control and Prevention guidelines (*2*), including COVID-19 pneumonia, and were classified as pneumonia-associated. Those visits were monitored and analyzed against 2021–2023 figures, disaggregated by age groups (<1 year, 1–4 years, 5–17 years, 18–64 years, and ≥65 years). The data in this article were last updated on November 4, 2024.

Total ED visits (Appendix Figure 1, https://wwwnc.cdc.gov/EID/article/31/5/24-1790-App1.pdf) were constantly elevated throughout 2024, most notable in summer during July (week 27 total 70,599 vs. historic maximum of 67,835) and August (week 35 total 67,540 vs. historic maximum of 60,710). Concurrently, a considerable increase in pneumonia-associated visits was recorded from week 18 of 1,164 visits, compared with the previous maximum of 959 visits in 2021 (Figure 1), largely among those 5–17 years of age.

During June–September 2024, there were 10,022 pneumonia-associated hospitalizations compared with 8,118 in 2023. Most hospitalizations were coded as pneumonia, organism unspecified (3,602 cases), bacterial pneumonia, unspecified (1,906 cases), or bronchopneumonia, unspecified organism (1,515 cases). Compared with the summer of 2023, a marked increase was observed for pneumonia caused by *Mycoplasma pneumoniae* (769 cases in 2024 vs. 53 cases in 2023, a 14.5-fold increase). Likewise, 85 cases of pneumonia caused by *Chlamydophila pneumoniae* were recorded in the summer 2024 versus 33 cases in 2023 (2.6-fold increase). In addition, 3 cases of pneumonia caused by *Bordetella pertussi* were reported in the summer of 2024 summer compared with none in 2023.

Because of our findings, we reviewed data from 3 other regional surveillance systems, focusing on the notification of infectious diseases, community syndromic surveillance, and virologic surveillance of respiratory viruses in EDs, to identify trends or outbreaks of causes of pneumonia that may have gone unnoticed. Our search focused on diseases reported through the statutory regional notification system for infectious diseases, including pneumonia caused by *M. pneumoniae* as a mandatory notification at the regional level since December 2023. In total, 366 notifications of pneumonia caused by *M. pneumoniae* were recorded, and high weekly frequency occurred during week 18 (April 29, 2024) through week 45 (November 4, 2024). Notifications of pneumonia caused by *M. pneumoniae* peaked in week 29 (July 15, 2024), when 24 cases were reported (Figure 2, panel A), mostly in hospitalized persons (72%, n = 263) and in persons 5–17 years old (52%, n = 189). For pertussis, 180 cases were recorded in 2024 (vs. 4 in 2023; 44-fold increase), mostly in persons <1 year of age (23%, n = 42) and 5–17 years of age (46%, n = 83). Notifications of pertussis reached peaks in June (30 cases) and July (34 cases) (Figure 2, panel B).

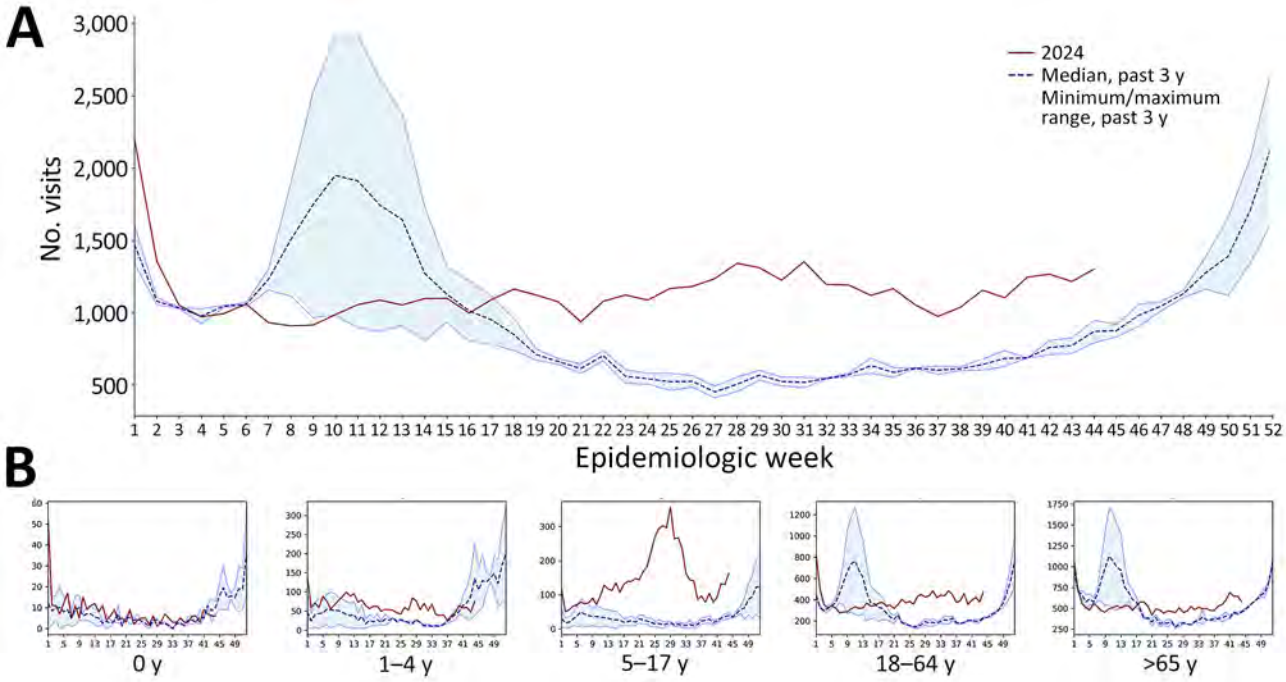

Figure 1. Increasing number of pneumonia-related emergency department visits for all causes, northern Italy, June–October 2024, compared with previous 3 years. A) Weekly number of pneumonia-associated emergency department visits across all patients. B) Weekly number of pneumonia-associated emergency department visits by age group.

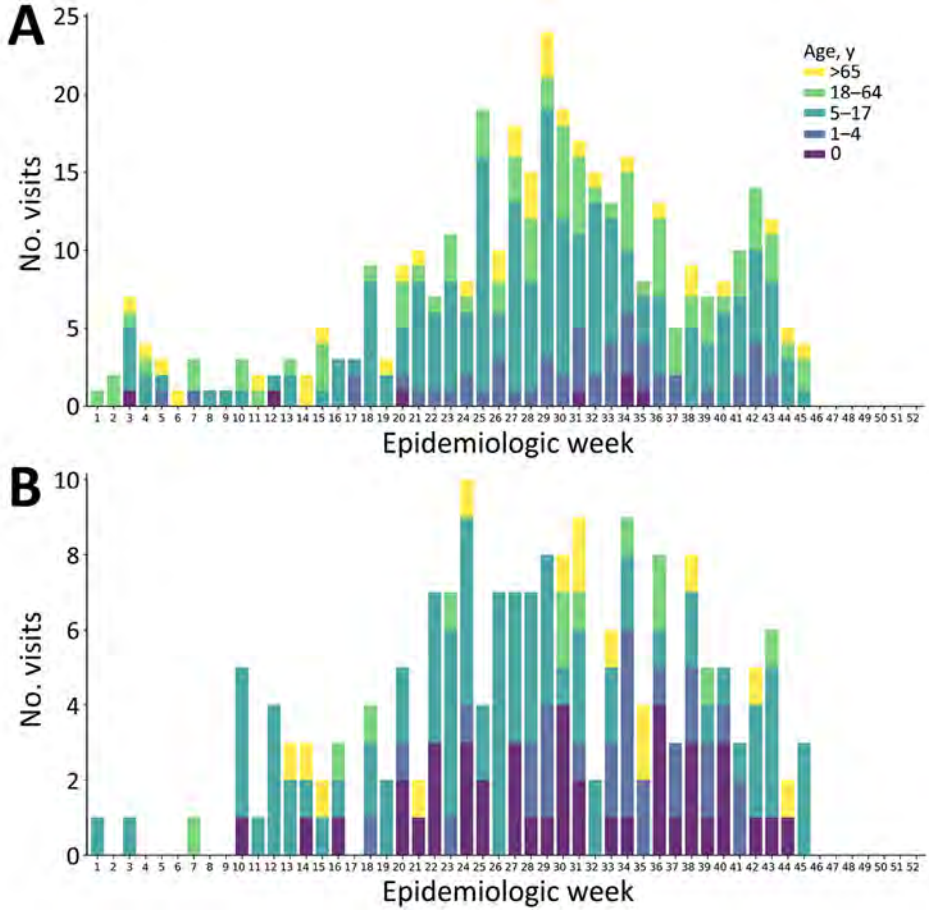

Figure 2. Increasing number of pneumonia-related emergency department visits for *Mycoplasma pneumoniae* (A) and pertussis (B), by age group, northern Italy, June–October 2024. Cases were notified by the regional infectious disease surveillance systems.

The surveillance system for influenza-like illness (ILI), part of the surveillance network (RespiVirNet, https://www.iss.it/en/respivirnet) of Italy, which uses data reported by general practitioners and pediatricians, was unable to identify any major change in ILI incidence (Appendix Figure 2). Likewise, existing virologic surveillance of ILI-associated ED visits during summer 2024 did not detect increased activity of any viral pathogens.

Because of the stringent measures implemented to curb the increase of COVID-19 cases in 2020, the population was less exposed to periodic small epidemics of common respiratory infections (*3*), and immunization programs were slowed down or halted, including immunization of pregnant women and children against pertussis (*4*). Other countries observed increased cases of pneumonia caused by *M. pneumoniae*, starting at the end of 2023, when China reported clusters of respiratory diseases in children (*5*). More recently, the United Kingdom (*6*) and the United States (*7*) also reported increased cases of those causes of pneumonia. Likewise, after a decline in cases of pertussis was observed during the COVID-19 pandemic, the disease returned to pre-pandemic levels or higher, as reported by some countries (*8*). Despite no decrease in vaccination coverage, an immunity debt might be the underlying reason for the increase in cases (*9*). Other pathogens, or a combination of pathogens, might be responsible for the observed increase in pneumonia-associated ED visits (*10*).

In conclusion, in northern Italy, we are extending ED surveillance to include bacteria such as *M. pneumoniae* and *B. pertussis*. We have found the newly implemented EDSyS is a promising tool for early detection of infectious diseases outbreaks; additional improvements to the system are in development. In particular, the range of syndromes covered will be expanded to include gastrointestinal syndromes, and automatic alerts for outbreak detection will strengthen overall pandemic preparedness.

Author contributions: conceptualization D.C. G.D.C., and F.B.; data curation M.M., G.B., and V.N.P.; data analysis M.M., G.B., and S.V.; supervision D.C., and G.D.C; manuscript drafting S.V.; manuscript review, editing, and approval all authors.

About the Author

Dr. Villa is a medical resident in public health at the University of Milan and a master of science candidate in epidemiology at the London School of Hygiene and Tropical Medicine. His research interest is the epidemiology and burden of infectious diseases such as tuberculosis, COVID-19, and human papillomavirus.

References

1. Ageron FX, Hugli O, Dami F, Caillet-Bois D, Pittet V, Eckert P, et al. Lessons from COVID-19 syndromic surveillance through emergency department activity: a prospective time series study from western Switzerland. BMJ Open. 2022;12:e054504. https://doi.org/10.1136/bmjopen-2021-054504
2. Centers for Disease Control and Prevention's National Syndromic Surveillance Program Community of Practice. ICD-10-CM master mapping reference table [cited 2024 Nov 4]. https://knowledgerepository.syndromicsurveillance.org/icd-10-cm-master-mapping-reference-table
3. Meyer Sauteur PM, Beeton ML, Pereyre S, Bébéar C, Gardette M, Hénin N, et al.; European Society of Clinical Microbiology and Infectious Diseases Study Group for Mycoplasma and Chlamydia Infections, and the ESGMAC Mycoplasma pneumoniae Surveillance study group. *Mycoplasma pneumoniae*: delayed re-emergence after COVID-19 pandemic restrictions. Lancet Microbe. 2024; 5:e100–1. https://doi.org/10.1016/S2666-5247(23)00344-0
4. Tessier E, Campbell H, Ribeiro S, Rai Y, Burton S, Roy P, et al. Impact of the COVID-19 pandemic on *Bordetella pertussis* infections in England. BMC Public Health. 2022;22:405. https://doi.org/10.1186/s12889-022-12830-9
5. World Health Organization. WHO statement on reported clusters of respiratory illness in children in northern China. 2023 November 22 [cited 2024 Nov 4]. https://www.who.int/news/item/22-11-2023-who-statement-on-reported-clusters-of-respiratory-illness-in-children-in-northern-china
6. Todkill D, Lamagni T, Pebody R, Ramsay M, Woolham D, Demirjian A, et al. Persistent elevation in incidence of pneumonia in children in England, 2023/24. Eurosurveill. 2024;29:pii=2400485. https://doi.org/10.2807/1560-7917.ES.2024.29.32.2400485
7. Centers for Disease Control and Prevention. *Mycoplasma pneumoniae* infection surveillance and trends. 2024 Oct [cited 2024 Nov 4]. https://www.cdc.gov/mycoplasma/php/surveillance
8. European Centre for Disease Prevention and Control. Increase of pertussis cases in the EU/EEA. 2024 May 8 [cited 2024 Nov 4]. https://www.ecdc.europa.eu/sites/default/files/documents/Increase%20in%20pertussis%20cases%20in%20the%20EU-EEA%20-%20May%202024%20FINAL.pdf
9. Reicherz F, Golding L, Lavoie PM, Abu-Raya B. Decay of anti-*Bordetella pertussis* antibodies in women of childbearing age following COVID-19 non-pharmaceutical measures. Vaccine. 2022;40:3746–51.
10. Pariani E, Piralla A, Pellegrinelli L, Giardina F, Porrello VN, Romano G, et al. Enhanced laboratory surveillance of respiratory infection disclosed the rapid rise of enterovirus D68 cases, northern Italy, August to September 2024. Eurosurveillance. 2024;29:pii=2400645. https://doi.org/10.2807/1560-7917.ES.2024.29.41.2400645

Address for correspondence: Simone Villa, Department of Biomedical Sciences for Health, University of Milan, Via Pascal, 36, Milan, 20133, Italy; email: simone.villa@unimi.it

Clinical and Epidemiologic Characteristics of Mpox Cases, Dominican Republic, July 2022–February 2023

Robert Paulino-Ramirez, Wilfredo Rafael Matias, Hector Lora-Rodríguez, Grey Benoît, Joel Ureña, Monica Thormann, Ronald Skewes-Ramm

Author affiliations: Universidad Iberoamericana, Santo Domingo, Dominican Republic (R. Paulino-Ramirez, H. Lora-Rodriguez); Brigham and Women's Hospital, Boston, Massachusetts, USA (W.R. Matias); Massachusetts General Hospital, Boston (W.R. Matias); Ministry of Health, Santo Domingo (G. Benoît, M. Thormann, R. Skewes-Ramm); Ministry of Defense, Santo Domingo (J. Ureña)

DOI: https://doi.org/10.3201/eid3105.241299

During July 2022–February 2023, mpox was confirmed in 71 of 283 suspected cases in the Dominican Republic; 32.4% of patients were women, and 22.5% children <10 years of age. We found differences in transmission compared with global trends, emphasizing the need for continued surveillance, diagnostics, and public health interventions.

Mpox is a zoonotic disease caused by the monkeypox virus (MPXV), which belongs to clade I (formerly Congo Basin clade) or clade II (formerly West Africa clade) (*1*). First identified in humans in the Democratic Republic of the Congo, mpox has become a global public health concern (*2*). As of December 2024, a total of 124,753 cases and 272 deaths have been reported in 128 countries; 54% of cases occurred in the Americas (*3*). Mpox spreads through close physical contact and fomites (*4*). Although sexual contact played a key role in the 2022–2023 mpox outbreak, nonsexual transmission also occurs, especially in children (*5*). In Latin America and the Caribbean, MPXV has circulated with varying disease outbreak intensity (*6*).

In the Dominican Republic, the first confirmed mpox case was reported in July 2022. We reviewed clinical and epidemiologic characteristics of reported cases to elucidate the epidemic in the Dominican Republic and guide public health efforts.

We conducted a retrospective review of the Dominican Republic's national mpox database, which contains epidemiologic data collected by the Ministry of Public Health. Mpox is a reportable disease in the Dominican Republic, requiring healthcare workers to complete forms for suspected and confirmed cases, which are then uploaded to the national database. We analyzed data representing the

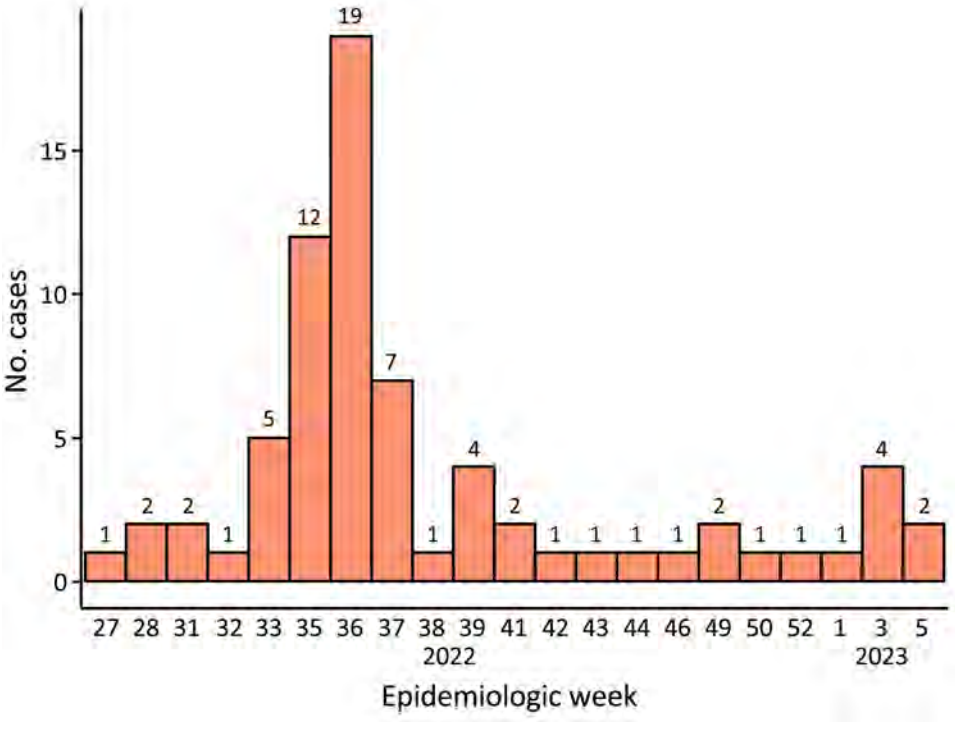

Figure. Number of confirmed mpox cases, by epidemiologic week, in study of clinical and epidemiologic characteristics of mpox, Dominican Republic, July 2022–February 2023. Numbers at the top of each bar indicate the actual number of cases for that week.

initial outbreak period during July 2022–February 2023 and defined cases as suspected, probable, or confirmed by using World Health Organization criteria (*7*). Medical authorities interviewed patients suspected of having mpox and collected sociodemographic and clinical information; samples for MPXV testing were taken from lesions, exudates, crusts, and blood (if no rash was present). The National Public Health Laboratory conducted sample testing by MPXV PCR, targeting G2R and C3L loci according to World Health Organization guidelines (*8*); a positive PCR result confirmed diagnosis of mpox. After confirmation, Ministry of Public Health epidemiologists conducted mandatory reporting, contact tracing, and household contact testing. We categorized suspected cases as confirmed or negative. We used R version 4.3.2 (The R Project for Statistical Computing, https://www.r-project.org) for analyses.

After the first mpox case was identified (July 2022), cases peaked in September and declined thereafter (Figure). Among 283 suspected cases, 71 (25.1%) were confirmed. Among confirmed mpox patients, 48 (67.6%) were male and 23 (32.4%) female; most (49.3%) male patients were 20–39 years of age. Sixteen (22.5%) confirmed mpox patients were children <10 years of age. Most (95.8%) confirmed mpox patients were born in the Dominican Republic; most (n = 39) cases occurred in the O Metropolitana region, encompassing Santo Domingo (Appendix Figure, https://wwwnc.cdc.gov/EID/article/31/5/24-1299-App1.pdf). We compiled sociodemographic and clinical characteristics (Table; Appendix Table). Most (90.1%) confirmed mpox patients manifested a rash, and 73.2% reported fever (>37.9°C; self-reported with or without a thermometer or measured by the person conducting household visits).

The Dominican Republic's mpox outbreak revealed unique epidemiologic patterns compared with other outbreaks; a higher percentage of women (32.4%) and children <10 years of age (22.5%) was observed. The patterns resemble those in endemic countries in Africa but contrast with global trends during the 2022–2023 outbreak, where most cases occurred in adult men who have sex with men (MSM) and only 3.6% of women and 1.1% of children <17 years of age globally (*9*). This divergence reflects either genuine differences in transmission dynamics or underreporting among MSM because of stigma and homophobia, which are common in the Dominican Republic and heightened by the intersectionality of HIV (*10*). Societal stigma against MSM in the Dominican Republic might influence sexual networks, leading to concurrent relationships with both men and women, promoting mpox transmission into heterosexual households. Within households, mpox might spread via close contact, caregiving, and shared personal items, contributing to more cases among women and children. Those findings highlight the need for comprehensive public health approaches, including stigma reduction and fostering community trust. Further research is needed to clarify transmission and guide interventions.

Table. Clinical and epidemiologic characteristics of suspected mpox cases in the Dominican Republic, July 2022–February 2023*

Patient characteristics	Confirmed cases	Negative cases
Total	71 (100.0)	212 (100.0)
Sex		
M	48 (67.6)	124 (58.5)
F	23 (32.4)	88 (41.5)
Age range, y		
0–9	16 (22.5)	55 (25.9)
10–19	6 (8.5)	22 (10.4)
20–29	19 (26.8)	41 (19.3)
30–39	16 (22.5)	45 (21.2)
40–49	4 (5.6)	15 (7.1)
50–59	7 (9.9)	15 (7.1)
≥60	3 (4.2)	19 (9.0)
Country of birth		
Dominican Republic	68 (95.8)	202 (95.3)
Other†	3 (4.2)	10 (4.7)
Highest education level		
None	10 (14.1)	38 (17.9)
Elementary school	8 (11.3)	23 (10.9)
Middle school	7 (9.9)	17 (8.0)
High school	14 (19.7)	47 (22.2)
College or technical school	11 (15.5)	24 (11.3)
Missing	21 (29.6)	63 (29.7)
Health region of residence		
I Valdesia	13 (18.3)	19 (9.0)
II Cibao Norte	11 (15.5)	25 (11.8)
III Cibao Nordeste	0	11 (5.2)
IV Enriquillo	0	10 (4.7)
O Metropolitana	39 (54.9)	122 (57.5)
V Este	6 (8.5)	11 (5.2)
VI Del Valle	0	2 (0.9)
VII Cibao Occidental	1 (1.4)	9 (4.2)
VIII Cibao Central	1 (1.4)	3 (1.4)
Health insurance type		
Private	23 (32.4)	55 (25.9)
Government subsidized	8 (11.3)	20 (9.4)
No reported insurance	11 (15.5)	53 (25.0)
Unknown	29 (40.8)	84 (39.6)
Time from symptom onset to seeking care, d (range)	5.0 (2.5–7.0)	4.0 (2.0–7.0)
Underlying illness		
Chronic diseases‡	5 (7.0)	8 (3.8)
HIV/AIDS	7 (9.9)	3 (1.4)
Malnutrition	0 (0.0)	2 (0.9)
Obesity/overweight	0 (0.0)	3 (1.4)
None	29 (40.8)	99 (46.7)
Missing	30 (42.3)	97 (45.8)

*Values are no. (%) except as indicated.
†Includes Germany, Belgium, United States, Haiti, Italy, Democratic Republic of Congo, Switzerland, and Venezuela.
‡Includes diabetes, chronic respiratory disease, hypertension, or other cardiovascular disease.

Positive mpox cases were clinically similar to negative cases; most patients experienced a rash and fever. Although using rash and fever as screening criteria assists case identification, their lack of specificity poses challenges, particularly in settings with limited diagnostic capabilities. Combining clinical criteria with exposure history or risk profiles might improve testing efficiency in diagnostic-constrained settings. Expanding access to diagnostics and developing easy-to-use tests for resource-limited settings are critical for accurate case identification and optimized resource allocation.

The first limitation of our study is that data collected during outbreak investigations likely underestimate true incidence. Second, because of the evolving nature of the outbreak, comprehensive data, including sexual orientation, were not available.

In conclusion, we describe the initial mpox outbreak during July 2022–February 2023 in the Dominican Republic; the percentage of infected women and children was higher than expected compared with the global outbreak predominantly affecting MSM. Although the country successfully implemented mandatory reporting and vaccine deployment, challenges remain, such as incomplete data capture, limited access to PCR, and barriers to healthcare access. Addressing those gaps will be essential to improve outbreak detection and prepare for future mpox outbreaks.

Acknowledgments

We thank the National Reference Laboratory for handling mpox samples and diagnostics, the Hospital Militar Ramón De Lara for their rapid installation of an isolation unit for mpox cases and reporting, and the provincial epidemiologists for their rapid deployment and reporting of mpox cases.

This study was approved by the Universidad Iberoamericana Institutional Review Board (approval no. CEI-2024-26).

W.R.M. was supported by the US National Institutes of Allergy and Infectious Diseases (grant no. T32 AI007433. Funding sources played no role in study design; in the collection, analysis, and interpretation of data; in the writing of the report; or in the decision to submit the paper for publication.

About the Author

Dr. Paulino-Ramirez is a principal investigator at Instituto de Medicina Tropical and Salud Global at Universidad Iberoamericana (UNIBE) in Santo Domingo, Dominican Republic. His research and clinical interests focus on infectious diseases, HIV, emerging viruses, public health, and the implementation of preventive strategies, such as preexposure prophylaxis.

References

1. Mitjà O, Ogoina D, Titanji BK, Galvan C, Muyembe JJ, Marks M, et al. Monkeypox. Lancet. 2023;401:60–74. https://doi.org/10.1016/S0140-6736(22)02075-X
2. Ladnyj ID, Ziegler P, Kima E. A human infection caused by monkeypox virus in Basankusu Territory, Democratic Republic of the Congo. Bull World Health Organ. 1972;46:593–7.
3. World Health Organization. Mpox: multi-country external situation report no. 46, published 28 January 2025 [cited 2025 Jan 30]. https://cdn.who.int/media/docs/default-source/documents/emergencies/mpox-multi-country-external-situation-report-no.-46.pdf
4. Alakunle EF, Okeke MI. Monkeypox virus: a neglected zoonotic pathogen spreads globally. Nat Rev Microbiol. 2022;20:507–8. https://doi.org/10.1038/s41579-022-00776-z
5. Low N, Bachmann LH, Ogoina D, McDonald R, Ipekci AM, Quilter LAS, et al. Mpox virus and transmission through sexual contact: defining the research agenda. PLoS Med. 2023;20:e1004163. https://doi.org/10.1371/journal.pmed.1004163
6. Quispe AM, Castagnetto JM. Monkeypox in Latin America and the Caribbean: assessment of the first 100 days of the 2022 outbreak. Pathog Glob Health. 2023;117:717–26. https://doi.org/10.1080/20477724.2023.2201979
7. World Health Organization. Surveillance, case investigation and contact tracing for mpox (monkeypox). Interim guidance, 20 March 2024 [cited 2024 Nov 27]. https://iris.who.int/bitstream/handle/10665/376306/WHO-MPX-Surveillance-2024.1-eng.pdf
8. Pan American Health Organization, World Health Organization. Laboratory guidelines for the detection and diagnosis of monkeypox virus infection [cited 2024 Aug 24]. https://www.paho.org/en/documents/laboratory-guidelines-detection-and-diagnosis-monkeypox-virus-infection
9. Laurenson-Schafer H, Sklenovská N, Hoxha A, Kerr SM, Ndumbi P, Fitzner J, et al.; WHO mpox Surveillance and Analytics team. Description of the first global outbreak of mpox: an analysis of global surveillance data. Lancet Glob Health. 2023;11:e1012–23. https://doi.org/10.1016/S2214-109X(23)00198-5
10. Yigit I, Paulino-Ramírez R, Waters J, Long DM, Turan JM, Budhwani H. A moderated mediation analysis of HIV and intersectional stigmas and antiretroviral adherence in people living with HIV in the Dominican Republic. AIDS Behav. 2024;28:3258–69. https://doi.org/10.1007/s10461-024-04425-9

Address for correspondence: Robert Paulino-Ramirez, Instituto de Medicina Tropical & Salud Global, Universidad Iberoamericana (UNIBE), Calle Majoma 13, Los Ríos, Santo Domingo, CP 10604, Dominican Republic; email: r.paulino1@unibe.edu.do

Corrections

Vol. 30, No. 3

The author list was incorrect in Larone's Medically Important Fungi: A Guide to Identification, 7th Edition (M.M. Azar). The article has been corrected online (https://wwwnc.cdc.gov/eid/article/30/3/23-1623_article).

Vol. 31, No. 2

Some of the data were inaccurate in Figure 1, panels C and D, in Comparison of Contemporary and Historic Highly Pathogenic Avian Influenza A(H5N1) Virus Replication in Human Lung Organoids (M. Flagg et al.). The article has been corrected online (https://wwwnc.cdc.gov/eid/article/31/2/24-1147_article).

Vol. 31, No. 3

A grant was missing from the funding list in Annual Hospitalizations for COVID-19, Influenza, and Respiratory Syncytial Virus, United States, 2023–2024 (K. Bi et al.). The article has been corrected online (https://wwwnc.cdc.gov/eid/article/31/3/24-0594_article).

Adolphe Philippe Millot (1857–1921). *Champignons-couleurs 2* (*Mushrooms color plate 02*) (detail). Public domain illustration from Larousse du XX^{e} siècle, 1932 Éditions.

The Oldest Art

Byron Breedlove

"Nature alone is antique, and the oldest art a mushroom" is an enduring quote from Scottish historian and writer Thomas Carlyle. This month's cover image, a color plate titled *Champignons*—the French word for mushrooms—from the 1932 edition *Larousse du XX^{e} siècle* (*Larousse of the 20th century*), celebrates examples of "the oldest art." Developed under the direction of editor and lexicographer Paul Augé, this six-volume *Larousse* comprised an estimated 235,000 articles, spanned 6,523 pages, and served as an encyclopedia and dictionary of the French language.

Author affiliation: Centers for Disease Control and Prevention, Atlanta, Georgia, USA

DOI: https://doi.org/10.3201/eid3105.AC3105

This natural history plate is the handiwork of Adolphe Philippe Millot, a painter, lithographer, and entomologist. Details about Millot's life are scant. Historian and curator William B. Ashworth notes that Millot "was the senior illustrator at the Museum of Natural History in Paris, at the end of the 19th century and the beginning of the 20th. But that's all we know. He presumably had a family, knew many French naturalists who *are* well known, and perhaps even had a certain social standing." Ashworth adds, "Millot went on to do thousands of illustrations for the *Larousse Encyclopedias* that appeared in various forms in the early 20th century."

Contemporary viewers will quickly recognize—before consulting the minuscule type in the figure's legend—that this colorful compendium includes

fungi other than mushrooms. During Millot's lifetime (and for nearly another half century), fungi were thought to be plants, and classifying fungal species was a nascent endeavor. The spell of Swedish botanist and taxonomist Carl Linnaeus, who had concluded in the mid-1700s that living organisms were either plants or animals, still lingered. During the 1960s, American plant ecologist Robert Whittaker determined that fungi are not plants and devised a taxonomic classification of the world's biota into five kingdoms: Animalia, Plantae, Fungi, Protista, and Monera.

Fungi are strong contenders for being the earth's least understood organism. Recent molecular studies demonstrate that fungi are more closely related to animals than to plants and fundamentally differ from plants at the cellular level. Cell walls of fungi are composed of chitin, also found in the exoskeletons of insects and crustaceans and in squid beaks, whereas cell walls of plants are made from cellulose. Fungi absorb nutrients from soil or other organic sources, such as rotting trees, whereas plants make their own food through photosynthesis. There is no decisive estimate on the number of fungi in existence. For instance, the authors of a 2024 article in the journal *IMA Fungus* estimated the number of fungal species to be between 1.5 and 10 million.

Science writer Cody Cottier offers this perspective: "Point to a patch of dirt, a body of water, even the air you're breathing, and odds are that it is teeming with mushrooms, molds and yeasts (or their spores) that no one has ever seen. In ocean trenches, Tibetan glaciers and all habitats between, researchers are routinely detecting DNA from obscure fungi. By sequencing the snippets, they can tell they're dealing with new species, thousands of them, that are genetically distinct from any known to science. They just can't match that DNA to tangible organisms growing out in the world."

Humans have found myriad uses for fungi, including as food; nearly 2,200 species of mushrooms can be safely consumed, and an estimated 100 species of known mushrooms can poison people. Fungi function as a leavening agent for breads; enable fermentation of cheeses and olives; and convert sugars from grains and fruits into beer, cider, and wine. At least 300 species of mushrooms contain psychoactive components—something indigenous cultures across the world have known for centuries—and contemporary clinicians and therapists are using such compounds for treating depression, posttraumatic stress disorder, substance abuse, and chronic pain. Antibiotics developed from fungi, such as penicillin and cyclosporine, have saved untold lives.

On the other hand, fungi also sicken and kill people. Hundreds of species of fungi, enough to fill perhaps 10 of Millot's color plates, are known to cause infections in humans. The Centers for Disease Control and Prevention notes that more than 1 billion people around the world experience a fungal infection each year. Aspergillosis, blastomycosis, candidiasis, coccidioidomycosis, cryptococcosis, histoplasmosis, and mucormycosis are fungal diseases that pose serious health concerns and are potentially deadly.

Microbiologist Arturo Casadevall explains, "Fungal diseases are difficult to manage because they tend to be chronic, hard to diagnose, and difficult to eradicate with antifungal drugs." Climate change, antimicrobial resistance, and various other factors are likely to lead to the emergence of fungal infections.

Bibliography

1. Ashworth WB. Scientist of the day—Adolphe Millot [cited 2025 Mar 31]. https://www.lindahall.org/about/news/scientist-of-the-day/adolphe-millot
2. Carlyle T. Sartor Resartus Book II, Chapter 3. The works of Thomas Carlyle in thirty volumes, Vol 1. London: Chapman and Hall Limited; 1896. p. 82.
3. Casadevall A. Fungal diseases in the 21st century: the near and far horizons. Pathog Immun. 2018;3:183–96. https://doi.org/10.20411/pai.v3i2.249
4. Cazabonne J, Walker AK, Lesven J, Haelewaters D. Singleton-based species names and fungal rarity: does the number really matter? IMA Fungus. 2024;15:7. https://doi.org/10.1186/s43008-023-00137-2
5. Centers for Disease Control and Prevention. About fungal diseases [cited 2025 Mar 31]. https://www.cdc.gov/fungal/about/index.html
6. Cottier C. Out of sight, 'dark fungi' run the world from the shadows [cited 2025 Apr 6]. https://www.scientificamerican.com/article/mysterious-dark-fungi-are-lurking-everywhere
7. Graeme KA. Mycetism: a review of the recent literature. J Med Toxicol. 2014;10:173–89. https://doi.org/10.1007/s13181-013-0355-2
8. Johnston E. What in earth? Understanding what fungi really are [cited 2025 Mar 31]. https://www.kew.org/read-and-watch/whats-a-fungi
9. Li H, Tian Y, Menolli N Jr, Ye L, Karunarathna SC, Perez-Moreno J, et al. Reviewing the world's edible mushroom species: a new evidence-based classification system. Compr Rev Food Sci Food Saf. 2021;20:1982–2014. https://doi.org/10.1111/1541-4337.12708
10. Rokas A. Evolution of the human pathogenic lifestyle in fungi. Nat Microbiol. 2022;7:607–19. https://doi.org/10.1038/s41564-022-01112-0
11. Whittaker RH. New concepts of kingdoms or organisms. Evolutionary relations are better represented by new classifications than by the traditional two kingdoms. Science. 1969;163:150–60. https://doi.org/10.1126/science.163.3863.150

Address for correspondence: Byron Breedlove, EID Journal, Centers for Disease Control and Prevention, 1600 Clifton Rd NE, Mailstop H16-2, Atlanta, GA 30329-4018, USA; email: byronbreedlove23@gmail.com

EMERGING INFECTIOUS DISEASES®

Upcoming Issue
Vectorborne Diseases

- Long-Term Clinical Outcomes of Adults Hospitalized for COVID-19 Pneumonia
- Prospective Multicenter Surveillance of *Helicobacter pylor*i and Non–*H. pylori Helicobacter* Infections during Medical Checkups, Japan, 2022
- Safety and Immunogenicity of Poultry Vaccine for Protecting Critically Endangered Avian Species against Highly Pathogenic Avian Influenza Virus, United States
- Diagnostic Accuracy of 3 Mpox Lateral Flow Assays for Antigen Detection, Democratic Republic of the Congo and United Kingdom
- Characterization of Adult and Pediatric Healthcare-Associated and Community-Associated *Clostridioides difficile* Infections, Canada, 2015–2022
- Force of Infection Model for Estimating Time to Dengue Virus Seropositivity among Expatriate Populations, Thailand
- *Baylisascaris procyonis* Roundworm in Common Raccoons, Mexico
- Nosocomial Transmission of *Plasmodium falciparum* Malaria, Spain, 2024
- Genesis and Spread of Novel Highly Pathogenic Avian Influenza A(H5N1) Clade 2.3.4.4b Virus Genotype EA-2023-DG Reassortant, Western Europe
- Clinical Manifestations, Risk Factors, and Disease Burden of Rickettsiosis, Cambodia, 2007–2020
- Negligible Neutralization of Influenza A(H5N1) Virus by Quadrivalent Seasonal Vaccines, United Kingdom, 2021–2024
- *Mycoplasma arginini* Cellulitis, Tenosynovitis, and Arthritis in a Kidney Transplant Recipient, Slovenia, 2024
- Cadaveric Human Growth Hormone–Associated Creutzfeldt-Jakob Disease with Long Latency Period, United States
- Use of Oral Flea Preventative to Control Rickettsia typhi–Infected Fleas on Reservoir Opossums, Galveston, Texas, USA, 2023–2024
- Global Prevalence of Nitroimidazole-Refractory Giardiasis, 2008–2020
- Highly pathogenic avian influenza A(H5N1) clade 2.3.4.4b virus isolated from a dairy farm worker in Michigan transmits through the air in a ferret model

Complete list of articles in the June issue at https://wwwnc.cdc.gov/eid/#issue-322

Earning CME Credit

To obtain credit, you should first read the journal article. After reading the article, you should be able to answer the following, related, multiple-choice questions. To complete the questions (with a minimum 75% passing score) and earn continuing medical education (CME) credit, please go to http://www.medscape.org/journal/eid. Credit cannot be obtained for tests completed on paper, although you may use the worksheet below to keep a record of your answers.

You must be a registered user on http://www.medscape.org. If you are not registered on http://www.medscape.org, please click on the "Register" link on the right hand side of the website.

Only one answer is correct for each question. Once you successfully answer all post-test questions, you will be able to view and/or print your certificate. For questions regarding this activity, contact the accredited provider, CME@medscape.net. For technical assistance, contact CME@medscape.net. American Medical Association's Physician's Recognition Award (AMA PRA) credits are accepted in the US as evidence of participation in CME activities. For further information on this award, please go to https://www.ama-assn.org. The AMA has determined that physicians not licensed in the US who participate in this CME activity are eligible for AMA PRA Category 1 Credits™. Through agreements that the AMA has made with agencies in some countries, AMA PRA credit may be acceptable as evidence of participation in CME activities. If you are not licensed in the US, please complete the questions online, print the AMA PRA CME credit certificate, and present it to your national medical association for review.

Article Title

Features of Invasive Aspergillosis Caused by *Aspergillus flavus*, France, 2012–2018

CME Questions

1. What was the most common risk factor for immune aspergillosis (IA) in the current study?

A. Treatment with chemotherapy
B. Diabetes mellitus
C. Hematologic malignancy
D. Solid organ transplantation

2. Which of the following findings were characteristic of patients with IA and diabetes vs other baseline risk conditions in the current study?

A. Older age
B. Shorter duration between onset of symptoms and diagnosis
C. Higher rate of pleuropulmonary involvement
D. Higher rates of disseminated IA

3. Which of the following statements regarding the anatomic site of IA infections in the current study is most accurate?

A. Approximately half of IA infections were disseminated
B. Most infections were in the pleuropulmonary space
C. Pleuropulmonary infections were associated with older age and a longer duration of symptoms vs ENT infections
D. 5% of patients with pulmonary IA had a fungal co-infection

4. Which of the following statements regarding prophylaxis and treatment of IA in the current study is most accurate?

A. Nearly three-quarters of patients were receiving antifungal prophylaxis before IA
B. The most common antifungal agent prescribed was voriconazole
C. Aspergillosis flavus was more susceptible to amphotericin B vs voriconazole
D. The case-fatality rate of IA was 2%

Earning CME Credit

To obtain credit, you should first read the journal article. After reading the article, you should be able to answer the following, related, multiple-choice questions. To complete the questions (with a minimum 75% passing score) and earn continuing medical education (CME) credit, please go to http://www.medscape.org/journal/eid. Credit cannot be obtained for tests completed on paper, although you may use the worksheet below to keep a record of your answers.

You must be a registered user on http://www.medscape.org. If you are not registered on http://www.medscape.org, please click on the "Register" link on the right hand side of the website.

Only one answer is correct for each question. Once you successfully answer all post-test questions, you will be able to view and/or print your certificate. For questions regarding this activity, contact the accredited provider, CME@medscape.net. For technical assistance, contact CME@medscape.net. American Medical Association's Physician's Recognition Award (AMA PRA) credits are accepted in the US as evidence of participation in CME activities. For further information on this award, please go to https://www.ama-assn.org. The AMA has determined that physicians not licensed in the US who participate in this CME activity are eligible for AMA PRA Category 1 Credits™. Through agreements that the AMA has made with agencies in some countries, AMA PRA credit may be acceptable as evidence of participation in CME activities. If you are not licensed in the US, please complete the questions online, print the AMA PRA CME credit certificate, and present it to your national medical association for review.

Article Title

Nationwide Observational Case–Control Study of Risk Factors for *Aerococcus* Bloodstream Infections, Sweden

CME Questions

1. Aerococci are most implicated in infection of which organ system?

A. Upper respiratory
B. Lower respiratory
C. Genitourinary
D. Skin

2. What were the most prominent characteristics of patients with bloodstream infections (BSIs) due to aerococci in the current study?

A. Either very young (aged <3 years) or very old (aged >70 years)
B. Middle-aged adults with either diabetes or chronic kidney disease
C. Age over 60 years and male sex
D. Living in an urban environment and a history of multiple sexual partners

3. Chronic illness of which organ systems were most associated with aerococcal BSIs in the current study?

A. Cardiac and pulmonary
B. Cardiac and renal
C. Rheumatologic and hepatic
D. Urinary and neurologic

4. Which of the following antibiotics was associated with a higher risk for subsequent aerococcal BSIs in the current study?

A. Nitrofurantoin
B. Clindamycin
C. Azithromycin
D. Tetracycline